

ROCKET RADIATION HANDBOOK

VOLUME I

"ROCKET RADIATION PHENOMENOLOGY AND THEORY"

AF CONTRACT F33657-72-C-0850

June 1974

ADA 042640



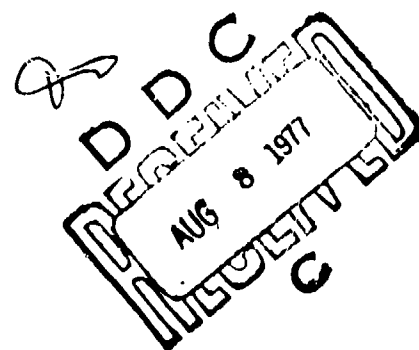
AD No. _____
DDC FILE COPY

Prepared for

Foreign Technology Division
United States Air Force
Wright-Patterson Air Force Base
Ohio 45433



AIRESEARCH MANUFACTURING COMPANY
OF CALIFORNIA



NOT FOR RELEASE
EXCEPT BY AUTHORITY OF
THE AIR FORCE

July 13, 1974 (expanded)
(Supersedes July 11 Erratta)

ERRATTA

VOLUME I, ROCKET RADIATION HANDBOOK

29 Nov 76

Place	Correction
✓ p. iii, line 5 from top	45933 should read 45433 ✓
✓ p. 141, Eq. (3.114)	$\frac{\text{Watts}}{\text{ster} \cdot \text{THz}}$ should read $\frac{\text{Watts}}{\text{ster} \cdot \mu\text{m}}$ ✓
✓ p. 242, Eq. (3.315)	2.8549×10^{18} should read 2.8549×10^6 ; multiply last two factors of equation by $\left(1 + \frac{1}{g_1}\right)$ ✓
✓ p. 243, Eq. (3.316)	2.8549×10^{18} should read 2.8549×10^6 ; multiply last two factors of equation by $\left(1 + \frac{\alpha}{g_\alpha}\right)$ ✓
✓ p. 264	Replace with corrected page 264 attached ✓
✓ p. 265	Replace with corrected page 265 attached ✓
✓ p. 282, Figure 4-3	Divide all power of 10^m on the ordinate by 10^2 (e.g. $10^9 \rightarrow 10^7$, etc.) ✓
✓ p. 285, Table 4-1	Replace with corrected table 4-1 attached ✓
✓ p. 365, third line from top	D_r should read D_v ✓
✓ p. 490	Add to $D_p = \dots$, defined by Eq. (C.40). ✓
✓ p. 490	Add: D_q = Diameter used in view-factor calculations defined by Eq. (C.41). ✓
✓ p. 513	Add: θ_s = Solar zenith angle, radians or degrees ✓
✓ p. 515	Add: μ = Special parameter used in view-factor calculations, defined by Eq. (C.47). ✓
✓ p. 521	Add: x_p, x_q, x_r, x_v = special dimensionless ratios used in view-factor calculations defined by Eqs. (C.43) through (C.46) ✓
✓ p. 521	Add: x_c = Factor used to calculate the average Core temperature. See Eq. (3.115). ✓
✓ p. 172, fourth line from bottom	D_e in Eq. (3.194) should read D_t ✓

ERRATTA
VOLUME 1, ROCKET RADIATION HANDBOOK

18 July 1974

29 Nov 74

PAGE	LOCATION	CORRECTION
✓ iii	line 3 in paragraph on "SPONSORSHIP"	change zip code to 45433 ✓
✓ 111	line 4 after EQ. 3.66	"and the other..." should begin at the left hand margin
✓ 120	definition of w_1, ϵ_1	✓ should read "statistical weight and energy respectively of level 1" ✓
150	last line of text before EQ. 3.141	change 3.64 to 3.66 ✓
151	definition of \bar{p}_I	units should be bars ✓
152	EQ. 3.143	exponent of p_a/p_e should be $3(\gamma-1)/(2\gamma)$ ✓
165	definition of γ	should read "ratio of specific heats at constant..." ✓
172	EQ. 3.194	change D_e to D_t ✓
242	EQ. 3.315	change 10^{18} to 10^6 ✓
243	EQ. 3.316	change 10^{18} to 10^6 ✓
264	first equation	change equation number to 3.362 ✓
282	Figure 4-3	divide all ordinate values by 100 (10 ⁹ becomes 10 ⁷ , etc.) ✓
285	Table 4-1	multiply all entries for $D_t(m)$ by 2 (0.206 becomes 0.412, etc.) ^t ✓
365	line 3 from top	D_r should read D_v ✓
490	definition of D_p bottom of page	add to end of definition ", defined by EQ. (C.40) ✓ add "D = Diameter used in view-factor calculations, defined by EQ. (C.41) ✓
513	top of page	add " μ = Special parameter used in view-factor calculations, defined by EQ. (C.47) ✓
521	between definitions of χ and ψ	add " $\chi_p, \chi_q, \chi_r, \chi_v$ = Special dimensionless ratios used in viewfactor calculations defined by EQs. (C.43) through (C.46) ✓

ADDITIONAL ERRATA

July 31, 1974
(Page 1 of 2)

VOLUME I, ROCKET RADIATION HANDBOOK

29

Location	Correction
p. 11, second line from top	Cross out:, as we shall show in Chapter 3
p. 150, second line from bottom	Eq. (3.64) should read Eq. (3.66) ✓
p. 151	Replace with new page attached ✓
p. 152, Eq. (3.145)	$T_{\text{exh}}^{3/2}$, should read $T_{\text{exh}} T_e^{1/2}$ ✓
p. 172, Eq. (3.193)	Replace with new page attached ✓
p. 173, Eq. (3.195)	Replace with new page attached ✓
p. 198, Eq. (3.265)	$\exp\left(-\frac{\epsilon_i}{kT_a}\right)$, should read $\exp\left(-\frac{h\nu_i}{kT_a}\right)$ ✓
	$\exp\left(-\frac{h\nu_a}{kT_a}\right)$, should read $\exp\left(-\frac{h\nu_a}{kT_a}\right)$ ✓
p. 198, Eq. (3.266)	$\exp\left(-\frac{\epsilon_i}{kT_a}\right)$, should read $\exp\left(-\frac{14,388.5}{\lambda_i T_a}\right)$ ✓
p. 204, second line from bottom	ϵ should read E ✓
p. 213, Eq. (3.286)	1.21 should read 1.39 ✓
p. 213, Eq. (3.287)	8.00 should read 9.19 ✓
p. 233, third line from top	ten should read six ✓
✓ p. 219, Eq. (3.293), and fourth line from top	<p>Cross out subscripts m on: $L_m(\nu_i)$, $L_m(\lambda_i)$, $L_m(\nu_{\text{ion}})$, $L_m(\lambda_{\text{ion}})$, etc.</p> <p>Should read: $L(\nu_i)$, $L(\lambda_i)$, $L(\nu_{\text{ion}})$, $L(\lambda_{\text{ion}})$, etc.</p>
P. 233, Eq. (3.295), Eq. (3.297), and fifth line from top	
p. 225, Eq. (3.301)	
p. 231, Eq. (3.305) ✓	
✓ p. 232, Eq. (3.307), Eq. (3.308)	
p. 233, fifth line from top ✓	
p. 234, Eq. (3.310) ✓	
p. 238, Eq. (3.313) ✓	
p. 239, Eq. (3.314), and fourth line from bottom ✓	

ADDITIONAL ERRATAJuly 31, 1974
(page 2 of 2)

VOLUME I, ROCKET RADIATION HANDBOOK

Location	Correction
p. 257, fifth line from topvibroni...., should read: vibronic
p. 259, sixth line from top	$k = 1$, should read: $k = i$
p. 261, fourth line from bottom approxi ated..., should read: approximated
p. 407, sixth line from bottom let, should read: led
p. 461, third line from top d_p , should read: α_p
p. 498	Add: $L(\lambda), L(\nu)$ = Contour function of special solar UV line defined by Eq. (3.292).

June 1974

18 17
FTD/CW-01-01-74-Vol-1
Vol. I

VOLUME I

6 ROCKET RADIATION HANDBOOK.

Volume I.

ROCKET RADIATION PHENOMENOLOGY
AND THEORY

10 Jozef W. / Eerkens

11 JUNE 1974

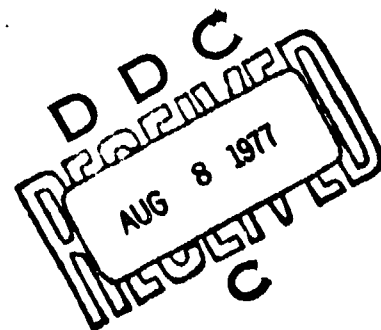
101-2-A007 746

12 562 p

AF CONTRACT F33657-72-C-0850

15

14 74-9903-Vol-1

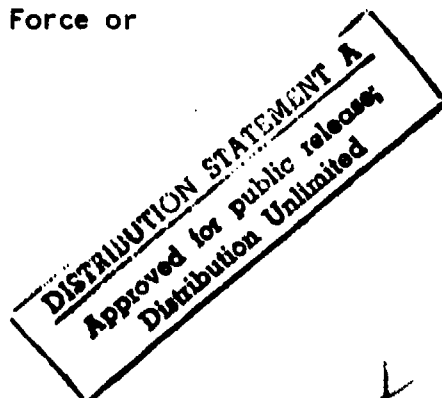


This document was prepared for the United States Air Force by the AiResearch Manufacturing Division of the Garrett Corporation. It has been reviewed by the USAF Foreign Technology Division, WPAFB, Ohio, 45433, but does not necessarily reflect the opinions of the US Air Force or the Department of Defense.



AIRESEARCH MANUFACTURING COMPANY
Los Angeles, California

404 881



mt

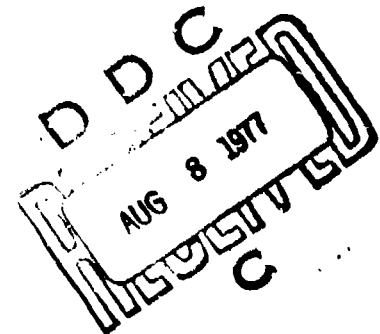
June 1974

FTD-CW-01-01-74
Vol. I

VOLUME I ROCKET RADIATION HANDBOOK

"ROCKET RADIATION PHENOMENOLOGY AND THEORY"

JUNE 1974



AF CONTRACT F33657-72-C-0850

This document was prepared for the United States Air Force by the AIRESEARCH Manufacturing Division of the Garrett Corporation. It has been reviewed by the USAF Foreign Technology Division, WPAFB, Ohio, 45433, but does not necessarily reflect the opinions of the US Air Force or the Department of Defense.



AIRESEARCH MANUFACTURING COMPANY
Los Angeles, California

N O T I C E S

SPONSORSHIP

The work reported herein was sponsored by the Foreign Technology Division (FTD), of the United States Air Force (USAF), Wright-Patterson AFB, Dayton, Ohio ^{48V33}~~45933~~, under Contract F33657-72-C-0850, with Capt. R. Chardon as Technical Project Monitor, Capt. J. Johnson as Administrative Project Monitor, and Mr. T. Larson as Project Director.

AUTHORSHIP

This report was prepared by the Garrett Corporation, AiResearch Division, of Los Angeles, California, under contract with FTD, USAF.

Dr. J. W. Eerkens was the main author and principle investigator in the program which was carried out under the general technical direction of Mr. H. Lopez, Director of Engineering.

DISTRIBUTION

The unclassified volumes of the Rocket Radiation Handbook may be distributed without restriction. The classified volumes will be distributed in accordance with a list held by Mr. T. Larson of FTD, USAF.

FINAL DISPOSITION OF CLASSIFIED VOLUMES

After the classified document has served its purpose, military organizations may destroy it in accordance with applicable directives; Department of Defense contractors may destroy it in accordance with the provisions of the Industrial Security Manual for Safeguarding Classified Information.

Section <input checked="" type="checkbox"/>		
Section <input type="checkbox"/>		
Section <input type="checkbox"/>		
BY <input type="checkbox"/>		
DISTRIBUTION/AVAILABILITY CODES		
Dist.	AVAIL. and/or	SPECIAL
A		

P R E F A C E

The present monograph is the first volume of the Rocket Radiation Handbook series. The unclassified volumes of the series are entitled:

- I. ROCKET RADIATION PHENOMENOLOGY AND THEORY
- II. MODEL EQUATIONS FOR PHOTON EMISSION RATES AND ABSORPTION CROSS-SECTIONS
- III. FUNDAMENTALS OF PHOTONICS
- IV. GAS DYNAMICS AND FLOW-FIELDS OF ROCKET EXHAUSTS
- V. ATMOSPHERIC PROPERTIES AND OPTICAL TRANSMISSION
- VI. RADIATION SENSING SYSTEMS THEORY

Although each volume supports the others and covers a subject that is essential to rocket radiation science, most volumes stand on their own and their material can be used in other fields of applied physics and engineering.

The new Rocket Radiation Handbook contains the results of six years of fundamental research and experimental data analyses of the radiant emissions produced by rockets as they traverse the atmosphere and travel into space. At the present level of development, the theory appears to predict most observed radiations to within the margin of accuracy imposed by uncertainties in the values of some input parameters and observational conditions.

Some earlier attempts to derive theoretical models for observed rocket emissions were rather incomplete and unsatisfactory causing engineers in the field to become skeptical of any theoretical work. As a result the

tendency has been to rely primarily on empirical information and the belief was held by many that satisfactory analytic expressions derived from theory, would be impossible to obtain in view of the perplexing multitude of phenomena which appear to be taking place simultaneously. It is my hope that the work presented here will dispel this notion.

That theoretical physics can correctly predict the overall results of a complex mixture of man-made physical events, if the theory is worked out properly and the basic phenomena are understood, was dramatically demonstrated during World War II by Enrico Fermi. Fermi and his associates developed the theory of neutron transport and nuclear chain reactors and designed the first nuclear reactor entirely from theory without the benefit of any data on an operating reactor. Their first nuclear reactor, when built, performed almost exactly according to calculation.

Another interesting example is the laser. Although the basic theory that could have predicted the principle of the laser existed in 1930, unfamiliarity of applied scientists and engineers with this theory, delayed the discovery of the laser until 1960.

The current Rocket Radiation Handbook, which is a complete revision and considerable expansion of an earlier version, was sponsored by the Foreign Technology Division of USAF-AFSC. In particular credit is due Capt. Roy Chardon who was the Technical Program Manager of the effort and who pushed most vigorously to have it compiled and issued. Col. G. R. Weinbrenner, Commander of FTD, Col. J. H. Mann, Mr. Ken Miller, Mr. Ted Larson, and Capt. Jeff Johnson under whose direction the work was carried out, also deserve full credit for backing this work.

June 1974

FTD-CW-01-01-74
Vol. I

In addition to the USAF, the Special Programs Office of the NASA must be mentioned. They sponsored most of the early work (1966-1970) on which the present Handbook is based. In particular Mr. Larry Gilchrist, Technical Program Manager, and Mr. Duff Gintner, Program Office Director at NASA H.Q. are thanked for their earlier support.

Finally I wish to express my gratitude to Dr. K. N. Satyendra under whose direction most of the early work which led to the present effort was initiated and to Mr. H. Lopez, Director of Engineering of the Garrett Corporation who saw to it that it was continued. For many valuable suggestions and assistance over the past six years I am indebted to Dr. R. Fairley, Dr. J. Robe, Mr. R. Proffitt, Mr. B. Bartholow, Dr. B. Stallwood, Dr. A. Bhattacharjie, Mr. C. Brooks, Mr. A. Gaede, and Mr. P. Dias. Many thanks also go to my Technical Typist, Editor, and Illustrator, Miss Frances Rossiter whose conscientious work and devotion made it possible to get all the material in a presentable form.

Data, figures, and derivations employed in the text which were obtained from other authors and organizations are too numerous to mention. They are referenced throughout the Handbook and use of their information is hereby gratefully acknowledged.

J. W. Eerkens

ABSTRACT

A review is given of various mechanisms responsible for the generation of infrared, visible, and ultraviolet radiation from aerospace rockets. Key mechanisms responsible for most of the observed radiation are identified by examining the order-of-magnitude of the energy that is fed to each one. For the exhaust, the major mechanisms are:

Undisturbed Core Relaxation (CORE); Afterburning (AB); Air Shock Collisional Deceleration (CD); Atmospheric Pumping (ATMP); Solar Scattering by Particles (SOSP); Solar Ultraviolet Absorption and Reradiation (SUAR).

While radiation from vehicle hardware is primarily caused by:

Vehicle Body Solar Reflections (VBSR); Vehicle Body Earthshine Reflections (VBER); Vehicle Body Self-Emissions (VBSE).

The AB and CD mechanisms are coupled and abbreviated ABCD. CORE and ABCD radiation are produced in different regions of the rocket plume and it is shown that they can be analyzed separately; together they are responsible for most of the infrared emissions from a thrusting rocket. ATMP is a weak infrared afterglow radiation from the slowed-down exhaust cloud that is active only at medium-high altitudes. It decays slowly but is usually not observed because of its dilution and because it is outside the field-of-view of a vehicle-tracking sensor.

SOSP and SUAR are primarily operative in the visible part of the spectrum. SUAR is important at altitudes above 135 km and is shown to be the origin of several spectacular emissions in the visible observed during the Apollo space flights.

After a qualitative survey, detailed quantitative expressions are developed for each of the main mechanisms. These expressions provide the spectral radiance as a function of altitude for different types of fuel/exhaust species, rocket hardware parameters, and rocket trajectories. In the derivation of the analytical expressions for ABCD and CORE radiances, a new approach is presented which differs from most earlier techniques. The new approach consists of applying the conservation law to the rate of production and loss of excited states in the plume, the use of Gauss divergence theorem to the radiating region, and the application of generalized spectral broadening functions which are evaluated in Volume II. Although some inevitable approximations are used, the new technique appears to give results that are more tractable, more general, and more exact than those obtained by earlier methods.

Examples are finally presented on how to calculate altitude dependent rocket-radiation signatures in the infrared. Computer-calculated curves of the integrated radiation in selected spectral ranges of the $2.66 \mu\text{m}$ H_2O band and the $4.26 \mu\text{m}$ CO_2 band are shown as a function of flight time for two different rockets. Computer-calculated NIR and UVIS spectral emissions are also presented as a function of wavelength for a given altitude.

TABLE OF CONTENTS

<u>Chapter</u>	<u>Page</u>
NOTICES.	iii
PREFACE.	v
ABSTRACT	ix
LIST OF FIGURES.	xv
LIST OF TABLES	xxiii
1. INTRODUCTION	1
2. SOURCES AND PHENOMENOLOGY OF NATURAL ROCKET RADIATION. . . .	13
2.1 GENERAL REVIEW OF ROCKET RADIATION SOURCES	13
2.2 VEHICLE BODY EMISSIONS	20
2.3 ROCKET EXHAUST RADIATIONS.	24
2.3.1 Survey of Radiation Mechanisms	24
2.3.2 Energy Considerations.	25
2.4 PHENOMENOLOGY OF THE MAJOR ROCKET RADIATION MECHANISMS	46
3. QUANTITATIVE THEORY OF ROCKET RADIATION.	67
3.1 PRELIMINARY DEFINITIONS.	67
3.2 VEHICLE BODY RADIATIONS.	76
3.2.1 Vehicle Body Solar Reflections (VBSR).	76
3.2.2 Vehicle Body Earthshine Reflections (VBER) . .	92
3.2.3 Vehicle Body Self-Emissions (VBSE)	100

<u>Chapter</u>	<u>Page</u>
3.3 ROCKET EXHAUST RADIATIONS.	104
3.3.1 General Comments	104
3.3.2 Plume Radiation in a Vacuum (Deep-Space Plume Radiation; DSPR)	106
3.3.3 Undisturbed Core or Mach Cone Radiation (CORE)	137
3.3.4 Afterburning and Collisional Deceleration Radiation (ABCD).	155
3.3.5 Atmospheric Pumping Radiation (ATMP)	191
3.3.6 Solar Radiation Scattering by Particles (SOSP)	201
3.3.7 Solar Ultraviolet Absorption and Reradiation (SUAR)	214
3.3.8 Spectral Considerations.	241
3.3.9 View Factors	261
3.3.10 Parametric Error Analysis and Adjustments. . .	264
4. APPLICATIONS AND EXAMPLES.	279
4.1 ROCKET RADIATION SIGNATURES.	279
4.2 PLUME EMISSION SPECTRA	295
4.3 CONCLUSIONS AND COMMENTS	300
APPENDIX A — REFLECTIVITIES AND EMISSIVITIES OF TYPICAL MATERIALS.	305
APPENDIX B — SPECTRAL CHARACTERISTICS OF BLACKBODY RADIATORS AND SELECTED ILLUMINATORS.	327
B.1 BLACKBODY RADIATORS.	327
B.2 SOLAR AND PLANETARY ILLUMINATORS	341
APPENDIX C — VIEW FACTORS FOR DIFFUSE EXHAUST PLUMES	349
C.1 PRELIMINARY CONSIDERATIONS	349

<u>Chapter</u>	<u>Page</u>
C.2 SPHERICAL BODY OF GAS.	353
C.3 CYLINDRICAL BODY OF GAS.	358
C.4 CONICAL BODY OF GAS.	371
APPENDIX D - SOLUTIONS OF THE DIFFERENTIAL EQUATION FOR INWARDS CYLINDRICAL DIFFUSION.	375
APPENDIX E - REACTION CHEMISTRY OF ROCKET PLUME AFTERBURNING	383
E.1 AFTERBURNING CHEMISTRY	383
E.2 AFTERBURNING OF H_2	387
E.3 AFTERBURNING OF CO	400
E.4 SAMPLE CALCULATIONS AND FINAL RESULTS.	404
APPENDIX F - HIGH-ALTITUDE JET FLARE ANGLE AND PLUME LENGTH CALCULATIONS.	429
APPENDIX G - PHOTON IONIZATION AND SCATTERING CROSS-SECTIONS	441
G.1 PHOTOIONIZATION.	442
G.2 RAYLEIGH SCATTERING.	444
APPENDIX H - ATMOSPHERIC TRANSMISSION OF SOLAR ULTRAVIOLET RADIATION AT HIGH ALTITUDES.	449
APPENDIX I - EFFECTIVE THROAT AND PLUME DIAMETERS FOR MULTIPLE-NOZZLED ROCKETS	473
NOMENCLATURE AND UNITS	487
UNITS AND CONVERSION FACTORS	523
BASIC PHYSICAL CONSTANTS	528
REFERENCES	533
DISTRIBUTION	537

LIST OF FIGURES

<u>Figure</u>		<u>Page</u>
1-1.	BAKER-NUNN PHOTOGRAPHY OF APOLLO-8 TRANSLUNAR INJECTION BURN OVER HAWAII ON 21 DECEMBER 1968.	3
1-2.	BAKER-NUNN PHOTOGRAPHY IN SPAIN OF LOX/LH2 FUEL DUMP CLOUD BY APOLLO-8 DURING TRANSLUNAR COASTING ON 21 DECEMBER 1968	4
1-3.	TYPICAL PLUME RADIATION IN THE ν_3 BAND OF H_2O	5
1-4.	TYPICAL RADIANT EMISSION CURVE OF A TWO-STAGE ROCKET.	6
2-1.	ILLUSTRATION OF SPATIAL DISTRIBUTION AND RADIATION PROCESSES OF A HIGH-ALTITUDE ROCKET EXHAUST	16
2-2.	ILLUSTRATION OF IMPORTANCE OF VIEWING CONDITIONS.	18
2-3a.	IMPORTANT PROPERTIES OF THE EARTH ATMOSPHERE (TEMPERATURE, PRESSURE, DENSITY, AND MOLECULAR WEIGHT), ACCORDING TO U.S. STANDARD ATMOSPHERE, 1962	52
2-3b.	IMPORTANT PROPERTIES OF THE EARTH ATMOSPHERE (NUMBER DENSITY, COLLISION FREQUENCY, MEAN FREE PATH, AND MOLECULAR SPEED), ACCORDING TO U.S. STANDARD ATMOSPHERE, 1962	53
2-3c.	IMPORTANT PROPERTIES OF THE EARTH ATMOSPHERE (CONCENTRATIONS OF MAIN CONSTITUENTS)	54
2-4.	SOLAR ILLUMINATION CURVES BELOW AND ABOVE THE EARTH ATMOSPHERE.	59
2-5.	COMPARISON OF WATER VAPOR PRESSURE WITH ATMOSPHERIC CONDITIONS.	62
2-6.	CALCULATED ROCKET PLUME DIAMETERS	64
3-1.	ANGLES USED IN THE CALCULATION OF THE OPTICAL CROSS-SECTION OF THE DIFFUSELY REFLECTION CYLINDER, CONE, AND HEMISPHERE. .	79

<u>Figure</u>		<u>Page</u>
3-2.	DIFFUSE REFLECTION CROSS-SECTIONS σ_s OF THE ATLAS ROCKET MODEL FOR $\phi_s = 0^\circ$	85
3-3.	DIFFUSE REFLECTION CROSS-SECTIONS σ_s OF THE ATLAS ROCKET MODEL FOR $\phi_s = 30^\circ$	86
3-4.	DIFFUSE REFLECTION CROSS-SECTIONS σ_s OF THE ATLAS ROCKET MODEL FOR $\phi_s = 45^\circ$	87
3-5.	GEOMETRIC PARAMETERS FOR SPECULAR REFLECTION.	90
3-6.	RADIANT FLUX DIAGRAM.	94
3-7.	SUN-EARTH-TARGET CONFIGURATION.	94
3-8.	EARTHSHINE IRRADIANCE FACTOR, F, AND VISIBLE EARTHSHINE TARGET IRRADIANCE, H, VERSUS TARGET ALTITUDE FOR VARIOUS SOLAR ZENITH ANGLES θ_s	97
3-9.	SELF-EMISSION CROSS-SECTION OF TYPICAL CONE-SHAPED SPACE VEHICLE	103
3-10.	DEEP-SPACE (VACUUM) ROCKET PLUME GEOMETRY	107
3-11.	ILLUSTRATION OF CORE REGION OF MEDIUM-ALTITUDE ROCKET EXHAUST FLOW FIELD	138
3-12.	ILLUSTRATION OF DIFFUSION FRONT PENETRATION INTO HYPOTHETICAL STRAIGHT-CYLINDER JET.	139
3-13.	ILLUSTRATION OF MIXING PROBLEM.	170
3-14.	BACK SCATTERING ($\theta_s = \pi$) CROSS-SECTIONS OF Al_2O_3 AND H_2O PARTICLES	205
3-15.	ANGULAR DEPENDENCE OF Al_2O_3 AND H_2O PARTICLE SCATTERING CROSS-SECTIONS.	206
3-16.	EXPERIMENTAL CORRELATION OF MEAN Al_2O_3 PARTICLE DIAMETER $\bar{d}_{Al_2O_3}$ WITH NOZZLE THROAT DIAMETER.	207
3-17.	THEORETICAL Al_2O_3 PARTICLE SIZE DISTRIBUTION WITH NOZZLE LOCATION	208

<u>Figure</u>		<u>Page</u>
3-18.	Al ₂ O ₃ PARTICLE SIZE DATA OBTAINED FROM SMALL ROCKET MOTORS.	209
3-19.	ILLUSTRATION OF SUSPECTED SOLAR-UV-EXCITED DISSOCIATIONS OF H ₂ O AND UVIS EMISSIONS FROM OH IN HIGH-ALTITUDE ROCKET EXHAUST PLUMES.	235
4-1.	CALCULATED RADIATION SIGNATURES OF BALLISTIC ATLAS ROCKET IN 2.74 AND 4.45 MICRON BANDS	280
4-2.	CALCULATED RADIATION SIGNATURES OF BALLISTIC TITAN II ROCKET IN 2.74 AND 4.45 MICRON BANDS	281
4-3.	CALCULATED RADIATION SIGNATURES OF SPACE-LAUNCHING TITAN 3B/AGENA ROCKET IN 2.74 AND 4.45 MICRON BANDS.	282
4-4.	CALCULATED RADIATION SIGNATURES OF SPACE-LAUNCHING TITAN 3D ROCKET IN 2.74 AND 4.45 MICRON BANDS.	283
4-5.	CALCULATED PURE MACH CORE RADIATION (TITAN II ROCKET).	291
4-6.	CALCULATED UNATTENUATED INFRARED RADIATION SPECTRUM OF TITAN-II SECOND STAGE	296
4-7.	CALCULATED UNATTENUATED UVIS SPECTRUM FROM AN AMINE-FUELED 300 KG(F) ROCKET MAKING A POST-BOOST MANEUVER BURN AT A THRUST ANGLE OF 135 DEGREES.	297
4-8.	CALCULATED ATMOSPHERE-ATTENUATED INFRARED RADIATION SPECTRUM OF TITAN-II SECOND STAGE.	299
A-1.	REFLECTANCE OF FRESHLY EVAPORATED FILMS.	308
A-2.	ANGULAR DEPENDENCE OF EMITTANCE OF METALS.	308
A-3.	ANGULAR DEPENDENCE OF EMITTANCE OF NONCONDUCTORS	308
A-4.	TYPICAL SPECTRAL REFLECTIVITIES OF SPACE VEHICLE SURFACES.	310
A-5.	SPECTRAL REFLECTIVITIES OF ALUMINUM SURFACES	311
A-6.	SPECTRAL REFLECTIVITIES OF ALUMINUM SURFACES	311

<u>Figure</u>		<u>Page</u>
A-7.	SPECTRAL REFLECTIVITIES OF COPPER SURFACES.	312
A-8.	SPECTRAL REFLECTIVITIES OF GOLD SURFACES.	312
A-9.	SPECTRAL REFLECTIVITIES OF SILICON SURFACES	313
A-10.	SPECTRAL REFLECTIVITIES OF PAINTED SURFACES	313
A-11.	SPECTRAL EMITTANCE CURVES AT 900°F FOR TYPE 321 STAINLESS STEEL SPECIMENS WITH DIFFERENT SURFACE TREATMENTS (COATING THICKNESS APPROXIMATELY 2 MILS)	321
A-12.	SPECTRAL EMITTANCE CURVES AT 1800°F FOR TYPE 321 STAINLESS STEEL SPECIMENS WITH DIFFERENT SURFACE TREATMENTS (COATING THICKNESS APPROXIMATELY 2 MILS)	321
A-13.	SPECTRAL EMITTANCE CURVES AT 900°F FOR INCONEL SPECIMENS WITH DIFFERENT SURFACE TREATMENTS (COATING THICKNESS APPROXIMATELY 2 MILS)	322
A-14.	SPECTRAL EMITTANCE CURVES AT 1800°F FOR INCONEL SPECIMENS WITH DIFFERENT SURFACE TREATMENTS (COATING THICKNESS APPROXIMATELY 2 MILS)	322
A-15.	NORMAL TOTAL EMISSIVITY AND TOTAL SOLAR ABSORPTIVITY OF INCONEL X.	323
A-16.	HEMISPHERIC TOTAL EMISSIVITY AND TOTAL SOLAR ABSORPTIVITY OF MOLYBDENUM.	323
A-17.	NORMAL TOTAL EMISSIVITY AND TOTAL SOLAR ABSORPTIVITY FOR K-MONEL	323
A-18.	NORMAL TOTAL EMISSIVITY AND TOTAL SOLAR ABSORPTIVITY FOR 301 STAINLESS STEEL	324
A-19.	NORMAL TOTAL EMISSIVITY AND TOTAL SOLAR ABSORPTIVITY FOR 316 STAINLESS STEEL	324
A-20.	NORMAL TOTAL EMISSIVITY AND TOTAL SOLAR ABSORPTIVITY FOR 347 STAINLESS STEEL	324
A-21.	NORMAL TOTAL EMISSIVITY FOR 18-8 STAINLESS STEEL.	325

<u>Figure</u>		<u>Page</u>
A-22.	HEMISPHERICAL TOTAL EMISSIVITY, NORMAL TOTAL EMISSIVITY, AND TOTAL SOLAR ABSORPTIVITY FOR TANTALUM.	325
A-23.	HEMISPHERICAL TOTAL EMISSIVITY OF TUNGSTEN	325
B-1.	SPECTRAL RADIANCE CURVES OF A BLACKBODY PER UNIT WAVELENGTH.	335
B-2.	SPECTRAL RADIANCE CURVES OF A BLACKBODY PER UNIT FREQUENCY.	336
B-3.	SPECTRAL RADIANCES PER UNIT WAVELENGTH AND PER UNIT FREQUENCY FOR BLACKBODIES AT VARIOUS TEMPERATURES ($^{\circ}$ K) PLOTTED ON ARITHMETIC SCALES	337
B-4.	SPECTRAL PHOTON FLUENCE PER UNIT WAVELENGTH FROM A BLACKBODY AT VARIOUS TEMPERATURES ($^{\circ}$ K)	338
B-5.	SPECTRAL PHOTON FLUENCE PER UNIT FREQUENCY FROM A BLACKBODY AT VARIOUS TEMPERATURES ($^{\circ}$ K).	339
B-6.	PHOTON FLUENCES EMITTED BY BLACKBODIES AT VARIOUS TEMPERATURES ($^{\circ}$ K) PLOTTED ON ARITHMETIC SCALES	340
B-7.	SOLAR RADIATION INTENSITY ABOVE THE ATMOSPHERE AT EARTH'S DISTANCE FROM THE SUN.	342
B-8.	SOLAR ULTRAVIOLET RADIATION OUTSIDE THE EARTH'S ATMOSPHERE	343
B-9.	RELATIVE SPECTRAL DISTRIBUTION OF ALBEDO RADIATION UNDER VARIOUS SKY CONDITIONS	345
B-10.	A TYPICAL SPECTRAL EMISSIVE POWER CURVE FOR THE THERMAL RADIATION LEAVING THE EARTH.	345
C-1.	ILLUSTRATION OF EXHAUST PLUME VIEWING SITUATION.	351
C-2.	DEPICTION OF SPHERICAL PLUME VIEWING GEOMETRY.	354
C-3.	ILLUSTRATION OF CYLINDRICAL PLUME VIEWING GEOMETRY	360
C-4.	VIEW FACTOR F_v FOR CYLINDRICAL PLUME WITH $\lambda = 3$	364

<u>Figure</u>		<u>Page</u>
C-5.	ILLUSTRATION OF VEHICLE OBSCURATION PROBLEM WHEN $D_v > D_p$	366
E-1.	PLOT OF $H_2 \rightarrow H_2O$ BURNING FUNCTION $h(\xi_{H_2O})$	410
E-2.	PLOT OF $CO \rightarrow CO_2$ BURNING FUNCTION $f(\xi_{CO_2})$	419
H-1.	PHOTON SCATTERING CROSS-SECTIONS	450
H-2.	ULTRAVIOLET EXTINCTION COEFFICIENTS OF N_2 , O_2 , N , O	451
H-3.	ULTRAVIOLET EXTINCTION COEFFICIENTS OF H_2O , CO_2	452
H-4.	ULTRAVIOLET EXTINCTION COEFFICIENTS OF N_2O , NO , CH_4 , O_3 .	453
H-5.	VISIBLE EXTINCTION COEFFICIENTS OF N_2 , O_2 , O_3 , H_2O	454
H-6.	MOLECULAR CONCENTRATIONS OF MAIN CONSTITUENTS IN THE EARTH ATMOSPHERE.	456
H-7.	CONCENTRATIONS OF EXCITED SPECIES AND TRACE ELEMENTS AT DIFFERENT ALTITUDES IN THE EARTH ATMOSPHERE.	457
H-8.	CONCENTRATIONS OF EXCITED SPECIES AND TRACE ELEMENTS AT DIFFERENT ALTITUDES IN THE EARTH ATMOSPHERE.	458
H-9.	CONCENTRATIONS OF EXCITED SPECIES AND TRACE ELEMENTS AT DIFFERENT ALTITUDES IN THE EARTH ATMOSPHERE.	459
H-10.	CONCENTRATIONS OF EXCITED SPECIES AND TRACE ELEMENTS AT DIFFERENT ALTITUDES IN THE EARTH ATMOSPHERE.	460
H-11.	AEROSOL EXTINCTION COEFFICIENT AT SEA LEVEL, $\alpha_p(o)$, Vs WAVELENGTH, FOR AN AVERAGE CLEAR DAY	462
H-12.	AEROSOL NUMBER DENSITY Vs ALTITUDE FOR THE CLEAR STANDARD ATMOSPHERE MODEL.	464
I-1.	ILLUSTRATION OF THE MODELING OF TWO EFFECTIVE HALF NOZZLES .	476
I-2.	MODEL FOR SIX NOZZLES.	477

<u>Figure</u>	<u>Page</u>
I-3. MODEL FOR FIVE NOZZLES (PENTAGON).	477
I-4. MODEL OF FIVE NOZZLES (CROSS).	478
I-5. MODEL OF FOUR NOZZLES.	478
I-6. MODEL OF THREE NOZZLES (LINEAR).	479
I-7. MODEL OF THREE NOZZLES (TRIANGULAR).	479
I-8. MODEL OF TWO NOZZLES	480
I-9. GENERALIZATION OF MODEL TO INCLUDE SEPARATION BETWEEN NOZZLES.	480

LIST OF TABLES

<u>Table</u>		<u>Page</u>
2-1.	PLUME RADIATION MECHANISMS AND MAXIMUM EMISSION RATES. . . .	44
2-2.	TYPICAL PROPELLANTS AND THRUSTS OF U.S. ROCKETS.	47
2-3.	TYPICAL EXHAUST PRODUCTS OF ROCKET PROPELLANTS	48
2-4.	SOLAR SPECTRAL IRRADIANCE FOR QUIET SUN, OUTSIDE THE EARTH'S ATMOSPHERE AT THE MEAN SUN-TO-EARTH DISTANCE; $H_0 = 1390 \text{ W m}^{-2}$	60
2-5.	SUMMARY OF MAJOR RADIATION-PRODUCING MECHANISMS OF ROCKET EXHAUSTS.	66
3-1.	MOLECULAR COLLISION PARAMETERS	194
3-2.	SOLAR UV LINES BELOW 182 NANOMETERS.	217
3-3.	ABSORPTIVE ELECTRONIC IONIZATION, EXCITATION, AND PREDISSOCIATION WAVELENGTHS (FREQUENCIES) OF ROCKET EXHAUST SPECIES	220
3-4.	DISSOCIATION ENERGIES AND FREQUENCIES OF ROCKET EXHAUST MOLECULES	221
3-5.	MAIN ELECTRONIC EMISSION LINES OF EXHAUST ATOMS IN THE UVIS REGION OF THE SPECTRUM.	228
3-6.	MAJOR VIBRONIC EMISSION BANDS OF EXHAUST MOLECULES IN THE UVIS REGION OF THE SPECTRUM.	229
3-7.	DISSOCIATION RATES OF EXHAUST MOLECULES IN THE EXOSPHERE UNDER SOLAR ULTRAVIOLET IRRADIATION.	240
3-8.	FREQUENCIES AND EINSTEIN RATES OF THE MORE IMPORTANT INFRARED-ACTIVE VIBRATION BANDS OF ROCKET EXHAUST MOLECULES.	248
3-9.	ROTATIONAL CONSTANTS OF SELECTED EXHAUST MOLECULES	258



<u>Table</u>	<u>Page</u>
4-1. ROCKET HARDWARE PARAMETERS OF FOUR TYPICAL ROCKETS.	285
4-2. MOLECULAR COMPOSITION OF THE EXHAUST OF FOUR TYPICAL ROCKETS (MOLES/KGM)	286
4-3. TRAJECTORY DATA OF FOUR TYPICAL ROCKETS	287
4-4. ASSUMED PARAMETER UNCERTAINTIES FOR ERROR ANALYSIS.	294
A-1. SPECTRAL EMISSIVITIES OF SOME SELECTED METALS	314
A-2. NORMAL SPECTRAL EMISSIVITIES AT 295°K	315
A-3. SPECTRAL EMISSIVITIES OF SOME SELECTED METAL OXIDES AND ORGANIC SUBSTANCES.	316
A-4. TOTAL NORMAL EMISSIVITY	317
B-1. BLACKBODY RADIATION FUNCTIONS	329
B-2. TOTAL BLACKBODY RADIATION	331
E-1. MAIN H ₂ AFTERBURNING REACTIONS AND RATE CONSTANTS	384
E-2. MAIN CO AFTERBURNING REACTIONS AND RATE CONSTANTS	386
G-1. EFFECTIVE CHARGE NUMBERS AND IONIZATION FREQUENCIES OF OUTER (VALENCE) SHELL FOR THE FIRST 36 ELEMENTS OF THE PERIODIC TABLE	445
G-2. EFFECTIVE CHARGE NUMBERS AND IONIZATION FREQUENCIES OF OUTER (VALENCE) SHELL FOR MISCELLANEOUS MOLECULES	446
H-1. AVERAGED SEA-LEVEL AEROSOL EXTINCTION COEFFICIENT, $\alpha_p(\lambda)$ AS A FUNCTION OF WAVELENGTH λ	463
H-2. AEROSOL NUMBER DENSITIES, n_p AT VARIOUS ALTITUDES, h , FOR THE MODEL CLEAR STANDARD ATMOSPHERE	465

1. INTRODUCTION

In the last decade, a considerable amount of experimental information has been obtained on the radiant emissions by rockets and their exhaust gases in the aerospace environment. Measurements ranging from the far-ultraviolet to the far-infrared have been made from such assorted platforms as satellites, balloons, aircraft, and from ground-based observatories (Refs. 1 thru 16). These measurements contain a great wealth of information regarding high-altitude and deep-space chemical reactions, radiative excitations and resonant transfer collisions between not only common molecules like H_2O , CO_2 , CO , O_2 , and H_2 , but also less available species such as OH , O and O_3 , which can exist in large quantities in the upper atmosphere and in space. In short, rocket exhaust emissions from high altitudes and deep space provide an extremely valuable laboratory for studies on interactions of important biospheric molecules between themselves as well as with photons.

It is the objective of this first volume in the Rocket Radiation Handbook Series, to review and discuss the major mechanisms responsible for the radiant emissions from rockets and their exhausts, and to develop quantitative theoretical expressions which can predict these emissions. Once such equations are available, and if shown to be substantially correct by comparing calculations with measurements, they can in principle be used in reverse to deduce important properties of various molecules from the

observed radiations, and thus increase our understanding of high-altitude and deep-space reactions and phenomena.

In Figures 1-1 and 1-2, some very spectacular emissions obtained during the Apollo-8 flight to the moon are shown as observed and photographed by the SAO Baker-Nunn cameras in Hawaii and Spain (Ref. 7).^{*} Although these observations were made with black-and-white film and thus are in the visible part of the spectrum, obviously the emissions may be expected to extend into the infrared as well. In Figure 1-3, the strong near-infrared emissions from the ν_3 vibrational band of H_2O (the most abundant rocket exhaust product) of a rocket plume are shown in the vicinity of $2.8 \mu m$ (Ref. 14). The absolute value of the emission strength depends of course on the exhaust product mass flow rate or the rocket thrust. As will be seen later it varies further with rocket velocity or altitude in a manner as illustrated in Figure 1-4 for a satellite-launching rocket such as the Atlas-Agena-B or Saturn.

The task before us is to theoretically predict and calculate the spectral radiations and their intensities as a function of rocket exhaust gas parameters and atmospheric/exospheric conditions. In doing this one finds that a satisfactory and complete theoretical treatment of rocket radiation phenomena requires intimate knowledge of a wide variety of scientific disciplines, chief among which are (see for example Refs. 1 through 24):

- (1) Compressible Viscous Fluid Dynamics which includes gas mixing and two-phase flow theory

^{*}SAO = Smithsonian Astronomical Observatory. SAO has a worldwide network of telescopes and assisted NASA during the Apollo flights.

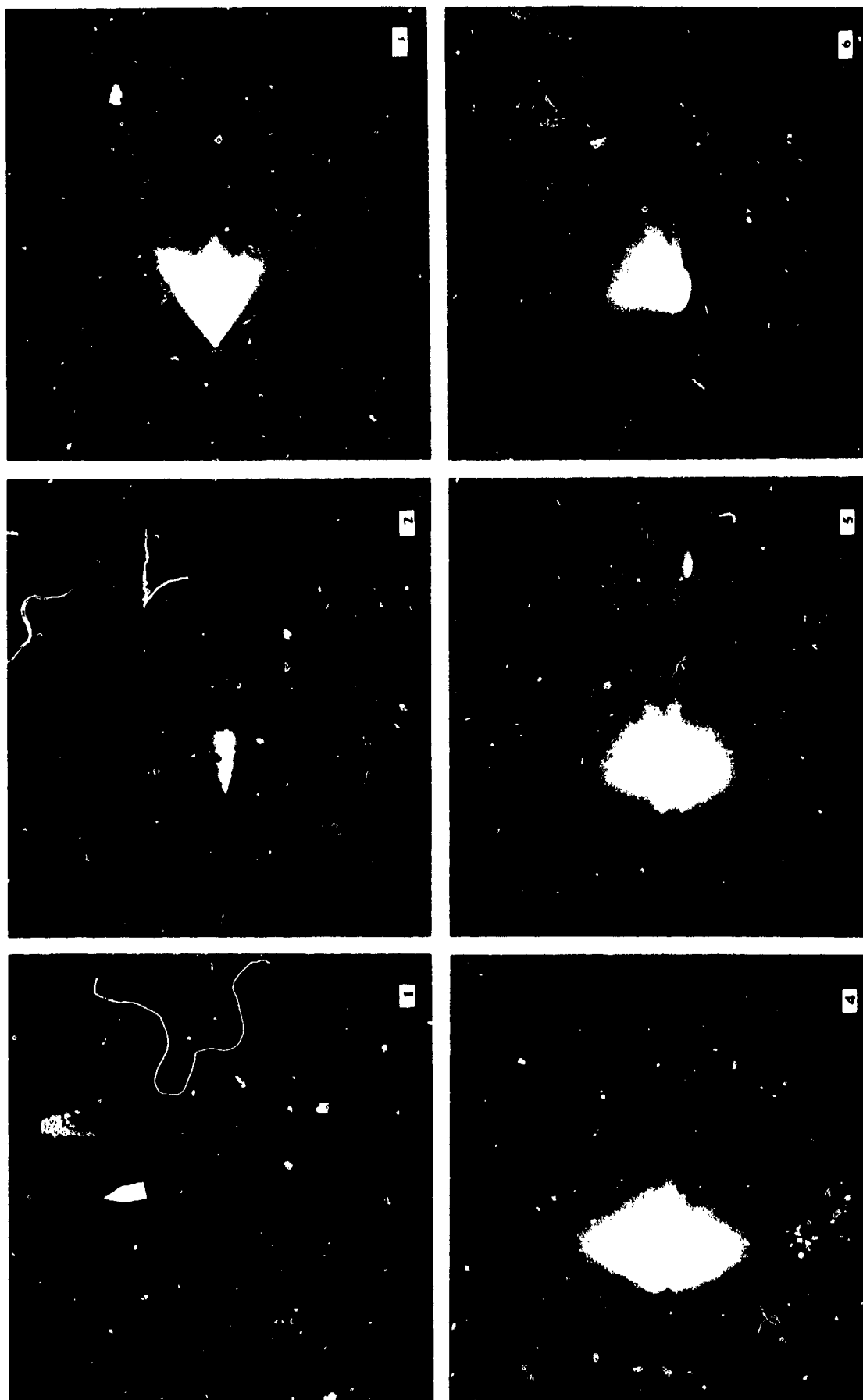


FIGURE 1-1. BAKER-NUNN PHOTOGRAPHY OF APOLLO-8 TRANSLUNAR INJECTION
BURN OVER HAWAII ON 21 DECEMBER 1968

June 1974

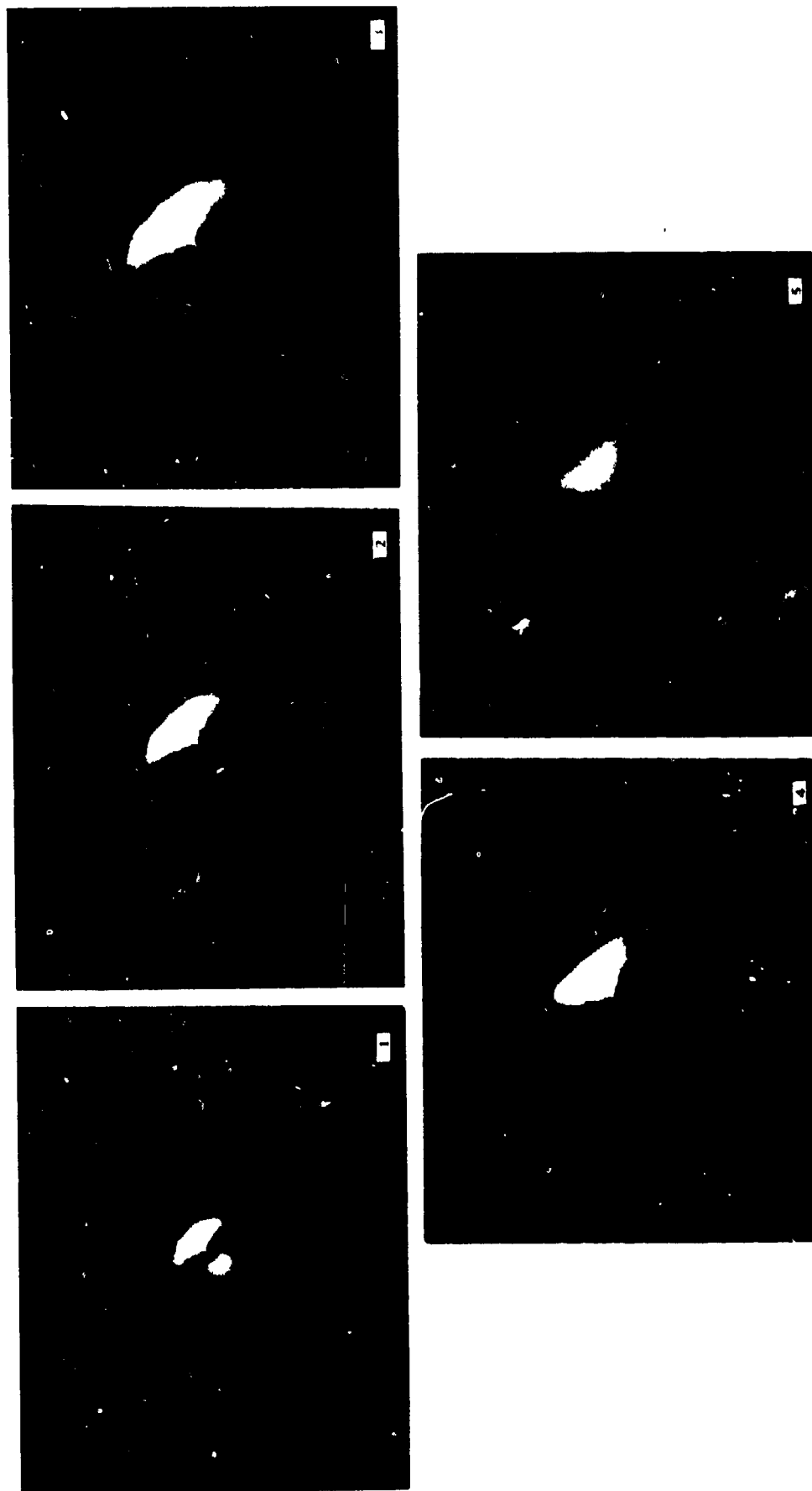


FIGURE 1-2. BAKER-NUNN PHOTOGRAPHY IN SPAIN OF LOX/LH2 FUEL DUMP CLOUD
BY APOLLO-8 DURING TRANSLUNAR COASTING ON 21 DECEMBER 1968

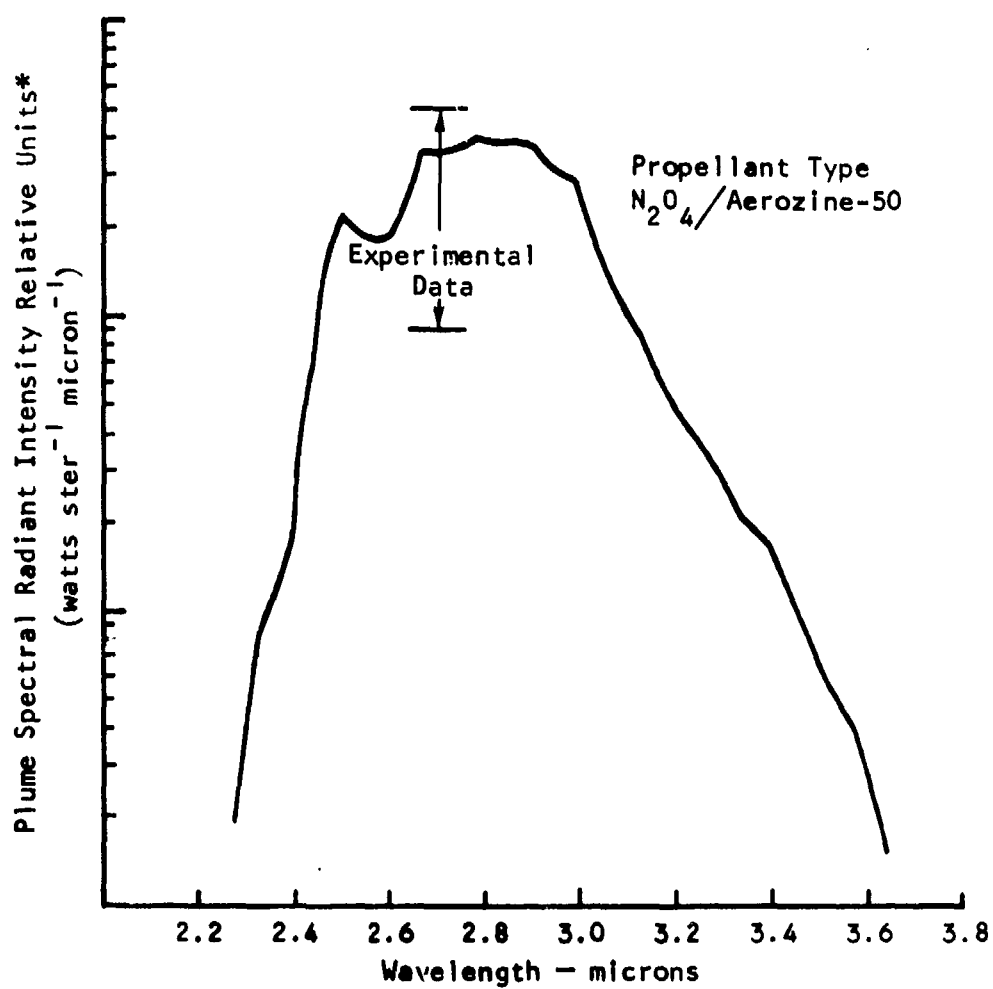


FIGURE 1-3. TYPICAL PLUME RADIATION IN THE ν_3 BAND OF H_2O
(Ref. 14)

*The absolute value varies with propellant mass flow rate
(or rocket thrust) and altitude.

June 1974

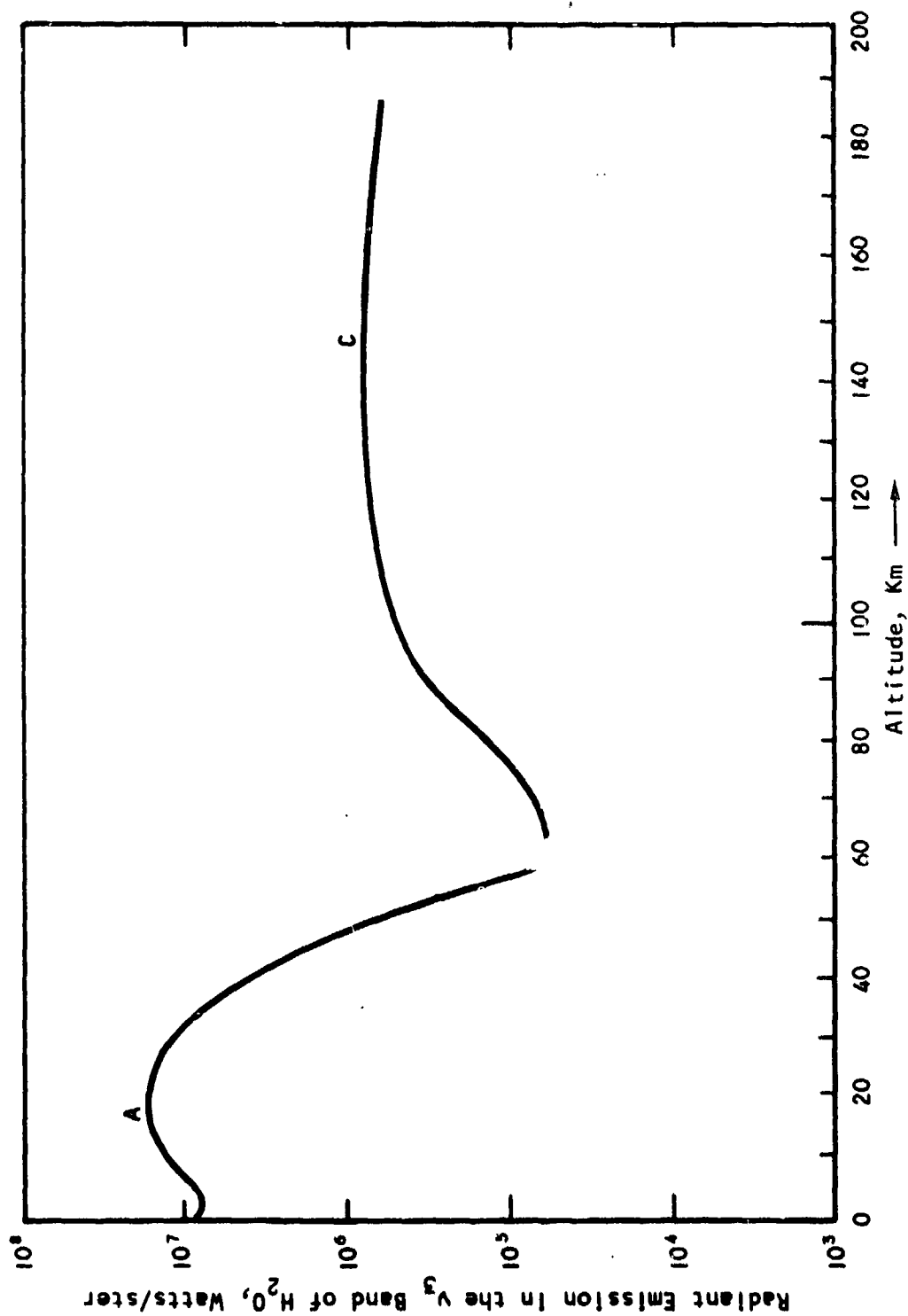


FIGURE I-4. TYPICAL RADIANT EMISSION CURVE OF A TWO-STAGE ROCKET

- (2) Rocket Propulsion
- (3) Kinetic Theory of Gases
- (4) Chemical Reaction Kinetics and Combustion
- (5) Quantum Theory of Radiation
- (6) Internal Physics of Molecules
- (7) Spectroscopy
- (8) Spectral Line-Broadening and Band-Broadening Theory
- (9) Macroscopic Diffusion and Transport Theory
- (10) Atmospheric Sciences and Atmospheric Transmission
- (11) Solar Radiation
- (12) Orbital Mechanics
- (13) Sensor Systems Theory
- (14) Detectability and Information Theory
- (15) Geometric Optics

With such a variety of fields, it will clearly be difficult to cover all topics to an extent that meets everyone's particular interests. Therefore for a number of subjects, special Appendices are provided which briefly review some relations that have been developed which may not be too familiar to the average reader. For more widely-known topics however, references are given to the original literature and no further elaboration is given.

For a complete discussion of some new approaches that were developed by the author for treating certain problems in rocket exhaust dynamics and radiation, a simple Appendix turned out to be inadequate. Thus three additional separate volumes were added to the Rocket Radiation Handbook Series to deal with these special topics, namely "Model Equations

for Photon Emission Rates and Absorption Cross-Sections" (Vol. II), "Fundamentals of Photonics" (Vol. III), and "Gas Dynamics and Flow-Fields of Rocket Exhausts" (Vol. IV).

In the chapter that follows, the mechanisms that are responsible for the emission of rocket radiation in the aerospace environment will first be described and pre-examined. In that chapter primarily the phenomenological aspects of these mechanisms are reviewed so that a feeling can be obtained for the kind of problems that one has to deal with and their dimensions. The criteria of energy conservation and energy flow will be used to determine which of the mechanisms receive most of the available kinetic and potential energy. By assuming reasonable bounds on the possible efficiencies for the conversion of this energy into radiation via each mechanism, it will be shown which of the mechanisms are most important and which may be neglected. In eliminating weak mechanisms in comparison with strong ones, one has to be careful of course that comparisons are made in all parts of the spectrum. A particular radiation-producing mechanism may be weak in one part of the spectrum when compared to others, but it may be the only one in another portion of the spectrum where it cannot be ignored.

After the preliminary survey in Chapter 2, detailed expressions are developed in Chapter 3 for the spectral radiant intensity of the most important mechanisms. These expressions give the emission strength for each mechanism as a function of photon frequency, altitude, and rocket parameters, and take into account spectral broadening and view factors. Though perhaps arbitrary, the study of rocket radiations in this monograph have been limited to the launch phase and the space travel phase, omitting the reentry phase for which ablation radiation plays a major role. Reentry radiation is well covered by such recent publications as Ref. 25.

The theoretical approach used for calculating radiant emissions from gaseous rocket exhausts used in this monograph differs in some important respects from most other methods that have been employed heretofore. Leaving a rigorous mathematical proof to Chapter 3, it may be of interest to point out here what the gross features of this new approach are.

The main feature of the new approach is the realization that under steady-state conditions the total rate (in all directions) at which photons escape from a hot exhaust gas, when multiplied and integrated over the various quantum energies that these photons carry, must equal the total rate at which energy is supplied to excited molecular states in the gas, regardless of whether the gas is optically thick or thin. An optically thick volume of gas merely acts as a "delay circuit" or "resistance" to the outflow or escape of photons from the surface that bounds the volume of gas. The total rate at which photons escape is unaffected however whether the gas is optically thick or thin and is equal to the total rate of photon creation throughout the exhaust gas volume at any instant. If this were not so there would be no steady state.

The difference between an optically thick and optically thin gas is that it takes an average photon emitted near the center of a dense gas cloud a lot longer to reach the surface and escape than if the photon was born in an optically thin gas. In the denser gas, an emitted photon is reabsorbed and reemitted many times and even annihilated due to collisional deexcitation. However because in a dense gas the collisional excitation rate equals the collisional deexcitation rate*, collisional annihilation of virtual photons

*This is the so-called LTE (Local Thermodynamic Equilibrium) hypothesis which can be invoked on the basis of the law of microscopic reversibility.

is exactly balanced by collisional creation of them. The net result is that photons are simply retarded as they diffuse outwards in the gas towards the surface; for each one that starts out, eventually one will escape.

In Volume III of this handbook, the distribution of photons in a finite volume of gas will be treated in detail. It is shown there that for an optically dense volume of gas, the omnidirectional photon flux or fluence is constant and has the same value everywhere at the surface of the gas volume. The photon emission from the surface of such a dense gas volume is then "Lambertian" (like for solid materials), which means that the radiant intensity in a particular direction coming from an element of surface area is proportional to the cosine of the angle that this direction makes with the surface. Since (as we shall see in Chapter 3) we can calculate the total photon production rate at any instant (and their spectral distribution) which is equal to the total photon escape rate from a rocket exhaust, we can in the case of an optically dense low-altitude exhaust calculate the radiant intensity in any direction by simply multiplying the total emission rate by a geometrical "view factor" which only depends on the shape of the exhaust gas volume and the angle at which it is viewed.

For optically thin or non-dense exhausts that occur at high altitudes, the photon fluence at the surface is not constant in general. In Volume III, expressions are provided which allow the calculation of the photon fluence in non-dense gases and the emission intensity in various directions from the surface of various standard geometric volumes of gas (cylinder, cone, etc.). In the limit of a completely transparent gas, the emission is completely isotropic and the total observed steradianance is proportional to the volume of gas in the observer's field-of-view divided by 4π steradians. Again it is

June 1974

FTD-CW-01-01-74
Vol. 1

possible to multiply the total steady photon emission rate from a thin exhaust by a simple geometric view factor, ~~as we shall show in Chapter 3.~~

The above-outlined methods for calculating the radiant emission from a rocket exhaust plume or cloud may sound complicated but are actually much simpler to carry out than the commonly-employed technique of "slicing" the gas volume into sections and calculating the emission from each section, taking into account the absorption by intervening sections between it and the observer. The total radiation is then obtained by summing over all sections (see for example Ref. 14).

At the end of Chapter 3 the sensitivities are examined of the radiant intensities to changes in the values of key parameters used in the expressions developed in the earlier sections of Chapter 3. In Chapter 4, examples and applications are given of radiation signature calculations based on the equations developed in Chapter 3. A series of appendices and a nomenclature list finally conclude this first volume of the Rocket Radiation Handbook.

FTD-CW-01-01-74
Vol. I

June 1974

2. SOURCES AND PHENOMENOLOGY OF NATURAL ROCKET RADIATION

2.1 GENERAL REVIEW OF ROCKET RADIATION SOURCES

In this chapter, the main sources will be surveyed that are responsible for rocket radiation and preliminary order-of-magnitude estimates are obtained of their contribution to the total emission.

If one wishes to be all-inclusive, one may list four types of photon* radiation that can emanate from a rocket, namely:

- (1) "Passive" or "Natural" radiation due to body and exhaust heat, and due to illumination by Solar, Lunar, Earth, or Celestial radiation.
- (2) "Activated" radiation due to artificial illumination of the rocket with radar or laser beams. This radiation can be "pure reflection radiation" or "luminescent reemission" (see Ref. 54).
- (3) "Nuclear" photon radiation, that is gammas and X-rays emitted by a radioactive material carried by the rocket. This may for example occur in the case of a nuclear rocket, or a radioisotope-power-package carrying rocket.
- (4) "Elint" radiation due to telemetry signals emitted from guidance-and-control and communication systems carried by the rocket.

*Other emanations (e.g., electrons, neutrons, etc.) are of course also possible in principle.

June 1974

In this Handbook only Item (1) will be considered, that is the passive or natural radiations which emit most strongly somewhere in the 10^{-7} meter (= 100 nm) to 10^{-3} meter (= 1 mm) wavelength region of the photon spectrum, that is from the ultraviolet through the visible, infrared, and into the radarwave region.* Thus even if the other photon radiations are present there is no interference from nuclear radiation which emits in the 10^{-13} to 10^{-8} meter region of the spectrum, and little interference from radar or telemetry which usually employ the 10^{-4} to 10^3 meter wavelength range (GHz to kHz frequencies).

Even if there is some spectral overlap between the natural rocket radiations and communication waves, the latter are confined to very narrow frequency bands and are man-modulated (i.e., they are spatially- and phase-coherent), whereas the natural rocket emissions in the radarwave region are random (incoherent) and distributed over a large spectrum. Thus they are easily distinguished. In fact in telemetry or communications technology the natural rocket emissions in the radarwave part of the spectrum are treated as noise.

The same can be said for laser and radar beam reflection or reemissions whose wavelengths do fall in the UVIR range. They are also confined to a narrow region of the spectrum and they are at least partially coherent. Thus they are again easily distinguished from natural radiation in case they happened to be present, if the radiation observations are highly resolved spectrally. For broad-band rocket radiation sensors, the presence

*We shall call this region UVIR for short. Further we shall often employ the abbreviations UV = Ultraviolet, VIS = Visible, IR = Infrared, and RW = Radarwave or Microwave.

of some laser-induced radiation from a laser-illuminator would be unnoticeable* since the total spectrum-integrated natural radiation usually far exceeds the reflection or reemitted (narrow line) laser radiation in intensity (see also Ref. 54).

The natural rocket radiations may be subdivided into two major groups: (a) Vehicle Hardware Emissions, and (b) Rocket Exhaust Emissions. Of these, the vehicle hardware emissions are easiest to understand as they involve solid surfaces and simple solar reflections from them or deal with solid surface self-emissions. In section 2.2 they are briefly reviewed.

The emissions produced by the rocket exhaust gases and condensables^{***} are more complex in nature as they involve a multitude of internal and external interactions. It is profitable to consider a rocket exhaust as being composed of two distinct parts; namely (1) the fast-moving region directly behind the nozzle which is in the process of mixing with the ambient atmosphere and is colliding and slowing down with respect to it — which region we shall call the "plume," and (2) the exhaust gases and condensables which have slowed down and come into equilibrium with respect to the atmosphere — termed the "cloud." Figure 2-1 illustrates these two regions.

Whereas the plume exists only as long as there is thrusting, the life of the cloud is theoretically infinite, although in practice the exhaust contained within a fixed observer's field-of-view decreases due to rapid expansion of the cloud by diffusional and/or free escape processes. If

*This applies only if a laser-illuminator is under consideration. For a high-energy laser-beam-powered rocket, this statement does not hold of course.

**Typical exhaust gases are H_2O , H_2 , CO_2 , CO , HCl ; condensables are Al_2O_3 , C_2 , and H_2O .

June 1974

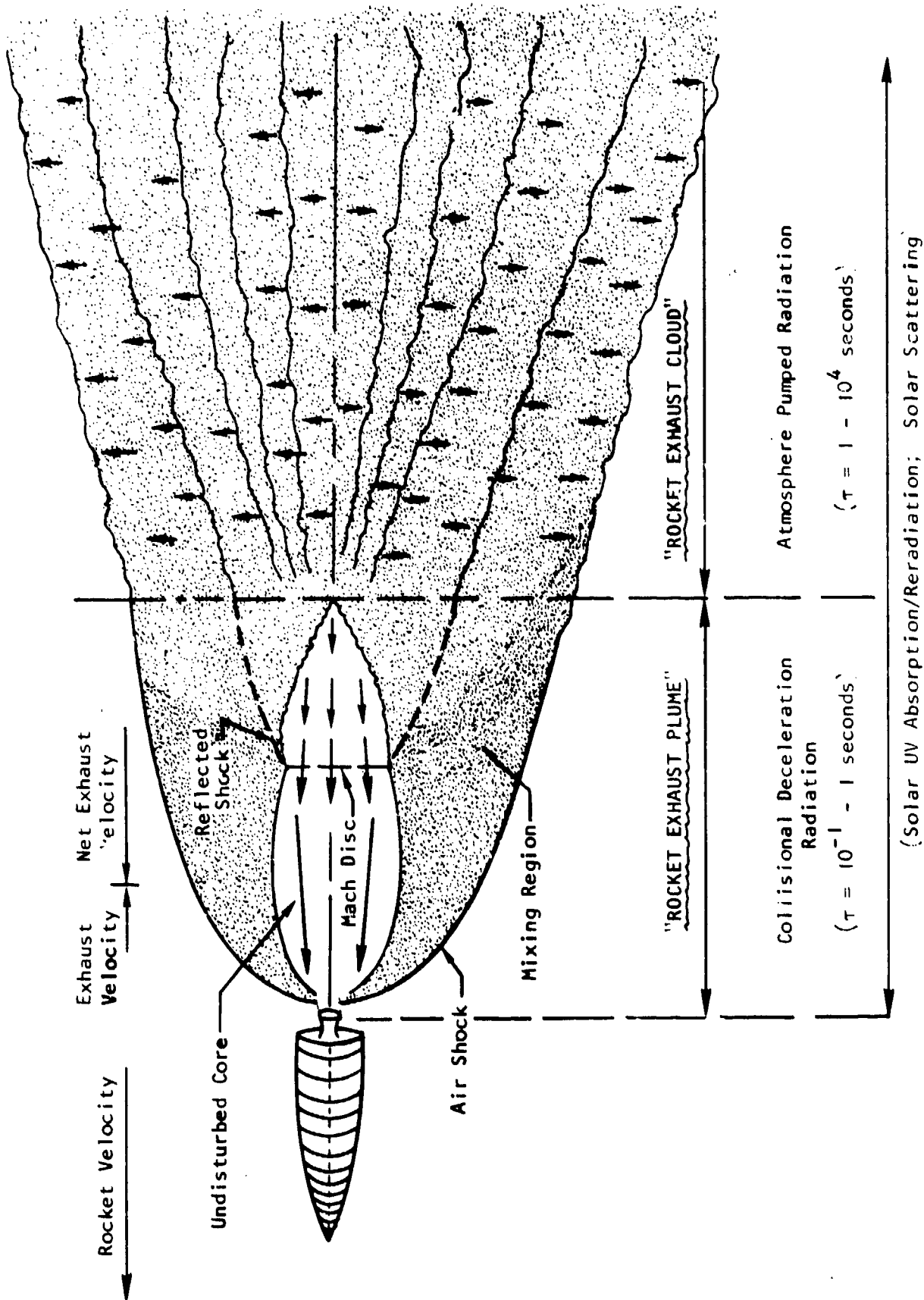


FIGURE 2-1. ILLUSTRATION OF SPATIAL DISTRIBUTION AND RADIATION PROCESSES OF A HIGH-ALTITUDE ROCKET EXHAUST

observed from large distances however (for example from a deep-space orbit), the cloud may remain totally within an observer's field-of-view for some time as illustrated in Figure 2-2. If in this case cloud radiations such as atmospheric pumping or solar fluorescence are operative, significant contributions from these sources may be expected, which continue after thrust cessation. Atmospheric pumping and solar fluorescence will be discussed in section 2.3.

The total integrated persistent radiation from the entire cloud may be substantial although the radiation intensity per unit surface area of the cloud (Watts/m^2) is several orders of magnitude smaller than that of the plume. If only a small portion of the cloud is viewed, as for example in the case of observing a rocket launch from a low-altitude satellite (LAS) such as SKYLAB or from an aircraft (see Figure 2-2), the radiant emission from the rocket plume, which is much more localized and higher in intensity (Watts/m^2), would far exceed the persistent radiations from the rocket cloud so that the latter can be ignored. For a high-altitude satellite (HAS) observer such as APOLLO however, the persistent radiation from the cloud ejected by the boosters may be as large as the plume of the upper stage and unless some technique to discriminate between cloud and plume radiation is employed, such a deep-space sensor would observe persistent rocket cloud radiations in certain unfavorable viewing situations.

For the observation of short-duration rocket maneuvers or fuel dumps during midcourse flights or in deep space, an observer on the ground, in an aircraft, LAS or HAS will usually also have to reckon with both rocket cloud and plume radiations, since his field-of-view will usually cover both the cloud and the plume. Thus in this case also, one has to reckon with possible continuing cloud radiation after thrust cessation.

June 1974

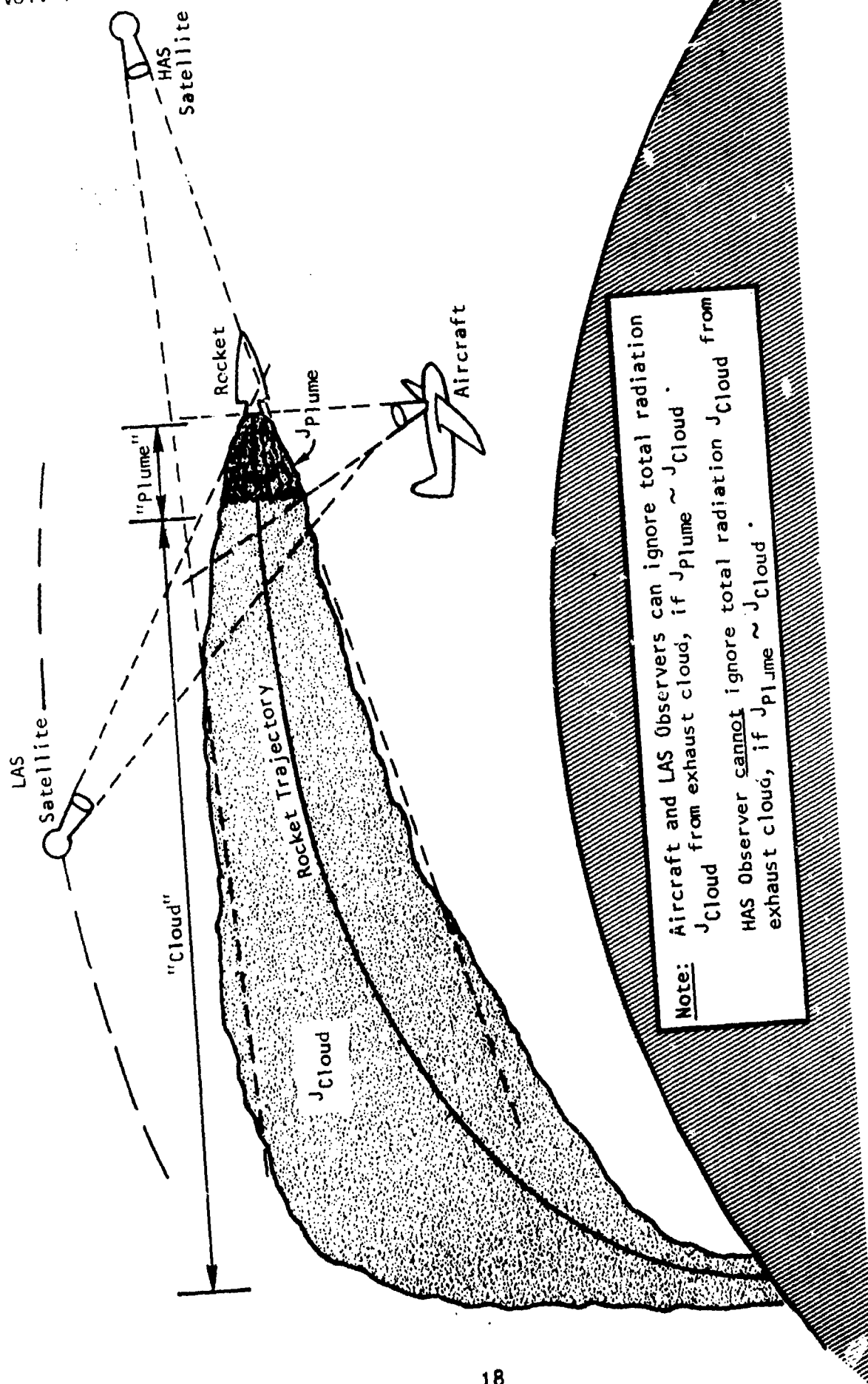


FIGURE 2-2. ILLUSTRATION OF IMPORTANCE OF VIEWING CONDITIONS

An important factor to be considered in rocket radiation work is the wavelength region in which most of the radiation is emitted. The peak-radiation wavelength region varies considerably with the rocket velocity of altitude as the detailed analyses to be given in Chapter 3 will show. These analyses reveal that for large rocket launchings such as an Atlas, most of the emission is in the near-infrared for the major part of the trajectory, with peak radiations shifting slowly from lower to higher frequencies as the rocket picks up speed. Near the burnout point when the vehicle has reached velocities in the neighborhood of 7 to 8 km/sec, even ultraviolet and visible emissions start to become significant. If after the launch phase a maneuver such as a retrofiring is executed, the peak exhaust radiation is often in the ultraviolet or visible instead of the infrared, though the latter is enhanced as well of course. For reentries, the highest levels of radiation are usually also in the ultraviolet and visible although again infrared emissions are substantial as well.

The wavelength region in which most radiation energy is emitted may not always be the best region for observation of course. For ground-based and airborne observations, atmospheric attenuation severely limits which regions of the spectrum can be used. For example the high-altitude UV emissions which occur near burnout or during space maneuvers cannot be observed even by high-flying aircraft or balloons because of the UV-absorbing ozone layer. Satellite observers on the other hand can observe the UV emissions. In addition to attenuation considerations, the background and foreground radiations must be considered before a final optimum observational band can be chosen. This applies to all types of observations (ground-, air-, and space-based).

2.2 VEHICLE BODY EMISSIONS

Space vehicle bodies can emit two types of passive radiation:

- (a) Reflected Sunlight (daytime only)
- (b) Body Self-Radiation (day or night)

For both radiations (a) and (b), the vehicle body cross-section $\sigma(m^2)$ is the most important parameter. Since the solar constant is about 556 Watts/ m^2 for the visible ($0.4 < \lambda < 0.7 \mu m$) part of the spectrum, one finds that an isotropically-reflecting* surface of σm^2 and reflectivity ρ would give rise to a radiant intensity of:

$$J \left(\begin{array}{l} \text{Vehicle} \\ \text{Reflected} \\ \text{Sunlight} \\ 0.4 < \lambda < 0.7 \mu m \end{array} \right) = \frac{556}{2 \pi} \rho \sigma = 88.6 \rho_{VIS} \sigma \quad , \quad \frac{\text{Watts}}{\text{ster}} \quad (2.1)$$

Most space vehicle surfaces reflect diffusely** instead of isotropically and Eq. (2.1) must be modified:

$$J \left(\begin{array}{l} \text{Vehicle} \\ \text{Reflected} \\ \text{Sunlight} \\ 0.4 < \lambda < 0.7 \mu m \end{array} \right) = 177 f(\psi) \rho_{VIS} \sigma \quad , \quad \frac{\text{Watts}}{\text{ster}} \quad (2.2)$$

* Isotropically reflecting = reflecting equally in all directions.

**Diffusely reflecting = reflecting in a direction θ from the surface normal with a relative intensity proportional to $\cos\theta$.

where $f(\psi)$ is a function varying from 0 to 1, that depends on the vehicle's surface geometry and on the sun-target-observer angle ψ .

Solar UV at wavelengths below $\lambda = 0.2 \mu\text{m}$ will be completely absorbed by most ordinary rocket or space vehicle surfaces and thus no reflective contributions below this wavelength are normally seen. The solar UV illumination between 0.2 and $0.4 \mu\text{m}$ amounts to about 120 Watts/ m^2 , so that reflected radiant intensities in this wavelength region are:

$$J_{\left(\begin{array}{c} \text{Vehicle} \\ \text{Reflected} \\ \text{Sunlight} \\ 0.2 < \lambda < 0.4 \mu\text{m} \end{array} \right)} = 19.1 \rho_{UV} \sigma \left(\text{m}^2 \right), \frac{\text{Watts}}{\text{ster}}, \quad (2.3)$$

for an isotropically-reflecting surface, and:

$$J_{\left(\begin{array}{c} \text{Vehicle} \\ \text{Reflected} \\ \text{Sunlight} \\ 0.2 < \lambda < 0.4 \mu\text{m} \end{array} \right)} = 38.2 f(\psi) \rho_{UV} \sigma \left(\text{m}^2 \right), \frac{\text{Watts}}{\text{ster}}, \quad (2.4)$$

for a diffuse surface.

Typical space vehicle bodies have cross-sections ranging from $\sigma = 1 \text{ m}^2$ to $\sigma = 100 \text{ m}^2$. Thus maximum radiant intensities from reflected sunlight will range from 177 to 17,700 Watts in the visible (0.4 to $0.7 \mu\text{m}$) with $\rho_{VIS} = 1$, and 8 to 800 Watts in the near-ultraviolet (0.2 to $0.4 \mu\text{m}$), with typical values of $\rho_{UV} = 0.2$.

June 1974

The self- or black-body emission by a space vehicle depends on the vehicle's temperature T . For a diffusely emitting surface, the black-body emission is given by:

$$\left(\begin{array}{c} \frac{dJ}{d\lambda} \\ \text{Self-Emission} \\ \text{by Vehicle} \end{array} \right) = \frac{3.80 \times 10^{-13} f(\psi) \sigma \epsilon}{\lambda^5 \left\{ \exp\left(\frac{1.438}{\lambda T}\right) - 1 \right\}}, \quad \frac{\text{Watts}}{\text{ster} \cdot \mu\text{m}} \quad (2.5)$$

where ϵ is the emissivity of the vehicle's surface, and λ is the wavelength in μm .

For a vehicle body temperature of $T = 273^\circ\text{K}$, the peak emissions occurs in the neighborhood of $\lambda = 10 \mu\text{m}$, and the total emission in the 8 to 12 μm region for example is:

$$\left(\begin{array}{c} J \\ \text{8 to 12 } \mu\text{m} \\ \text{Vehicle} \\ \text{Self-Emission} \end{array} \right) = \int_{\lambda = 8 \mu\text{m}}^{12 \mu\text{m}} \frac{dJ}{d\lambda} d\lambda = 6 f(\psi) \sigma \epsilon, \quad \frac{\text{Watts}}{\text{ster}} \quad (2.6)$$

Thus typical space vehicles with $\sigma = 1 \text{ m}^2$ to $\sigma = 100 \text{ m}^2$ will emit a maximum ($\epsilon = 1$; $f = 1$) of 6 Watts/ster to 600 Watts/ster in the 8 to 12 μm band.

It is found that the emissions by a rocket plume in the infrared part of the spectrum are some 1000 to 10,000 times higher than the intensities one obtains from Eqs. (2.5) or (2.6) for infrared body radiation. Thus when the rocket is thrusting, the vehicle body self-emissions can be neglected. However during midcourse or deep-space coasting, only body

June 1974

FTD-CW-01-01-74
Vol. I

self-emission occurs and thus under these circumstances the latter is the dominant mechanism in the infrared.

The visible and ultraviolet reflections of sunlight by the rocket vehicle are dominant of course during most of a rocket's launch trajectory although near burnout, the visible and ultraviolet contributions by the exhaust may exceed the hardware reflections for certain types of rockets.

In conclusions, it is evident that both (visible) solar reflections and (infrared) body self-emissions must be included in any theory that has to account for all rocket radiations under any circumstances (thrusting or non-thrusting). In Chapter 3, complete expressions for these radiation mechanisms will be given.

2.3 ROCKET EXHAUST RADIATIONS

2.3.1 Survey of Radiation Mechanisms

Rocket plume emissions have been investigated for more than 20 years during which time a large number of mechanisms have been proposed as the cause of the emission of exhaust radiation. The main mechanisms that have been considered or investigated are the following (see for example Refs. 1 to 21):

- (1) Undisturbed Core or Mach Cone Radiation
- (2) Afterburning Radiation
- (3) Collisional Deceleration or Plume/Air Shock Radiation
- (4) Internal Shock Radiation
- (5) Atmospheric Pumping Radiation
- (6) High-Altitude Atomic Oxygen Reactions and Radiations
- (7) High-Altitude Molecular Association/Dissociation Radiations
- (8) Airglow from Rocket Vehicle Air Impact Friction
- (9) Scattering of Rocket Chamber Radiation by Solid and Gaseous Exhaust Products in the Plume
- (10) Scattering of Solar Radiation by Solid Exhaust Particles
- (11) Scattering of Solar Radiation by Molecular Exhaust Species
- (12) Solar Radiation Absorption and UV, VIS, IR Reemission
- (13) Plume Reflected Earthshine

It is probable that all mechanisms listed above play some part in plume emission, but fortunately several types of emissions radiate much stronger than others so that the others can be safely ignored in most cases of interest.

To determine approximately what the relative strengths of the emissions are of the different mechanisms, in the next subsection the

source, magnitude, and distribution of the energy responsible for driving each mechanism will be considered. By assuming some reasonable bounds for the efficiency of conversion of this energy into radiation for each mechanism, we can then put them in perspective and estimate which ones are most important.

2.3.2 Energy Considerations

As a starting point, consider the distribution of the energy produced by the rocket propellant combustion process. The energy created in this process is first of all divided between the rocket vehicle which gains kinetic energy, and the expelled exhaust gases which get the balance (see Ref. 22). Here, the rocket exhaust energy is of prime interest. The total energy carried by the exhaust materials may be envisioned to be in four forms as follows:

$$\begin{aligned} \left(\frac{dU}{dt}\right)_{\text{Total Exhaust Gases}} &= \left(\frac{dU}{dt}\right)_{\text{Exhaust Heat}} + \left(\frac{dU}{dt}\right)_{\text{Latent Chemical Energy}} + \\ &+ \left(\frac{dU}{dt}\right)_{\text{Dynamic Energy with respect to atmosphere}} + \left(\frac{dU}{dt}\right)_{\text{Potential Energy with respect to earth surface}}, \text{ Watts} \end{aligned} \quad (2.7)$$

where:

$$\left(\frac{dU}{dt}\right)_{\text{Exhaust Heat}} = \dot{W} g_c \Delta H_c \left(\frac{T_e}{T_c}\right), \text{ Watts} \quad (2.8)$$

June 1974

$$\left(\frac{dU}{dt}\right)_{\substack{\text{Latent} \\ \text{Chemical} \\ \text{Energy}}} = \dot{W} g_F \Delta H_c, \text{ Watts} \quad (2.9)$$

$$\left(\frac{dU}{dt}\right)_{\text{Dynamic}} = 500,000 \dot{W} \bar{V}_r^2, \text{ Watts} \quad (2.10)$$

$$\left(\frac{dU}{dt}\right)_{\text{Potential}} = 9,800 \dot{W} h, \text{ Watts} \quad (2.11)$$

Here a balance was written for the rate at which energy is released rather than the total energy, since it is the rate which is of main interest.

The various parameters in Eqs. (2.8) through (2.11) are defined as:

$\dot{W} = F/I_{sp} =$ Rocket mass expulsion rate, kgms/sec

$F =$ Rocket thrust, kgm (force)

$I_{sp} =$ Specific impulse, sec

$g_c =$ Moles/kg of propellant fuel burned in rocket chamber

$g_F =$ Moles/kg of unburned fuel leaving rocket nozzle

$\Delta H_c =$ Molar heat of combustion of rocket fuel, Joules/mole

$\bar{V}_r = \bar{V}_r(h) = \bar{V}_v(h) - V_{\text{exh}} =$ Relative velocity of exhaust with respect to earth-fixed coordinates, km/sec

$V_v(h) =$ Rocket velocity with respect to earth-fixed coordinates, km/sec

$\bar{V}_{\text{exh}} = 0.98 \times 10^{-2} I_{sp} =$ Average exhaust velocity with respect to rocket, km/sec

h = Altitude, km

T_e = Temperature of exhaust gases in exit plane of rocket nozzle, $^{\circ}\text{K}$

T_c = Total temperature of exhaust gases in combustion chamber, $^{\circ}\text{K}$

Except for outside sources such as the sun or energy sources stored in the upper atmosphere, Eq. (2.7) gives the maximum amount of energy that could possibly be available for the production of plume radiation. Of the four sources listed, the fourth one given by Eq. (2.11) is not known to drive any mechanism resulting in plume radiation unless one considers reentry. It will not be considered further.

The first component in Eq. (2.7), exhaust heat, is the remaining thermal energy that the exhaust gases and condensables possess after they have done work and propelled the rocket, that is:

$$U_{\text{Exhaust Heat}} = U_{\text{Combustion Energy}} - U_{\text{Rocket Dynamic Energy}} - U_{\text{Exhaust Dynamic Energy}} \quad (2.12)$$

Usually the rocket gas flow parameters are expressed in terms of Euler's one-dimensional gas dynamic equations which together with the laws of thermodynamics and the assumption of adiabatic conditions give the heat content of the gas and its velocity as it exits from the rocket nozzle (see Rocket Radiation Handbook, Volume IV).

In the combustion of rocket fuel, typical values of the heat of combustion ΔH_c are $\Delta H_c = 250,000$ Joules/mole, $T_e/T_c \approx 0.5$, while

June 1974

$g_c \approx 10$ moles/kg, $g_f \approx 10$ moles/kg, and \bar{V}_r may vary from -3 km/sec at sea-level to 0 km/sec at 60 to 90 km altitude to +5 km/sec at burnout (~ 150 km). Thus for a rocket with a thrust of $F = 100,000$ kg(F) and $I_{sp} = 286$ sec, or for $\dot{W} = 350$ kg(M)/sec we have that:

$$\left(\frac{dU}{dt}\right)_{\text{Exhaust Heat}} \approx 4.38 \times 10^8 \text{ Watts} \quad (2.13)$$

$$\left(\frac{dU}{dt}\right)_{\text{Latent Chemical Energy}} \approx 8.75 \times 10^8 \text{ Watts} \quad (2.14)$$

$$\left(\frac{dU}{dt}\right)_{\text{Dynamic}} = \begin{cases} 15.8 \times 10^8 \text{ Watts (h = 0 km)} & (2.15a) \\ 0 \text{ Watts (60} \lesssim h \lesssim 90 \text{ km)} & (2.15b) \\ 43.8 \times 10^8 \text{ Watts (h} \sim 150 \text{ km)} & (2.15c) \end{cases}$$

Clearly the maximum amounts of available energy are enormous. Of course the energies (2.13) through (2.15) do not give the radiation energy yet since we still have to consider how efficiently this energy is converted into radiation.

Let us next investigate how the available energy might feed or drive the radiation mechanisms (1) through (13) considered above. Core Radiation is radiation due to the deexcitation of hot exhaust species in a region directly behind the nozzle called the "Undisturbed Core" or "Mach Cone" where no air mixing has taken place yet. If the mean transit time of the exhaust

molecules in the core region is $\bar{\tau}_M$ before they enter the air/exhaust mixing region and if the mean time for radiant emission of a photon is τ_r then, as we shall show rigorously in section 3.4, a fraction $\left[1 - \exp(-\bar{\tau}_M/\tau_r)\right]$ will radiate in the core region.

As already mentioned, the energy for Core Radiation originates in the rocket's heat of combustion or more precisely that portion of this heat which is not converted into mechanical motion. If T_a is the ambient temperature, the maximum possible total Core Radiation energy is according to the second law of thermodynamics:

$$\left(\frac{dU}{dt}\right)_{\substack{\text{Maximum Core} \\ \text{Radiation} \\ \text{(All Wavelengths)}}} \approx \left[1 - \exp\left(-\frac{\bar{\tau}_M}{\tau_r}\right)\right] \left(\frac{T_e - T_a}{T_e}\right) \left(\frac{dU}{dt}\right)_{\substack{\text{Exhaust} \\ \text{Heat}}} \quad (2.16)^*$$

Typical values of $T_e \approx 1500^\circ\text{K}$, $\bar{\tau}_M \approx 10$ millisecond, $\tau_r \approx 10$ millisecond, while $T_a \approx 150^\circ\text{K}$. Therefore:

$$\begin{aligned} \left(\frac{dU}{dt}\right)_{\substack{\text{Maximum Core} \\ \text{Radiation} \\ \text{(All Wavelengths)}}} &\approx 0.63 \times 0.83 \left(\frac{dU}{dt}\right)_{\substack{\text{Exhaust} \\ \text{Heat}}} = \\ &= 2.30 \times 10^6 \text{ Watts for a rocket with } \dot{W} = 350 \text{ kg(M)/sec} \end{aligned} \quad (2.17)$$

*The amount of heat radiation under consideration here should not be confused with the intensity of radiation which is of course proportional to T^4 .

June 1974

The amount given by (2.17) is clearly substantial. Of course this amount of radiation is distributed over many different wavelengths which for most rockets usually fall primarily in the infrared part of the electromagnetic spectrum. The conclusion is that Core radiation is an important infrared contributor in rocket plume radiations.

The next mechanism, "afterburning radiation," is due to combustion in the air of unburned fuel that is still present in the exhaust that leaves the nozzle. Because much higher I_{sp} 's are obtained with fuel-rich exhausts, propellants are mixed so that 50 to 80 mole percent of a rocket exhaust contains unburned H_2 and CO which can react with O_2 in the atmosphere if the latter's density is high enough. Since afterburning is the process of converting the remaining latent chemical energy to heat and radiation, we have:

$$\left(\frac{dU}{dt} \right)_{\substack{\text{Maximum} \\ \text{Afterburning} \\ \text{Radiation} \\ \text{(All Wavelengths)}}} = \eta_{AB} \left(\frac{T_r - T_a}{T_a} \right) \left(\frac{dU}{dt} \right)_{\substack{\text{Latent} \\ \text{Chemical} \\ \text{Energy}}} \quad (2.18)$$

where η_{AB} is the fractional degree of reaction of the fuel components in the exhaust in the afterburning process and T_r is the mean temperature of the exhaust and air after mixing and partial combustion. The parameter η_{AB} is on the order of 0.3 at the lower altitudes, dropping to 0 at the higher altitudes due to the lack of oxygen (see section 3.5). Further $T_r \approx 1000^\circ K$ and $T_a \approx 250^\circ K$. Thus:

$$\left(\frac{dU}{dt}\right)_{\text{Max. Afterburning Radiation (All Wavelengths) (h} \sim 20 \text{ km)}} \approx 1.97 \times 10^8 \text{ Watts, for a rocket with } \dot{W} = 350 \text{ kg(M)/sec} \quad (2.19)$$

Afterburning radiation from rocket exhausts is also mostly in the infrared part of the spectrum usually.

Collisional deceleration or plume/air shock radiation as well as internal shock radiation both result from a conversion of bulk dynamic energy into heat and thence to radiation. This energy source is represented by the third term in Eq. (2.7) and given by (2.10). Thus:

$$\begin{aligned} \left(\frac{dU}{dt}\right)_{\text{Total Collisional Deceleration or Shock Radiation (All Wavelengths)}} &= \left(\frac{T_r - T_a}{T_a}\right) \left(\frac{dU}{dt}\right)_{\text{Dynamic}} = \\ &= \begin{cases} 11.8 \times 10^8, & \text{Watts (h = 0 km ; } \bar{V}_r \approx +3 \text{ km/sec)} \\ 0 & \text{, Watts (60 } \lesssim h \lesssim 90 \text{ km)} \\ 32.8 \times 10^8, & \text{Watts (h } \sim 150 \text{ km ; } \bar{V}_r \approx -5 \text{ km/sec)} \end{cases} \\ &\text{, for a rocket with } \dot{W} = 350 \text{ kg(M)/sec} \end{aligned} \quad (2.20)$$

Again it is clear that collisional deceleration (CD) radiation* is very important and stronger than any of the others that we have considered so far at the low (h ~ 0 to 20 km) and high (h ~ 150 km) altitudes.

*Some prefer the term "thermalization" or "air shock" radiation.

June 1974

The fifth mechanism on the list, "atmospheric pumping radiation" derives its energy from the upper atmosphere, and not from any energy reservoirs contained in the plume. At high altitudes (above 90 km), a large fraction of N_2 and O_2 molecules are in vibrationally-excited states N_2^* and O_2^* due to the high temperatures that exist there (this energy came originally from the sun of course). Because N_2 and O_2 are homonuclear diatomic molecules whose vibrational dipole moment is zero, they cannot emit (to first-order) vibrational radiation and can only transfer or receive excitation energy via collisions. Thus if N_2^* and O_2^* encounter exhaust molecules such as H_2O and CO_2 which do radiate well, excitation energy is first transferred from N_2^* and O_2^* to H_2O and CO_2 by collisions and then emitted as radiation. The H_2O and CO_2 molecules dumped into the upper atmosphere by rocket exhausts therefore act as siphons which release the otherwise "locked-up" vibrational energy stored in N_2 and O_2 . Since the "pumping" or energy transfer process can occur over and over again because of the infinite supply of excited N_2^* and O_2^* , "atmospheric pumping radiation" is proportional to the total number of radiatable molecules dumped in the upper atmosphere. That is:

$$\left(\frac{dU}{dt}\right)_{\text{Atmospheric Pumping}} = z_c^* \epsilon_Y g_X \dot{W} t_{AP}, \text{ Watts,} \quad (2.21)$$

where:

$$z_c^* = z_c^*(h) = \text{Collisional excitation rate, sec}^{-1}$$

$$\epsilon_Y = \text{Quantum energy of emitted photon, Joules/mole}$$

g_X = Moles/kg of exhaust of radiatable molecules X

\dot{W} = Exhaust mass flow rate, kg/sec

t_{AP} = Rocket burn time at altitudes where atmospheric pumping is effective, sec

Typical values in (2.21) are $z_c^* = 1 \text{ sec}^{-1}$, $\epsilon_Y = 36,000 \text{ Joules/mole}$, and $g_X = 20 \text{ moles/kg}$, so that:

$$\left(\frac{dU}{dt}\right)_{\text{Atmospheric Pumping}} \sim 720,000 \dot{W} t_{AP}, \text{ Watts} \quad (2.22)$$

Thus for a model rocket with $F = 100,000 \text{ kg(F)}$ or $\dot{W} = 350 \text{ kg(M)/sec}$, and $t_{AP} \approx 10 \text{ seconds}$, one gets:

$$\left(\frac{dU}{dt}\right)_{\text{Atmospheric Pumping}} = 25.2 \times 10^8, \text{ Watts}, \quad (2.23)$$

which is quite substantial. Of course atmospheric pumping radiation occurs over the entire length of the high-altitude portion of the rocket trail where atmospheric pumping takes place and thus over a much larger region in space than the other mechanisms considered so far which take place within a kilometer or so behind the rocket. Thus a better way to estimate the effect of atmospheric pumping radiation is to write:

$$\left(\frac{dU}{dt}\right)_{\text{Atm. Pump.}} \cdot S_{AP}^{-1} = 0.50 \times 10^8, \text{ Watts/km}, \quad (2.24)$$

June 1974

where $S_{AP} = V_v t_{AP} \sim 5 \text{ km/sec} \times 10 \text{ sec} = 50 \text{ km}$.

Though weaker than the other mechanisms on a per kilometer basis, and occurring primarily at altitudes between 90 and 150 kilometers, it appears that atmospheric pumping radiation cannot be entirely ignored particularly if the sensor of the observer has a large part of the rocket trail in its field-of-view (see Figure 2-2). The wavelengths at which atmospheric pumping radiation are emitted fall mainly in the mid- and far-infrared.

The possibility of radiations that accompany high-altitude chemical reactions between exhaust species and atomic oxygen (e.g., $\text{H}_2\text{O} + \text{O} \rightarrow \text{H}_2\text{O}_2$ and $\text{CO} + \text{O} \rightarrow \text{CO}_2$), and high-altitude dissociations of exhaust species (e.g., $\text{CO}_2 \rightarrow \text{CO} + \text{O}$ and $\text{H}_2\text{O} \rightarrow \text{OH} + \text{O}$), Items (6) and (7) on the list, have also been considered. These processes are similar to "atmospheric pumping," except that each chemical reaction-excitation process can occur only once for a particular exhaust molecule and not repeatedly as is the case for atmospheric pumping. This is because the suppliers for this radiation are the exhaust molecules which can be consummated only once in a chemical reaction, whereas in atmospheric pumping they remain chemically the same.

Of course if high-altitude chemical reactions or dissociations are very rapid compared to the atmospheric pumping rate, the exhaust molecules will never get a chance to experience atmospheric pumping. This latter situation occurs at very high altitudes and in the presence of solar ultraviolet radiation. However between 90 and 130 kilometers, atmospheric pumping is definitely operative even for a daytime launch.

The emission of high-altitude chemical reaction radiation is estimated to be:

$$\left(\frac{dU}{dt}\right)_{\text{High-Altitude Chemical Reactions}} \sim \epsilon_Y z_C^r g_X \dot{W} t_{\text{HACR}} \sim 7200 \dot{W} t_{\text{HACR}}, \text{ Watts}, \quad (2.25)$$

since the rate of chemical reaction z_C^r (sec^{-1}) is estimated to be about a hundred times slower than the vibrational excitation rate z_C^* for atmospheric pumping and very roughly $\epsilon_Y \approx 40,000$ Joules/mole. Here t_{HACR} is the travel time of the burning rocket through that portion of the atmosphere where high-altitude chemical reactions can take place. For $\dot{W} = 350$ kg/sec, $t_{\text{HACR}} \approx 10$ sec, and assuming a trail length of $S_{\text{HACR}} = V_{\text{HACR}} \times t_{\text{HACR}} = 70$ kilometers we then get:

$$\left(\frac{dU}{dt}\right)_{\text{HACR}} / S_{\text{HACR}} \approx 3.6 \times 10^3, \text{ Watts/km}, \quad (2.26)$$

since the radiation from these reactions will also extend over a large portion of the rocket's trail (but only back to a point where these reactions are complete or have come to equilibrium). Because of its weakness, high-altitude chemical reactions (HACR) will not be further considered for the infrared region. The other mechanisms reviewed earlier clearly dominate in the infrared. Only solar UV-induced dissociations that cause UV or visible emissions will be investigated later in some detail as part of mechanism (12), "solar UV absorption and reemission"

Airglow from friction or impact of high-altitude molecules with the rocket vehicle body, Item (8) on the list, has been considered as a possible source by some. However the total energy available for this type of radiation is at most:

June 1974

$$\begin{aligned} \left(\frac{dU}{dt} \right)_{\substack{\text{Vehicle Friction} \\ \text{Airglow} \\ \text{(All Wavelengths)}}} &\approx 10^9 \eta_{AG} (n_{air} V_v) \left(\frac{\pi}{4} D_v^2 \right) \left(\frac{1}{2} M_{air} V_v^2 \right) = \\ &= 2.48 \times 10^{-17} n_{air} D_v^2 V_v^3 \eta_{AG} , \text{ Watts} \end{aligned} \quad (2.27)$$

where:

$n_{air} = n_{air}(h) = \text{air density, molecules/m}^3$

$D_v = \text{Diameter of rocket vehicle, m}$

$V_v = V_v(h), \text{ velocity of rocket vehicle; km/sec}$

$M_{air} = \text{Mass of air molecule, kgm}$

$\eta_{AG} = \text{Conversion efficiency of heat to airglow radiation for vehicle air friction process}$

At an altitude of say $h = 100$ km in the vicinity of which peak dynamic heating of an ascending rocket takes place usually, one has that $n_{air} \approx 10^{19}$ molecules/m³, $V_v \approx 3$ km/sec, while $D_v \approx 10$ meters for a large rocket. Then:

$$\left(\frac{dU}{dt} \right)_{\substack{\text{Vehicle Friction} \\ \text{Airglow}}} \sim 6.70 \times 10^5 \eta_{AG} , \text{ Watts } (h \sim 100 \text{ km}) \quad (2.28)$$

which is negligible compared to the other sources of plume energy even if

$\eta_{AG} = 1$. Therefore vehicle-induced airglow at high altitudes will not be considered any further. Of course during reentry, when high-density air is

encountered, radiation from body friction is very large. However in this monograph only pre-reentry rocket radiation phenomena are considered.

Radiation generated in the rocket combustion chamber that escapes through the nozzle and which is subsequently scattered or refracted by gaseous molecules and solid particles in the rocket plume (mechanism (9))* is another possible source of radiation which has been suggested. Since a rocket chamber behaves almost like an ideal block-body the maximum available energy can be calculated directly from Stefan's Law:

$$\left(\frac{dU}{dt}\right)_{\text{Maximum Plume-Scattered Chamber Radiation}} \approx 5.67 \times 10^{-8} T_c^4 \left(\frac{\pi D_t^2}{4}\right), \text{ Watts}, \quad (2.29)$$

where D_t is the nozzle throat diameter in meters and T_c is the combustion chamber temperature in °K. Taking a typical value** of $T_c = 3600$ °K and $D_t = 0.3$ meter, one gets that:

$$\left(\frac{dU}{dt}\right)_{\text{Maximum Plume-Scattered Chamber Radiation}} \approx 6.73 \times 10^5, \text{ Watts}, \quad (2.30)$$

Again this radiation, which is primarily in the infrared, is negligible compared to the Core and Thermalization radiation and will not be considered further.

*This radiation has also been called the "searchlight effect" (Ref. 17).

**Of course this value of T_c is related to the combustion energy production rate $(dU/dt)_{\text{Combustion Energy}}$ and chamber hardware parameters.

Next to be considered are the three solar-illuminated produced plume radiations, Items (10) through (12) on the list. The total illumination by the sun is about 1390 Watts/m² distributed over the well-known solar spectrum. For scattering by solid exhaust particles in the plume, the total scattered radiation amounts to:

$$\left(\frac{dU}{dt}\right)_{\text{Particle-Scattered Solar Radiation}} = 1390 \bar{\sigma}_p N_p, \text{ Watts} \quad (2.31)$$

where:

N_p = Number of particles in the plume

$\bar{\sigma}_p$ = Average scattering cross-section of an exhaust particle, m²

The number of particles in an exhaust plume or cloud is given by:

$$N_p = \frac{1000 f_p \dot{W} t_b}{\frac{\pi}{6} d_p^3 \rho_p} \quad (2.32)$$

where:

\dot{W} = Rocket mass expulsion rate, kg/sec

t_b = Burn time, sec

f_p = Weight fraction in combustion products of condensable species p

d_p = Average diameter of particles, cm

ρ_p = Average density of particles, gm/cm³

Typically $d_p \approx 10^{-4}$ cm, $\rho_p \approx 3.5$ gm/cm³ and $f_p \approx 1$ percent so that:

$$N_p \sim 5.46 \times 10^{12} \dot{W} t_b, \text{ particles} \quad (2.33)$$

The scattering cross-section σ_p varies considerably with particle size, particle chemistry and wavelength. For values of $d_p \approx 1 \mu\text{m}$, which apply for typical Al_2O_3 particles, and for $\lambda = 0.5 \mu\text{m}$ we have $\sigma \approx 2.5 \times 10^{-14}$ m². Thus from Eqs. (2.31) and (2.33) one obtains as upper limit on the radiation due to solar scattering:

$$\left(\frac{dU}{dt}\right)_{\text{Particle-Scattered Solar Radiation}} \approx 190 \dot{W} t_b, \text{ Watts}, \quad (2.34)$$

or per kilometer of trail:

$$\left(\frac{dU}{dt}\right)_{\text{Particle-Scattered Solar Radiation}} \approx 190 \dot{W}/V_v, \text{ Watts/km} \quad (2.35)$$

Though the radiation given by (2.34) or (2.35) may appear to be much less than that of the self-produced plume emissions, Items (1) through (4), the range of wavelengths over which most of these latter emissions occur is in the infrared, whereas the solar-reflected radiations are in the visible which is much easier to detect. Also solar-reflected radiation from exhaust plumes and clouds is continuous and extends over the entire trail whereas the plume self-emissions occur only during thrusting and extend to a distance of only

June 1974

a few kilometers behind the rocket. Substituting typical values of $\dot{W} = 350 \text{ kg/sec}$ and $V_v = 3 \text{ km/sec}$ in (2.35) one gets for example:

$$\left(\frac{dU}{dt}\right)_{\text{Particle-Scattered Solar Radiation}} = 22,167 \text{ Watts/km} \quad (2.36)$$

Clearly particle-reflected solar radiation in the visible can be quite important.

The emission due to molecular-Rayleigh scattering of solar radiation is given by:

$$\left(\frac{dU}{dt}\right)_{\text{Molecular-Rayleigh Scattering of Solar Radiation}} = 1390 \bar{\sigma}_{\text{Rayleigh}} \cdot \frac{\dot{W}}{M_e} t_b, \text{ Watts}, \quad (2.37)$$

where $\bar{\sigma}_{\text{Rayleigh}}$ is the wavelength-averaged cross-section in m^2 for Rayleigh scattering of solar photons by an (averaged) exhaust molecule, M_e is the average mass of the exhaust molecules in kilograms, and the other parameters are the same as before. Typical values in (2.37) are $\bar{\sigma}_{\text{Rayleigh}} = 10^{-31} \text{ m}^2$ (see Appendix G), and $M_e = 4.15 \times 10^{-26} \text{ kg}$, so that:

$$\left(\frac{dU}{dt}\right)_{\text{Molecular-Rayleigh Scattering of Solar Radiation}} \sim 3.35 \times 10^{-3} \dot{W} t_b, \text{ Watts}, \quad (2.38)$$

or assuming again a velocity of $V_v = 3 \text{ km/sec}$ and $\dot{W} = 350 \text{ kg/sec}$:

$$\left(\frac{dU}{dt}\right)_{\text{Molecular-Rayleigh Scattering of Solar Radiation}} \approx 0.39 \text{ Watts/km} \quad (2.39)$$

This is more than 10,000 times weaker than the particle-produced scattered radiation given by (2.36). Because it is so weak, molecular-scattered solar radiation will not be considered any further.

The solar spectrum contains photons which are resonant with respect to vibrational and electronic transitions in the exhaust species. Thus solar photon absorptions followed by reemissions can occur in rocket plumes (Item (12)). Of these resonant absorptions, the infrared ones which cause vibrational excitations and which reemit in the infrared are usually weak compared to the infrared emissions by the other mechanisms we discussed. However very bright visible and ultraviolet reemissions have been observed for the ultraviolet/visible absorptions at the higher altitudes ($h \geq 130$ km) which cause electronic excitations in the exhaust molecules. For solar photons with $\lambda \leq 2400 \text{ \AA}$, the illumination intensity is $I(\lambda \leq 2400 \text{ \AA}) \approx 6 \text{ W/m}^2$, so that:

$$\left(\frac{dU}{dt}\right)_{\text{Absorption/Reemission of Solar UV}} = 6 \bar{\sigma}_{aUV} \left(\frac{\dot{W}}{M_e} t_b\right), \text{ Watts} \quad (2.40)$$

where all parameters are the same as before and the absorption cross-section for solar UV photons $\bar{\sigma}_{aUV} \approx 10^{-21} \text{ m}^2$. Taking $M_e = 4.15 \times 10^{-26} \text{ kg}$ again, and $\dot{W} = 350 \text{ kg/sec}$, $V_v = 3 \text{ km/sec}$, one finds then that:

June 1974

$$\left(\frac{dU}{dt}\right)_{\text{Absorption/Reemission of Solar UV}} \approx 6.5 \times 10^4 \dot{W} t_b, \text{ Watts}$$

$$= 6.5 \times 10^4 \dot{W}/V_v, \text{ Watts/km} = 7.58 \times 10^6 \text{ Watts/km of trail} \quad (2.41)$$

This amount is enormous when compared with Eqs. (2.36) and (2.39). The reemission that follows the absorption of solar UV by exhaust plumes and clouds can of course be partially in the infrared part of the spectrum as well as in the visible and ultraviolet. For many exhaust molecules, the solar UV absorption causes dissociation and excitation of one or more dissociated atoms or radicals. The emission of these dissociated and excited radicals (e.g., OH) is usually in the near-UV or visible with little or no contributions in the infrared.

Finally consider plume-reflected earthshine radiation (Item (13)). The illumination is mostly in the far-IR ($\lambda = 8$ to $14 \mu\text{m}$) and amounts for near-earth altitudes ($h \leq 400 \text{ km}$) to about $I_{\text{IR Earthshine}} \approx 10^{-7} \text{ Watts/m}^2$. This amount when scattered from solid plume particles gives rise to a radiation of at most:

$$\left(\frac{dU}{dt}\right)_{\text{Plume-Reflected IR Earthshine}} \sim 5 \times 10^{-7} \dot{W}/V_v = 5.85 \times 10^{-5}, \text{ Watts/km}, \quad (2.42)$$

where the same parameters as in Eq. (2.34) were used except that $\sigma_{\text{PIR}} \approx 10^{-12} \text{ m}^2$ instead of $\sigma_{\text{PVIS}} \approx 2.5 \times 10^{-14} \text{ m}^2$, and again $\dot{W} = 350 \text{ kg/sec}$, $V_v \approx 3 \text{ km/sec}$.

Obviously (2.42) is too weak to be of any significance when compared to any of the previous radiations. For Rayleigh-scattering by exhaust molecules, the reflected energy would be even less than (2.42). Only molecular resonant absorption and reemission of earthshine could yield higher values than (2.42) but the atmosphere-filtered earthshine is composed of just those photons that are also transparent to most exhaust clouds. So this possibility does not occur unless unusual molecular species are present in the exhaust which absorb in the 8 to 12 μm wavelength region.

In the above, only very rough estimates were obtained of the possible importance of various mechanisms on the basis of total available energies and with minimum regard of the spectral distributions of the radiations or the spatial extent over which the emissions take place. In practical applications, a more detailed analysis of each mechanism is required of course which must include the precise spectral regions in which the radiations occur, the dependence of the plume emissions on altitude, and the spatial extent over which the emissions are spread.

Though crude, the estimates obtained above for the radiation strengths of various mechanisms do give some insight into the relative importance of the mechanisms and allow one to disregard some obviously unimportant ones. For convenience and for comparison, the results of the estimated energy supply and radiation rate calculations are summarized in Table 2-1.

It should be emphasized again here, that most of the expressions used for estimates are incomplete in the theoretical physics sense, since we simply inserted various parameters such as T_e , V_v , etc., from experimental knowledge. Physics establishes rigid relations for example between the exit temperature T_e

TABLE 2-1. PLUME RADIATION MECHANISMS AND MAXIMUM EMISSION RATES

Mechanism		Approximate Maximum Spectrum-Integrated Energy Supply Rates for an Exhaust With $\dot{W} = 350$ kg/sec*	Spectral Region
1	Core Radiation	2.30×10^8 , Watts	IR
2	Afterburning Radiation	1.97×10^8 , Watts ($h \lesssim 50$ km)	IR
3	Collisional Deceleration Radiation	11.8×10^8 , Watts ($h = 0$ km)	IR/VIS/UV
4	Internal Shock Radiation	0 , Watts ($60 \lesssim h \lesssim 90$ km)	
		32.8×10^8 , Watts ($h \gtrsim 200$ km)**	
5	Atmospheric Pumping Radiation	5×10^7 , Watts/km ($90 \lesssim h \lesssim 130$ km)	IR
6	Atomic Oxygen Chemiluminescence	3.6×10^5 , Watts/km ($h \gtrsim 130$ km)	IR/VIS/UV
7	High-Altitude Molecular Association/Dissociation Radiation		
8	Airglow from Rocket Vehicle Friction	6.70×10^5 , Watts ($h \sim 100$ km)	IR/VIS/UV
9	Scattering of Chamber Radiation by Plume	6.73×10^5 , Watts	IR
10	Solar Radiation Scattered by Solid Particles in Plume	2.2×10^4 , Watts/km	VIS
11	Solar Radiation Scattered by Gaseous Species in Plume	0.39 , Watts/km	VIS
12	Absorption of Solar UV by Plume Gases and Reemission in UV, VIS. and IR	7.58×10^6 , Watts/km	UV/VIS/IR
13	Plume-Reflected Earthshine	5.85×10^{-5} , Watts/km	IR

*The ascending rocket is assumed to follow a typical trajectory for near-earth-orbit injection; h = rocket altitude. Radiations given in Watts/km refer to km of trail length with $V_v \sim 3$ km/sec.

**This value is for $\dot{W} = 350$ kg/sec. Usually at this altitude, a second or third stage is burning with $\dot{W} \sim 50$ kg/sec, and the radiation should be scaled down by a factor of $350/50 = 7$.

and the mass flow rate \dot{W} , the rocket chamber pressure p_c and chamber temperature T_c , or the photon flux that leaves the surface of a body of gas. From such physics relations one obtains for example Stefan's T^4 radiation law for optically dense gases and solids, and by applying such relationships throughout one can develop more precise expressions for rocket radiation that are internally consistent.

In conclusion, the calculations given are only good for order-of-magnitude estimates. They are unsatisfactory in that they require a priori knowledge of several physical parameters that are not independent but related to each other by well-established laws of physics. However they do allow a quick assessment of the major radiation mechanisms without lengthy and rigorous calculations. The latter will be carried out in Chapter 3.

2.4 PHENOMENOLOGY OF THE MAJOR ROCKET RADIATION MECHANISMS*

Having identified the major sources of rocket radiation, let us next review each mechanism in more depth. In this section the physical aspects of the mechanisms are examined qualitatively only, though with some anticipation of the quantitative calculations that are given in Chapter 3.

The vehicle body radiations require little additional discussion over what was said in section 2.2.** Thermal self-emission in the infrared occurs of course for all bodies whose temperatures are nonzero and is well understood in terms of the theories developed originally by Maxwell, Boltzmann, Wien, and Planck (see for example Chapter 2 of Ref. 2). Reflected solar radiation from solid surfaces is likewise a well-studied and well-understood phenomenon.

Afterburning radiation, as the name indicates, is due to the further combustion of unburnt rocket fuel in the atmosphere after it has been expelled from the rocket into the atmosphere. Most rockets attain the highest specific impulse (I_{sp}) for a given propellant/oxidant combination if the mixture is burnt "fuel-rich," that is if an excess of hydrogen or hydrogen-bearing propellant is provided over and above the stoichiometric amount required for complete combustion. The exhausts of most rockets therefore contain large amounts of unburnt H_2 , CO , or hydrocarbons C_xH_y which, if conditions are right, will undergo combustion with the oxygen of the atmosphere in the air/exhaust mixing region of the plume (see Figure 2-1). Tables 2-2 and 2-3 list typical rocket fuels and their exhaust products.

*Some of the material presented in this section is slightly repetitive when compared to the discussion given in section 2.3. This is done in the interest of completeness.

**We shall abbreviate the two vehicle body radiations by VBSR = Vehicle Body Solar Reflections and VBSE = Vehicle Body Self-Emissions.

TABLE 2-2. TYPICAL PROPELLANTS AND THRUSTS OF U.S. ROCKETS*

Rocket Type	Fuel	Oxidizer	Approximate Thrust F_{vac} , kg(F)
Thor	RP-1 ⁽¹⁾	O ₂ (Liq)	80,000
Atlas - 1st Stage - 2nd Stage (Sustainer)	RP-1 ⁽¹⁾	O ₂ (Liq)	208,000
	RP-1 ⁽¹⁾	O ₂ (Liq)	36,000
Agna B - Upper Stage	UDMH ⁽²⁾	IRFNA ⁽³⁾	7,000
Centaur - Upper Stage	H ₂ (Liq)	O ₂ (Liq)	14,000 (2 Engines)
Titan - 1st Stage - 2nd Stage	50m/o UDMH / 50m/o H ₂ H ₄ ⁽²⁾	N ₂ O ₄	200,000
	50m/o UDMH / 50m/o H ₂ H ₄	N ₂ O ₄	45,000
Saturn-IC (1st Stage)	RP-1 ⁽¹⁾	O ₂ (Liq)	3,400,000 (5 Engines)
-II (2nd Stage)	H ₂ (Liq)	O ₂ (Liq)	500,000 (5 Engines)
-IVB (3rd Stage)	H ₂ (Liq)	O ₂ (Liq)	90,000
-SPS (4th Stage)	50m/o UDMH / 50m/o H ₂ H ₄ ⁽²⁾	N ₂ O ₄	9,000
<p>(1) RP-1 = C₁₀H₂₀ (Kerosene)</p> <p>(2) UDMH = Unsymmetric Di-Methyl Hydrazine = (CH₃)₂N₂H₂ ; 50m/o UDMH / 50m/o N₂H₄ is also called Aerozine-50.</p> <p>(3) IRFNA = Inhibited Red Fuming Nitric Acid = 77.03 m/o HNO₃ + 7.02 m/o N₂O₄ + 13.80 m/o H₂O + 1.59 m/o HF + 0.55 m/o NO₂ ; Note that m/o = mole percent.</p>			

*Data are from Refs. 22 and 28.

June 1974

TABLE 2-3. TYPICAL EXHAUST PRODUCTS OF ROCKET PROPELLANTS*

Exhaust Species	Fuel/Oxidizer				Solid Propellant***
	RP-1 / LOX	Aerozine-50 / N ₂ O ₄ **	H ₂ / O ₂		
	Exhaust Species Concentration (moles/kg)	Exhaust Species Concentration (moles/kg)	Exhaust Species Concentration (moles/kg)		
H ₂	6	3	71.5	12	
H ₂ O	15	19	47.5	4	
OH	0.02	—	0.02	—	
CO	14	2	—	10	
CO ₂	7.5	3.7	—	7	
N ₂	—	15	—	3	
HCl	—	—	—	5.5	
C (s)	≤ 0.001	—	—	—	
Al ₂ O ₃ (s)	—	—	—	3	

*Data are from Refs. 13, 22, 26, and 27.

**Aerozine-50 = 50m/o UDMH / 50m/o N₂H₄.

***Data estimated from p. 19-5 of Ref. 22.

The heat liberated by the Afterburning (AB) process together with the heat produced by the air-shock or "Collisional Deceleration" (CD)^{††} of the exhaust causes a substantial temperature rise in the air/exhaust mixing region (see Figure 2-1) which gives rise to what we shall term "ABCD" (Afterburning and Collisional Deceleration) radiation for short. At the lower altitudes, ABCD radiation is responsible for some 90% of the total infrared rocket radiation with Mach Cone or Undisturbed Core radiation^{***} (to be discussed later) generating most of the remainder. If the sun is shining, vehicle body solar reflections will give most of the visible signal although there is also "spill-over" visible radiation from the ABCD mechanism at low altitudes that causes the plume to be visible when the rocket lifts off.

As a rocket reaches altitudes above 60 kilometers, Afterburning ceases to be important in comparison with Core and Collisional Deceleration radiations because the atmospheric oxygen supply (which sustains afterburning) is very low in concentration at these altitudes. Thus although we shall often continue to use the term "ABCD" radiation for convenience, the Afterburning contribution to this radiation mechanism ceases to be important at the higher altitudes.

When a rocket reaches a velocity of about $V_v = 3$ km/sec, the average air-related velocity $\bar{V}_r = V_v - \bar{V}_{exh}$ of the exhaust is $\bar{V}_r \approx 0$ since the exhaust velocity $\bar{V}_{exh} \approx 3$ km/sec.^{***} When this happens (usually at an altitude of $70 \lesssim h \lesssim 90$ km), the radiation from Collisional Deceleration is minimal and primarily Core Radiation is emitted from the plume (point B in Figure 1-4).

*Still another name sometimes given to this mechanism is "Rethermalization."

**We shall often abbreviate this to CORE or Core Radiation.

***The parameter designated V_e is reserved for the mean exhaust velocity in the nozzle exit plane (see section 3); \bar{V}_{exh} is the maximum mean exhaust velocity which may be equal to or larger than V_e .

June 1974

However above an altitude of about 80 to 100 km, where the vehicle velocity V_v begins to exceed 3 km/sec (and thus $\bar{V}_r = V_v - \bar{V}_{exh}$ becomes positive, since $\bar{V}_{exh} \sim 3$ km/sec), the radiation due to Collisional Deceleration (CD) becomes important again. Near burnout, both Core and CD radiation have high values, unless the altitude is above 200 km where CD fades out.

It is primarily Collisional Deceleration and Afterburning radiation that produces the first maximum (point A) at low altitudes and is responsible for the minimum at point B of Figure 1-4. The second maximum at high altitudes (point C) is due to both Core and CD radiation. As we shall see in Chapter 3, Collisional Deceleration radiation is proportional to the factor $F(\bar{V}_r) = \exp\left\{-B/(\lambda_o \bar{V}_r^2)\right\}$, where λ_o is the band-center emission wavelength, and B is a constant. When the rocket vehicle velocity V_v increases from 0 to 8 km/sec, \bar{V}_r varies from -3 km/sec through 0 km/sec, ending at +5 km/sec since $\bar{V}_{exh} \approx 3$ km/sec. Thus since $F(\bar{V}_r)$ is larger, the larger the value of \bar{V}_r^2 is, a maximum of radiation (for constant B and λ_o) occurs at lift-off when $\bar{V}_r = -3$ km/sec, a minimum appears at $\bar{V}_r = 0$ km/sec and a second maximum occurs at $\bar{V}_r = +5$ km/sec at burnout. The constant B has such a value that when $1 \lesssim |\bar{V}_r| \lesssim 4$ km/sec, the factor $F(\bar{V}_r)$ is high for values of λ_o that fall in the infrared region due to pure vibrational transitions. For values of \bar{V}_r that exceed 4 km/sec, ultraviolet/visible emissions from allowed electronic transitions become also quite important. Of course the infrared emissions get higher too as the value of \bar{V}_r increases from 4 to 5 km/sec.

All these comments apply only of course as long as there is air for the exhaust to collide with. Above about 200 km the mean path between collisions exceeds the field-of-view and as a result CD radiation fades out above this altitude.

When the exhaust gas molecules leave the rocket engine, a fair portion is in excited vibrational states. These molecules will deexcite in a time on the order of ten milliseconds with the emission of an infrared photon.* The emission takes place directly behind the nozzle shown in Figure 2-1 where ambient air cannot mix with the exhaust. This Undisturbed Core Region, also called the Mach Cone Region, is roughly conical in shape. It is relatively small at low altitudes becoming larger and larger at the higher altitudes. Its boundary is determined by the speed with which ambient air diffuses inwards into the exhaust jet by turbulent diffusion. At sea-level the length of the core is on the order of two nozzle exit plane diameters (~ 1 meter), while at burnout altitudes ($h \sim 150$ km), it is on the order of 1 km due to the fact that the air is extremely thin there and the mean free path for a collision has become almost 1 km. Figure 2-3 shows the exponential changes of the key atmospheric parameters with altitude according to the U.S. standard 1962 atmosphere composed by AFCRL (Ref. 24).

The radiation emitted by the Core region is always present throughout powered flight. Its magnitude is about one to two orders-of-magnitude smaller than Collisional Deceleration radiation at the lower altitudes, but it starts to rise at about 25 km reaching a maximum constant level at 120 km that is of the same magnitude as CD radiation. Above 200 km, where CD radiation fades out, Core radiation is the main source of rocket radiation from a burning rocket.

After passage through the undisturbed Core region where they shed some of their internal excitation energy, the exhaust molecules enter the air/exhaust mixing region where they encounter air molecules with which

*For a discussion of the various types of excitations and emissions that a molecule can experience, see Chapter 1 of Vol. II, Rocket Radiation Handbook.

June 1974

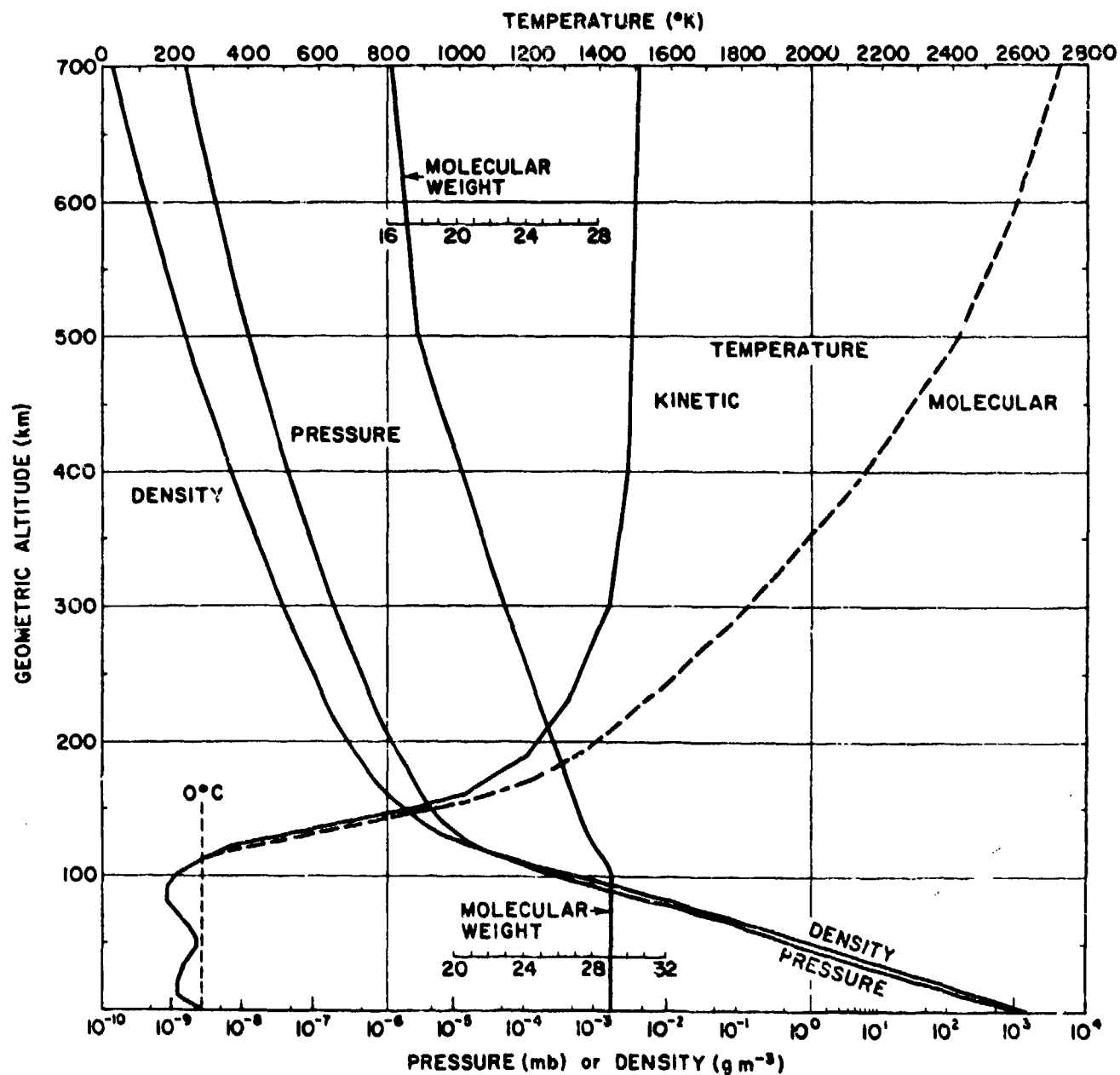


FIGURE 2-3a. IMPORTANT PROPERTIES OF THE EARTH ATMOSPHERE
(TEMPERATURE, PRESSURE, DENSITY, AND MOLECULAR WEIGHT),
ACCORDING TO U.S. STANDARD ATMOSPHERE, 1962
(After Ref. 24)

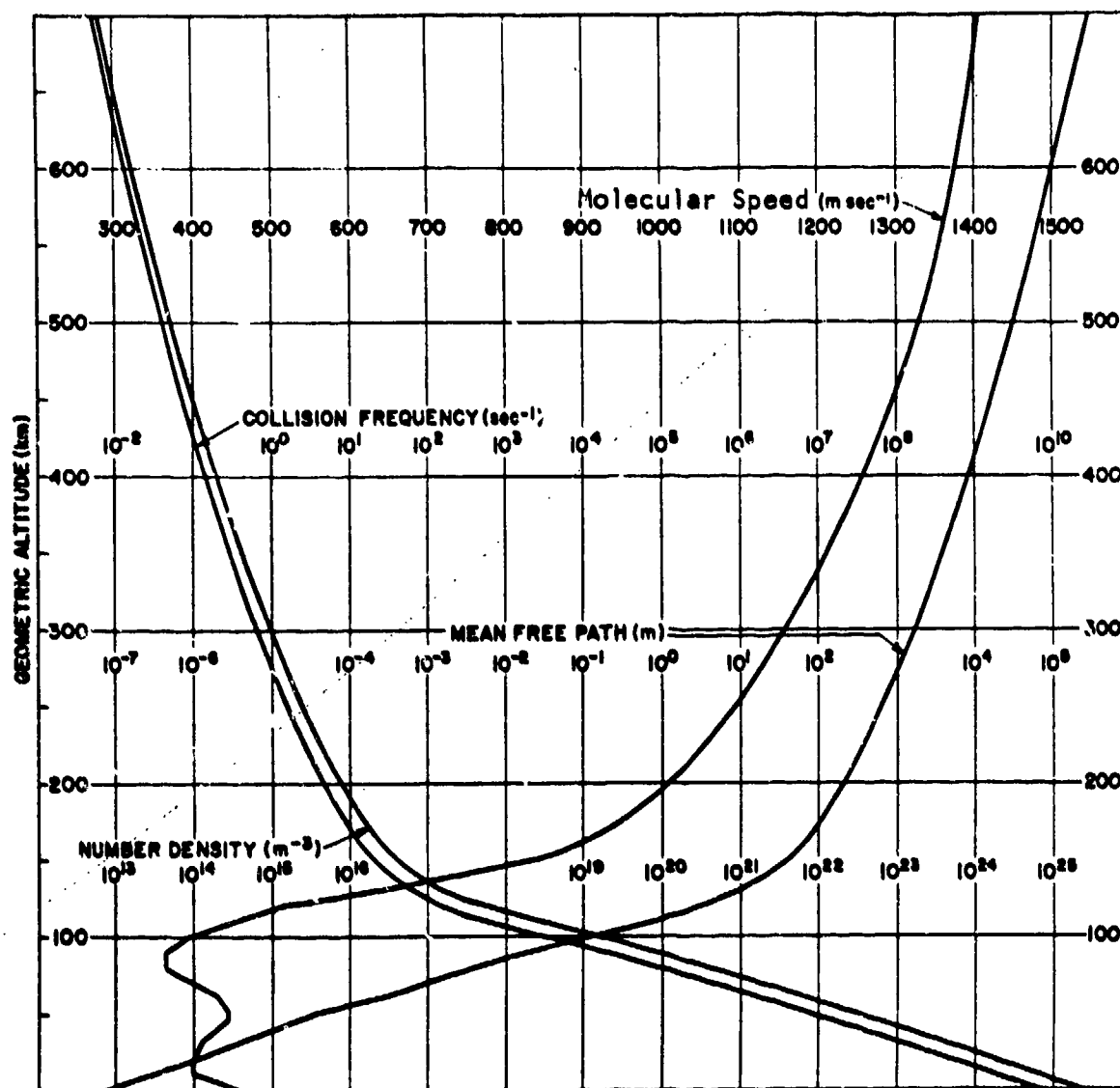


FIGURE 2-3b. IMPORTANT PROPERTIES OF THE EARTH ATMOSPHERE (NUMBER DENSITY, COLLISION FREQUENCY, MEAN FREE PATH, AND MOLECULAR SPEED), ACCORDING TO U.S. STANDARD ATMOSPHERE, 1962
(After Ref. 24)

June 1974

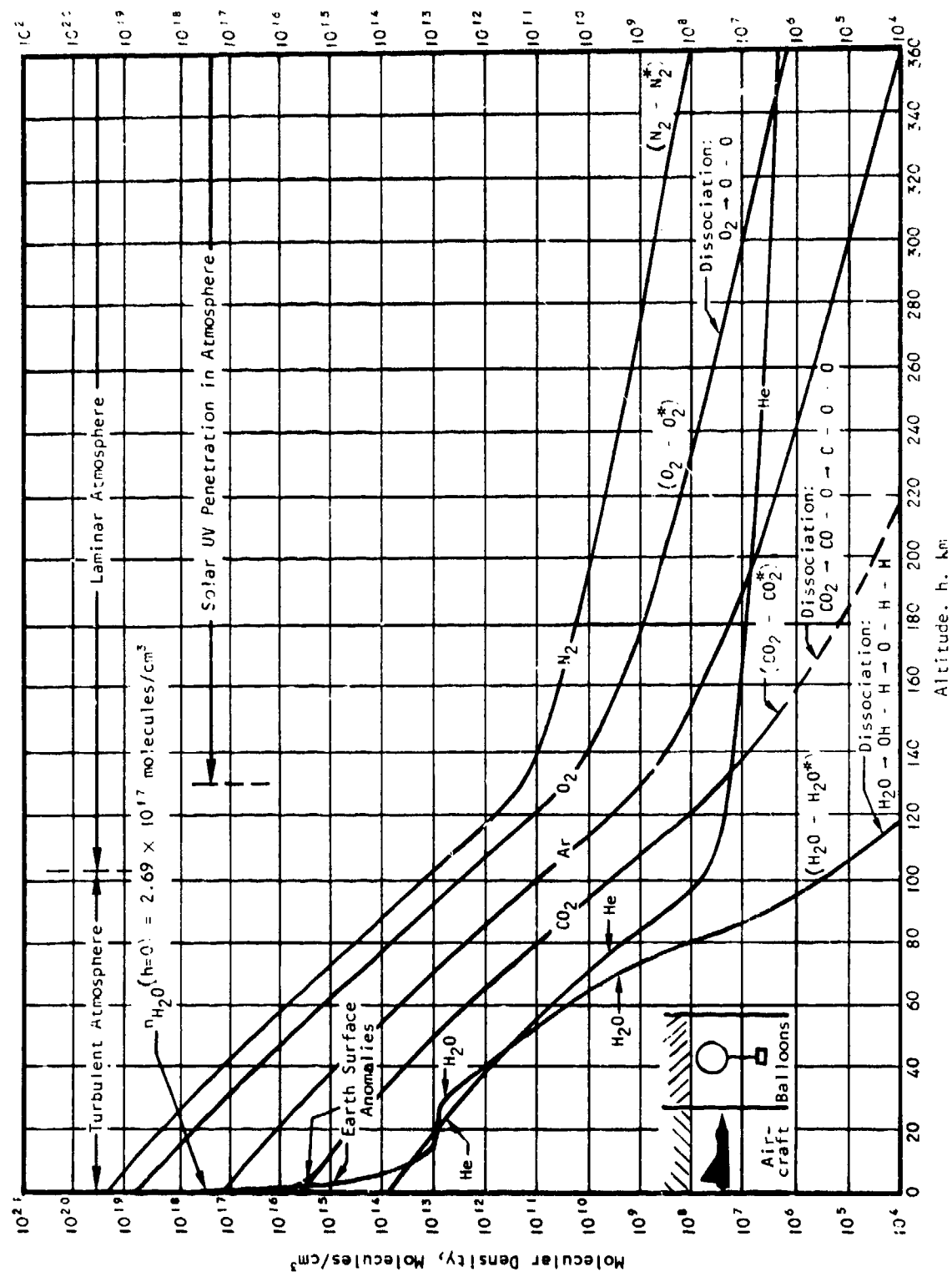


FIGURE 2-3c. IMPORTANT PROPERTIES OF THE EARTH ATMOSPHERE (CONCENTRATIONS OF MAIN CONSTITUENTS)

they collide (see Figure 2-1). Due to the high relative velocities of the exhaust molecules with respect to the atmospheric molecules ($\bar{V}_r = 2$ to 6 km/sec for boosters and 7 to 9 km/sec for orbital maneuvers), vibrational ($(\bar{V}_r)_{\min} \approx 1$ km/sec) and electronic ($(\bar{V}_r)_{\min} \approx 4$ km/sec) excitations will be induced in both the exhaust and atmospheric molecules and atoms during these collisions. The subsequent emission of radiation after these excitations occurs within microseconds for electronic excitations and in milliseconds for the vibrational excitations.

Since the first fast collisions with air molecules occur within a millisecond to seconds after the exhaust molecules have left the nozzle and since subsequent emission of radiation occurs within milliseconds, the Collisional Deceleration radiation produced by a rocket exhaust is essentially operative only as long as the rocket is thrusting. Within seconds after thrust cessation (the exact decay time depends of course on altitude), all of the last exhausted molecules have experienced at least their first slowing-down collision and nearly all have had two, three, or more additional collisions and have essentially slowed down to ambient molecular speeds at altitudes not exceeding 200 kilometers. We conclude from this therefore that Collisional Deceleration radiation ceases immediately after thrust cessation, and while the rocket is burning it is directly proportional to rocket thrust which determines the number of molecules exhausted per second and thus the number of collisions and emissions per second.

After having slowed down in about 0.1 to 10 seconds, the exhaust molecules next engage in energy exchange interactions with the ambient atmosphere at equilibrium (slowed-down) speeds in the process we called "Atmospheric Pumping" in section 2.3. As we shall see in Chapter 3, at

June 1974

altitudes between 90 and 150 kilometers, exhaust molecules such as H_2O and CO_2 can be continuously "pumped" by the atmosphere and allowed to radiate efficiently in their characteristic vibrational wavelength bands. Since Atmospheric Pumping (ATMP) is repeated over and over again, the radiation from this process is persistent and can be observed as long as the exhaust cloud is reasonably dense and in the field-of-view of the observer, and of course if its radiation intensity is above any backgrounds. ATMP radiation is weak in intensity ($Watts/m^2$) when compared to ABCD and CORE radiation and behaves similarly to a high-altitude atmospheric cloud of water vapor.

The key altitude-dependent parameters of the earth atmosphere important to the Atmospheric Pumping process are shown in Figure 2.3. Probably the most important parameters are the atmospheric collision frequency (or mean free path) and the ambient temperature. Figure 2-3b shows above 90 kilometers the collision frequency between species is less than 10^4 sec^{-1} or the time between collisions is more than 10^{-4} seconds. Since, as mentioned, most molecular vibrational states deexcite spontaneously at decay times of 10^{-4} to 10^{-3} seconds, this means that a vibrationally-excited molecule has sufficient time to release its excitation energy via the emission of radiation, before a collision takes place in which this energy is transferred and redistributed as translational kinetic energy. In macroscopic language, energized gases at densities above altitudes of 90 km dissipate excited vibrational energy more efficiently through radiation than via conduction and convection, provided they are infrared-active.

Excited molecules such as H_2O^* and CO_2^* , or other infrared-active molecules can radiate efficiently and strongly in their vibrational bands when present in the atmosphere. N_2 and O_2 on the other hand do not radiate vibrational energy in first-order transitions because they do not possess

a vibrational dipole moment.* Instead they transfer vibrational energy to other N_2 and O_2 molecules, or to H_2O and CO_2 molecules if present, by collisions. Quadrupole or higher-order vibrational radiative transitions are possible for N_2 and O_2 but they have decay times of seconds to minutes so that at the altitudes under consideration a collision has occurred (with radiationless energy transfer) long before the excited N_2 or O_2 molecule can radiate a quantum. At higher altitudes where the density is low enough, the higher-order transitions can efficiently produce radiation. However few N_2 and O_2 molecules exist any more at these altitudes since prolonged solar irradiation has caused these molecules to dissociate to atoms there.

It is clear from the above that large amounts of H_2O or CO_2 dumped in the atmosphere at altitudes above 90 km and below about 300 km, if vibrationally excited, are very efficient radiators. The atmospheric temperature above an altitude of 110 km rises sharply from 300 °K to 1500 °K at 300 km producing a large population of vibrationally-excited O_2^* and N_2^* which do not radiate. With H_2O or CO_2 thrown in however the atmosphere-stored excitation energy can be siphoned off in collisional transfers, and then radiated away via collisions like $N_2^* + CO_2 \rightarrow CO_2^* + N_2 \rightarrow CO_2 + N_2 + h\nu$ and $O_2^* + H_2O \rightarrow H_2O^* + O_2 \rightarrow H_2O + O_2 + h\nu$. Because the air density drops exponentially and exhaust molecules get more and more rapidly dissociated at high altitudes, atmospheric pumping at altitudes above about 200 km is extremely dilute and for most practical purposes, only at altitudes between 90 and 150 km can atmospheric pumping radiation be strong enough (if captured by the sensor's field-of-view) to be noticeable.

*See Vol. II, Rocket Radiation Handbook for more details on the radiation physics of molecules.

June 1974

The basic energy source responsible for Atmospheric Pumping radiation is the earth's upper atmosphere, or going one step further back, the sun which excited the O_2 and N_2 in the upper atmosphere. Although in day-time illumination by solar UV radiation at high altitudes will cause ultimate dissociation of most exhaust molecules, the rate of this dissociation appears to be too slow to cause an appreciable effect on the molecular exhaust gas population at altitudes below 150 km. Therefore Atmospheric Pumping radiation during usual observation times (minutes) is usually unaffected by this dissociation at altitudes between 90 and 150 km.

The solar UV effects just mentioned bring us to the fifth important radiation generating mechanism in the rocket exhaust. In addition to, and simultaneously with the "ABCD," "CORE," and "ATMP" radiation mechanisms, ultraviolet illumination by the sun which exists above altitudes of 150 kilometers will promote strong absorptions and excitations of the exhaust molecules, which then reradiate the absorbed energy at various characteristic wavelengths. UV absorption cross-sections are extremely high for all molecules and several order-of-magnitudes higher than IR absorption cross-sections.

Because the sun's spectrum drops very steeply in the UV as shown in Figure 2-4 and Table 2-4, the highest UV wavelength λ_{UV} which a molecule still absorbs becomes very important. For rocket exhaust gases, the OH molecule is the species which has the highest UV wavelength absorption cut-off ($\lambda_{UV} \approx 3100$ Angstroms), and thus the more OH (or H_2O from which it dissociates) is present in a rocket exhaust, the stronger the emission is from the UV absorption/reemission or fluorescence process.* Most other exhaust molecules

*We shall abbreviate this process to SUAR = Solar Ultraviolet Absorption and Reradiation. The term "fluorescence" is also appropriate though some authors have restricted the word "fluorescence" to phenomena that involve only electronic excitations and deexcitations in solid materials.

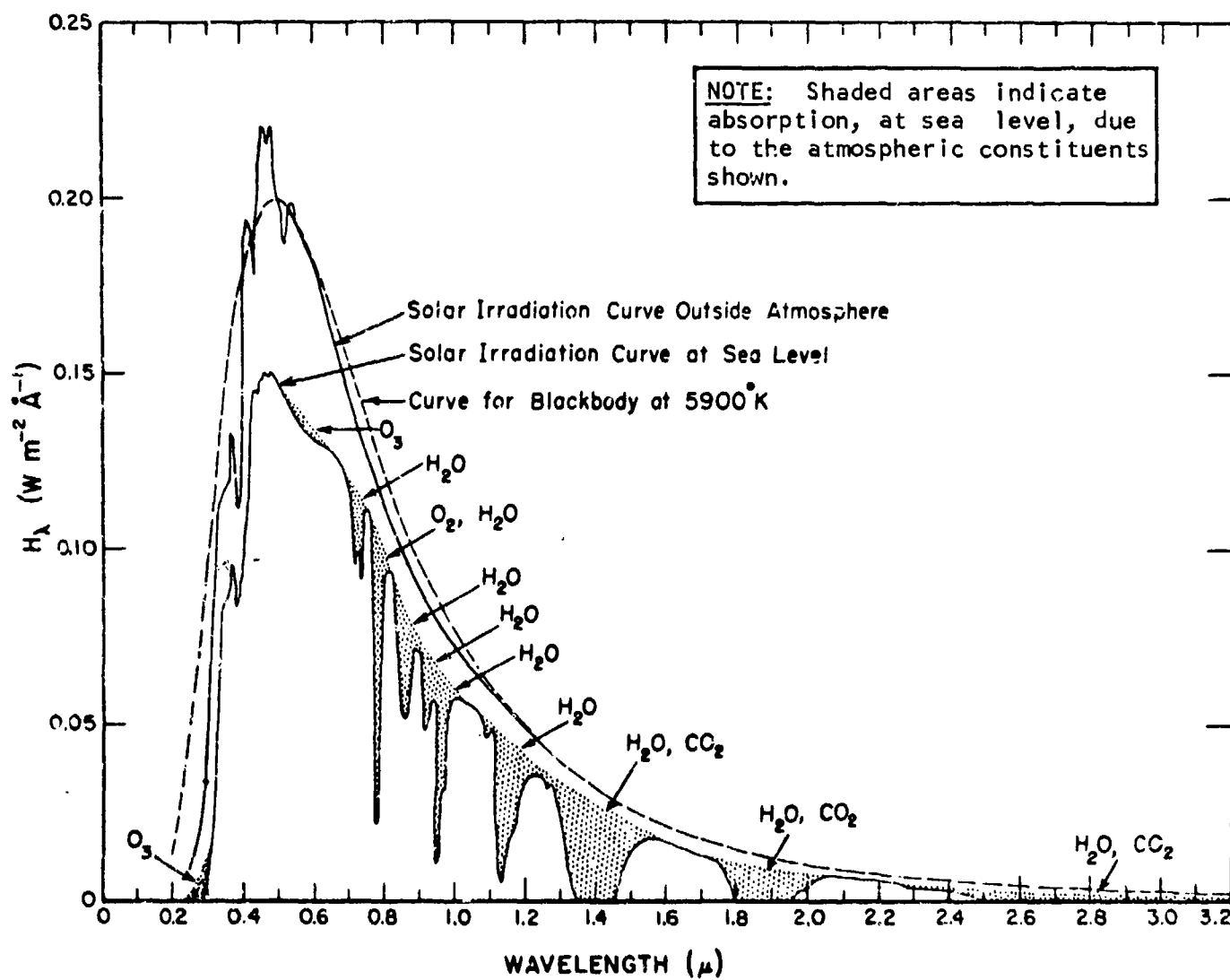


FIGURE 2-4. SOLAR ILLUMINATION CURVES BELOW AND ABOVE THE EARTH ATMOSPHERE

TABLE 2-4. SOLAR SPECTRAL IRRADIANCE FOR QUIET SUN, OUTSIDE THE EARTH'S
ATMOSPHERE AT THE MEAN SUN-TO-EARTH DISTANCE; $H_0 = 1390 \text{ W m}^{-2}$

Wavelength Interval	$H_{\Delta\lambda}$ ($\text{W m}^{-2} \Delta\lambda^{-1}$)	$H_{\Delta\lambda}/H_0$ (%)	Wavelength Interval	$H_{\Delta\lambda}$ ($\text{W m}^{-2} \Delta\lambda^{-1}$)	$H_{\Delta\lambda}/H_0$ (%)
(A)			(μ)		
1-8	$< 10^{-9*}$	$< 10^{-11*}$	0.5-0.6	193	13.9
8-31	10^{-7**}	$7 \times 10^{-9**}$	0.6-0.7	162	11.7
31-165	$0.70 \times 10^{-3\dagger}$	$4.9 \times 10^{-5\dagger}$	0.7-0.8	128	9.2
165-303	1.18×10^{-3}	8.3×10^{-5}	0.8-0.9	101	7.2
304	0.25×10^{-3}	1.8×10^{-5}	0.9-1.0	81	5.8
305-460	3.15×10^{-3}	2.2×10^{-4}	1.0-1.1	66	4.8
460-1215	1.74×10^{-3}	1.2×10^{-4}	1.1-1.2	55	4.0
1216	4.40×10^{-3}	3.1×10^{-4}	1.2-1.3	45	3.2
1216-1800	3.30×10^{-2}	2.3×10^{-3}	1.3-1.5	66	4.7
1800-2250	0.9	6.5×10^{-2}	1.5-2.0	84	6.1
(μ)			1.0-3.0	54	3.9
0.225-0.3	17	1.3	3.0-11.0	27	1.9
0.3-0.4	110	7.9	11.0-30.0	0.7	0.05
0.4-0.5	200	14.4	1 cm-30 m	$10^{-11\dagger\dagger}$	$< 10^{-13\dagger\dagger}$

*Increases 10^3 and 10^5 for disturbed sun and for Class 3 flare respectively.
 **Increases by factor of at least 50 for disturbed sun.
 †Increases by factor of 7 for disturbed sun.
 ††Increases by factor of 10^3 for disturbed sun.

have cut-off wavelengths at approximately 2000 Angstroms, where the solar photon flux is less than one-tenth of that between 2000 to 3000 Angstroms.

Besides solar absorption and reradiation, solar photons can also be scattered by rocket exhausts as discussed already in section 2.3. Calculations show that only scattering from solid particles present in a rocket exhaust are significant.* Rayleigh scattering from molecules is so weak that it can be ignored for all practical purposes. Since solid particles form primarily in the exhausts of solid rockets (Al_2O_3 particles and H_2O condensation on them), solar scattering is usually important only for solid rockets, at high altitudes. At low altitudes where the atmosphere is still dense, H_2O vapor from liquid rockets can also condense (see Figure 2-5). However above 90 kilometers, this can happen only in the presence of a sufficient number of solid particle nuclei, which are usually absent in the exhausts of liquid-propellant rockets.

Whereas ABCD and CORE radiation are proportional to flow rate or thrust ($\dot{W} = F/I_{sp}$) and are emitted within a kilometer or so behind the rocket in the plume region, the emission from the other three mechanisms (ATMP, SUAR, and SOPS) is proportional to the total amount of exhaust product (W) that is released in the cloud region which occupies the entire rocket trail (see Figures 2-1 and 2-2). It is thus more appropriate to express the amount of radiation from the latter three mechanisms on a per kilometer-of-trail basis or even better on the basis of a square kilometer in the field-of-view of a sensor. It is clearly important then to know how the exhaust spreads and distributes itself in the atmosphere.

*We shall abbreviate the solar photon particle scattering mechanism to SOPS in what follows.

June 1974

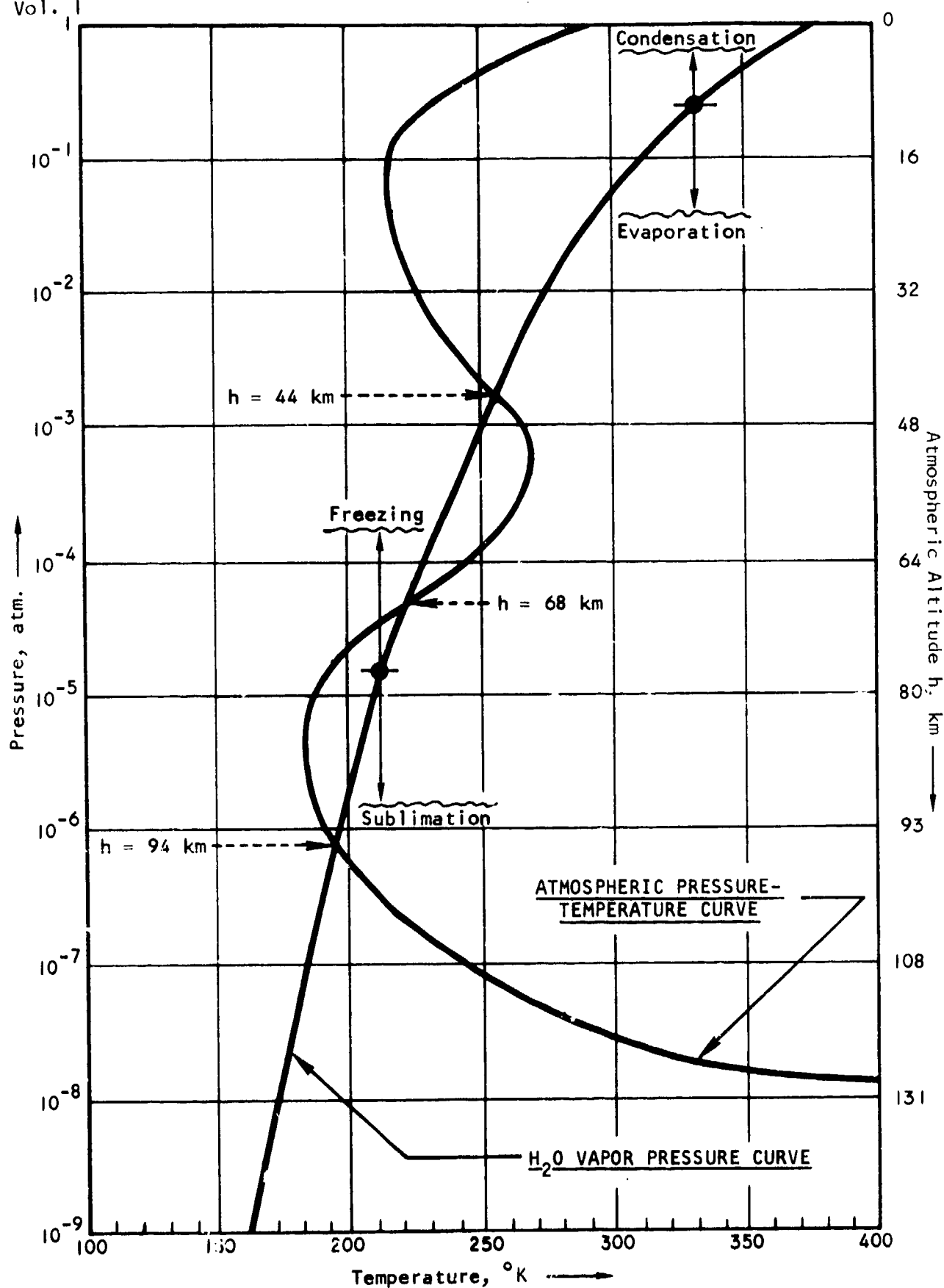


FIGURE 2-5. COMPARISON OF WATER VAPOR PRESSURE WITH ATMOSPHERIC CONDITIONS

Immediately after leaving the rocket nozzle, the exhaust molecules expand as a supersonic jet with a shock structure as illustrated in Figure 2-1. At high altitudes, the shocks are very thick and merge with the air/plume mixing region, because of the thinness of the air. After passing through the undisturbed core region in about 10^{-3} to 10^{-2} seconds, the exhaust molecules enter the mixing region where they remain for approximately 10^{-2} to 10^{-1} seconds and where they undergo the slowing-down collisions mentioned before. The maximum diameter of the plume's supersonic region occurs where the jet has expanded to a pressure that equals the atmospheric pressure. Typical plume diameters vary between 1 and 4 km at altitudes between 150 and 250 kilometers (see Figure 2-6 and Ref. 4). These are only gross descriptions and for more details, Vol. IV of the Rocket Radiation Handbook should be consulted which discusses the fluid dynamics and geometry of the exhaust plume in depth.

After slowing down, the molecules begin to diffuse outward into space and into the atmosphere with a density distribution determined by the diffusion laws and/or free expansion physics depending on the atmospheric density. The speed of average lateral diffusion is on the order of meters/second at the lower altitudes ($h \sim 100$ km) to km/sec in the hard vacuum of space. It is during this second expansion phase, that the molecules participate in the infrared ATMP process (at altitudes between about 90 and 150 kilometers) which may be observed for minutes to hours, depending on the solid angle that the observer subtends at the cloud and provided the background intensity is not too high (ATMP radiation may be substantial when all of it is considered but it is dilute and thus weak in intensity). Similarly the SOPS and SUAR emissions in the visible may be observed for extended periods of time under the appropriate circumstances.

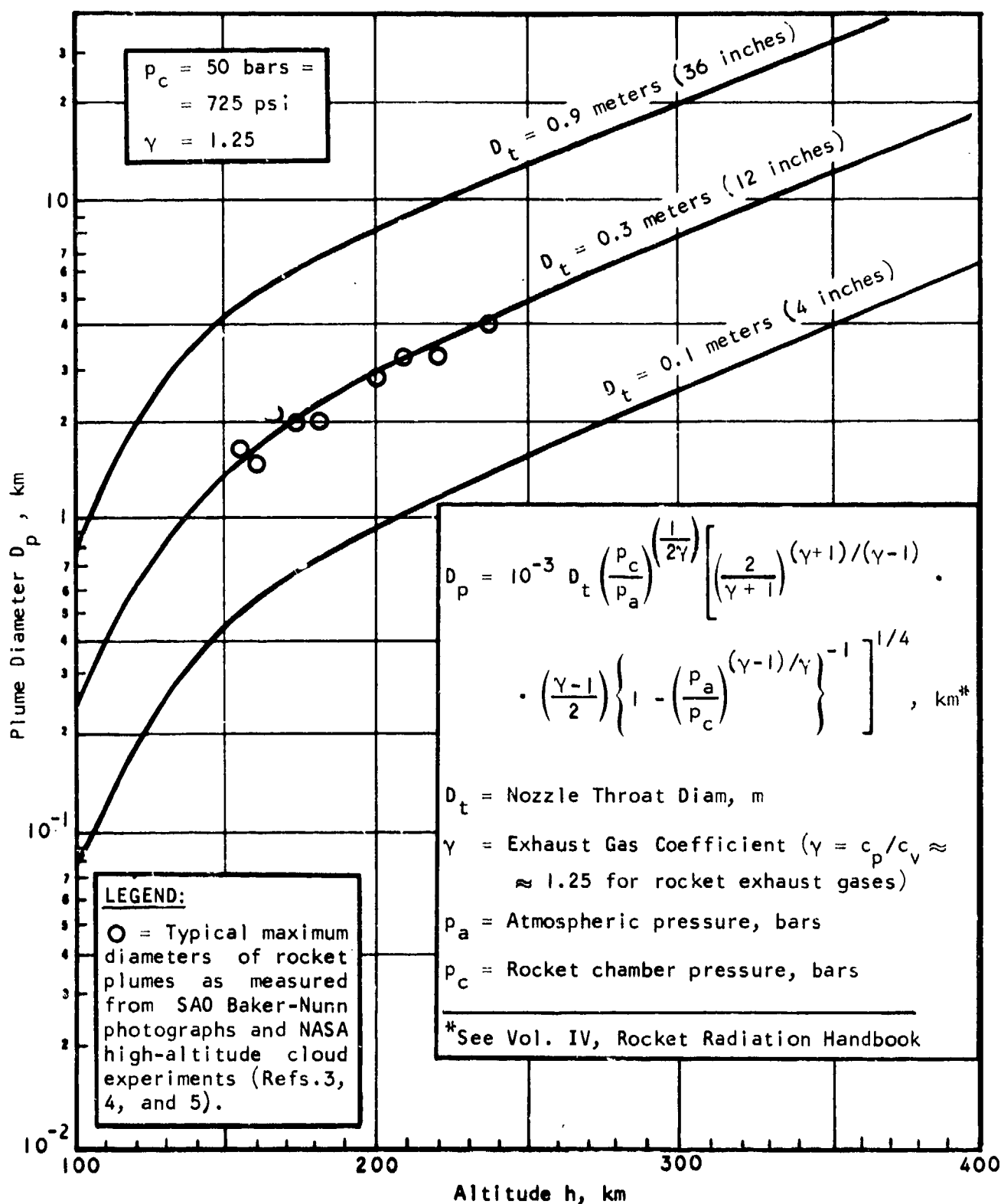


FIGURE 2-6. CALCULATED ROCKET PLUME DIAMETERS

To summarize in addition to the two vehicle body radiation processes of solar reflection and self-emission, there are six important radiation-producing mechanisms for rocket exhausts which take place in two distinct stages of exhaust gas expansion into the atmosphere. Table 2-5 summarizes the main phenomenological aspects of the six exhaust radiation mechanisms while Figure 2-1 illustrates the two steps in exhaust gas spatial behavior. Order-of-magnitude estimates of the radiation strengths of the six mechanisms were listed in Table 2-1.

TABLE 2-5. SUMMARY OF MAJOR RADIATION-PRODUCING MECHANISMS OF ROCKET EXHAUSTS

Mechanism	Source of Energy*	Strongest Emission Wavelength Region	Altitude Region	Time Behavior (Region of Exhaust)
1. Afterburning (Day or Night)	Atmospheric Oxygen (Radiation $\propto \dot{W} = F/I_{sp}$)	Combined with mechanism (3) to give: IR for $2 < V_r < 4$ km/sec UV/VIS for $4 < V_r < 9$ km/sec	$\lesssim 80$ km	Short-lived - only occurs during thrusting (Plume)
2. Undisturbed Core (Day or Night)	Rocket Chamber Combustion (Radiation $\propto \dot{W} = F/I_{sp}$)	IR	Any altitude	Short-lived - only occurs during thrusting (Plume)
3. Collisional Deceleration (Day or Night)	Relative kinetic velocity (V_r) of exhaust with respect to atmosphere (Radiation $\propto \dot{W} = F/I_{sp}$)	IR for $2 < V_r < 4$ km/sec UV/VIS for $4 < V_r < 9$ km/sec	100 to 600 km (the higher, the more spread out the radiation is)	Short-lived - only occurs during thrusting (Plume)
4. Atmospheric Pumping (Day or Night)	Temperature and excited states of upper atmosphere (Radiation $\propto W$)	IR	90 to 200 km (the higher, the more spread out the radiation is)	Long-lived - minutes to hours (Cloud)
5. Solar UV Absorption/Re-radiation (Daytime only)	Sun (Radiation $\propto W$)	UV, VIS, IR	$\gtrsim 130$ km	Long-lived - minutes to hours (Plume and Cloud)
6. Solar Radiation Scattering from Particles (Daytime only)	Sun (Radiation $\propto W$)	VIS	Any Altitude	Long-lived - minutes to hours (Plume and Cloud)

*F = Rocket Thrust (lbs); I_{sp} = Specific Impulse (sec); \dot{W} = Exhaust Flow Rate, kg/sec;
W = Total Exhaust Released, kg.

3. QUANTITATIVE THEORY OF ROCKET RADIATION

3.1 PRELIMINARY DEFINITIONS

The physical quantities of prime interest in optical sensing of space objects are the radiation flux $H_T(\lambda)$ in Watts/m² or spectral flux $dH_T(\lambda)/d\lambda$ in Watts/(m²·μm) coming from the object or target at the sensor location, and that from any background $H_B(\lambda)$ which may be present. Both $H_T(\lambda)$ and $H_B(\lambda)$ are assumed to have values in a certain portion of the electromagnetic spectrum at wavelength λ .

In nearly all cases of interest, the targets may be considered point sources of radiation, or may be treated as an equivalent point source. The background radiation is always an extended source however. The radiant flux of an extended source must be integrated over all solid angles within the angular field-of-view (fov) of the optics of the sensor. Background radiations and other sensor relations are covered in Vol. VI of the Rocket Radiation Handbook and we shall not consider them further here. In this volume we concentrate on analyzing the radiation coming from man-made space objects which may be considered point sources or equivalent point sources.

The optical radiation emitted by space objects can be divided into two categories: (1) that emitted due to scattering of incident radiation from a separate illuminating source, and (2) that emitted by a space object from its thermal or chemical energy reservoir, (either self-provided or with the help of nature (e.g., ATP)) which we shall term "self-emission."

In the first case the radiation spectrum will be characteristic of the illuminating source while in the second case the spectrum is characteristic of the rocket's exhaust or hardware.

Sources of illumination of space objects can be point sources such as the sun, the moon, a laser, or a radar. Or they are extended sources like the reflected solar radiation from the earth's surface. We shall primarily consider natural point source illuminators here. Since the moon is so much weaker than the sun, usually only the sun will be of interest in most applications.

The self-emission of radiation by a solid body in space is determined by the temperature of the object whose value is established by the balance of energy absorption and emission. For most space objects the absorbed energy comes from solar heating and earth radiation. Self-emission by rocket exhaust gases is also strongly dependent on the gas temperature, but in contrast to vehicle hardware, its value is determined by the various mechanisms discussed in Chapter 2.

The radiation flux from a target at a sensor is in general dependent on wavelength, source strength and the distance from the sensor to the target. The various dependencies are most conveniently separated in terms of target cross-sections, reflectivities or emissivities and illumination or self-emittance strengths. For illuminated space objects, the radiation intensity $H_T(\lambda, \eta, \alpha_s)$ at a sensor a distance S away may be expressed by the relation:

$$H_T(\lambda, \eta, \alpha_s) = \frac{\sigma_s(\eta, \alpha_s) \rho(\lambda) H_I(\lambda)}{4\pi S^2}, \text{ Watts/m}^2 \quad (3.1)$$

(reflection)

where:

- $\sigma_s(\eta, \alpha_s)$ = Apparent isotropic reflection cross-section of the space object, m^2
- η = Illuminator-target-observer angle, degrees
- α_s = Orientation angle of space object with respect to illuminating source, that is angle between the space object axis and object-to-sun line.
- α_o = Orientation angle of space object with respect to observer, that is angle between the space object axis and the object-to-observer line.
- $\rho(\lambda)$ = Reflectivity of the space object at wavelength λ for normal incidence
- $H_I(\lambda)$ = Illumination strength at the space object of general illuminator I, Watts/ m^2
- $H_S(\lambda)$ = Solar illumination strength, Watts/ m^2
- S = Distance from sensor to space object, meters
- $H_T(\lambda, \eta, \alpha_s)$ = Radiation intensity at the sensor location, Watts/ m^2

By expressing H_T in terms of σ_s , ρ , H_I , and S , we may conveniently separate effects due to geometry, due to wavelength, and due to the illumination source strength. The apparent reflection cross-section $\sigma_s(\eta, \alpha_s)$ depends only on the relative angle η between the observer, the space object, and the illuminating source, and on the orientation angle α_s of the space object with respect to the illuminator. The apparent cross-section σ_s as defined by Eq. (3.1), namely $\sigma_s = 4\pi R^2 H_T / \rho H_I$, is that of an equivalent isotropic point scatterer. This definition appears more general

June 1974

than if σ were defined according to the relation $\sigma' = A_p = \pi S^2 H_T / \rho H_I$ which is a special result for diffuse scattering, or $\sigma'' = A'' \delta\left(\frac{\eta}{2} - \alpha_s\right)$ which applies to specular reflections. Here A'' is an optically flat specularly reflecting surface facing the illuminator and $\delta(x)$ is the Dirac delta function, that is $\delta(x=0) = 1$ and $\delta(x \neq 0) = 0$. A_p is the projected surface area of a diffusely emitting surface of constant emission intensity. The difference between the diffuse and isotropic scattering definition of σ involves a factor of 4 and is unimportant as long as the same consistent defining equation is used to calculate H_T . In section 3.2 analytical cross-sections σ_s for body-scattered radiation will be derived for both diffuse and specularly reflecting surfaces of various vehicle geometrics.

The normal reflectivity $\rho(\lambda)$ can often be assumed constant, that is a spectrum-averaged value can be taken for example in the visible region for illumination by the sun. Values of the reflectivity ρ for typical aerospace structural materials are given in Appendix A. In textbooks on optical physics, ρ is often shown to vary with angle of incidence for the case of specular reflection. Here we shall incorporate all angular dependences in the cross-section σ , and always take for ρ the value corresponding to normal incidence (see also section 3.2).

The illumination flux H_s from the sun has a spectral distribution discussed in Appendix B. The total energy flux from the sun near the top of the earth atmosphere is 1390 Watts/m² of which approximately 40 percent or 556 Watts/m² is in the visible between 4000 and 7000 Angstroms.

Pulsed laser fluxes H_L of $10^{-2} - 10^{-4}$ Watts/m² are obtainable with current lasers at a laser to target distance of 100 km (approximately 60

miles). For lasers the radiation is extremely monochromatic ($\Delta\lambda/\lambda = 10^{-6}$ to 10^{-14}), and no spectrum averaging is required. We shall not consider laser illuminators in any detail in this monograph* and only mention them as a basis for comparison with solar illumination.

For reflection from condensed particles in the rocket exhaust, Eq. (3.1) still applies except that we must now sum or integrate over all the cross-sections $\sigma_s(\eta, \alpha_s)$ of all the particles in the exhaust cloud which will have a multitude of orientations α_s . Instead of integrating over $\sigma_s(\eta, \alpha_s)$, it is usually simpler to consider the scattering cross-section $\sigma_p(\eta, \alpha_s, \lambda)$ defined by:

$$\sigma_p(\eta, \alpha_s, \lambda) = \sigma_s(\eta, \alpha_s) \rho(\lambda) \text{ , m}^2 \text{ ,} \quad (3.2)$$

when we analyze photon scattering from small particles. That is we incorporate the reflection coefficient in the cross-section. In section 3.3, we shall investigate photon-particle scattering cross-sections in detail.

The radiation intensity that is observed due to self-emission by objects in space depends on the source's projected area or cross-section σ_e as viewed by the observer, on the surface emissivity ϵ , and on the source's blackbody emission W_{BB} (determined by the temperature T):

$$\frac{dH_T(\lambda)}{d\lambda} = \frac{\sigma_e(\alpha_o) \epsilon(\lambda) dW_{BB}/d\lambda}{4\pi S^2} \text{ , } \frac{\text{Watts}}{\text{um} \cdot \text{m}^2} \quad (3.3)$$

(emission)

*Because of its special nature, laser illumination and sensing of objects in space or in the atmosphere is treated in a separate document.

Here S is again the distance between observer and radiating object in meters, and:

$\epsilon(\lambda)$ = Emissivity of radiating object

$\sigma_e(\alpha_o)$ = Equivalent isotropic emission cross-section of object as seen by observer, m^2

α_o = Angle between the target body axis and the line-of-sight of the observer, degrees

λ = Radiation wavelength, μm

$dW_{BB}/d\lambda$ = Blackbody radiant emission, Watts/($m^2 \cdot \mu m$)

Analytical expressions and curves for $dW_{BB}/d\lambda$ of standard blackbody radiation are given in Appendix B. If $\epsilon(\lambda)$ can be assumed constant as a function of wavelength, that is $\epsilon(\lambda) \rightarrow \bar{\epsilon}$, Eq. (3.3) can be integrated over λ for any desired wavelength interval say between λ_1 and λ_2 :

$$H_T(\lambda_2 \leftrightarrow \lambda_1) = \frac{\sigma_e(\alpha_o) \bar{\epsilon} W_{BB}(\lambda_2 \leftrightarrow \lambda_1)}{4\pi S^2}, \quad \frac{\text{Watts}}{m^2} \quad (3.4)$$

(emission)

Tables allowing the calculation of $W_{BB}(\lambda_2 \leftrightarrow \lambda_1)$ for any given temperature T and any wavelength interval are given in Appendix B, while emissivities ϵ of typical space vehicle materials are listed in Appendix A.

We find that the main problem in determining H_T for solid vehicle bodies in space is that of determining the geometric cross-sections $\sigma_e(\alpha_o)$ or $\sigma_e(\alpha_o)$ of the target, which will be taken up in sections 3.2.1,

3.2.2, and 3.2.3. The other parameters ρ , ϵ , and H_S are nearly always constants, while W_{BB} can always be calculated if T is known. The distance S is of course a variable and is therefore left as an explicit parameter in the expressions for H_T .

For self-emissions by the gaseous rocket exhaust molecules, one could also use (3.3) in principle by integrating it over all molecules. However for molecules it is more expedient to use a cross-section $\sigma_e(\alpha_o, \lambda)$ defined by:

$$\sigma_e(\alpha_c, \lambda) = \sigma_e(\alpha_o) \epsilon(\lambda), \text{ m}^2 \quad (3.5)$$

instead of $\sigma_e(\lambda)$. In fact, as we shall see in section 3.3, we shall rewrite the entire product $\sigma_e(\alpha_o) \cdot \epsilon(\lambda) \cdot dW_{BB}/d\lambda$ of Eq.(3.3) and use different expressions for the energy source term $dW_{BB}/d\lambda$.

Because a division by the square of the observer-to-target range S^2 always occurs for point targets, it is convenient to write all radiation expressions in terms of the "radiant intensity" $J(\lambda)$ or $dJ/d\lambda$ instead of $H_T(\lambda)$ or $dH_T(\lambda)/d\lambda$ (see Ref. 2). The "radiant intensity" $J(\lambda)$ and the energy flux or "irradiance" $H_T(\lambda)$ are simply related by:

$$H_T(\lambda) = \frac{J(\lambda)}{S^2}, \quad \frac{\text{Watts}}{\text{m}^2} \quad (3.6)$$

$$J(\lambda) = S^2 H_T(\lambda), \quad \frac{\text{Watts}}{\text{ster}} \quad (3.7)$$

June 1974

$$\frac{dH_T(\lambda)}{d\lambda} = \left(\frac{1}{S^2} \right) \frac{dJ(\lambda)}{d\lambda} , \quad \frac{\text{Watts}}{\text{m}^2 \cdot \mu\text{m}} \quad (3.8)$$

$$\frac{dJ(\lambda)}{d\lambda} = (S^2) \frac{dH_T(\lambda)}{d\lambda} , \quad \frac{\text{Watts}}{\text{ster} \cdot \mu\text{m}} \quad (3.9)$$

In all that follows we shall develop expressions for the parameters $J(\lambda)$ or $dJ/d\lambda$ instead of $H(\lambda)$ and $dH/d\lambda$ although in any application the latter are actually required.

Note that the total "radiant power" $P(\lambda)$ emitted by a radiation source is given by:

$$P(\lambda) = \int_{\Omega} J(\lambda) d\Omega = \int_{\Omega} S^2 H_T(\lambda) d\Omega , \text{ Watts} \quad (3.10)$$

Applying this to Eqs. (3.1) and (3.4) yields:

$$P(\lambda)_{\text{reflection}} = \rho(\lambda) H_s(\lambda) \int_{\Omega} \frac{\sigma_s(\eta(\Omega), \alpha_s(\Omega))}{4\pi} d\Omega , \text{ Watts} \quad (3.11)$$

and:

$$P(\lambda_1 \rightarrow \lambda_2)_{\text{self-emission}} = \bar{\epsilon} W_{\text{BB}}(\lambda_1 \rightarrow \lambda_2) \int_{\Omega} \frac{\sigma_e(\alpha_o(\Omega))}{4\pi} d\Omega , \text{ Watts} \quad (3.12)$$

Equations (3.11) and (3.12) show that if σ_s and σ_e were constant and independent of direction Ω (isotropic scatterer) or if they can be

approximated by average values, the integration over Ω yields simply 4π and thus $\sigma_s(\eta, \alpha_s) \rightarrow \bar{\sigma}_s = \text{constant}$, and $\sigma_e(\alpha_o) \rightarrow \bar{\sigma}_e = \text{constant}$. It is for this reason that we defined our cross-sections as equivalent isotropic cross-sections and normalized with 4π rather than with π . Thus for a flat surface of area A which reflects or emits diffusely according to the cosine law (see sections 3.2 and 3.3), we have that ($\sigma = \sigma_s$ or $\sigma = \sigma_e$):

$$\int_{\Omega} \sigma \, d\Omega = 4\pi \bar{\sigma} = \pi A, \, \text{m}^2, \quad (3.13)$$

and thus:

$$\bar{\sigma} = \frac{A}{4}, \, \text{m}^2 \quad (3.14)$$

Before concluding this section on preliminary definitions, one additional item must be considered. In observing the radiation from rocket exhaust gases, a sensor's field-of-view can either follow the moving rocket vehicle, or it can be fixed and non-moving while looking at the region of space where the exhaust cloud dwells. We shall call the first operational mode the Target Tracking Observation mode (labeled TTO for short), and the second case the Integrated Cloud Observation (ICO) mode. Usually TTO is used in studying earth-to-space launching rockets, while ICO is employed for the study of space maneuvers with short burntimes.

3.2 VEHICLE BODY RADIATIONS

3.2.1 Vehicle Body Solar Reflections (VBSR)

The radiant intensity of reflected light from a point source such as the sun which illuminates a body in space, depends on the body geometry and on the orientation of the body with respect to the illuminating source and the observer. Most space vehicles can be considered to be composed of spherical, cylindrical, and conical components of anodized aluminum with some or all surfaces coated with paint. The radiation reflected from these surfaces may therefore be a combination of both specular and diffuse reflections, though usually the emission approaches that of a diffuse reflector.

As discussed in section 3.1, the observed radiant intensity J due to vehicle-body solar reflections may be expressed by:

$$\left(\frac{dJ}{d\lambda} \right)_{VBSR} = \frac{\sigma_s(\eta, \alpha_s) \rho(\lambda)}{4\pi} \frac{dH_I(\lambda)}{d\lambda}, \quad \frac{\text{Watts}}{\text{ster} \cdot \text{Hz}} \quad (3.15)$$

Of the various parameters in (3.15), η and α_s are viewing angles defined later, $\rho(\lambda)$ is a materials parameter to be obtained from the tables in Appendix A, while $dH_I/d\lambda$ can be obtained from Appendix B if the illuminator is the sun. Thus in evaluating $(dJ/d\lambda)_{VBSR}$ for a given rocket, one needs only to calculate the varying cross-section parameter $\sigma_s(\eta, \alpha_s)$ as a

function of time, since σ_s depends on the viewing parameters and thus on the rocket's time-dependent trajectory. The other parameters $\rho(\lambda)$ and $(dH_I/d\lambda)$ are only dependent on wavelength and thus they are independent of the rocket's trajectory, unless ultraviolet solar radiation is considered for which $dH_I/d\lambda$ varies with altitude.

To determine the variation of $(dJ/d\lambda)_{VBSR}$ with rocket altitude or with time, one has only to calculate $\sigma_s(t) = \sigma_s(\eta(t), \alpha_s(t))$ if visible solar radiation is considered. Here $\eta(t)$ and $\alpha_s(t)$ are time-dependent values of the viewing angles η and α_s defined below. For ultraviolet radiation, $dH_I(t)/d\lambda$ must also be known.

Closed solutions have been derived (Ref. 29) for the optical cross-sections $\sigma_s(\eta, \alpha_s)$ of the diffusely reflecting sphere, cylinder, cone, and truncated cone, where the point source illuminator and observer can occupy any position at distances large compared to the dimensions of the object. For the hemisphere which is illuminated by a beam parallel to its base, a numerical integration is necessary to obtain the optical diffuse-reflection cross-section (see Eqs. (3.25) through (3.27) below). The expressions for the optical cross-section of these three basic shapes can be easily programmed for a computer and can be used to determine the overall cross-section of any typical rocket or space vehicle composed of spherical, cylindrical, and conical components.

Analytically, the radiant intensity J (Watts/ster) of a diffusely reflecting object is obtained by multiplying the normal radiant intensity of each surface element by the cosine of the angle between the normal to the surface element and the direction of observation, and then integrating this product over the portion of the surface which is both irradiated and observed.

June 1974

The equivalent isotropic scattering cross-section σ_s , as used in (3.15) and defined in section 3.1, is then equal to the radiant power divided by the reflectivity ρ and the incident irradiance H :

$$\sigma_s = 4\pi \frac{J}{\rho H} \quad (3.16)$$

The solutions for σ_s for various shapes are given below using the notation and the angles shown in Figure 3-1. The center of the x-y-z coordinate system may be placed anywhere along the space object's axis since it is assumed that both the illuminating source and the observer are located at infinity. We have (Ref. 29):

a. Sphere

$$\sigma_s = \frac{2}{3} R^2 \left\{ \sin \eta_s + (\pi - \eta_s) \cos \eta_s \right\}, m^2, \quad (3.17)$$

where:

R = radius of sphere, m

η_s = Sun-target-observer angle

c. Cylinder

$$\sigma_s = \frac{rL}{2} \sin \alpha_s \sin \alpha_o \left\{ \sin \psi + (\pi - \psi) \cos \psi \right\}, m^2, \quad (3.18)$$

where:

June 1974

r = radius of cylinder, m

L = length of cylinder, m

α_s = angle between direction of irradiation and axis of cylinder

α_o = angle between direction of observation and axis of cylinder

$\cos \psi = \frac{\cos \eta_s - \cos \alpha_s \cos \alpha_o}{\sin \alpha_s \sin \alpha_o}$ = dihedral angle between planes of α_s and α_o

c. Cone

$$\sigma_s = \left\{ \frac{1}{4} (a_1 + a_2) l \cos \delta \right\} f(s), m^2, \quad (3.19)$$

where:

a_1, a_2 = radii of the bases, m

l = altitude of the cone, m

δ = generating angle of cone

$\frac{\pi}{2} + \gamma_s$ = limiting angle of irradiation in plane of ψ

$$\sin \gamma_s = \frac{\tan \delta}{\tan \alpha_s}$$

$\frac{\pi}{2} + \gamma_o$ = limiting angle of observation in plane of ψ

$$\sin \gamma_o = \frac{\tan \delta}{\tan \alpha_o}$$

The phase factor $f(s)$ in (3.19) is given for five different cases:

Case I (Cone)

Entire surface both seen and irradiated, that is $\alpha_s \leq \delta$, $\alpha_o \leq \delta$:

$$f(s) = 2\pi \left\{ 2 \cos \alpha_s \cos \alpha_o \tan^2 \delta + \cos \psi \sin \alpha_s \sin \alpha_o \right\} \quad (3.20)$$

Case II (Cone)

Entire surface is seen but not fully irradiated, that is $\alpha_s \geq \delta$, $\alpha_o \geq \delta$:

$$\begin{aligned} f(s) = & 2 (\pi + 2 \gamma_s) \cos \alpha_s \cos \alpha_o \tan^2 \delta + 4 \cos \psi \cos \gamma_s \cdot \\ & \cos \alpha_s \sin \alpha_o \tan \delta + 4 \cos \gamma_s \sin \alpha_s \cos \alpha_o \tan \delta + \\ & + \left\{ (\pi + 2 \gamma_s) - 2 \sin \gamma_s \cos \gamma_s \right\} \cos \psi \sin \alpha_s \sin \alpha_o \end{aligned} \quad (3.21)$$

Case III (Cone)

Entire surface is irradiated but not fully seen, that is $\alpha_s \leq \delta$, $\alpha_o \geq \delta$; or entire surface is neither fully seen nor fully irradiated but the portion that is seen is fully irradiated, that is $\alpha_s \geq \delta$, $\alpha_o \geq \delta$, $\gamma_s - \gamma_o \geq \psi$:

$$\begin{aligned} f(s) = & 2 (\pi + 2 \gamma_o) \cos \alpha_s \cos \alpha_o \tan^2 \delta + 4 \cos \psi \cos \gamma_o \sin \alpha_s \cdot \\ & \cos \alpha_o \tan \delta + 4 \cos \gamma_o \cos \alpha_s \sin \alpha_o \tan \delta + \\ & + \left\{ (\pi + 2 \gamma_o) - 2 \sin \gamma_o \cos \gamma_o \right\} \cos \psi \sin \alpha_s \sin \alpha_o \end{aligned} \quad (3.22)$$

June 1974

Case IV (Cone)

Entire surface is neither fully seen nor fully irradiated and only one band of irradiation apparent, that is $\alpha_s \geq \delta$, $\alpha_o \geq \delta$,

$$\gamma_s + \gamma_o \leq \pi - \psi :$$

$$\begin{aligned} f(s) = & 2 \left\{ (\pi - \psi) + (\gamma_s + \gamma_o) \right\} \cos \alpha_s \cos \alpha_o \tan^2 \delta + \\ & + 2 \left\{ \cos (\psi - \gamma_s) + \cos \gamma_o \right\} \cos \alpha_s \sin \alpha_o \tan \delta + \\ & + 2 \left\{ \cos \gamma_s + \cos (\psi - \gamma_o) \right\} \sin \alpha_s \cos \alpha_o \tan \delta + \\ & + \left[\left\{ (\pi - \psi) + (\gamma_s + \gamma_o) - \sin \gamma_s \cos \gamma_s + \right. \right. \\ & \left. \left. + \sin (\psi - \gamma_o) \cos (\psi - \gamma_o) \right\} \cos \psi + \left\{ \cos^2 \gamma_s - \right. \right. \\ & \left. \left. - \cos^2 (\psi - \gamma_o) \right\} \sin \psi \right] \sin \alpha_s \sin \alpha_o \end{aligned} \quad (3.23)$$

Case V (Cone)

Entire surface neither fully seen nor fully irradiated and two bands of irradiation are apparent, that is $\alpha_s \geq \delta$, $\alpha_o \geq \delta$,

$$\gamma_s + \gamma_o \geq \pi - \psi :$$

$$\begin{aligned} f(s) = & 4 (\gamma_o + \gamma_s) \cos \alpha_s \cos \alpha_o \tan^2 \delta + 4 (\cos \gamma_o + \\ & + \cos \gamma_s \cos \psi) \cos \alpha_s \sin \alpha_o \tan \delta + 4 (\cos \gamma_s + \\ & + \cos \gamma_o \cos \psi) \sin \alpha_s \cos \alpha_o \tan \delta + 2 \left\{ (\gamma_s + \gamma_o) + \right. \\ & \left. - \sin \gamma_s \cos \gamma_s - \sin \gamma_o \cos \gamma_o \right\} \cos \psi \sin \alpha_s \sin \alpha_o \end{aligned} \quad (3.24)$$

d. Hemisphere

For this particular geometry, the illuminating source (sun) is constrained to lie in the x-y plane. The observer may be in any direction within the limits $0 \leq \psi \leq \pi$, $-\frac{\pi}{2} \leq \phi_0 \leq \frac{\pi}{2}$. The resulting expressions may be divided into two cases:

Case I (Hemisphere)

For $0 \leq \psi \leq \pi$, $0 \leq \phi_0 \leq \frac{\pi}{2}$:

$$\sigma_s = R^2 \left[\left\{ \frac{1}{3} \sin \phi_0 (1 + \cos \psi) + \frac{\pi}{3} \cos \phi_0 \cos \psi \right\} - \int_{\beta = \frac{\pi}{2}}^{\psi} f(\psi, \phi_0, \beta) d\beta \right], m^2 \quad (3.25)$$

Case II (Hemisphere)

For $0 \leq \psi \leq \pi$, $-\frac{\pi}{2} \leq \phi_0 \leq 0$:

$$\sigma_s = R^2 \left[\left\{ \frac{1}{3} \sin \phi_0 (1 + \cos \psi) \right\} + \int_{\beta = \psi - \frac{\pi}{2}}^{\frac{\pi}{2}} f(\psi, \phi_0, \beta) d\beta \right], m^2 \quad (3.26)$$

where β is an integration variable in a plane parallel to the x-y plane, and the function $f(\psi, \phi_0, \beta)$ is given by:

June 1974

$$f(\psi, \phi_0, \beta) = \cos \phi_0 \cos \beta \cos(\psi - \beta) \left[\sin \left\{ \tan^{-1} \left\{ -\cot \phi_0 \cdot \right. \right. \right. \\ \left. \left. \left. \cos(\psi - \beta) \right\} \right\} - \frac{1}{3} \sin^3 \left\{ \tan^{-1} \left\{ -\cot \phi_0 \cos(\psi - \beta) \right\} \right\} \right] + \\ - \frac{1}{3} \cos^3 \left\{ \tan^{-1} \left\{ -\cot \phi_0 \cos(\psi - \beta) \right\} \right\} \sin \phi_0 \cos \beta \quad (3.27)$$

If one models the Atlas rocket for example by an equivalent cylinder 20 meters long, 3.5 meters in diameter, for the first stage which is connected to the second stage by a truncated cone of length 8 meters and $a_2 = 1.75$ meters and $a_1 = 0.75$ meters (see Figure 3-1), and topped by a second short cylinder with dimensions $L = 2.4$ m, $D = 1.5$ m and hemisphere of 0.75 meters radius, one obtains representative reflection cross-sections as shown in Figures 3-2 through 3.4. Note that ϕ_s in these figures equals $90^\circ - \alpha_s$ or vice versa $\alpha_s = 90^\circ - \phi_s$.

For specular reflection from an optically flat surface, the scattering cross-section is given by:

$$(\sigma_s)_{\text{spec}} = \frac{64 A_{\text{eff}}^2}{\pi (1.22 \lambda)^2} f_r(\eta_s, \lambda) = 13.687 f_r(\eta_s, \lambda) \left(\frac{A_{\text{eff}}}{\lambda} \right)^2, \text{ m}^2 \quad (3.28)$$

where:

$$A_{\text{eff}} = \int_A dA(\psi_s, \psi_0, \alpha_s) \cdot \delta(\psi_0) \delta(\psi_s) \delta(\pi - (\alpha_0 + \alpha_s)), \text{ m}^2 \quad (3.29)$$

If the optically flat surface is a polished metal (the usual case for space vehicles), then:

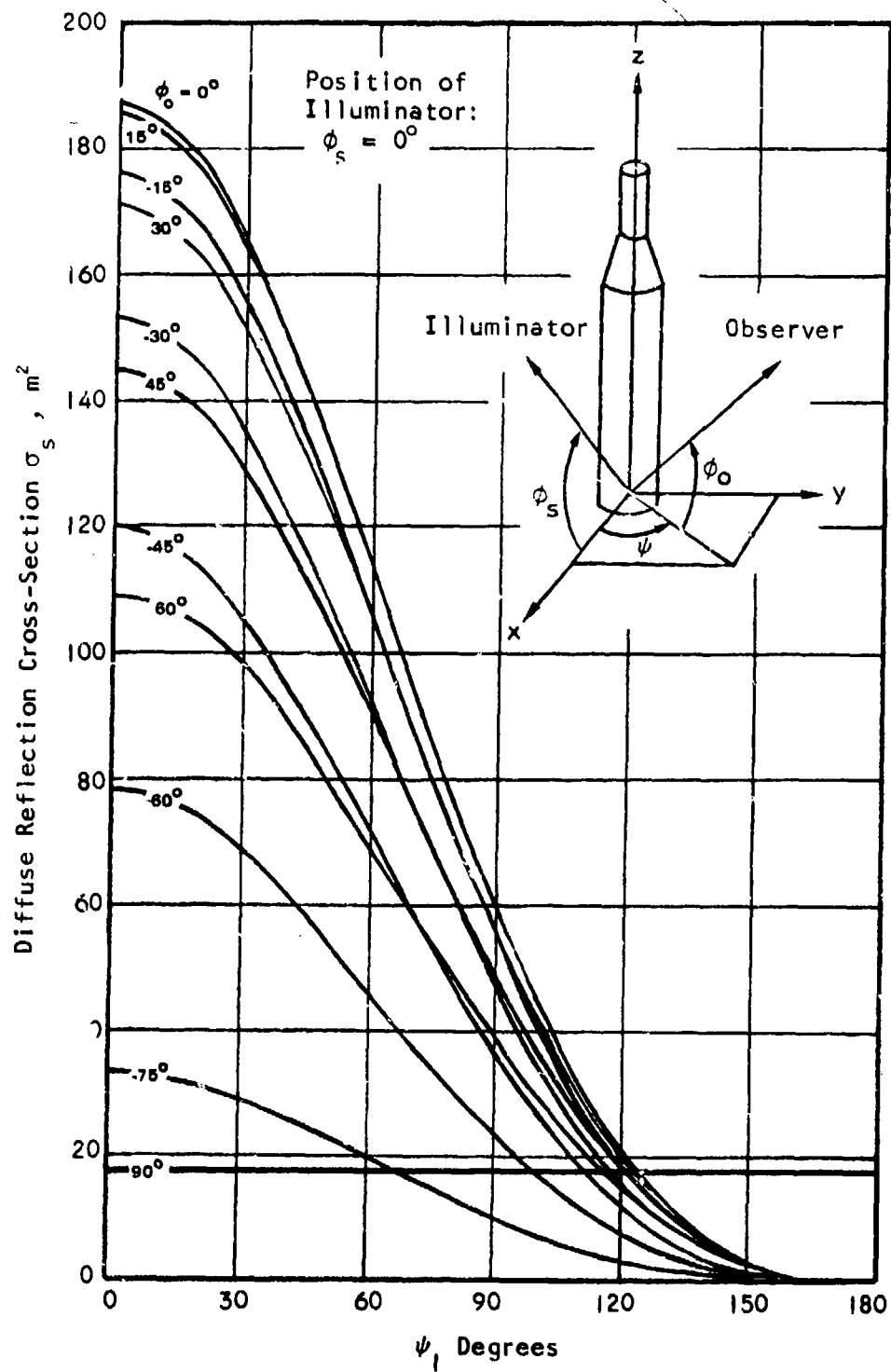


FIGURE 3-2. DIFFUSE REFLECTION CROSS-SECTIONS σ_s OF THE ATLAS ROCKET MODEL FOR $\phi_s = 0^\circ$

June 1974

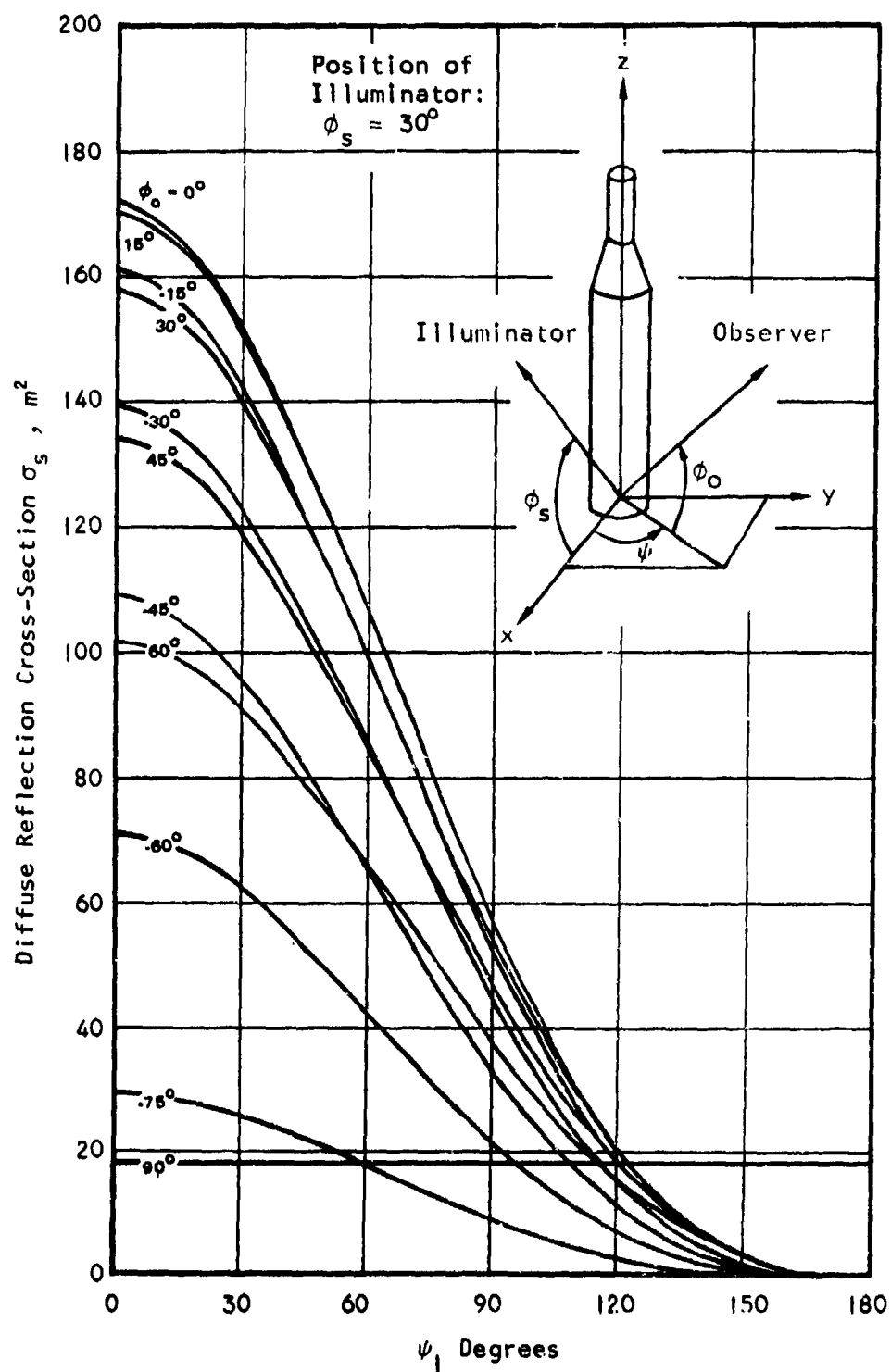


FIGURE 3-3. DIFFUSE REFLECTION CROSS-SECTIONS σ_s OF THE ATLAS ROCKET MODEL FOR $\phi_s = 30^\circ$

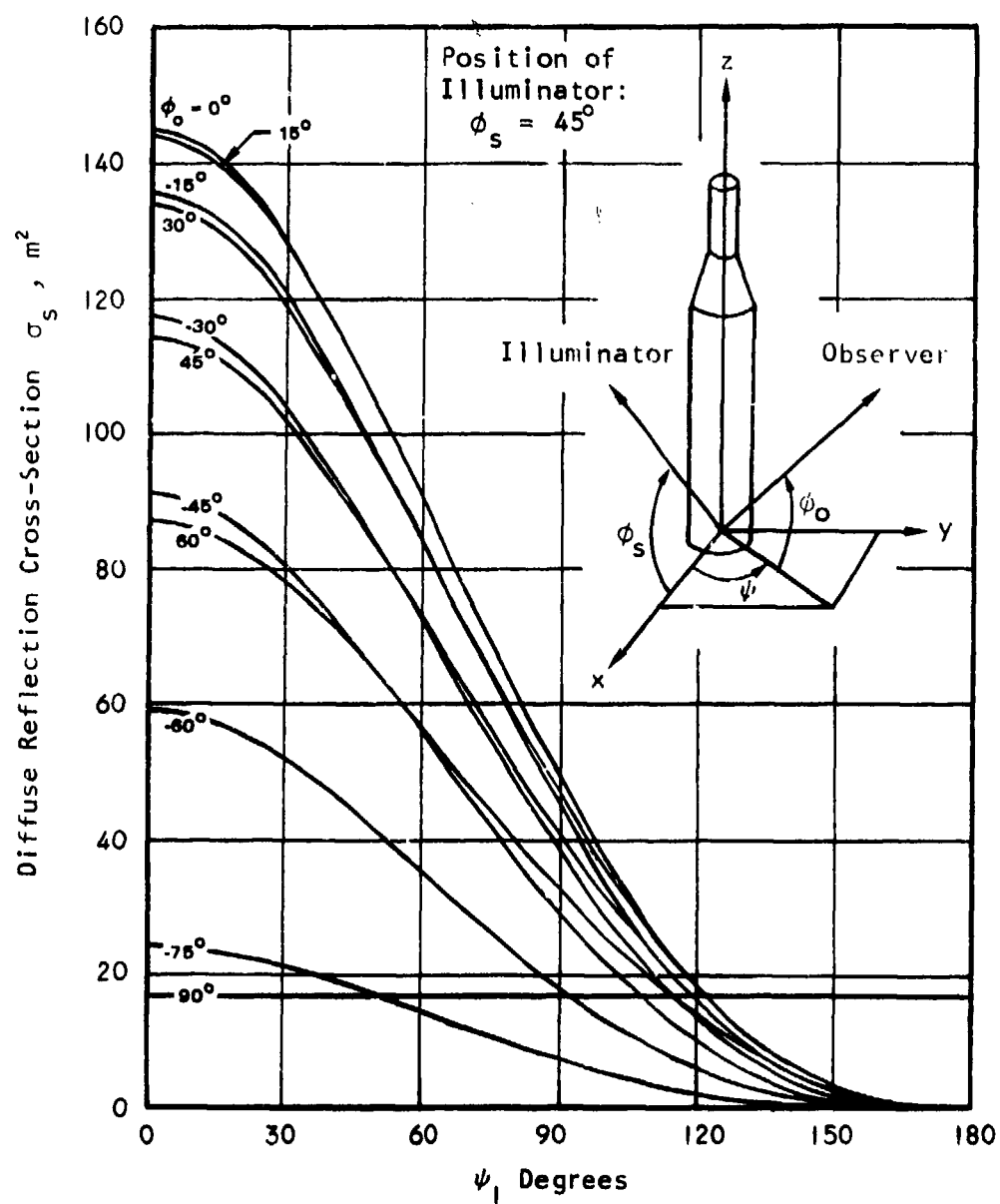


FIGURE 3-4. DIFFUSE REFLECTION CROSS-SECTIONS σ_s OF THE ATLAS ROCKET MODEL FOR $\phi_s = 45^\circ$

June 1974

$$f_r(\eta_s, \lambda) = f_r^{\text{metal}}(\eta_s, \lambda) = 0.5 f_{r\perp}^{\text{metal}}(\eta_s, \lambda) + 0.5 f_{r//}^{\text{metal}}(\eta_s, \lambda), \quad (3.30)$$

where:

$$f_{r//}^{\text{metal}}(\eta_s, \lambda) = \left[\frac{(m+1)^2 + \kappa_o^2}{(m-1)^2 + \kappa_o^2} \right] \left[\frac{\left(m - \frac{1}{\cos(\eta_s/2)}\right)^2 + \kappa_o^2}{\left(m + \frac{1}{\cos(\eta_s/2)}\right)^2 + \kappa_o^2} \right] \quad (3.31)$$

$$f_{r\perp}^{\text{metal}}(\eta_s, \lambda) = \left[\frac{(m+1)^2 + \kappa_o^2}{(m-1)^2 + \kappa_o^2} \right] \left[\frac{\left(m - \cos(\eta_s/2)\right)^2 + \kappa_o^2}{\left(m + \cos(\eta_s/2)\right)^2 + \kappa_o^2} \right] \quad (3.32)$$

$$\kappa_o = \frac{\lambda}{4\pi} \Sigma_o \quad (= \text{Extinction Coefficient}) \quad (3.33)$$

λ = Photon Wavelength, m

Σ_o = $\Sigma_s + \Sigma_a$ = Macroscopic photon extinction cross-section of polished metal surface, m^{-1}

Σ_s = $\Sigma_s(\lambda)$ = Macroscopic photon scattering cross-section of polished metal surface, m^{-1}

Σ_a = $\Sigma_a(\lambda)$ = Macroscopic photon absorption cross-section of polished metal surface, m^{-1}

m = Refractive index of polished metal surface

The function $\delta(x)$ in (3.29) is the Dirac delta function defined

by:

$$\delta(x) = 1, \text{ if } x = 0 \quad (3.34a)$$

$$\delta(x) = 0, \text{ if } x \neq 0 \quad (3.34b)$$

The geometric parameters α_0 , α_s , ψ_0 , ψ_s , and η_s are illustrated in Figure 3-5.

The angular dependence $f_r(\eta_s, \lambda)$ of the specular reflectivity is incorporated here in the cross-section (3.28) in keeping with the convention that we adopted earlier to include all angular dependencies in the parameter σ_s . The specular reflectivity $\rho(\lambda)$ of polished metals at normal incidence ($\eta_s = 0^\circ$) is (Ref. 30):

$$\rho(\lambda)_{(\eta_s = 0^\circ)} = \frac{(m+1)^2 + \kappa_0^2}{(m-1)^2 + \kappa_0^2} \quad (3.35)$$

Appendix A lists values of $\rho(\lambda)$ for various metals.

The parameters $f_{r\perp}^{\text{metal}}$ and $f_{r//}^{\text{metal}}$ given by (3.31) and (3.32) are the angular dependencies of specular reflection by metals for respectively the case of perpendicular (\perp) polarized light and parallel ($//$) polarized light with respect to the plane of incidence (Ref. 30). For light coming from a natural source such as the sun, approximately 50% is \perp polarized and 50% is $//$ polarized, and therefore Eq. (3.30) applies. If the illumination source has polarized photons such as from a laser, $f_r(\eta_s, \lambda)$ to be used in (3.28) is instead of (3.30) equal to:

$$f_{r, \text{polar.}}^{\text{metal}}(\eta_s, \lambda) = f_{r\perp}^{\text{metal}} \sin \omega + f_{r//}^{\text{metal}} \cos \omega, \quad (3.36)$$

June 1974

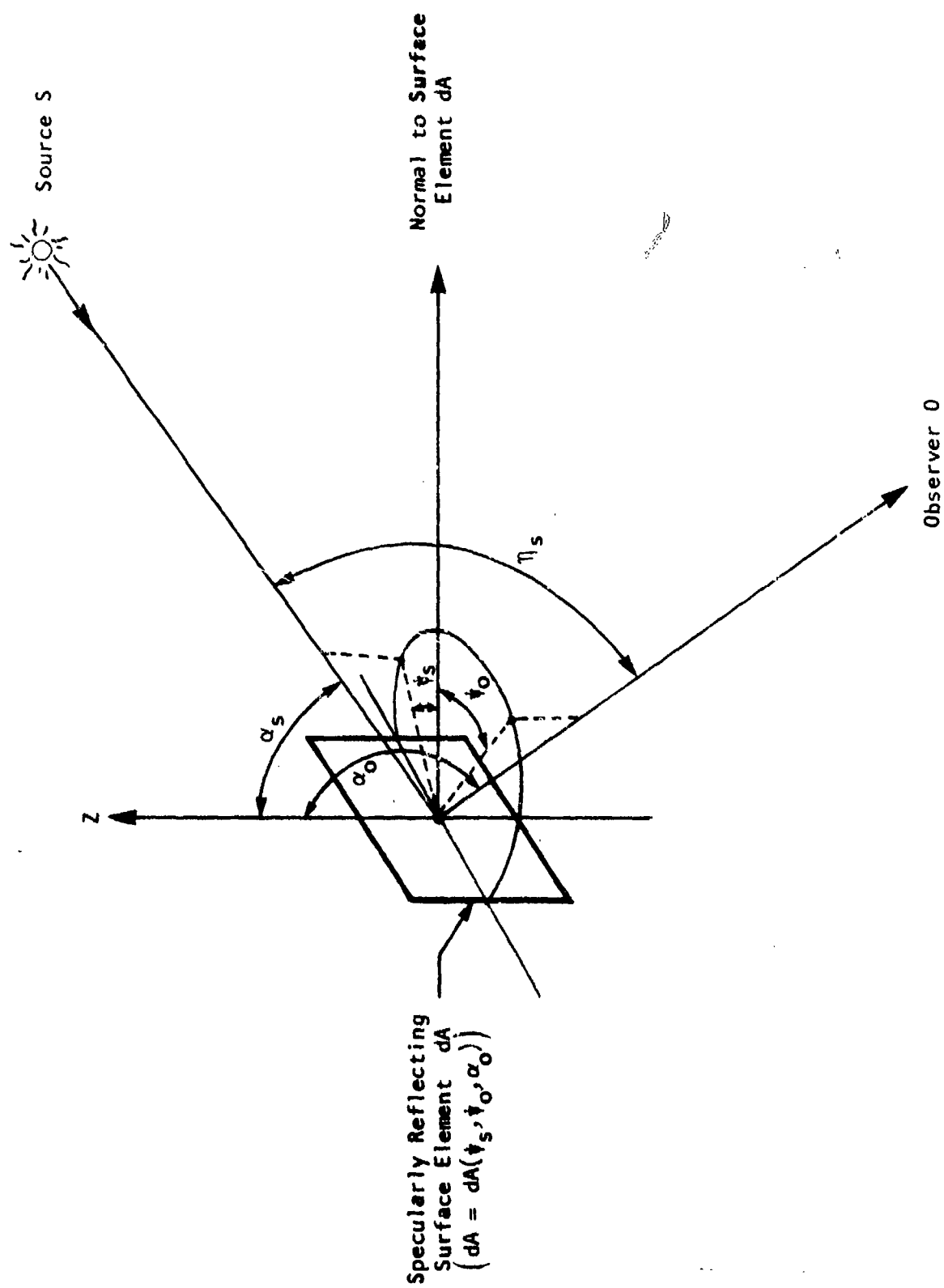


FIGURE 3-5. GEOMETRIC PARAMETERS FOR SPECULAR REFLECTION

where ω is the angle between the direction of polarization and the plane of incidence.

For infrared photons with wavelength λ larger than $5 \mu\text{m}$, one can use the relation:

$$m = \sqrt{30 \sigma \lambda} \quad , \quad \lambda \gtrsim 5 \mu\text{m} \quad (3.37a)$$

$$\kappa_0 \approx 0 \quad , \quad \lambda \gtrsim 5 \mu\text{m} \quad (3.37b)$$

in Eqs. (3.31) and (3.32), where:

σ = Electrical conductivity of the metal, ohm-cm

λ = Photon wavelength, μm

Equation (3.37) may be used even down to $\lambda = 2 \mu\text{m}$ as an approximation, but below $\lambda = 2 \mu\text{m}$ the assumptions inherent in relation (3.37) become invalid.

If the optically flat surface is not metallic but a dielectric (e.g., glass), the function $f_r(\eta_s, \lambda)$ given by Eqs. (3.30), (3.31), and (3.32) must be changed to:

$$f_r(\eta_s, \lambda) = \overset{\text{dielectric}}{f_r(\eta_s, \lambda)} = \frac{1}{2} \frac{\sin^2\left(\frac{\eta_s}{2} - \chi\right)}{\sin^2\left(\frac{\eta_s}{2} + \chi\right)} \cdot \left[1 + \frac{\cos^2\left(\frac{\eta_s}{2} + \chi\right)}{\cos^2\left(\frac{\eta_s}{2} - \chi\right)} \right], \quad (3.38)$$

where:

$$\chi = \sin^{-1} \left\{ \frac{\sin(\eta_s/2)}{m} \right\} \quad (3.39)$$

June 1974

Equation (3.38) applies to unpolarized light from natural sources. For a source of polarized light (e.g., from a laser), we have instead of (3.38):

$$f_r(\eta_s, \lambda)_{\text{polar.}}^{\text{dielectric}} = \left[\frac{\sin^2\left(\frac{\eta_s}{2} - X\right)}{\sin^2\left(\frac{\eta_s}{2} + X\right)} \right] \sin \omega + \left[\frac{\tan^2\left(\frac{\eta_s}{2} - X\right)}{\tan^2\left(\frac{\eta_s}{2} + X\right)} \right] \cos \omega \quad (3.40)$$

where ω is again the angle between the direction of polarization and the optical plane of incidence.

In Eq. (3.28) only the central disk of reflected light is considered, that is only the zero-order diffraction region. The higher-order diffraction rings are too weak to be of practical interest for the typical aerospace distances between observer and space vehicles. The specularly reflected light beam coming from the space vehicle's flat surface element dA to the observer is in (3.28) further assumed to disperse into a cone with a diffraction-limited apex angle given by:

$$\theta_d = \frac{1.22 \lambda}{\sqrt{\frac{4}{\pi} A_{\text{eff}}}}, \text{ radians} \quad (3.41)$$

3.2.2 Vehicle Body Earthshine Reflections (VBER)

If the illuminating source cannot be considered as a point, an integration must be carried out over all incident illuminating angles. The main illumination source that falls in this category is solar radiation reflected from the earth and its atmosphere also called earthshine. In this case, an extended source with many elements of sunlit surface area on

a spherical atmosphere must be considered which contribute to the irradiance of the target. The illumination will obviously depend on the zenith angle of the sun and the altitude and orientation of the target.

In the following we give an abbreviated version of the earthshine problem from Refs. 31 and 32. Assume an element of source area dC consisting of many point sources, each contributing to the irradiance of an element of target surface area dA . The solar-illuminated upper atmosphere surface is assumed to be a perfectly diffuse Lambert's-law radiator which has the property that the radiance N of any particular surface element dC is the same when viewed from any direction within 90° from the normal to the surface element. Therefore, the amount of radiant flux dP (Watts) emitting from dC and directed within the small solid angle subtended by dA at a distance S is proportional to the projected area of dC as well as the solid angle (see Figure 3-6). Thus:

$$dP = N \cdot dC \cos \eta \cdot \frac{dA \cos \psi}{S^2} \quad (3.42)$$

where N (Watts/m²-ster) is the radiance of the surface element dC , $dC \cos \eta$ is the projected area of dC and $\frac{dA \cos \psi}{S^2}$ is the solid angle subtended by the projected target surface element (Figure 3-6). A perfectly diffuse white surface receiving an irradiance H_E will have a radiance in any direction equal to:

$$N = \frac{H_E}{\pi} \quad (3.43)$$

Considering a solar-illuminated spherical Lambertian surface, the irradiance H_E of an element of area dC is given by $\bar{H}_E \cos \beta_E$ where \bar{H}_E is the irradiance

June 1974

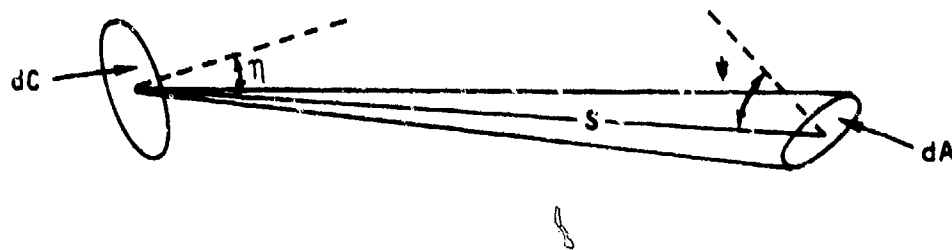


FIGURE 3-6. RADIANT FLUX DIAGRAM

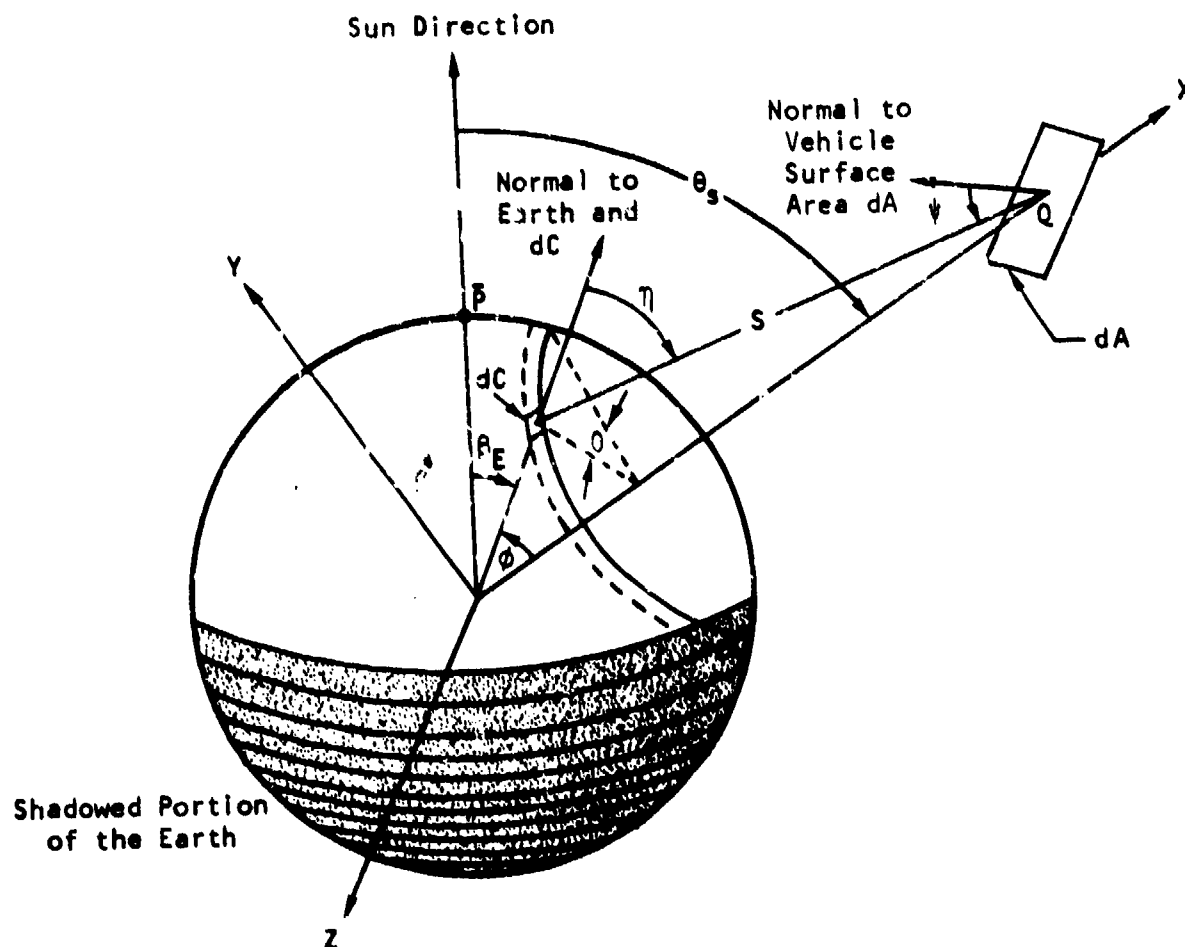


FIGURE 3-7. SUN-EARTH-TARGET CONFIGURATION

of the point \bar{P} on the surface nearest the sun and β_E is the angle between the direction of the sun and that of the normal of dC relative to geocenter (Figure 3-7). For a surface of less than 100 percent reflectivity, the radiance of dC is decreased to $\frac{H_E}{\pi}$ times the albedo a at dC (albedo a = ratio of reflected to incident illumination). Equation (3.42) becomes then:

$$dP = a \frac{\bar{H}_E}{\pi} \cos \beta_E \cos \eta \frac{\cos \psi}{S^2} dC dA \quad (3.44)$$

The irradiance H of a surface is defined as the radiant flux incident per unit area so that the irradiance of the target area dA equals:

$$dH = \frac{dP}{dA} = a \frac{\bar{H}_E}{\pi} \cos \beta_E \cos \eta \frac{\cos \psi}{S^2} dC \quad (3.45)$$

Calculating the irradiance at any point due to a source of finite area requires the integration of Eq. (3.45) over this area. The region concerned here is that earth surface area which is both sunlit and can be seen from the point in space at which the target is located.

$$H = \iint a \frac{\bar{H}_E}{\pi} \cos \beta_E \cos \eta \frac{\cos \psi}{S^2} dC \quad (3.46)$$

In Ref. 31, a simple and efficient numerical technique is presented by which numerical results for Eq. (3.46) for various target altitudes and orientations may be obtained assuming a flat target surface. Using the angles in the diagram, the element of source area becomes:

June 1974

$$dG = R_E \sin \phi \, d\theta \cdot r_E \, d\phi \quad (3.47)$$

Equation (3.46) then reads:

$$H = a \bar{H}_E \int_{\phi_L}^{\phi_U} \int_{\theta_L}^{\theta_U} \frac{R_E^2}{\pi} \cdot \frac{\sin \phi \cos \beta_E \cos \eta \cos \psi}{s^2} \, d\theta \, d\phi = a \bar{H}_E F \quad (3.48)$$

The F term of Eq. (3.48) was evaluated numerically in Ref. 31 using Simpson's rule with integration limits of:

$$\phi_L = 0, \phi_U = \cos^{-1}\left(\frac{R_E}{R}\right), \theta_L = 0, \theta_U = 2\pi \quad (3.49)$$

Reference 31 gives the resulting values of the irradiance factor F for several zenith angles of the sun and target altitudes as a function of the angle between the vehicle surface normal at Q and the X-axis. The curves indicate that a maximum F is obtained when the target is in the same direction as the sun; i.e., $\theta_s = 0$, and the normal to its surface is directed along the X-axis. For our purposes, F values have been plotted versus target altitude in Figure 3-8 for various solar zenith angles assuming that the flat target surface is perpendicular to the geocentric range vector at all times. The irradiance factor is seen to decrease with altitude, for although more of the earth's surface area can be seen from the target as it increases in altitude, the intensity of the radiation is falling off with the square of the distance between the target and each element of area on the earth surface. The illumination of the target also decreases with increasing zenith angle, for as θ_s increases, the target is moving away from the more highly irradiated portion of the earth.

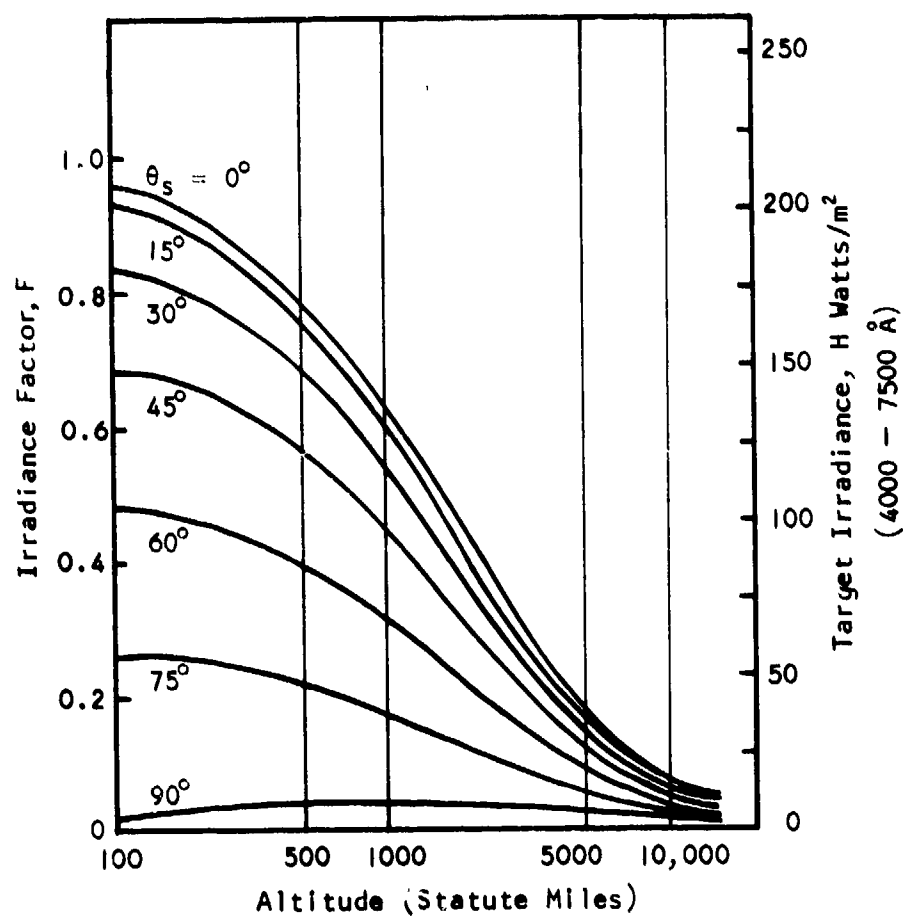


FIGURE 3-8. EARTHSHINE IRRADIANCE FACTOR, F , AND VISIBLE EARTHSHINE TARGET IRRADIANCE, H , VERSUS TARGET ALTITUDE FOR VARIOUS SOLAR ZENITH ANGLES θ_s
(After Ref. 31)

If the space vehicle is spherical, closed solutions for earthshine illumination by an extended spherical earth can be obtained as shown in Ref. 32.

Returning to Eq. (3.48), $H = a \bar{H}_E F$, it is necessary to assume a value of solar irradiance \bar{H}_E incident at the top of the earth's atmosphere and a value of albedo a , both of which depend on the spectral region of interest. For direct daytime solar reflection which varies with the nature of the earth's surface and cloud cover, the radiation peaks in the visible region of the spectrum. In the wavelength interval $4000 - 7500 \text{ \AA}$, the solar irradiance at the top of the atmosphere is $\bar{H}_E = 559 \text{ Watts/m}^2$.

The average albedo a of the earth for visible sunlight is about 39 percent with fluctuations between 32 percent in July and 52 percent in October. Cloud albedo measurements have an average value of 0.5 but may vary between 0.8 and 0.01 according to cloud conditions. For the ultraviolet, the albedo $a \rightarrow 0$ due to molecular absorption in the upper atmosphere.

The average target irradiance H is given by the value of F multiplied by a constant factor $a \cdot \bar{H}_E = 0.39 \times 559 = 218 \text{ Watts/m}^2$, which is shown in Figure 3-8 on the right-hand ordinate. It is obvious that the F numbers can be used to obtain results in any bandwidth if the proper scaling factors of albedo and incident solar energy are known.

To calculate exact cross-sections σ and radiant intensities $J = \rho H \sigma / 2\pi$ of a space target illuminated by solar earthshine would require rather elaborate integrations. As an approximation we may employ the expressions for σ given in section 3.2.1 for point illuminators, using for the effective illuminator angle α_I the value:

$$\alpha_I^{\text{eff}} = \alpha_{\text{sun}} + (\pi - \theta_s)/2, \quad (3.50)$$

where θ_s is the solar zenith angle at the space target with respect to a geocentric line. This has the effect of replacing the extended illuminating source by an effective point-source illuminator placed at the approximate center of the sun-illuminated portion of the earth atmosphere as seen by the space vehicle. Denoting cross-sections so obtained by:

$$\bar{\sigma}_{\text{eff}} = \sigma (\alpha_I^{\text{eff}}) = \sigma \left(\alpha_{\text{sun}} + \frac{\pi - \theta_s}{2} \right), \text{ m}^2 \quad (3.51)$$

the spectral radiant intensity $dJ/d\lambda$ becomes:

$$\left(\frac{dJ}{d\lambda} \right)_{\text{VBER}} = \rho(\lambda) \frac{d(a \bar{H}_E F)}{d\lambda} \frac{\bar{\sigma}_{\text{eff}}}{4\pi} = \frac{\bar{\rho} \bar{a} F \bar{\sigma}_{\text{eff}}}{4\pi} \frac{d \bar{H}_E}{d\lambda}, \frac{\text{Watts}}{\text{ster} \cdot \text{Hz}},$$

(3.52)

where in the visible and infrared (but not in the UV) usually an average value for $\rho(\lambda)$ and $a(\lambda)$ can be assumed, and $d \bar{H}_E/d\lambda$ has the spectral distribution of the sun.

The effect of earthshine on the optical intensity (in the visible) of a solar-illuminated space target is to increase the direct-solar-reflected intensity by about 10 percent on the average and by about 37 percent in the most favorable situation. Of course if the target is shaded by the earth, but still subjected to earthshine, the radiant intensity is determined by earthshine only.

June 1974

3.2.3 Vehicle Body Self-Emissions (VBSE)

The spectral radiant intensity for vehicle body self-emission may be expressed by (see section 3.1):

$$\left(\frac{dJ}{d\lambda}\right)_{VBSE} = \frac{\sigma_e(\alpha_o) \epsilon(\lambda)}{4\pi} \frac{dW_{BB}}{d\lambda}, \quad \frac{\text{Watts}}{\text{ster} \cdot \text{Hz}} \quad (3.53)$$

Here the emissivity $\epsilon(\lambda)$ is a purely materials-dependent parameter which may be obtained from the tables in Appendix A, while the black-body radiation function $dW_{BB}/d\lambda$ may be gotten from Appendix B.

For a surface which behaves as a diffuse emitter, the cross-section $\sigma_e(\alpha_o)$ (as defined in section 3.1) is four times the projected area of the emitter that can be seen by the observer. This is due to the fact that for a diffuse emitter the emission per unit solid angle in a direction at an angle θ with the normal to the surface element dA equals $\frac{\epsilon W_{BB}}{\pi} dA \cos\theta$ Watts/ster, whereas the projected area through which this flux passes equals $dA \cos\theta$ thus making the radiance $N = \frac{\epsilon W_{BB}}{\pi} dA \cos\theta / (dA \cos\theta) = \epsilon W_{BB} / \pi$ Watts/(m² · ster) which is constant. The total radiant intensity J from the emitter is then:

$$J = \frac{A_{proj} \epsilon W_{BB}}{\pi}, \quad \text{Watts/ster} \quad (3.54)$$

and the irradiance at a distance S is:

$$H_T = \frac{A_{\text{proj}} \epsilon W_{\text{BB}}}{\pi S^2}, \text{ Watts/m}^2 \quad (3.55)$$

Then the cross-section σ_e to be used in (3.53), according to our definition given in section 3.1 is:

$$\sigma_o = \sigma_e(\alpha_o) = 4 A_{\text{proj}}, \text{ m}^2 \quad (3.56)$$

Assuming the same geometry as shown in Figure 3-1, the cross-sections for a sphere, cylinder, cone, truncated cone, and hemisphere become:

a. Sphere (Radius R):

$$\sigma_e = 4\pi R^2, \text{ m}^2 \quad (3.57)$$

b. Finite Cylinder (Radius r, Length L):

$$\sigma_e = 8 L r \sin \alpha_o + 4\pi r^2 |\cos \alpha_o|, \text{ m}^2 \quad (3.58)$$

(Side) (End)

c. Truncated Cone (Radii a_1, a_2 ; Cone Half-Angle δ ; $a_1 > a_2$):

$$\sigma_e = 4\pi a_1^2 \cos \alpha_o, \text{ m}^2, \text{ for } 0 \leq \alpha_o \leq \delta \quad (3.59a)$$

(End)

$$\sigma_e = 4(a_1^2 - a_2^2)(\cos \alpha_o) \left(-\frac{\pi}{2} + \sin^{-1} \beta + \frac{1}{\beta} \sqrt{1 - \beta^2} \right) + \quad (3.59b)$$

(Side)

$$+ 4\pi a_1^2 \cos \alpha_o, \text{ m}^2, \text{ for } \delta \leq \alpha_o \leq \frac{\pi}{2} \quad (3.59b)$$

(End)

$$\sigma_e = 4 (a_1^2 - a_2^2) \left| \cos \alpha_o \right| \left(\frac{\pi}{2} + \sin^{-1} \beta + \frac{1}{\beta} \sqrt{1 - \beta^2} \right) + \quad (3.59c)$$

$$+ 4\pi a_2^2 \left| \cos \alpha_o \right|, \text{ m}^2, \text{ for } \frac{\pi}{2} \leq \alpha_o \leq (\pi - \delta)$$

(Side)
(End)

$$\sigma_e = 4\pi (a_1^2 - a_2^2) \left| \cos \alpha_o \right| + 4\pi a_2^2 \left| \cos \alpha_o \right|, \text{ m}^2, \quad (3.59d)$$

(Side)
(End)

for $(\pi - \delta) \leq \alpha_o \leq \pi$

where:

$$\beta = \frac{|\cot \alpha_o|}{\cot \delta} \quad (3.60)$$

d. Hemisphere (Radius R):

$$\sigma_e = 2\pi R^2 (1 + \cos \alpha_o) \quad (3.61)$$

In all of the above expressions α_o is the angle between the axis of the cylinder, truncated cone, hemisphere, and target observer direction.

By approximating space vehicle configurations with hemispherical, cylindrical, and conical surfaces, the self-emission cross-section can be calculated for any observation angle α_o . As an example, in Figure 3-9 values of σ_e are plotted versus α_o for a cone-shaped body with a base diameter of 2 meter and apex half-angle of 11.3 degrees which approximates a typical space vehicle.

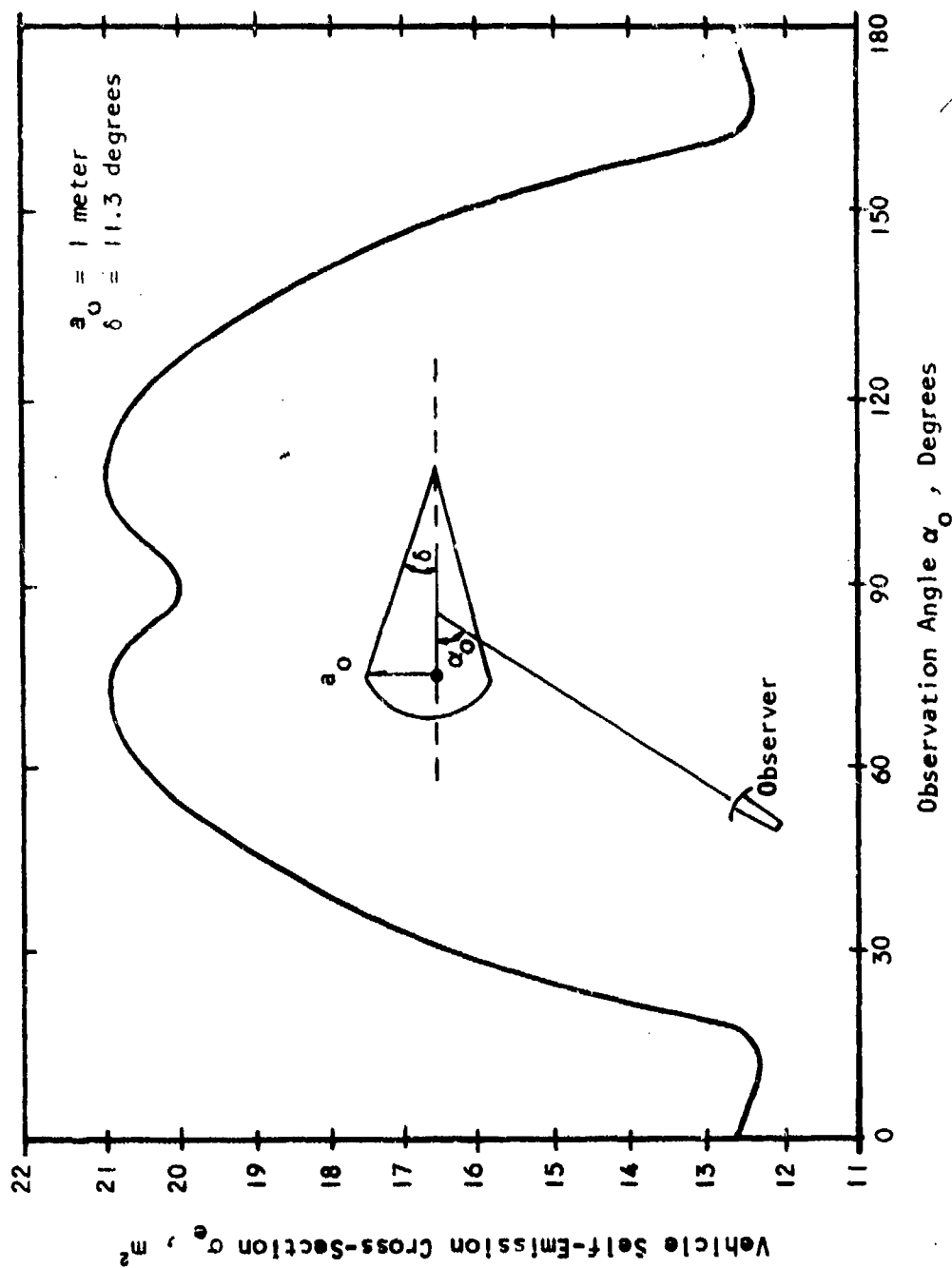


FIGURE 3-9. SELF-EMISSION CROSS-SECTION OF TYPICAL CONE-SHAPED SPACE VEHICLE

3.3 ROCKET EXHAUST RADIATIONS

3.3.1 General Comments

The theory of exhaust gas radiation which is presented below includes three powerful new approaches to the problem which do not appear to have been considered previously elsewhere. These are:

1. Application of Gauss' divergence theorem to the mathematics of the detailed balancing of excitation quanta in intermolecular V-V and V-T energy exchanges* and photon-molecule interactions in the exhaust.
2. Rigorous application of the basic "Law of Spectroscopic Stability" to all molecular spectral broadening processes.
3. Development of a more comprehensive theory of photon kinetics ("photonics") by transplanting the results of "neutronics" theory for neutrons in nuclear reactors to that of photons drifting through gaseous bodies.

The result of applying (1) is the discovery that for engine exhaust plumes, the number of excited-energy states flowing out of the engine has to equal the number of photons emitted through the boundaries of the exhaust plume. If used properly, this result allows a considerable simplification in the analytical calculation of exhaust gas radiation over other methods which have been developed. The technique will be discussed in detail in the next subsection 3.3.2.

*A V-V molecular collision is one in which internal excitation energy (V) is exchanged, while in a V-T collision, excitation energy (V) is transferred to translational kinetic energy (T).

The application of (2) leads to simplified expressions for spectral broadening and band contour functions for use in the theory of exhaust gas spectral radiation. Detailed derivations and discussions are given in Volume II of the Rocket Radiation Handbook.

Application of method (3), that of treating the migration of photons in gas clouds by a well-established analogous theory for neutrons in nuclear reactors, yields a much improved understanding of the spatial distribution of photons in gas clouds for both optically dense as well as optically thin gases and all intermediate cases. Basic principles of "photonics" are discussed in Volume III of the Rocket Radiation Handbook.

Knowing and understanding what the magnitude and spectrum is of the radiation emitted by hot exhaust gases from rocket engines is obviously also useful in fields that study exhausts from aircraft, automobiles, and other types of combustion engines. To date, most interest in exhaust radiation analysis has come from military applications. Recently however the air pollution monitoring field is developing requirements for a better understanding of engine exhaust radiations as well, and the material presented below, though applied to rocket exhausts, can be adapted with little modification to such fields as:

- a. Air Pollution Monitoring
- b. Anti-Air-Pollution Fuel Design
- c. Aircraft Engine Performance Monitoring and Measurements
- d. Weather and Meteorological Effects
- e. Anti-Aircraft Heat-Seeking Missile Sensors

- f. Aircraft Anti-Missile-Countermeasures
 - 1. Radiation Suppression Techniques
 - 2. Radiation Decoying Techniques
- g. Aircraft Intelligence-Gathering Sensors

3.3.2 Plume Radiation in a Vacuum (Deep-Space Plume Radiation; DSPR)

As will become apparent later, the analytically most simple case of rocket exhaust radiation is the one in which the rocket exhaust* does not interact with the atmosphere. For this reason, we shall treat this case first although a rocket usually experiences this situation last in a space mission.

In Figure 3-10, the geometry is illustrated for a rocket exhaust discharging into the vacuum of deep space. Near the nozzle exit plane and in the core region of the plume, the gas is optically dense (the photon mean free path is less than the plume dimensions), but in the outer regions where the gas molecules escape into the vacuum without further intermolecular collisions, the gas becomes obviously optically transparent. Since gas molecules in photon-active excited states take a finite time to deexcite to the ground state, a region of space behind the nozzle can be defined enclosed by the surface C_e (see Figure 3-10) within which essentially all exhaust molecules have experienced deexcitation and beyond which all molecules may be considered "cold" or "dead," that is radiationless. The characteristic linear dimension of the radiation emitting region or plume bounded by C_e would be:

*Although the exhaust from a rocket is usually gaseous, solid particles may be present sometimes. Therefore the terms "exhaust gases" and "rocket gases" are avoided, and "exhaust" is assumed to include both gases and entrained particles.

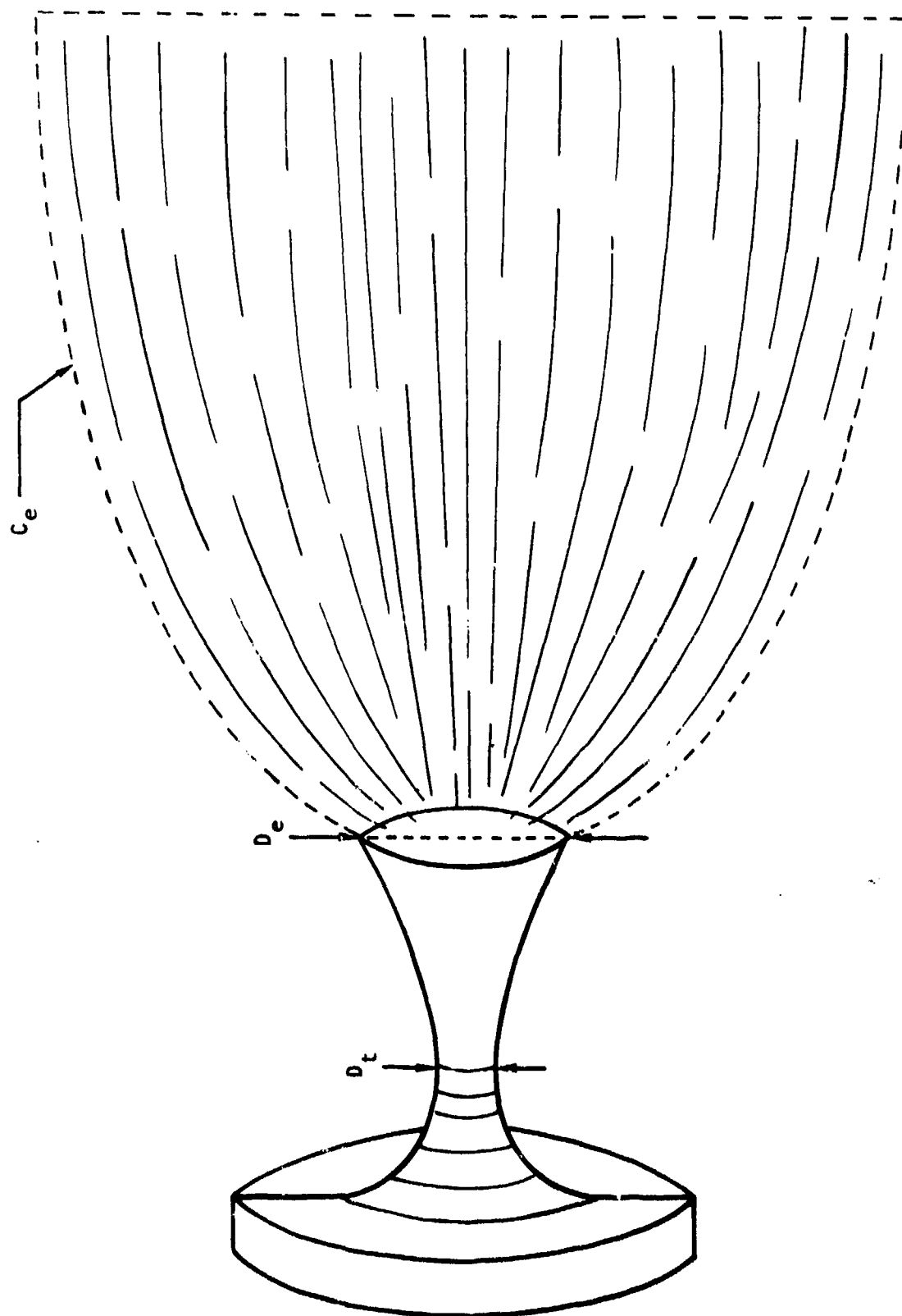


FIGURE 3-10. DEEP-SPACE (VACUUM) ROCKET PLUME GEOMETRY

$$L_p \approx L_c + 5 c_c \left[\sum_i \left(\frac{1}{\tau_i} \right) \right]^{-1}, \quad m \quad (3.62)$$

where:

L_c = Linear dimension of the plume core, m

c_c = Average molecular velocity of molecules escaping from core region, m/sec

τ_i = Excitation lifetime ($\tau_i = A_i^{-1}$ = Einstein coefficient) of molecule for state i, sec

Equation (3.62) gives the mean distance at which molecules have decayed about 5 e-folds after reaching the collisionless region of the plume, that is only a fraction $\exp(-5) \approx 0.0067$ would still be excited beyond C_e .

Consider now the number of excited species X_i in a unit volume du of gas anywhere within the region bounded by C_e . For this unit volume du we can write the excited-state conservation (or balancing) equation:

$$\begin{aligned} \frac{\partial n(X_i)}{\partial t} = & \frac{\partial G(X_i)}{\partial u} - \frac{\partial D(X_i)}{\partial u} + \frac{\partial R(X_i)}{\partial u} - \frac{\partial S(X_i)}{\partial u} + \frac{\partial P(X_i)}{\partial u} - \\ & - \frac{\partial L(X_i)}{\partial u} + \frac{\partial C(X_i)}{\partial u} - \frac{\partial B(X_i)}{\partial u} + \frac{\partial F(X_i)}{\partial u}, \quad \frac{\text{molecules } X_i}{m^3 \cdot \text{sec}}, \quad (3.63) \end{aligned}$$

In which:

$n(X_i) = n_i$ = Density of excited molecules X_i , molecules/ m^3 .

X_i = Molecule X in excited state i.

$\frac{\partial G(X_i)}{\partial v}$ = Net Influx (or outflux) of excited molecules X_i into (or out of) unit volume per unit time due to transport.

$\frac{\partial D(X_i)}{\partial v}$ = Rate of destruction (decay) of excited molecules per unit volume due to emission of radiation (radiative decay).

$\frac{\partial R(X_i)}{\partial v}$ = Rate of production of excited species X_i due to resonant energy transfer in collisions-of-the-second-kind (V-V transfers) between molecules X and excited molecules Y .

$\frac{\partial S(X_i)}{\partial v}$ = Rate of destruction of excited molecules due to resonant energy transfer in collisions-of-the-second-kind (V-V transfers) between excited molecules X_i and other species Y .

$\frac{\partial P(X_i)}{\partial v}$ = Rate of production of excited molecules X_i in unit volume due to Kinetic collision with other molecules (T-V collisions).

$\frac{\partial L(X_i)}{\partial v}$ = Rate of destruction of excited molecules X_i in unit volume due to Kinetic collisions with other molecules (V-T collisions).

$\frac{\partial C(X_i)}{\partial v}$ = Rate of production of excited molecules X_i in unit volume due to resonant capture of photons by molecules in lower-lying energy states.

$\frac{\partial B(X_i)}{\partial v}$ = Rate of destruction of excited molecules X_i due to stimulated emission by resonant photons.

$\frac{\partial F(X_i)}{\partial v}$ = Rate of production of excited molecules X_i due to decay of higher energy levels m that transition to i .

June 1974

The nine terms on the right-hand side of Eq. (3.63) can be expressed in terms of gas transport variables and microscopic parameters as follows. The migration term is given by:*

$$\frac{\partial G_i}{\partial v} = \vec{v} \cdot n_i \vec{V}_i + \vec{v} \cdot \mathcal{D}_X \vec{\nabla} n_i, \quad \frac{\text{molecules}}{\text{m}^3 \cdot \text{sec}} \quad (3.64)$$

in which:

$\vec{V}_i = \vec{V}_i(\vec{r}) =$ Bulk dynamic velocity of molecules X_i at \vec{r} , m/sec

$\vec{r} =$ Position coordinate (fixed with respect to the observer)
in plume region

$\mathcal{D}_X =$ Diffusion coefficient of molecules X , m^2/sec

The molecular diffusion coefficient \mathcal{D}_X may according to the kinetic theory of gases (Refs. 33 and 34), be expressed in terms of other gas parameters by the relation:

$$\mathcal{D}_X = \frac{0.4234 k_d}{n_{\text{tot}} \bar{\sigma}_{c_i}} \left(\frac{8 kT}{\pi \bar{M}_X} \right)^{1/2} = \frac{91.19 k_d}{n_{\text{tot}} \bar{\sigma}_{c_i}} \left(\frac{T}{\bar{M}_X} \right)^{1/2}, \quad \frac{\text{m}^2}{\text{sec}} \quad (3.65)$$

where:

$T =$ Kinetic temperature, $^{\circ}\text{K}$

$\bar{M}_X = \frac{2 M_X M_Y}{M_X + M_Y} =$ Effective mass of molecules X , a.m.u.
(atomic mass units)

$n_{\text{tot}} =$ Total molecular density, m^{-3}

*We shall use subscripts i instead of (X_i) to denote dependence on the excited state i of species X in all of the following.

$\bar{\sigma}_{cX}$ = Average elastic collision cross-section for collisions of molecules X with other molecules Y (including Y = X), m^2 .

k_d = Collision factor; $k_d = 1.000$ for hard-sphere molecules, $k_d = 1.2652$ for "inverse-fifth-power-repulsion" molecules (Ref. 34)*.

Using the gas law $p = n RT$, Eq. (3.65) can be written in the more convenient form:

$$\mathcal{D}_X = 2.358 \times 10^{-7} \left[\frac{k_d T^{3/2}}{p_{\text{tot}} \bar{\sigma}_{cX} \bar{M}_X^{1/2}} \right], \text{ m}^2/\text{sec} \quad (3.66)$$

*where now:

p_{tot} = Total gas pressure in bars.

$\bar{\sigma}_{cX}$ = Collision cross-section in $\text{\AA}^2 = 10^{-16} \text{ cm}^2 = 10^{-20} \text{ m}^2$
 ← and the other parameters are as before.

The first term on the right-hand side of Eq. (3.64) is the bulk convective migration term while the second is the local kinetic diffusion term.

The radiative decay term in Eq. (3.63) is:

$$\frac{\partial \mathcal{D}_1}{\partial v} = \int_{\lambda} \frac{dA_1}{d\lambda} n_1 d\lambda, \frac{\text{molecules}}{\text{m}^3 \cdot \text{sec}}, \quad (3.67)$$

*Reference 34 gives the Maxwell-Chapman-Enskog numerical factors $c_d = 1.200 \times 0.499 = 0.5988$ for hard-sphere molecules in the expression $\mathcal{D} = c_d \bar{v} l_c$ and $c_d = 1.543 \times 0.491 = 0.7576$ for "inverse-fifth-power" molecules. We normalize to the hard-sphere molecular model and define here $k_d = c_d / (c_d)_{\text{hard-sphere}}$.

in which:

$$\frac{dA_i}{d\lambda} = \text{Spontaneous emission (or "decay") rate constant (Einstein "A" coefficient) for excited state } i \text{ of species } X \text{ in the wavelength range } d\lambda, \text{ sec}^{-1} \cdot \mu\text{m}^{-1}$$

Explicit expressions for $dA_i/d\lambda$ are given in Volume II of the Handbook.

The resonant-transfer excitation* term in Eq. (3.63) can be expressed by:

$$\frac{\partial R_i}{\partial v} = \sum_Y n_j v_{YX} (\bar{\sigma}_{jX})_i n_X, \quad \frac{\text{molecules}}{\text{m}^3 \cdot \text{sec}}, \quad (3.68)$$

while the resonant-transfer deexciting* term in (3.63) is given by:

$$\frac{\partial S_i}{\partial v} = \sum_k \sum_Y n_Y v_{YX} (\bar{\sigma}_{Yi})_k n_i, \quad \frac{\text{molecules}}{\text{m}^3 \cdot \text{sec}} \quad (3.69)$$

In the above:

$n_j \equiv n_{Yj}$ = Density of excited species j of molecules Y , molecules/ m^3

$n_i \equiv n_{Xi}$ = Density of excited species i of molecules X , molecules/ m^3

n_Y, n_X = Density of unexcited (ground-state) molecules Y and X respectively, molecules/ m^3

$(\bar{\sigma}_{jX})_i$ = Average resonant energy transfer (V-V) cross-section for interactions between excited molecules Y_j and ground-state molecules X , resulting in excited molecules X_i , m^2

*These interactions are also called "V-V" exchange collisions (V = Molecular Potential Energy).

$(\bar{\sigma}_{Yi})_k$ = Average resonant energy transfer cross-section for interactions between ground-state molecules Y and excited molecules X_i , resulting in deexcitation of molecules X_i and excitation of Y to Y_k , m^2

v_{YX} = Average molecular velocity of molecules Y with respect to molecules X, m/sec. According to the kinetic theory of gases (Ref. 34):

$$v_{YX} = \sqrt{\frac{4}{\pi} \frac{kT}{M_{YX}}} = 102.897 (T/M_{YX})^{1/2}, \text{ m/sec} \quad (3.70)$$

$$M_{YX} = \frac{M_Y M_X}{M_Y + M_X} \equiv \text{Reduced Mass, amu} \quad (3.71)$$

M_Y, M_X = Molecular mass of species Y and X respectively, amu (atomic mass units)

T = Gas temperature, $^{\circ}\text{K}$

If excitations of i from other excited levels q in molecule X have a good probability of occurring, then $(\bar{\sigma}_{jX})_i$ should be replaced by $(\bar{\sigma}_{jX})_i + \sum_q Z_q^{-1} \left[\exp\left(-\frac{\epsilon_q}{kT}\right) \right] w_q (\bar{\sigma}_{jq})_i$, where the sum over q extends over all excited states in the molecule X (except the ground state) and $w_q Z_q^{-1} \exp\left\{-(\epsilon_q)/(kT)\right\}$ is the population of excited states q (Z_q is the normalization constant for excitations q, w_q is the weight of state q, and ϵ_q is its energy level). Similarly if V-V transitions from other excited states s in molecule Y are important $(\bar{\sigma}_{Yi})_k$ must be replaced by $(\bar{\sigma}_{Yi})_k + \sum_s Z_s^{-1} \left[\exp\left(-\frac{\epsilon_s}{kT}\right) \right] w_s (\bar{\sigma}_{si})_k$ where the sum over s is over all excited states in molecule Y except the ground state. Usually however the first terms are sufficient.

The thermal production rate in Eq. (3.63) is:

$$\frac{\partial P_i}{\partial v} = \sum_Y n_Y v_{YX} (\bar{\sigma}_{YX})_i n_X, \quad \frac{\text{molecules}}{\text{m}^3 \cdot \text{sec}}, \quad (3.72)$$

in which:

$(\bar{\sigma}_{YX})_i$ = Average microscopic cross-section for inelastic kinetic excitation collisions* between species Y and X in which X is excited to state i, m^2

v_{YX} = Given by Eq. (3.70)

n_X, n_Y = Molecular densities of X and Y, m^{-3}

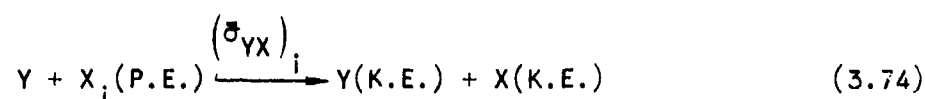
Similarly the thermal destruction rate in Eq. (3.63) is given by:

$$\frac{\partial L_i}{\partial v} = \sum_Y n_Y v_{YX} (\bar{\sigma}_{YX})_i n_i, \quad \frac{\text{molecules}}{\text{m}^3 \cdot \text{sec}}, \quad (3.73)$$

where the parameters are as defined before.

The difference between destruction rates (3.69) and (3.73) is that the cross-section $(\bar{\sigma}_{Yi})_k$ in (3.69) is restricted to interactions in which the molecule Y, after hitting excited molecule X_i , is excited to excited state Y_k . The cross-section $(\bar{\sigma}_{YX})_i$ of (3.73) on the other hand accounts for inelastic interactions between molecules Y and excited molecules X_i in which potential energy of X_i is converted to kinetic energy between outgoing molecules Y and X, that is by the "reaction":

*These interactions are also called V-T exchange collisions (V = Potential Energy; T = Kinetic Energy).



The photon-absorptive excitation and photon-stimulated deexcitation terms in (3.63) may be expressed by:

$$\frac{\partial C}{\partial u} = \int_{\lambda} \frac{dn_Y}{d\lambda} c \sigma_{Yi}(\lambda) n_X d\lambda, \quad \frac{\text{molecules } X_i}{\text{m}^3 \cdot \text{sec}}, \quad (3.75a)$$

and:

$$\frac{\partial B}{\partial u} = \int_{\lambda} \frac{dn_Y}{d\lambda} c \sigma_{iY}(\lambda) n_i d\lambda, \quad \frac{\text{molecules } X_i}{\text{m}^3 \cdot \text{sec}},$$

where:

$$\frac{dn_Y}{d\lambda} = \text{Photon density per unit wavelength range } d\lambda, \text{ photons}/(\text{m}^3 \cdot \mu\text{m})$$

$$c = \text{Velocity of light} = 3 \times 10^8 \text{ m/sec}$$

$$\sigma_{Yi}(\lambda) = \text{Absorption cross-section of photons of wavelength } \lambda \text{ by molecules } X \text{ resulting in their excitation to state } i, \text{ m}^2$$

$$\sigma_{iY}(\lambda) = \text{Stimulated deexcitation cross-section by photons of wavelength } \lambda \text{ for excited molecules } X_i \text{ resulting in their deexcitation, m}^2$$

The cascade production term $\partial F(X_i)/\partial u$ in (3.63) finally is given

by:

$$\frac{\partial F(X_i)}{\partial u} = \sum_k \frac{\partial E_{ki}}{\partial u}, \quad \frac{\text{molecules } X_i}{\text{m}^3 \cdot \text{sec}}, \quad (3.76)$$

June 1974

where E_{ki} is the net radiative decay of higher-lying states k that transition to i .

Now the theory of statistical mechanics shows that in a gas at equilibrium with the walls of an enclosure which is at uniform temperature T , one must have for each excited level i :

$$\frac{\partial P(X_i)}{\partial u} + \frac{\partial C(X_i)}{\partial u} + \frac{\partial F(X_i)}{\partial u} = \frac{\partial L(X_i)}{\partial u} + \frac{\partial D(X_i)}{\partial u} + \frac{\partial B(X_i)}{\partial u} \quad (3.77a)$$

Here we have neglected V-V resonance transfers for simplicity.

The collisional population and depopulation terms $\partial P(X_i)/\partial u$ and $\partial L(X_i)/\partial u$ in (3.77a) are many orders of magnitude larger than the molecule-radiation field interaction terms $\partial C(X_i)/\partial u$, $\partial F(X_i)/\partial u$, $\partial D(X_i)/\partial u$, and $\partial B(X_i)/\partial u$, for gases at ordinary temperatures and pressures. This can be verified by substitution of typical measured cross-sections and other microscopic parameters in expressions (3.67) through (3.76); the situation actually stems from the more generally recognized condition of "weak coupling" between radiation fields and matter. Because of weak coupling, one can write therefore that:

$$\frac{\partial P(X_i)}{\partial u} \approx \frac{\partial L(X_i)}{\partial u}, \quad (3.77b)$$

which states that in a region of uniform temperature T , the collisional excitation rate of excited level i must equal the collisional deexcitation of level i .

If a gas is flowing and not enclosed by a wall at uniform temperature, so that radiation can escape from it, the four radiation-field dependent

terms (C, F, D, and B) in (3.77a) will no longer balance each other. In regard to the terms P and L however, if the unit volume ∂u is taken small enough so that the temperature T in it may be considered constant, P and L will still balance. There is no physical reason to expect Eq. (3.77b) to change since there is no change in the molecular collision rates if the gas is at temperature T whether a radiation field is present or not. The condition (3.77b) applied to local regions in a non-stationary gas is often referred to as the LTE (= Local Thermodynamic Equilibrium) condition and we shall assume it in what follows.

In case of a steadily-emitting exhaust plume, one has that $\partial n_i / \partial t = 0$, and for small volume elements in the radiation core of the plume one may assume Eq. (3.77b) to apply. Thus according to (3.63) and (3.77b) one has in the radiating core of a steady-state plume that:

$$\frac{\partial G_i}{\partial u} + \frac{\partial R_i}{\partial u} + \frac{\partial C_i}{\partial u} + \frac{\partial F_i}{\partial u} = \frac{\partial D_i}{\partial u} + \frac{\partial S_i}{\partial u} + \frac{\partial B_i}{\partial u} \quad (3.78)$$

Now because one must have conservation of photons, the total radiative decay rate D_i of molecules X_i in the entire radiating core minus the net photon capture rate C'_i must equal the total photon emission rate E_i from level i, that is:

$$E_i = D_i - C'_i, \quad \frac{\text{photons}}{\text{sec}} \quad (3.79)$$

Here:

$$\begin{aligned} C'_i &\equiv C_i - B_i = \int_{\text{Potential Cone}} du \left[c \int_{\lambda} \frac{dn_Y}{d\lambda} \left\{ \sigma_{Yi} n_X - \sigma_{iY} n_i \right\} d\lambda \right] = \\ &= \int_{\text{Potential Cone}} du \int_{\lambda} \frac{dn_Y}{d\lambda} \left\{ 1 - \rho_i \right\} \sigma_{Yi} n_X d\lambda, \end{aligned} \quad (3.80)$$

June 1974

In which:

$$\rho_i = \frac{\sigma_{Yi}}{\sigma_{iY}} \frac{n_i}{n_X} = \frac{w_X}{w_{X_i}} \frac{n_i}{n_X} = \frac{1}{w_{X_i}} \frac{n_i}{n_X} \quad (3.81)$$

w_{X_i} = Degeneracy of excited state i of molecule X

w_X = 1 = Degeneracy of ground-state of molecule X

Here we used the well-known fact that the ratio of the photon absorption and stimulated emission cross-sections for transitions from a lower level n to a higher level m equals w_n/w_m (see Volume II, Rocket Radiation Handbook).

Usually $\rho_i \ll 1$, in which case (3.80) reduces to:

$$C'_i = C_i = \int_{\text{Radiating Core}} d\nu \int_{\lambda} \frac{dn_Y}{d\lambda} \sigma_{Yi}(\lambda) n_X d\lambda \quad (3.82)$$

Returning to Eqs. (3.78) and (3.79), we can write:

$$\begin{aligned} E_i &= \int_{\text{Radiating Core}} d\nu \left[\frac{\partial D_i}{\partial \nu} - (1 - \rho_i) \frac{\partial C_i}{\partial \nu} \right] = \\ &= \int_{\text{Radiating Core}} d\nu \left[\frac{\partial G_i}{\partial \nu} + \frac{\partial R_i}{\partial \nu} - \frac{\partial S_i}{\partial \nu} + \frac{\partial F_i}{\partial \nu} \right], \quad \frac{\text{photons}}{\text{sec}} \quad (3.83) \end{aligned}$$

From Eq. (3.64) and the application of Gauss' divergence theorem, we can write:

$$\begin{aligned}
 G_i &= \int_{\text{Radiating Core}} dV \left(\frac{\partial G_i}{\partial V} \right) = \int_{\text{Core}} dV \left[\vec{\nabla} \cdot n_i \vec{V}_i + \vec{\nabla} \cdot \mathcal{D}_i \vec{\nabla} n_i \right] = \\
 &= \int_{\text{Surface Boundary } C_e \text{ of Radiating Core}} d\vec{s} \cdot \left[n_i \vec{V}_i + \mathcal{D}_i \vec{\nabla} n_i \right], \quad \frac{\text{molecules}}{\text{sec}} \quad (3.84)
 \end{aligned}$$

Here:

$d\vec{s}$ = Unit surface area vector with a direction normal to the surface boundary of the enclosed volume over which the integration is to be carried out.

In nearly all exhaust plume situations, the molecular diffusion term $\mathcal{D}_i \vec{\nabla} n_i$ is small compared to the convective term $n_i \vec{V}_i$ in Eq. (3.84). Furthermore since the inflow of excited species X_i into the base of the radiating core takes place only through the nozzle exit plane of diameter D_e at velocity V_e it is clear that Eq. (3.84) can be rewritten as:

$$\left(G_i \right)_{\text{in}} = \int_{\text{Base of Radiating Core}} d\vec{s} \cdot n_i \vec{V}_i = \left(n_i \right)_{\text{Base of Radiating Core}} V_e \frac{\pi}{4} D_e^2, \quad \text{molecules } X_i / \text{sec} \quad (3.85)$$

Now the number of excited molecules X_i that cross the nozzle exit plane per unit time may be expressed in terms of the exhaust mass flow rate and the Boltzman factor. We have that:

$$\dot{W} = \rho_e V_e \frac{\pi}{4} D_e^2, \quad \frac{\text{kgms}}{\text{sec}} \quad (3.86)$$

June 1974

$$\dot{N} = \dot{W}/M_e = n_e V_e \frac{\pi}{4} D_e^2, \text{ molecules/sec} \quad (3.87)$$

$$y_X = n_X/n_e \quad (3.88)$$

$$(n_i)_{\text{Base of Core}} = \frac{n_X w_i}{Z_V} \exp\left(-\frac{\epsilon_i}{kT_e}\right), \quad \frac{\text{excited molecules}}{m^3} \quad (3.89)$$

Here:

y_X = Mole fraction of species X in exhaust

\dot{W} = Mass flow rate from exhaust-producing engine, $\frac{\text{kgms}}{\text{sec}}$

n_e = Density of exhaust gas in nozzle exit plane of diameter D_e , $\frac{\text{kgms}}{m^3}$

M_e = Average molecular weight of exhaust gases in nozzle exit plane, kgms

n_e = Molecular density of exhaust in nozzle exit plane, m^{-3}

w_i, ϵ_i = Statistical weight and energy, *respectively* of level i

Z_V = Partition or "sum-of-states" function (Normalization Constant) for internal molecular excitations

$$Z_V = \text{Vibrational partition function} = \left\{ 1 - \exp\left(-\frac{\epsilon_1}{kT_e}\right) \right\}^{-1} \quad (3.90)$$

The partition function (3.90) applies to molecular vibrational states only. This is usually the case of interest. For rotational and electronic excited states other expressions must be used (see Volume II, Rocket Radiation Handbook).

Using the relations (3.86) through (3.89) in Eqs. (3.85) finally yields:

$$\begin{aligned} (G_i)_{in} &= \frac{y_X \dot{W}}{M_e} \frac{w_i \exp\{-\epsilon_i/(kT_e)\}}{Z_V} = \\ &= 6.025 \times 10^{23} g_X \dot{W} \frac{w_i \exp\{-\epsilon_i/(kT_e)\}}{Z_V}, \quad \frac{\text{molecules}}{\text{sec}}, \end{aligned} \quad (3.91)$$

where for convenience we abbreviate:

$$g_X = \frac{y_X}{A_o M_e} = \frac{y_X}{A_o \sum_Y y_Y M_Y}, \quad \frac{\text{moles}}{\text{kgm}} \quad (3.92)$$

Here A_o is Avogadro's number and the partition function Z_V in (3.91) must be evaluated at $T=T_e$, that is $Z_V = Z_V(T_e)$.

Since by definition, molecules which have passed beyond the surface C_e (Figure 3-10) are "dead," we have that $(G_i)_{out} = 0$, and thus returning to Eq. (3.83), we can write with the aid of (3.91) and (3.76):

$$\begin{aligned} E_i &= \left\{ (G_i)_{in} - (G_i)_{out} \right\} + (R_i - S_i) + \sum_k E_{ki} = \\ &= 6.025 \times 10^{23} g_X \dot{W} \frac{w_i \exp\{-\epsilon_i/(kT_e)\}}{Z_V(T_e)} + (R_i - S_i) + \\ &+ \sum_k E_{ki}, \quad \frac{\text{photons emitted from states } i}{\text{second}} \end{aligned} \quad (3.93)$$

Equation (3.93) is a very important result and fundamental to all plume radiation calculations. It is an expression which simply asserts conservation of excited quanta. Though the result (3.93) was proven by a step-by-step mathematical analysis via Eqs. (3.63) through (3.93), it could also have been predicted directly if one applies the fundamental conservation law of physics to the quanta of excitation and radiation.

In Eq. (3.93) R_i is the net production rate of excited states i by V-V resonant transfer collisions and S_i is the net loss of excited species i by such V-V collisions. In many applications one has that $R_i = S_i = 0$, but for the case that special radiation-spectrum-shifting molecules* are present which cause a negative value of $R_i - S_i$ (thus a positive value for $\Delta S_i = S_i - R_i$), one may evaluate these terms further as follows. A mean V-V-transfer decay time for excited states i may be defined by:

$$\tau_{qi} = \left[\int du \left\{ \sum_k \sum_Y n_Y v_{YX} (\bar{\sigma}_{Yi})_k n_i - \sum_j n_j v_{jX} (\bar{\sigma}_{jX})_i n_X \right\} \right]^{-1}, \text{ sec}, \quad (3.94)$$

where the integration over du is over the volume of the radiating plume.

Then if τ_i is the radiative decay time, the fraction of molecules that experience V-V transfers will be:

$$f_{qi} = \tau_{qi}^{-1} / (\tau_{qi}^{-1} + \tau_i^{-1}) \quad (3.95)$$

*The overall effect from the presence of different V-V excitation-robbing molecules is that the excitation energy is redistributed over other quanta of excitation which ultimately are emitted as radiation in another (longer wavelength) part of the spectrum. We shall interchangeably call such molecules "suppressants" or "spectrum-shifters," since they do suppress the radiation in one part of the spectrum but also shift this radiation to another wavelength region.

We can write therefore:

$$\Delta S_i = - (R_i - S_i) = \left\{ (G_i)_{in} - (G_i)_{out} \right\} \left\{ \frac{\tau_{qi}^{-1}}{\tau_{qi}^{-1} + \tau_i^{-1}} \right\} \quad (3.96)$$

Then Eq. (3.93) for level i may be rewritten:

$$E_i = \sum_j E_{ij} = 6.025 \times 10^{23} g_X \dot{W} \left\{ \frac{w_i \exp(-\epsilon_i/kT_e)}{Z_V} \right\} \left\{ \frac{\tau_i^{-1}}{\tau_i^{-1} + \tau_{qi}^{-1}} \right\} +$$

$$+ \sum_k E_{ki} , \frac{\text{photons emitted from state i}}{\text{second}} \quad (3.97a)$$

Similarly we have for level k:

$$E_k = \sum_i E_{ki} = 6.025 \times 10^{23} g_X \dot{W} \left\{ \frac{w_k \exp(-\epsilon_k/kT_e)}{Z_V} \right\} \left\{ \frac{\tau_k^{-1}}{\tau_k^{-1} + \tau_{qk}^{-1}} \right\} +$$

$$+ \sum_m E_{mk} , \frac{\text{photons emitted from state k}}{\text{second}} , \quad (3.97b)$$

and so on for all levels l, m, p, \dots of interest. The levels j in (3.97a) and i in (3.97b) must of course be levels that are lower in energy than respectively levels i and k , and also they must be such that radiative transitions $i \rightarrow j$ and $k \rightarrow i$ are allowed. As mentioned, in many applications $\tau_{qi} = \infty$ and $\tau_{qk} = \infty$, in which case the terms $\tau_i^{-1}/(\tau_i^{-1} + \tau_{qi}^{-1})$ and $\tau_k^{-1}/(\tau_k^{-1} + \tau_{qk}^{-1})$ in (3.97a) and (3.97b) equal unity.

June 1974

Writing for convenience:

$$G'_i = 6.025 \times 10^{23} g_X \dot{w} \frac{w_i \exp\{-\epsilon_i/(kT_e)\}}{Z_V} \left\{ \frac{\tau_i^{-1}}{\tau_{qi}^{-1} + \tau_i^{-1}} \right\}, \quad (3.97c)$$

Eqs. (3.97a) and (3.97b) can be written in the form:

$$E_i = G'_i + \sum_k f_{ki} \left[G'_k + \sum_m f_{km} \left\{ G'_m + f_{mn} \sum_n (G'_n + \dots) \right\} \right] \quad (3.97d)$$

In what follows, we shall first examine the sum (3.97d) for vibrational transitions. Neglecting $\Delta v = 2$ transitions (which are much weaker than $\Delta v = 1$ transitions - see Vol. II) and anharmonic effects, the sum in (3.97d) reduces for diatomic molecules to:

$$\begin{aligned} (E_i)_{\text{vib.}} &= G'_i + G'_k + G'_m + G'_n + \dots = \\ &= \sum_{n=1}^{\infty} G'_i \approx 6.025 \times 10^{23} g_X \dot{w} \left\{ \frac{\tau_i^{-1}}{\tau_{qi}^{-1} + \tau_i^{-1}} \right\} \cdot \\ &\cdot \left\{ 1 - \exp\left(-\frac{h\nu_0}{kT_e}\right) \right\} \sum_{n=1}^{\infty} \exp\left(-\frac{nh\nu_0}{kT_e}\right) \end{aligned} \quad (3.97e)$$

since for diatomic molecules:

$$w_i = w_n = 1$$

$$\epsilon_i = h\nu_i \approx h\nu_0 \text{ (anharmonic terms neglected)}$$

$$\nu_0 = \text{Fundamental vibrational frequency}$$

$$f_{ij} = 1 \text{ for } \Delta v = 1 \text{ transitions (see Eq. (3.101))}$$

$$(Z_V)_{\text{vib.}} = \sum_{n=0}^{\infty} \exp\left(-\frac{nh\nu_0}{kT_e}\right) = \frac{1}{1 - \exp(-h\nu_0/kT_e)} = [1 - u^{-1}]^{-1}$$

and the sum in (3.97e) can be shown to equal:

$$\Sigma_i = \sum_{n=1}^{\infty} u^{-n} = \frac{u}{u-1} = \frac{1}{1-u^{-1}} \quad (3.97f)$$

where $u = \exp\{(h\nu_0)/(kT_e)\}$. The factor $\{\tau_i^{-1} + \tau_{qi}^{-1}\}$ in the summation (3.97e) is constant to first order (i.e., anharmonicity is neglected), since in this case all $\tau_i = \tau_j = \tau_k = \dots$ and $\tau_{qi} = \tau_{qj} = \tau_{qk} = \dots$. Carrying out the summation using (3.97f), one obtains then that:

$$(E_i)_{\text{vib.}} = 6.025 \times 10^{23} g_X \dot{W} \left\{ \exp\left(-\frac{h\nu_0}{kT_e}\right) \left\{ \frac{\tau_i^{-1}}{\tau_i^{-1} + \tau_{qi}^{-1}} \right\} \right. , \quad \left. \frac{\text{photons emitted from level } i}{\text{second}} \right\} \quad (3.97g)$$

June 1974

The same result (3.97g) is obtained for polyatomic molecules if again all second-order (weaker) $\Delta v_\alpha \neq 1$ and combination-band transitions are neglected in comparison with $\Delta v_\alpha = 1$ transitions for all the normal vibrations α (with fundamental frequency ν_α), and if degenerate vibrations are treated mathematically as independent normal vibrations which happen to have the same frequency (see Vol. II, Rocket Radiation Handbook).

For pure rotational transitions, Eqs. (3.97c) or (3.97d) becomes:

$$(E_i)_{\text{rot}} = 6.025 \times 10^{23} g_X \dot{W} \frac{\tau_J^{-1}}{\tau_J^{-1} + \tau_{qJ}^{-1}} \sum_{J'=J}^{\infty} \frac{(2J'+1) \exp\left\{-J'(J'+1) \frac{h\nu_B}{kT_e}\right\}}{(Z_V)_{\text{rot}}} =$$

(i=J)

$$\approx 6.025 \times 10^{23} g_X \dot{W} \frac{\tau_J^{-1}}{\tau_J^{-1} + \tau_{qJ}^{-1}} \frac{(Z_V)_{\text{rot}} - \int_{J'=0}^J \left\{ \exp\left(-m^2 \frac{h\nu_B}{kT_e}\right) \right\} d(m^2)}{(Z_V)_{\text{rot}}}$$

$$(E_i)_{\text{rot}} = 6.025 \times 10^{23} g_X \dot{W} \left[\exp\left\{-J(J+1) \frac{h\nu_B}{kT_e}\right\} \right] \left\{ \frac{\tau_J^{-1}}{\tau_J^{-1} + \tau_{qJ}^{-1}} \right\}$$

(i=J)

$$, \quad \frac{\text{photons from level } i=J}{\text{second}}, \quad (3.97h)$$

where τ_J is the mean radiative life of rotational level J and (see Rocket Radiation Handbook, Vol. II):

$$(Z_V)_{\text{rot}} = \frac{h\nu_B}{kT_e} + \frac{1}{3} + \frac{1}{15} \frac{kT}{h\nu_B} + \dots \approx \frac{h\nu_B}{kT_e} \quad (3.97i)$$

The result (3.97h) is the same as (3.97g) if we set $\epsilon_i = ih\nu_0$ and $\epsilon_i = J(J+1) h\nu_B$ respectively for the vibrational and rotational case. For electronic transitions, $(Z_V)_{elc} \approx 1$, and the value of the sum of Boltzmann factors of higher-lying states ($k > i$) is small compared to the Boltzmann factor for the state i of interest. Thus again an equation like (3.97h) and (3.97g) results and we shall assume without further proof that in general:

$$E_i = 6.025 \times 10^{23} g_X \dot{w} \left\{ \frac{\tau_i^{-1}}{\tau_i^{-1} + \tau_{qi}^{-1}} \right\} \left\{ \exp\left(-\frac{\epsilon_i}{kT_e}\right) \right\},$$

, $\frac{\text{photons emitted from level } i}{\text{second}}$,

(3.97j)

where ϵ_i is the energy level of an excited rotational, vibrational, or electronic state. Note that the statistical weight w_i of level i and the partition function Z_V are not factors in (3.97j).

Now the photons emitted from state i will in general have energies $\epsilon_{yi} = \epsilon_{ij} = h\nu_{ij}$ where j is a lower-lying energy state to which the molecule X_i relaxes. If the transition is "ground-state-connected," we have of course that:

$$\epsilon_{yi} = h\nu_{yi} = h\nu_{ij} = \epsilon_{ij} = \epsilon_i = h\nu_i, \quad (3.98)$$

since in this case $j = 0$ and $\epsilon_{i=0} = 0$ is usually assumed.

The photons are not all emitted with "sharp" energies $\epsilon_{yi} = \epsilon_{ij}$, but are "broadened" over a range of frequencies in the immediate vicinity of $h^{-1}\epsilon_{ij}$. The various frequency broadening processes are discussed in detail

June 1974

in Volume II of the Rocket Radiation Handbook. It is shown there that the number of photons $N_{\gamma i}$ emitted in frequency range $d\nu$ is given by:

$$\frac{d^2 N_{\gamma i}}{dt d\nu} = \left(\frac{dN_{\gamma i}}{dt} \right) \frac{b(\nu, \nu_{ij}, \Delta\nu_{ij})}{\Delta\nu_{ij}} = E_{ij} \frac{b(\nu, \nu_{ij}, \Delta\nu_{ij})}{\Delta\nu_{ij}} \quad (3.99)^*$$

where $b(\nu, \nu_{ij}, \Delta\nu_{ij})$ is the so-called line- or band-shape function, and $\Delta\nu_{ij}$ is the line- or band-spread for the transitions $i \rightarrow j$, while $(dN_{\gamma i}/dt) = E_{ij}$ for an exhaust plume. Explicit expressions for the functions $b(\nu, \nu_{ij}, \Delta\nu_{ij})$ and $\Delta\nu_{ij}$, which depend on gas temperature (and gas pressure in the case of single lines), are given in Volume II for the three cases of (a) electronic, (b) vibrational, and (c) rotational transitions.

With the aid of (3.99) and (3.97j), the total photonic energy emitted per unit time and per unit frequency range at the general photon frequency ν may be written:

$$\begin{aligned} \frac{dP(\nu)}{d\nu} &= h\nu \sum_X \sum_i \sum_j (E_i)_X f_{ij} \frac{b(\nu, \nu_{ij}, \Delta\nu_{ij})}{\Delta\nu_{ij}} = \\ &= 3.9917 \times 10^{-10} \dot{W}_\nu \sum_i \sum_j g_i f_{ij} \cdot \\ &\cdot \left\{ \frac{b(\nu, \nu_{ij}, \Delta\nu_{ij})}{\Delta\nu_{ij}} \right\} \left\{ \frac{\tau_i^{-1}}{\tau_i^{-1} + \tau_{qi}^{-1}} \right\} \left\{ \exp - \frac{\epsilon_i}{kT_e} \right\}, \text{ Watts Hz}^{-1} \quad (3.100)^* \end{aligned}$$

*The temperature-dependent (and sometimes pressure-dependent) parameter $\Delta\nu_{ij}$ must be evaluated at a mean temperature (and mean pressure) in the core of the plume, since the actual temperature- or pressure-perturbed transition $i \rightarrow j$ resulting in a photon, takes place at various positions in the plume. A coarse approximation would be $T_C \approx \frac{2}{3} T_g$ for DSPR radiation (see also Vol. IV). T_C is constant and independent of altitude for DSPR of course.

Here we set $g_{X_i} \equiv g_i$, while $h = 6.6252 \times 10^{-34}$ Joules/Hz, \dot{W} is in kg/sec, and all frequencies ν are in Hz. The relative deexcitation rate parameter f_{ij} is given by:

$$f_{ij} = \frac{A_{ij}^0}{\sum_j A_{ij}^0} \quad (3.101)$$

where A_{ij}^0 is the Einstein coefficient for a $i \rightarrow j$ transition, whose value can be obtained for a particular case from the relations presented in Volume II of the Rocket Radiation Handbook.

Now for vibrational transitions (but not for rotational or electronic transitions), the band center frequencies ν_{ij} for all the $\Delta v = 1$ transitions $\nu_i = 5 \rightarrow \nu_j = 4$, $\nu_i = 4 \rightarrow \nu_j = 3$, etc., are almost the same except for small anharmonic shifts. Thus the vibrational emission bands (comprising in general P-, Q-, and R-branches — see Vol. II) from these transitions practically overlap except for these small anharmonic shifts. If we use the vibrational band contour function $b_v(\nu, \nu_{ij}, \Delta \nu_{ij}) / \Delta \nu_{ij}$ in Eq. (3.100) which assumes that the rotational lines in the band are smeared out anyway, we can simply set all ν_{ij} in Eq. (3.100) equal to $\nu_{ij} = \nu_\alpha$ and $\epsilon_i = i h \nu_\alpha$. Then:*

*If higher resolution spectral emissions are desired, Eq. (3.100) must be used, except that for vibrational transitions $f_{ij} \approx 1$ may be assumed so that the summation over j can be omitted. The more detailed rovibrational contour function $b_{rov}(\nu, \nu_{ij}, \Delta \nu_{ij})$ given in Volume II must be used in this case instead of $b_v(\nu, \nu_{ij}, \Delta \nu_{ij})$, and the anharmonic shifts $\Delta_i = \nu_{ij} - \nu_\alpha$ must be calculated which may be done via relations given in Volume II.

June 1974

$$\left(\frac{dP}{d\nu}\right)_{\text{vib.}} = 3.9917 \times 10^{-10} \dot{W} \nu \sum_{\alpha} g_{\alpha} \left\{ \frac{\tau_{\alpha}^{-1}}{\tau_{\alpha}^{-1} + \tau_{q\alpha}^{-1}} \right\} \cdot$$

$$\cdot \left\{ \frac{b_{\nu}(\nu, \nu_{\alpha}, \Delta\nu_{\alpha})}{\Delta\nu_{\alpha}} \right\} \left\{ \frac{\exp\left(-\frac{h\nu_{\alpha}}{kT_e}\right)}{1 - \exp\left(-\frac{h\nu_{\alpha}}{kT_e}\right)} \right\}, \frac{\text{Watts}}{\text{Hz}} \quad (3.102)^*$$

Here the summation is over the various normal vibrations α with fundamental frequency ν_{α} of various molecules X but not over the levels of a certain normal vibration. (Note that for polyatomic molecules such as H_2O for example, $(g_{H_2O})_{\alpha=1} = (g_{H_2O})_{\alpha=2} = (g_{H_2O})_{\alpha=3} = g_{H_2O}$.)

In some applications, it is desirable to express the spectral radiant intensity in terms of wavelength λ instead of frequency ν . Since

$$\nu = c\lambda^{-1}, \quad (3.103a)$$

$$d\nu = -\frac{c}{\lambda^2} d\lambda = \nu \frac{d\lambda}{\lambda}, \quad (3.103b)$$

where $c = 2.94793 \times 10^{14} \mu\text{m/sec}$, we can rewrite the general equation (3.100) in the form (we include summations over species X in the summation i , that is $g_{X1} = g_i$):

*See footnote to Eq. (3.100).

$$\begin{aligned}
 \frac{dP(\lambda)}{d\lambda} &= \frac{dP}{dv} \frac{dv}{d\lambda} = \frac{3.5876 \times 10^{19}}{\lambda^3} \sum_i \sum_j f_{ij} g_i \left(\frac{b(v, v_i, \Delta v_i)}{\Delta v_i (\text{Hz})} \right) \cdot \\
 &\quad \cdot \left\{ \exp\left(-\frac{s_i}{kT_e}\right) \right\} \left\{ \frac{\tau_i^{-1}}{\tau_i^{-1} + \tau_{qi}^{-1}} \right\}, \quad \frac{\text{Watts}}{\mu\text{m}} \quad (3.104)^*
 \end{aligned}$$

Equations (3.100), (3.102), or (3.104) give the total spectral emission from the exhaust plume which escapes through the surface C_e (see Figure 3-10). The amount of radiation that is observed by a sensor viewing the plume depends of course on the field-of-view (fov) of the sensor, the angle between the plume axis and the sensor's viewing direction, and the range or distance between sensor and plume. If the photon density or fluence distribution in the dense region of the plume were constant, the leak rate of photons leaving the surface of the plume would also be constant, and in that case the number of photons sensed by an observer would only depend on the geometry of the plume and the intersection of the fov with the plume.

The theory of photon distributions inside exhaust gas plumes and clouds termed "photonics," is discussed in Volume III of the Rocket Radiation Handbook. An investigation of the photonics in rocket plumes shows that the assumption of a constant photon fluence (and thus a constant emission current) at the boundaries of the optically dense core region of a plume is reasonable for first-order calculations. This means that three-dimensional

*See footnote to Eq. (3.100).

June 1974

viewing-geometry-dependent variations in the radiant intensity as observed by a distant sensor can be expressed via a simple view factor F_v . Equations for F_v are discussed in detail in Appendix C for various plume geometries (sphere, cylinder, and cone). F_v is normalized there to $F_v = 1$ for isotropic $\frac{1}{4\pi}$ plume emission. Note that the assumption of a constant photon fluence near the surface of a radiation-containing body is precisely the condition that makes the body a "diffuse" emitter (following the "cosine law").

Actually for a deep-space rocket plume, the optically dense, diffusely emitting core region is surrounded by an optically thin emitting region (particularly in the rearward direction) where the photon fluence is no longer constant and where emission is isotropic instead of diffuse. Thus a blend of both diffusely and isotropically emitted radiation will be received by a sensor that views a deep-space rocket plume. Nevertheless, since most radiation usually emanates from the optically dense core, the use of a view factor F_v based on the assumption that the entire plume emits diffusely, usually gives sufficiently accurate results for most cases of interest. View factors for isotropically emitting, optically thin gas clouds and for hybrid cases are discussed in Volumes III and IV of the Rocket Radiation Handbook and may be used in cases that the assumption of diffuse emission is totally invalid. Of course experimentally derived view factors F_v can also be employed if available.

Another factor that must be taken into account before we can write a final radiation equation, is the atmospheric transmission $Tr = Tr(v, S)$. This applies in the case that atmosphere is present between the sensor and the rocket plume, causing the radiation to be partially absorbed or scattered as it travels a distance S from the plume to the sensor. $Tr(v, S) = 1$

of course if there is no intervening atmosphere. Volume V of the Rocket Radiation Handbook gives expressions of $Tr(\nu, S)$ for various portions of the spectrum.

Returning to Eqs. (3.100) and (3.102) then, and adding a view factor and transmission factor, the view-dependent radiant intensity as observed by a sensor may be expressed by:

$$\left(\frac{dJ(\nu)}{d\nu} \right)_{\text{DSR}} = \frac{d^2 P(\nu)}{d\nu d\Omega} = \frac{F_v}{4\pi} \frac{dP(\nu)}{d\nu} = 31.765 \times 10^{-11} \dot{W} \nu Tr(\nu, S) F_v \cdot$$

$$\cdot \sum_i \sum_j g_i f_{ij} \left[\frac{b(\nu, \nu_{ij}, \Delta\nu_{ij})}{\Delta\nu_{ij}} \right] \left[\exp\left(-\frac{\epsilon_i}{kT_e}\right) \right] \left[\frac{\tau_i^{-1}}{\tau_i^{-1} + \tau_{qi}^{-1}} \right],$$

$$, \quad \frac{\text{Watts}}{\text{ster} \cdot \text{THz}},$$

$$(\nu, \Delta\nu_{ij} = \text{THz})$$

(3.105)*

where $Tr(\nu, S) = 1$ outside the earth atmosphere, and $F_v = 1$ for a spherically symmetric emitting plume. In Eq. (3.105), ν and $\Delta\nu_{ij}$ are in THz ($= 10^{12}$ Hz) which is a more natural unit than the Hz in the optical region of the spectrum. In many approximate analyses, one might set $F_v \approx 1$, if the plume geometry is not accurately known.

Similarly Eq. (3.104) becomes:

*See footnote to Eq. (3.100).

$$\frac{dJ(\lambda)}{d\lambda} = 2.8549 \times 10^8 \left(\frac{\dot{W}}{\lambda^3 (\mu m)} \right) \cdot Tr(\lambda, S) \cdot F_v \cdot \sum_i \sum_j g_i f_{ij} \left(\frac{b(\lambda, \lambda_{ij}, \Delta v_{ij})}{\Delta v_{ij} (THz)} \right) \cdot \left[\exp\left(-\frac{\epsilon_i}{kT_e}\right) \right] \cdot \left\{ \frac{\tau_i^{-1}}{\tau_i^{-1} + \tau_{qi}^{-1}} \right\}, \frac{\text{Watts}}{\mu m \cdot \text{ster}}$$

(3.106)*

Equations (3.105) and (3.106) give the spectral steradiancies of deep-space rocket plumes in any desired part of the spectrum. To use these relations, one has to know only the rocket mass flow rate \dot{W} , the exit temperature T_e , and the exhaust species composition $g_i = g_{X_i} = g_X$.** Once the spectral region of interest is specified, expressions for $b(v, v_i, \Delta v_i)$ and for Δv_i can be written from the relations given in Volume II. To get the total steradiance for a certain portion of the wavelength spectrum, one can of course simply integrate Eqs. (3.105) or (3.106) numerically (or analytically if the expressions for $b(v, v_i, \Delta v_i)$, etc., allow it) over the spectral range of interest.

In Eqs. (3.105) and (3.106), all plume geometry effects are contained in the view factor F_v , which is on the order of 1. This formulation is clearly much simpler (and also more accurate) than that developed in other approaches (see for example Ref. 14) where plume geometry is first

*See footnote to Eq. (3.100).

**In the sum over excited states i in Eqs. (3.105) and (3.106), many of the g_i have the same value. For example H_2O has three vibrational infrared-active levels, which we might label $i = 1$, $i = 2$, and $i = 3$. Then $g_1 = g_2 = g_3$. The index $i = 4$ might be assigned to the vibrational level of CO , and thus $g_4 \neq g_3$, etc.

calculated from an approximate theoretical aerodynamics model and then the radiation emitted by small volume elements in the plume summed over the entire plume. Approximate averaged values for gas self-absorption and emission factors are further used to account for intervening gas between the observer and the volume elements.

The relations developed above are for a steadily burning rocket. If the rocket ceases burning, the source term $G(X_i)$ in (3.63) drops out, and if we assume the terms $R(X_i)$, $S(X_i)$, and $B(X_i)$ to be negligibly small (we may still assume $P(X_i) = L(X_i)$ under LTE conditions), we get:

$$\begin{aligned} \frac{\partial N(X_i)}{\partial t} &\equiv \frac{\partial N_i}{\partial t} = D(X_i) + C(X_i) = \\ &= \int_{\lambda} \left[-\frac{dA_i}{d\lambda} N_i + N_X \frac{dn_Y}{d\lambda} c \sigma_{Yi} \right] d\lambda = -p_i A_i^0 N_i \quad (3.107)^* \end{aligned}$$

Here $N_i \equiv N(X_i)$ is the total number of i -excited X molecules in the plume, N_X is the total number of X molecules, and p_i is the probability for photons emitted from excited molecular level i to escape from the plume. Expressions for the escape probability p_i of photons of wavelength λ close to $\lambda_i = c h / \epsilon_i$ are given in Volume III of the Rocket Radiation Handbook. The equality of the last two members of (3.107) is also discussed in Volume III.

The solution of (3.107) is of course simply:

$$N_i(t') = N_i(t'=0) \exp(-(p_i A_i^0 t')) \quad (3.108)$$

*As shown in Volume II, we have $dA_i/dv = A_i^0 \sum_j (f_{ij}/\Delta v_{ij}) b(v, v_{ij}, \Delta v_{ij})$.

June 1974

where t' is measured from the moment of rocket thrust cessation, and $N_i(t'=0)$ equals the total number of i -excited X molecules before thrust cessation. Since J and $dJ/d\lambda$ are proportional to $\sum_i N_i$, we have that:

$$\left(\frac{dJ}{d\lambda}\right)_{t'} = \sum_i \left(\frac{dJ_i}{d\lambda}\right)_{t'=0} \exp(-p_i A_i^0 t') \quad (3.109)$$

where $\left(\frac{dJ_i}{d\lambda}\right)_{t'=0}$ refers to the steradian due to emissions from the i -th level only (Eq. (3.106) with the summation sign over i omitted) at time $t' = 0$.

The escape probability parameter p_i is unity for an optically thin plume and becomes small for an optically thick plume. It depends in a complicated way on plume geometry, plume temperature and pressure, and other parameters (see Volume III).

From the results we obtained above, it is clear that for a steadily burning rocket, the radiant emission is in first approximation independent of whether the plume is optically thick or thin (except for the view factor). That is whether a photon released from level i in the plume is reabsorbed and reemitted 1000 times on the average before it escapes from the plume, or whether it experiences absorption and reemission 10 times is of no consequence to the total outgoing photon current that leaves the plume as long as the supply rate and decay rate of excited levels are balanced, that is under steady-state operating conditions. The photon eventually escapes the plume and its average hold-up time in the plume is not important.

When the supply rate of i -excited molecules is suddenly stopped however, the radiance $dJ/d\lambda$ will decay exponentially with time, and now the

average resistance for a photon to escape or the average hold-up time does become important, and is incorporated in the escape parameter p_i . The calculation of p_i for various plume geometries is given in Volume III.

3.3.3 Undisturbed Core or Mach Cone Radiation (CORE)

When a rocket engine exhausts into the atmosphere, the plume radiation can no longer be treated quite as simply as in the case of a discharge into the vacuum of deep-space, because of the interaction of the exhaust with the ambient atmosphere. In this case it is necessary to consider separately the radiation emitted from (a) the undisturbed core region of the plume, (b) the mixing region of the plume, and (c) the slowed-down exhaust cloud which is left in the atmosphere (see Chapter 2).

As discussed in sections 2.3 and 2.4, CORE or Mach Cone radiation is essentially due to radiative deexcitations beyond the rocket nozzle of molecules which were originally thermally excited inside the high-temperature rocket chamber. However only those deexcitations which occur in the "Undisturbed Core" or "Mach Cone" as shown in Figures 3-11 and 3-12 (see also Figure 2-1) will be considered to contribute to CORE radiation*. Outside this region the molecules are reheated due to collisions with molecules from the atmosphere. This requires separate consideration and will be treated in the next section.

Clearly the total radiation from the core is equal to that emitted by the exhaust in deep space (DSPR), minus an amount that would have been emitted by still-excited molecules that travel beyond the core region boundary into the mixing region. If one can calculate therefore the mean dwell time τ_M of molecules in the Mach Cone region and one knows the mean radiative

*The terms "Mach Core" and "Mach Cone" will be used interchangeably from here on.

June 1974

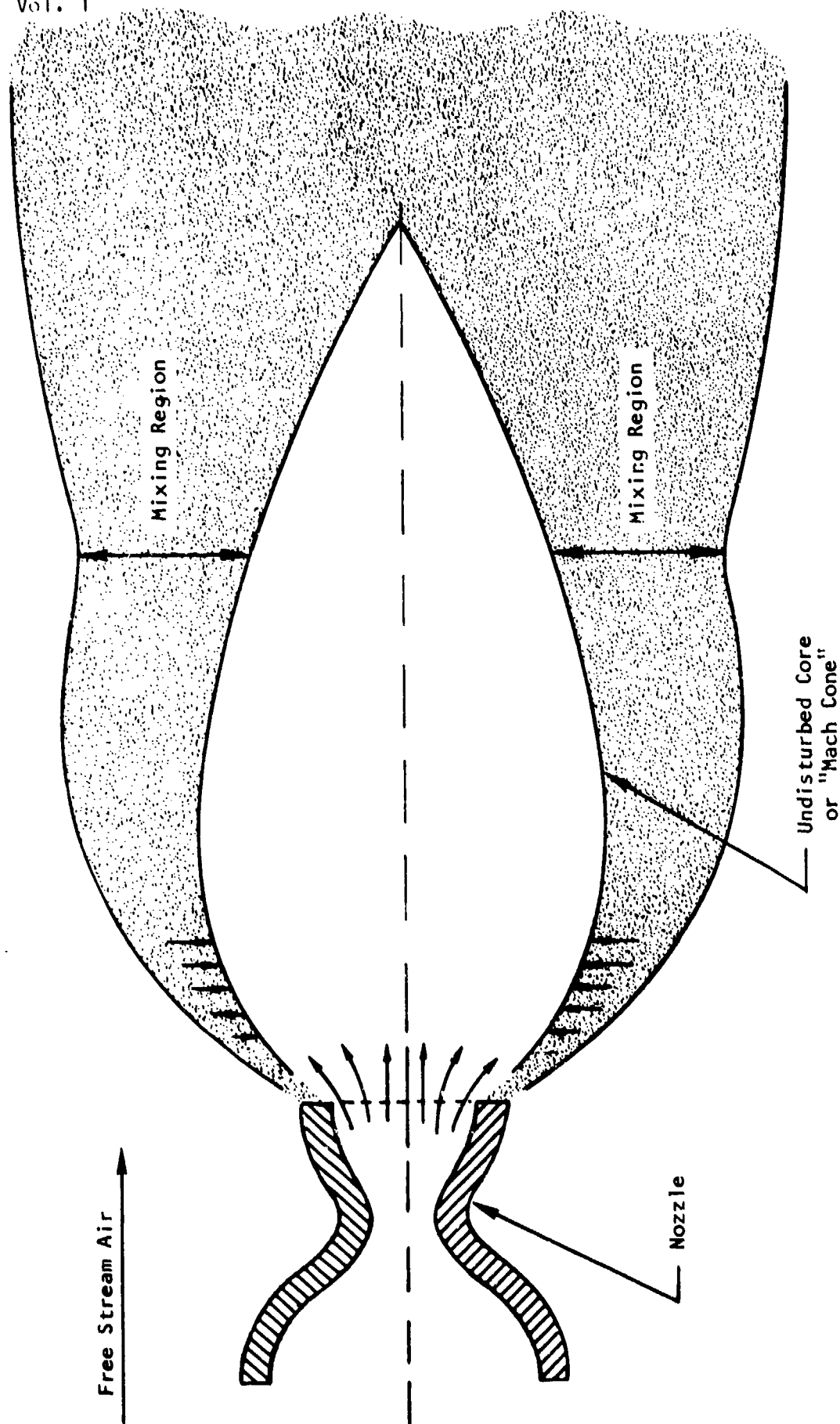


FIGURE 3-11. ILLUSTRATION OF CORE REGION OF MEDIUM-ALTITUDE ROCKET EXHAUST FLOW FIELD
(See also Schlieren photographs of Figures 47 to 49 of Ref. 36)

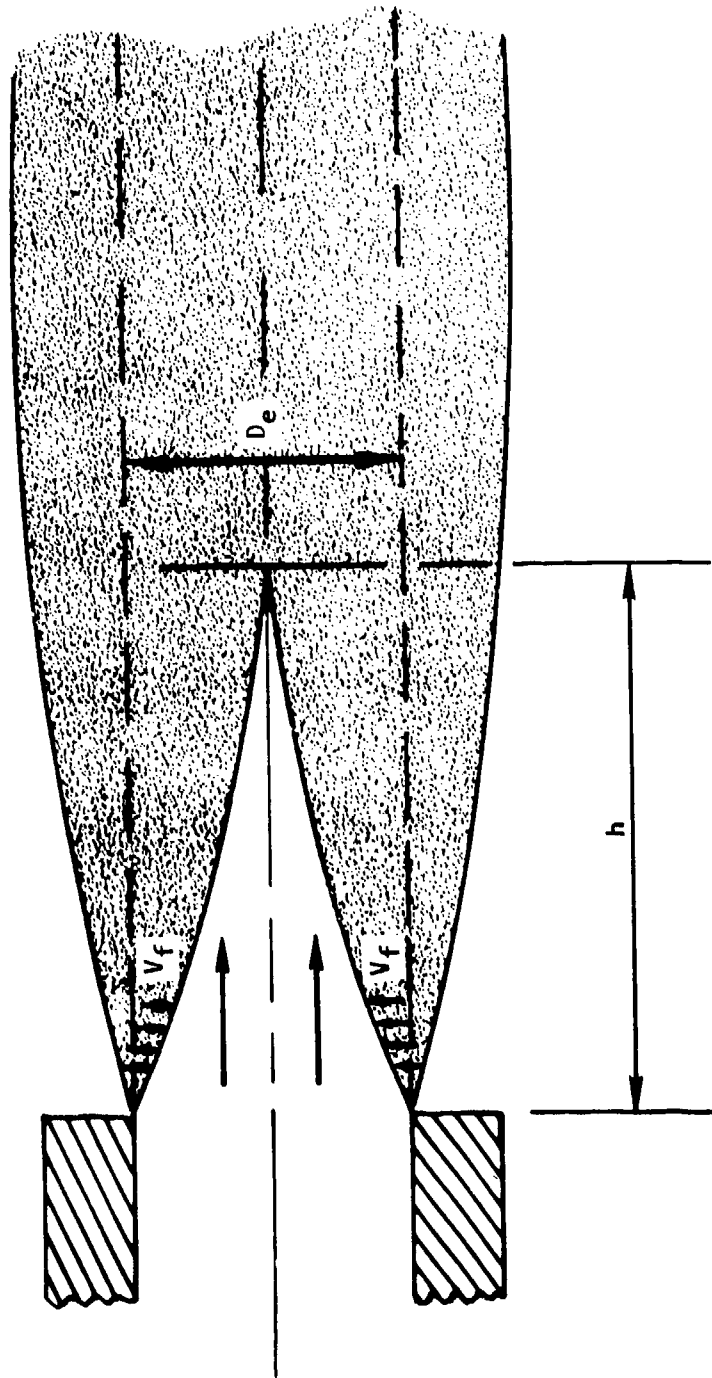


FIGURE 3-12. ILLUSTRATION OF DIFFUSION FRONT PENETRATION INTO HYPOTHETICAL STRAIGHT-CYLINDER JET

emission time τ_i and suppressant transfer time τ_{qi} (see Eq. (3.94)), one can obtain the total radiation emitted from level i from the CORE region, by multiplying the solution for the DSPR case by the non-survival fraction F_i of excitations i in the core:

$$F = 1 - \exp\left(-\frac{\tau_M}{(\tau_i^{-1} + \tau_{qi}^{-1})^{-1}}\right) \quad (3.110)$$

The radiative decay time τ_i must be used in (3.110) and not the collisional mean life of an excited level i of a molecule, since according to LTE, the collisional excitation rate equals the collisional deexcitation rate everywhere in the core (see the previous section) and therefore the net radiative decay time of level i for the bulk flow is τ_i . Often τ_i^{-1} is zero in (3.110).

The total radiation emitted from the CORE region is thus given by:

$$\begin{aligned} \left(\frac{dP(\nu)}{d\nu}\right) &= 3.9917 \times 10^{-10} \dot{W} \nu \cdot \sum_i \sum_j g_i f_{ij} \left[\frac{b(\nu, \nu_{ij}, \Delta\nu_{ij})}{\Delta\nu_{ij}} \right] \cdot \\ &\cdot \left[\exp\left(-\frac{e_i}{kT_e}\right) \right] \left[\frac{\tau_i^{-1}}{\tau_i^{-1} + \tau_{qi}^{-1}} \right] \left[1 - \exp\left(-\frac{\tau_M}{(\tau_i^{-1} + \tau_{qi}^{-1})^{-1}}\right) \right], \quad \frac{\text{Watts}}{\text{Hz}} \quad (3.111) \end{aligned}$$

or in terms of wavelengths:

$$\begin{aligned} \left(\frac{dP(\lambda)}{d\lambda}\right) &= 3.5876 \times 10^{19} \left(\frac{\dot{W}}{\lambda^3(\mu m)}\right) \cdot \sum_i \sum_j g_i f_{ij} \left[\frac{b(\lambda, \nu_{ij}, \Delta\nu_{ij})}{\Delta\nu_{ij}(\text{Hz})} \right] \cdot \\ &\cdot \left[\exp\left(-\frac{e_i}{kT_e}\right) \right] \left[\frac{\tau_i^{-1}}{\tau_i^{-1} + \tau_{qi}^{-1}} \right] \left[1 - \exp\left(-\frac{\tau_M}{(\tau_i^{-1} + \tau_{qi}^{-1})^{-1}}\right) \right], \quad \frac{\text{Watts}}{\mu m} \quad (3.112) \end{aligned}$$

In applications where one deals with ground-state connected transitions, $j = 0$ and $f_{ij} = 1$ so that the summation over j is unnecessary.

Equations (3.111) or (3.112) now contain a strong altitude-dependent parameters, namely τ_M (and a weaker one, Δv_{ij}). This is in contrast to the DSPR equations which were free of altitude-dependent factors, except for the view factor F_V . Equations (3.111) and (3.112) still must be multiplied by the view factor $F_V/4\pi$ and the transmission factor $Tr(v)$ to obtain the direction-dependent steradian. Thus (using units of THz for v and Δv_{ij}):

$$\left(\frac{dJ(v)}{dv} \right)_{\text{CORE}} = 31.765 F_V Tr(v) \frac{\dot{W}}{(\text{kg/s})} \frac{v}{(\text{THz})} \cdot \sum_i \sum_j g_i f_{ij} \left[\frac{b(v, v_{ij}, \Delta v_{ij})}{\Delta v_{ij} (\text{THz})} \right] \cdot \left[\exp\left(-\frac{\epsilon_i}{kT_e}\right) \right] \left[\frac{\tau_i^{-1}}{\tau_i^{-1} + \tau_{qi}^{-1}} \right] \left[1 - \exp\left(-\frac{\tau_M}{(\tau_i^{-1} + \tau_{qi}^{-1})^{-1}}\right) \right], \frac{\text{Watts}}{\text{ster} \cdot \text{THz}}$$

(3.113)

$$\left(\frac{dJ(\lambda)}{d\lambda} \right)_{\text{CORE}} = 2.8549 \times 10^6 \left(\frac{\dot{W}}{\lambda^3 (\mu\text{m})} \right) F_V Tr(\lambda) \cdot \sum_i \sum_j g_i f_{ij} \left[\frac{b(\lambda, \lambda_{ij}, \Delta v_{ij})}{\Delta v_{ij} (\text{THz})} \right] \cdot \left[\exp\left(-\frac{\epsilon_i}{kT_e}\right) \right] \left[\frac{\tau_i^{-1}}{\tau_i^{-1} + \tau_{qi}^{-1}} \right] \left[1 - \exp\left(-\frac{\tau_M}{(\tau_i^{-1} + \tau_{qi}^{-1})^{-1}}\right) \right], \frac{\text{Watts}}{\text{ster} \cdot \text{THz}}$$

(3.114)

Expressions for the molecular spectrum parameters $b(\nu, \nu_{ij}, \Delta\nu_{ij})$, $\Delta\nu_{ij}$, τ_i , τ_{qi} , w_i , ϵ_i , Z_V , etc., are given in Volume II of the Rocket Radiation Handbook, while the rocket hardware parameters \dot{W} , g_i , and T_e are assumed to be specified.

The spectral band or line-spread $\Delta\nu_{ij}$ depends on the mean temperature in the Mach core T_M and therefore also on altitude. As an approximation we may take for T_M in the core:

$$T_M = \frac{2}{3} T_e + \frac{1}{3} T_{\text{exh}}, \text{ } ^\circ\text{K} \quad (3.115)^*$$

where:

$$T_{\text{exh}} = T_c \left(\frac{p_a}{p_c} \right)^{(\gamma-1)/\gamma} = T_e \left(\frac{p_a}{p_e} \right)^{(\gamma-1)/\gamma}, \text{ } ^\circ\text{K} \quad (3.116)$$

in which:

T_e = Mean temperature of exhaust gas in nozzle exit plane, $^\circ\text{K}$

T_c = Combustion chamber temperature, $^\circ\text{K}$

p_e = Pressure of exhaust gas in nozzle exit plane,
bars (1 bar = 14.5 psi)

p_c = Rocket chamber pressure, bars

p_a = Ambient atmosphere pressure, bars

γ = Rocket exhaust gas coefficient ($\gamma \sim 1.2$ usually)

*A more rigorous approach would be to set $(T_M)_{\text{CORE}} = (1-x_c) T_e + x_c T_{\text{exh}}$, and to determine x_c experimentally instead of setting $x_c \approx 1/3$.

Note that T_M is defined in such a way that $(T_M)_{\text{CORE}} \rightarrow (T_C)_{\text{DSPR}} \approx \frac{2}{3} T_e$ when $p_a \rightarrow 0$. Equation (3.116) can be derived from one-dimensional rocket exhaust flow dynamics (see Volume IV, Rocket Radiation Handbook). The altitude dependence of Δv_{ij} enters thus via p_a into T_{exh} and thence into T_M on which Δv_{ij} depends.

The remaining, more strongly altitude-dependent parameter which one needs in Eqs. (3.113) and (3.114) is the CORE dwell time τ_M . If the mean bulk velocity of molecules in the Mach Core region is \bar{v}_M (m/sec) and the mean travel distance through the core equals $\bar{L}_M(m)$, then clearly:

$$\tau_M = \bar{L}_M / \bar{v}_M, \text{ sec} \quad (3.117)$$

Now, as illustrated in Figure 3-11, in the free jet or plume the air molecules will start to diffuse inwards into the core, while at the same time the exhaust diffuses outwards into the air. The velocity of the diffusion front of the inwards-moving air we shall label v_f and it may be a function of time, that is $v_f = v_f(t)$. The exhaust gas moves at the same time rearwards (with respect to the nozzle) with an average velocity $v_M = v_M(t)$. Time t is defined here as the elapsed time since the exhaust molecules left the nozzle exit plane.

Now as illustrated in Figure 3-11, due to the pear-shaped core flow, whose general features may be calculated in first approximation from the frictionless Euler equations of fluid dynamics (and which has various types of shocks in it*), the inwards diffusion front also follows a pear-shaped contour.

*It should be mentioned here that in spite of the presence of internal shocks inside the undisturbed core, the Gauss divergence theorem still holds throughout the core, even through shocks. Thus the result (3.93) still applies.

If the jet did not first blossom and then contract, but instead flowed everywhere in straight lines parallel to its axis as a straight cylinder, the diffusion front of the inwards-diffusing air would proceed as shown in Figure 3-12.* For this case relatively simple relations can be developed to calculate the undisturbed conical core height h and thence the average travel length \bar{L}_M . Before treating the blossoming supersonic jet case, let us first consider therefore the inward diffusion of air into the simpler cylindrical jet model of Figure 3-12.

The height of the undisturbed cone h (see Figure 3-12), which is the point where the inwards-diffusing air has reached the centerline of the cone, is given by:

$$h = \frac{D_e}{2} \frac{\int_0^{t_f} V_M(t) dt}{\int_0^{t_f} V_f(t) dt} = \frac{D_e}{2} \frac{\bar{V}_M}{\bar{V}_f}, \quad m \quad (3.118)$$

Here \bar{V}_M and \bar{V}_f are time-averaged velocities.

The diffusive propagation velocity V_f is in general composed of a molecular diffusion component V_{fd} and a turbulent diffusion component V_{ft} , that is:

*The situation of Figure 3-12 is actually close to that which exist for a subsonic aircraft exhaust jet.

$$V_f = V_{fd} + V_{ft} , \text{ m/sec} \quad (3.119)$$

If the air-related exhaust velocity \bar{V}_r given by:

$$V_r = |V_v - \bar{V}_M| , \text{ m/sec} \quad (3.120)$$

is large, the turbulent term V_{ft} usually dominates and $V_f = V_{ft}$. If on the other hand $\bar{V}_r = 0$, no turbulence can exist and $V_f = V_{fd}$. In (3.120) V_v is the rocket vehicle velocity.

Now as shown in Appendix D, the inward velocity of a diffusion front for a cylindrical geometry is given by:

$$V_{fd} = \left(\frac{\mathcal{D}}{t} \right)^{1/2} = \frac{2\mathcal{D}}{a_e - r_f} , \text{ m/sec} , \quad (3.121)$$

where:

\mathcal{D} = Molecular gaseous diffusivity, m^2/sec

$a_e = \frac{D_e}{2}$ = original radius of axisymmetric exhaust plume
at time $t = 0$, m

r_f = Radial distance from plume axis of diffusion
front from plume axis, m

we have also according to Appendix D that:

$$r_f = a_e - \sqrt{4\mathcal{D}t} , \text{ m} \quad (3.122)$$

The time of travel t_f for the diffusion front to reach the axis is then according to Eq. (3.122) given by:

$$t_f = \frac{a_e^2}{4D} , \text{ sec} \quad (3.123)$$

Then the average molecular diffusion front velocity \bar{V}_{fd} is:

$$\bar{V}_{fd} = \frac{a_e}{t_f} = \frac{4D}{a_e} = \frac{8D}{D_e} , \text{ m/sec} , \quad (3.124)$$

where D_e is the nozzle exit diameter.

The average inward velocity due to turbulent diffusion, \bar{V}_{ft} , is similarly given by:

$$\bar{V}_{ft} = \frac{8D_t}{D_e} = 4 V_* \quad (3.125)$$

where the "friction velocity" is defined by (Refs. 37 and 38):

$$V_* = \frac{D_t}{a_e} = \frac{2D_t}{D_e} \quad (3.126)$$

and:

D_t = Turbulent diffusion coefficient, m^2/sec

A theoretical value for V_* derived from Von Karman's theory of turbulence (Ref. 37) is:

$$V_* = 0.150 V_r \text{Re}^{-0.125} , \text{ m/sec} \quad (3.127)$$

where the Reynolds number Re is given by:

$$Re = \frac{V_r D_e}{\mu/\rho} = \frac{k_d V_r D_e}{\mathcal{D}} \approx 1.4 \frac{V_r D_e}{\mathcal{D}} \quad (3.128)$$

In Eq. (3.128) μ/ρ is the "kinematic viscosity" and \mathcal{D} is the "molecular diffusivity" which equals $\mathcal{D} = k_d \mu/\rho$. Here $k_d = 1.200$ for hard-sphere molecules and $k_d = 1.543$ for molecules which repel each other according to the inverse-fifth-power of the distance (Ref. 34). For the exhaust gases of interest we shall take $k_d \approx 1.4$.

The velocity V_{ft} is according to Eq. (3.125) and (3.127) then:

$$\bar{V}_{ft} = 0.60 \bar{V}_r Re^{-0.125} \quad (3.129)$$

where \bar{V}_r must be time-averaged over the time interval t_f . Usually $\bar{V}_M =$ constant and $\bar{V}_r = V_v - \bar{V}_M =$ constant, during the time interval t_f . That is no significant changes occur in the plume for a steadily moving rocket during a time interval $t_f \approx 10^{-3}$ to 10^{-2} seconds.

Substituting (3.129) and (3.124) into Eq. (3.119) we obtain for the average diffusion front velocity \bar{V}_f :

$$\bar{V}_f = \frac{8\mathcal{D}}{D_e} + 0.60 \bar{V}_r Re^{-0.125}, \text{ m/sec}, \quad (3.130)$$

and from (3.118):

$$h = \frac{D_e}{2} \bar{V}_M \left[\frac{8D}{D_e} + 0.60 \bar{V}_r \text{Re}^{-0.125} \right]^{-1} =$$

$$= \frac{D_e}{2} \bar{V}_M \left[\frac{8D}{D_e} + 0.5516 \bar{V}_r \left(\frac{D}{\bar{V}_r D_e} \right)^{0.125} \right]^{-1}, \text{ m} \quad (3.131)$$

Values of h calculated from Eq. (3.131) agree surprisingly well with experiment. For example for the case that $V_r = 100$ m/sec, $D_e = 1$ inch $= 2.5 \times 10^{-2}$ m, and with $D = D_{\text{air}} = 1.6 \times 10^{-5}$ m²/sec, we calculate from (3.131) that $h/D_e = 4.02$ while experiments with subsonic jets (Ref. 39) show that $h/D_e \approx 4.25$ in this case.

We can also obtain the time-dependent radial diffusion front velocity $V_f = V_f(t)$ which according to Eqs. (3.121), (3.127), and (3.128) is:

$$V_f(t) = \left\{ D + 0.06895 D_e \bar{V}_r \left(\frac{D}{\bar{V}_r D_e} \right)^{0.125} \right\}^{0.5} t^{-0.5}, \text{ m/sec} \quad (3.132)$$

The mean distance of travel \bar{L}_M for a molecule through the undisturbed cone, prior to entering the mixing region, is given by:

$$\bar{L}_M = \int_{r=0}^{a_e} \frac{2\pi r dr}{\pi a_e^2} \bar{V}_M t = \bar{V}_M \int_{r=0}^{a_e} \left(\frac{2\pi r}{\pi a_e^2} \right) \left(\frac{(a_e - r)^2}{4 D_{\text{tot}}} \right) dr =$$

$$\bar{L}_M = \frac{a_e^2}{24} \frac{\bar{V}_M}{D_{\text{tot}}} = \frac{D_e^2}{96} \frac{\bar{V}_M}{D_{\text{tot}}} = \frac{1}{6} h, \quad \text{m}, \quad (3.133)$$

since

$$h = \frac{a_e^2 \bar{V}_M}{4 \mathcal{D}_{\text{tot}}} = \frac{D_e^2 \bar{V}_M}{16 \mathcal{D}_{\text{tot}}}, \quad (3.134)$$

Here we define \mathcal{D}_{tot} to be:

$$\mathcal{D}_{\text{tot}} = \mathcal{D} + \mathcal{D}_t, \text{ m}^2/\text{sec} \quad (3.135)$$

where,

$$\mathcal{D}_t = 0.06895 D_e \bar{V}_r \left(\frac{\mathcal{D}}{\bar{V}_r D_e} \right)^{0.125} \quad (3.136)$$

Written out thus:

$$\bar{L}_M = \frac{D_e \bar{V}_M}{12} \left[\frac{8 \mathcal{D}}{D_e} + 0.5516 \bar{V}_r \left(\frac{\mathcal{D}}{\bar{V}_r D_e} \right)^{0.125} \right]^{-1}, \text{ m} \quad (3.137)$$

The mean residence time τ_M for a molecule in the undisturbed cone is finally:

$$\tau_M = \frac{\bar{L}_M}{\bar{V}_M} = \frac{D_e}{12} \left[\frac{8 \mathcal{D}}{D_e} + 0.5516 \bar{V}_r \left(\frac{\mathcal{D}}{\bar{V}_r D_e} \right)^{0.125} \right]^{-1}, \text{ sec} \quad (3.138)$$

The result (3.138) applies to the cylindrical straight jet. For the blossoming supersonic jet shown in Figure 3-11, one could as an approximation replace D_e by D_{exh} , where D_{exh} is the diameter of the jet upon adiabatic expansion from pressure p_e to pressure p_a according to one-dimensional flow

June 1974

theory (see Vol. IV). This approximation might be reasonable at the lower altitudes, but at the higher altitudes where D_{exh} is large it would be physically unreasonable to expect that atmospheric air would not have penetrated the plume to a considerable extent before the exhaust has expanded to diameter D_{exh} . A more agreeable though coarse approximation is to replace D_e by $D_M = \frac{1}{2} (D_e + D_{\text{exh}})$ in Eq. (3.138), where D_{exh} is the diameter at full expansion (see Vol. IV):

$$D_{\text{exh}} = D_t \left(\frac{\gamma - 1}{2} \right)^{1/4} \left(\frac{2}{\gamma + 1} \right)^{\frac{\gamma + 1}{4(\gamma - 1)}} \left(\frac{p_c}{p_a} \right)^{\frac{1}{2\gamma}} \left[1 - \left(\frac{p_a}{p_c} \right)^{\frac{\gamma - 1}{\gamma}} \right]^{-1/4}, \text{ m} \quad (3.139)$$

Here p_c is the combustion chamber or total pressure of the jet, p_a is the ambient air pressure, and D_t is the nozzle throat diameter (m). Then:

$$\left(T_M \right)_{\text{super-sonic jet core}} \approx \frac{D_e + D_{\text{exh}}}{24} \left[\frac{16 \mathcal{D}}{D_e + D_{\text{exh}}} + 0.5516 \bar{v}_r \left(\frac{2 \mathcal{D}}{\bar{v}_r (D_e + D_{\text{exh}})} \right)^{0.125} \right]^{-1}, \text{ sec} \quad (3.140)$$

We shall assume (3.140) in what follows.

Now the "molecular diffusivity" \mathcal{D} is a function of temperature and pressure. In Eq. (3.140) the value for \mathcal{D} must be evaluated at the Core Gas/Mixed Region Interface. We can write approximately for \mathcal{D} (see Eq. (3.64)):

$$\mathcal{D} = 2.358 \times 10^{-7} \frac{(\bar{T}_I)^{3/2}}{\bar{p}_I \bar{\sigma}_{a/e} \bar{M}_e^{1/2}}, \text{ m}^2/\text{sec} \quad (3.141)$$

where:

- \bar{T}_I = Average temperature in interface region, °K
- \bar{p}_I = Average gas pressure in interface region, atm
- M_e = Mean molecular weight of exhaust gas, a.m.u.
- $\bar{\sigma}_{a/e}$ = $\pi(r_A + r_X)^2$ = Average collision cross-section between air molecules A and exhaust molecules X; in units of $\text{\AA}^2 = 10^{-16} \text{ cm}^2 = 10^{-20} \text{ m}^2$
- r_A, r_X = Average collision radii of molecules A and X respectively, \AA

For most rocket exhaust gases the product $(\bar{\sigma}_{a/e} M_e^{1/2})$ is nearly constant and we may set:

$$(\bar{\sigma}_{a/e} M_e^{1/2}) \approx 46, \quad \text{\AA}^2 \cdot (\text{a.m.u.})^{1/2}, \quad (3.142a)$$

In Eq. (3.141). Further we shall assume that:

$$\bar{p}_I \approx p_a \quad (3.142b)$$

$$\bar{T}_I^{3/2} \approx T_e^{1/2} T_{exh} = T_e^{3/2} \left(\frac{p_a}{p_e} \right)^{(\gamma-1)/\gamma} \quad (3.142c)^*$$

With the values (3.142a) through (3.142c) substituted in (3.141), we obtain finally for \mathcal{D} :

*The choice for this estimate is based on the requirement that the CORE dimensions must attain a constant finite value in deep-space where $p_a \rightarrow 0$ (see Eq. (3.144)). If we took $\bar{T}_I^{3/2} = T_e^{3/2} (p_a/p_e)^{3(\gamma-1)/2\gamma}$, the CORE dimensions would grow (very slowly) to infinity as $p_a \rightarrow 0$. This we know is incorrect (see section 3.3.2).

where:

\bar{T}_I = Average exhaust gas temperature in interface region, °K

\bar{p}_I = Average gas pressure in interface region, ^{BARS} atm

M_e = Mean molecular weight of exhaust gas, a.m.u.

$\bar{\sigma}_{a/e}$ = $\pi(r_A + r_X)^2$ = Average collision cross-section between air molecules A and exhaust molecules X; in units of $\text{\AA}^2 = 10^{-16} \text{ cm}^2 = 10^{-20} \text{ m}^2$

r_A, r_X = Average collision radii of molecules A and X respectively, \AA

For most rocket exhaust gases the product $(\bar{\sigma}_{a/e} \bar{M}_e^{1/2})$ is nearly constant and we may set:

$$(\bar{\sigma}_{a/e} \bar{M}_e^{1/2}) \approx 46, \quad \text{\AA}^2 \cdot (\text{a.m.u.})^{1/2}, \quad (3.142a)$$

in Eq. (3.141). Further we shall assume that:

$$\bar{p}_I \approx p_a \quad (3.142b)$$

$$\bar{T}_I \approx T_{\text{exh}} = T_e \left(\frac{p_a}{p_e} \right)^{(\gamma-1)/\gamma} \quad (3.142c)$$

With the values (3.142a) through (3.142c) substituted in (3.141), we obtain finally for \mathcal{D} :

* See New Page.

June 1974

$$\mathcal{D} \approx 5.126 \times 10^{-9} \frac{T_{\text{exh}}^{3/2} T_e}{p_a} = 5.126 \times 10^{-9} \frac{T_e^{3/2} (p_a/p_e)^{\frac{3(\gamma-1)}{2}}}{p_a}, \text{ m}^2/\text{sec}$$

(3.143)

Note that the parameter τ_M as defined by (3.140) approaches a limiting value at very high altitudes (where $p_a \rightarrow 0$) which is given by:

$$(\tau_M)_{p_a \rightarrow 0} \rightarrow \tau_{MH} = \frac{D_{\text{exh}}^2}{384 \mathcal{D}} = 5.080 \times 10^5 \left(\frac{\gamma-1}{2} \right)^{\frac{1}{2}} \left(\frac{2}{\gamma+1} \right)^{\frac{\gamma+1}{2(\gamma-1)}} \left(\frac{p_c}{p_e} \right)^{\frac{1}{\gamma}} \cdot \frac{D_e^2 p_e}{T_e^{3/2}}, \text{ sec}$$

(m² . bars . °K^{-3/2})

(3.144)

Here D_e is in meters, p_e is in bars, and T_e is in °K. When $p_a \rightarrow 0$, the molecular diffusion part (the first member) in the brackets of (3.140) becomes much larger than the turbulent diffusion part (the second member) so that the latter can be neglected. The resultant expression then becomes equal to (3.144) which is independent of p_a .

The mean core length similarly approaches in deep space the value:

$$(\bar{L}_M)_{p_a \rightarrow 0} \rightarrow \bar{L}_{MH} = \frac{\bar{V}_M D_{\text{exh}}^2}{348 \mathcal{D}} = 5.080 \times 10^5 \left(\frac{\gamma-1}{2} \right)^{1/2} \left(\frac{2}{\gamma+1} \right)^{\frac{\gamma+1}{2(\gamma-1)}} \left(\frac{p_c}{p_e} \right)^{\frac{1}{\gamma}} \frac{D_e^2 \bar{V}_M p_e}{T_e^{3/2}}, \text{ m}$$

(3.145)

Thus even in a vacuum, a CORE region can be defined which cannot be penetrated by whatever ambient molecule is encountered. This is as it must be physically

according to our definition of the Mach Core. For typical values of $\gamma = 1.25$, $p_c = 40$ bars, $p_e = 0.5$ bars, $V_e = 2000$ m/sec, and $T_e = 1500^\circ\text{K}$, we find for example from (3.143) and (3.144) that $\tau_{MH} = 30$ sec, and $\bar{L}_{MH} = 60$ kilometers.

One other parameter which needs to be determined more precisely before we can use Eq. (3.140), is the absolute mean relative velocity $\bar{V}_r = |V_v - \bar{V}_M|$. Now we know that \bar{V}_M must have a value somewhere in between V_e and V_{exh} , that is somewhere between the velocity in the nozzle exit plane where the temperature is T_e (and the pressure p_e), and the velocity at the fully expanded point where $T = T_{\text{exh}}$ (and the pressure p_a). Using the adiabatic isentropic flow relation (see Vol. IV):

$$V = V_e \left[\frac{1 - (p/p_c)^{(\gamma-1)/\gamma}}{1 - (p_e/p_c)^{(\gamma-1)/\gamma}} \right]^{1/2} = V_e \left(\frac{T_c - T}{T_c - T_e} \right)^{1/2}, \quad \text{m/sec}, \quad (3.146)$$

and the approximation (3.115), one may set:

$$\bar{V}_M \approx V_e \left(\frac{T_c - \frac{2}{3}T_e - \frac{1}{3}T_{\text{exh}}}{T_c - T_e} \right)^{1/2} = V_e \left\{ 1 + \frac{1}{3} \left(\frac{T_e - T_{\text{exh}}}{T_c - T_e} \right) \right\}^{1/2}, \quad \text{m/sec} \quad (3.147)^*$$

Here T_{exh} is given by Eq. (3.116), T_c is the combustion chamber temperature, T_e is the exhaust gas temperature in the nozzle exit plane, and V_e is the velocity of the exhaust gas in the nozzle exit plane which is given by:

*The same remark applies here as was given in connection with Eq. (3.115), that is in a more rigorous approach, the factor $1/3$ in Eq. (3.147) should be replaced by χ_c which may be obtained experimentally or analytically.

June 1974

$$V_e = 129 \left[\left(\frac{\gamma}{\gamma - 1} \right) \frac{T_c}{\bar{M}_e} \left\{ 1 - \left(\frac{P_e}{P_c} \right)^{(\gamma-1)/\gamma} \right\} \right]^{1/2}, \text{ m/sec} \quad (3.148)$$

In Eq. (3.148), \bar{M}_e is the mean molecular weight of the exhaust gases (grammoles), γ is their specific heat ratio and the factor $129 \approx \sqrt{2R} = 128.973$ m/sec, where R is the gas constant.

In conclusion, we have obtained an expression for the radiant intensity of the CORE region of a rocket plume (Eqs. (3.113) and (3.114)) which is theoretically rigorous except for the estimates or approximations (3.115) and $D_M = (D_e + D_{exh})/2$. Both approximations enter into the parameter τ_M via relations (3.140) and (3.147), while Δv_{ij} depends only on the approximation (3.115).

Because of the approximations that were used, it may be argued that the result (3.113) or (3.114) gives no large improvement over the usual calculations based on a computer sum over the radiation from many small volume elements of a mathematically calculated flow field. However it should be remembered that the theoretically calculated flow field as well as the averaging over photon mean free paths, emissivities, etc., which are always made in such computations, also contain many approximations that cause the final result to have an uncertainty as large as (and usually worse than) the one inherent in calculations based on (3.113) or (3.114). When a signature of $dJ/d\lambda$ as a function of altitude h is needed, Eqs. (3.113) and (3.114) can give immediate answers, but if the usual "cellularized field" approach is employed, a new elaborate computer calculation is needed for each altitude point. Clearly, Eqs. (3.113) and (3.114) are much superior in such a case.

Even if the calculation via Eq. (3.113) or (3.114) gave a result that was slightly too high or too low, this effect would be carried through at all altitudes, and thus would not influence the general shape or trend of an altitude signature.

3.3.4 Afterburning and Collisional Deceleration Radiation (ABCD)

Because most rocket exhausts are fuel-rich and contain considerable fractions of unoxidized H_2 , CO , H , and OH , reactions with O_2 of the atmosphere will take place in a rocket plume. In these so-called "afterburning" reactions heat is liberated which will cause additional vibrational excitations in some of the exhaust molecules and thus additional emissions of radiation. At the lower altitudes, the air density is high and thus the supply of oxygen plentiful to sustain afterburning. However as a rocket reaches the higher altitudes, the thinness of the atmosphere causes a gradual fade-out of afterburning and thus a subsidence of afterburning-initiated radiation.

In addition to heat released from afterburning, heat is generated in the mixing region from the conversion of dynamic velocity energy of the plume relative to air. This radiation-generating "collisional deceleration" takes place in the air shock (see Figure 2-1) and must be considered together with "afterburning" since their heating effects occur concurrently so that the total temperature rise and therefore the radiation rate is higher than if the temperature rise due to each mechanism were considered separately. The two mechanisms are thus coupled and we shall use the label ABCD to indicate their combined effect in the general case. However at high altitudes where afterburning ceases, collisional deceleration is the only significant radiation-producing mechanism left of course.

Now formally we can write for the ABCD radiant emission coming from the mixing region:

$$\frac{dJ}{dv} = \frac{h\nu F_v \text{Tr}(\nu)}{4\pi} \int_{\text{ABCD Volume}} \sum_i \frac{dA_i}{dv} p_i \frac{dn_i}{dv} dv, \quad \frac{\text{Watts}}{\text{ster} \cdot \text{Hz}}, \quad (3.149)$$

where the integration is over excited molecules i in the mixing region (or ABCD) volume, and the other parameters are as defined before. To evaluate (3.149), we shall use an approach similar to the one given in section 3.3.2, and obtain an explicit expression for the quantity beyond the integral sign in (3.149).

We shall again assume local thermodynamic equilibrium (LTE) throughout the ABCD region so that P and L terms in the equivalent of Eq. (3.63) cancel each other, and we are left with:

$$\left(\frac{\partial n_i}{\partial t} \right)_{\text{ABCD}} = \left(\frac{\partial G_i}{\partial v} \right)_{\text{ABCD}} - \left(\frac{\partial D_i}{\partial v} \right) - \left(\frac{\partial C_i}{\partial v} \right) + \left(\frac{\partial F_i}{\partial v} \right) \quad (3.150)$$

Here D_i , C_i , and F_i are as defined before in section 3.3.2, but now the radiation-generating term $(G_i)_{\text{ABCD}}$ is different. We have neglected the stimulated emission term B_i here as well as the V-V exchange terms R_i and S_i of Eq. (3.63) since they are usually negligibly small. If V-V exchange is important, a correction term $\tau_i^{-1}/(\tau_i^{-1} + \tau_{qi}^{-1})$ may be factored into the relations we shall develop below in the same manner as we did for the DSPR and CORE radiation cases.

June 1974

FTD-CW-01-01-74
Vol. 1.

We can formally write for the source term:

$$(G_i)_{ABCD} = \vec{v} \cdot \vec{V}_{ABCD} [n_F \xi_i + n_X \eta_i] , \quad (3.151)$$

where we neglected again kinetic diffusion effects (see the discussion following Eq. (3.84)), and where:

\vec{V}_{ABCD} = Bulk velocity of molecules in the ABCD region,
m/sec

n_X = Density of molecules X, m^{-3}

n_F = Density of fuel molecules F, m^{-3}

ξ_i = AB chemical reaction conversion parameter giving
the number of excited states X_i produced due to
reactions of fuel molecules F with atmospheric
oxygen, per fuel molecule F

η_i = Fraction of molecules X excited to state i in
ABCD region due to the ABCD temperature increase

The product $n_F \xi_i$ equals the number of excited states X_i created per unit volume due to AB chemical reaction (not due to any other already existing X_i 's), that is:

$$(n_i)_{\text{reaction}} = \xi_i n_F \quad (3.152)$$

We shall discuss the parameters ξ_i and η_i in detail below, but first let us carry out an integration over the ABCD emission volume in the same manner

June 1974

as we did for the Mach Core case. We again assume steady-state conditions so that $\partial n_i / \partial t = 0$ in (3.150). Then we have that:

$$(D_i)_{ABCD} = (C_i + F_i)_{ABCD} + \int_{\substack{ABCD \\ \text{Volume}}} \vec{\nabla} \cdot \vec{V}_{ABCD} (\xi_i n_F + \eta_i n_X) dV \quad (3.153)$$

Or, since $(C_i)_{ABCD}$ represents the number of photons absorbed per unit time in the ABCD region, the net rate of escaping photons is:

$$\begin{aligned} (E_i)_{ABCD} &= (D_i - C_i)_{ABCD} = \int_{\substack{ABCD \\ \text{Volume}}} A_i^0 p_i \frac{dn_i}{dV} dV = \\ &= \int_{\substack{ABCD \\ \text{Volume}}} \vec{\nabla} \cdot \vec{V}_{ABCD} (\xi_i n_F + \eta_i n_X) dV, \quad \frac{\text{photons}}{\text{sec}} \end{aligned} \quad (3.154)^*$$

which when converted to a surface integral over the entire surface of the ABCD volume yields:

$$\begin{aligned} (E_i)_{ABCD} &= \int_{\substack{ABCD \\ \text{Volume}}} A_i^0 p_i \frac{dn_i}{dV} dV = \iint_{\substack{\text{Surface of} \\ \text{ABCD Region}}} \vec{V}_{ABCD} (\xi_i n_F + \eta_i n_X) d\vec{s}, \\ &\quad , \quad \frac{\text{photons}}{\text{sec}} \end{aligned} \quad (3.155)$$

where $d\vec{s}$ is the directional unit surface normal to the surface. We recognize $\vec{V}_{ABCD} n_F$ and $\vec{V}_{ABCD} n_X$ to be the influx of unburned fuel and excitable molecules to the ABCD region, and $\vec{V}_{ABCD} n_F \xi_i$ and $\vec{V}_{ABCD} n_X \eta_i$ as the influx of excited

* A_i^0 is the total spontaneous emission rate from level i (see Vol. II, Rocket Radiation Handbook). The contribution to excited levels i from the cascade term $F_i = \sum_k E_{ki}$ (see Eq. (3.93)) is here incorporated in factors ξ_i and η_i .

molecules X_i due to respectively afterburning reaction and thermal excitation (including cascade contributions). We shall assume the ABCD region to extend to some distance L_{ABCD} behind the rocket, beyond which no or very few excited molecules X_i exist so that the outflux of X_i is zero. Then if we assume ξ_i and η_i to be constant throughout all or a portion of the ABCD region including the entrance boundary*, but zero elsewhere and at the exit boundary (we shall take appropriate averages), we see that (3.155) reduces

$$\begin{aligned} (E_i)_{ABCD} &= \int_{\substack{ABCD \\ \text{Volume}}} p_i A_i^0 \frac{dn_i}{dv} dv = A_i^0 N_i = A_i^0 (N_{i \text{ reaction}} + N_{i \text{ exhaust}}) = \\ &= 6.025 \times 10^{23} \dot{W} (g_F \xi_i + g_i \eta_i) , \quad \frac{\text{photons}}{\text{sec}} \end{aligned} \quad (3.156)$$

where $6.025 \times 10^{23} g_F \dot{W}$ and $6.025 \times 10^{23} g_i \dot{W}$ is the total influx of unburned fuel and excitable molecules per second. Substituting (3.156) in (3.149), using the relation $dA_i/dv = \sum_j A_i^0 (f_{ij}/\Delta v_{ij}) b(v, v_{ij}, \Delta v_{ij})$, one obtains:**

$$\begin{aligned} \left(\frac{dJ}{dv} \right)_{ABCD} &= 31.765 \dot{W} \frac{v}{(\text{THz})} F_v \text{Tr}(v) \sum_i \sum_j \left(\frac{f_{ij}}{\Delta v_{ij}} \right) b(v, v_{ij}, \Delta v_{ij}) \cdot \\ &\cdot \left\{ g_F \xi_i + g_i \eta_i \right\} , \quad \frac{\text{Watts}}{\text{ster} \cdot \text{THz}} \end{aligned} \quad (3.157)$$

Equation (3.157) is very similar to (3.113) except for the parameters ξ_i and η_i which we shall evaluate next.

*Usually most chemical reaction represented by ξ_i and collisional deceleration represented by η_i take place in the air shock which is rather thin. We can thus consider this as a planar source region which feeds excited molecules to the ABCD region of the plume.

**See Volume II for expressions for A_i^0 , $b(v, v_{ij}, \Delta v_{ij})$, etc.

One can visualize the ABCD region as a rocket-following chemical reactor of equivalent diameter D_{ABCD} and equivalent length L_{ABCD} to which ambient air and fuel and excitable species are fed. The feed rate of fuel and excitable is of course:

$$d(\text{Fuel})/dt = g_F \dot{W}, \text{ moles/sec} \quad (3.158)$$

$$d(\text{Excitables})/dt = g_i \dot{W}, \text{ moles/sec} \quad (3.159)$$

while atmospheric oxygen and nitrogen are supplied at rates of approximately:

$$\frac{d(O_2)}{dt} = 0.2 V_a m_a \left(\frac{\pi}{4} D_a^2 \right), \frac{\text{moles}}{\text{second}} \quad (3.160)$$

$$\frac{d(N_2)}{dt} = 0.8 V_a m_a \left(\frac{\pi}{4} D_a^2 \right), \frac{\text{moles}}{\text{second}} \quad (3.161)$$

in which:

$V_a = V_a(h)$ = Effective average air inflow velocity into ABCD region, m/sec

$m_a = m_a(h)$ = Molar air density, moles/m³

$D_a = D_a(h)$ = Effective air inlet diameter of ABCD region, m

We shall develop expressions for V_a and D_a later on.

In nearly all rocket exhausts, the only important fractions of unburned fuel are H_2 and CO, at mole concentrations of g_{H_2} and g_{CO} moles/kgm.

The chemical combustion reactions which these species can undergo when mixed with O_2 are listed in Tables E-1 and E-2 of Appendix E.

From Appendix E we find that the number of excitable molecules produced in the ABCD zone due to AB chemical reaction may be expressed by:

$$\left(N_{H_2O} \right)_{AB \text{ reaction}} = N_{H_2} \xi_{H_2O} \quad (3.162)$$

$$\left(N_{CO_2} \right)_{AB \text{ reaction}} = N_{CO} \xi_{CO_2} \quad (3.163)$$

where ξ_{H_2O} and ξ_{CO_2} are the degrees of conversion in the ABCD region of H_2 molecules to H_2O , and CO molecules to CO_2 respectively, which are given by the expressions:

$$\xi_{H_2O} = \xi_O H(\xi_h - \xi_O) + \xi_h H(\xi_O - \xi_h) \quad (3.164)$$

$$\xi_{CO_2} = \xi_O H(\xi_c - \xi_O) + \xi_c H(\xi_O - \xi_c) \quad (3.165)$$

Here the Heaviside function $H(x)$ is defined by:

$$H(x) = 1, \text{ for } x > 0 \quad (3.166a)$$

$$H(x) = 0, \text{ for } x < 0 \quad (3.166b)$$

June 1974

and according to the analysis given in Appendix E we have:

$$\xi_o = \frac{1}{1 + \left(\frac{\pi}{4} D_a^2 \right) \frac{\rho_a V_a}{1000 \dot{W}}} \quad (3.167)$$

$$\xi_h = \frac{13.64}{g_{H_2}} \left\{ \frac{\left(\frac{\pi}{4} D_a^2 \right) \frac{\rho_a V_a}{1000 \dot{W}}}{1 + \left(\frac{\pi}{4} D_a^2 \right) \frac{\rho_a V_a}{1000 \dot{W}}} \right\} \quad (3.168)$$

$$\xi_c = \frac{13.64}{g_{CO}} \left\{ \frac{\left(\frac{\pi}{4} D_a^2 \right) \frac{\rho_a V_a}{1000 \dot{W}}}{1 + \left(\frac{\pi}{4} D_a^2 \right) \frac{\rho_a V_a}{1000 \dot{W}}} \right\} \quad (3.169)$$

In Eqs. (3.167) through (3.169) we have:

V_a = Effective air flow velocity into plume, m/sec

ρ_a = Air density, gm/m³

\dot{W} = Rocket mass expulsion rate, kgs/sec

g_{H_2}, g_{CO} = Concentration of H₂ and CO in rocket exhaust
at the nozzle exit, moles per kgm

Other parameters are as defined before.

Of the AB reaction-produced molecules given by (3.162) and (3.163), the number that are in excited states with energy ϵ_{X_i} in a freely radiating gas is according to Eq. (3.97j) given by:

$$(N_{X_i})_{\text{reaction}} = N_X \exp\left(-\frac{\epsilon_{X_i}}{kT_r}\right) = N_F \xi_X \exp\left(-\frac{\epsilon_{X_i}}{kT_r}\right) \quad (3.170)$$

Here X stands for H_2O or CO_2 and F for H_2 or CO respectively. Comparison with (3.156) shows that:

$$\xi_i = \xi_X \exp\left(-\frac{\epsilon_{X_i}}{k T_r}\right), \quad (3.171)$$

where:

T_r = Mean temperature in ABCD reaction region, $^{\circ}K$

ϵ_{X_i} = Excitation level i in molecule X from which emissions occur, Joules

k = Boltzmann's constant = 1.3804×10^{-23} Joules/ $^{\circ}K$

The number of CD-produced excited molecules X_i is of course also related by the Boltzmann factor to the number of unexcited molecules X in the ABCD region. Thus η_i in Eqs. (3.156) and (3.157) is simply:

$$\eta_i = \exp\left(-\frac{\epsilon_{X_i}}{k T_r}\right) \quad (3.172)$$

Equation (3.171) can therefore also be written:

$$\xi_i = \xi_X \eta_i \quad (3.173)$$

The ABCD-produced temperature T_r in the ABCD region may be expressed by:

$$T_r = T_{mix} + \Delta T_{AB} + \Delta T_{CD} \quad (3.174)$$

June 1974

Here:

$$T_{mix} = \frac{N_{exh} C_e T_Q + N_a C_a T_a}{N_{exh} C_e + N_a C_a} = \frac{T_Q + \mu_{a/e} T_a}{1 + \mu_{a/e}} \quad (3.175)$$

and ΔT_{AB} and ΔT_{CD} are the average temperature rises in the ABCD region due to liberated heat from afterburning and collisional deceleration. In (3.175), T_a and T_Q are the air and exhaust temperatures ($^{\circ}K$) prior to entrance of the air and the exhaust into the ABCD region, while C_a , N_a and C_e , N_{exh} are the molecular heat capacity and total number of air and exhaust molecules respectively in the ABCD region. The "mixing ratio" $\mu_{a/e}$ in (3.175) is given by:

$$\mu_{a/e} = \frac{C_a N_a}{C_e N_{exh}} \approx \frac{N_a}{N_{exh}} \quad (3.176)$$

The second approximation in (3.176) is usually good since $C_a \approx C_e$.

The temperature T_Q in (3.175) must have a value somewhere between the exit temperature T_e and the temperature T_{exh} corresponding to complete adiabatic isentropic expansion of the jet to the ambient air pressure p_a , given by:

$$T_{exh} = T_e \left(\frac{p_a}{p_e} \right)^{(\gamma-1)/\gamma} = T_c \left(\frac{p_a}{p_c} \right)^{(\gamma-1)/\gamma}, \quad ^{\circ}K \quad (3.177)$$

The actual expansion of the jet to ambient pressures is not quite adiabatic since Mach Core radiation occurs. To correct for this we multiply T_{exh} by

a radiative correction factor β_M (to be discussed below) and obtain the corrected temperature:

$$T_h = \beta_M T_{\text{exh}} = \beta_M T_c \left(\frac{p_a}{p_c} \right)^{\frac{\gamma-1}{\gamma}} = \beta_M T_e \left(\frac{p_a}{p_e} \right)^{\frac{\gamma-1}{\gamma}}, \quad ^\circ\text{K} \quad (3.178)$$

The exhaust velocity at the expansion point where the gas has reached temperature T_h and pressure p_a is then:

$$v_h = \beta_M^{1/2} v_{\text{exh}} = 129 \beta_M^{1/2} \left[\left(\frac{\gamma}{\gamma-1} \right) \frac{T_c}{\bar{M}_e} \left\{ 1 - \left(\frac{p_a}{p_c} \right)^{\frac{\gamma-1}{\gamma}} \right\} \right]^{1/2}, \quad \text{m/sec}$$

(3.179)

In (3.177) through (3.179), we have:

T_c = Rocket combustion chamber temperature, $^\circ\text{K}$

p_c = Rocket chamber pressure, bars

p_a = Ambient air pressure, bars

γ = c_p/c_v = Ratio of specific heats ^{at} and constant pressure and constant volume of exhaust gas ≈ 1.24

\bar{M}_e = Mean molecular weight of exhaust, grams/mole (= a.m.u.)

129 = $\sqrt{2R} = 10^{-2} (2 \times 8.317 \times 10^7)^{1/2} = 128.973 \text{ m/sec}$

R = Gas constant = 8.317×10^7 , ergs $\cdot (^\circ\text{K})^{-1} \text{ mole}^{-1}$

June 1974

By using p_c and T_c instead of p_e and T_e in Eqs. (3.177) and (3.178), these relations are applicable also at near-the-ground altitudes where the design nozzle exit pressure $p_e = p_o$ is lower than the ambient air pressure p_a and the design exit velocity $V_e = V_o$ value is higher than V_h as given by (3.179). The exhaust simply expands to the ambient pressure p_a in the nozzle at these lower altitudes and then separates from the nozzle at some point upstream before it reaches the exit plane, thus not utilizing a portion of the nozzle.

Clearly the average exhaust gas temperature T_Q just before it enters the mixing region has a value less than T_e but larger than T_h . We shall delay the evaluation of an expression for T_Q until later, after we first complete the derivation of relations for the other temperature-affecting contributions in Eq. (3.175).

The parameter β_M in Eqs. (3.178) and (3.179) is equal to the fraction of the total exhaust gas energy not lost by radiation from the Mach Core. From an energy balance we obtain for the radiative correction factor β_M :

$$\beta_M = \frac{\dot{W} H(T_e) - P_{CORE}}{\dot{W} H(T_e)} = 1 - \frac{P_{CORE}}{\dot{W} H(T_e)} \quad (3.180)$$

where $H(T_e)$ is the enthalpy in Joules per kilogram of the exhaust gas in the nozzle exit plane and P_{CORE} is the total radiation (Watts) emitted from the Mach Core. Now for nearly all rockets the CORE radiation is in the infrared and due to vibrational transitions. Thus Eq. (3.102) applies, and:

$$P_{\text{CORE}} = \int_{v=0}^{\infty} \left(\frac{dP}{dv} \right)_{\text{CORE}} dv \equiv 3.9917 \times 10^{-10} \dot{W} \sum_i g_i v_i \cdot \left[\exp\left(\frac{e_i}{kT_e}\right) - 1 \right]^{-1} \cdot \left[1 - \exp(-\tau_M/\tau_i) \right], \text{ Watts}, \quad (3.181)^*$$

where we assumed $\tau_{qi}^{-1} = 0$ for convenience. In obtaining (3.181) from (3.111) we used the relation (see Vol. II, Rocket Radiation Handbook):

$$\int_0^{\infty} v \left\{ \frac{b(v, v_{ij}, \Delta v_{ij})}{\Delta v_{ij}} \right\} dv = v_{ij} \approx v_i \quad (3.182)^{***}$$

The enthalpy $H(T_e)$ in (3.180) can be approximated by (Ref. 33):

$$H(T_e) = \bar{c}_p T_e = R T_e \sum_i g_i \left(\frac{\phi_i + 2}{2} \right), \text{ Joules/kgm}, \quad (3.183)$$

where:

ϕ_i = Degrees of freedom of molecular species i

R = Gas constant = $8.317 \text{ Joules} \cdot ^\circ\text{K}^{-1} \cdot \text{mole}^{-1}$

With (3.183) and (3.181) substituted in (3.180) and using the relation $v_i = c/\lambda_i$, then:

* We have neglected the V-V transfer correction term in (3.181).

***The result $v_{ij} \approx v_i$ only applies to vibrational transitions of course.

$$\beta_M = 1 - 14,388.5 \tau_e^{-1} \cdot \left[\frac{\sum_i g_i \lambda_i^{-1} \{ \exp(h\nu_i/kT_e) - 1 \}^{-1} \{ 1 - \exp(-\tau_M/\tau_i) \}}{\sum_i g_i (\phi_i + 2)/2} \right] \quad (3.184)$$

where λ_i is in μm and the summation over i is over the various normal vibrations ν_i of the exhaust molecules X . The degrees of freedom ϕ_i for diatomic molecules such as OH, CO, etc., is $\phi_i \approx 5$, while for the triatomic molecules H_2O and CO_2 , $\phi_i \approx 7$.

Equation (3.184) can be written in a more compact form by defining:

$$q_i = \frac{14,388.5}{T_e \lambda_i} \quad (3.185)$$

($^{\circ}\text{K}$) (μm)

Then:

$$\beta_M \approx 1 - \frac{\sum_i g_i \left\{ 1 - \exp\left(-\frac{\tau_M}{\tau_i}\right) \right\} q_i \left\{ \exp(q_i) - 1 \right\}^{-1}}{\sum_i g_i (\phi_i + 2)/2} \quad (3.186)$$

Note from Eq. (3.186) that $\beta_M \rightarrow 1$, if $\tau_M \rightarrow 0$ which occurs at high altitudes where $p_a \rightarrow 0$. It might appear at first that β_M could become negative if $q_i > 1$. However q_i also appears in the exponential and the factor $[q_i/(\exp(q_i)-1)]$ can never be larger than 1. Therefore β_M can never become negative for any combination of values of T_e and λ_i .

Returning to the mixing ratio $\mu_{a/e}$ defined by Eq. (3.176), let us next find relations for N_a and N_{exh} for the ABCD mixing region. Referring

to Figure 3-13, the question requiring an answer is what molar ratio of air to exhaust exists for the mixed gas flowing through the plane B-B'.* At the lower altitudes the rocket's velocity V_v is less than the average jet exhaust velocity \tilde{V}_x along the rocket trajectory, so that the velocity of air relative to the initial portion of the jet $V_k = \tilde{V}_x - V_v$ which is away from the jet in the forwards direction, as illustrated in case (a) of Figure 3-13. At higher latitudes however, the air velocity relative to the jet equals $V_k = V_v - \tilde{V}_x$ and is in the rearward direction relative to the jet, as shown in Figure 3-13, case (b). However for both cases (a) and (b), the turbulent inward diffusion process is only a function of the absolute value of V_k that is of $|V_k| = |V_v - \tilde{V}_x| = |\tilde{V}_x - V_v|$. The same degree of turbulence results whether the shear stresses in the exhaust/air interface are in one direction or in the other.

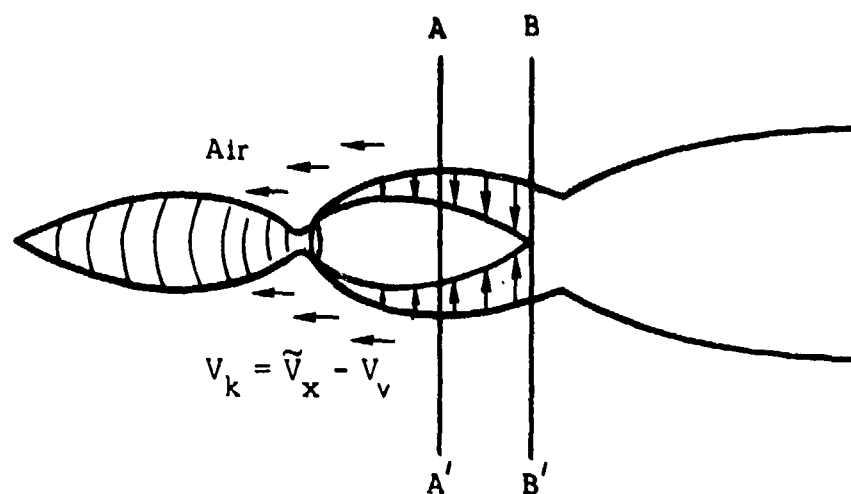
In Appendix D it is shown that the number of air molecules that have diffused inward into the plume over a distance $L_p = z_f$, that is in the region prior to plane B-B', is given by:

$$N_a = 0.98 m_I \pi a_e^2 z_f = 0.98 m_I \pi a_e^2 \bar{V}_M t_f, \text{ moles} \quad (3.187)$$

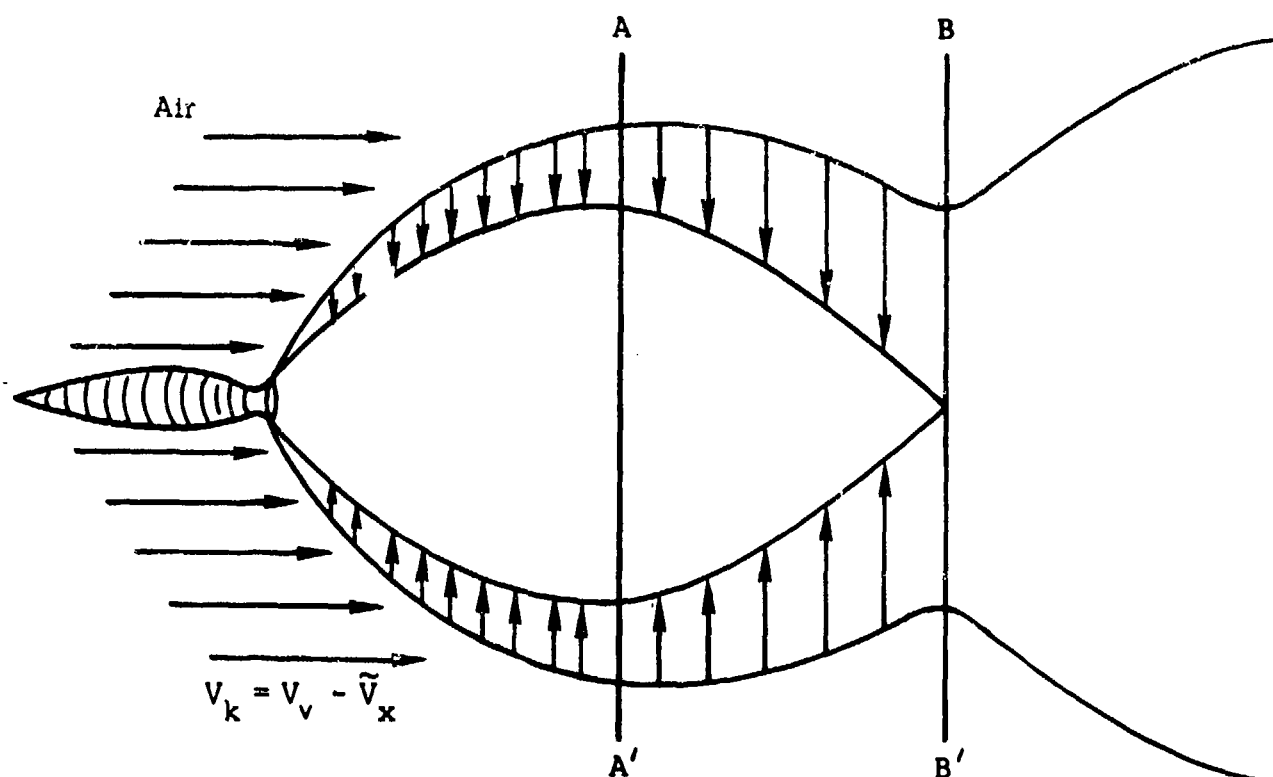
Here t_f is the time of travel required for the air to penetrate to the center of the plume and z_f is (see Appendix B):

$$z_f = \bar{V}_M t_f = \frac{\bar{V}_M a_e^2}{4 D}, \text{ m} \quad (3.188)$$

*We are calculating here an average mixing ratio for the ABCD region of the plume. Actually the mixing ratio varies axially of course, and at large distances from the nozzle exit where the exhaust gases have come to rest with respect to the atmosphere (i.e., in the exhaust "cloud") $\mu_{a/e} \rightarrow \infty$ as $t \rightarrow \infty$.



Case (a) $\tilde{V}_x > V_v$



Case (b) $V_v > \tilde{V}_x$

FIGURE 3-13. ILLUSTRATION OF MIXING PROBLEM

\bar{V}_M is the average bulk velocity of the exhaust in the core given by Eq. (3.147) and z_e is the average radius of the plume (see Appendix D) which can be approximated by:

$$z_e \approx \frac{D_e + D_h}{4}, \quad m \quad (3.189)$$

Here D_e is the nozzle exit diameter, as before, and D_h is the diameter of the fully expanded plume (see below). The parameter m_I in (3.187) is the molar density (moles/m³) of air at the pure air/plume interface.

The amount of exhaust gas in the region prior to plane B-B' is given by:

$$N_{\text{exh}} = \frac{1000 \dot{W}}{\bar{M}_e} t_f = \frac{\pi}{4} D_e^2 V_e t_f m_e, \quad \text{moles} \quad (3.190)$$

where m_e is the molar density (moles/m³) of the exhaust in the nozzle exit plane. Then the average air/exhaust mixing ratio $\mu_{a/e}$ is given by:

$$\mu_{a/e} = \frac{N_a}{N_{\text{exh}}} = \frac{0.98}{4} \left(\frac{D_e + D_h}{D_e} \right)^2 \frac{\bar{V}_M}{V_e} \frac{m_I}{m_e} \quad (3.191)$$

The molar densities m_I and m_e are given by:

$$m_I = \frac{\rho_I}{\bar{M}_a} = \frac{p_I}{RT_I} = \frac{1000 p_I}{0.08317 T_I}, \quad \frac{\text{moles}}{\text{m}^3} \quad (3.192a)$$

$$m_e = \frac{1000 p_e}{0.08317 T_e}, \quad \frac{\text{moles}}{\text{m}^3} \quad (3.192b)$$

June 1974

Here p_I and T_I are the pressure and temperature in the air/plume interface layer. Now $p_I = p_a$ is a good approximation, but $T_I \neq T_a$. In fact $T_I \approx (T_{\text{exh}} + T_e)/2 \approx T_e$ is a reasonable approximation since the air is heated in the interface region. With these assumptions ($p_I = p_a$; $T_I = T_e$) then, the mixing ratio becomes (setting the factor $0.98 \approx 1$):

$$\mu_{a/e} = \frac{p_a}{p_e} \frac{\bar{V}_M}{V_e} \left\{ \frac{D_e + D_h}{2D_e} \right\}^2 = \frac{1}{4} \frac{p_a}{p_e} \frac{\bar{V}_M}{V_e} \cdot \left[1 + \left(\frac{\gamma-1}{2} \right)^{1/4} \left(\frac{2}{\gamma+1} \right)^{\frac{\gamma+1}{4(\gamma-1)}} \left(\frac{p_c}{p_a} \right)^{\frac{1}{2\gamma}} \beta_M^{1/2} \cdot \left\{ 1 - \left(\frac{p_a}{p_c} \right)^{\frac{\gamma-1}{\gamma}} \right\}^{-1/4} \right]^2$$

(3.193)

In the second part of (3.193), the expression for the fully expanded exhaust flow diameter D_h is written out which can be shown to equal (see Vol. IV):

$$D_h = \beta_M^{1/2} D_{\text{exh}} = D_{\text{exh}} \left(\frac{\gamma-1}{2} \right)^{1/4} \left(\frac{2}{\gamma+1} \right)^{\frac{\gamma+1}{4(\gamma-1)}} \beta_M^{1/2} \cdot \left(\frac{p_c}{p_a} \right)^{\frac{1}{2\gamma}} \left[1 - \left(\frac{p_a}{p_c} \right)^{\frac{\gamma-1}{\gamma}} \right]^{-1/4}, \quad m \quad (3.194)$$

Here β_M given by Eq. (3.186) is the correction factor to account for radiation losses from the core for the otherwise adiabatically expanding jet.

* See New Page

June 1974

Here p_I and T_I are the pressure and temperature in the air/plume interface layer. Now $p_I = p_a$ is a good approximation, but $T_I \neq T_a$. In fact according to Eq. (3.142c), $T_I \approx T_e (p_a/p_e)^{2(\gamma-1)/3\gamma}$ is a more reasonable estimate for the interface region. With these assumptions ($p_I = p_a$; $T_I = T_e (p_a/p_e)^{2(\gamma-1)/3\gamma}$), the mixing ratio becomes (setting the factor $0.98 \approx 1$):

$$\mu_{a/e} = \left(\frac{p_a}{p_e} \right)^{\frac{\gamma+2}{3\gamma}} \frac{\bar{v}_M}{v_e} \left\{ \frac{D_e + D_h}{2D_e} \right\}^2 = \frac{1}{4} \left(\frac{\bar{v}_M}{v_e} \right) \left(\frac{p_a}{p_e} \right)^{\frac{\gamma+2}{3\gamma}} \cdot \left[1 + \beta_M^{1/2} \left(\frac{p_e}{p_a} \right)^{\frac{1}{2\gamma}} \left\{ \frac{1 - (p_e/p_c)^{(\gamma-1)/\gamma}}{1 - (p_a/p_c)^{(\gamma-1)/\gamma}} \right\}^{1/4} \right]^2 \quad (3.193)$$

In the second part of (3.193), the expression for the fully expanded exhaust flow diameter D_h is written out which can be shown to equal (see Vol. IV):

$$D_h = \beta_M^{1/2} D_{exh} = D_t \left(\frac{\gamma-1}{2} \right)^{1/4} \left(\frac{2}{\gamma+1} \right)^{\frac{\gamma+1}{4(\gamma-1)}} \beta_M^{1/2} \cdot \left(\frac{p_c}{p_a} \right)^{\frac{1}{2\gamma}} \left[1 - \left(\frac{p_a}{p_c} \right)^{\frac{\gamma-1}{\gamma}} \right]^{-1/4}, \quad m \quad (3.194)$$

Here β_M given by Eq. (3.186) is the correction factor to account for radiation losses from the core for the otherwise adiabatically expanding jet.

If we assume Eq. (3.147) for \bar{V}_M , the mixing ratio expression (3.193) can be expressed finally in the form:

$$\mu_{a/e} = \frac{1}{4} \left(\frac{p_a}{p_e} \right)^{\frac{\gamma+2}{2\gamma}} \left\{ 1 + \frac{1}{3} \frac{T_e}{T_c - T_e} \left(1 - \left(\frac{p_a}{p_e} \right)^{\frac{\gamma-1}{\gamma}} \right) \right\}^{1/2} \cdot \left[1 + \beta_M^{1/2} \left(\frac{p_e}{p_a} \right)^{\frac{1}{2\gamma}} \left\{ \frac{1 - (p_e/p_c)^{(\gamma-1)/\gamma}}{1 - (p_a/p_c)^{(\gamma-1)/\gamma}} \right\}^{1/4} \right]^2$$

(3.195)

Here p_a and p_e are the ambient air and nozzle exit plane pressures, and we used Eq. (3.116) for T_{exh} in the expression for \bar{V}_M .

Equation (3.195) still contains one difficulty in that the pressure, temperature, and velocity in the nozzle exit plane, p_e , T_e , and V_e are constant and equal to the design value only as long as $p_a < p_e$. If $p_a > p_e$, which occurs usually at rocket launch altitudes (that is near the ground), the exhaust will separate from the nozzle wall upstream from the exit plane (overexpanded nozzle case). In this case p_e , T_e , and V_e are different from the nozzle design values p_0 , T_0 , and V_0 . To account for this situation, we therefore must write:

$$p_e = p_0 H(p_0 - p_a) + p_a H(p_a - p_0), \text{ bars} \quad (3.196)$$

If we assume Eq. (3.147) for \bar{V}_M , the mixing ratio expression (3.193) can be expressed finally in the form:

$$v_{a/e} = \frac{1}{4} \left(\frac{p_a}{p_e} \right) \left\{ 1 + \frac{1}{3} \frac{T_e}{T_c - T_e} \left(1 - \left(\frac{p_a}{p_e} \right)^{\frac{\gamma-1}{\gamma}} \right) \right\}^{1/2} \cdot \left[1 + \left(\frac{\gamma-1}{2} \right)^{1/4} \left(\frac{2}{\gamma+1} \right)^{\frac{\gamma+1}{4(\gamma-1)}} \left(\frac{p_c}{p_a} \right)^{\frac{1}{2\gamma}} \beta_M^{1/2} \cdot \left\{ 1 - \left(\frac{p_a}{p_c} \right)^{\frac{\gamma-1}{\gamma}} \right\}^{-1/4} \right]^2 \quad (3.195)$$

Here p_a and p_e are the ambient air and nozzle exit plane pressures, and we used Eq. (3.116) for T_{exh} in the expression for \bar{V}_M .

Equation (3.195) still contains one difficulty in that the pressure, temperature, and velocity in the nozzle exit plane, p_e , T_e , and V_e are constant and equal to the design value only as long as $p_a < p_e$. If $p_a > p_e$, which occurs usually at rocket launch altitudes (that is near the ground), the exhaust will separate from the nozzle wall upstream from the exit plane (overexpanded nozzle case). In this case p_e , T_e , and V_e are different from the nozzle design values p_o , T_o , and V_o . To account for this situation, we therefore must write:

$$p_e = p_o H(p_o - p_a) + p_a H(p_a - p_o), \text{ bars} \quad (3.196)$$

*SEE NEW PAGE.

$$T_e = T_o H(p_a - p_o) + T_c \left(\frac{p_a}{p_c} \right)^{(\gamma-1)/\gamma} H(p_o - p_a), \text{ } ^\circ K \quad (3.197)$$

$$V_e = V_o H(p_a - p_o) + 129 \left[\left(\frac{\gamma}{\gamma-1} \right) \frac{T_c}{\bar{M}_e} \left\{ 1 - \left(\frac{p_a}{p_c} \right)^{(\gamma-1)/\gamma} \right\} \right]^{1/2} \cdot H(p_o - p_a), \text{ m/sec} \quad (3.198)$$

$$V_o = 129 \left[\left(\frac{\gamma}{\gamma-1} \right) \frac{T_c}{\bar{M}_e} \left\{ 1 - \left(\frac{p_o}{p_c} \right)^{(\gamma-1)/\gamma} \right\} \right]^{1/2}, \text{ m/sec} \quad (3.199)$$

Here p_c and T_c are the rocket combustion chamber (static) pressure and temperature, \bar{M}_e and γ are the molecular weight (grammoles) and specific heat ratio of the exhaust gas.

Thus by using p_e , T_e , and V_e as defined by (3.196) through (3.199) in Eq. (3.193) or Eq. (3.195), a satisfactory expression for the mixing ratio results. Of course p_e , T_e , and V_e are simply equal to the design values p_o , T_o , and V_o at the higher altitudes where $p_a < p_o$.

Having evaluated the parameters necessary to calculate T_{mix} via Eq. (3.175), we next calculate the temperature increments ΔT_{AB} and ΔT_{CD} due to afterburning and collisional deceleration. We must have from a simple heat balance that:

$$\begin{aligned} \Delta T_{AB} &= \frac{\left(y_{H_2} \xi_{H_2O} \Delta H_{H_2} + y_{CO} \xi_{CO} \Delta H_{CO} \right) N_{exh}}{N_{exh} C_e + N_a C_a} = \\ &= \frac{C_e^{-1} \left(y_{H_2} \xi_{H_2O} \Delta H_{H_2} + y_{CO} \xi_{CO_2} \Delta H_{CO} \right)}{1 + \mu_{a/e}}, \text{ } ^\circ K \end{aligned} \quad (3.200)$$

Here:

y_{H_2}, y_{CO} = Mole fractions of H_2 and CO respectively
in the exhaust in the nozzle exit plane

$$y_{H_2} = \bar{M}_e \frac{g_{H_2}}{1000} \quad (3.201)$$

$$y_{CO} = \bar{M}_e \frac{g_{CO}}{1000} \quad (3.202)$$

g_{H_2}, g_{CO} = Moles of H_2 and CO per kilogram of exhaust
gas

ξ_{H_2O}, ξ_{CO_2} = Degree of completion of combustion of
 $H_2 \rightarrow H_2O$ and $CO \rightarrow CO_2$ respectively given
by Eqs. (3.164) and (3.165)

$\Delta H_{H_2}, \Delta H_{CO}$ = Heat of combustion of $H_2 \rightarrow H_2O$ and $CO \rightarrow CO_2$
reactions, Joules \cdot mole $^{-1}$

C_e, C_a = Specific heat (constant pressure) of exhaust
and air respectively, Joules $^{\circ}K^{-1} \cdot$ mole $^{-1}$

The measured heats of combustion for the gaseous reactions
 $H_2 + \frac{1}{2} O_2 \rightarrow H_2O$ and $CO + \frac{1}{2} O_2 \rightarrow CO_2$ are $\Delta H_{H_2} = 285,000$ Joules/mole and
 $\Delta H_{CO} = 281,000$ Joules/mole respectively, while the specific heat for most
exhausts that are rich in H_2O and CO_2 is $C_e \approx 34.1$ Joules mole $^{-1} \cdot$ $^{\circ}K^{-1}$.
Substituting these values in (3.200) gives:

$$(\Delta T)_{AB} = \frac{8.3578 \bar{M}_e \left(y_{H_2} \xi_{H_2O} + 0.986 g_{CO} \xi_{CO_2} \right)}{1 + \mu_{a/e}}, \quad ^{\circ}K \quad (3.203)$$

June 1974

Turning next to the temperature rise from collisional deceleration, we have if we assume that the relative dynamic energy between the plume and ambient air along the trajectory is converted adiabatically to heat (that is

$$\left(\frac{\gamma}{\gamma-1}\right) R \Delta T_{CD} = \frac{1}{2} \bar{M}_e V_k^2)^*:$$

$$\begin{aligned} (\Delta T)_{CD} &= \frac{x_{CD} \bar{M}_e V_k^2 N_{exh}}{M_{exh} + N_a} = \\ &= \left(\frac{x_{CD} \bar{M}_e}{1 + \mu_{a/e}} \right) \left\{ V_v^2 + 2 V_v V_Q \cos(\theta - \varphi) + V_Q^2 \cos^2(\theta - \varphi) \right\}, \text{ } ^\circ K, \quad (3.204) \end{aligned}$$

where the factor x_{CD} is given by:

$$x_{CD} = \left(\frac{\gamma-1}{\gamma} \right) \left(\frac{1}{2R} \right) = 60.12 \times 10^{-6} \left(\frac{\gamma-1}{\gamma} \right), \frac{^\circ K \text{ mole}}{g \cdot m^2} \quad (3.205)$$

and where:

\bar{M}_e = Average mass of exhaust molecules, grams per mole (\therefore a.m.u.)

V_v = Rocket vehicle velocity, m/sec

V_Q = Average velocity of the exhaust in the ABCD region relative to the rocket vehicle, m/sec

θ = Angle between rocket thrust direction and direction of motion of rocket, degrees

φ = Jet flare angle, degrees

γ = c_p/c_v = Specific heat ratio of the exhaust/air mixture

*The dynamic energy component in the radial direction, $\frac{1}{2} \bar{M}_e \tilde{V}_y^2$, is consumed by the work needed for expansion of the plume from pressure p_e to ambient pressure p_a .

In Eq. (3.204) we generalized the relations for the exhaust velocity to the case that the jet axis (or rocket thrust direction) does not coincide with the direction of motion of the rocket vehicle, as for example for a vernier engine or retro thruster. With V_Q as the averaged bulk velocity of the exhaust gas in the ABCD region relative to the rocket, one can write the relations:

$$V_k = (V_v - \tilde{V}_x) = (V_v + V_Q \cos(\theta - \varphi)) \quad (3.206)$$

$$\tilde{V}_x = V_Q \cos(\pi - \theta + \varphi) = -V_Q \cos(\theta - \varphi) \quad (3.207)$$

$$\tilde{V}_y = V_Q \sin(\pi - \theta + \varphi) = -V_Q \sin(\theta - \varphi) \quad (3.208)$$

$$\tilde{V}_x^2 + \tilde{V}_y^2 = V_Q^2 \quad (3.209)$$

Here φ is the average flare angle of the jet and θ is the angle measured between the forwards direction of motion of the rocket and the thrust vector direction.

For a large booster rocket, $\theta = 180^\circ$ of course and Eqs. (3.206) and (3.208) reduce to:

$$V_k^2 = (V_v - V_Q \cos \varphi)^2 \quad (3.210)$$

$$\tilde{V}_y = V_Q \sin \varphi \quad (3.211)$$

June 1974

Equations (3.210) and (3.211) usually apply to most cases of interest.

For diatomic molecules $\gamma = 1.4$ and we obtain $\chi_{CD} = 17.2$ from Eq. (3.205), while for $\gamma = 1.25$, we get $\chi_{CD} = 12 \times 10^{-6}$. Since most of the air/exhaust mixing region contains diatomic molecules, we shall take $\chi_{CD} \approx 17 \times 10^{-6}$ in Eq. (3.204) and thus:

$$\Delta T_{CD} = \frac{17 \times 10^{-6} \bar{M}_e (V_v^2 + V_v V_Q \cos(\theta - \varphi) + V_Q^2 \cos^2(\theta - \varphi))}{1 + \mu_{a/e}} \text{ , } ^\circ\text{K} \quad (3.212)$$

In Eq. (3.212), V_v and V_Q are in meters per second.

Adding the contributions (3.175), (3.203), and (3.212) we can write finally for the total temperature T_r in the mixing region:

$$\Theta = \frac{T_r}{T_a} = \frac{T_Q + \mu_{a/e} T_a + 17 \times 10^{-6} \bar{M}_e (V_v + V_Q \cos(\theta - \varphi))^2}{T_a (1 + \mu_{a/e})} + \frac{8.3578 \bar{M}_e (g_{H_2} \xi_{H_2O} + 0.986 g_{CO} \xi_{CO_2})}{T_a (1 + \mu_{a/e})} \quad (3.213)$$

It remains to find expressions for V_a , D_a , V_Q , and the flare angle φ . From a comparison of Eqs. (3.160) and (3.161) with Eqs. (3.187) and (3.190), it is clear that we may write for the air inflow into the plume:

$$V_a = 0.98 \bar{V}_M, \text{ m/sec} \quad (3.214)$$

$$D_a = 2a_e = \frac{D_e + D_h}{2}, \text{ m} \quad (3.215)$$

where D_h was defined by Eq. (3.194), D_e is the nozzle exit diameter, and \bar{V}_M was given by Eq. (3.147). With these definitions for V_a and D_a , Eqs. (3.167) through (3.169) can be written:

$$\xi_o = \frac{1}{1 + \mu_{a/e}(\bar{M}_a/\bar{M}_e)} \quad (3.216)$$

$$\xi_h = \left(\frac{13.64}{g_{H_2}} \right) \left(\frac{\mu_{a/e}(\bar{M}_a/\bar{M}_e)}{1 + \mu_{a/e}(\bar{M}_a/\bar{M}_e)} \right) \quad (3.217)$$

$$\xi_c = \left(\frac{13.64}{g_{CO}} \right) \left(\frac{\mu_{a/e}(\bar{M}_a/\bar{M}_e)}{1 + \mu_{a/e}(\bar{M}_a/\bar{M}_e)} \right) \quad (3.218)$$

Of course ξ_{H_2O} and ξ_{CO_2} are still given by (3.164) and (3.165) with ξ_o , ξ_h , and ξ_c given by (3.216) through (3.218). That is:

$$\xi_{H_2O} = \xi_o, \text{ if } \xi_o < \xi_h \quad (3.219a)$$

June 1974

$$\xi_{H_2O} = \xi_h, \quad \text{if } \xi_h < \xi_o \quad (3.219b)$$

$$\xi_{CO_2} = \xi_o, \quad \text{if } \xi_o < \xi_c \quad (3.220a)$$

$$\xi_{CO_2} = \xi_c, \quad \text{if } \xi_c < \xi_o \quad (3.220b)$$

In Eqs. (3.216) through (3.218) we used the relation:

$$\mu_{a/e} = \frac{(\rho_a / \bar{M}_a) V_a \left(\frac{\pi}{4} \right) D_a^2}{1000 \dot{W} / \bar{M}_e} = \left(\frac{\bar{M}_e}{\bar{M}_a} \right) \left(\frac{\rho_a V_a}{1000 \dot{W}} \right) \left(\frac{\pi}{4} D_a^2 \right) \quad (3.221)$$

Next, expressions for V_Q and φ will be developed. At low altitudes where the plume exhibits little blossoming $\tilde{V}_x = V_Q \approx (V_e + V_h)/2$. That is the average velocity of the exhaust in the atmosphere relative to the rocket has a value between that at the nozzle exit and the value attained at the point where it is fully expanded to ambient pressure. However at higher altitudes the bulk velocity in the air shock region (where the exhaust collides with atmospheric air) is no longer mostly in the rearward direction but instead it is sideways due to the flare-out of the jet. If this mean flare angle is φ in the air shock region, then \tilde{V}_x and \tilde{V}_y are:

$$\tilde{V}_x \approx V_Q \cos \varphi, \quad \text{m/sec} \quad (3.222)$$

$$\tilde{V}_y \approx V_Q \sin \varphi, \quad \text{m/sec}, \quad (3.223)$$

where:

$$V_Q \approx \frac{1}{2} (V_e + V_h), \quad \text{m/sec} \quad (3.224)$$

Here V_h was given by Eq. (3.179). Though a coarse approximation, we shall assume the simple average expressed by Eq. (3.224) for the velocity V_Q in the ABCD region in what follows.

Turning next to the flare angle ϕ , according to frictionless Eulerian fluid dynamics (see Vol. IV), there is a maximum expansion angle for a supersonic jet. The (approximate) Prandtl-Meyer theory gives for this maximum angle of the bulk fluid flow:

$$\left(\phi_{\max}\right)_{\text{Prandtl-Meyer}} = \left(\sqrt{\frac{\gamma + 1}{\gamma - 1}} - 1 \right) \frac{\pi}{4}, \text{ radians}, \quad (3.225)$$

which for typical rockets with $\gamma = 1.25$ yields $\phi_{\max} = 180$ degrees. Clearly this result is unreasonable and counter to observations. The result is not completely surprising however since Eq. (3.225), which is based on Eulerian fluid flow theory, does not account for molecular diffusion and mixing effects.

An improved method (over that of Prandtl and Meyer) for the calculation of maximum jet flare angles is presented in Appendix F. It is based on the approximate high-altitude flow theory of Hill and Draper (see Vol. IV). The high-altitude Hill-Draper jet-flow theory is also based on Eulerian frictionless flow. However it assumes further a Gaussian exhaust-gas density distribution (as a function of the polar angle about the jet axis) for gas jets that discharge into a vacuum or very thin atmosphere. This assumption, though somewhat ad hoc, introduces real gas behavior (that is some of the molecular nature of a gas) into the otherwise mathematically continuous and frictionless fluid postulated by the Euler equations.

The expression for the maximum (high-altitude) jet flare angle $(\varphi_{CD})_{\max}$, based on the Hill-Draper theory, is given by (see Appendix F):

$$(\varphi_{CD})_{\max} = \cos^{-1} \left[1 - \zeta (\pi \ln B)^{1/2} \right], \quad (3.226)$$

where ζ is the Hill-Draper parameter given by:

$$\zeta = \frac{1}{\gamma} \left(\frac{p_e}{p_c} \right)^{\frac{\gamma-1}{\gamma}} \left[\left(\frac{2}{\gamma-1} \right) \left\{ 1 - \left(\frac{p_e}{p_c} \right)^{\frac{\gamma-1}{\gamma}} \right\} \right]^{-1}, \quad (3.227)$$

and:

$$B \approx 4.6 \times 10^5 D_e \left(\frac{p_c}{T_c} \right) \left(\frac{p_c}{p_e} \right) \left(\frac{\gamma}{E^2} \right) \left(\frac{2}{\gamma+1} \right)^{\frac{\gamma+1}{\gamma-1}} \quad (3.228)$$

Here the nozzle expansion ratio E is given by:

$$E = \left(\frac{D_e}{D_t} \right)^2 = \left(\frac{2}{\gamma+1} \right)^{\frac{\gamma+1}{2(\gamma-1)}} \left(\frac{p_c}{p_e} \right)^{\frac{1}{\gamma}} \left[\left(\frac{2}{\gamma-1} \right) \left\{ 1 - \left(\frac{p_e}{p_c} \right)^{\frac{\gamma-1}{\gamma}} \right\} \right]^{-\frac{1}{2}} \quad (3.229)$$

In the above relations, the nozzle exit diameter D_e and throat diameter D_t are in meters, the combustion chamber pressure p_c and nozzle exit plane pressure p_e are in bars and the combustion chamber temperature T_c is in degrees Kelvin.

For typical booster rockets with $\gamma = 1.25$, $\zeta = 0.075$, and $B = 3000$, we find from Eq. (3.226) the value $(\varphi_{CD})_{\max} = 51.4$ degrees. This result is much closer to the observed high-altitude jet flare angles than the value $\varphi_{\max} = 180$ degrees which one obtains from the Prandtl-Meyer equation (3.225).

Now as a rocket moves up from the ground into the upper atmosphere, the jet expands from an average flare angle of $\varphi_{CD} \approx 0$ degrees to $(\varphi_{CD})_{\max} \approx 51.4$ degrees. To obtain a relation giving the dependence of $\varphi \equiv \varphi_{CD}$ with altitude, we shall make the semi-empirical estimate:

$$\varphi \approx (\varphi_{CD})_{\max} \exp\left\{-\frac{D_e}{D_{\text{exh}}}\right\} =$$

$$\varphi = (\varphi_{CD})_{\max} \exp\left[\left(\frac{p_a}{p_e}\right)^{\frac{1}{2\gamma}} \left(\frac{1 - (p_a/p_c)^{\frac{\gamma-1}{\gamma}}}{1 - (p_o/p_e)^{\frac{\gamma-1}{\gamma}}}\right)^{\frac{1}{4}}\right] \quad (3.230)$$

Here p_e is given by Eq. (3.196). Equation (3.230) shows the proper altitude-dependent behavior for the flare angle. For $(D_e/D_{\text{exh}}) \ll 1$, which occurs at high altitudes, we have:

$$\varphi \approx (\varphi_{CD})_{\max} \left(1 - \frac{D_e}{D_{\text{exh}}}\right) \approx (\varphi_{CD})_{\max} \left(\frac{D_{\text{exh}} - D_e}{D_{\text{exh}}}\right) \quad (3.231)$$

which gives the proper scaling since $\varphi \rightarrow 0$ if $D_{\text{exh}} = D_e$ and $\varphi \rightarrow (\varphi_{CD})_{\max}$ when $D_{\text{exh}} \gg D_e$. The exponential form (3.230) is preferable over the linear

June 1974

form (3.231) however since it prevents the angle ϕ from going negative at very low (launch-point) altitudes where $D_{\text{exh}} < D_e$ for most rockets.

With relation (3.230), all parameters except T_0 in Eq. (3.213) can now be completely determined from the basic rocket hardware parameters, the rocket's flight trajectory, and the atmosphere's pressure and temperature behavior with altitude.

There remains still one problem in using Eq. (3.213) for all altitudes. This is the fact that as a rocket moves into the vacuum of space, the collisional mean free path becomes infinite so that the region in which conversion of kinetic energy into heat takes place via the CD process becomes also infinite in extent.

In deriving expression (3.213), it was assumed that the AB, CD, and mixing exchange processes all took place within a relatively confined region, that is in a thin air shock and sharp afterburning combustion zone. At very high altitudes, this assumption is no longer true and a thick air shock and practically no combustion exist. Although the view factor F_v (see section 3.3.9) accounts for some of the spreading of the CD source energy and radiation as the effective plume length $L_p \rightarrow \infty$ (one has that $F_v \rightarrow 0$, for $L_p \rightarrow \infty$), at near-vacuum altitudes we have to further correct Eq. (3.213) and allow the $(\Delta T)_{\text{CD}}$ contribution to vanish as the altitude $h \rightarrow \infty$ (and therefore $L_p \rightarrow \infty$).

The reason for requiring such a correction is that at deep-space altitudes, the sum of the CORE and ABCD radiation expressions must go over into the expression for DSPR radiation developed in section 3.3.2. Since the CORE region becomes rather large at very high altitudes where $p_a \rightarrow 0$ (see the discussion following Eq. (3.145)), most of the molecules relax and radiate within the CORE, long before encountering an air molecule via which they

could experience CD excitations. Thus essentially the CORE radiation approaches the DSPR radiation and the temperature T_Q of molecules entering the CD region must approach the value T_h when $\tau_M \gg \tau_i$. Further, even after molecules have moved beyond the undisturbed core, their chance of colliding with an air molecule within the field-of-view of the observer become vanishingly small of course as $p_a \rightarrow 0$.*

An inspection of Eq. (3.213) shows that the afterburning contributions (ϵ_{H_2O} and ϵ_{CO_2}), and the air enthalpy contributions ($\mu_{a/e} T_a$) to the effective ABCD zone temperature T_r , vanish as $p_a \rightarrow 0$ as they should. The two remaining terms are the mean exhaust temperature contribution T_q which, as stated, should approach the value T_h , and the CD contribution $\Delta T_{CD} = 17 \times 10^{-6} \bar{M}_e [V_v + V_Q \cos(A-\phi)]^2$ which should vanish as $p_a \rightarrow 0$.

Now in the formal radiation expressions that were developed in sections 3.3.2 and 3.3.3 two temperatures are needed. One temperature, say T_1 , is needed to represent the average temperature of excited source molecules that flow through an imaginary boundary into a region where the molecules emit radiation, while the second temperature, say T_2 , represents the average temperature in the radiating region. Since radiation means a drop in temperature we have always that $T_2 < T_1$. The temperature T_1 is needed in the Boltzmann population factors $\exp\{-\epsilon_i/(kT)\}$ used in the radiation equations, while T_2 is required in the expressions for the band-width function $\Delta\nu_{mn}$. For the DSPR case we had:

$$(T_1)_{\text{DSPR}} = T_e \quad (3.232)$$

*Theoretically all kinetic energy of the exhaust relative to the atmosphere is ultimately converted to heat and radiation and could be observed if the field-of-view were large enough, and as long as $p_a \neq 0$.

June 1974

$$(T_2)_{\text{DSPR}} = T_C \approx \frac{2}{3} T_e, \quad (3.233)$$

while for CORE radiation we had:

$$(T_1)_{\text{CORE}} = T_e \quad (3.234)$$

$$(T_2)_{\text{CORE}} = T_M \approx \frac{2}{3} T_e + \frac{1}{3} T_{\text{exh}} \quad (3.235)$$

To assure that $T_Q \rightarrow T_h$ at altitudes where τ_M becomes very large compared to τ_i , and to account for the fact that $T_2 < T_1$, we shall therefore make the following estimates for $(T_Q)_1$ and $(T_Q)_2$:

$$(T_Q)_1 = \frac{1}{3} T_h + \frac{2}{3} \left[T_e \frac{\tau_i}{\tau_M + \tau_i} + T_h \frac{\tau_M}{\tau_M + \tau_i} \right], \text{ } ^\circ\text{K} \quad (3.236)$$

$$(T_Q)_2 = \frac{1}{2} T_h + \frac{1}{2} \left[T_e \frac{\tau_i}{\tau_M + \tau_i} + T_h \frac{\tau_M}{\tau_M + \tau_i} \right], \text{ } ^\circ\text{K} \quad (3.237)$$

Here τ_M was given by Eq. (3.140), and T_h by Eq. (3.178).

Adjusting further the ΔT_{CD} term so it vanishes at high altitudes, we shall write it as:

$$\Delta T_{\text{CD}} = 17 \times 10^{-6} \bar{M}_e \left[V_v + V_Q \cos(\theta - \varphi) \right]^2 f_{\text{CD}}, \text{ } ^\circ\text{K}, \quad (3.238)$$

where for TTO and ICO observations respectively:

$$(f_{CD})_{TTO} = \frac{\tau_s}{\tau_s + \tau_{CD}} = \frac{1}{1 + V_v \tau_{CD}/D_s} \quad (3.239a)$$

$$(f_{CD})_{ICO} = \frac{D_s}{D_s + \lambda_{CD}} = \frac{1}{1 + \lambda_{CD}/D_s} \quad (3.239b)$$

Here V_v is the rocket vehicle velocity (m/sec), D_s is the sensor's field-of-view diameter (m) at the plume, and τ_{CD} is the mean time (sec) and λ_{CD} the mean path (m) between collisions for an air molecule that penetrates the plume. The latter parameters can be shown to equal:

$$\begin{aligned} \tau_{CD} &= \left[|V_v + V_Q \cos(\theta - \varphi)| n_a \sigma_{a/X} \right]^{-1} = \\ &= 3.456 \times 10^{-9} \left(\frac{T_a(^{\circ}K)}{p_a(\text{bars})} \right) \frac{|V_v + V_Q \cos(\theta - \varphi)|^{-1}}{(\text{m/sec})}, \text{ sec} \end{aligned} \quad (3.240)$$

$$\lambda_{CD} = (n_a \sigma_{a/X})^{-1} = 8.748 \times 10^{-10} \left(\frac{T_a(^{\circ}K)}{p_a(\text{bars})} \right), \text{ m} \quad (3.241)$$

Here n_a is the molecular density of air and $\sigma_{a/X}$ is the average microscopic collision cross-section between exhaust and air molecules which is taken as $\sigma_{a/X} \approx 16 \times 10^{-20} \text{ m}^2$ (see Table 3-1) for the high altitudes where air is partially dissociated.

The factor f_{CD} gives the probability that a collision can occur (and thus ΔT_{CD} be created) during a sensor's time of observation τ_s of the plume ($\tau_s = D_s/V_v$) and/or in its field-of-view diameter D_s .

With the above final adjustments, we obtain:

$$\Theta_1 - \frac{(T_r)_1}{T_a} = \left[(1 + \mu_{a/e}) T_a \right]^{-1} \cdot \left[\mu_{a/e} T_a + \frac{1}{3} T_h + \frac{2}{3} \left\{ T_e \left(\frac{\tau_i}{\tau_M + \tau_i} \right) + \right. \right. \\ \left. \left. + T_h \left(\frac{\tau_M}{\tau_M + \tau_i} \right) \right\} + 17 \times 10^{-6} \bar{M}_e \cdot (V_v + V_Q \cos(\theta - \varphi))^2 f_{CD} + \right. \\ \left. + 8.3578 \bar{M}_e (g_{H_2} \xi_{H_2O} + 0.986 g_{CO} \xi_{CO_2}) \right]$$

(3.242)

$$\Theta_2 = \frac{(T_r)_2}{T_a} = \left[(1 + \mu_{a/e}) T_a \right]^{-1} \cdot \left[\mu_{a/e} T_a + \frac{1}{2} T_h + \frac{1}{2} \left\{ T_e \left(\frac{\tau_i}{\tau_M + \tau_i} \right) + \right. \right. \\ \left. \left. + T_h \left(\frac{\tau_M}{\tau_M + \tau_i} \right) \right\} + 17 \times 10^{-6} \bar{M}_e \cdot (V_v + V_Q \cos(\theta - \varphi))^2 f_{CD} + \right. \\ \left. + 8.3578 \bar{M}_e (g_{H_2} \xi_{H_2O} + 0.986 g_{CO} \xi_{CO_2}) \right]$$

(3.243)

Here $\mu_{a/e}$ is the mixing ratio given by Eq. (3.195); T_a is the ambient air temperature ($^{\circ}K$); T_e is the exhaust temperature in the rocket nozzle exit

plane; T_h is the fully expanded exhaust temperature given by Eq. (3.178); V_v is the rocket vehicle velocity (m/sec), V_0 is the exhaust velocity given by (3.224) in m/sec; ξ_{H_2O} and ξ_{CO_2} are given by (3.216) through (3.220); θ is the thrust vector angle; φ is the jet flare angle; \bar{M}_e is the mean molecular weight of the exhaust (grams/mole); and g_{H_2} and g_{CO} are the moles per kilogram of H_2 and CO that exit from the nozzle into the atmosphere.

Returning to Eq. (3.157), and using Eqs. (3.171), (3.172), (3.173), (3.242), and (3.243), one obtains the following relation for ABCD radiation:

$$\left(\frac{dJ}{dv}\right)_{ABCD} = 31.756 \times 10^{-11} \frac{\dot{W}}{(\text{kg/s})(\text{THz})} v F_v \text{Tr}(v, S) \cdot$$

$$\cdot \sum_i \sum_j g'_i f_{ij} \left[\frac{b(v, v_{ij}, \Delta v_{ij})}{\Delta v_{ij} (T_a \Theta_2)} \right] \left[\exp \left\{ -\frac{\epsilon_i}{k T_a \Theta_1} \right\} \right], \frac{\text{Watts}}{\text{ster} \cdot \text{THz}}$$

(3.244)

Here $\Delta v_{ij} = \Delta v_{ij}(T_a \Theta_2)$ and $\exp\{-\epsilon_i/(k T_a \Theta_1)\}$ are the band-spread and Boltzmann factor which must be evaluated respectively at $T = (T_r)_2 = T_a \Theta_2$, and $T = (T_r)_1 = T_a \Theta_1$. The parameter g_i gives the moles per kilogram of the various species X with excitable levels i in the exhaust, augmented by any H_2O and CO_2 that is formed in the AB process and depleted by H_2 and CO consumed in the same AB process. That is:

$$g'_i = g_i \begin{pmatrix} 1 \neq H_2O & ; & 1 \neq H_2 \\ 1 \neq CO_2 & ; & 1 \neq CO \end{pmatrix} \quad (3.245a)$$

June 1974

$$g'(i = H_2O) = g_{H_2O} + g_{H_2} \epsilon_{H_2O} \quad (3.245b)$$

$$g'(i = CO_2) = g_{CO_2} + g_{CO} \epsilon_{CO_2} \quad (3.245c)$$

$$g'(i = H_2) = g_{H_2} (1 - \epsilon_{H_2O}) \quad (3.245d)$$

$$g'(i = CO) = g_{CO} (1 - \epsilon_{CO_2}) \quad (3.245e)$$

Rewriting (3.244) in terms of wavelengths λ instead of ν , one has alternatively:

$$\left(\frac{dJ}{d\lambda} \right)_{ABCD} = 2.8549 \times 10^6 \frac{\dot{W}}{(\text{kg/s})} \left(\frac{\text{Tr}(S) F_v}{\lambda^3 (\mu\text{m})} \right) \cdot \sum_i \sum_j (g_i + \psi_i) f_{ij} \left[\frac{b(\lambda, \lambda_{ij}, \Delta\nu_{ij})}{\Delta\nu_{ij} (T_a \Theta_2)} \right] \left[\exp\left(-\frac{\epsilon_i}{kT_a \Theta_i}\right) \right], \frac{\text{Watts}}{\text{ster} \cdot \mu\text{m}} \quad (3.246)$$

Here we wrote $g'_i = g_i + \psi_i$ in the alternative form:

$$\psi_i = g_{H_2} \epsilon_{H_2O}, \quad \text{for } i = H_2O \quad (3.247a)$$

$$\psi_i = g_{CO} \epsilon_{CO_2}, \quad \text{for } i = CO_2 \quad (3.247b)$$

$$\psi_i = -g_{H_2} \xi_{H_2O} \quad , \quad \text{for } i = H_2 \quad (3.247c)$$

$$\psi_i = -g_{CO} \xi_{CO_2} \quad , \quad \text{for } i = CO \quad (3.247d)$$

$$\psi_i = 0 \quad , \quad \text{for all other } i \quad (3.247e)$$

In Eqs. (3.244) and (3.246), the parameters $Tr(\lambda, S)$ and F_v are the atmospheric transmission and view factor as discussed before in sections 3.3.2 and 3.3.3.

Although the final relations (3.244) and (3.246) for ABCD radiation contain a number of approximating assumptions, they have the advantage of showing directly how the radiation depends on such parameters as altitude, exit temperatures, etc. The same comments that were given in the last paragraph of section 3.3.3 for Mach or Core radiation, also apply to the ABCD radiation formulas developed above.

3.3.5 Atmospheric Pumping Radiation (ATMP)

Due to the fact that atmospheric temperatures are very high at high altitudes (see Figure 2.3a), rocket exhaust molecules will get repeatedly excited vibrationally after they have slowed down and come into equilibrium with the atmosphere. In this "cloud" region, the exhaust gas has reached pressure p_a and temperature T_a . This repetitive excitation phenomena, called "atmospheric pumping" is important only at high altitudes ($h \gtrsim 90$ km), where the atmospheric temperature is high enough to induce vibrational excitation in molecules. Because atmospheric pumping occurs only at high altitudes, we do not have to consider reabsorptions and photon escape probabilities (see Vol. III), and can consider the exhaust cloud to be optically thin.

June 1974

The collision rate between exhaust and air molecules per unit volume is given by:

$$\frac{d^2N}{dt d(Vol)} = \bar{v}_{a/X} \sigma_{a/X} n_a(h) n_X, \quad \frac{\text{collisions}}{\text{sec} \cdot \text{m}^3} \quad (3.248)$$

where n_X is the molecular density of exhaust species X, $n_a(h)$ is the atmospheric molecular density in molecules/m³, and $\sigma_{a/X}$ is the total microscopic cross-section for momentum and energy exchanging collisions between air and exhaust molecules in m². The mean velocity $\bar{v}_{a/X}$ (m/sec) is given by:

$$\bar{v}_{a/X} = 147 \left(\frac{T_a}{\left(\frac{2 M_a M_X}{M_a + M_X} \right)} \right)^{1/2}, \quad \text{m/sec} \quad (3.249)$$

in which:

M_X = Molecular weight of exhaust species X, a.m.u.

$T_a = T_a(h)$ = Kinetic temperature of atmosphere, °K

M_a = Molecular weight of air, a.m.u.

$$M_a = 28.8, \quad \text{a.m.u.}, \quad \text{for } 0 < h \leq 100 \text{ km} \quad (3.250a)$$

$$M_a = 28.8 (1.100 - 0.001 h), \quad \text{a.m.u.}, \quad \text{for } 100 < h \leq 400 \text{ km} \quad (3.250b)$$

$$M_a = 40.93 - 7.50 \times 10^{-2} h + 5.77 \times 10^{-5} h^2, \quad \text{a.m.u.},$$

for $400 < h \leq 600 \text{ km} \quad (3.250c)$

$$M_a = 20.23 - 5.80 \times 10^{-3} h, \text{ a.m.u.}, \text{ for } 600 < h \leq 988 \text{ km} \quad (3.250d)$$

$$M_a = 14.4, \text{ a.m.u.}, \text{ for } 988 < h \leq \infty \text{ km} \quad (3.250e)$$

The cross-section $\sigma_{a/X}$ in (3.248) may be expressed by:

$$\sigma_{a/X} = \pi (d_a + d_X)^2 = \frac{1}{2} \left[(\sigma_c)_a + (\sigma_c)_X \right], \text{ m}^2 \quad (3.251)$$

Here d_m is the diameter of molecule m ($m=a, X$). In Table 3-1, measured values of a_m and $(\sigma_c)_m$ for some selected molecules are listed.

If the probability of exciting vibrational level i during a collision is designated by p_{oi} , the number of i -exciting collisions is given by:

$$\frac{d^2 N_{oi}}{dt d(\text{Vol})} = \bar{v}_{a/X} \sigma_{a/X} p_{oi} n_a(h) n_X, \frac{\text{excitations}}{\text{sec} \cdot \text{m}^3} \quad (3.252)$$

Similarly if the probability of deexciting an excited level i during a collision is p_{oi} , the number of i -deexciting collisions is given by:

$$\frac{d^2 N_{oi}}{dt d(\text{Vol})} = - \left\{ A_i^0 + \bar{v}_{a/e} \sigma_{a/X} p_{io} n_a(h) \right\} (n_X)_i, \frac{\text{deexcitations}}{\text{sec} \cdot \text{m}^3} \quad (3.253)$$

Here A_i^0 is the total spontaneous photon emission rate (sec^{-1}) for state i (see Vol. II), and $(n_X)_i$ is the density of excited exhaust molecules.

TABLE 3-1. MOLECULAR COLLISION PARAMETERS

Gas	Average Velocity \bar{v} in m/sec		Mean Free Path λ_c in μm , $(\lambda_c = \frac{1}{n \sigma_c})$				Collision Frequency z_c in sec^{-1}	Molecular Diameter, d_m in Angstroms				Self-Collision Cross-Section σ_c in m^2
	0°C	20°C	Boltzmann		Meyer	$z_c = \bar{v}/\lambda_c$	From Viscosity	From Van der Waal's Equation	From Heat Conductivity	Average	Average	
			0°C; 1 atm	20°C; 1 atm								20°C; 1 atm
Air	447	463	—	—	—	—	—	—	—	—	—	
Ammonia	583	604	5.92×10^{-2}	6.60×10^{-2}	5.83×10^{-2}	915×10^7	2.97	3.08	—	3.05	29.20×10^{-20}	
Argon	381	395	8.98×10^{-2}	9.88×10^{-2}	8.73×10^{-2}	400×10^7	2.88	2.94	2.86	2.89	26.24×10^{-20}	
Carbon Monoxide	454	471	8.46×10^{-2}	9.23×10^{-2}	8.16×10^{-2}	510×10^7	3.19	3.12	—	3.15	31.20×10^{-20}	
Carbon Dioxide	362	376	5.56×10^{-2}	6.15×10^{-2}	5.44×10^{-2}	612×10^7	3.34	3.23	3.40	3.32	34.64×10^{-20}	
Helium	1208	1252	25.25×10^{-2}	27.45×10^{-2}	33.10×10^{-2}	454×10^7	1.90	2.65	2.30	2.28	16.36×10^{-20}	
Hydrogen	1696	1755	16.00×10^{-2}	17.44×10^{-2}	15.40×10^{-2}	1006×10^7	2.40	2.34	2.32	2.35	17.36×10^{-20}	
Krypton	263	272	9.5×10^{-2}	—	—	—	—	(3.69)	3.14	3.14	31.04×10^{-20}	
Mercury	170	176	—	(14.70×10^{-2})	(13.0×10^{-2})	—	—	3.01	—	3.01	28.28×10^{-20}	
Neon	538	557	—	—	—	—	—	—	—	—	—	
Nitrogen	454	471	8.50×10^{-2}	9.29×10^{-2}	8.21×10^{-2}	507×10^7	3.15	3.15	3.53	3.28	33.92×10^{-20}	
Oxygen	425	440	9.05×10^{-2}	9.93×10^{-2}	8.78×10^{-2}	443×10^7	2.98	2.92	—	2.95	27.40×10^{-20}	
Water Vapor	566	587	—	(8.39×10^{-2})	—	(700×10^7)	—	—	—	(3.26)	32.40×10^{-20}	
Xenon	210	218	5.6×10^{-2}	—	—	—	—	4.02	3.42	3.72	43.60×10^{-20}	

Now according to statistical mechanics, one has (see section 5.3, Vol. II):

$$\frac{p_{oi}}{p_{io}} = \frac{w_i \exp(-(\epsilon_i/kT_a))}{Z_V} = w_i \left[\exp\left(-\frac{\epsilon_i}{kT_a}\right) \right] \left[\prod_{\alpha} \left\{ 1 - \exp\left(-\frac{h\nu_a}{kT_a}\right) \right\} \right] \quad (3.254)$$

Here w_i and ϵ_i are the weight and energy of level i , and the product is over all the normal vibrations α of the molecule. Then if we define the collisional deexcitation cross-section σ_* by:

$$\sigma_* = p_{io} \sigma_{a/X} , \quad m^2 , \quad (3.255)$$

and use the steady-state condition which requires that the excitation rate equals the deexcitation rate:

$$\frac{d^2 N_{oi}}{dt d(Vol)} = - \frac{d^2 N_{oi}}{dt d(Vol)} , \quad (3.256)$$

we can solve for $(n_X)_i$:

$$(n_X)_i = \left[\frac{\bar{\nu}_{a/X} \sigma_* n_a(h) n_X}{A_i^o + \bar{\nu}_{a/X} \sigma_* n_a(h)} \right] \left[w_i \exp\left(-\frac{\epsilon_i}{kT_a}\right) \right] \left[\prod_{\alpha} \left\{ 1 - \exp\left(-\frac{h\nu_a}{kT_a}\right) \right\} \right] ,$$

, $\frac{\text{i-excited molecules X}}{m^3}$

(3.257)

The radiant intensity due to the emission of photons of energy $h\nu$ is then given by:

June 1974

$$\left[\frac{d^2 J}{dv d(Vol)} \right]_{ATMP} = (hv) (Tr(v)) \left(\frac{F_v}{4\pi} \right) \sum_i \frac{dA_i}{dv} (n_X)_i = 0.5272 \times 10^{-10} n_X \cdot$$

$$\cdot \frac{v}{(THz)} Tr(v) F_v \cdot \sum_i \sum_j w_i f_{ij} \left[\frac{b(v, v_{ij}, \Delta v_{ij})}{\Delta v_{ij} (THz)} \right] \left[\frac{A_i^0 \bar{v}_{a/X} \sigma_* n_a(h)}{A_i^0 \bar{v}_{a/X} \sigma_* n_a(h)} \right]$$

$$\cdot \left[\exp\left(-\frac{\epsilon_i}{kT_a}\right) \right] \left[\prod_{\alpha} \left\{ 1 - \exp\left(-\frac{hv_{\alpha}}{kT_a}\right) \right\} \right] , \frac{\text{Watts}}{\text{THz} \cdot \text{ster} \cdot \text{m}^3} \quad (3.258)$$

Here we added the usual atmospheric transmission factor $Tr(v)$ and view factor $F_v/(4\pi)$, and we made use of the relation (see Vol. II):

$$\frac{dA_i}{dv} = A_i^0 \sum_j f_{ij} \frac{b(v, v_{ij}, \Delta v_{ij})}{\Delta v_{ij}} , \text{ Hz}^{-1} \quad (3.259)$$

$$f_{ij} = \frac{A_{ij}^0}{\sum_j A_{ij}^0} \quad (3.260)$$

The total radiant intensity dJ/dv from a cloud containing N_X exhaust molecules is of course also given by (3.258) with n_X substituted by N_X .

In applied rocket radiation observation work, one needs a relation for N_X in terms of other rocket hardware and trajectory parameters. The amount of exhaust deposited in the atmosphere by a rocket which will be in the field-of-view of a sensor, is given by:

$$N_X = \int_{Vol} n_X d(Vol) = 6.023 \times 10^{23} g_X \dot{W} \tau_s , \text{ molecules} , \quad (3.261)$$

where for TT0 (= target tracking observations; see section 3.1):

$$\tau_s = t H(t_s - t) + t_s H(t - t_s) H(t_b - t) + (t_s + t_b - t) H(t_b + t_s - t) H(t - t_b), \text{ sec} \\ (\text{TT0})$$

(3.262)

and for ICO (= integrated cloud observations; see section 3.1):

$$\tau_s = t H(t_b - t) + t_b H(t - t_b), \text{ sec} \\ (\text{ICO})$$

(3.263)

Here $H(x)$ is the Heaviside unit step function defined by Eq. (3.166), and:

$$t_s = \frac{D_s}{V_v \sin \alpha} = \frac{S \theta}{V_v \sin \alpha}, \text{ sec}$$

(3.264)

t_b = Rocket burn time, sec

θ = Field-of-view angle, radians

α = Angle between line-of-sight and rocket vehicle trajectory, radians

S = Distance between rocket exhaust cloud and sensor, m

$D_s = S\theta$ = Effective diameter of sensor field-of-view at the cloud target, m

V_v = Rocket vehicle velocity, m/sec

With Eq. (3.261) substituted in (3.258), we obtain for atmosphere-pumped exhaust cloud radiation:

June 1974

$$\begin{aligned} \left(\frac{dJ}{dv}\right)_{ATMP} &= 31.765 \frac{\dot{W}}{(\text{kg/s})(\text{THz})} \nu \text{Tr}(\nu) F_v \cdot \\ &\cdot \sum_i \sum_j g_i w_i f_{ij} \left[\frac{b(\nu, \nu_{ij}, \Delta\nu_{ij})}{\Delta\nu_{ij}(\text{THz})} \right] \left[\frac{\tau_s}{\tau_{i*}} \right] \left[\exp\left(-\frac{h\nu_i}{kT_a}\right) \right] \cdot \\ &\cdot \left[\prod_{\alpha} \left\{ 1 - \exp\left(-\frac{h\nu_{\alpha}}{kT_a}\right) \right\} \right] , \frac{\text{Watts}}{\text{THz} \cdot \text{ster}} , \end{aligned} \quad (3.265)$$

or in terms of wavelengths λ :

$$\begin{aligned} \left(\frac{dJ}{d\lambda}\right)_{ATMP} &= 2.8549 \times 10^6 \frac{\dot{W}}{\lambda^3(\mu\text{m})} \text{Tr}(\lambda) F_v \cdot \\ &\cdot \sum_i \sum_j g_i w_i f_{ij} \left[\frac{b(\lambda, \lambda_{ij}, \Delta\nu_{ij})}{\Delta\nu_{ij}(\text{THz})} \right] \left[\frac{\tau_s}{\tau_{i*}} \right] \cdot \\ &\cdot \left[\exp\left(-\frac{h\nu_i}{kT_a}\right) \right] \left[\prod_{\alpha} \left\{ 1 - \exp\left(-\frac{h\nu_{\alpha}}{kT_a}\right) \right\} \right] , \frac{\text{Watts}}{\mu\text{m} \cdot \text{ster}} \end{aligned} \quad (3.266)$$

Here we abbreviated for convenience $g_i \equiv g_{\lambda_i}$ and:

$$\tau_{i*} = \tau_i^0 + \left(\tau_a / \chi \right)_i , \quad \text{sec} \quad (3.267)$$

$$\tau_i^0 = (A_i^0)^{-1} , \quad \text{sec} \quad (3.268)$$

$$(\tau_{a/X})_i = [\bar{v}_{a/X} \sigma_* n_a(h)]^{-1}, \text{ sec} \quad (3.269)$$

The kinetic velocity $\bar{v}_{a/X}$ in (3.269) is given by:

$$\bar{v}_{a/X} \approx 19.6 \left(\frac{28.3 + M_X}{M_X} \right)^{1/2} T_a^{1/2}, \text{ m/sec} \quad (3.270)$$

while $\sigma_* \sim \sigma_{a/X}$ which was given by Eq. (3.251). Thus if the atmospheric molecular density $n_a(h)$ is known, $(\tau_{a/X})_i$ can be obtained from (3.269). The radiative decay time $\tau_i^0 = (A_i^0)^{-1}$ can be obtained from the tables and relations given in Volume II for a particular molecule X and excited level i.

An inspection of (3.265) or (3.266) shows that the two most influential altitude-dependent parameters in these relations are the air density $n_a(h)$ (which enters into τ_{i*} via Eq. (3.269)) and the ambient temperature $T_a = T_a(h)$. Since T_a increases with altitude, one can expect ATMP radiation to increase as a rocket rises upwards through the atmosphere. At the higher altitudes however $\tau_{i*} \rightarrow \infty$ since $n_a \rightarrow 0$ and thus ATMP radiation will rapidly approach zero at higher altitudes. Because of the counteracting effects of $T_a(h)$ and $n_a(h)$ with altitude h, ATMP radiation goes through a peak usually at altitudes between 150 to 175 kilometers.

Although ATMP radiation is weak compared to ABCD and CORE radiation because the cloud is more diluted than the plume, it has persistence which the other two radiation mechanisms do not possess. Thus if a rocket ceases to thrust and the slowly expanding stationary exhaust cloud is observed that was left in the atmosphere by the rocket (rather than following

June 1974

the moving rocket), one would observe a slowly decaying weak radiative glow in the infrared from this cloud. The water-band radiation from these exhaust clouds should be very similar to that from high-altitude rainclouds, but for the carbon-dioxide emissions there would be no comparable nature-made phenomenon except perhaps the high-altitude clouds produced by volcanic eruptions.

If an exhaust cloud is dumped above an altitude of 130 km during daytime so that it is illuminated by the sun, the solar UV (see section 3.3.7) will dissociate the exhaust molecules. For ICO observations, the parameter τ_s given by Eq. (3.263) must be replaced in this case by:

$$\begin{aligned} \tau_{sX} \left(\begin{array}{l} h > 135 \text{ km} \\ \text{daytime} \end{array} \right) = \tau_{X_d} \left[\left\{ 1 - \exp\left(-\frac{t}{\tau_{X_d}}\right) \right\} H(t_b - t) + \left\{ 1 - \exp\left(-\frac{t_b}{\tau_{X_d}}\right) \right\} \right. \\ \left. \cdot \left\{ \exp\left(-\frac{t - t_b}{\tau_{X_d}}\right) \right\} H(t - t_b) \right] , \text{ sec} \quad (\text{ICO}) , \end{aligned} \quad (3.271)$$

while for TT0 observations of exhausts under solar UV illumination, τ_s in Eq. (3.262) must be replaced by:

$$\begin{aligned} \tau_{sX} \left(\begin{array}{l} h > 135 \text{ km} \\ \text{daytime} \end{array} \right) = \tau_{X_d} \left[\left\{ 1 - \exp\left(-\frac{t}{\tau_{X_d}}\right) \right\} \cdot H(t_s - t) + \left\{ 1 - \exp\left(-\frac{t_s}{\tau_{X_d}}\right) \right\} \right. \\ \cdot H(t - t_s) H(t_b - t) + \left\{ 1 - \exp\left(-\frac{t_b + t_s - t}{\tau_{X_d}}\right) \right\} \left\{ \exp\left(-\frac{t - t_b}{\tau_{X_d}}\right) \right\} \cdot \\ \left. \cdot H(t - t_b) H(t_b + t_s - t) \right] , \text{ sec} \quad (\text{TT0}) \end{aligned} \quad (3.272)$$

Here τ_{X_d} is the photodissociation decay time for exhaust species X (listed in Table 3-7, section 3.3.7) and t_s was defined before in (3.264). The time t (seconds) is the elapsed time since rocket burn initiation, and t_b (seconds) is the rocket burn cutoff time. From Table 3-7 one finds that most common exhaust species with the exception of CO_2 will experience significant photodissociation under solar illumination above 135 kilometers during typical observation times. Note that τ_{sX} participates in the summation over species X and thus over i in Eqs. (3.265) and (3.266).

3.3.6 Solar Radiation Scattering by Particles (SOSP)

The incident solar spectrum near the earth was shown in Figure 2-4 (see also Figures B-7 and B-8 of Appendix B). It is clear that the illumination levels in the visible are high and that space clouds and plumes can be observed if the cloud scatters or reflects the radiation significantly.

As mentioned in Chapter 2, only solar photon scattering by particles (if present) in a rocket plume gives significant signals. The Rayleigh scattering of solar radiation by gaseous exhaust molecules is so weak that it can hardly be observed in most practical cases of interest.* The question of whether or not visible scattered radiation can be observed thus turns to whether or not the exhaust has solid particles. Solid propellants are known to exhaust micron-sized particles of Al_2O_3 , MgO , and/or BeO (see Refs. 17, 18), while liquid rocket exhausts may sometimes contain small quantities of solid carbon or soot. In addition H_2O , which is present in both liquid and solid rockets, can freeze out at the lower altitudes ($0 \lesssim h \lesssim 94$ km) where the ambient temperature is below 273°K (see Fig. 2.5).

*It is insignificant also when compared to solar ultraviolet absorption and reemission in the visible (to be discussed in section 3.3.7).

June 1974

Aside from scattering, at altitudes above 130 kilometers, solar illumination produces also visible radiation due to solar ultraviolet absorption and visible reemission by exhaust molecules which will be discussed in section 3.3.7. Whereas the latter produces visible radiation with a spectrum that is characteristic of exhaust molecules and their dissociation products, the particle-scattered solar radiation has essentially the spectrum of the sun. The scattered solar spectrum may be modified slightly due to Mie scattering resonances at certain wavelengths, if all particles were spherical and had the same diameter. Since the actual particles in an exhaust cloud are not exactly spherical and have different diameters, the spectrum-modifying effects due to Mie scattering resonances at certain wavelengths of the solar spectrum are smoothed out considerably and hardly noticeable.

The exospheric solar illumination in the vicinity of the earth in the visible (VIS) and near-infrared (NIR) part of the spectrum may be approximated by the expression:

$$\left(\frac{dH_s}{d\lambda} \right)_{(VIS/NIR)} = \frac{8.20 \times 10^{15}}{\lambda^5 \left\{ \exp\left(\frac{2440}{\lambda}\right) - 1 \right\}} \cdot \frac{\text{Watts}}{\text{m}^2 \cdot \text{nm}}, \quad (3.273)$$

where λ is the solar photon wavelength in nanometers.* The visible solar radiation scattered from solid exhaust particles of a rocket exhaust is then:

$$\left(\frac{dJ}{d\lambda} \right)_{\text{Particle-Scattered Solar VIS/NIR}} = \frac{8.20 \times 10^{15} \dot{W} \tau_s}{\lambda^5 \left\{ \exp\left(\frac{2440}{\lambda}\right) - 1 \right\}} \sum_i c_{p_i} \tilde{\sigma}_{p_i}(\beta_s) \cdot \frac{\text{Watts}}{\text{ster} \cdot \text{nm}}, \quad (3.274)$$

* 1 nm = 1 nanometer = 10^{-9} meters = 10 Angstroms

where \dot{W} is the rocket's mass expulsion rate (kgm/sec), λ is again the wavelength in nm, and where τ_s is given by Eq. (3.262) or (3.263) presented in the previous subsection 3.3.5. The parameter $\tilde{\sigma}_{p_i}(\beta_s)$ is the mean photon scattering cross-section which we shall discuss further below, while the specific particle production factor C_{p_i} in (3.274) is given by:

$$C_{p_i} = 10^{12} \frac{g_{p_i} M_{p_i}}{\rho_i \bar{d}_i^3}, \frac{\text{particles } p_i}{\text{kgm}} \quad (3.275)$$

in which:

- g_{p_i} = Moles of condensable species i in exhaust, moles/kgm
- M_{p_i} = Molecular weight of condensable species i , a.m.u.
- ρ_i = Density of solidified species i , gms/cm³
- \bar{d}_i = Mean particle size of species i in exhaust, μm

The wavelength-averaged and particle-size averaged scattering cross-section for visible light $\tilde{\sigma}_{p_i}(\beta_s)$ (in units of m² ster⁻¹) for the particles of species i depends on the mean wavelength $\bar{\lambda}$, the mean particle size \bar{d}_i , the chemical nature of the particle p_i , and the particle surface quality. This cross-section is furthermore dependent on the solar photon scattering angle β_s or the sun-cloud-observer angle $\eta_s = \pi - \beta_s$.

The most important condensables in rocket exhausts are H₂O and Al₂O₃. For H₂O, we have $\rho_{\text{H}_2\text{O}} = 1 \text{ gm/cm}^3$ and $M_{\text{H}_2\text{O}} = 18 \text{ a.m.u.}$, so that:

June 1974

$$C_{H_2O} = 1.80 \times 10^{13} \left(\frac{g_{H_2O}}{d_{H_2O}^3} \right), \frac{H_2O \text{ particles}}{\text{kgm}} \quad (3.276)$$

For Al_2O_3 , we have $\rho_{Al_2O_3} = 3.5 \text{ gms/cm}^3$ and $M_{Al_2O_3} = 102 \text{ a.m.u.}$, so that:

$$C_{Al_2O_3} = 2.91 \times 10^{13} \left(\frac{g_{Al_2O_3}}{d_{Al_2O_3}^3} \right), \frac{Al_2O_3 \text{ particles}}{\text{kgm}} \quad (3.277)$$

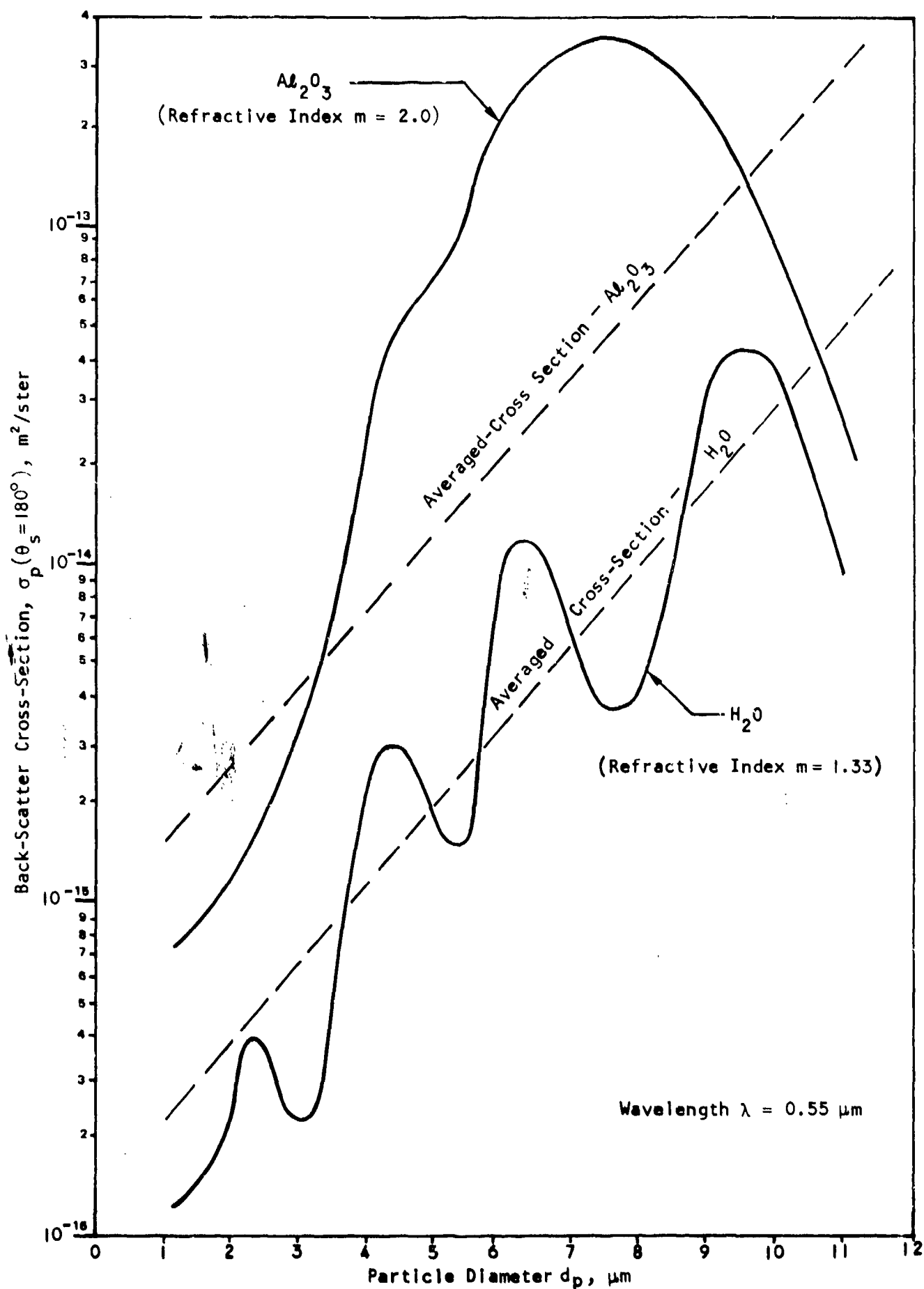
Then Eq. (3.274) may be written:

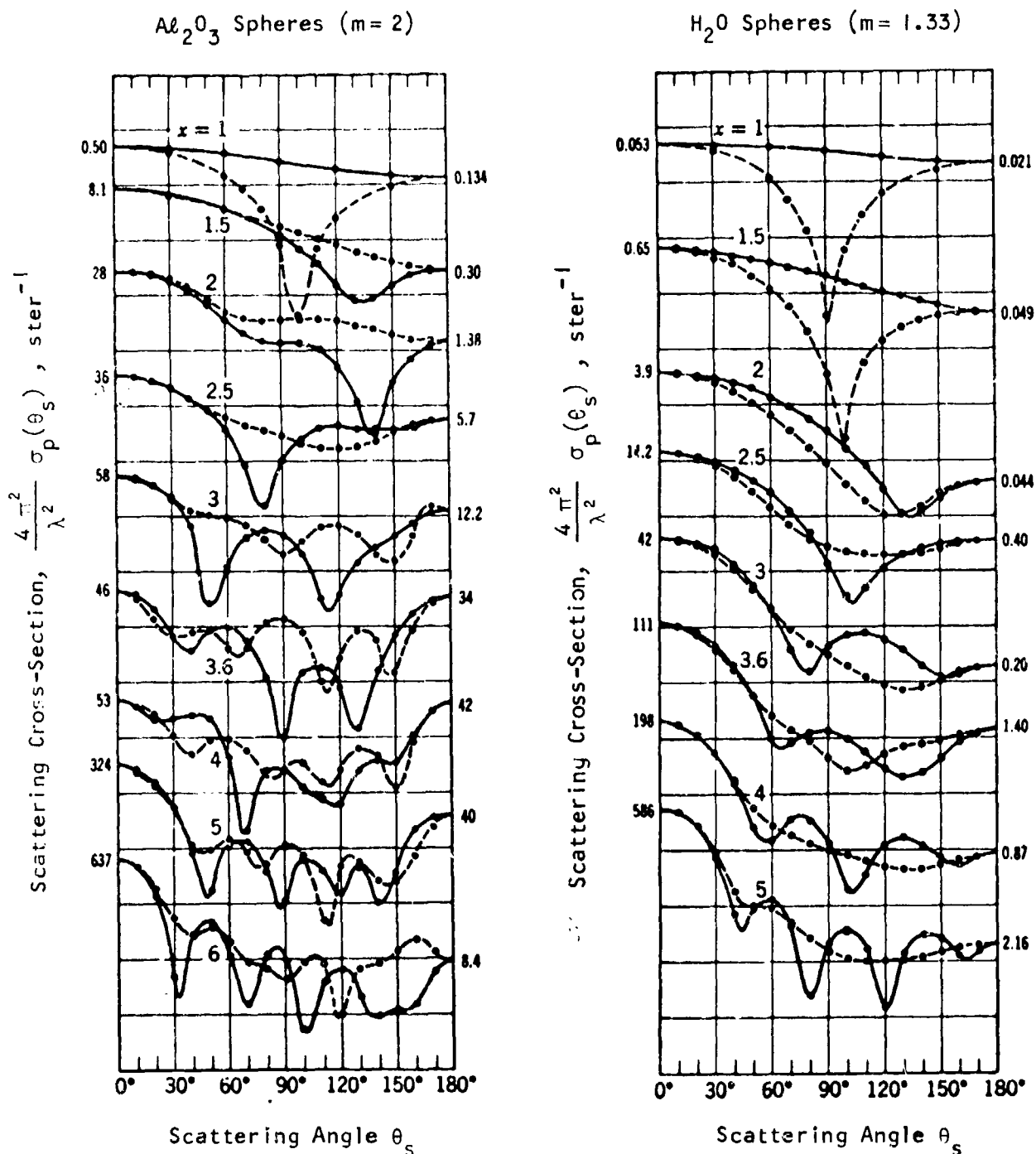
$$\left(\frac{dJ}{d\lambda} \right)_{Al_2O_3 \text{ and } H_2O \text{-Scattered}}^{\text{Solar Visible}} = \frac{2.386 \times 10^{29} \dot{W} \tau_s}{\lambda^5 \left\{ \exp\left(\frac{2440}{\lambda}\right) - 1 \right\}} \cdot \left\{ \frac{g_{Al_2O_3} \tilde{\sigma}_{Al_2O_3}(\beta_s)}{d_{Al_2O_3}^3} + \frac{0.62 \xi_{fr} g_{H_2O} \tilde{\sigma}_{H_2O}(\beta_s)}{d_{H_2O}^3} \right\}, \frac{\text{Watts}}{\text{ster} \cdot \text{nm}} \quad (3.278)$$

where $\xi_{fr} = \xi_{fr}(h)$ is the mole fraction of H_2O in the exhaust that has frozen out.

In Figures 3-14 and 3-15, the dependences of $\sigma_{H_2O}(\beta_s)$ and $\sigma_{Al_2O_3}(\beta_s)$ are shown as a function of incident wavelength, particle size, and scattering angle β_s *. Measurements of the size of Al_2O_3 particles produced by solid rockets are shown in Figures 3-16 through 3-18. One finds that for rockets with expansion ratios ϵ larger than 1, which is almost always the case of interest, one can use the empirical relation (see Figure 3-16):

*The curves show an index of refraction for Al_2O_3 of $m=2$ (curves with $m=2$ were readily available), whereas in the literature a value of $m \approx 1.67$ is reported for Al_2O_3 . Since the cross-sections are subsequently averaged anyway, this discrepancy is of little consequence.

FIGURE 3-14. BACK SCATTERING ($\theta_s = \pi$) CROSS-SECTIONS OF Al_2O_3 AND H_2O PARTICLES



- NOTE:**
- Solid curves are for perpendicular and dashed curves for parallel polarized light.
 - Cross-section for natural light is $\sigma = \frac{1}{2} (\sigma_{\perp} + \sigma_{\parallel})$.
 - Ordinate scales are logarithmic and one division equals a factor of 10.
 - $x = \pi d/\lambda$, where d = particle diameter and λ = wavelength.

FIGURE 3-15. ANGULAR DEPENDENCE OF Al_2O_3 AND H_2O PARTICLE SCATTERING CROSS-SECTIONS (After Ref. 41)

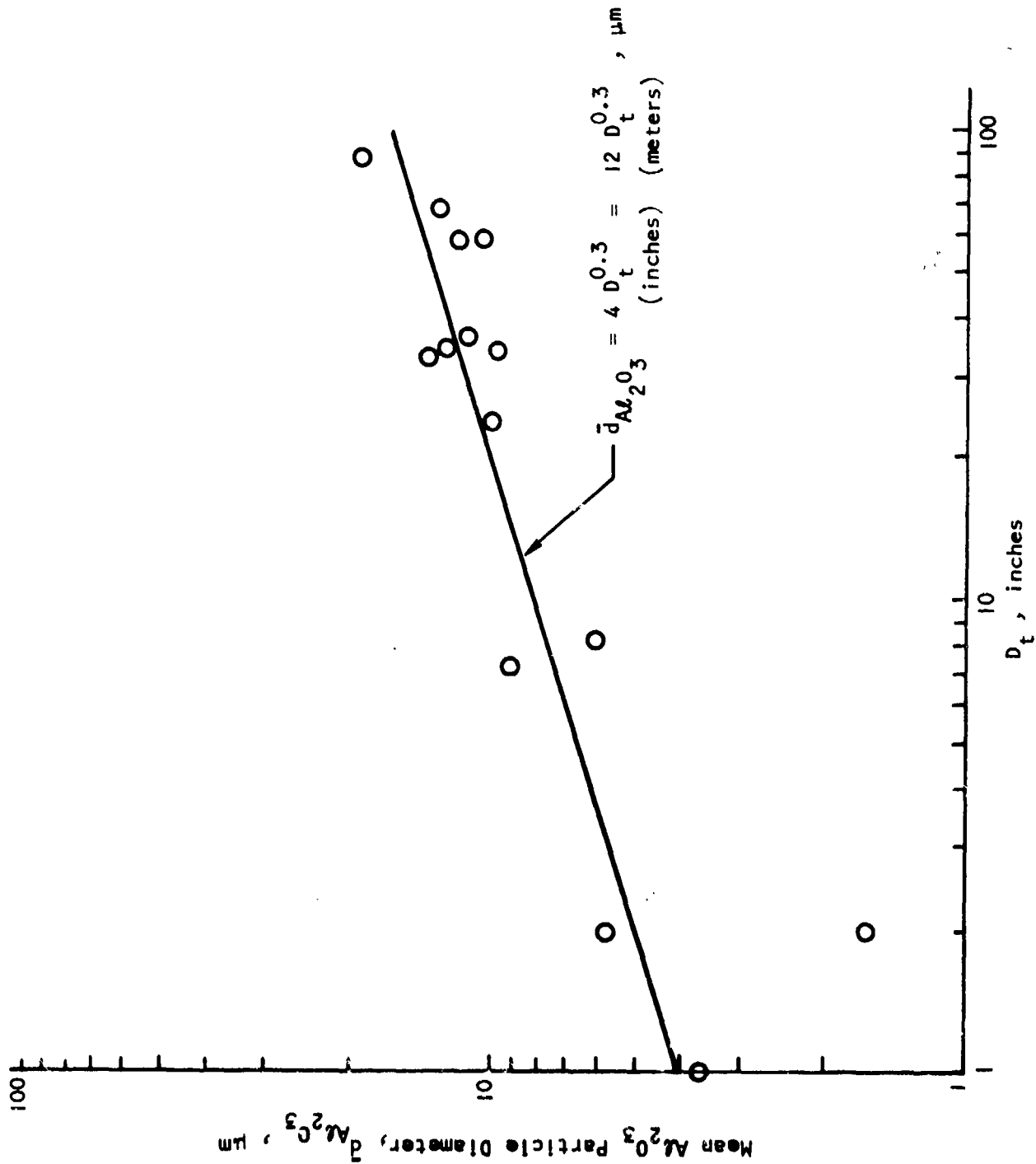


FIGURE 3-16. EXPERIMENTAL CORRELATION OF MEAN Al_2O_3 PARTICLE DIAMETER $d_{Al_2O_3}$ WITH NOZZLE THROAT DIAMETER (Adapted from Ref. 42)

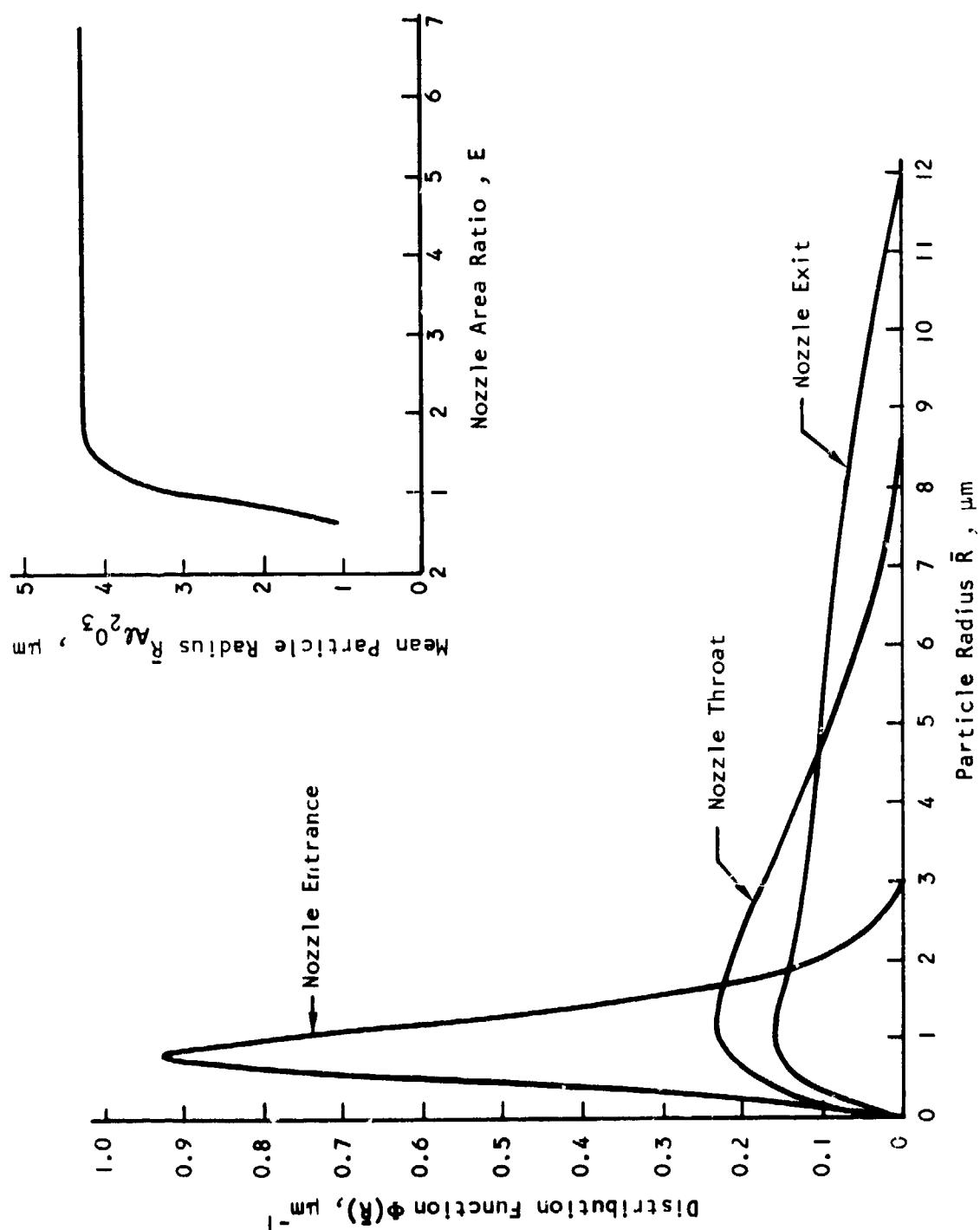


FIGURE 3-17. THEORETICAL Al_2O_3 PARTICLE SIZE DISTRIBUTION WITH NOZZLE LOCATION
(Adapted from Ref. 42)

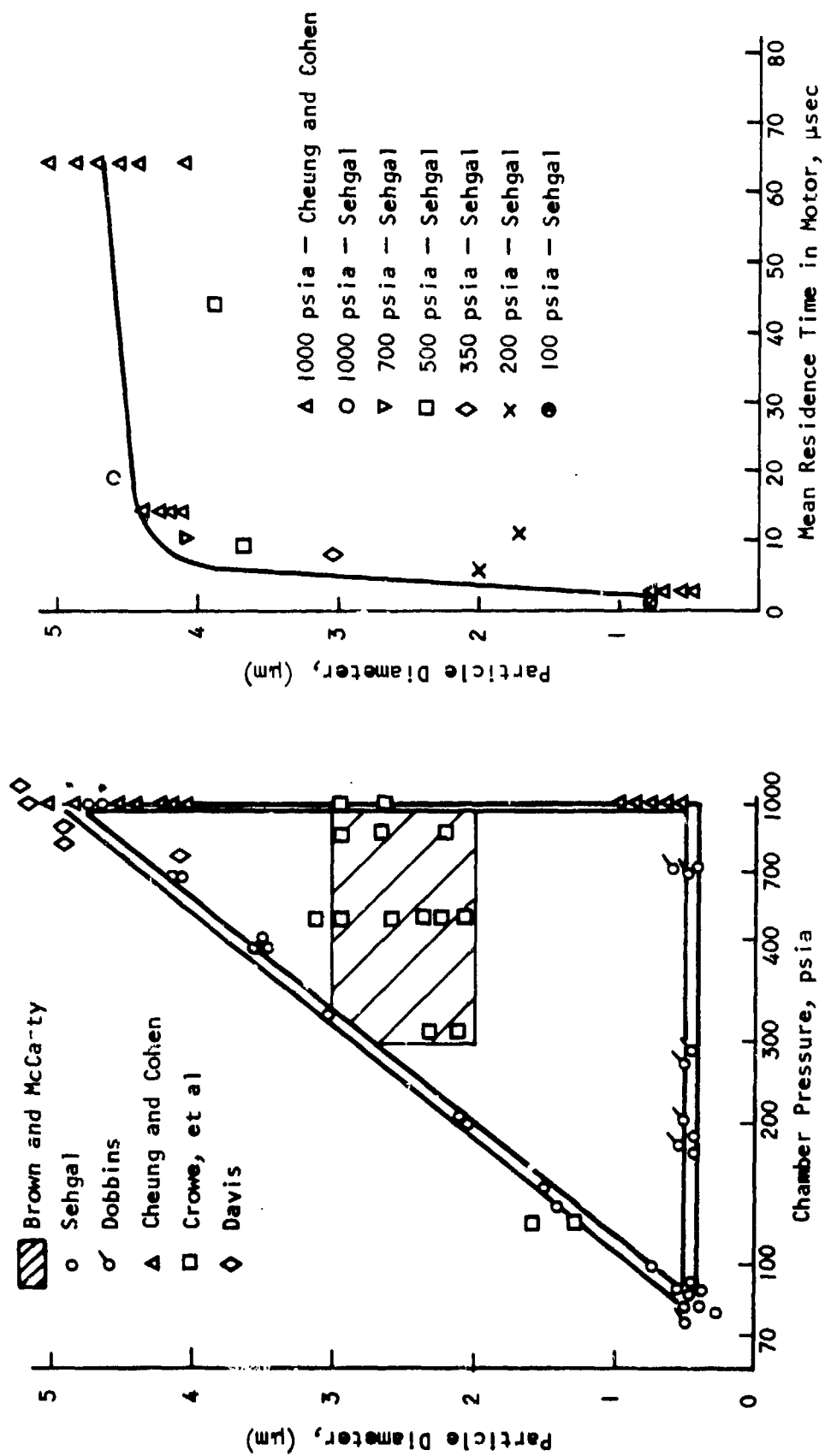


FIGURE 3-18. Al_2O_3 PARTICLE SIZE DATA OBTAINED FROM SMALL ROCKET MOTORS
(Adapted from Ref. 42)

June 1974

$$\bar{d}_{Al_2O_3} = 12 D_t^{0.3} \text{ (meters)} , \mu m \quad (3.279)$$

where $\bar{d}_{Al_2O_3}$ is in μm and the nozzle throat diameter D_t is in meters.

Whereas the mean diameter for Al_2O_3 particles is independent of altitude, this is not the case for H_2O . The average diameter \bar{d}_{H_2O} depends on altitude (primarily via the ambient temperature) and on the presence in the exhaust of other nucleating particles such as Al_2O_3 for solid rockets and C (soot) in liquid-fueled rocket exhausts. Similarly the freezing fraction ξ_{fr} depends on the altitude and the presence of other particles. In general, condensation of H_2O can occur only at altitudes between 0 and 94 kilometers where ambient pressures and temperatures favor the condensed state of H_2O (see Figure 2-5). If conditions are favorable, condensation occurs several kilometers downstream from the nozzle exit where the exhaust has cooled down and after it has experienced afterburning and collisional deceleration.

If Al_2O_3 or C particles are present in the exhaust, a good portion of the H_2O will freeze out on these particles, particularly at the higher altitudes ($68 \lesssim h \lesssim 94$ km). If these nucleating particles are not present, the H_2O will freeze out very slowly and a good fraction will remain in the vapor form because of expansion and diffusion of the H_2O to density levels that are too low to favor condensation.

At altitudes above 94 kilometers, the H_2O in the exhaust will remain in the vapor state due to the vapor-favoring ambient temperatures and pressures (see Figure 2-5). In deep space where a vacuum exists, the H_2O density will always be too low and the temperature too high to sustain

condensation of hot H_2O exhaust molecules. Even if dumped as a liquid, H_2O will first freeze but then evaporate very slowly if released in the earth shadow (due to earthshine), or quickly if illuminated by the sun (due to UV absorption).

Because of the above-mentioned complications, it will be necessary to make some simplifying assumptions regarding the formation of ice particles, if excessive (and uncertain) calculations are to be avoided. We shall assume an average H_2O particle size of:

$$\bar{d}_{H_2O} \approx 2 \mu m, \quad (3.280)$$

and it will be assumed that particles can exist only at certain altitudes determined by Figure 2-5. Although $\xi_{fr}(h)$ will in reality have values between 0 and 1 at the altitudes where liquid or solid H_2O particles can form, we shall assume for the H_2O released from rocket exhausts (see Figure 2-5):

$$\xi_{fr}(h) = 0.6, \quad 0 < h < 44 \text{ km} \quad (3.281a)$$

$$\xi_{fr}(h) = 0, \quad 44 < h < 68 \text{ km} \quad (3.281b)$$

$$\xi_{fr}(h) = 0.6, \quad 68 < h < 94 \text{ km} \quad (3.281c)$$

$$\xi_{fr}(h) = 0, \quad h > 94 \text{ km} \quad (3.281d)$$

The formation of these condensed H_2O particles will further be assumed to occur several plume diameters downstream from the rocket.

June 1974

For the solar visible spectrum, the mean wavelength is $\lambda \approx 5500$ Angstroms. Taking $\bar{d}_{H_2O} = 2 \mu m$ and assuming $\bar{d}_{Al_2O_3} = 8 \mu m^*$, using $D_t = 0.25 m$, which applies approximately for many large rockets, we find from Figure 3-14 that:

$$\tilde{\sigma}_{H_2O}(\beta_s = \pi) = 2.2 \times 10^{-16} \frac{m^2}{ster} \quad (3.282)$$

$$\tilde{\sigma}_{Al_2O_3}(\beta_s = \pi) = 3.0 \times 10^{-13} \frac{m^2}{ster} \quad (3.283)$$

From Figure 3-15 we can then obtain an estimated curve-fitted angular dependence for the cross-sections:

$$\tilde{\sigma}_{H_2O}(\beta_s) = 2.2 \times 10^{-[15 + 0.057 (\beta_s - 0.00384 \beta_s^2)]} \frac{m^2}{ster} \quad (3.284)$$

$\left(\begin{array}{l} \lambda = 0.55 \mu m; \\ \bar{d} = 2 \mu m \end{array} \right)$

and:

$$\tilde{\sigma}_{Al_2O_3}(\beta_s) = 3.0 \times 10^{-[12 + 0.057 (\beta_s - 0.00384 \beta_s^2)]} \frac{m^2}{ster} \quad (3.285)$$

$\left(\begin{array}{l} \lambda = 0.55 \mu m; \\ \bar{d} = 8 \mu m \end{array} \right)$

where $0 < \beta_s < 180^\circ$, and β_s is measured in degrees. For lack of better experimental information, we shall assume Eqs. (3.284) and (3.285) for the average photon scattering cross-sections of H_2O and Al_2O_3 particles.

Substituting the above results in Eq. (3.278), we finally obtain the estimate:

*Average diameters of soot (C) particles in rocket exhausts (if present) are about $\bar{d}_C = 0.1 \mu m$. Modern rockets produce very little solid C however.

$$\begin{aligned}
 \left(\frac{dJ}{d\lambda} \right)_{\text{Al}_2\text{O}_3 \text{ and H}_2\text{O}}^{\text{SOSP}} &= \frac{1.39}{1.24 \times 10^4} \frac{15 - 0.057 (\beta_s - 0.00384 \beta_s^2)}{\lambda^5 \left\{ \exp\left(\frac{2440}{\lambda}\right) - 1 \right\}} \\
 &\cdot \text{Tr}(\lambda) F_v \dot{W} \tau_s \left(g_{\text{Al}_2\text{O}_3} + 0.0292 \xi_{fr} g_{\text{H}_2\text{O}} \right), \quad \frac{\text{Watts}}{\text{ster} \cdot \text{nm}} \quad (3.286)
 \end{aligned}$$

where the scattering angle β_s is measured in degrees and is related to the sun-cloud-observer angle η_s by $\eta_s = 180^\circ - \beta_s$; $g_{\text{Al}_2\text{O}_3}$ and $g_{\text{H}_2\text{O}}$ are the number of moles of Al_2O_3 and H_2O in the exhaust per kilogram of exhaust; ξ_{fr} is given by Eq. (3.281); \dot{W} is the rocket's mass expulsion rate in kgm/sec, and τ_s (seconds) is given by Eq. (3.262) or (3.263).

Instead of the scattering angle β_s , it is often more convenient to express (3.286) in terms of the sun-target-observer angle $\eta_s = 180 - \beta_s$, degrees. We obtain in this case:

$$\begin{aligned}
 \left(\frac{dJ}{d\lambda} \right)_{\text{Al}_2\text{O}_3 \text{ and H}_2\text{O}}^{\text{SOSP}} &= \frac{9.19}{8.00 \times 10^4} \frac{11 - 0.02165 (\eta_s - 0.0101 \eta_s^2)}{\lambda^5 \left\{ \exp\left(\frac{2440}{\lambda}\right) - 1 \right\}} \\
 &\cdot \text{Tr}(\lambda) F_v \dot{W} \tau_s \left(g_{\text{Al}_2\text{O}_3} + 0.0292 \xi_{fr} g_{\text{H}_2\text{O}} \right), \quad \frac{\text{Watts}}{\text{ster} \cdot \text{nm}} \quad (3.287)
 \end{aligned}$$

In Eqs. (3.286) and (3.287) we have added the atmospheric transmission factor Tr and the view factor F_v to account for cloud shapes other than spherical ones. Summarizing the units of the various parameters in (3.286) and (3.287), we have:

June 1974

η_s	=	Sun-target-sensor angle, degrees
λ	=	Photon wavelength, nm
$g_{Al_2O_3}, g_{H_2O}$	=	Moles of Al_2O_3 and H_2O in rocket exhaust per kilogram of exhaust
ξ_{fr}	=	Freezing fraction determined by Eq. (3.281)
\dot{W}	=	Rocket mass expulsion rate, kgm/sec
τ_s	=	Time (sec) parameter given by Eqs. (3.262) or (3.263)

Because solid Al_2O_3 particles do not dissociate under solar UV illumination and condensed H_2O does not form above 130 km where the solar UV is present, we do not have to correct the parameter τ_s for any solar photodissociation effects.

3.3.7 Solar Ultraviolet Absorption and Reradiation (SUAR)

At altitudes above 130 kilometers (see Figure 2-3c), ultraviolet photons from the sun (if present) will excite and ionize exhaust molecules causing subsequent emission of ultraviolet (UV), visible (VIS), and infrared (IR) radiation. The ionized molecules will recombine with the freed electrons very rapidly creating excited electronic states. The electrons will return to the ground state from these excited levels via a number of transitions to intermediate energy levels with concomitant characteristic spectral emissions of the neutral exhaust molecule. The same applies of course to the directly excited molecular states. A fraction of the ionized molecules will get excited a second time by the solar UV photons before they have recombined with electrons. This will cause emissions from excited ionic states of the exhaust molecules.

In addition to excitation and ionization, many exhaust molecules can be "predissociated" by UV photons, if the photon energy lies above the dissociation energy of the molecule but below its ionization level. One or both of the fragments of the dissociated molecule can then be in an excited state and emit radiation shortly (within microseconds) after the dissociation event.

As mentioned in Chapter 2, the solar UV absorption by gases in space is strong and considerable reradiation may be expected from this mechanism. A number of experiments (Refs. 4 through 11 and 53) have verified the importance of solar UV absorption/reradiation by gas clouds in space. There is also some solar IR absorption and reradiation but the cross-sections are much lower so that even with the higher photon flux levels that exist in the solar IR (compared to the flux levels in the solar UV), the net result is a much weaker emission compared to that produced by the solar UV.

From data on the solar spectrum shown in Figure B-8, Appendix B, we find that the continuum solar energy flux and the photon number flux in the UV in the exosphere can be approximated by the relations:

$$\frac{dH}{d\lambda} (\text{UV}; \lambda < 300 \text{ nm}) = \frac{dH}{d\lambda} = \frac{8.20 \times 10^{15}}{\lambda^5 \left[\left\{ \exp\left(\frac{2440}{\lambda}\right) \right\} - 1 \right]}, \frac{\text{Watts}}{\text{m}^2 \cdot \text{nm}} \quad (3.288)$$

$$\frac{d\phi}{d\lambda} (\text{UV}; \lambda < 300 \text{ nm}) = \frac{4.13 \times 10^{31}}{\lambda^4 \left[\left\{ \exp\left(\frac{2440}{\lambda}\right) \right\} - 1 \right]}, \frac{\text{photons}}{\text{m}^2 \cdot \text{sec} \cdot \text{nm}} \quad (3.289)$$

where λ is the solar photon wavelength in nm ($1 \text{ nm} = 1 \text{ nanometer} = 10^{-9} \text{ meters}$).

June 19/4

Sometimes it is convenient to have the energy and photon number flux per unit frequency instead of per unit wavelength. In frequency units, Eqs. (3.288) and (3.289) become:

$$\frac{dH}{d\nu} (\text{UV}; \nu > 1000 \text{ THz}) = \frac{1.01 \times 10^{-6} \nu^3}{\left[\left\{ \exp\left(\frac{\nu}{123}\right) \right\} - 1 \right]}, \frac{\text{Watts}}{\text{m}^2 \cdot \text{THz}} \quad (3.290)$$

$$\frac{dN}{d\nu} (\text{UV}; \nu > 1000 \text{ THz}) = \frac{1.52 \times 10^{15} \nu^2}{\left[\left\{ \exp\left(\frac{\nu}{123}\right) \right\} - 1 \right]}, \frac{\text{photons}}{\text{m}^2 \cdot \text{sec} \cdot \text{THz}} \quad (3.291)$$

Here ν is the solar photon frequency in units of terahertz ($1 \text{ THz} = 10^{12} \text{ Hz}$).

The photon flux and energy flux given by Eqs. (3.288) through (3.291) give approximately the continuum radiation of the solar UV. At wavelengths below 180 nm the solar spectrum has, in addition to the continuum, a number of intense atomic lines superimposed on the continuum as listed in Table 3-2. The individual intensities of these lines are many times higher than the continuum. The most intense line is the Lyman- α line of hydrogen at 121.6 nm, which has a peak intensity 250 times the value of the continuum.

To account for the discrete lines we shall therefore multiply the expressions (3.288) through (3.291) by the discrete line parameter $L(\lambda) = L(\nu)$, defined by:

TABLE 3-2. SOLAR UV LINES BELOW 182 NANOMETERS*

Element	Center Wavelength, λ_c (nm)	Estimated Linewidth, $\Delta\lambda_c$ (nm)	Estimated Maximum Line Intensity, $L_m = I_{\text{line max.}} / I_{\text{continuum}}$
Si II } Doublet	181.72	0.10	16
Si II }	180.76	0.07	8
Fe II, Al II	166.76	0.06	6
C I	165.63	0.20	12
He II	163.87	0.06	6
C I	155.90	0.16	5
C IV } Doublet	154.90	0.06	10
C IV }	154.86	0.07	16
Si II } Doublet	153.33	0.05	5
Si II }	152.76	0.05	5
Si IV } Doublet	140.12	0.05	7
Si IV }	139.33	0.07	15
O I } Doublet	135.47	0.04	3
O I }	135.05	0.03	2
C II Doublet	133.57	0.20	50
O I } (2 Lines)	130.45	0.20	15
O I } Triplet	130.05	0.08	10
Si II	126.47	0.05	8
S II	125.88	0.08	5
N V	124.19	0.07	5
N V	123.90	0.07	7

*The data in this table were obtained from a spectrogram made during an Aerobee-Hi Rocket Flight on March 13, 1959, by the Naval Research Laboratory ("Sky and Telescope," March 1970).

TABLE 3-2. SOLAR UV LINES BELOW 182 NANOMETERS* (Cont.)

Element	Center Wavelength, λ_c (nm)	Estimated Linewidth, $\Delta\lambda_c$ (nm)	Estimated Maximum Line Intensity, $L_m = I_{line}/I_{continuum}$
H I (Ly α)	121.57	0.92	250
Si III	120.52	0.09	80
N I	119.24	0.09	3
N I (r)	118.99	0.06	2
C III	117.38	0.11	35
N II	108.29	0.13	15
O VI } Doublet	103.43	0.14	75
O VI }	102.86	0.10	80
H I (Ly β)	102.07	0.14	90
N III	98.65	0.06	5
C III	97.17	0.11	85
H I (Ly δ)	94.61	0.08	8
H I (Ly ϵ)	93.34	0.07	4
O II, III	82.95	0.09	5
O IV } Doublet	78.58	0.05	2
O IV }	78.46	0.05	2
(?)	77.61	0.05	2
(?)	76.66	0.05	3
(?)	62.48	0.05	8
O IV	57.57	0.05	8
He I	58.18	0.05	8

*The data in this table were obtained from a spectrogram made during an Aerobee-HI Rocket Flight on March 13, 1959, by the Naval Research Laboratory ("Sky and Telescope," March 1970).

$$L = L(\lambda) = L_m \exp - \left(\frac{\nu - \nu_c}{0.565 \Delta \nu_c} \right)^2 = L_m \exp - \left(\frac{\lambda - \lambda_c}{0.565 \Delta \lambda_c} \right)^2, \text{ if } L(\lambda) > 1 \quad (3.292a)^*$$

$$L = 1, \text{ if } L(\lambda) \leq 1 \quad (3.292b)$$

where:

$$L_m = L_m(\lambda_c) = \frac{I(\lambda)_{\text{line maximum}}}{I(\lambda)_{\text{continuum}}} \quad (3.293)$$

Values for $L_m(\lambda_c)$, λ_c , and $\Delta \lambda_c$ are listed in Table 3-2.

In Tables 3-3 and 3-4, the UV photon wavelengths below which the various exhaust species are ionized, and the wavelengths below which molecular species are dissociated, are listed.

Many exhaust molecules absorb semi-continuously at wavelengths below the first electronic excitation wavelength λ_1 . The atoms on the other hand absorb continuously only for wavelengths below the ionization wavelength. For many molecules, dissociation occurs nearly continuously at wavelengths below the predissociation wavelength, or at least within a broad band below the predissociation wavelength.

Most molecules will not dissociate however for wavelengths starting somewhat above the ionization value down to values of λ far below this level

*If $\Delta \nu_c / \nu$ and $\Delta \nu_c / \nu_c \ll 1$ as is the case here, we have $\Delta \nu_c / \nu_c = -\Delta \lambda_c / \lambda_c$ and

$$\text{thus } \left(\frac{\nu - \nu_c}{\Delta \nu_c} \right)^2 = \left(\frac{\nu}{\Delta \nu_c} - \frac{\nu_c}{\Delta \nu_c} \right)^2 = \left(\frac{\lambda_c}{\Delta \lambda_c} - \frac{\lambda}{\Delta \lambda_c} \right)^2 = \left(\frac{\lambda - \lambda_c}{\Delta \lambda_c} \right)^2.$$

TABLE 3-3. ABSORPTIVE ELECTRONIC IONIZATION, EXCITATION,
AND PREDISSOCIATION WAVELENGTHS (FREQUENCIES)
OF ROCKET EXHAUST SPECIES

Atom	Ionization		First Excitation		Second Excitation	
	λ_{ion} (nm)*	ν_{ion} (THz)**	λ_1 (nm)*	ν_1 (THz)**	λ_2 (nm)*	ν_2 (THz)**
H	91.1	3290	121.57	2466	97.1	3909
O	91.0	3300	135.56	2210	130.22	2300
N	85.3	3520	120.07	2500	(112)	(2680)
Cl	110.0	2725	296.72	1011	165.7	1812
C	95.5	3140	138.98	2160	134.73	2227
F	71.1	4210	97.65	3075	95.48	3142
Molecule	Ionization		First Excitation		Predissociation	
	λ_{ion} (nm)*	ν_{ion} (THz)**	λ_1 (nm)*	ν_1 (THz)**	λ_{pd} (nm)*	ν_{pd} (THz)**
H ₂	80.7	3720	109.0	2750	88.7	3381
O ₂	99.2	3023	630.0;*** 296.2 ***	476;*** 1011 ***	144.0	2080
N ₂	66.0	4450	144.3	2078	126.4	2373
C ₂	97.0	3095	258.0	1162		
OH	(168)	(1784)	308.6	972	(268)	1128
CO	88.0	3410	200	1500	125.0	2220
HCl	89.9	3338	227.2	1320	230.0	1303
NO	130.4	2300	230.0	1303	(220)	(1363)
AlCl	(90)	(3337)	261.4	1148		
H ₂ O	98.6	3042	186.0	1612	184.9	1622
CO ₂	89.9	3340	175.0	1713	(80)	(3750)

*1 nm = 1 nanometer = 10^{-9} meter

**1 THz = 1 terahertz = 10^{12} Hz

***These are first-order forbidden transitions with respect to the ground-state.

TABLE 3-4. DISSOCIATION ENERGIES AND FREQUENCIES OF ROCKET EXHAUST MOLECULES

Molecule	Dissociation	Dissociation Energy, ϵ_d (eV)	Dissociation Frequency, ν_d (THz)	Dissociation Wavelength, λ_d (nm)	Predissociation Lower Limit (nm)
H ₂	H + H	4.4763	1082	274.3	88.7
O ₂	O + O	5.080	1229	244.1	173.5
N ₂	N + N	9.756	2360	127.1	126.4
C ₂	C + C	3.6	871	344.1	(300)
OH	O + H	4.35	1052	285.2	268.0
CO	C + O	9.9	2398	125.2	125.0
HCl	H + Cl	4.430	1071	280.0	230.0
NO	N + O	5.296	1280	234.2	(220.0)
AlCl	Al + Cl	3.1	750	400.0	(350.0)
H ₂ O	H + OH	5.1136	1235	242.8	184.9
CO ₂	O + CO	4.453	1078	278.2	(80)

in the ionization continuum. Thus although ionization energies are higher than the dissociation energies, the molecule will remain intact if the energy of the interacting photon is high enough for ionization to occur.

When photon absorption by molecules results in molecular dissociation, the dissociated atoms will radiate away part of the excitation energy at their own characteristic atomic frequencies. The dissociated atoms of a molecule may recombine sometimes with the emission of a photon (e.g., $\text{CO} + \text{O} \rightarrow \text{CO}_2 + h\nu$). However usually most molecules in a high-altitude ($h \gtrsim 140$ km) exhaust cloud will remain dissociated once this event has occurred. As we shall see, the rate of dissociation of most exhaust molecules except for CO_2 , H_2 , and N_2 is reasonably fast. It takes for example ten minutes for 90 percent of the H_2O in an exhaust cloud to dissociate, but about thirty hours for 90 percent of the N_2 to decompose (see Table 3-7).

In Volume II of this handbook, expressions are given for photon absorption cross-sections for atoms and molecules resulting in excitation or dissociation, while Appendix G gives expressions for photo-ionization. In the following, photoionization will be considered first. From Appendix G we have for $\nu \geq \nu_{\text{ion}}$ that:

$$\sigma_{\text{ion}} = 6.30 \times 10^{-22} \frac{H(\nu - \nu_{\text{ion}})}{Z_{\text{eff}}^2} \left\{ \left(\frac{\nu_{\text{ion}}}{\nu} \right)^{5/2} - 0.087 \left(\frac{\nu_{\text{ion}}}{\nu} \right)^{3/2} \right\}, \text{ m}^2, \quad (3.294)$$

Here $H(x)$ is the unit step function, Z_{eff} is the effective charge, and ν_{ion} is the ionization frequency of the outer electron shell of the molecule (see Tables G-1 and G-2 in Appendix G). Thus for W_X kgm of exhaust molecules X

with molecular weight M_X , we have for the ionization rate in the exosphere using Eqs. (3.291) and (3.292):

$$\begin{aligned} \frac{d [\text{Ionizations of X}]}{dt} &= 6.025 \times 10^{26} \frac{W_X}{M_X} \int_{\nu=\nu_{\text{ion}}}^{\infty} \sigma_{\text{ion}}(\nu) \frac{d\rho_Y}{d\nu} d\nu = \\ &\approx 6.48 \times 10^{22} \frac{W_X \nu_{\text{ion}}^2 L_m(\nu_{\text{ion}})}{M_X Z_{X,\text{eff}}^2} \exp\left(-\frac{\nu_{\text{ion}}}{123}\right), \quad \frac{\text{ionizations}}{\text{second}} \end{aligned} \quad (3.295)$$

where $L_m(\nu_{\text{ion}})$ is usually $L_m(\nu_{\text{ion}}) = 1$, unless the ionization frequency of the molecule under consideration coincides with one of the strong discrete lines listed in Table 3-3 for which values of L_m are listed. In performing the integration over ν indicated in (3.295), we approximated Eq. (3.291) by:

$$\frac{d\rho_Y}{d\nu} = 1.52 \times 10^{15} \nu^2 \exp\left(-\frac{\nu}{123}\right), \quad \frac{\text{photons}}{\text{m}^2 \cdot \text{sec} \cdot \text{THz}}, \quad (3.296)$$

which is almost exact in the frequency region of interest ($\nu \gtrsim 1000$ THz).

At altitudes below 130 km, atmospheric attenuation of UV radiation must be considered. Using the approximate relation $\text{Tr}_s(\lambda, \theta_s, h) = \text{Tr}_s(\nu, \theta_s, h)$ for high-altitude solar transmission given in Appendix H, one has instead of (3.295):

$$\begin{aligned} \frac{d [\text{Ionizations of X}]}{dt} &= 6.48 \times 10^{22} \frac{W_X L_m(\nu_{\text{ion}}) \nu_{\text{ion}}^2}{M_X Z_{X,\text{eff}}^2} \cdot \\ &\cdot S_s(\nu_{\text{ion}}) \exp\left(-\frac{\nu_{\text{ion}}}{123}\right), \quad \frac{\text{ionizations}}{\text{second}} \end{aligned} \quad (3.297)$$

where:

$$S_s = S_s(\theta_s, h, \nu_{ion}) = \frac{1}{112.3} \int_{\nu=\nu_{ion}}^{\infty} Tr_s(\theta, h, \nu) \left\{ \left(\frac{\nu_{ion}}{\nu} \right)^{-1/2} - 0.087 \left(\frac{\nu_{ion}}{\nu} \right)^{1/2} \right\} \cdot \left\{ \exp - \left(\frac{\nu - \nu_{ion}}{123} \right) \right\} d\nu \quad (3.298)$$

Note that in the exosphere where $Tr_s = \text{constant} = 1$, the integral (3.298) may be evaluated approximately by assuming the slowly varying factor $\{(\nu_{ion}/\nu)^{-1/2} - 0.087 (\nu_{ion}/\nu)^{1/2}\}$ to be constant in comparison with the rapidly varying factor $\exp\{-(\nu - \nu_{ion})/123\}$ in the integration, and evaluating the slowly varying factor at $\nu = \nu_{ion}$. If one does this (with $Tr_s = 1$), $S_s = 1$. This is the approximation assumed in (3.295).

If $Tr_s(\theta_s, h, \nu)$ is assumed to have the altitude and frequency dependence as assumed in Appendix H, the integration (3.298) is best carried out on a computer. A reasonably fair analytic approximation to the integral (3.298) may be obtained however as follows. First we approximate:

$$\begin{aligned} S_s &\approx \frac{1}{112.3} \left\{ \left(\frac{\nu_{ion}}{\nu} \right)^{-1/2} - 0.087 \left(\frac{\nu_{ion}}{\nu} \right)^{1/2} \right\}_{\nu=\nu_{ion}} \cdot \int_{\nu=\nu_{ion}}^{\infty} Tr_s(\theta, h, \nu) \left\{ \exp - \left(\frac{\nu - \nu_{ion}}{123} \right) \right\} d\nu = \\ &= \frac{1}{123} \int_{\nu=\nu_{ion}}^{\infty} Tr_s(\theta_s, h, \nu) \left\{ \exp - \left(\frac{\nu - \nu_{ion}}{123} \right) \right\} d\nu \quad (3.299) \end{aligned}$$

Now the frequency dependence of $Tr_s(\theta_s, h, \nu)$ varies moderately slowly over the e-folding range $(\nu - \nu_{ion}) = 123$ THz of the exponential factor $\exp\{(\nu - \nu_{ion})/123\}$ in (3.299) as may be seen by inspection of the various transmission factors given in Appendix H. Therefore as a coarse approximation, we may take $Tr_s(\theta_s, h, \nu)$ outside the integral sign, and write:

$$S_s \approx \frac{Tr_s(\theta_s, h, \nu = \nu_{ion})}{123} \int_{\nu = \nu_{ion}}^{\infty} \left\{ \exp\left(-\frac{\nu - \nu_{ion}}{123}\right) \right\} d\nu = Tr_s(\theta_s, h, \nu = \nu_{ion}) \quad (3.300)$$

Each ionization event as given by (3.297) is eventually followed by an electron-ion recombination event. If in the ion-electron recombination process, radiation due to transitions from free electron states to bound electron states are neglected (the so-called Bremstrahlung), and if it is further assumed that most electrons are captured into one of the many upper (near the ionization level) electronic levels of a molecule (or atom) and that they all cascade back to the ground level through the same one, two, three, or more electronic levels of the molecule, one can write:

$$\begin{aligned} \left(\frac{dJ}{d\nu}\right)_{\text{SUAR Ioniz.}} &= \frac{F_v}{4\pi} Tr(\nu) h\nu \left(\frac{d(\text{Ionization})}{dt}\right) \sum_i \sum_j f'_{ij} \frac{b_e(\nu, \nu_{ij}, \Delta\nu_{ij})}{\Delta\nu_{ij}} = \\ &= 3.42 \times 10^{-3} \frac{\dot{W}}{(\text{kg/s})} \frac{F_v}{(\text{THz})} \nu Tr(\nu) \sum_i \sum_j f'_{ij} \frac{b_e(\nu, \nu_{ij}, \Delta\nu_{ij})}{\Delta\nu_{ij}(\text{THz})} \cdot \\ &\cdot \left(\frac{g_i \tau_{si} L_m(\nu_{ion}) Tr_s(\theta_s, h, \nu_{ion})}{M_i Z_{i\text{eff}}^2} \right) \frac{\nu_{ion}^2}{(\text{THz})} \exp\left(-\frac{\nu_{ion}}{123}\right), \frac{\text{Watts}}{\text{ster} \cdot \text{THz}} \end{aligned}$$

(3.301)

June 1974

Here ν , ν_{ion}^i , and $\Delta\nu_{ij}$ are all in units of THz ($= 10^{12}$ Hz). The usual view factor F_v and atmospheric transmission $Tr(\nu)$ have been added also in (3.301) for completeness.

Explicit expressions for the line or band shape function $b_e(\nu, \nu_{ij}, \Delta\nu_{ij})/\Delta\nu_{ij}$ of electronic or vibronic transitions are given in Volume II of the Rocket Radiation Handbook for various types of molecules. The summation over i in (3.301) is over all molecules X with excited electronic levels i through which the recombined electron cascades in returning to the ground level, while the j are the levels to which a level i can relax. The weighting factor f'_{ij} in (3.301) is composed of two component factors, that is:

$$f'_{ij} = f_{rci} f_{ij} = f_{rci} \frac{A_{ij}^0}{\sum_j A_{ij}^0}, \quad (3.302)$$

where A_{ij}^0 is the electronic spontaneous emission rate for which explicit expressions are given in Volume II, and where f_{rci} is the probability that a recombining electron will follow a ground-level-returning cascade that passes through level i . If after recombination only one cascade is followed always, $f_{rci} = 1$, but if say 30 percent of the time cascade A is followed which passes through level i , and 70 percent of the time cascade B results which includes another level k , we have $f_{rci} = 0.3$ and $f_{rck} = 0.7$ of course. Theoretical and experimental data on the factors f_{rci} are rare and difficult to obtain and for lack of any knowledge one often sets $f_{rci} \approx 1$, and thus $f'_{ij} \approx f_{ij}$.

In Eq. (3.301) we also used the relation:

$$\frac{w_X}{M_X} = 0.001 g_X \dot{W} \tau_{sX}, \quad \text{moles} \quad (3.302)$$

where \dot{W} is the rocket mass expulsion rate in kgm/sec, $g_X \equiv g_i$ gives the moles per kgm of exhaust species X and $\tau_{sX} \equiv \tau_{si}$ is the effective average time the exhaust species X dwells in the field-of-view of the observer. For TTO (Target Tracking Observations) τ_{sX} is given by Eq. (3.272), while in the case of ICO (Integrated Cloud Observations) observations, Eq. (3.271) should be used.

Often it is convenient to express the radiant intensity in terms of wavelengths λ instead of ν . In this case Eq. (3.301) changes to:

$$\left(\frac{dJ}{d\lambda}\right)_{\text{SUAR Ioniz.}} = \frac{c}{\lambda^2} \left(\frac{dJ}{d\nu}\right)_{\text{SUAR Ioniz.}} = 2.76 \times 10^{19} \left(\frac{\dot{W} F_v \text{Tr}(\lambda)}{\lambda_{(\text{nm})}^3}\right) \sum_i \sum_j \left(\frac{b_e(\lambda, \lambda_{ij}, \Delta\nu_{ij})}{\Delta\nu_{ij}(\text{THz})}\right) \cdot \left(\frac{f'_{ij} g_i \tau_{si} L_m(i\lambda_{\text{ion}}) \text{Tr}_s(\theta_s, h, i\lambda_{\text{ion}})}{Z_{i\text{eff}}^2 i\lambda_{\text{ion}(\text{nm})}^2}\right) \exp\left(-\frac{2437}{i\lambda_{\text{ion}}}\right), \frac{\text{Watts}}{\text{ster} \cdot \text{nm}}$$

(3.303)

Here λ and $i\lambda_{\text{ion}}$ are in nm (nanometers) and $\Delta\nu_{ij}$ is in THz.

The emissions i in Eq. (3.303) are a series of characteristic temperature-and-pressure-broadened lines for monoatomic exhaust species ($X = \text{H}, \text{Cl}, \text{O}, \text{etc.}$), and a series of rotationally-broadened vibronic bands for the case of molecular exhaust species ($X = \text{CO}_2, \text{H}_2\text{O}, \text{CO}, \text{OH}, \text{HCl}, \text{etc.}$). Center wavelengths, λ_{ij} , of some of the stronger transitions that have been observed are given in Tables 3-5 and 3-6. Clearly, the SUAR radiation spectrum (3.303) provides a characteristic spectral "fingerprint" of the exhaust species, in contrast to SOSP radiation which only transfers the

June 1974

TABLE 3-5. MAIN ELECTRONIC EMISSION LINES OF EXHAUST ATOMS IN THE
UVIS REGION OF THE SPECTRUM (Data from Refs. 51 and 52)

Atom	Transition Wavelength λ_{ij} (nm)*	Relative Intensity**	Atom	Transition Wavelength λ_{ij} (nm)*	Relative Intensity**
H	$i \rightarrow 0$		C	$i \rightarrow 0$	
	97.4	5		155.8	5
	102.8	7		165.7	7
	121.6	10	C+	247.9	5
	$i \rightarrow 1$			133.6	10
	434.0	4		426.7	5
	486.1	6	N	$i \rightarrow 0$	
O	656.3	8		119.8	2
	$i \rightarrow 0$			$i \rightarrow j$	
	130.1	8		409.9	2
	135.6	8		411.0	5
	$f \rightarrow 0$			444.7	3
	297.2	1		493.5	3
	$i \rightarrow j$		N+	108.3	7
	394.7	2		566.7	5
	436.8	2		568.0	5
	533.6	2	O+	$i \rightarrow j$	
O+	615.8	3		479.5	5
	777.2	5		481.0	5
	411.9	4		481.9	4
	464.9	4			

* $i \rightarrow j$ = Non-ground state connected transition.
 $i \rightarrow 1$ = First excited state connected transition.
 $i \rightarrow 0$ = Ground state connected transition.
 $f \rightarrow 0$ = "Forbidden" ground state connected transition.

**These values are rough estimates.

TABLE 3-6. MAJOR VIBRONIC EMISSION BANDS OF EXHAUST MOLECULES IN THE
UVIS REGION OF THE SPECTRUM (Data from Refs. 46, 47, and 48)

Molecule	Wavelength Region of Band, (nm)*	Relative Intensity**	Molecule	Wavelength Region of Band, (nm)*	Relative Intensity**
H ₂ O	130 - 140		H ₂	406.7 - 421.3	
	161 - 178			449.8 - 508.4	
	569 - 574			519.6 - 642.8	
	588.6 - 594.1			716.9 - 725.3	
	649.6 - 654.4			752.5	
	694.4 - 701.6			816.5 - 835.0	
	718.6 - 790.2				
OH	260.8 - 262.2	3	CO	200 - 280	
	267.7 - 269.1	2		283 - 280	
	281.1 - 282.9	6		412 - 662	
	287.5 - 289.3	3	CO ₂	287.4	
	294.5 - 296.2	1		303.4 - 316.5	
	302.1 - 308.9	10		324.5 - 328.4	
	312.1 - 312.6	1		337.0 - 340	
	318.5 - 320.9	1		350.3 - 356.6	
	342.8 - 347.2	2		362.1 - 369.1	
	386.4 - 388			376.1 - 389	
	421.6 - 423			396.1 - 416	
	433.7 - 435		CO ₂ ⁺	288.3 (sharp)	
	458.7 - 460			289.6 (sharp)	
	473.0 - 474		HCl	198 - 237.5	
	495.7 - 497			283 - 396.6	
	512.3 - 514				
	548.0 - 550				
OH ⁺	356 - 360				

*The center wavelength λ_{ij} of the electronic transition is approximately in the middle of each band.

**These values are rough estimates.

solar spectrum (except for possible secondary spectral effects due to particle-size-related Mie resonances).

Before concluding the analysis on ionization-produced SUAR radiation, one additional comment is in order. If a cloud of atoms with a low ionization potential (e.g., Cs, K, Na, etc.) is released at high altitudes, the rapid electron recombination that was postulated above does not apply. In this case it is possible (see Ref. 5) that the earth's magnetic field will force ionized atoms out of the cloud of neutrals with the result that two separated space-charge-balanced clouds are formed, one containing neutral atoms and electrons, and the other ions. The ions are also excited by solar UV (see below) and one observes characteristic spectral emissions (e.g., blue) from the neutral cloud that are different from the characteristic spectral emissions of the ion cloud (e.g., purple). It is possible to develop expressions similar to the ones given above for these special cases (magnetic fields, etc., must be considered to determine the populations in the ion and neutral cloud), but we shall not discuss them here.

In addition to ionization-recombination-generated SUAR radiation, there is of course also SUAR radiation due to excitation (possibly followed by dissociation). In fact the contribution from excitations in the total amount of SUAR radiation usually far exceeds that contributed by ionization/recombinations.

The cross-section for solar photon absorption (in the UVIS region) is approximately given by (see Vol. II, section 5.1):

$$\sigma_{\text{abs}_X} = (\sigma_{01})_X \approx 4.422 \times 10^{-19} w_i \frac{b_e(\nu, \nu_{10}, \Delta\nu_{10})}{\Delta\nu_{10}(\text{THz})}, \text{ m}^2 \quad (3.304)$$

where w_i is the statistical weight of the electronic excited level i , and $b_e(\nu, \nu_{i0}, \Delta\nu_{i0})$ is the electronic transition shape function for which expressions are given in Volume II. The band or line-spread $\Delta\nu_{i0}$ is in THz, as before. Equation (3.304) applies only for allowed transitions $0 \rightarrow i$ (for selection rules, see Vol. II). For first-order-forbidden magnetic-dipole transitions, the cross-section is about 5×10^{-5} times smaller, while for electric quadrupole transitions the cross-section is still smaller (by a factor of about 10^{-8} to 10^{-10}).

Using expression (3.296) for the solar UV flux, Eq. (3.304) for the cross-section, Eq. (3.302) for the amount of exhaust molecules under observation, and approximation (3.300) to account for upper-atmosphere filtering of solar UV photons, one obtains:

$$\begin{aligned} \frac{d(\text{Excitations } X_i)}{dt} &= 6.025 \times 10^{23} g_X \dot{W} \tau_{sX} \int_{\nu=0}^{\infty} (\sigma_{oi})_X \frac{d\phi_Y}{d\nu} \text{Tr}_s(\theta_s, h, \nu) d\nu = \\ &= 4.05 \times 10^{20} g_X \dot{W} \tau_{sX} L_{\nu_i}(\nu_i) \text{Tr}_s(\theta_s, h, \nu_i) w_i \nu_i^2 \exp\left(-\frac{\nu_i}{123}\right), \frac{\text{Excitations } X_i}{\text{second}} \end{aligned} \quad (3.305)$$

Here we used the relation (see Vol. II):

$$\int_{\nu=0}^{\infty} \frac{b_e(\nu, \nu_{ij}, \Delta\nu_{ij})}{\Delta\nu_{ij}} f(\nu) d\nu = f(\nu_{ij}) \quad (3.306)$$

Also note that $\nu_{oi} = \nu_i$, where ν_i is the frequency of excited level i .

The subsequent reemission of radiation due to solar UV excitation is then:

June 1974

$$\left(\frac{dJ}{dv}\right)_{\text{SUAR Excit.}} = 2.135 \times 10^{-2} \dot{W} F_v \frac{v}{(\text{THz})} \text{Tr}(v) \sum_i \sum_j g_i \tau_{si} L_p(v_i) \text{Tr}_s(\theta_s, h, v_i) \cdot$$

$$\cdot f_{ij} w_i v_i^2 \left\{ \exp\left(-\frac{v_i}{123}\right) \right\} \frac{b_e(v, v_{ij}, \Delta v_{ij})}{\Delta v_{ij}(\text{THz})}, \quad \frac{\text{Watts}}{\text{ster} \cdot \text{THz}}$$

(3.307)

Again, the view-factor $F_v/4\pi$ and atmospheric transmission $\text{Tr}(v)$ were added for completeness.

Rewriting (3.307) in terms of wavelength λ , results finally in the expression:

$$\left(\frac{dJ}{d\lambda}\right)_{\text{SUAR Excit.}} = 1.725 \times 10^{20} \left(\frac{\dot{W} F_v \text{Tr}(\lambda)}{\lambda_{(\text{nm})}^3} \right) \sum_i \sum_j g_i \tau_{si} L_p(\lambda_i) \text{Tr}_s(\theta_s, h, \lambda_i) \cdot$$

$$\cdot f_{ij} w_i \left\{ \frac{\exp\left(-\frac{2437}{\lambda_i}\right)}{\lambda_i^2(\text{nm})} \right\} \frac{b_e(\lambda, \lambda_{ij}, \Delta v_{ij})}{\Delta v_{ij}(\text{THz})}, \quad \frac{\text{Watts}}{\text{ster} \cdot \text{nm}}$$

(3.308)

As before, $\tau_{si} = \tau_{sx}$ is given by Eqs. (3.271) and (3.272) for respectively ICO and TIO observations. Note that for SUAR excitation the simple factor f_{ij} applies, that is:

$$f_{ij} = \frac{(A_{ij}^0)_{\text{elc}}}{\sum_j (A_{ij}^0)_{\text{elc}}}, \quad (3.309)$$

in contrast to the ionization-recombination case for which $f'_{ij} = f_{rci} f_{ij}$ must be used. Also it should be noted by comparing (3.308) with (3.303) that excitation SUAR radiation is at least ^{f_{ij}} ~~ten~~ times more intense than ionization SUAR radiation, unless a special solar spectral line coincides with ν_{ion} so that $L(\nu_{ion}) \gg 1$.

In Eq. (3.308), only direct excitations i due to solar UV photon absorptions and subsequent emissions from $i \rightarrow j$ transitions are accounted for. The emissions from subsequent transitions $j \rightarrow k$, $k \rightarrow l$, etc., lower down in the cascade are not included in expression (3.308). Usually this omission is justified since due to the steep decline of the photon flux with increasing frequency in the UV region, direct excitations of level j (lying lower in energy than level i) are much stronger than direct excitations of level i (which is at a higher energy) from which some additional population of level j results due to downward cascading of $i \rightarrow j \rightarrow k$.

The only times that cascading contributions "from above" cannot be neglected occurs when (a) the frequency ν_{oi} of the higher level i of the molecule coincides with one of the special strong lines in the solar UV spectrum listed in Table 3-2, or (b) if the level j reached in the cascade $i \rightarrow j$ cannot be optically excited from the ground level o , that is if the transition $o \rightarrow j$ is optically forbidden, but emissions $j \rightarrow k \rightarrow o$ are allowed. These special cases can be easily included however by adding to Eq. (3.308) the following expression for such special levels j_i which are populated by cascades $i \rightarrow j_i$ or $i \rightarrow p \rightarrow q \rightarrow \dots j_i$.

$$\left(\frac{dJ}{d\lambda}\right)_{\text{(SUAR Excit.) } j_i} = 1.725 \times 10^{20} \left\{ \frac{\dot{W} F_v \text{Tr}(\lambda)}{\lambda_{(\text{nm})}^3} \right\} \sum_i \sum_k g_i \tau_{s_i} L_{\text{eff}}(\lambda_i) \text{Tr}_s(\theta_s, h, \lambda_i) \cdot$$

$$\cdot w_i \left\{ \frac{\exp\left(-\frac{2437}{\lambda_i}\right)}{\lambda_{i(\text{nm})}^2} \right\} f_{j_i k} \left\{ \frac{b_e(\lambda, \lambda_{j_i k}, \Delta\nu_{j_i k})}{\Delta\nu_{j_i k} \text{ (THz)}} \right\}, \frac{\text{Watts}}{\text{ster. nm}}$$

(3.310)

In most practical applications, once the exhaust molecules have been identified, the levels can be established by consultation with the literature such as Refs. 46, 47, and 48, and a determination can be made if any special levels j_i should be considered.

In addition to the special consideration of populations of excited levels from "upstream cascades," one might also examine the possibility of double- or multiple-photon up-pumping. However the probability for the occurrence of such events is extremely small, since both the solar photon flux density and the exhaust gas density are too low and lifetimes of electronic excited states are too short. (Only with laser beams can double and multiple absorptions be significant.) One may therefore safely ignore two- or three-step excitations in a single (undissociated) molecule.

A different situation than the one just discussed can exist however in the case that a molecule is dissociated by solar UV. For example H_2O may dissociate due to solar UV absorption into H and OH. The OH formed in the dissociation is usually in a high excited vibrational level and not in the ground vibrational state as shown in Figure 3-19. Because excited vibrational

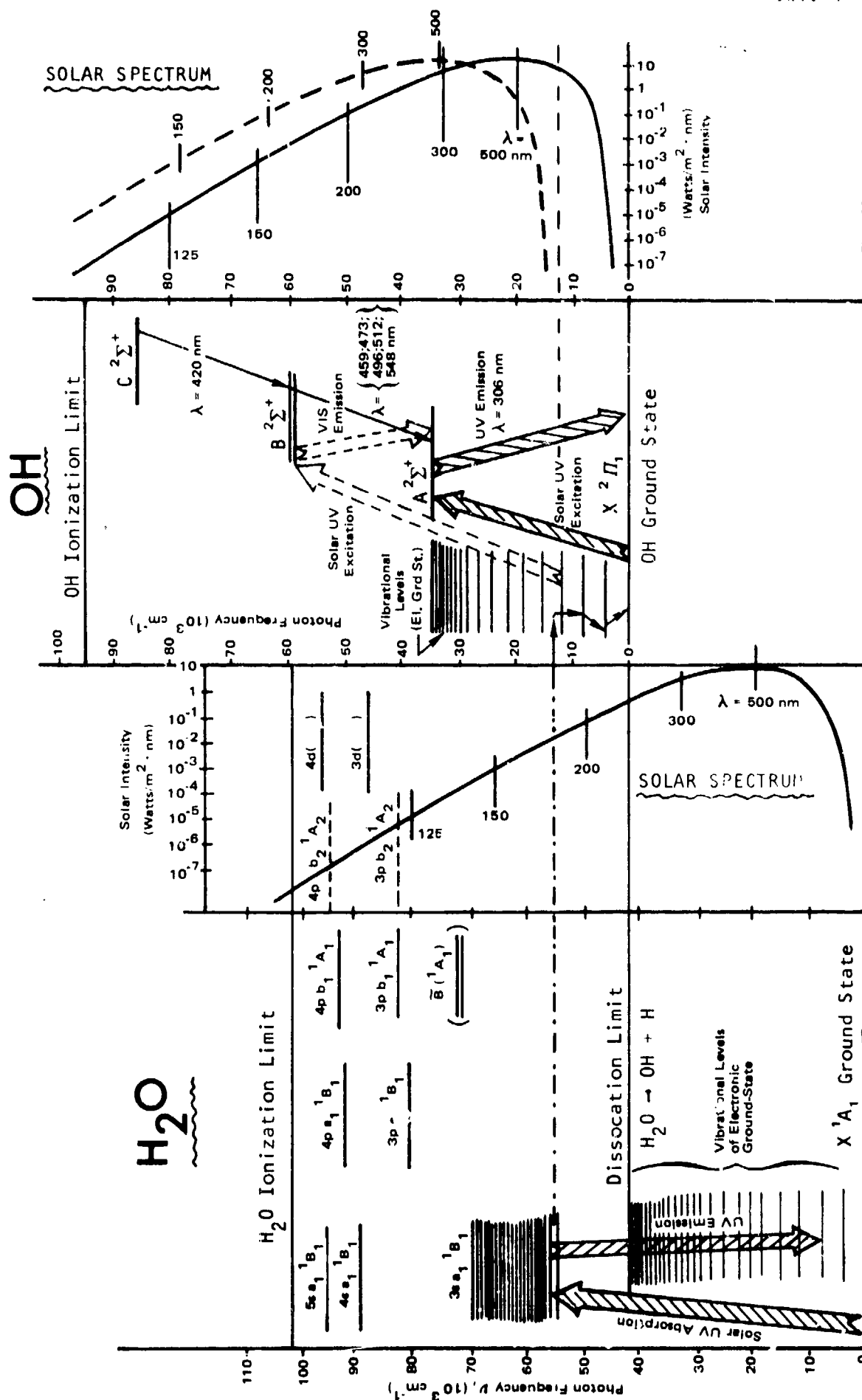


FIGURE 3-19. ILLUSTRATION OF SUSPECTED SOLAR-UV-EXCITED DISSOCIATIONS OF H_2O AND UVIS EMISSIONS FROM OH IN HIGH-ALTITUDE ROCKET EXHAUST PLUMES

June 1974

levels have much longer lifetimes (~ 4 ms) compared to excited electronic level lifetimes (~ 1 μ s), it is possible for additional solar photons to excite the OH to higher levels than would be possible under normal circumstances if the OH were in the ground vibrational state to start with.

In Figure 3-19 for example, it is speculated that OH formed in the dissociation of H_2O by solar UV photons is left in the $v = 3$ vibrational level. Additional solar UV photons (with $\lambda \sim 225$ nm) then excite OH to the $B^2\Sigma^+$ electronic level which decays to the $A^2\Sigma^+$ electronic level with the emission of several strong visible bands. This excitation scheme is postulated in order to explain the bright visible emission (Ref. 53) that was observed during the lunar-injection-burn of Apollo-8 above Hawaii as shown in Figure 1-1. In the first frame of Figure 1-1, the Apollo-8 vehicle had just moved from the dark side to the light side of the earth and was illuminated by atmosphere-filtered visible (but not UV) solar radiation. Only the vehicle body which reflected this visible radiation is observed in this first frame. As Apollo-8 became fully illuminated by non-atmosphere-filtered solar radiation which included the UV, the exhaust gases behind the vehicle (which contained H_2 and H_2O) suddenly began to radiate very brightly in the visible as shown in frames 2, 3, etc. Clearly, solar UV had to be the origin of this new radiation which was absent in frame 1 of Figure 1-1 (see Ref. 53).

Now inspection of Figure 3-19 shows that non-dissociated H_2O would reradiate in the UV. Similarly OH, if excited from its ground state, would mostly reemit UV from $A^2\Sigma^+ \rightarrow X^2\Pi_1$ transitions. If only UV was emitted, the exhaust radiation could not have been observed from the ground. The $B^2\Sigma^+ \rightarrow A^2\Sigma^+$ transitions are in the visible however and can be produced by assuming that the scheme shown by the dotted lines is operative as described

above. Since visible radiation was observed, only the latter mechanism could explain the observations.

The intensity of the observed visible radiation from the Apollo-8 exhaust plume is also orders of magnitude higher than could be explained by assuming that solar radiation was scattered by the exhaust gases (Rayleigh scattering). Scattering from frozen particles (see section 3.3.6) was impossible since temperatures in the exhaust plume were too high to allow any freezing there. Further, if scattering had been operative, one should also have observed scattered solar radiation from the exhaust in the first frame of the sequence shown in Figure 1-1; but it was not.

In addition to the just-described $\text{H}_2\text{O} \rightarrow \text{OH}^* + \text{H}$ case in which OH^* is generated in an excited vibrational level, the photodissociation process can sometimes also create electronically excited atoms. For example the photodissociation of O_2 in the exosphere (e.g. from LOX dumps; see Figure 1-2) can result in the formation of atomic oxygen in the ^1S and ^1D excited levels which are metastable but which do eventually relax (via magnetic dipole or electric quadrupole interaction) to the ^3P ground state with the emission of sharp line radiations in the visible (see Ref. 9).

Photodissociation by solar UV occurs for many molecules at frequencies that lie in the vicinity of the first allowed electronic excited state. The solar UV photon wavelength below which dissociation plus dissociated radical excitation can occur is of course given by:

$$\lambda_{d*1} \leq \frac{3 \times 10^5}{\nu_d(\text{XY}) + \nu_1(\text{Y})} \quad , \quad \text{nm} \quad , \quad (3.311)$$

June 1974

where XY is a molecule with atomic or radical partners X and Y, and where Y is the dissociated atom or radical in the excited state i. The frequencies ν_d and ν_i are defined by:

$\nu_d = \nu_d(XY)$ = Photodissociation frequency of molecule XY, THz

$\nu_i = \nu_i(Y)$ = Frequency of excitation of atom or radical Y during dissociation process, THz

The number of XY photodissociations and Y_i excitation events is clearly:

$$\frac{d [\text{Dissociations XY}]}{dt} = \frac{d [\text{Excitations } Y_i]}{dt} = \sum_{\nu_k > \nu_{d* k}}^{\infty} \int_{\nu = \nu_{d* k}}^{\infty} \sigma_{\text{abs}}(\nu, \nu_k) L(\nu) \frac{d\rho}{d\nu} d\nu, \text{ sec}^{-1} \text{ per molecule XY} \quad (3.312)$$

The summation over the allowed molecular electronic levels k at frequencies ν_k can usually be replaced by an integration since the states k lie close to each other in the region where dissociation can occur. Since the term $\exp(-\nu/123)$ in the solar flux expression changes most rapidly under the integrals, one obtains for the radiant intensity due to Y_i reradiation (converting all ν 's to λ 's via $\lambda = c/\nu$):

$$\left(\frac{dJ}{d\lambda} \right)_{\substack{\text{SUAR} \\ \text{Photodiss.} \\ + \text{Excit.}}} = 1.725 \times 10^{20} \left(\frac{\dot{W}_V F_V \text{Tr}(\lambda)}{\lambda_{(\text{nm})}^3} \right) \sum_k \sum_i \sum_j g_k \tau_{sk} w_k L_{\text{su}}(\lambda_{d* k}) \cdot \text{Tr}_s(\theta_s, h, \lambda_{d* k}) \left\{ \frac{\exp\left(-\frac{2437}{\lambda_{d* k}(\text{nm})}\right)}{\lambda_{d* k}^2(\text{nm})} \right\} f_{ij} \left\{ \frac{b(\lambda, \lambda_{ij}, \Delta\nu_{ij})}{\Delta\nu_{ij}(\text{THz})} \right\}, \frac{\text{Watts}}{\text{ster} \cdot \text{nm}}$$

Here the summation over k is over photodissociatable molecular species XY that form excited species Y_i , and λ_{d*k} is the dissociation wavelength for molecule k . The parameter $\tau_{sk} = \tau_{sX}$ is again given by Eqs. (3.217) and (3.272) for respectively ICO and TTO observations, while f_{ij} is again given by (3.309) and w_k is the statistical weight of the dissociation-producing electronic level of molecule XY .

The emission shape function $b(\lambda, \lambda_{ij}, \Delta\nu_{ij})/\Delta\nu_{ij}$ is equal to a doppler or collision-broadening line function (see Vol. II) in the case that Y is an atom, or equal to a vibronic shape function (see Vol. II) if the dissociation product Y is a multiatomic radical or molecule.

The total photodissociation rate z_d is usually somewhat higher than the rate given by Eq. (3.312) since for frequencies between ν_d and ν_{d*1} , radiationless dissociations can occur. The total photodissociation rate is given by:

$$\begin{aligned}
 z_{X_d} &= \sum_{\nu_k = \nu_{pd}}^{\infty} \int_{\nu_{pd}}^{\infty} \sigma_{abs}(\nu, \nu_k) L(\nu) \frac{d\phi(\nu)}{d\nu} d\nu = \\
 &= 6.72 \times 10^{-4} \text{Tr}_s(\theta_s, h, \nu_{pd}) w_d \nu_{pd}^2 L(\nu_{pd}^I) \exp\left(-\frac{\nu_{pd}}{123}\right), \frac{\text{sec}^{-1}}{\text{molecule}}
 \end{aligned}
 \tag{3.314}$$

where $L(\nu_{pd}^I)$ is the value of any special solar line at a frequency equal to or slightly higher than the pre-dissociation frequency $\nu_{pd} = 3 \times 10^5/\lambda_{pd}$, and w_d is the statistical weight of the electronic level that leads to dissociation.

TABLE 3-7. DISSOCIATION RATES OF EXHAUST MOLECULES IN THE EXOSPHERE UNDER SOLAR ULTRAVIOLET IRRADIATION

Molecule X	Calculated		Decay Time* $\tau_{X_d} = \frac{1}{z_d}$
	ν_{pd} (THz)	Dissociation Rate z_d (sec^{-1})	
H ₂ O	1622	3.31×10^{-3}	5.03 m**
CO ₂	3750	5.43×10^{-10}	58.4 y
CO	2400	1.30×10^{-5}	21.4 h
OH	1120	9.36×10^{-2}	10.7 s
HCl	1304	2.84×10^{-2}	35.2 s
NO	1364	1.91×10^{-2}	52.4 s
O ₂	2083	1.29×10^{-4}	2.16 h
N ₂	2373	1.58×10^{-5}	17.56 h
H ₂	3382	8.80×10^{-9}	3.60 y

* $\tau_{X_d} = 1488 \nu_d^{-2} \exp(\nu_d/123)$, sec.

** s = seconds; m = minutes; h = hours; y = years.

In Table 3-7, calculated dissociation rates and decay times $\tau_d = 1/z_d$ are listed for exhaust species of major interest exposed to solar UV in the exosphere ($Tr_s = 1$). Because the various exhaust species have different decay times, it is possible to identify a particular exhaust molecule not only from the characteristic emission spectrum of its dissociation product species Y_i but also from the radiation intensity decay time of the line emissions of Y_i . Thus a double check is possible which allows one to distinguish between different species with emissions in the same part of the spectrum. For example an exhaust cloud of H_2O will show emission lines from excited OH^* at $\lambda = 306 \pm 5$ nm which decays at an e-folding rate of 5 minutes, that is at the dissociation decay rate of H_2O (the OH dissociates faster and thus the H_2O decay rate is controlling). Another species with emissions in the 306 ± 5 nm region of the spectrum would decay at a different rate.

3.3.8 Spectral Considerations

The total radiant intensity from a rocket exhaust in a certain part of the spectrum is of course equal to the sum of any contributions in that region from any of the six main mechanisms discussed in the previous sections. If only infrared emissions are of interest, CORE and ABCD are the main mechanisms under daytime or nighttime TTO (= target-tracking-observation) conditions. In addition to CORE and ABCD, ATMP radiation should also be considered if observations are made under wide fov angle and/or ICO (= integrated cloud observations) conditions. In the latter case, it is necessary that one specifies further whether the observations are made at night or during the day since solar UV will dissociate the molecular species in the exhaust cloud in daytime but not at night.

June 1974

For visible and ultraviolet (UVIS) emissions, ABCD, SOSP, and SUAR must all be considered. Daytime conditions are essential of course for both SOSP and SUAR. ABCD radiation in the UVIS occurs when the exhaust velocity relative to the air is large which happens at take-off, at near-orbital velocities, and during deorbiting retrofirings.* Of course ABCD radiation in the UVIS can occur both at night and in daytime, but in daytime the background radiation is usually stronger than any UVIS emissions that are present so that it is often not observed.

The total radiation from both CORE and ABCD may be conveniently lumped into the one formula:

$$\left(\frac{dJ}{d\lambda}\right)_{\text{ABCD+CORE}} = 2.8549 \times 10^{16} \left(\frac{\dot{W}}{\lambda^3 (\mu\text{m})}\right) F_v \text{Tr}(\lambda, S, h) \cdot \sum_i \sum_j g_i f_{ij} \frac{\tau_i^{-1}}{\tau_i^{-1} + \tau_{qi}^{-1}} \cdot$$

$$\cdot \left[\left\{ \frac{b(\lambda, \lambda_{ij}, \Delta\lambda_{ij})}{\Delta\nu_{ij} (T = T_M)} \right\} \left\{ 1 - \exp\left(-\frac{\tau_M}{(\tau_i^{-1} + \tau_{qi}^{-1})^{-1}}\right) \right\} \left\{ \exp\left(-\frac{\epsilon_i}{kT_e}\right) \right\} + \right.$$

$$\left. + \left\{ \frac{b(\lambda, \lambda_{ij}, \Delta\lambda_{ij})}{\Delta\nu_{ij} (T = T_a \Theta_2)} \right\} \left\{ \exp\left(-\frac{\epsilon_i}{kT_a \Theta_1}\right) \right\} \right], \frac{\text{Watts}}{\mu\text{m} \cdot \text{ster}}$$

MULTIPLY LAST 2 FACTORS OF EQ. BY $\left(1 + \frac{V_e}{3c}\right)$ (3.315)

Here $\epsilon_i = h\nu_i$ is the energy level from which photon emissions take place, which in general can be an electronic level, a vibrational level, or a rotational level. Expressions for parameters such as τ_M , Θ_1 , and Θ_2 were given in sections 3.3.3 and 3.3.4.

*These emissions are primarily due to several vibrational combination bands of H_2O that emit in the visible (see Table 3-8).

As mentioned in section 3.3.2 in connection with Eq. (3.102), for vibrational emissions one can sum Eq. (3.315) over all the levels of each one of the normal vibrations α (see Vol. II) of the different molecules if emissions are observed in the strong $\Delta v_\alpha = 1$ emission bands, since one can assume $v_{ij} \approx v_\alpha$ for all $\Delta v_\alpha = v_{\alpha i} - v_{\alpha j} = 1$ transitions. This assumption is excellent, if one is not interested in fine spectral details. One obtains in this case:

$$\begin{aligned}
 \left(\frac{dJ}{d\lambda} \right)_{\substack{\text{ABCD+} \\ \text{CORE} \\ \text{(Infrared)} \\ \Delta v_\alpha = 1}} &= 2.8549 \times 10^6 \left(\frac{\dot{W}}{\lambda^3 (\mu\text{m})} \right) F_v \text{Tr}(\lambda, S, h) \cdot \sum_{\alpha} g_{\alpha} \left(\frac{\tau_{\alpha}^{-1}}{\tau_{\alpha}^{-1} + \tau_{q\alpha}^{-1}} \right) \cdot \\
 &\cdot \left[\left\{ \frac{b_v(\lambda, \lambda_{\alpha}, \Delta v_{01})}{\Delta v_{01} (T = T_M)} \right\} \left\{ 1 - \exp \left(- \frac{\tau_M}{(\tau_{\alpha}^{-1} + \tau_{q\alpha}^{-1})^{-1}} \right) \right\} \left\{ \exp \left(\frac{14,388.5}{\lambda_{\alpha} T_e} \right) - 1 \right\}^{-1} + \right. \\
 &\quad \left. + \left\{ \frac{b_v(\lambda, \lambda_{\alpha}, \Delta v_{01})}{\Delta v_{01} (T = T_a \Theta_2)} \right\} \left\{ \exp \left(\frac{14,388.5}{\lambda_{\alpha} T_a \Theta_1} \right) - 1 \right\}^{-1} \right] \cdot \frac{\text{Watts}}{\text{ster} \cdot \mu\text{m}}
 \end{aligned}$$

(3.316)

The summation over α in (3.316) is over the infrared-active normal vibrations only. For diatomic molecules there is only one value for λ_{α} , while for triatomic molecules there are usually three different values* of λ_{α} like in

*For H_2O , $\lambda_{\alpha=1} \neq \lambda_{\alpha=2} \neq \lambda_{\alpha=3}$, but $g_{\alpha=1} = g_{\alpha=2} = g_{\alpha=3}$ of course.

the case of H_2O . However for linear triatomic molecules such as CO_2 there are only two infrared-active λ_α 's since the third one is infrared-inactive (see Vol. II).

If one is primarily interested in those regions of the infrared vibrational spectrum where most of the radiant energy is released, one needs only to consider the fundamental $\Delta v_\alpha = 1$ transitions, since the emission from overtone transitions $\Delta v_\alpha = 2, 3, \dots$ and combination band transitions $\Delta v = \sum_\alpha \Delta v_\alpha \geq 1$, are always much weaker than those of the $\Delta v_\alpha = 1$ transitions. However if one is interested in special regions of the vibrational spectrum where only overtone and multi-band transitions are active, the latter can of course not be ignored. For such vibrational multi-band or overtone transitions, Eq. (3.315) must be used and f_{ij} evaluated, which was given by Eq. (3.101).

For vibrational transitions, the radiative decay constant or Einstein coefficient can be expressed by the general relation (see Vol. II, Tables 5-1 and 5-2):

$$A_{ij}^0 = 2.6833 \times 10^{-21} \frac{v_{ij}^3}{(\text{Hz})^3} w_j \frac{R_{ij}^2}{(\text{cm}^2)}, \quad \text{sec}^{-1}, \quad (3.317)$$

where the transition matrix R_{ij}^2 is given by:

$$(R_{ij}^2)_{\text{vib.}} = \frac{h z_{ij}^2}{8\pi^2 M_{ij} v_{ij} x_{ij}} \prod_\alpha \left(\frac{v_{\alpha i}!}{v_{\alpha j}!} \right)^{\delta_\alpha} \left\{ \frac{x_\alpha^{|v_{\alpha i} - v_{\alpha j}|}}{(|v_{\alpha i} - v_{\alpha j}| + 1)^2} \right\}, \quad \text{cm}^2, \quad (3.318)$$

in which:

$$\delta_{\alpha} = 1, \text{ if } v_{\alpha_i} > v_{\alpha_j}; \delta_{\alpha} = -1, \text{ if } v_{\alpha_i} < v_{\alpha_j} \quad (3.319)$$

$$M_{ij} = \left[\sum_{\alpha} M_{\alpha}^{-1/2} |v_{\alpha_i} - v_{\alpha_j}| \right]^{-2}, \text{ a.m.u.} \quad (3.320)$$

$$x_{ij} = \left[\sum_{\alpha} x_{\alpha}^{-1/2} |v_{\alpha_i} - v_{\alpha_j}| \right]^{-2} \quad (3.321)$$

$$\phi = 1 - \frac{1}{2} \left(\frac{(\sum_{\alpha} |v_{\alpha_i} - v_{\alpha_j}|)! - 1}{(\sum_{\alpha} |v_{\alpha_i} - v_{\alpha_j}|)! + 1} \right) \quad (3.322)$$

$$z_{ij} = (v_{ij} M_{ij} x_{ij})^{1/2} \left| \sum_{\alpha} \left(\frac{|v_{\alpha_i} - v_{\alpha_j}| + 1}{|v_{\alpha_i} - v_{\alpha_j}|} \right) \left(\frac{z_{\alpha} \vec{e}_{\alpha}}{M_{\alpha}^{1/2} v_{\alpha}^{1/2} x_{\alpha}^{1/2}} \right) \right| \quad (3.323)$$

$$v_{ij} = \sum_{\alpha} (v_{\alpha_i} - v_{\alpha_j}) v_{\alpha}, \quad \text{Hz} \quad (3.324)$$

The v_{α_i} and v_{α_j} are the vibrational quantum numbers of levels i and j respectively of the normal vibration α . In (3.317), w_j is the statistical weight of level j . If j is the ground state $w_j = 1$. The parameter x_{ij} is the transition-averaged anharmonic constant, M_{ij} is the effective vibrational mass of the transition $i \rightarrow j$, v_{ij} is the frequency of the vibrational transition $i \rightarrow j$, and z_{ij} is the transition-averaged first-derivative dipole-charge (see Vol. II, section 3.3, and Appendix B). The four parameters v_{α} ,

M_α , x_α , and z_α are the fundamental constants of a normal vibration α .

Values of these constants for different molecules are given in Volume II.

For $\Delta v_\alpha = v_{\alpha_i} - v_{\alpha_j} = 1$ transitions, Eqs. (3.318) through (3.324) simplify to:

$$\left(R_{ij}^2 \right)_{\text{vib.}} \bigg|_{(\Delta v_\alpha = 1)} = \frac{h z_\alpha^2}{16\pi^2 M_\alpha v_\alpha} (v_{\alpha_i} + v_{\alpha_j} + 1) \text{ , cm}^2 \quad (3.325)$$

$$v_{ij} = v_\alpha \quad (3.326)$$

$$M_{ij} = M_\alpha \quad (3.327)$$

$$z_{ij} = 2z_\alpha \quad (3.328)$$

$$\phi = 1 \quad (3.329)$$

Thus for $\Delta v_\alpha = 1$ transitions, the Einstein factor (3.317) is:

$$\begin{aligned} \left(A_{ij}^0 \right)_{\text{vib.}} \bigg|_{(\Delta v_\alpha = 1)} &= 0.6095 \times 10^{-4} \left(\frac{z_\alpha^2 v_\alpha^2}{M_\alpha} \right) w_j (v_{\alpha_j} + v_{\alpha_i} + 1) = \\ &= 6098.6 \left(\frac{z_\alpha^2}{M_\alpha \lambda_\alpha^2} \right) w_j (v_{\alpha_j} + v_{\alpha_i} + 1) \text{ , sec}^{-1} \text{ ,} \end{aligned} \quad (3.330)$$

(amu · μm²)

where ν_α is in cm^{-1} , λ_α is in μm , and M_α is in a.m.u. (atomic mass units).

In Table 3-8, the Einstein factors for the more important vibrational levels of exhaust molecules are listed which give rise to infrared emissions. For $\Delta\nu_\alpha = 1$ emission bands, the factor $f_{ij} \approx 1$ since transitions $i \rightarrow j$ with $\Delta\nu_\alpha \neq 1$ have A_{ij}^0 factors that are much smaller than the A_{ij}^0 factors for $\Delta\nu_\alpha = 1$ transitions.* For example for the $(\nu_1 + 3\nu_3)$ emission of H_2O , we have:

$$f_{\substack{i=\nu_1+3\nu_3 \\ j=0}} = \frac{A_{i=(\nu_1+3\nu_3) \rightarrow j=0}^0}{A_{i=(\nu_1+3\nu_3) \rightarrow j=2\nu_3}^0 + A_{i=(\nu_1+3\nu_3) \rightarrow j=3\nu_3}^0 + A_{i=(\nu_1+3\nu_3) \rightarrow j=0}^0} =$$

$$= 0.040472 \quad (\text{for } \text{H}_2\text{O}) \quad , \quad (3.331)$$

while for the $(\nu_1 + \nu_3)$ emission of CO_2 , one obtains:

$$f_{\substack{i=\nu_1+\nu_3 \\ j=0}} = \frac{A_{i=(\nu_1+\nu_3) \rightarrow j=0}^0}{A_{i=(\nu_1+\nu_3) \rightarrow j=\nu_1}^0 + A_{i=(\nu_1+\nu_3) \rightarrow j=0}^0} =$$

$$= 0.007353 \quad (\text{for } \text{CO}_2) \quad (3.332)$$

Note here that in the $(\nu_1 + \nu_3)$ case for CO_2 , one has $A_{i=(\nu_1+\nu_3) \rightarrow j=\nu_3}^0 = 0$, since ν_1 is not infrared-active. Also note that for the H_2O case,

$$A_{i=(\nu_1+3\nu_3) \rightarrow j=(\nu_1+2\nu_3)}^0 = 3 A_{i=(\nu_3) \rightarrow j=0}^0$$

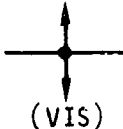
*The $f_{ij} = 1$ assumption was also used in deriving Eq. (3.316).

TABLE 3-8. FREQUENCIES AND EINSTEIN RATES OF THE MORE IMPORTANT
INFRARED-ACTIVE VIBRATION BANDS OF ROCKET EXHAUST MOLECULES

Molecule	Vibration Band*	Band Frequency ν_{ij} (cm^{-1})	Band Wavelength λ_{ij} (μm)	Einstein Factor A_{ij}^0 (sec^{-1})	f_{ij}
<u>DIATOMIC</u>					
CO	ν_e	2,170	4.608	33.23	1
	$2\nu_e$	4,330	2.309	1.9180	0.028048
	$3\nu_e$	6,485	1.542	0.8605	0.008557
OH	ν_e	3,735	2.677	15.51	1
	$2\nu_e$	7,465	1.340	1.0772	0.033561
	$3\nu_e$	11,180	0.895	0.5684	0.012068
HCl	ν_e	2,990	3.344	7.591	1
	$2\nu_e$	5,970	1.675	1.0363	0.063899
NO	ν_e	1,904	5.252	56.04	1
	$2\nu_e$	3,790	2.639	3.737	0.032267
HF	ν_e	4,139	2.416	6.2	1
<u>TRIATOMIC</u>					
CO ₂	ν_2	667.3	14.986	2.04	1
	ν_3	2,349.2	4.377	244.9	1
	$3\nu_2$	1,932.5	5.175	1.095×10^{-3}	0.000179
	$\nu_1 + \nu_2$	2,076.5	4.816	0.1151	0.053408
	$2\nu_2 + \nu_3$	3,609	2.771	0.3518	0.001413
	$\nu_1 + \nu_3$	3,710	2.695	1.8162	0.007353
	$4\nu_2 + \nu_3$	4,860.5	2.057	2.435×10^{-3}	0.000299
	$\nu_1 + 2\nu_2 + \nu_3$	4,983.5	2.007	2.999×10^{-2}	0.000120
	$2\nu_1 + \nu_3$	5,100	2.961	0.3544	0.001447

*All listed transitions are to the ground state, that is $j = 0$. For transitions $\nu_\alpha \nu_\alpha \rightarrow (\nu_\alpha - 1)\nu_\alpha$, that is for $\Delta\nu_\alpha = 1$ transitions not involving the ground state, one has $A_{ij}^0 = \nu_\alpha A_{i-1,j}^0$.

TABLE 3-8. FREQUENCIES AND EINSTEIN RATES OF THE MORE IMPORTANT INFRARED-ACTIVE VIBRATION BANDS OF ROCKET EXHAUST MOLECULES (Cont.)

Molecule	Vibration Band*	Band Frequency ν_{ij} (cm^{-1})	Wavelength λ_{ij} (μm)	Einstein Factor A_{ij}° (sec^{-1})*	f_{ij}
<u>TRIATOMIC</u>					
H_2O <div style="text-align: center;">  <p>(NIR)</p><p>(VIS)</p> </div>	ν_1	3,651.7	2.738	95.289**	1
	ν_2	1,595.0	6.270	22.225**	1
	ν_3	3,755.8	2.663	43.490**	1
	$2\nu_2$	3,151.4	3.173	0.4124***	0.0126
	$\nu_2+\nu_3$	5,332.0	1.875	4.756	0.0675
	$2\nu_2+\nu_3$	6,874.0	1.455	1.153	0.0129
	$\nu_1+\nu_3$	7,251.6	1.379	20.422	0.1283
	$\nu_1+\nu_2+\nu_3$	8,807.5	1.135	2.949****	0.0180
	$2\nu_1+\nu_3$	10,613.12	0.9422	24.661	0.0953
	$3\nu_3$	11,032.36	0.9064	6.241	0.0457
	$2\nu_1+\nu_2+\nu_3$	12,151.22	0.8230	1.607	0.00623
	$\nu_2+3\nu_3$	12,565.01	0.7959	3.606	0.02307
	$3\nu_1+\nu_3$	13,830.92	0.7230	7.263	0.02158
	$\nu_1+3\nu_3$	14,318.77	0.6984	9.522	0.04047
	$3\nu_1+\nu_2+\nu_3$	15,347.90	0.6516	1.089	0.00309
	$\nu_1+\nu_2+3\nu_3$	15,832.47	0.6316	1.348	0.00541
	$3\nu_1+2\nu_2+\nu_3$	16,821.61	0.5945	0.144	0.00039
	$4\nu_1+\nu_3$	16,899.01	0.5918	6.858	0.01588
	$2\nu_1+3\nu_3$	17,495.48	0.5716	2.281	0.00705

*All listed transitions are to the ground state, that is $j = 0$.

****For transitions $v_\alpha v_\alpha \rightarrow (v_\alpha - 1)v_\alpha$, that is for $\Delta v_\alpha = 1$ transitions not involving the ground state, one has $A_{ij}^0 = v_\alpha A_{10}^0$. Thus for $2v_1 \rightarrow v_1$, $A_{21}^0 = 2 \times 95.3 = 190.6 \text{ sec}^{-1}$, etc.**

***For $3\nu_2 \rightarrow \nu_2$ one finds $\nu_{31} = 3110 \text{ cm}^{-1}$, $A_{31}^0 = 1.696$, $f_{31} = 0.0248$; for $4\nu_2 \rightarrow 2\nu_2$..., etc.

***For $v_1 + 2v_2 + v_3 \rightarrow v_1 + v_2 + v_3$, $A_{11}^0 = 5.899 \text{ sec}^{-1}$, $f_{11}^0 = 0.0360$.

Table 3-8 shows also the H_2O combination bands in the visible below $0.6516 \mu m = 651.6 \text{ nm}$. Though weak, these bands are responsible for a large portion of the visibly observed emissions of a rocket plume as a rocket leaves the launching pad. In addition to the vibrational bands in the visible, electronic transitions with concomitant UVIS emissions can also occur if the temperature in the Boltzmann factors of Eq. (3.315) are high enough. Usually for most rockets $T_e \sim 2000^\circ K$, so that significant amounts of electronic excitation cannot occur in the Mach Core. However $(T_r)_1 = T_a \Theta_1$, used in the ABCD Boltzmann factor, can have values between 3000 and $6000^\circ K$ (due primarily to the $M_e V_k^2$ term from CD) and at these temperatures significant population of electronic excited levels can take place. The more important UVIS emission bands of various exhaust molecules were listed in Table 3-6.

For emissions from electronic transitions as well as from combination-band vibrational transitions, Eq. (3.315) must be used instead of (3.316). Unless a cascade is well known, it usually is a rather good approximation to assume that $f_{ij} \approx 1$ in (3.315) for electronic transitions, and that the sum over i is over electronic levels with different major emission wavelengths λ_{ij} . There is rarely a series of electronic or vibronic deexcitations $i \rightarrow j$ with nearly the same λ_{ij} as one finds in vibrational decay. Thus a summation over i which led to Eq. (3.316) for vibrational emissions cannot be performed for electronic transitions. For electronic transitions, A_{ij}^0 is again given by Eq. (3.317), but the matrix element R_{ij}^2 is in this case different from (3.318). A coarse approximation for R_{ij}^2 for electronic transitions is (see Table 5-2, Vol. II):

$$(R_{ij}^2)_{\text{elc}} \approx \frac{1.536 \times 10^{-12}}{\nu_{ij}(\text{cm}^{-1})}, \text{ cm}^2 \quad (3.333)$$

and thus:

$$(A_{ij}^0)_{\text{elc}} \approx \frac{0.111 \nu_{ij}^2 \omega_j}{(\text{cm}^{-1})^2}, \text{ sec}^{-1} \quad (3.334)$$

Since $f_{ij} \approx 1$ for most electronic emissions of interest, Eq. (3.334) is usually not needed for the calculation of f_{ij} values.

For pure rotational transitions, Eq. (3.315) can again be used (not (3.316)). Since only $\Delta J = J_i - J_j = +1$ transitions give rise to an emission, and the selection rule is $\Delta J = 0, \pm 1$, we can set $f_{ij} = 1$ in (3.315) for all pure rotational transitions. A sum over states i leading to (3.316) as was carried out for the vibrational case, cannot be done for the pure rotational case since the rotational energy levels are not (even approximately) equally spaced for varying values of the rotational quantum number J (see Vol. II). Expressions for $(R_{ij}^2)_{\text{rot}}$ and $(A_{ij}^0)_{\text{rot}}$ are given in Volume II but are not needed, since always $f_{ij} = 1$ in Eq. (3.315) for pure rotational emissions.

When UVIS or VIS radiations are being considered, Eqs. (3.287) and (3.308) for SOSP and SUAR contributions must of course be added to the ABCD expression (3.315), if observations are made under solar illumination.* For the far-infrared on the other hand only Eq. (3.315) is needed for

*Note that (3.287) and (3.308) are given in Watts/ster. nm. Before adding UVI contributions from ABCD as given by Eq. (3.315) in Watts/ster. μm the latter must first be adjusted to the same units of course ($1 \text{ W/ster. } \mu\text{m} = 10^{-3} \text{ W/ster. nm}$).

June 1974

contributions of pure rotational transitions from various level $\epsilon_i = h\nu_B J(J+1)$ and (3.316) for far-infrared vibrational emissions. In parts of the spectrum where strong vibrational bands exist, the pure rotational emission contribution can usually be neglected, and Eq. (3.316) is sufficient.

The most important spectrum-dependent function in the radiant emission expressions (3.315) or (3.316) are the shape or contour functions $b(\lambda, \lambda_{ij}, \Delta\nu_{ij})/\Delta\nu_{ij}$ which are the main subject of Volume II. These functions have in general a maximum near the wavelength $\lambda = \lambda_{ij}$ (or frequency $\nu = \nu_{ij}$) and drop off exponentially or quadratically for wavelengths λ larger than or smaller than λ_{ij} . The dimensionless function $b(\lambda, \lambda_{ij}, \Delta\nu_{ij}) \equiv b(\nu, \nu_{ij}, \Delta\nu_{ij})$ is usually so defined that:

$$b(\nu = \nu_{ij}, \nu_{ij}, \Delta\nu_{ij}) = 1 \quad (3.335)$$

It also has the property that:

$$\int_{\nu=0}^{\infty} b(\nu, \nu_{ij}, \Delta\nu_{ij}) d\nu = \Delta\nu_{ij} \quad , \text{ Hz} \quad (3.336)$$

Thus it follows also that:

$$\int_{\nu=0}^{\infty} \frac{b(\nu, \nu_{ij}, \Delta\nu_{ij})}{\Delta\nu_{ij}} d\nu = 1 \quad (3.337)$$

The spectral or differential Einstein factor is (see Vol. II):

$$\frac{dA_{ij}}{dv} = A_{ij}^0 \frac{b(v, v_{ij}, \Delta v_{ij})}{\Delta v_{ij}}, \quad \text{sec}^{-1} \cdot \text{Hz}^{-1}, \quad (3.338)$$

and clearly:

$$\int_{v=0}^{\infty} \frac{dA_{ij}}{dv} dv = \int_{v=0}^{\infty} A_{ij}^0 \frac{b(v, v_{ij}, \Delta v_{ij})}{\Delta v_{ij}} dv = A_{ij}^0, \quad \text{sec}^{-1} \quad (3.339)$$

because Eq. (3.337).

The shape function $b_v(v, v_{ij}, \Delta v_{ij})$ and "spread" Δv_{ij} for vibrational emission bands is given by (see Vol. II):

Case I: All diatomic species and ν_3 bands of linear triatomic molecules (e.g. CO_2 , N_2O).

$$b_v(v, v_{ij}, \Delta v_{ij}) = \frac{|v - v_{ij}|}{\Delta v_{ij}} \exp\left(-\left(\frac{v - v_{ij}}{\Delta v_{ij}}\right)^2\right) \quad (3.340)$$

$$\Delta v_{ij} = (4\nu_B kT/h)^{1/2} = 1.6698 (\nu_B \cdot T)^{1/2}, \quad \text{cm}^{-1} \quad (3.341)^*$$

($\text{cm}^{-1} \cdot ^\circ\text{K}$)

*Because of CO_2 's symmetry, the value $(\nu_B)_{\text{eff}} = 2(\nu_B)_{\text{CO}_2}$ must be used here.

Case II: All ν_2 bands of linear triatomic molecules
(e.g. CO_2 , N_2O).

$$b_v(\nu, \nu_{ij}, \Delta\nu_{ij}) = \frac{2}{3} \frac{|\nu - \nu_{ij}|}{\Delta\nu_{ij}} \left\{ \exp - \left(\frac{\nu - \nu_{ij}}{\Delta\nu_{ij}} \right)^2 \right\} + \frac{4\nu_B}{3 \xi_B \Delta\nu_{ij}} \left\{ \exp - \left(\frac{4\nu_B |\nu - \nu_{ij}|}{\xi_B \Delta\nu_{ij}^2} \right) \right\} \quad (3.342)$$

$\Delta\nu_{ij}$ is again given by (3.341).

The right-hand side of (3.340) and the first part of the expression on the right-hand side of (3.342) give the so-called P- and R-branches of an emission band, while the second part in (3.342) gives the Q-branch. Diatomic molecules and stretching vibrations of linear molecules as given by (3.340) do not possess a Q-branch. The function $H(x)$ in (3.342) is the Heaviside unit-step function defined before by (3.166); ν_B is the rotational constant of the molecule and $\xi_B = (\xi_B)_\alpha$ is the rotational anharmonic coefficient of an α -vibration that possesses a Q-branch.

The nonlinear H_2O molecule has three infrared-active vibrations that emit bands which all have Q-branches. The $b_v(\nu, \nu_{ij}, \Delta\nu_{ij})$ expressions for H_2O are (see Vol. II):

Case III: The ν_3 bands of nonlinear molecules such as H_2O :

$$b_v(\nu, \nu_{ij}, \Delta\nu_{ij}) = \frac{2}{3} \frac{|\nu - \nu_{ij}|}{\Delta\nu_{ij}} \exp\left(-\left(\frac{\nu - \nu_{ij}}{\Delta\nu_{ij}}\right)^2\right) +$$

(Bands with $i = \nu_3\nu_3$)

$$+ \frac{2(\nu_B + \nu_C) H(\nu_{ij} - \nu)}{3 \xi_{BC} \Delta\nu_{ij}} \exp\left\{-\frac{2(\nu_B + \nu_C) |\nu_{ij} - \nu|}{\xi_{BC} \Delta\nu_{ij}^2}\right\}$$

(3.343)

Case IV: The ν_1 and ν_2 bands of nonlinear molecules such as H_2O :

$$b_v(\nu, \nu_{ij}, \Delta\nu_{ij}) = \frac{2}{3 \Delta\nu_{ij}} \left(\frac{\nu_B + \nu_C}{2\pi \nu_A}\right)^{1/2}$$

(Bands with $i = \nu_1\nu_1$ and $i = \nu_2\nu_2$)

$$\cdot \left[\exp\left(-\left(\frac{\nu - \nu_{ij}}{\Delta\nu_{ij}}\right)^2\right) - \exp\left\{-\frac{\nu_B + \nu_C}{2\nu_A} \left(\left(\frac{\nu_B + \nu_C}{\Delta\nu_{ij}}\right)^2 \left(\frac{\nu_A}{|\nu_B + \nu_C - \nu_A|} - 1\right)^2 + 1\right)\right\} \right] +$$

$$+ \frac{2|\nu - \nu_{ij}|}{3 \Delta\nu_{ij}} \left(\frac{\nu_B + \nu_C}{2\nu_A}\right) \left(\frac{\nu_B + \nu_C}{2\nu_A - \nu_B - \nu_C}\right)^{1/2} \cdot \left[\exp\left\{-\frac{\nu_B + \nu_C}{2\nu_A} \left(\frac{\nu - \nu_{ij}}{\Delta\nu_{ij}}\right)^2\right\} \right] \cdot$$

$$\cdot \left[\operatorname{erf}\left\{\left(\frac{\nu_A}{|\nu_B + \nu_C - \nu_A|} - 1\right) \left(\frac{(\nu_B + \nu_C)^2}{2\nu_A(2\nu_A - \nu_B - \nu_C)}\right) \left(\frac{|\nu - \nu_{ij}|}{\Delta\nu_{ij}}\right)\right\} + \right.$$

June 1974

Case IV (Cont.)

$$\begin{aligned}
 & - \operatorname{erf} \left\{ \left(\frac{v_A - v_B}{v_A} \right)^{\frac{1}{2}} \left(\frac{|v - v_{IJ}|}{\Delta v_{IJ}} \right) \right\} + \begin{matrix} \textcircled{H}(v_{IJ} - v) \\ \textcircled{H}(v - v_{IJ}) \end{matrix} \left(\frac{v_B + v_C}{3 \xi_{BC} \Delta v_{IJ}} \right) \left(\frac{2v_A}{2v_A - v_B - v_C} \right)^{\frac{1}{2}} \\
 & \cdot \left[\exp - \left\{ \frac{(v_B + v_C)(2\xi_{BC}|v - v_{IJ}| - 2v_A + v_B + v_C)}{\xi_{BC}^2 \Delta v_{IJ}^2} \right\} \right] \left[\operatorname{erf} \left\{ \left(\frac{(v_B + v_C)(2v_A - v_B - v_C)}{\xi_{BC}^2 \Delta v_{IJ}^2} \right)^{\frac{1}{2}} \right. \right. \\
 & \quad \cdot \left. \left. \left(\frac{2v_A - v_B - v_C}{v_B + v_C} \left(\left\{ \frac{2\xi_{BC}(v_B + v_C)|v_{IJ} - v|}{(2v_A - v_B - v_C)^2} + 1 \right\}^{\frac{1}{2}} - 1 \right) - 1 \right) \right\} + \right. \\
 & \quad \left. \left. + \operatorname{erf} \left\{ \left(\frac{(v_B + v_C)(2v_A - v_B - v_C)}{\xi_{BC}^2 \Delta v_{IJ}^2} \right)^{\frac{1}{2}} \cdot \left(\frac{2v_A - v_B - v_C}{v_B + v_C} \left(\left\{ \frac{2\xi_{BC}(v_B + v_C)|v_{IJ} - v|}{(2v_A - v_B - v_C)^2} + 1 \right\}^{\frac{1}{2}} + 1 \right) + 1 \right) \right\} \right]
 \end{aligned}$$

(3.344)

Here $\textcircled{H}(x)$ and $\textcircled{H}(x)$ in the second part of (3.344) refer to the v_1 and v_2 vibration respectively whichever applies.

The spread Δv_{IJ} to be used in Eqs. (3.343) and (3.344) is given by:

$$\Delta v_{IJ} = 1.1807 \left\{ \frac{(v_B + v_C) T}{(\text{cm}^{-1}) (\text{°K})} \right\}^{1/2}, \quad \text{cm}^{-1} \quad (3.345)$$

Table 3-9 lists values of ν_A , ν_B , ν_C , ξ_B , and ξ_{BC} of several exhaust molecules. For combination-band vibrational transitions in nonlinear molecules such as $(\nu_1 + \nu_3)$, Eq. (3.344) may be used.

For electronic transitions in molecules, expressions for the vibronic band-system contour $b_e(\nu, \nu_{ij}, \Delta\nu_{ij})/\Delta\nu_{ij}$ are also available and given in Volume II. We shall not list them here as they are rather lengthy and complicated. The vibronic contour functions usually exhibit two peaks. However for broad-band observations one may employ as a coarse approximation, the semi-Gaussian fit:

$$\frac{b_e(\nu, \nu_{ij}, \Delta\nu_{ij})}{\Delta\nu_{ij}} \approx \frac{\exp\left\{-2 \frac{|\nu - \nu_{ij}|}{\Delta\nu_{ij}}\right\}}{\Delta\nu_{ij}}, \quad (3.346)$$

with:

$$\Delta\nu_{ij} = (\Delta\nu_{ij})_{elc} = \left\{ \frac{2kT/(\hbar\rho_j)}{1 + 2\{1 + (\nu_{ij} - \nu_q)/\nu_p\}^{1/2}} \right\} \cdot \exp\left\{ \frac{\nu_{ij} - \nu_q + \nu_p \left(1 + 2\sqrt{1 + \frac{\nu_{ij} - \nu_q}{\nu_p}}\right)}{kT/(\hbar\rho_j)} \right\}, \text{ cm}^{-1} \quad (3.347)$$

where for diatomic molecules:

$$\rho_j = \left[1 - \left(\frac{\nu_{ej}}{\nu_{ei}}\right)^2 \left\{ \exp - 2\beta_j (r_{ei} - r_{ej}) \right\} \right]^{-1} \quad (3.348)$$

TABLE 3-9. ROTATIONAL CONSTANTS OF SELECTED EXHAUST MOLECULES

Molecule	Rotational Constant (cm^{-1})	Anharmonic Coefficient for Q-Branches*
CO	$\nu_B = 1.93$	—
OH	$\nu_B = 18.87$	—
HCl	$\nu_B = 10.59$	—
HF	$\nu_B = 20.94$	—
NO	$\nu_B = 1.70$	—
CO ₂	$\nu_B = 0.390$	$(\xi_B)_2 = 0.001846$
N ₂ O	$\nu_B = 0.419$	$(\xi_B)_2 = 0.001337$
H ₂ O	$\nu_A = 27.88$	$(\xi_{BC})_1 = 0.03342$
H ₂ O	$\nu_B = 14.51$	$(\xi_{BC})_2 = 0.00183$
H ₂ O	$\nu_C = 9.29$	$(\xi_{BC})_3 = 0.02026$

*The subscript on ξ_B or ξ_{BC} indicates the normal vibration α for which the coefficient applies.

$$\nu_q = \nu_{ij} - \nu_{dj} \left\{ 1 - \exp[-\beta_j(r_{e_i} - r_{e_j})] \right\}^2 \left(\frac{\nu_{e_j}}{\nu_{e_i}} \right)^2, \text{ cm}^{-1} \quad (3.349)$$

$$\nu_p = \nu_{dj} \frac{\{1 - \exp[-\beta_j(r_{e_i} - r_{e_j})]\}^2}{(\nu_{e_i}/\nu_{e_j})^2 \{ \exp[-2\beta_j(r_{e_i} - r_{e_j})] - 1 \}}, \text{ cm}^{-1} \quad (3.350)$$

Here ν_{d_k} , ν_{e_k} , β_k , and r_{e_k} are respectively the dissociation frequency, the fundamental vibrational frequency, the Morse coefficient and the equilibrium spacing constant of the Morse potential of the vibration in state k ($k=i$ and $k=j$). For polyatomic molecules $\Delta\nu_{ij}$ must be averaged over the normal vibrations α and Volume II should be consulted. It should be noted further that $\Delta\nu_{ij}$ is proportional to T if the exponential in (3.347) is small. As a coarse estimate, one may take for the vibronic spreads $\Delta\nu_{ij}$ the wavelength ranges listed in Table 3-6.

The $b(\nu, \nu_{ij}, \Delta\nu_{ij})/\Delta\nu_{ij}$ function for pure rotational line emissions are usually given by the well-known collision-broadened line function (see Vol. II):

$$b_c(\nu, \nu_{ij}, \Delta\nu_{ij}) = \frac{\{(\Delta\nu_{ij})_c/\pi\}^2}{(\nu - \nu_{ij})^2 + \{(\Delta\nu_{ij})_c/\pi\}^2} \quad (3.351)$$

$$(\Delta\nu_{ij})_c = 1.1288 \times 10^{16} \sigma_{1-2} p (\mu_{1-2} T)^{-1/2}, \text{ cm}^{-1} \quad (3.352)$$

(cm²) (atm) (amu) (°K)

Here σ_{1-2} is the oscillation-interrupting collision cross-section in cm² for collisions between molecules 1 and 2, μ_{1-2} is the reduced mass

June 1974

$\mu_{1-2} = M_1 M_2 / (M_1 + M_2)$ of the colliding partners in amu units, p is the gas pressure in atm, and T is the gas temperature in $^{\circ}\text{K}$. Values for σ_{1-2} for various gases are given in Volume II.

At very low pressures the pure rotational line function becomes equal to the doppler line-broadening function:

$$b_D(\nu, \nu_{ij}, \Delta\nu_{ij}) = \exp - \left\{ \pi \left(\frac{\nu - \nu_{ij}}{(\Delta\nu_{ij})_D} \right)^2 \right\} \quad (3.353)$$

$$(\Delta\nu_{ij})_D = \frac{\nu_{ij}}{c} \left(\frac{2\pi kT}{M} \right)^{1/2} = 7.625 \times 10^{-7} \frac{\nu_{ij}}{(\text{cm}^{-1})} T^{1/2} M^{-1/2}, \text{ cm}^{-1}, \quad (3.354)$$

(cm⁻¹)(^oK)(amu)

where $c = 3 \times 10^{10}$ cm/sec and M is the mass of the emitting molecule.

Eqs. (3.353) and (3.354) apply instead of (3.351) and (3.352) when

$(\Delta\nu_{ij})_C \ll (\Delta\nu_{ij})_D$. Note that $(\Delta\nu_{ij})_C$ is linearly proportional to pressure.

Only some of the more important spectral shape functions were reviewed in the above discussions. It was assumed in these relations that measurements are made over a wavelength interval that includes at least several rotational lines, so that mathematical band-averaging can be applied. If ultra-narrow spectral observations are made, which include only one rotational line or a portion of a line, fine-spectrum broadening functions b_{rov} and b_{vbc} (for vibrational and electronic transitions) must be used in place of the functions b_v and b_e given above. Expressions for fine-spectrum broadening functions, as well as broadening functions for some other special cases are given in Volume II. For most practical cases involving rocket radiation, the broadening functions given above should be adequate however.

As mentioned in section 3.3.3., in many cases of interest, resonant V-V transfers of excitation energy from the level of interest to a suppressant molecule are not present and in this case $\tau_{q\alpha}^{-1} = 0$ in Eqs. (3.315) and (3.316).

The atmospheric transmission factor $Tr(\lambda, S, h)$ that appears in (3.315) and (3.316) depends on the observer to rocket distance S and altitude h , as well as on wavelength λ . Relations for $Tr(\lambda, S, h)$ are given in Volume V of the Rocket Radiation Handbook and will not be further considered here.

3.3.9 View Factors

The view factor F_v appearing in Eqs. (3.315) and (3.316) depends only on the geometry of the exhaust plume. Although CORE and ABCD radiation are generated in separate portions of the plume, the photons emitted by the CORE have to travel through the outer ABCD region where they experience absorptions and reemissions before they finally leave the exhaust plume. Thus the CORE emission is blended spatially with ABCD radiation, and the use of a single view factor F_v for calculating the sensor-observed plume emission due to both radiation mechanisms is appropriate.

In Appendix C, analytic expressions of view factors F_v are developed for simple geometries such as a cylinder, cone, or sphere. Although an actual exhaust plume does not have such a geometry, it has cylindrical symmetry and may be approximated by an equivalent finite cylinder with equivalent length L_p , and diameter D_p . The view factor F_v for a finite cylinder is shown in Appendix C to depend primarily on the ratios:

June 1974

$$\lambda = L_p / D_p , \quad (3.355)$$

$$\rho = D_s / D_p , \quad (3.356)$$

and on the sensor's field-of-view and "aspect angle" α , that is the angle between the line-of-sight and the cylinder axis. Thus $(F_v)_{cyl} = F_v(D_s, \lambda, \rho, \alpha)$. Here D_s is the diameter of the (assumed) circular field-of-view of the observing sensor at the rocket plume.

Now α can be obtained directly from the rocket trajectory and the location of the sensor, while D_s can be calculated if the sensor's optics and field-of-view is known (see Vol. VI). If the sensor's field-of-view angle is θ_{fov} and the observer-to-rocket range is S , then clearly (in the usual small angle approximation):

$$D_s = S \theta_{fov} , m \quad (3.357)$$

The equivalent cylindrical rocket plume diameter D_p , may be approximately set equal to D_{exh} or D_h , given by Eqs. (3.139) or (3.194). To obtain an expression for the equivalent cylindrical plume length L_p we shall employ the Hill-Draper theory (Ref. 19) mentioned before. In Appendix F it is shown that for view-factor calculations we may take approximately:

$$L_p \approx \lambda D_p , m \quad (3.358)$$

where:

$$\lambda = \frac{L_p}{D_p} = 1.5 \cot \left[\left\{ \cos^{-1} (1 - \zeta \sqrt{\pi \ln B}) \right\} \left\{ \exp - \left(\frac{D_e^I}{D_p} \right) \right\} \right] \quad (3.359)$$

Here the parameters ζ and B are constants that depend only on the rocket hardware and fuel parameters. They were defined before by Eqs. (3.227) and (3.228) of section 3.3.4. D_e^I must equal $D_e^I = D_e H(D_p - D_e) + D_p H(D_e - D_p)$ in (3.359) to account for launch-altitude separations in the nozzle (see Eq. (3.196)).

As discussed in Appendix F, at ultra-high-altitudes the physical dimensions of the plume become larger than the radiation-active plume dimensions, and therefore when calculating view factors we shall take for D_p the relation:

$$D_p = D_{\text{exh}} H(D_r - D_{\text{exh}}) + D_r H(D_{\text{exh}} - D_r) \quad , \quad m \quad (3.360)$$

Here D_{exh} was given by Eq. (3.139), and:

$$D_r = \frac{D_t}{(p_r/p_c)^{\frac{1}{2\gamma}}} \left[\frac{\{2/(\gamma+1)\}^{\frac{\gamma+1}{\gamma-1}}}{\left(\frac{2}{\gamma-1}\right) \left\{ 1 - \left(\frac{p_r}{p_c}\right)^{\frac{\gamma-1}{\gamma}} \right\}} \right] \quad , \quad m \quad (3.361)$$

where p_r is given by (see Appendix F):

June 1974

$$p_r = \left[2.506 \times 10^{-11} T_c^{1/2} \bar{M}_e^{1/2} p_c^{\left(\frac{1-\gamma}{2\gamma}\right)} \right]^{\left(\frac{2\gamma}{\gamma+1}\right)}, \text{ bars} \quad (3.361)$$

(°K) (amu)(bars)

For a typical value of $\gamma = 1.25$, $T_c = 3000^\circ\text{K}$, $p_c = 50$ bars, and $\bar{M}_e \approx 30$ amu, one finds from Eq. (3.362) that $p_r = 6.09 \times 10^{-10}$ bars which corresponds to an altitude of about 250 kilometers according to Figure 2-3a. Thus for most near-earth orbit launching rockets, the radiative size limit $D_p = D_r$ will not be reached.

3.3.10 Parametric Error Analysis and Adjustments

Before investigating the effects of variances of the input parameters on the total output radiation, let us review what input parameters enter into a radiation calculation. For rocket radiation signature calculations involving the ABCD and CORE expressions (3.315) or (3.316), the following input parameters are required for each rocket stage:

a. Rocket Hardware Data

- \dot{W} = Exhaust mass flow rate, kgm/sec
- T_c = Combustion chamber temperature, °K
- p_c = Combustion chamber pressure, bars
- D_t = Nozzle throat diameter, m
- p_e = Nozzle exit plane design pressure, bars
- γ = Gas coefficient of exhaust gases
- θ = Rocket thrust angle, degrees

* See NEW PAGE

$$p_r = \left[2.506 \times 10^{-11} T_c^{1/2} \bar{M}_e^{1/2} p_c \left(\frac{1-\gamma}{2\gamma} \right) \right]^{\left(\frac{2\gamma}{\gamma+1} \right)}, \text{ bars} \quad (3.362)$$

For a typical value of $\gamma = 1.25$, $T_c = 3000^\circ\text{K}$, $p_c = 50$ bars, and $\bar{M}_e \approx 30$ amu, one finds from Eq. (3.362) that $p_r = 6.09 \times 10^{-10}$ bars which corresponds to an altitude of about 250 kilometers according to Figure 2-3a. Thus for most near-earth orbit launching rockets, the radiative size limit $D_p = D_r$ will not be reached.

3.3.10 Parametric Error Analysis and Adjustments

Before investigating the effects of variances of the input parameters on the total output radiation, let us review what input parameters enter into a radiation calculation. For rocket radiation signature calculations involving the ABCD and CORE expressions (3.315) or (3.316), the following input parameters are required for each rocket stage:

a. Rocket Engine Data

- T_c = Combustion chamber temperature, $^\circ\text{K}$
- p_c = Combustion chamber pressure, bars
- D_t = Nozzle throat diameter, m
- p_e = Nozzle exit plane design pressure, bars
- γ = Gas coefficient of exhaust gases
- θ = Rocket thrust angle, degrees

Of these six parameters, θ is usually fixed at $\theta = 180^\circ$ for booster rockets. Only if vernier-rocket burns are considered is $\theta \neq 180^\circ$. Thus for booster rockets there are basically five parameters. For any one of the basic five parameters one can substitute another parameter that is related to these five and can be calculated from them. For example instead of p_e one can specify the nozzle area ratio $E = D_e^2/D_t^2$, or the nozzle exit plane parameters T_e or D_e , and in place of D_t , \dot{W} may be specified. Each one of these other parameters can be calculated from the basic set of five parameters, T_c , p_c , D_t , p_e , and γ via ideal one-dimensional adiabatic rocket flow theory (see Vol. IV). Often the mass flow rate \dot{W} (kgm/sec) is given also as a sixth independent parameter. However for ideal flow it is related to T_c ($^\circ\text{K}$), p_c (bars), γ , D_t (m), and M_e (amu) via the expression $\dot{W} = 861.39 p_c D_t^2 [\gamma \{2/(\gamma+1)\}]^{(\gamma+1)/(\gamma-1)} \cdot (M_e/T_c)^{1/2}$ (see Vol. IV). If \dot{W} is independently specified, non-ideality factors are automatically included but \dot{W} should still be approximately given by the ideal relation. Not more than the basic six or five engine parameters should be used to avoid overdetermination and inconsistencies.

b. Rocket Trajectory and Relative Sensor Position

To calculate signatures (radiation versus time plots), the rocket's position and velocity relative to the earth must be specified as a function of time. Also the burn-start and burn-stop times for each stage must be given. The number of time points for each stage can vary between 5 and 50 depending on how smoothly varying or irregular the trajectory data are. Usually for

Of these seven parameters, θ is usually fixed at $\theta = 180^\circ$ for booster rockets. Only if vernier-rocket burns are considered is $\theta \neq 180^\circ$. Thus for booster rockets there are basically six parameters. For any one of the basic six parameters one can substitute another parameter that is related to these six and can be calculated from them. For example instead of p_e one can specify the nozzle exit plane diameter D_e , the nozzle "area-ratio" E , or the nozzle exit plane temperature T_e . Each one of these parameters can be calculated from the basic set of six parameters \dot{W} , T_c , p_c , D_t , p_e , and γ via one-dimensional adiabatic rocket flow theory (see Vol. IV). In performing radiation calculations, it is important that the number of input parameters do not exceed the basic set of six. Overdetermination may cause inconsistencies, particularly if input values are provided which are not exactly related by the standard one-dimensional rocket flow relations. The latter equations are assumed to hold throughout all expressions developed here.

b. Rocket Trajectory and Relative Sensor Position

To calculate rocket radiation signatures, that is to plot a radiation versus time curve, it is necessary that the rocket's position and velocity relative to the earth is specified as a function of time. Also the burn-start and burn-stop times for each stage must be given. The number of time points for each stage can vary between 5 and 50 depending on how smoothly varying or irregular the trajectory data are. Usually for

* See New Page.

June 1974

each stage, some 10 time points are sufficient. Thus for a typical three-stage rocket this means that some $3 \times 10 \times 4$ (altitude; range; azimuth; velocity) = 120 input numbers are required to specify the rocket trajectory.

In addition to the rocket trajectory giving a four-set of numbers as a function of time, it is necessary that the field-of-view diameter of the sensor at the rocket, $D_s = D_s(t)$, and the aspect angle $\alpha = \alpha(t)$, that is the angle between the rocket's direction of motion and the line-of-sight from the sensor to the rocket, be specified as a function of time. The determination of $D(t)$ and $\alpha(t)$ is best calculated together with the rocket trajectory calculations, and thus a six-set (h , LONG, LAT, V_v , α , D_s) as a function of time should be specified. Here the longitude (LONG) and latitude (LAT) are substituted for range and azimuth.

c. Exhaust Gas Molecular Composition

Several books, tabulations, and computer programs are available (Refs. 26 and 27) which give the molecular species composition of a rocket exhaust for a given propellant mix. For radiation calculations, the exhaust gas composition is expressed by the following parameters:

g_{H_2} = Moles of H_2 per kilogram of exhaust mass

g_{H_2O} = Moles of H_2O per kilogram of exhaust mass

g_{CO_2} = Moles of CO_2 per kilogram of exhaust mass

- g_{CO} = Moles of CO per kilogram of exhaust mass
 g_{HCl} = Moles of HCl per kilogram of exhaust mass
 $g_{Al_2O_3}$ = Moles of Al_2O_3 per kilogram of exhaust mass
 g_{NO} = Moles of NO per kilogram of exhaust mass
 g_{OH} = Moles of OH per kilogram of exhaust mass
 g_H = Moles of H per kilogram of exhaust mass
 g_{N_2} = Moles of N_2 per kilogram of exhaust mass
 g_{O_2} = Moles of O_2 per kilogram of exhaust mass

The above list is representative of most of the exhaust species that are present in a rocket exhaust. However, if present, the amounts of other species such as HF, NO_2 , etc., must be added to completely specify the molecular field.

If the species distribution is given in terms of moles of X per kgm of exhaust g_X , as is our convention, one additional parameter can be derived which is the species-averaged molecular weight $\bar{M}_e = \left[10^{-3} \sum_X g_X \right]^{-1}$, grams/mole. This constant appears in several subsidiary expressions and is treated as a semi-independent constant even though it depends on the sum over the g_X . In many data inputs, \bar{M}_e is therefore specified separately as though it were an independent parameter.

d. Molecular Constants

The molecular constants needed in radiation calculations may be divided into three groups, namely rotational, vibrational, and electronic constants:

(1) Rotational Constants (see also Vol. II)

$(\nu_A)_{H_2O}$, $(\nu_B)_{H_2O}$, $(\nu_C)_{H_2O}$ = Rotational constants for the three rotational axes of asymmetric nonlinear H_2O , (cm^{-1}) .

$(\nu_B)_{CO_2}$ = Rotation constant for linear CO_2 , (cm^{-1}) .

$(\nu_B)_{CO}$ = Rotation constant for CO , (cm^{-1}) .

⋮

etc., for all molecules listed under c.

$(\xi_{BC1})_{H_2O}$, $(\xi_{BC2})_{H_2O}$, $(\xi_{BC3})_{H_2O}$ = Second-order rotational coefficients due to the three normal vibrations of H_2O .

$(\xi_B)_{CO_2}$ = Second-order rotational coefficient of CO_2 .

⋮

etc., for all molecules listed under c.

(2) Vibrational Constants (see also Vol. II)

$(\nu_1)_{H_2O}$, $(\nu_2)_{H_2O}$, $(\nu_3)_{H_2O}$ = Fundamental frequencies (cm^{-1}) of the three normal vibrations of H_2O .

$(\nu_1)_{\text{CO}_2}$, $(\nu_2)_{\text{CO}_2}$, $(\nu_3)_{\text{CO}_2}$ = Fundamental frequencies
(cm^{-1}) of the three normal vibrations of CO_2 .

$(\nu_e)_{\text{CO}}$ = Fundamental vibrational frequency (cm^{-1}) of CO.

$(\nu_e)_{\text{HCl}}$ = Fundamental vibrational frequency (cm^{-1}) of HCl.

·
·
·

etc., for all molecules listed under c.

$(x_1)_{\text{H}_2\text{O}}$, $(x_2)_{\text{H}_2\text{O}}$, $(x_3)_{\text{H}_2\text{O}}$ = Anharmonic vibrational
constants of H_2O for normal vibrations ν_1 , ν_2 , and
 ν_3 respectively.

$(x_1)_{\text{CO}_2}$, $(x_2)_{\text{CO}_2}$, $(x_3)_{\text{CO}_2}$ = Anharmonic vibrational
constants of CO_2 for normal vibrations ν_1 , ν_2 , and
 ν_3 respectively.

$(x_e)_{\text{CO}}$ = Anharmonic vibrational constant of CO.

$(x_e)_{\text{HCl}}$ = Anharmonic vibrational constant of HCl.

·
·
·

etc., for all molecules listed under c.

$(z_1)_{\text{H}_2\text{O}}$, $(z_2)_{\text{H}_2\text{O}}$, $(z_3)_{\text{H}_2\text{O}}$ = First-derivative dipole
charges of H_2O for respectively the ν_1 , ν_2 , and ν_3
normal vibration.

$(z_1)_{\text{CO}_2}$, $(z_2)_{\text{CO}_2}$, $(z_3)_{\text{CO}_2}$ = First-derivative dipole
charges of H_2O for respectively the ν_1 , ν_2 , and ν_3
normal vibration. (Note that $(z_1)_{\text{CO}_2} = 0$.)

June 1974

$(z_1)_{CO}$ = First-derivative dipole charge of CO.

$(z_1)_{HCl}$ = First-derivative dipole charge of HCl.

·
·
·

etc., for all molecules listed under c.

$(M_1)_{H_2O}$, $(M_2)_{H_2O}$, $(M_3)_{H_2O}$ = Vibrational masses (amu)
of H_2O for the ν_1 , ν_2 , and ν_3 normal vibrations.

$(M_1)_{CO_2}$, $(M_2)_{CO_2}$, $(M_3)_{CO_2}$ = Vibrational masses (amu)
of CO_2 for the ν_1 , ν_2 , and ν_3 normal vibrations.

$(M)_{CO}$ = Vibrational reduced mass (amu) for CO.

$(M)_{HCl}$ = Vibrational reduced mass (amu) for HCl.

·
·
·

etc., for all molecules listed under c.

(3) Electronic Constants (see also Vol. II)

$(\nu_{i=1})_{H_2O}$, $(\nu_{i=2})_{H_2O}$, ... = Frequencies (cm^{-1}) of
electronic excited levels $i=1$, $i=2$, in H_2O .

$(\nu_{i=1})_{CO_2}$, $(\nu_{i=2})_{CO_2}$, ... = Frequencies (cm^{-1}) of
electronic excited levels $i=1$, $i=2$, in CO_2 .

$(\nu_{i=1})_{CO}$, $(\nu_{i=2})_{CO}$, ... = Frequencies (cm^{-1}) of
excited levels $i=1$, $i=2$, in CO.

·
·
·

etc., for all molecules listed under c.

$(\beta_{\alpha; i=0})_{H_2O}$, $(\beta_{\alpha; i=1})_{H_2O}$, ... = Morse potential exponential coefficients of H_2O for electronic excited levels $i=0$ (ground state), $i=1$,, for normal vibration α ($\alpha = 1, 2, 3$ for H_2O).

$(\beta_{\alpha; i=0})_{CO_2}$, $(\beta_{\alpha; i=1})_{CO_2}$, ... = Morse potential exponential coefficients of CO_2 for electronic excited levels $i=0$ (ground), $i=1$,, for normal vibration α ($\alpha = 1, 2, 3$ for CO_2).

$(\beta_{i=0})_{CO}$, $(\beta_{i=1})_{CO}$, ... = Morse potential exponential coefficients of CO for electronic excited levels $i=0$ (ground state), $i=1$,

$(\beta_{i=0})_{HCl}$, $(\beta_{i=1})_{HCl}$, ... = Morse potential exponential coefficients of HCl for electronic excited levels $i=0$ (ground state), $i=1$,

·
·
·

etc., for all molecules listed under c.

$(r_{\alpha; i=0})_{H_2O}$, $(r_{\alpha; i=1})_{H_2O}$, ... = Morse potential equilibrium separation (cm) of H_2O for electronic excited levels $i=0$ (ground state), $i=1$,, for normal vibration α ($\alpha = 1, 2, 3$ for H_2O).

$(r_{\alpha; i=0})_{CO_2}$, $(r_{\alpha; i=1})_{CO_2}$, ... = Morse potential equilibrium separation (cm) of CO_2 for electronic excited levels $i=0$ (ground state), $i=1$,, for normal vibration α ($\alpha = 1, 2, 3$ for CO_2).

June 1974

$(r_{e;i=0})_{CO}$, $(r_{e;i=1})_{CO}$, ... = Morse potential
equilibrium separation (cm) of CO for electronic excited
levels $i=0$ (ground state), $i=1$,
:
:
:
etc., for all molecules listed under c.

$(\nu_{d\alpha;i=0})_{H_2O}$, $(\nu_{d\alpha;i=1})_{H_2O}$, ... = Morse potential
dissociation frequency (cm⁻¹) of H₂O for electronic
excited levels $i=0$ (ground state), $i=1$, ... , for normal
vibration α ($\alpha = 1, 2, 3$ for H₂O).

$(\nu_{d\alpha;i=0})_{CO_2}$, $(\nu_{d\alpha;i=1})_{CO_2}$, ... = Morse potential
dissociation frequency (cm⁻¹) of CO₂ for electronic
excited levels $i=0$ (ground state), $i=1$, ... , for normal
vibration α ($\alpha = 1, 2, 3$ for CO₂).

$(\nu_{di=0})_{CO}$, $(\nu_{di=0})_{CO}$, ... = Morse potential
dissociation frequency for electronic excited levels
 $i=0$ (ground), $i=1$, ... , for normal vibration α .
:
:
:
etc., for all molecules listed under c.

c. Atmospheric Properties

Atmospheric pressure and temperature variations with altitude
strongly influence a rocket radiation signature. Atmospheric
composition changes with altitude are also important though

not as influential as the pressure and temperature. Thus in all radiation signature calculations, one must specify the parameters:

$p_a(h)$ = Atmospheric pressure (bars) versus altitude h (km).

$T_a(h)$ = Atmospheric temperature ($^{\circ}\text{K}$) versus altitude h (km).

$y_{\text{O}_2}(h), y_{\text{N}_2}(h), \dots$ = Mole fraction of O_2 , N_2 , of atmospheric molecules and atoms versus altitude h (km).

Although the above list of inputs appears quite formidable at first sight, it must be remembered that the input data of (d) are fixed by nature and once available can be stored permanently in a computer memory. The atmospheric parameters under (e) are semi-permanent and usually a model exponential atmosphere such as shown in Figure 2-3 (see also Ref. 24) is adequate for most radiation calculations.

The only purely rocket-dependent input parameters are those listed under items (a), (b), and (c). For these, the set of exhaust species listed under (c) is surprisingly constant for a given combination of rocket fuel and oxidizer; the typical values listed in Table 2-3 are often adequate for many radiation signature calculations.

The mean molecular weight \bar{M}_e varies little between fuels and normally has a value between 23 and 28 amu for amine, hydrocarbon, or solid-fueled rockets, and about 5 amu for H_2/O_2 rockets. The effect on rocket radiation intensity due to variations in the value of \bar{M}_e over the 23-28 amu range of hydrocarbon, amine, or solid rockets is usually small.

June 1974

The particular values of some of the parameters in the remaining two groups, namely (a) hardware constants and (b) trajectory six-sets, can effect the magnitude of a rocket radiation signature substantially. For example the gas coefficient γ , though it only has values between 1.000 and 1.667, effects the radiant emission strength strongly, since it appears as an exponent in many terms. For most rocket exhausts, γ has a value that lies within 5 percent of $\gamma = 1.23$. Trajectories can also strongly influence a rocket signature and considerably different signature profiles may result, depending on whether a given rocket is shot into a ballistic depressed, lofted, or space-injection orbit.

In carrying out signature calculations for multi-nozzle rockets, one often encounters the problem of what value one must choose for the throat diameter D_t or nozzle exit diameter D_e , which is a key parameter in the radiation equations (see section 3.3.8). In Appendix I it is shown that at high altitudes an equivalent value $(D_t)_N$, defined by:

$$(D_t)_N = N_N^{1/2} D_t, \text{ m}, \quad (3.363)$$

may be used for multi-nozzle rockets, where:

N_N = Number of nozzles

D_t = Throat diameter of each nozzle, m

or more generally:

$$(D_t)_N = \left[\sum_{i=1}^{N_N} (D_t)_i^2 \right]^{1/2}, \text{ m} \quad (3.364)$$

where $(D_t)_i$ is the throat diameter of each nozzle and the summation is over the total number of nozzles N_N .

At the lower altitudes however Eqs. (3.363) and (3.364) give rise to plume diameters that are too small, and instead a relation of the form:

$$(D_t)_G = D_t \{1 + f(E, F, K)\} , m \quad (3.365)$$

is required (see Appendix I). Here:

$$E = \left(\frac{\gamma-1}{2}\right)^{1/2} \left(\frac{2}{\gamma+1}\right)^{\frac{\gamma+1}{2(\gamma-1)}} \left(\frac{p_c}{p_e}\right)^{\frac{1}{\gamma}} \left[1 - \left(\frac{p_e}{p_c}\right)^{\frac{\gamma-1}{\gamma}}\right]^{-1/2} \quad (3.366)$$

$$F = \left(\frac{\gamma-1}{2}\right)^{1/4} \left(\frac{2}{\gamma+1}\right)^{\frac{\gamma+1}{4(\gamma-1)}} \left(\frac{p_c}{p_a}\right)^{\frac{1}{2\gamma}} \left[1 - \left(\frac{p_a}{p_c}\right)^{\frac{\gamma-1}{\gamma}}\right]^{-1/4} \quad (3.367)$$

$$K = S_N / D_t \quad (3.368)$$

Here S_N is the separation between nozzle skirts (see Appendix I). The function $f(E, F, K)$ depends on the particular multi-nozzle arrangement as follows (see also Appendix I):*

a. Two Nozzles

$$f(E, F, K) = \frac{\sqrt{E} + K}{F} \quad (3.369)$$

*These relations are due to R. Chardon.

June 1974

b. Three Nozzles (Triangular)

$$f(E, F, K) = \frac{\sqrt{E} + K}{F \cos(\pi/6)} \quad (3.370)$$

c. Three Nozzles (Linear)

$$f(E, F, K) = \frac{2 \sqrt{E} + 2 K}{F} \quad (3.371)$$

d. Four Nozzles

$$f(E, F, K) = \frac{\sqrt{2E} + K \sqrt{2}}{F} \quad (3.372)$$

e. Five Nozzles (Cross)

$$f(E, F, K) = \frac{2 \sqrt{E} + 2 K}{F} \quad (3.373)$$

f. Five Nozzles (Pentagon)

$$f(E, F, K) = \frac{\sqrt{E} + K}{F \sin(\pi/5)} \quad (3.374)$$

g. Six Nozzles (Hexagon)

$$f(E, F, K) = \frac{2\sqrt{E} + 2 K}{F} \quad (3.375)$$

As an approximation for all altitudes, one may take for the effective diameter D_t of a multi-nozzle rocket:

$$(D_t)_{\text{eff}} = (D_t)_N H(D_{t_N} - D_{t_G}) + (D_t)_G H(D_{t_G} - D_{t_N}), \quad m, \quad (3.376)$$

that is $(D_t)_{\text{eff}}$ is the larger of $(D_t)_N$ and $(D_t)_G$ calculated respectively by Eqs. (3.363) and (3.365).

Since usually the field-of-view diameter D_s covers the entire plume at the lower altitudes and since in this case the view-factor F_V is insensitive to the value of D_p (only the ratio $L_p/D_p = \lambda$ and the aspect angle α matter in this case), no great error results if Eq. (3.363) is assumed for all altitudes in the expressions for F_V . However for the Mach Core calculation of τ_M which depends on D_t , Eq. (3.376) should give an improvement over Eq. (3.363).

In the theory developed above, several ad hoc approximations (such as $\bar{T}_M = \frac{2}{3} T_e + \frac{1}{3} T_{\text{exh}}$; $\bar{V}_M = \frac{1}{2} V_e + \frac{1}{2} V_{\text{exh}}$, etc.) were used. In addition, many input parameters are often not accurately known. For this reason, it is profitable to carry out a sensitivity analysis and determine the variance of the radiant intensity J (or $dJ/d\lambda$) as a function of the uncertainties in the values of the various input parameters.

Since J (or $dJ/d\lambda$) depends on many exponentially varying functions, the calculation of the error or variance ΔJ in J will be based on logarithmic derivatives ($\Delta J = \Delta(\ln J)$) rather than on linear ones. Then according to standard error-analysis theory:

$$\begin{aligned} \Delta J &= \pm J_0 \left[\sum_i \left\{ \ln(J(x_i + \Delta x_i)) - \ln(J(x_i)) \right\}^2 \right]^{1/2} = \\ &= \pm J_0 \left[\sum_i \left\{ \ln \left(\frac{J(x_i + \Delta x_i)}{J(x_i)} \right) \right\}^2 \right]^{1/2} \end{aligned} \quad (3.377)$$

Here J_0 is the value of J evaluated with input parameters x_1, x_2, \dots at their nominal values, and the Δx_i are the errors or variances in the values of the x_i .

Expression (3.377) is not quite symmetric and applies strictly only in the limit of first-order error theory, for which $J(x_i + \Delta x_i)/J(x_i) = J(x_i)/J(x_i - \Delta x_i)$. This latter equality is not always well approximated, and therefore an improvement is obtained by rewriting Eq. (3.377) in the symmetric form:

$$\Delta J = \pm J_0 \left[\sum_i \left\{ \frac{1}{2} \ln \left(\frac{J(x_i + \Delta x_i)}{J(x_i)} \right) + \frac{1}{2} \ln \left(\frac{J(x_i)}{J(x_i - \Delta x_i)} \right) \right\}^2 \right]^{\frac{1}{2}} =$$

$$= \pm J_0 \left[\sum_i \left\{ \frac{1}{2} \ln \left(\frac{J(x_i + \Delta x_i)}{J(x_i - \Delta x_i)} \right) \right\}^2 \right]^{\frac{1}{2}} \quad (3.378)$$

In Chapter 4, examples will be given of the resulting uncertainty in J due to various uncertainties in the input parameters x_i , using Eq. (3.378). From such sample error calculations, an assessment may be made of how good or bad such assumptions as $\bar{T}_M = 2/3 T_e + 1/3 T_{exh}$ are in calculating a particular rocket radiation signature. The results indicate that the simplifying assumptions may lead to errors on the order of 10 to 20 percent in the signature. Though these errors may appear large at first, it should be remembered that the trends, shapes, and variations in a signature curve are less effected than the absolute values, since systematic errors produce biases in the output that are in the same direction.

4. APPLICATIONS AND EXAMPLES

4.1 ROCKET RADIATION SIGNATURES

One important application for the relations developed in Chapter 3 is the calculation of the radiant emission from a rocket as it rises from the launch pad into space. The radiation history of such an event, that is a plot of the radiant intensity (in a certain wavelength interval) as a function of altitude or time is referred to as a rocket "signature."

In Figures 4-1 through 4-4, TTO signature plots* are shown of the radiant intensity per unit wavelength range at $\lambda = 2.74 \mu\text{m}$ for four typical rockets and trajectories. The radiation at $2.74 \mu\text{m}$ is in the ν_3 vibrational band of H_2O and in a portion of the ν_2 band of H_2O (centered at $\lambda = 2.66 \mu\text{m}$), while the $\lambda = 4.45 \mu\text{m}$ radiation is in the ν_3 vibrational band of CO_2 . Thus both are in the strongest emission bands of H_2O and CO_2 . The signatures are based on Eq. (3.316) with τ_{qi} set equal to $\tau_{qi}^{-1} = 0$ and the atmospheric transmission factor Tr set equal to $\text{Tr} = 1$. That is, no infrared-radiation suppressing molecules are assumed to be present, and the signatures are "bare."

Actually observed signature intensities would be equal to the ones shown multiplied by $\text{Tr}(S, h, \lambda)$ and $R_s(\lambda)$ and integrated over λ , that is:

$$J_{\text{observed}} = \int_{\lambda_1 \leftrightarrow \lambda_2}^{\lambda_2} \left(\frac{dJ}{d\lambda} \right) R_s(\lambda) \text{Tr}(\lambda, S, h_s, h_v) d\lambda, \quad \frac{\text{Watts}}{\text{ster}}, \quad (4.1)$$

*TTO = Target Tracking Observations (see last paragraph, section 3.1).

June 1974

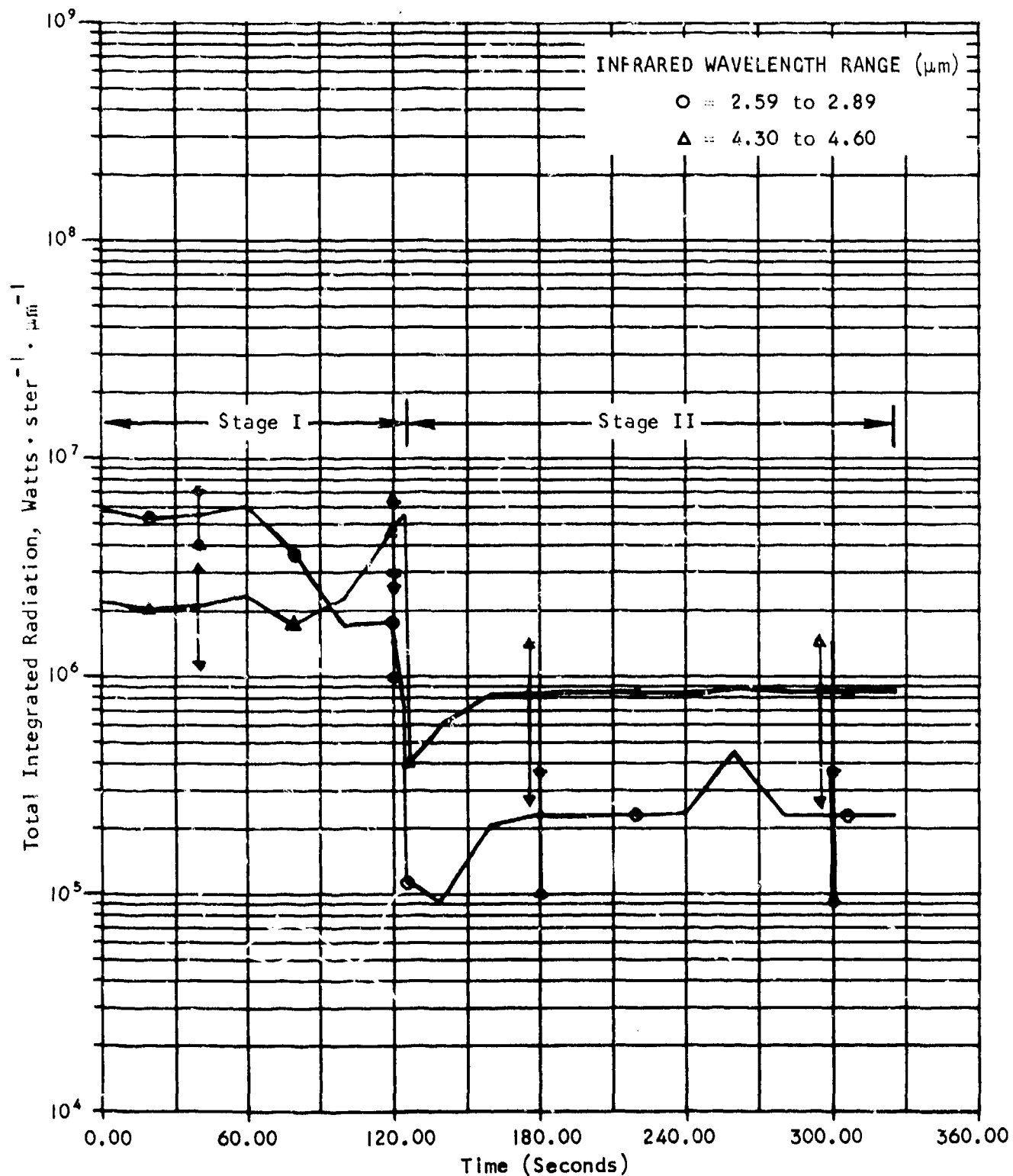


FIGURE 4-1. CALCULATED RADIATION SIGNATURES OF BALLISTIC ATLAS
ROCKET IN 2.74 AND 4.45 MICRON BANDS

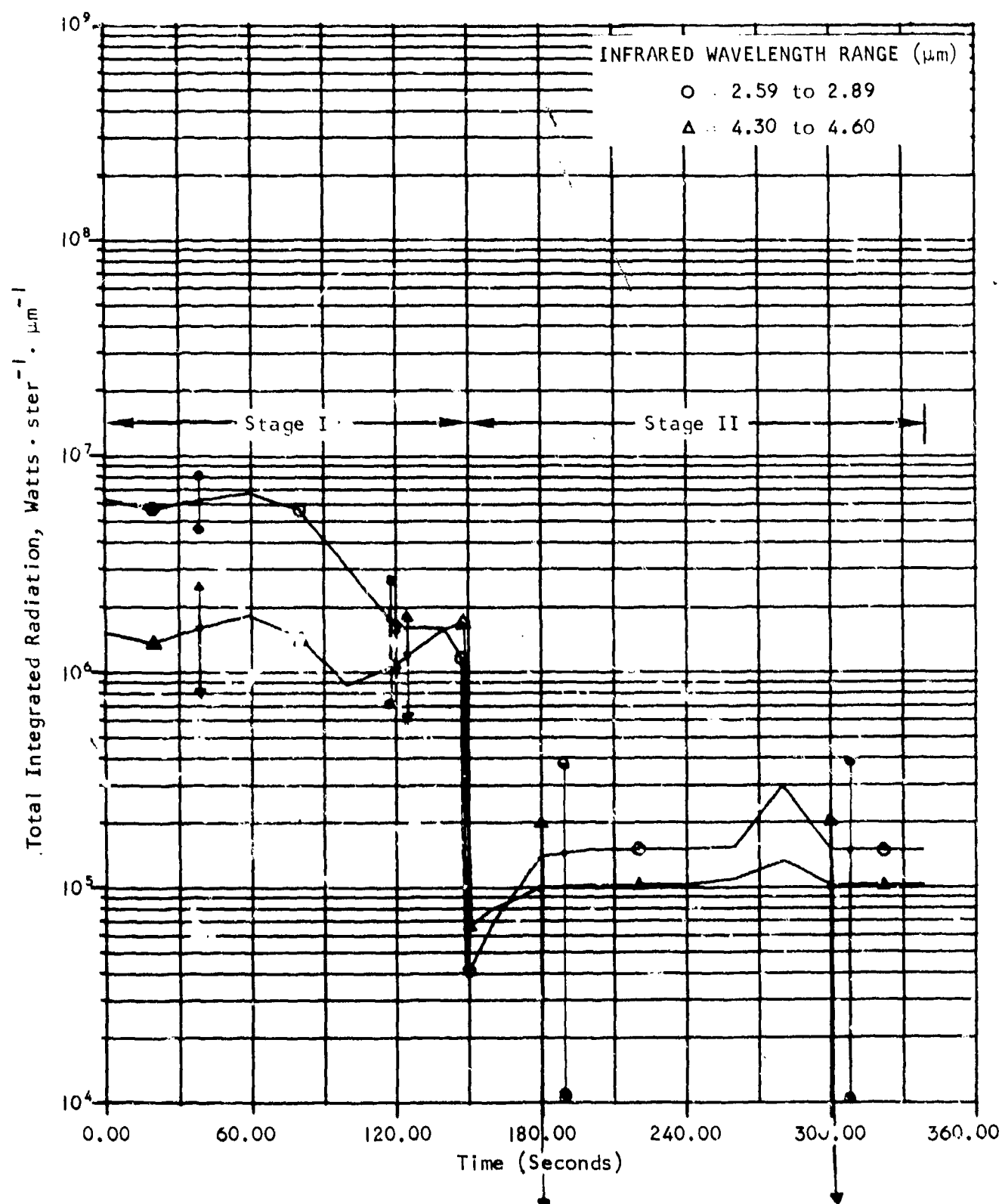


FIGURE 4-2. CALCULATED RADIATION SIGNATURES OF BALLISTIC TITAN II ROCKET IN 2.74 AND 4.45 MICRON BANDS

June 1974

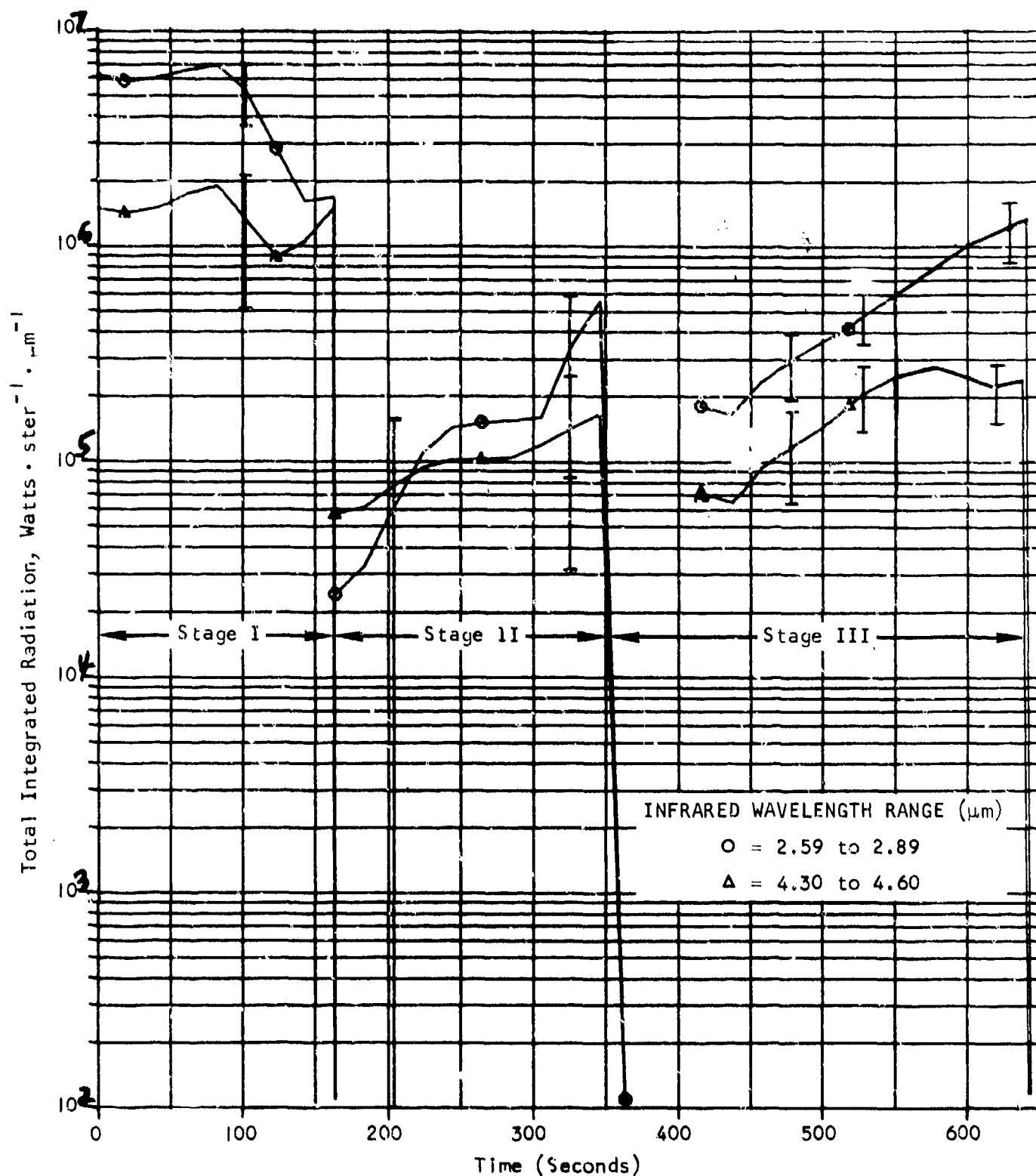


FIGURE 4-3. CALCULATED RADIATION SIGNATURES OF SPACE-LAUNCHING TITAN 3B/AGENA ROCKET IN 2.74 AND 4.45 MICRON BANDS

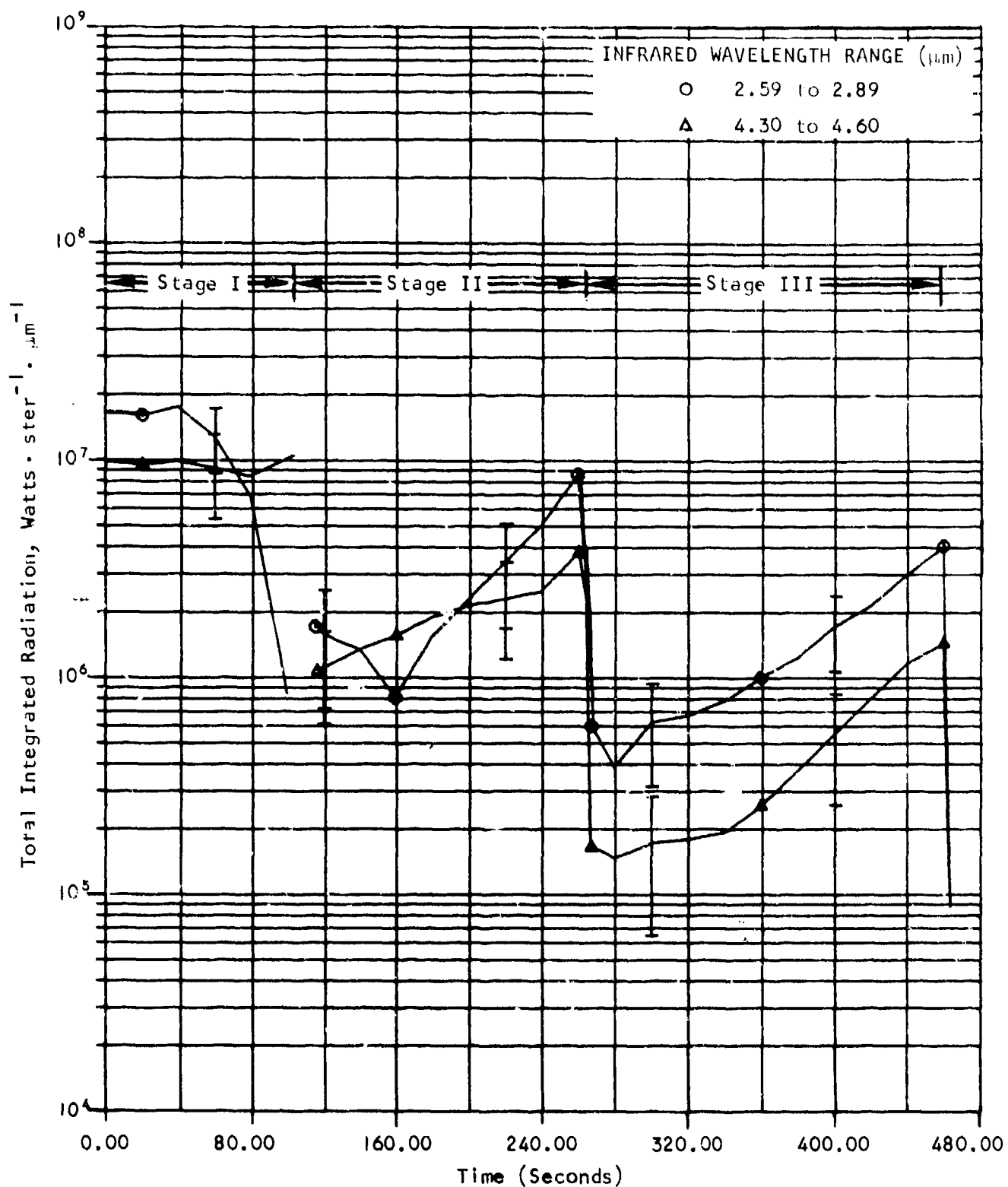


FIGURE 4-4. CALCULATED RADIATION SIGNATURES OF SPACE-LAUNCHING
TITAN 3D ROCKET IN 2.74 AND 4.45 MICRON BANDS

where:

$\left(\frac{dJ}{d\lambda}\right)$ = "Bare" radiant intensity, $\frac{\text{Watts}}{\text{ster} \cdot \mu\text{m}}$
(calculated from (3.316) with $Tr = 1$).

λ_1, λ_2 = Wavelength band limits set by sensor filter optics.

$R_s(\lambda)$ = Sensor response curve (see Vol. VI).

$Tr(\lambda, S, h_s, h_v)$ = Atmospheric transmission which depends on sensor-to-rocket distance S , rocket altitude h_v , and sensor altitude h_s (see Vol. V).

Any vehicle body radiations in the near-infrared can be shown to be small compared to the plume emissions during a launch, and may thus be conveniently neglected.

For simplicity it was assumed in Figures 4-1 through 4-4 that the sensor views the rocket plume "side-on," that is at $\alpha = 90^\circ$, and thus with a fixed view factor $F_v(\alpha = 90^\circ)$. Also the sensor's field-of-view diameter D_s at the rocket plume is assumed to have a constant value $D_s = 1 \text{ km}$.

The rocket hardware parameters, exhaust species distributions, and trajectory data used in the calculation of the four sample rocket radiation signatures appearing in Figures 4-1 through 4-4, are listed in Tables 4-1 through 4-3. The standard 1962 USAF-CRL model atmosphere was used also (see Figure 2-3, Ref. 24, or Vol. V) and molecular constants were taken from Refs. 47 and 48 as needed (see also section 3.3.8 and Vol. II).

All signatures show as main features two (for two stages) or three (for three stages) high level regions separated by minimum radiation regions

TABLE 4-1. ROCKET HARDWARE PARAMETERS OF FOUR TYPICAL ROCKETS

PARAMETER	BALLISTIC MISSILE ROCKETS				SPACE ORBIT LAUNCHING ROCKETS					
	Atlas, Stage 1	Atlas, Stage 2	Titan II, Stage 1	Titan II, Stage 2	Titan 3B-Agena, Stage 1	Titan 3B-Agena, Stage 2	Titan 3B-Agena, Stage 3	Titan 3D, Stage 1	Titan 3D, Stage 2	Titan 3D, Stage 3
\dot{W}_{tot} (kg/sec)	680	122	753	147.5	753	147.5	25	3265	753	147.5
No. of Nozzles	3	1	2	1	2	1	1	2	2	1
P_c (m)	0.412	0.234	0.388	0.232	0.388	0.232	0.118	1.880	0.388	0.232
T_c (°K)	3531	3556	3330	3335	3330	3335	3075	3300	3330	3335
P_c (bars)	39.7	48.3	54.1	56.9	54.1	56.9	34.9	34.5	54.1	56.9
P_e (bars)	0.726	0.193	0.946	0.0873	0.946	0.0873	0.1014	0.69	0.946	0.0873
T_e (°K)*	2143	1639	1896	1187	1896	1187	1213	2131	1896	1187
γ	1.2035	1.2189	1.2256	1.2500	1.2256	1.2500	1.1897	1.18	1.2256	1.2500
M_e (amu)	23.62	23.62	23.07	23.07	23.07	23.07	24.50	26.29	23.07	23.07
t_B (sec) (Burntime)	125	181	148	174	163	200	284	118	146	200

*This parameter is redundant and can be calculated from P_c , T_c , γ , and P_e (see also section 3.3.10).

TABLE 4-1. ROCKET HARDWARE PARAMETERS OF FOUR TYPICAL ROCKETS

PARAMETER	BALLISTIC MISSILE ROCKETS				SPACE ORBIT LAUNCHING ROCKETS					
	Atlas, Stage 1	Atlas, Stage 2	Titan II, Stage 1	Titan II, Stage 2	Titan 3B-Agena, Stage 1	Titan 3B-Agena, Stage 2	Titan 3B-Agena, Stage 3	Titan 3D, Stage 1	Titan 3D, Stage 2	Titan 3D, Stage 3
\dot{W}_{tot} (kg/sec)	600	122	753	147.5	753	147.5	25	3265	753	147.5
No. of Nozzles	3	1	2	1	2	1	1	2	2	1
D_t (m)	0.206 0.206	0.234 0.147	0.388 0.194	0.232 0.146	0.388 0.194	0.232 0.146	0.118 0.059	1.880 0.940	0.388 0.194	0.232 0.146
T_c (°K)	3531	3556	3330	3335	3330	3335	3075	3300	3330	3335
p_c (bars)	39.7	48.3	54.1	56.9	54.1	56.9	34.9	34.5	54.1	56.9
p_e (bars)	5.726	0.193	0.946	0.0873	0.946	0.0873	0.1014	0.69	0.946	0.0873
T_e (°K)*	2143	1639	1896	1187	1896	1187	1213	2131	1896	1187
γ	1.2035	1.2189	1.2256	1.2500	1.2256	1.2500	1.1897	1.18	1.2256	1.2500
M_e (amu)	23.62 23.62	23.62	23.67 23.67	23.07	23.07	23.07	24.50	26.29	23.07	23.07
t_B (sec) (Burntime)	125	181	148	174	163	200	284	118	146	200

*This parameter is redundant and can be calculated from p_c , T_c , γ , and p_e (see also section 3.3.10).

* See New Page

TABLE 4-2. MOLECULAR COMPOSITION OF THE EXHAUST OF FOUR TYPICAL ROCKETS (MOLES/KGM)

MOLECULE	BALLIST_C MISSILE ROCKETS				SPACE ORBIT LAUNCHING ROCKETS					
	Atlas, Stage 1	Atlas, Stage 2	Titan II, Stage 1	Titan II, Stage 2	Titan 3B-Agena, Stage 1	Titan 3B-Agena Stage 2	Titan 3B-Agena Stage 3	Titan 3D, Stage 1	Titan 3D, Stage 2	Titan 3D, Stage 3
CO	14.144	13.047	2.252	1.276	2.252	1.276	1.9	9.82	2.252	1.276
CO ₂	7.273	8.369	3.486	4.461	3.486	4.461	5.3	6.86	3.486	4.461
H	0.074	0.003	0.009	0	0.009	0	0	0	0.009	0
H ₂	5.793	6.913	2.975	3.952	2.975	3.952	4.0	11.72	2.975	3.952
H ₂ O	15.072	14.001	19.252	18.282	19.252	18.282	19.2	4.11	19.252	18.282
OH	0.025	0	0.004	0	0.004	0	0	0.004	0.004	0
O ₂	0.0003	0	0	0	0	0	0	0	0	0
N ₂	0	0	15.369	15.369	15.369	15.369	10.4	2.96	15.369	15.369
NO	0	0	0.0004	0	0.0004	0	0	0	0.0004	0
HCl	0	0	0	0	0	0	0	5.71	0	0
Cl	0	0	0	0	0	0	0	0.033	0	0
Al ₂ O ₃	0	0	0	0	0	0	0	2.99	0	0

June 1974

FTD-CW-01-01-74
Vol. 1.

TABLE 4-3. TRAJECTORY DATA OF FOUR TYPICAL ROCKETS

BALLISTIC TRAJECTORY							ORBIT INJECTION								
Atlas				Titan II			Titan 3B-Agena			Titan 3D					
Time (sec)	Thrust (Mg)	Altit. (km)	Veloc. (km/s)	Time (sec)	Thrust (Mg)	Altit. (km)	Veloc. (km/s)	Time (sec)	Thrust (Mg)	Altit. (km)	Veloc. (km/s)	Time (sec)	Thrust (Mg)	Altit. (km)	Veloc. (km/s)
20	181.5	1.075	.111	20	199.4	.757	.076	18.79	205.7	.378	.033	20	965.3	1.30	0.128
40	192.2	4.74	.279	40	204.6	3.31	.188	41.79	211.5	1.87	.105	40	867.5	5.30	0.287
60	202.4	11.5	.523	60	211.5	8.36	.353	61.89	220.4	4.89	.212	60	805.4	12.0	0.465
80	208.1	21.9	.918	80	216.4	16.4	.594	82.29	229.7	10.2	.382	80	764.2	21.2	0.713
100	211.1	37.0	1.52	100	218.1	28.0	.955	102.29	235.7	18.0	.635	100	734.8	32.8	1.05
120	214.0	58.2	2.41	120	218.4	43.6	1.47	123.09	238.2	28.6	1.027	116	322.9	44.3	1.35
125	215.0	64.8	2.71	140	218.5	64.3	2.19	143.09	238.4	41.3	1.552	117	503.3	45.0	1.36
126	37.3	66.1	2.72	148	218.5	74.5	2.57	162.49	238.4	56.6	2.249	120	392.4	47.2	1.40
140	37.0	85.1	2.84	150	46.4	77.2	2.57	163.19	0	57.2	2.264	127	251.8	52.4	1.46
160	36.9	111	3.05	160	46.4	90.6	2.68	163.79	42.0	57.8	2.266	140	238.2	61.6	1.60
180	36.9	137	3.30	180	46.4	116.7	2.89	183.99	45.7	74.5	2.409	160	238.1	75.0	1.53
200	36.8	163	3.60	200	46.4	142.4	3.15	204.19	46.3	89.5	2.586	180	238.5	87.3	2.11
220	36.5	188	3.95	208	46.4	152	3.30	224.19	46.6	103	2.792	200	238.4	98.1	2.47
240	36.5	213	4.38	220	46.4	168	3.46	244.49	46.7	114	3.034	220	237.7	108	2.91
260	36.7	238	4.90	240	46.4	194	3.83	264.69	46.9	124	3.314	240	237.3	117	3.46
280	36.7	264	5.57	260	46.4	222	4.26	285.49	47.0	133	3.644	260	237.0	126	4.16
300	36.6	291	6.47	280	46.4	251	4.81	305.69	47.0	141	4.017	265	155.0	128	4.37
306	36.6	300	6.81	300	46.4	284	5.50	325.59	47.2	147	4.446	267	43.9	129	4.38
307	0.635	301	6.83	322	46.4	326	6.56	346.19	47.2	152	4.974	280	45.0	134	4.50
325	0.635	327	6.81	323	0.754	328	6.57	363.49	47.2	157	5.502	300	45.8	141	4.71
				338	0.754	360	6.55	416.69	8.50	165.1	5.504	320	46.2	147	4.95
								437.59	7.72	165.0	5.661	340	46.4	151	5.21
								457.79	7.69	164	5.821	360	46.4	153	5.50
								478.59	7.67	161	6.000	380	46.5	154.7	5.83
								498.59	7.66	159	6.182	400	46.5	155.5	6.21
								518.59	7.64	155	6.376	420	46.6	155.7	6.63
								528.59	7.64	153	6.478	440	46.6	155.5	7.14
								549.59	7.62	149	6.705	460	46.6	155.2	7.74
								569.59	7.61	146	6.939	464	46.6	155.2	7.90
								589.59	7.61	142	7.193				
								610.59	7.60	140	7.485				
								630.59	7.59	138.4	7.795				
								647.29	7.59	138.5	8.082				

between them. The first high level region occurs during first-stage burning and exhibits a maximum point which occurs approximately where afterburning has its peak. The first deep minimum region which occurs almost always at the beginning of second-stage burning is due to (1) decreased mass flow rate of the second stage (compared to the first), and (2) decreased CD heating since the air-relative exhaust velocity V_k (see Eq. (3.206)) of the exhaust goes through a zero point near there. The second (and third) high-level regions which occur at high altitudes are due to the fact that (1) CORE radiation is approaching, or has approached, its maximum there (equal to DSPR radiation), and (2) CD heating is increasing again there, after having gone through its low point in the first deep trough. The vehicle velocity and thus the air-related exhaust velocity is getting very high again at the higher altitudes. However CD heating at the later stages is absent if an altitude over 200 km is reached since the air gets too thin there to allow a sufficient number of CD excitations to occur within the field-of-view of typical sensors.

The importance of altitude on CD heat is illustrated vividly by a comparison of the signatures from the ballistic trajectories of the Atlas and Titan II (Figures 4-1 and 4-2) which go to an altitude of 325 and 360 km, and the signatures of the orbit launching Titan 3B/Agena and the Titan 3D (Figures 4-3 and 4-4) which only reach an altitude of 138 and 155 km (see Table 4-3). The terminal vehicle velocities of the ballistic rockets are about $V_v = 6.8$ km/sec while the orbit launchers reach about $V_v = 8$ km/sec. The high $(V_v - \tilde{V}_x)^2$ peak heating effect near burnout altitude is in the case of the ballistic rockets not observed because they are well above 200 km there. Instead the steady maximum level CORE radiation (DSPR radiation)

prevails. However, as may be seen in Figures 4-3 and 4-4, CD heating is quite significant for the orbit-launchers which stay below 200 km and as a result show strong CD peaks towards the end of the second and third stage burns.

The last two peaks in Figures 4-3 and 4-4 are usually somewhat lower and rounded off in actual observations since in an orbit launch the rocket is about to get out-of-sight at that altitude, which means that the aspect angle is much more than (or less than) the 90° assumed in the calculations. This causes the view factor F_v to drop below the constant value of F_v ($\alpha = 90^\circ$) that was assumed. The radiation level will of course be lowered correspondingly. Only when the relative sensor and rocket positions are known accurately, can the precise reduction of the radiation level by the changing value of F_v be determined.

High-altitude CD peaks are not entirely absent from the ballistic rocket signatures and appear as small bumps on the otherwise level CORE radiation plateaus in the last portion of the signature curves.* The signature curves shown are a little jagged (the high-altitude CD bumps appear as triangles for example) due to the long time intervals of about 20 seconds that were taken in the computation of the curves. Shorter time intervals in computation should yield smoother curves.

An interesting difference between the $4.45 \mu\text{m}$ CO_2 radiation and the $2.74 \mu\text{m}$ H_2O radiation is that the signature of the former has a minimum that

*CD radiation bumps or spikes can also occur during stagings or when vernier burns are executed. In both cases gas is released with a higher-than-normal air-relative velocity V_k , causing increased V_k^2 -dependent CD radiation. During staging, it is the decreased exhaust velocity \tilde{V}_x of the "after-bell" gases that causes an increase in $V_k = V_v - \tilde{V}_x$. For the vernier burn it is the sideways thrust angle θ that causes $V_k = V_v - \tilde{V}_x(\cos\theta)$ to increase above the normal thrusting value with $\theta = 180^\circ$.

June 1974

occurs much earlier than the minimum of the latter. In fact for the Atlas rocket for example an upswing in radiation is observed already during first-stage burning, after a brief minimum. This is due to the fact that the radiative decay constant for the CO_2 transition is about 4 millisecond, compared to about 11 milliseconds for the H_2O band. As a result, more of potential CO_2 radiation is released in the Mach Core (before it is mixed with air) than H_2O radiation. Separate plots of only CORE radiation are shown in Figure 4-5 and from these curves it is clear why the CO_2 radiation attains its maximum level sooner than the H_2O CORE radiation.

The prediction of an earlier CO_2 Mach Core radiation peak compared to the H_2O Mach Core peak is a very sensitive function of the calculated radiative decay constant of $\tau_i = 4$ milliseconds for CO_2 versus $\tau_i = 11$ milliseconds for H_2O , as well as the Mach Core dwell time τ_M , which appears in the factor $\{1 - \exp(-\tau_M/\tau_i)\}$. Approximating errors in the calculation of τ_M may shift the CORE curves, but since τ_M must be the same for both curves, the relative position and slopes of the two CORE radiation curves should give information on the relative magnitudes of τ_i for the H_2O and CO_2 bands. This is valuable scientific information, and should encourage the simultaneous measurement of $2.74 \mu\text{m}$ and $4.45 \mu\text{m}$ rocket radiation signatures. Of course the measured radiation will be a composite of ABCD and CORE radiation and some analysis will be required to extract the pure CORE contribution.

The small dips shown in the very early parts of the signature curves occur when the ambient pressure $p_a = p_e$. This happens because before the occurrence of these small dips (at an altitude between 3 and 8 km), the exhaust gas will expand to ambient pressure p_a inside the nozzle and in this case, p_e in the mixing ratio expressions $\mu_{a/e}$ (Eq. (3.195)) is given by p_a .

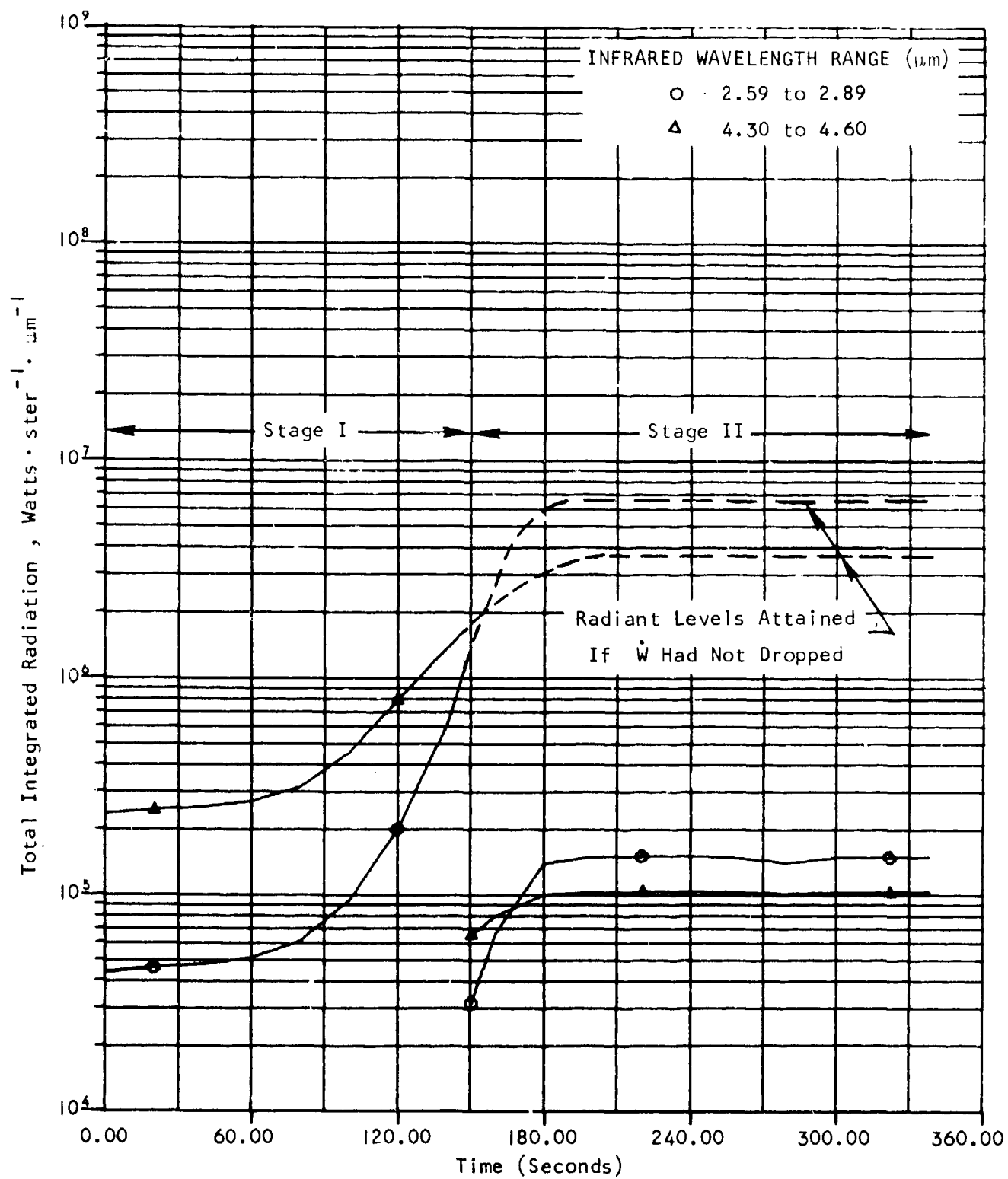


FIGURE 4-5. CALCULATED PURE MACH CORE RADIATION (TITAN II ROCKET)

June 1974

Thus fractionally more air cooling of the plume occurs relative to later times in the trajectory where $p_e = p_o = \text{constant}$ (see Eq. (3.196)). If observations of rocket launchings are made from satellites such as Skylab, the early part of the signature curve is not seen however, because of strong atmospheric absorption of infrared rocket radiation during the lift-off and low-altitude portion of the trajectory. Thus the first small dips are usually missed in satellite-observed signatures.

Several other inflection points, dips, and bumps are present in the signature curves, some of which depend critically on a particular physical parameter. However since many of the physical parameters are not exactly known, the predicted location of such special features may differ somewhat from what is actually observed. It is clear that an analysis of experimental rocket radiation signatures could provide a wealth of basic data and should assist in verifying, adjusting, or changing some of the molecular and gas constants used, many of which were calculated (e.g. the τ_i) from somewhat uncertain data. Also some of the approximate expressions (e.g. f_{CD}) that were used in the theory given in section 3.3 should be tested against actual field data.

For thorough signature analyses, it is essential that all "laboratory" parameters are accurately known, since observational conditions can strongly effect the signatures. For example the field-of-view diameter D_s at the target, which was taken as $D_s = 1 \text{ km}$ in Figures 4-1 through 4-4, will cause the sensed radiant intensity to decrease as soon as the plume length L_p and/or diameter D_p exceeds $D_s = 1 \text{ km}$.* Such "laboratory-induced" effects must of

*For D_p , this occurs at about 150 km (see Figure 2-6).

course be recognized and properly accounted for, and cannot be ascribed to a high-altitude physical process in the plume.

The signatures shown in Figures 4-1 through 4-4 exhibit also error bars which are based on Eq. (3.378) of section 3.3.10, and the assumption that certain input parameters have uncertainties in their values as shown in Table 4-4. Also shown in Table 4-4 are "influence coefficients" which give the fractional change in J due to the fractional change in one parameter with all others held constant. The figures in the table show that the gas coefficient γ and the combustion chamber temperature T_c appear to have the highest influence coefficients as one would expect. Note also that the influence coefficients of \dot{W} and g_{H_2O} are linear as expected.

For variances in γ , Eq. (3.378) which holds only for small perturbations, is inadequate in certain regions of the signature plots. For a $\Delta\gamma = \pm 0.05$ variance for example, one finds that near the signature "trough" region $+\Delta J \approx 2.5 J_0$ and $-\Delta J \approx 0.1 J_0$. Formula (3.378) takes $\Delta J = \pm(2.5 J_0 + 0.1 J_0)/2 = \pm 1.3 J_0$, from which one obtains $J_- = J_0 - \Delta J = -0.3 J_0$ and $J_+ = +2.3 J_0$. These results are clearly wrong. Thus in γ -ultrasensitive regions the effect of variations in γ should be calculated separately.

The signature computations plotted in Figures 4-1 through 4-4 included only emissions from the fundamental $\Delta v_\alpha = 1$ ($1 \rightarrow 0$; $2 \rightarrow 1$; $3 \rightarrow 2$; ...) vibrational transitions obtained via Eq. (3.316). Since overtone and combination-band emissions are much weaker and far away from the spectral regions considered, this is an excellent approximation.

June 1974

TABLE 4-4. ASSUMED PARAMETER UNCERTAINTIES FOR ERROR ANALYSIS

Parameter	Fractional Variance	Fractional Change in J*	Parameter	Fractional Variance	Fractional Change in J*
\dot{W}	± 0.1	± 0.100335	P_a	± 0.1	± 0.003702
T_c	± 0.1	± 0.277410	T_a	± 0.1	± 0.005316
P_c	± 0.1	± 0.055767	D_s (DFOV)	± 0.15	± 0.007785
P_e	± 0.1	± 0.058176	α (ASPCT)	± 0.1	± 0.000000
D_e	± 0.05	± 0.027765	g_{H_2O}	± 0.05	± 0.050047
γ	± 0.05	± 0.611489	g_{CO_2}	± 0.05	± 0.000005
\bar{H}_e	± 0.05	± 0.006193	g_{CO}	± 0.05	± 0.00013
V_V	± 0.05	± 0.001782			

*Values are for the $2.74 \mu m$ H_2O band at 160 km altitude.

4.2 PLUME EMISSION SPECTRA

In addition to rocket radiation signatures, that is plots of the band-integrated radiation intensity versus altitude or time, the radiation expressions developed in Chapter 3 also are capable of providing absolute emission spectra at any desired altitude, that is plots of intensity versus wavelength. Figures 4-6 and 4-7 are examples of such spectral plots.

Figure 4-6 shows calculations of the infrared emission spectrum produced by the exhaust of a Titan rocket (see Table 4-2) in the 2 to 10 μm region, where H_2O , CO , and CO_2 emit most strongly. Only the fundamental $\Delta v_{\alpha} = 1$ ($1 \rightarrow 0$, $2 \rightarrow 1$, $3 \rightarrow 2$, etc.) vibrational transitions are accounted for in Figure 4-6. The weaker overtones and combination-bands are usually not noticeable in the 2 to 10 μm region where most fundamentals of H_2O , CO_2 , and CO are active.

The spectrum shown in Figure 4-6 gives only the band contours, that is the minimum resolution is assumed to be several rotational line spacings. Detailed line spectra can also be readily calculated however by use of the rovibrational functions b_{rov} instead of b_v (see Vol. II and section 3.3.8). The curves of Figure 4-6 are based on the contour function b_v given in section 3.3.8.

Figure 4-7 shows the emission contour in the UVIS region at high altitudes due to SUAR and CD (with high V_k^2). Approximate vibronic contour functions were used in calculating the curve shown in Figure 4-7 (see Eq. (3.346) and the following discussion in section 3.3.8). Figure 4-7 gives therefore only the gross features of the UVIS spectrum and should be considered more as an example of what might in general be obtained. At

June 1974

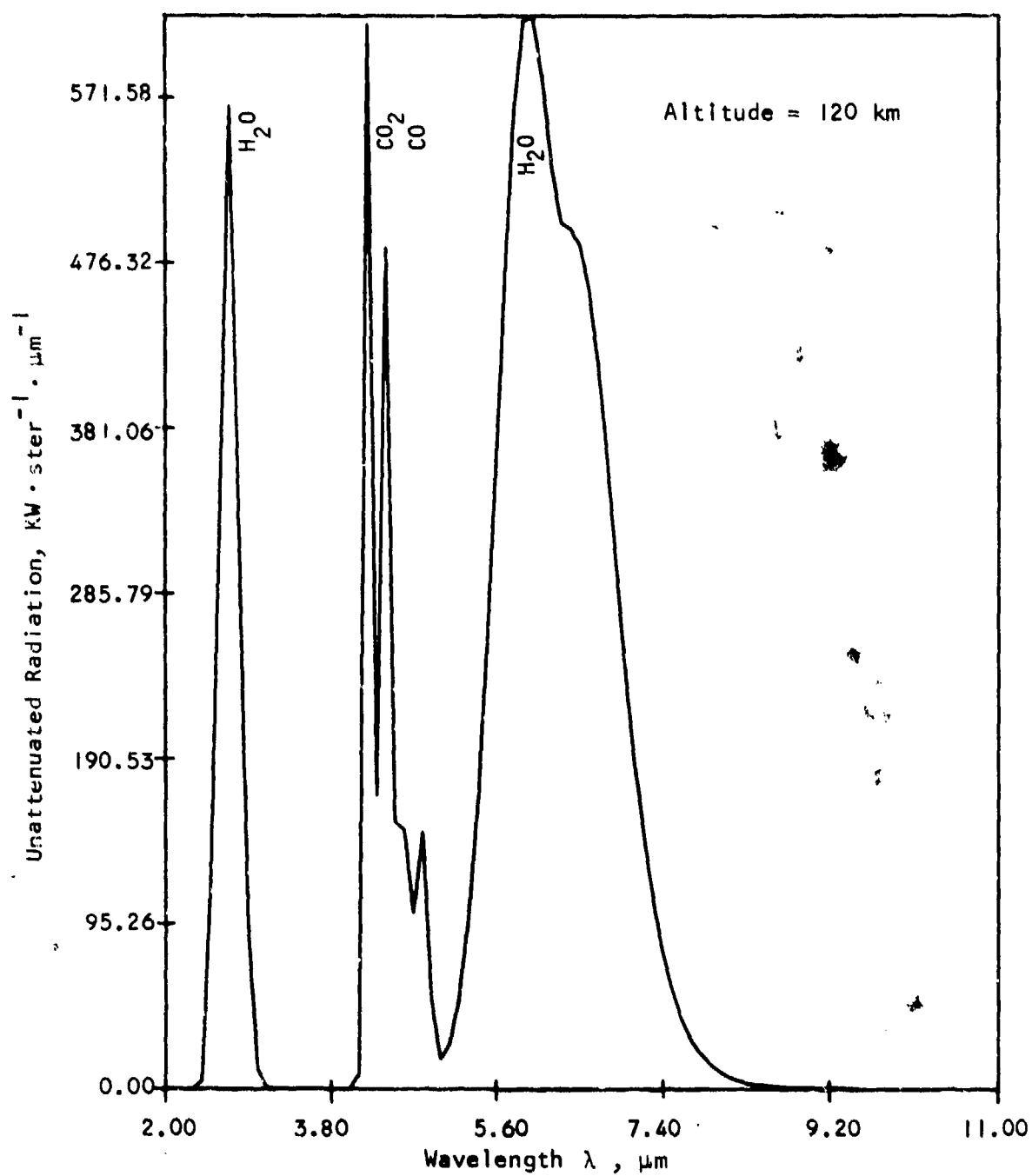


FIGURE 4-6. CALCULATED UNATTENUATED INFRARED RADIATION
SPECTRUM OF TITAN-II SECOND STAGE

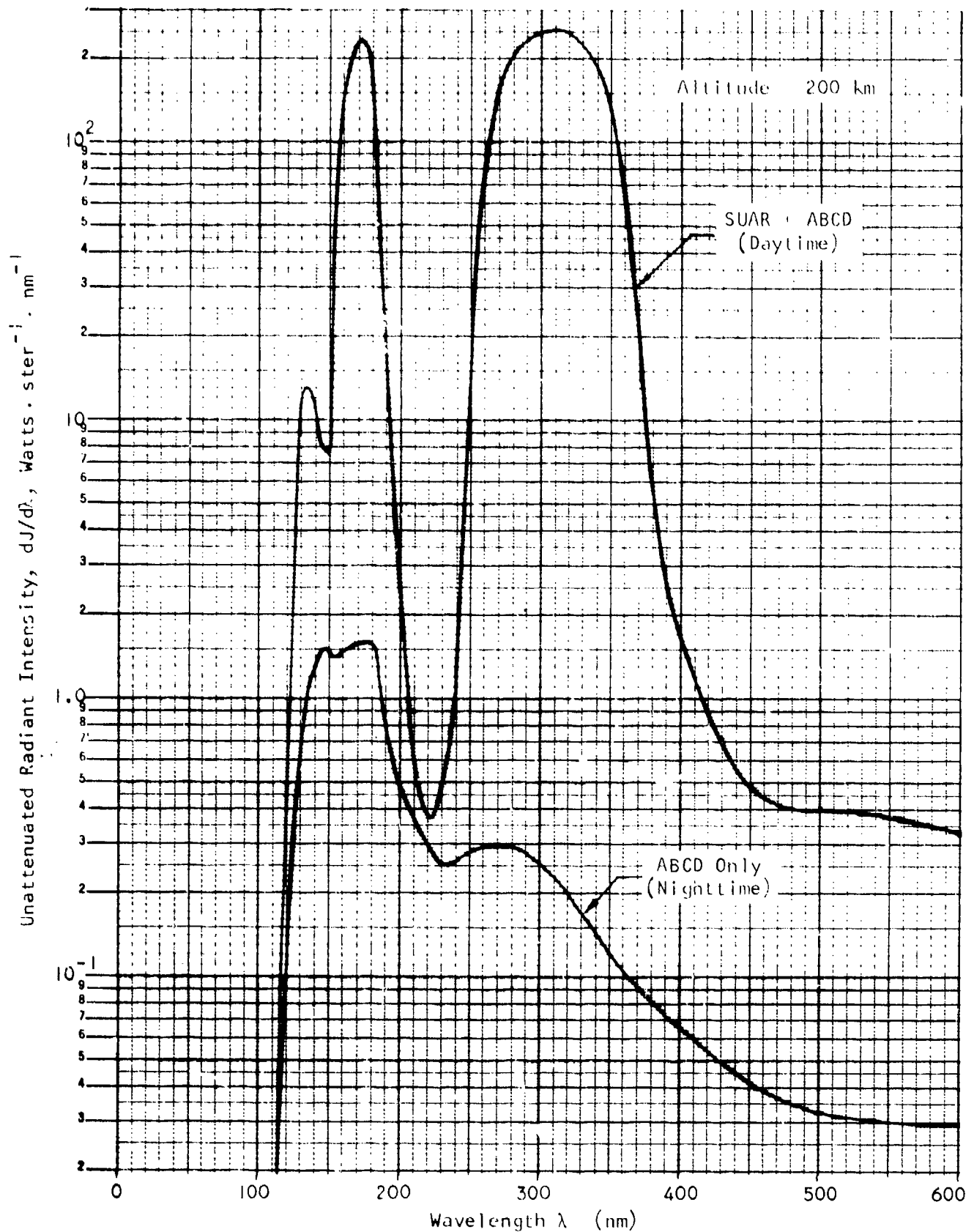


FIGURE 4-7. CALCULATED UNATTENUATED UVIS SPECTRUM FROM AN AMINE-FUELED 300 KG(F) ROCKET MAKING A POST-BOOST MANEUVER BURN AT A THRUST ANGLE OF 135 DEGREES

present, fundamental data on vibronic transitions (see section 3.3.10) are somewhat incomplete. Without such data it is not possible to use the more accurate vibronic contour functions developed in Volume II and hence the coarse contour relations of the form (3.346) together with the data in Table 3-6 had to be used in arriving at the coarse UVIS contour spectrum of Figure 4-7. If and when more complete vibronic data become available and more measurements are made to obtain such data, it should be possible to calculate better UVIS emission spectra using the more accurate vibronic and rovibronic contour functions given in Volume II.

The infrared spectrum of Figure 4-6 shows the non-attenuated rocket plume emissions observable from satellites. Figure 4-8 shows the atmosphere-filtered spectrum (see Volume V for atmospheric transmission) corresponding to Figure 4-6. The atmosphere contains a lot of H_2O and CO_2 and thus the rocket emissions in the H_2O and CO_2 bands are heavily filtered when observations involve a long atmospheric path between the observer and the rocket (e.g. for aircraft- or ground-based sensors). Because the exhaust gases are hotter than the air however, their emission bands are broader since the band-spread is proportional to $T^{1/2}$ (see for example Eq. (3.341)). As a result, emissions in the "wings" of the H_2O and CO_2 bands can still get through the atmosphere. Of course emissions from "foreign" exhaust gases such as CO or HCl can get through the atmosphere even better. Both of these effects are clearly shown in the atmosphere-attenuated curves of Figure 4-8.

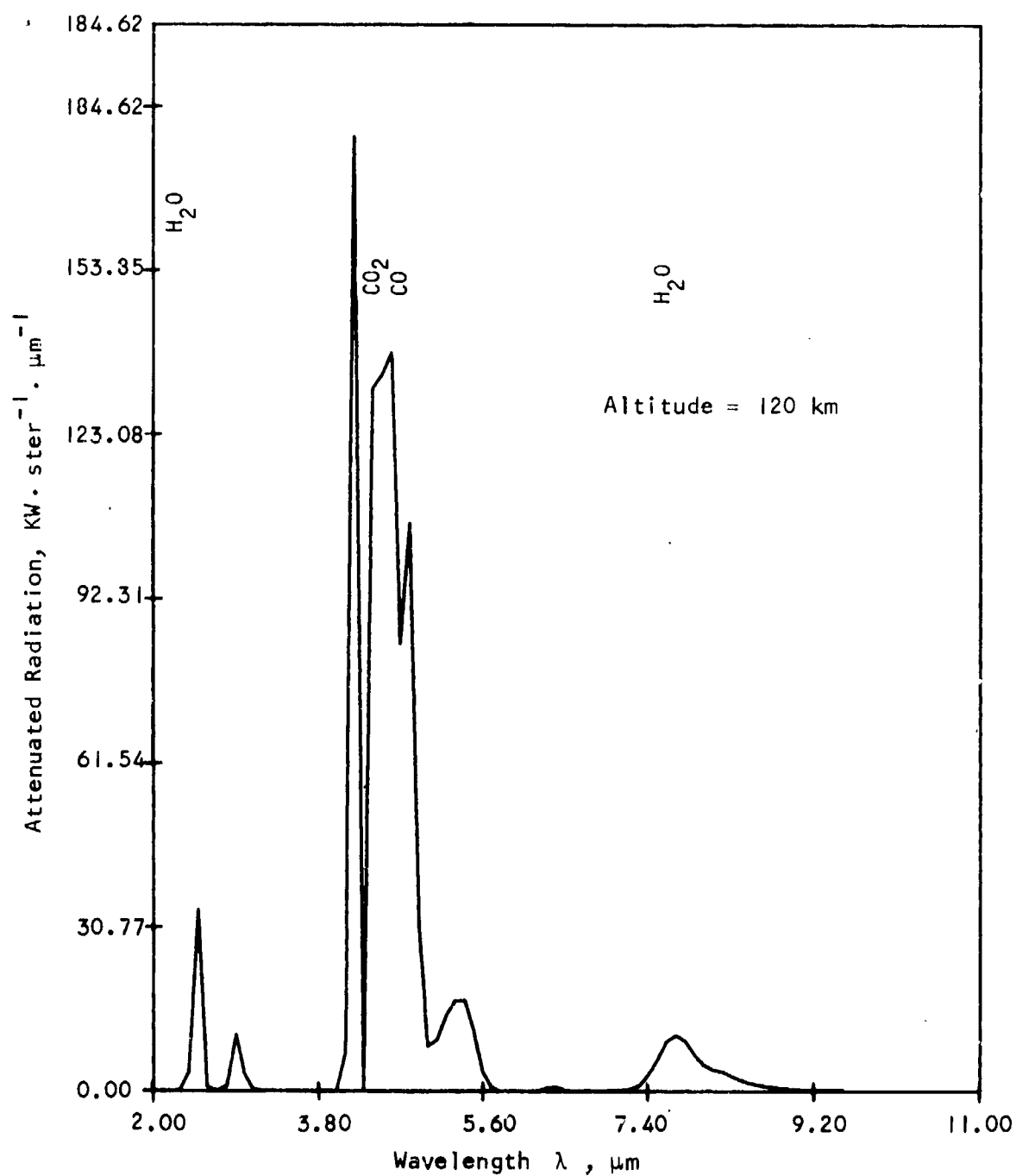


FIGURE 4-8. CALCULATED ATMOSPHERE-ATTENUATED INFRARED RADIATION SPECTRUM OF TITAN-II SECOND STAGE

4.3 CONCLUSIONS AND COMMENTS

The theory developed in Chapter 3 provides reasonably satisfactory relations for the calculation of rocket radiation "signatures" and spectra as shown in sections 4.1 and 4.2. However the theory developed so far does not yield relations for the detailed spatial distribution of the emitted radiation, that is the imagery of the rocket plume or cloud. Only gross spatial features and shapes of the plume and cloud were evaluated as needed for calculating view factors and a few other space-dependent parameters.

The theory of Chapter 3 employed some basically new approaches in answer to the questions of: (1) How many photons are emitted by the plume in total, and: (2) What is the spectral (not spatial) distribution of these photons. View factors were considered next in order to give an answer to the question of: (3) How many of all the emitted photons of certain wavelengths travel in a certain direction. However the question of: (4) How many photons with certain wavelengths are emitted from each unit surface area of the plume in a certain direction was not answered, since in most applications for which the theory of Chapter 3 was developed, this information is not needed. That is, with the exception of Baker-Nunn photography (see Chapter I), most rocket radiation tracking sensors collect only spectral radiance information and not imagery.

In principle however the spectral radiance theory as developed in this volume of the Rocket Radiation Handbook can be extended to include imagery calculations. This requires a detailed knowledge of the spatial distribution of the exhaust gas molecules in the plume as well as knowledge of the photon distribution in it. Volume III will cover photon migrations and distributions in gaseous media, while Volume IV provides theories and

methods for the calculation of rocket jet and plume structures and exhaust cloud expansions. From a known molecular density distribution in the plume as calculated via the relations given in Volume IV, the internal photon distribution and surface escape flux distribution can be obtained next by means of the theory provided in Volume III. Once the photon escape flux distribution is known as a function of plume surface position for a particular plume, the radiant intensities at any point on the surface of the plume can be calculated of course, starting with the known total emission rate and spectral distribution obtained with the theory given in Chapter 3. Thus imagery, or the spatial distribution of the emitted rocket radiation is in principle calculable as well.

It should be noted that the above-outlined procedure follows steps that are the reverse of those used in most other rocket radiation signature calculations. They usually start with plume surface emittance calculations based on a surface temperature distribution that is computed from some fluid dynamic model of the jet or plume. The unit surface emittances are then summed in order to obtain the total radiation from the plume. Thus one begins in these techniques with the most complex problem namely that of finding an answer to the intensity, spectral, directional, and spatial distribution of plume emission all at once. Having obtained such an answer by means of numerous approximations, one then integrates out and "loses" all spatial information since it is not needed. In the approach developed in Chapter 3 on the other hand, only an accounting of total emission intensity and spectral distribution is developed, while directionality is added later via the view factor formalism. This approach, it would appear, is in principle less redundant and should give more accurate results, even though it also makes use of various inevitable approximations.

In developing the explicit radiation equations of Chapter 3, several ad hoc or coarse approximating assumptions were employed such as $\bar{T}_M = \frac{2}{3} T_e + \frac{1}{3} T_{exh}$ and $\bar{V}_M = \frac{1}{2} V_e + \frac{1}{2} V_{exh}$. Such approximations are mathematically and physically not elegant and future efforts should be directed towards obtaining more exact expressions for these bulk-averaged parameters. Nevertheless, the savings in calculational effort that such simple approximations afford are immeasurable and much to be preferred over schemes that involve detailed flow-field calculations.

The fading of the CD mechanism at high altitudes due to the disappearance of an atmosphere, which was handled by the "fade-out" factor f_{CD} (Eq. 3.239), should also be examined in more detail. Similarly use of the "smoothing factors" $\exp(-\tau_M/\tau_i)$ which let $T_Q \rightarrow T_h$ in deep space, should be further scrutinized.

Another area finally that needs further examination is the effect of radiant and molecular energy exchange between solid Al_2O_3 particles and gas molecules in the exhaust plumes of solid rockets. Qualitatively one may expect that the particles will act in the manner of an added capacitance and delay the ultimate release of the exhaust gas energy via radiation. Thus the effective radiative plume length of two-phase plumes with entrained particles should be somewhat longer than the length of a purely gaseous plume.

Another difference between purely gaseous plumes and plumes that have entrained particles is that the particles, if heavy enough, will collectively form a tighter jet or beam with a smaller flare angle than that of the gaseous jet (Ref. 16). This separation of particle and gas flow should become more and more noticeable at the higher altitudes where the gaseous jet has a very large flare angle.

Because of the energy conservation law, the total radiation emitted from a plume containing particles should of course be the same as that from a pure gaseous plume but due to the effects mentioned above, the emission from a particle-laden plume will be distributed over a slightly longer equivalent cylinder. In addition to this modified spatial distribution, the presence of particles should also tend to change the otherwise pure molecular spectrum towards a continuous Planckian spectrum. The resultant spectrum from a two-phase plume should lie therefore between a Planckian and molecular distribution of photon frequencies.

All the above two-phase flow effects should be of second order however and the radiation as calculated by the formulas given in Chapter 3 should still be good to first-order for most solid-rocket plumes, particularly if observations are made in or near the stronger molecular emission bands.

One final comment that must be made here, is that it was tacitly assumed in the theory of Chapter 3 that the radiative decay times τ_i of the excited levels under consideration are much less than the view time $\tau_s = V_V/D_s$. That is we must have that $\tau_i V_V/D_s \ll 1$. If this is not so, as for example in the case of microwave emissions from pure rotational transitions, where $\tau_i \sim$ minutes, the radiant emission expressions give in Chapter 3 must be multiplied by the factor:

$$(f_{si})_{TTO} = \frac{\tau_i V_V}{D_s}, \quad \text{for target-tracking observations} \quad (4.2)$$

and:

$$(f_{si})_{ICO} = \frac{\tau_i \bar{v}_e p_{esc}}{D_s}, \quad \text{for integrated-cloud observations} \quad (4.3)$$

June 1974

Here τ_i is the radiative decay time of level i , V_v is the rocket vehicle velocity, \bar{v}_e is the mean kinetic velocity of an exhaust molecule, and $p_{\text{esc}} = p_{\text{esc}}(D_s)$ is the probability of escape of an exhaust molecule from the field-of-view of diameter D_s . Usually the condition $\tau_i V_v / D_s \ll 1$ is met however and the corrections (4.2) or (4.3) are unnecessary.

APPENDIX A
REFLECTIVITIES AND EMISSIVITIES OF TYPICAL MATERIALS

As stated in section 3.1, the irradiance received at a sensor from an illuminated or self-emitting object in space depends on four parameters, namely cross-section, illumination or self-emission intensity, reflectivity or emissivity, and the distance between the target and the observer. In this appendix we shall consider the material effects of the target's surface, namely the reflectivity ρ and emissivity ϵ .

For most space objects of interest, one has that the transmissivity $\tau = 0$, and in this case Kirchhoff's law states that the absorptivity $\alpha = \epsilon$, so that:

$$\epsilon = 1 - \rho \quad (\text{A.1})$$

Both ϵ and ρ depend on wavelength λ and temperature T :

$$\epsilon = \epsilon(\lambda, T) \quad (\text{A.2})$$

In textbooks on optical physics, ϵ and ρ are also considered to depend on the angle of incidence ϕ . For example for smooth surfaces whose roughness is less than the wavelength λ , so-called "specular" reflection occurs, and the angular dependence of ϵ or ρ in the case of a non-conductor may be derived from the relation:

June 1974

$$\rho_o = \frac{1}{2} \frac{\sin^2 (\phi - \chi)}{\sin^2 (\phi + \chi)} \left\{ 1 + \frac{\cos^2 (\phi + \chi)}{\cos^2 (\phi - \chi)} \right\} \quad (\text{A.3})$$

where:

$$\chi = \sin^{-1} \left\{ \left(\frac{1}{m} \right) \sin \phi \right\} \quad (\text{A.4})$$

ϕ = angle of incidence

m = refractive index of surface material

In the case of conductors, the specular reflectivity can be approximated by:

$$\rho_{\perp} = \frac{60 \lambda - 2 \sqrt{30 \sigma \lambda} \cos \phi + \cos^2 \phi}{60 \lambda + 2 \sqrt{30 \sigma \lambda} \cos \phi + \cos^2 \phi} \quad (\text{A.5})$$

$$\rho_{//} = \frac{60 \sigma \lambda \cos^2 \phi - 2 \sqrt{30 \sigma \lambda} \cos \phi + 1}{60 \sigma \lambda \cos^2 \phi + 2 \sqrt{30 \sigma \lambda} \cos \phi + 1} \quad (\text{A.6})$$

$$\rho_o = \rho_{\perp} + 0.5 \rho_{//} \quad (\text{A.7})$$

where:

λ = wavelength, cm

σ = electrical conductivity, ohm-cm

ρ_{\perp} = reflectivity for light with polarization perpendicular to plane of incidence

$\rho_{//}$ = reflectivity for light with polarization parallel to plane of incidence

ρ_o = reflectivity of unpolarized light

Equations (A.5) and (A.6) are valid for wavelengths λ above five microns as verified by experiment, but may be used down to two microns. Below this the assumption of Ohm's law used in the derivation of (A.5) and (A.6) becomes invalid and absorption resonances become important (see Figure A-1).

In Figures A-2 and A-3, curves are given of $\epsilon = 1 - \rho$ as a function of angle of incidence ϕ , based on Eqs. (A.3) and (A.7) for various metals and conductors. Figure A-1 gives the reflectance at normal incidence ($\phi = 0$) of a number of metals. For strongly-transmitting surfaces, ϵ can no longer be obtained via Eq. (A.1) and the relations (A.3) or (A.7). However, as stated, such materials are rarely used on spacecraft outer structures.

For surfaces which have irregularities (roughness) of dimensions large compared to the wavelength, the reflectivity ρ (or emissivity ϵ) will no longer follow the relations (A.3) or (A.7), and the angular dependence of ρ is the average of that due to a large number of randomly-oriented surface elements on and between which not only one but often several reflections can take place. For a large number of rough surfaces, one finds that the angular dependence of the reflectivity of the surface follows a cosine distribution, being highest in a direction normal to the surface and falling off to zero at grazing incidence. Such surfaces are said to be "diffuse" or "Lambertian" reflectors. Still other surfaces exist (such as a surface made up of many shiny small spheres) which reflect "isotropically," that is all incident or self-generated light is reemitted with equal probability in all directions and thus ρ is constant and independent of ϕ .

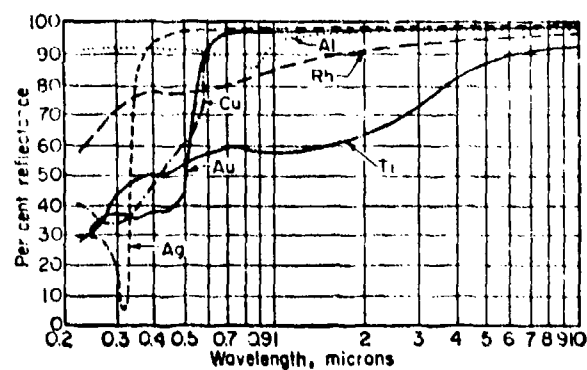


FIGURE A-1. REFLECTANCE OF FRESHLY
EVAPORATED FILMS
(After Ref. 22)

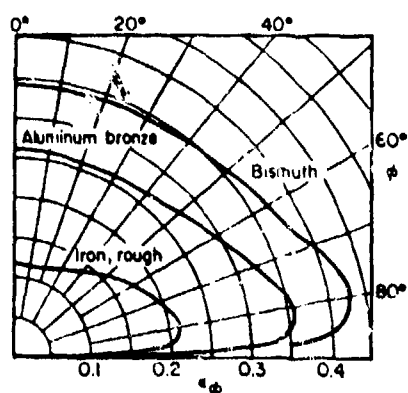


FIGURE A-2. ANGULAR DEPENDENCE
OF EMITTANCE OF METALS
(After Ref. 22)

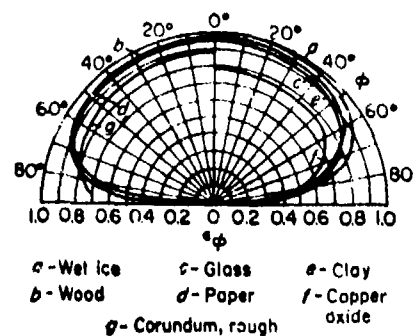


FIGURE A-3. ANGULAR DEPENDENCE
OF EMITTANCE OF NONCONDUCTORS
(After Ref. 22)

Instead of assuming ρ (or ϵ) to depend on the angle of incidence ϕ , we shall incorporate all angular dependences for specular, diffuse or isotropic reflection, in the expression for the cross-section which as we have stated in section 3.1 should contain by definition all geometrical effects. The value for ρ to be used in all relations in this monograph will therefore be that for normal incidence, that is $\rho = \rho(\phi=0)$. For diffusely-reflecting surfaces this value of ρ is best determined experimentally (it is not equal to $\rho(\phi=0)$ for a specularly-reflecting surface). Such experimental values of ρ (or ϵ) for diffuse surfaces are given in Figures A-1, and A-4 through A-10, and in Tables A-1 through A-4.

For most spacecraft the surface is close to that of a diffuse reflector and thus values for ϵ and ρ should be taken from Tables A-1 and A-2 and Figures A-4 through A-10. Together with the diffuse cross-sections given in section 3.2, these values for ρ and ϵ then give the radiant intensity of a space object.

Data on the spectral temperature dependence of ϵ or ρ are rather scarce. In many calculations, variations of ϵ or ρ with temperature are neglected and values at $T = 300^\circ\text{K}$ are assumed to apply. In Figures A-11 through A-14, the spectral temperature dependence of ϵ for various types of steel surfaces are shown. These curves indicate that the value of ϵ may change by as much as 50 percent, in going from 900°F (482°C) to 1800°F (982°C).

The total (infrared) spectrum-integrated emissivity changes with temperature have been measured more extensively for various materials. Figures A-15 through A-23 and Table A-4 show some of the published data on the change of $\bar{\epsilon} = \int_{\lambda} [\epsilon(\lambda)/d\lambda] d\lambda$ with temperature.

June 1974

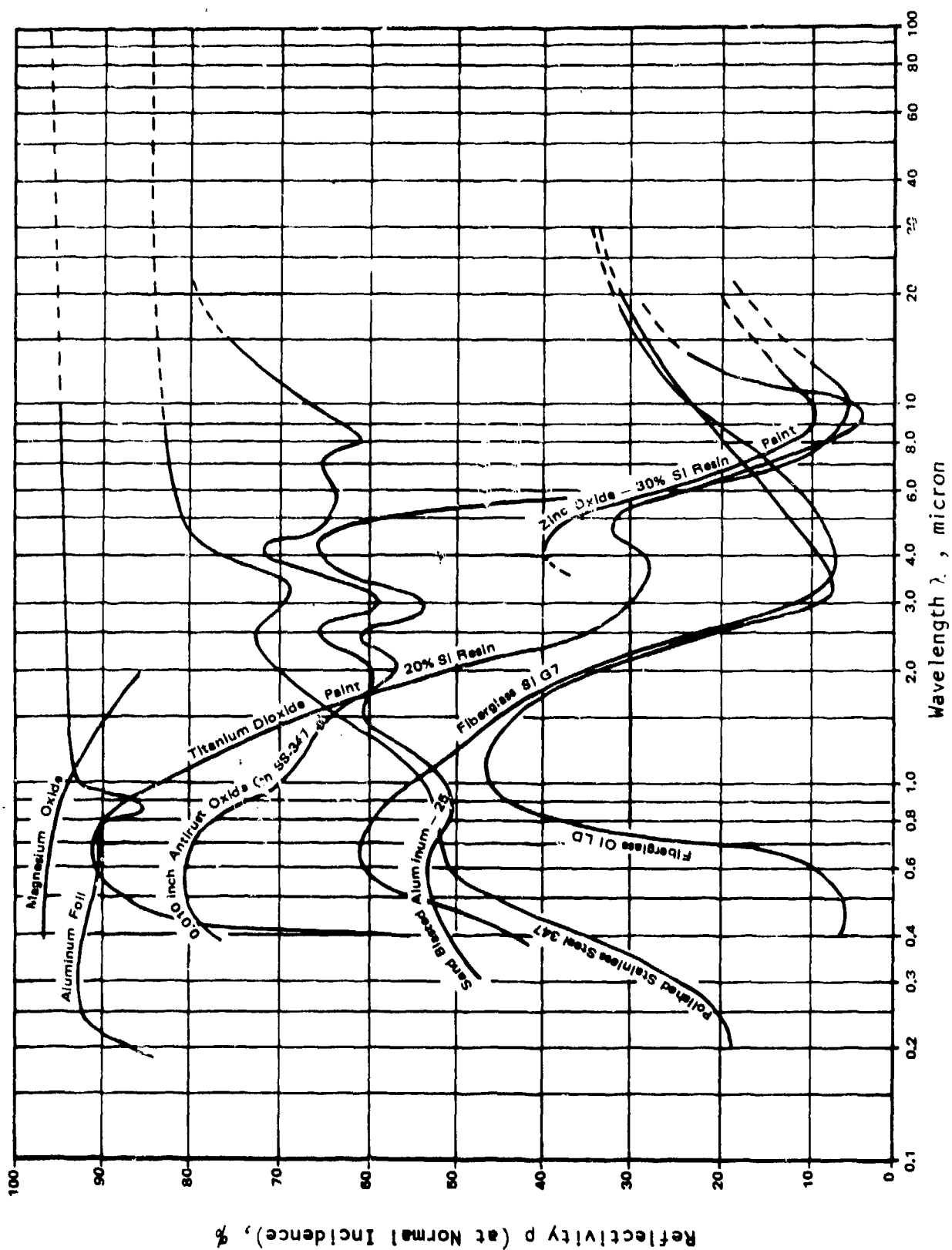


FIGURE A-4. TYPICAL SPECTRAL REFLECTIVITIES OF SPACE VEHICLE SURFACES

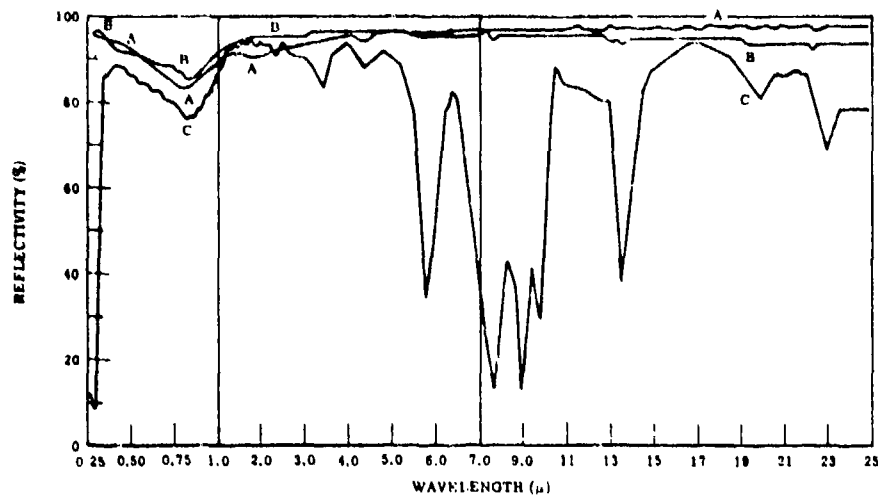


FIGURE A-5. SPECTRAL REFLECTIVITIES OF ALUMINUM SURFACES. A = evaporated aluminum, 25 μ inch on polished 6061-T6 aluminum; B = evaporated aluminum (0.2 μ) on 1/4-mil Mylar crumpled and stretched (looking at aluminum); C = evaporated aluminum (0.2 μ) on 1/4-mil Mylar crumpled and stretched (looking at Mylar).

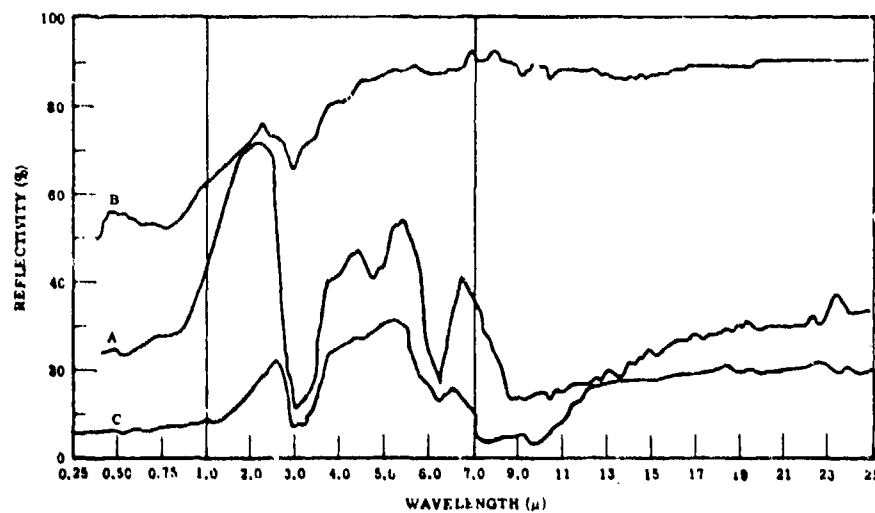


FIGURE A-6. SPECTRAL REFLECTIVITIES OF ALUMINUM SURFACES. A = chromic acid anodize on 24S-T81 aluminum; B = sulfuric acid anodize on 24S-T81 extruded aluminum, chemically milled; C = hard anodize (1 mil) on 6061-T6 aluminum (35 amp ft⁻², 45 volts, 20° F).

June 1974

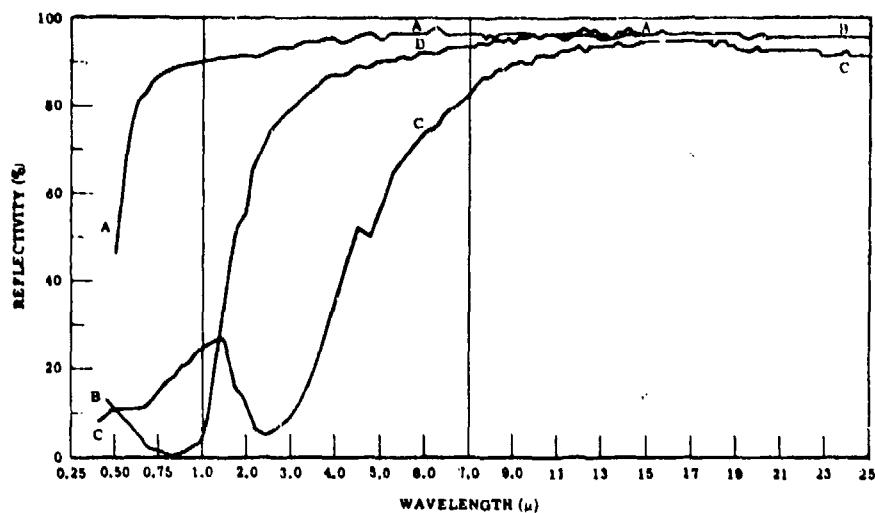


FIGURE A-7. SPECTRAL REFLECTIVITIES OF COPPER SURFACES.
A = polished copper, 17 mils thick; B = Tabor solar collector chemical treatment (110-30) on nickel-plated copper; C = Tabor solar collector chemical treatment (125-30) on nickel-plated copper; D = Tabor solar collector chemical treatment (110-30) on nickel-plated copper.

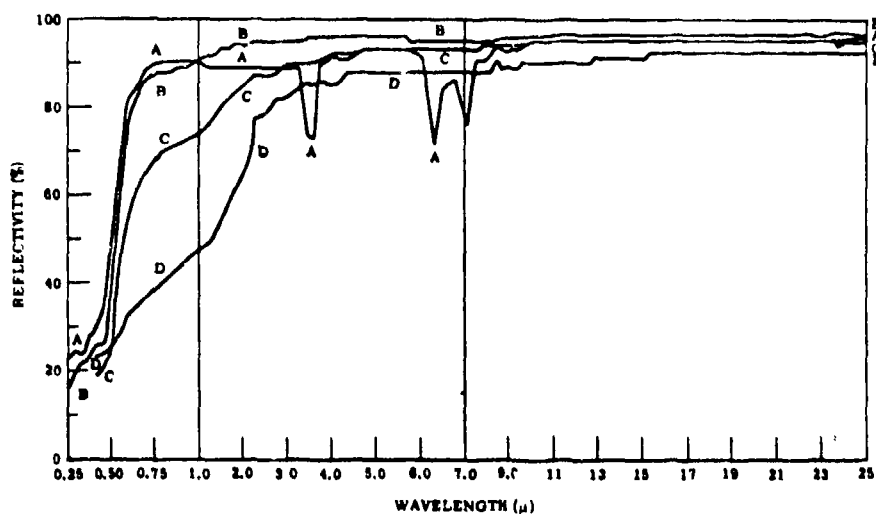


FIGURE A-8. SPECTRAL REFLECTIVITIES OF GOLD SURFACES.
A = immersion gold, approximately 0.03 mil, on nickel-plated copper plate on 6061-T6 polished aluminum, aged 6 months in air, unpolished; B = vacuum-evaporated gold on fiberglass laminate; C = gold ash (80 μ) on 0.4-mil silver on Epon glass; D = white gold on polished MIL-S-5059 steel.

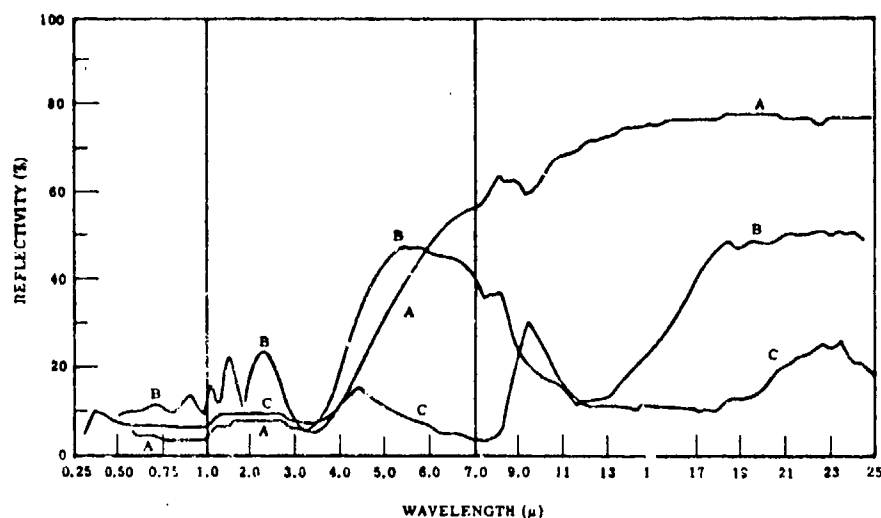


FIGURE A-9. SPECTRAL REFLECTIVITIES OF SILICON SURFACES. A = silicon solar cell of International Rectifier Corp; B = silicon solar cell, International Corp. 1.11- μ evaporated coat, SiO₂-fast deposition rate; C = silicon solar cell, Hoffman Corp. Type 120-C, 3-mil glass cover.

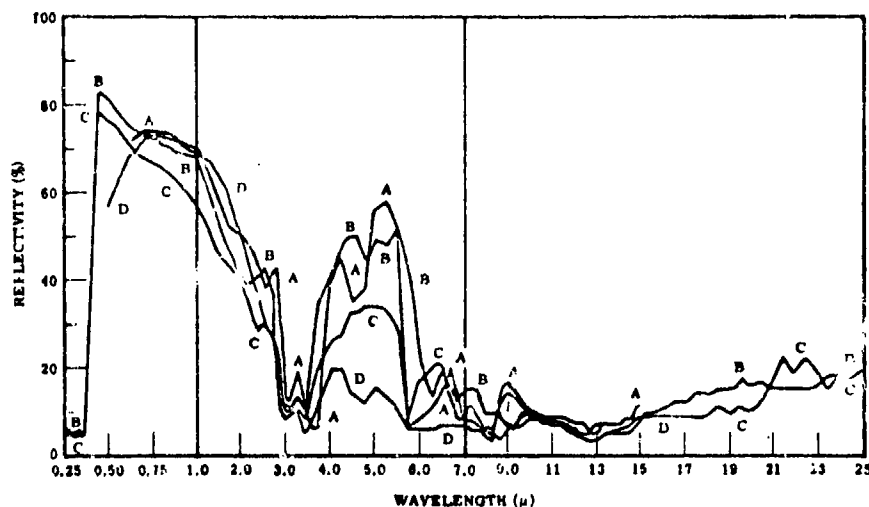


FIGURE A-10. SPECTRAL REFLECTIVITIES OF PAINTED SURFACES. A = flat white paint, Fuller No. 2882 on 2-mil polished aluminum; B = white epoxy resin paint of Mg; C = flat white acrylic resin, Sherwin-Williams M49WC6-CA-10144; MIL-C-15328A pretreatment wash coating on 22-mil 301 stainless steel 1/2 hard; D = white paint mixed with powdered glass, 7-mil on polished aluminum.

TABLE A-1. SPECTRAL EMISSIVITIES OF SOME SELECTED METALS (Ref. 22)

Wave-length, μ	Al foil	Al 25		SS 347		SS 302		Mg alloy 11K 31		Bettelle Mg-Li alloy	Si solar cells	Au		Cr		Be		Cu smooth
		Pol.	SB	Pol.	SB	Pol.	SB	Pol.	SB			Pol.	SB	Pol.	SB	Pol.	SB	
0.4	0.15	0.30	0.50	0.53	0.69	0.60	0.72	0.74	0.75	0.84	0.92	0.67	0.82					0.89
0.44	0.13	0.30	0.49	0.48	0.68	0.58	0.71	0.73	0.76	0.83	0.91	0.67	0.81					0.84
0.48	0.20	0.30	0.49	0.48	0.67	0.55	0.70	0.73	0.78	0.82	0.93	0.63	0.78					0.78
0.52	0.19	0.30	0.48	0.46	0.67	0.52	0.69	0.72	0.78	0.82	0.93	0.63	0.78					0.71
0.56	0.19	0.31	0.48	0.45	0.66	0.51	0.68	0.72	0.78	0.81	0.93	0.63	0.78					0.61
0.60	0.19	0.31	0.48	0.43	0.65	0.51	0.68	0.72	0.78	0.81	0.93	0.63	0.78					0.58
0.64	0.19	0.31	0.48	0.42	0.65	0.51	0.68	0.72	0.78	0.81	0.93	0.63	0.78					0.53
0.68	0.19	0.32	0.41	0.42	0.64	0.48	0.68	0.71	0.78	0.78	0.93	0.63	0.78					0.48
0.70	0.19	0.32	0.49	0.42	0.64	0.48	0.68	0.71	0.78	0.78	0.93	0.63	0.78					0.44
1.0	0.13	0.33	0.50	0.42	0.65			0.71	0.78	0.81	0.93	0.63	0.78					0.40
1.5	0.10	0.16	0.39	0.34	0.62			0.71	0.78	0.81	0.93	0.63	0.78					
2.0	0.07	0.15	0.42	0.31	0.64			0.71	0.78	0.81	0.93	0.63	0.78					
2.5	0.07	0.15	0.35	0.25	0.57			0.71	0.78	0.81	0.93	0.63	0.78					
3.0	0.16	0.42	0.32	0.32	0.54			0.71	0.78	0.81	0.93	0.63	0.78					
3.5	0.17	0.19	0.41	0.31	0.47			0.71	0.78	0.81	0.93	0.63	0.78					
4.0	0.06									0.75	0.84	0.03	0.17	0.07	0.14	0.04	0.31	
4.5	0.06									0.75	0.84	0.03	0.17	0.07	0.14	0.04	0.31	
5.0	0.07									0.75	0.84	0.03	0.17	0.07	0.14	0.04	0.31	
5.5	0.07									0.75	0.84	0.03	0.17	0.07	0.14	0.04	0.31	
6.0	0.06									0.75	0.84	0.03	0.17	0.07	0.14	0.04	0.31	
6.5	0.06									0.75	0.84	0.03	0.17	0.07	0.14	0.04	0.31	
7.0	0.07									0.75	0.84	0.03	0.17	0.07	0.14	0.04	0.31	
7.5	0.08									0.75	0.84	0.03	0.17	0.07	0.14	0.04	0.31	
8.0	0.08									0.75	0.84	0.03	0.17	0.07	0.14	0.04	0.31	
8.5	0.07									0.75	0.84	0.03	0.17	0.07	0.14	0.04	0.31	
9.0	0.08									0.75	0.84	0.03	0.17	0.07	0.14	0.04	0.31	
9.5	0.07									0.75	0.84	0.03	0.17	0.07	0.14	0.04	0.31	
10.0	0.07									0.75	0.84	0.03	0.17	0.07	0.14	0.04	0.31	
10.5	0.06									0.75	0.84	0.03	0.17	0.07	0.14	0.04	0.31	
11.0	0.06									0.75	0.84	0.03	0.17	0.07	0.14	0.04	0.31	
11.5										0.75	0.84	0.03	0.17	0.07	0.14	0.04	0.31	
12.0										0.75	0.84	0.03	0.17	0.07	0.14	0.04	0.31	
12.5										0.75	0.84	0.03	0.17	0.07	0.14	0.04	0.31	
13.0										0.75	0.84	0.03	0.17	0.07	0.14	0.04	0.31	
13.5										0.75	0.84	0.03	0.17	0.07	0.14	0.04	0.31	

Notes: SS = stainless steel
Pol. = polished
SB = sandblasted

TABLE A-2. NORMAL SPECTRAL EMISSIVITIES AT 295°K

	(Wavelength in microns)													
Material	0.50	0.60	0.80	1.0	2.0	3.0	4.0	5.0	7.0	9.0	10	12	14	
Aluminum				0.26	0.18	0.12	0.08	0.07	0.04	0.03	0.02	0.02		
Antimony		0.47	0.46	0.45	0.40	0.35	0.32	0.31	0.29	0.28	0.28		0.28	
Bismuth					0.32	0.25		0.23		0.19			0.17	
Cadmium				0.30	0.13	0.07	0.04	0.04	0.02	0.02	0.02	0.01	0.01	
Chromium	0.45	0.44		0.43		0.30		0.19		0.08				
Cobalt				0.32	0.28	0.23	0.19	0.15	0.07	0.04	0.03	0.03	0.03	
Copper	0.50	0.28		0.10		0.03		0.02		0.02				
Copper, electrolytically deposited	0.47	0.17												
Copper, commercially pure	0.56	0.28		0.10	0.05	0.03		0.03	0.02		0.02		0.02	
Gold				0.62		0.33		0.02		0.02			0.02	
Gold, electrolytically deposited	0.53	0.16		0.04	0.03	0.03	0.03	0.02	0.02	0.02	0.02		0.02	
Graphite	0.79	0.76	0.73	0.73	0.65	0.57	0.52	0.49	0.46	0.42	0.41		0.27	
Iridium				0.22	0.13	0.09	0.06	0.06	0.05	0.04	0.04	0.04		
Iron	0.45	0.43		0.35	0.22	0.16	0.12	0.09	0.07	0.06			0.05	
Lead								0.08		0.06			0.04	
Magnesium	0.28	0.27	0.26	0.23	0.22	0.20	0.16	0.14	0.09	0.07				
Molybdenum	0.55	0.52	0.48	0.42	0.18	0.12	0.10	0.08	0.07	0.06	0.06	0.05		
Nickel				0.27		0.12		0.06		0.04				
Nickel, electrolytically deposited	0.39	0.35		0.28	0.17	0.12	0.09	0.06	0.06	0.05			0.03	
Palladium				0.26	0.19	0.12	0.12	0.10	0.06	0.03	0.03	0.03	0.03	
Platinum		0.45		0.27	0.19	0.11	0.08	0.06	0.05		0.04	0.04	0.04	
Platinum, electrolytically deposited	0.42	0.30		0.27	0.20	0.11	0.09	0.06	0.05				0.04	
Rhodium	0.24	0.23	0.19	0.16	0.09	0.08	0.08	0.07	0.06	0.05	0.05			
Silicon	0.66	0.68	0.71	0.72	0.72		0.72		0.72		0.72			
Silver	0.10	0.07		0.04		0.05		0.03		0.01		0.01	0.01	
Silver, chemically deposited	0.09			0.03	0.02	0.02					0.014		0.01	
Tantalum	0.62	0.55	0.36	0.22	0.10	0.08	0.07	0.07	0.06	0.06			0.05	
Tellurium		0.61	0.52	0.50	0.48	0.47	0.43	0.43	0.32	0.22				
Tin				0.46	0.39	0.32	0.28	0.24	0.19	0.16	0.16	0.15		
Tungsten	0.50	0.18		0.38	0.16	0.06		0.05			0.04	0.04		
Vanadium	0.43	0.41		0.39	0.31	0.26	0.21	0.18	0.12	0.08				
Zinc				0.20	0.08	0.04	0.03	0.03	0.02	0.02	0.02	0.01	0.01	
Mach's magnalium (69 Al + 31 Mg)	0.17	0.17		0.18		0.13		0.11		0.10			0.08	
Steel untempered	0.45	0.45		0.37	0.23	0.17		0.11	0.07	0.07			0.04	
Stellite	0.36			0.31	0.25	0.21	0.18	0.15		0.12		0.11		
Brass, Trobridge				0.09				0.04	0.03	0.02				

Basic References

1. Hottel's table from McAdams, "Heat Transmission," 3d ed., McGraw-Hill Book Company, Inc., New York, 1954.
2. Smithells, "Metals Handbook," Interscience Publishers, Inc., New York, 1949.
3. T. S. Holden and J. J. Greenland, Report R. 6, "The Coefficient of Solar Absorptivity and Low Temperature Emissivity of Various Materials," A Review of Literature to 1951. Commonwealth Scientific and Industrial Research Organization, Division of Building Research, Victoria, Australia.
4. E. Schmidt and L. Furthmann, *Mit. Kaiser-Wilhelm, Inst. Eisenforsch. Dusseldorf* 109, 225 (1928). (Contains comprehensive bibliography.)
5. G. B. Wilkes, "Heat Insulation," John Wiley & Sons, Inc., New York, 1950.
6. R. B. Dingle, *Physica* 19, 311-347 (pt. I, 1953); 348-304 (pt. II, 1953); 729-736 (pt. III, 1953); 1187-1196 (pt. IV, 1953).
7. M. M. Reynolds and M. M. Fulk, unpublished data, NBS, AEC, CEL.
8. "International Critical Tables."
9. M. Jakob, "Heat Transfer," vol. I, John Wiley & Sons, Inc., New York, 1949.
10. G. Ribaud, *Traité de pyrométrie optique, Rev. opt.*, 1931.
11. Landolt-Börnstein tables.
12. "Temperature—Its Measurement and Control in Science and Industry," Reinhold Publishing Corporation, New York, 1941.

TABLE A-3. SPECTRAL EMISSIVITIES OF SOME SELECTED METAL OXIDES AND ORGANIC SUBSTANCES
(Ref. 22)

Wave- Length, μ	Rutile on stainless steel 547			Fiberglass		0.080" fused Si	TiO ₂ paint		ZnO paint, 30% Si resin	Effect of 6-hr UV on TiO ₂ paint, 40% resin	NiO standard	Gray paint, 60 TiO ₂ , 10 C, 23% Si	70% red FeO, 30% Si
	0.010" μ	0.020" μ	0.020" Z	91 L.D	Si G-7		20% Si resin*	50% resin					
0.4	0.23	0.22	0.00	0.94	0.57		0.55	0.55		0.55	0.025	0.50	0.75
0.44	0.22	0.18	0.49	0.94	0.55		0.20	0.20		0.20	0.025	0.79	0.74
0.48	0.20	0.16	0.40	0.94	0.49		0.17	0.17		0.17	0.025	0.78	0.72
0.52	0.20	0.15	0.33	0.94	0.45		0.15	0.15		0.15	0.025	0.79	0.60
0.56	0.21	0.15	0.27	0.93	0.43		0.13	0.13		0.13	0.025	0.73	0.50
0.60	0.22	0.15	0.24	0.91	0.41		0.12	0.13		0.13	0.025	0.60	0.49
0.64	0.22	0.15	0.23	0.85	0.39		0.11	0.13		0.13	0.025	0.80	0.36
0.68	0.22	0.14	0.23	0.79	0.39		0.10	0.13		0.13	0.03	0.80	0.36
0.72	0.22	0.14	0.23	0.76	0.39		0.09	0.13		0.13	0.03	0.80	0.35
1.0	0.30			0.55	0.42		0.15	0.20			0.045	0.15	0.22
1.5	0.34			0.66	0.53		0.30	0.40			0.07	0.16	0.27
2.0	0.44			0.66	0.53		0.46	0.52			0.11	0.17	0.42
2.5	0.39			0.92	0.92		0.65	0.65			0.13	0.17	0.59
3.0	0.46												
3.5	0.38												
4.0	0.35	0.36		0.90	0.93	0.85	0.72	0.70	0.60				0.68
4.5	0.34	0.40		0.88	0.93	0.60	0.64	0.66	0.60				0.65
5.0	0.41	0.43		0.89	0.92	0.63	0.68	0.66	0.63				0.67
5.5	0.54	0.53		0.87	0.90	0.90	0.71	0.74	0.68				0.76
6.0	0.71	0.66		0.87	0.86	0.91	0.81	0.77	0.73				0.84
6.5	0.62	0.76		0.83	0.86	0.91	0.86	0.79	0.77				0.90
7.0	0.85	0.79		0.82	0.86	0.89	0.88	0.81	0.80				0.91
7.5	0.89	0.52		0.82	0.55	0.92	0.88	0.85	0.85				0.90
8.0	0.90	0.87		0.81	0.54	0.77	0.91	0.90	0.87				0.94
8.5	0.93	0.67		0.81	0.64	0.55	0.92	0.93	0.90				0.95
9.0	0.90	0.90		0.78	0.76	0.41	0.90	0.92	0.89				0.92
9.5	0.96	0.85		0.77	0.76	0.61	0.88	0.90	0.87				0.91
10.0	0.77	0.79	0.75	0.77	0.74		0.87	0.90	0.87				0.91
10.5				0.76	0.77	0.83	0.90	0.93	0.88				0.94
11.0				0.76	0.76		0.93	0.95	0.89				0.94
11.5	0.71	0.65		0.75	0.76	0.90	0.95	0.95	0.91				0.94
12.0				0.76	0.76		0.95	0.95	0.89				0.94
12.5	0.75	0.68		0.75	0.76	0.89	0.93	0.92	0.89				0.94
13.0				0.74	0.74		0.91	0.87	0.85				0.94
13.5	0.71	0.62		0.74	0.74		0.91	0.87	0.85				0.94

*Crutile.

TABLE A-4. TOTAL NORMAL EMISSIVITY

Material	Temp., °K	Emissivity (total normal)
Aluminum, annealed (electropolished)	1000†	0.07
	500	0.04
	300	0.03
	300	0.018 (76°K)
	300	0.011 (4°K)
Aluminum oxide layer:		
0.25 μ thick	311	0.06
0.50 μ thick	311	0.11
1.0 μ thick	311	0.30
2.0 μ thick	311	0.65
3.0 μ thick	311	0.70
4.0 μ thick	311	0.70
7.0 μ thick	311	0.75
Aluminum lacquer layer:		
0.5 μ thick	311	0.05
1.0 μ thick	311	0.08
1.5 μ thick	311	0.15
2.0 μ thick	311	0.30
3.0 μ thick	311	0.38
4.0 μ thick	311	0.41
5.0 μ thick	311	0.45
8.0 μ thick	311	0.57
Aluminum:		
Commercial plate	373	0.09
Commercial plate, polished	373	0.05
Commercial plate dipped in HNO ₃	373	0.05
Commercial plate dipped in hot hydroxide	373	0.04
Al vaporized on 0.0005-in. Mylar plastic (both sides)	300	0.04 (76°K)
Antimony	295	0.28
Bismuth	1000†	0.3
	373	0.06-0.19
Brass:		
Polished	373	0.03
Rolled plate	300	0.06
Shim stock 65/35	295	0.029 (76°K)
	205	0.018 (4°K)
Oxidized	500	0.60
	373	0.60
Cadmium	300	0.02
Electroplate (mossy)	295	0.03 (76°K)
Chromium	300-1000	0.08-0.26†
Plated on copper	300	0.08 (76°K)
Plated on iron	370	0.08
Cobalt	295	0.03

TABLE A-4. TOTAL NORMAL EMISSIVITY (Cont.)

Material	Temp., °K	Emissivity (total normal)
Copper:		
Black oxidized.....	300	0.78
Scraped.....	300	0.07
Commercial polish.....	300	0.03
Electrolytic, careful polish.....	353	0.018
Electrolytic, careful polish.....	295	0.015 (76°K)
Chromic acid dip.....	295	0.017 (76°K)
Polished.....	295	0.019 (76°K)
Liquid honed.....	295	0.088 (76°K)
Electrolytic polish.....	295	0.008 (4°K)
Mechanical polish.....	295	0.015 (4°K)
Carefully prepared surface of pure Cu.....	295	0.008 (90°K)
Gold.....	300-1400†	0.02-0.03‡
0.0015-in. foil (on glass or Lucite plastic).....	295	0.01 (76°K)
0.0005-in. foil (on glass or Lucite plastic).....	295	0.016 (76°K)
0.000040-in. foil (on glass or Lucite plastic).....	295	0.023 (76°K)
0.000010-in. leaf (on glass or Lucite plastic).....	295	0.063 (76°K)
Au vaporized onto 2 sides of 0.0005-in. Mylar plastic.....	295	0.02 (76°K)
Au plate 0.0002 in. on stainless steel (1% Ag in Au).....	295	0.025 (76°K)
Au plate 0.0001 in. on stainless steel (1% Ag in Au).....	295	0.027 (76°K)
Au plate 0.00005 in. on stainless steel (1% Ag in Au).....	295	0.027 (76°K)
Au plate 0.0002 in. on copper (1% Ag in Au).....	295	0.025 (76°K)
Iridium.....	295	0.04
Iron:		
Electrolytic.....	450-500	0.05-0.065‡
	533	0.07
	373	0.05
	295	0.05
	300	0.017 (90°K)
Oxidized.....	1500	0.89
	373	0.74
Cast iron, polished.....	311	0.21
Cast iron, oxidized.....	311	0.63
Cast iron, oxidized.....	533	0.66
Cast iron, oxidized.....	811	0.76
Iron sheet, rusted red.....	295	0.69
Galvanized iron.....	365	0.07
Steels:		
Stainless, polished.....	373	0.08
Stainless, type 302.....	300	0.048 (76°K)
Stainless, oxidized.....	300-1000	0.79‡
Lead:		
Unoxidized, polished.....	400-500	0.057-0.075‡
Unoxidized, polished.....	373	0.05
0.004-in. foil.....	295	0.036 (76°K)
	295	0.011 (4°K)

TABLE A-4. TOTAL NORMAL EMISSIVITY (Cont.)

Material	Temp., °K	Em. sivity (total normal)
Oxidized at 473°K.....	473	0.63
Gray oxidized.....	295	0.28
Red lead.....	373	0.93
Magnesium.....	295	0.07
	533	0.13 (295°K)
	811	0.18 (295°K)
	1000	0.21 (295°K)
Manganin, bright rolled.....	391	0.048
	295	0.076 (295°K)
	295	0.073 (90°K)
Mercury.....	273-373†	0.09-0.12†
Molybdenum.....	2300	0.24
	1800	0.19
	1300	0.13
	373	0.07
	295	0.05
Nickel:		
Electrolytic.....	811	0.10
	533	0.07
	311	0.06
	295	0.04
Polished.....	395	0.045
Bright matte.....	395	0.041
0.004-in. foil.....	295	0.022 (76°K)
Electroplated on iron and polished.....	298	0.045
Electroplated on pickled iron and unpolished.....	295	0.11
Electroplated on copper.....	300	0.03 (76°K)
Oxidized.....	1500	0.85
Oxidized.....	500	0.37
Palladium.....	295	0.03
Platinum.....	1367	0.18
	811	0.10
	533	0.06
	373	0.05
	295	0.03
	200	0.016 (85°K)
Rhodium.....	295	0.05
Plated on stainless steel.....	295	0.078 (76°K)
Silver.....	811	0.03
	373	0.025
	295	0.022
	273	0.02
	295	0.008 (76°K)
Tantalum.....	2300	0.26
	1800	0.21
	205	0.05

TABLE A-4. TOTAL NORMAL EMISSIVITY (Cont.)

Material	Temp., °K	Emissivity (total normal)
Tellurium.....	295	0.22
Tin.....	373	0.05
0.001-in. foil.....	295	0.013 (76°K)
	295	0.012 (4°K)
1% indium.....	295	0.012 (4°K)
5% indium.....	295	0.017 (4°K)
Tinned iron sheet.....	297	0.064
Tungsten, filament.....	2300	0.28
	1800	0.23
	1300	0.15
	800	0.088
	500	0.053
	300	0.032
	300	0.019 (85°K)
Zinc.....	295	0.05
	295	0.026 (76°K)
Solder, 50-50 solder on Cu.....	295	0.032 (76°K)
Stellite.....	293	0.11
Monel metal:		
Polished.....	811	0.10 (295°K)
	1367	0.16 (295°K)
Smooth, not polished.....	366	0.16
Everdur, dull.....	366	0.11
Copper-nickel.....	373	0.059
Water.....	273-373	0.92-0.96†
Ice:		
Smooth, H ₂ O.....	273	0.96
Rough crystals.....	273	0.985
Glass.....	293	0.94
Lacquer:		
White.....	373	0.925
Black matte.....	373	0.97
Oil paints, all colors.....	273-373	0.92-0.96†
Enamel.....	295	0.90-0.95
Candlesoot.....	273-373	0.952
Plaster.....	273-373	0.91
Paper.....	373	0.92
Rubber, hard, glossy plate.....	297	0.946
Quartz (fused).....	295	0.932

† Liquid phase.

‡ Linear interpolation fairly accurate.

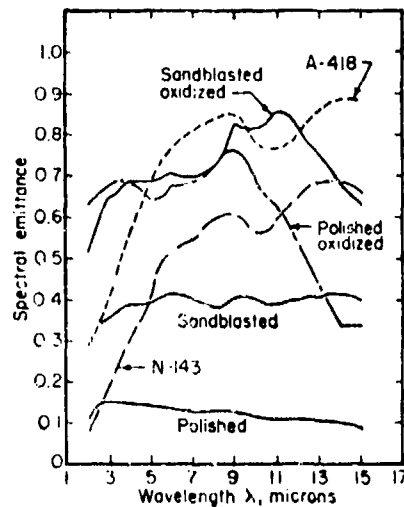


FIGURE A-11. SPECTRAL EMITTANCE CURVES AT 900°F FOR TYPE 321 STAINLESS STEEL SPECIMENS WITH DIFFERENT SURFACE TREATMENTS (COATING THICKNESS APPROXIMATELY 2 MILS). (Ref. 22)

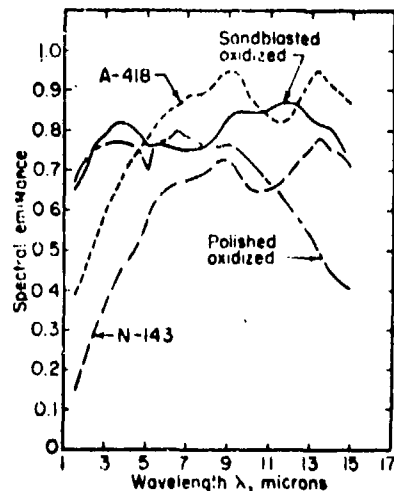


FIGURE A-12. SPECTRAL EMITTANCE CURVES AT 1800°F FOR TYPE 321 STAINLESS STEEL SPECIMENS WITH DIFFERENT SURFACE TREATMENTS (COATING THICKNESS APPROXIMATELY 2 MILS). (Ref. 22)

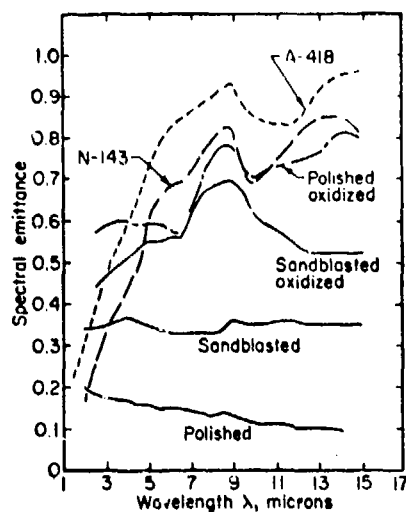


FIGURE A-13. SPECTRAL EMITTANCE CURVES AT 900°F FOR INCONEL SPECIMENS WITH DIFFERENT SURFACE TREATMENTS (COATING THICKNESS APPROXIMATELY 2 MILS). (Ref. 22)

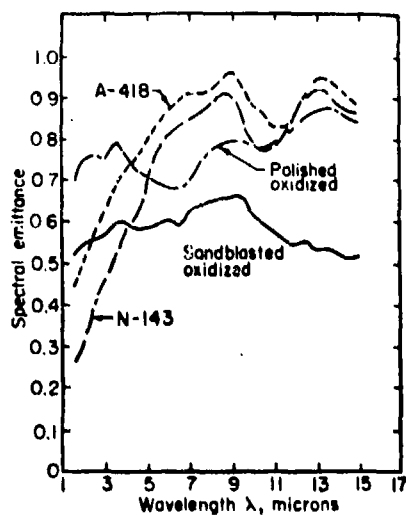


FIGURE A-14. SPECTRAL EMITTANCE CURVES AT 1800°F FOR INCONEL SPECIMENS WITH DIFFERENT SURFACE TREATMENTS (COATING THICKNESS APPROXIMATELY 2 MILS). (Ref. 22)

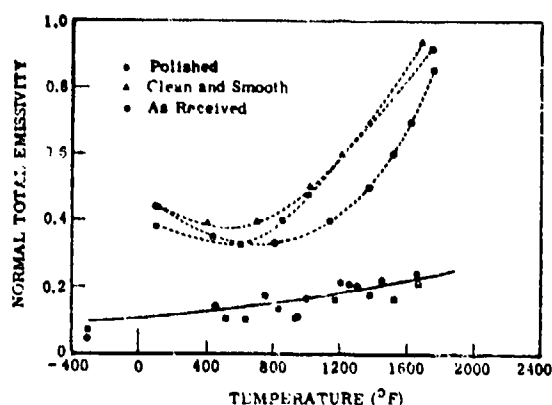


FIGURE A-15. NORMAL TOTAL EMISSIVITY AND TOTAL SOLAR ABSORPTIVITY OF INCONEL X. (Note: temperatures are those to which samples had been heated before tests.)

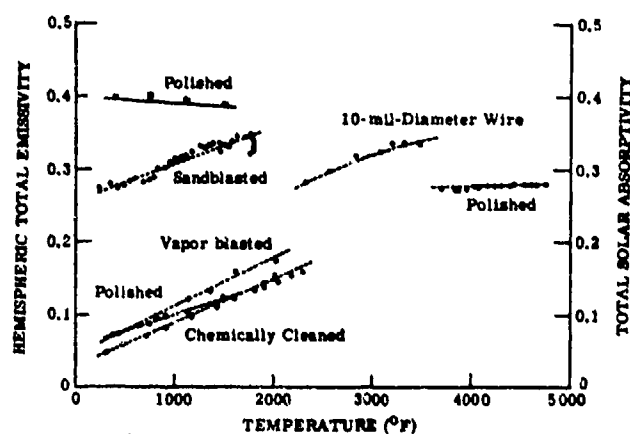


FIGURE A-16. HEMISPHERIC TOTAL EMISSIVITY AND TOTAL SOLAR ABSORPTIVITY OF MOLYBDENUM

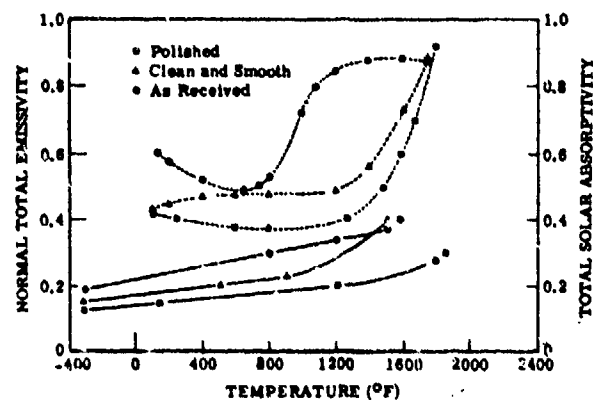


FIGURE A-17. NORMAL TOTAL EMISSIVITY AND TOTAL SOLAR ABSORPTIVITY FOR K-MONEL. (Note: temperatures are those to which samples had been heated before tests.)

June 1974

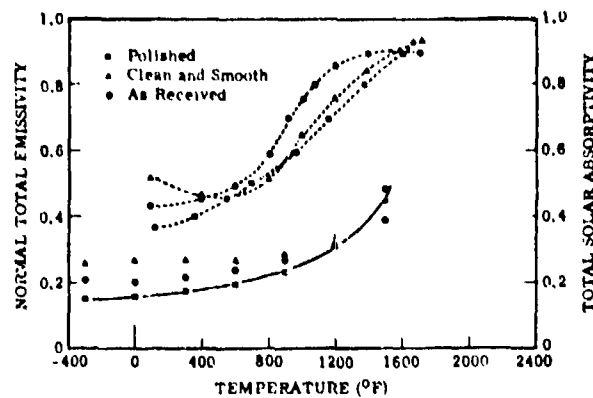


FIGURE A-18. NORMAL TOTAL EMISSIVITY AND TOTAL SOLAR ABSORPTIVITY FOR 301 STAINLESS STEEL. (Note. All measurements made at 100°F. Temperatures are those to which samples had been heated previous to tests.)

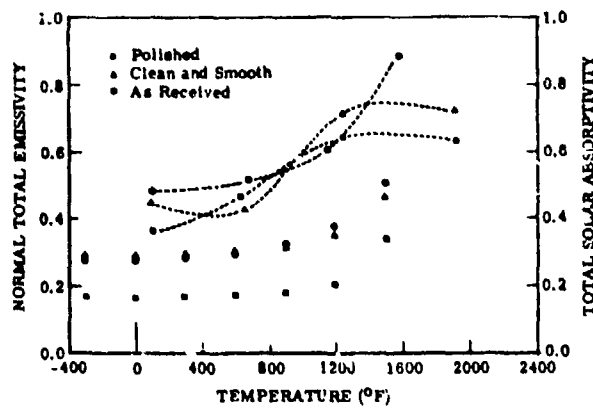


FIGURE A-19. NORMAL TOTAL EMISSIVITY AND TOTAL SOLAR ABSORPTIVITY FOR 316 STAINLESS STEEL. (Note: All measurements made at 100°F. Temperatures are those to which samples had been heated previous to tests.)

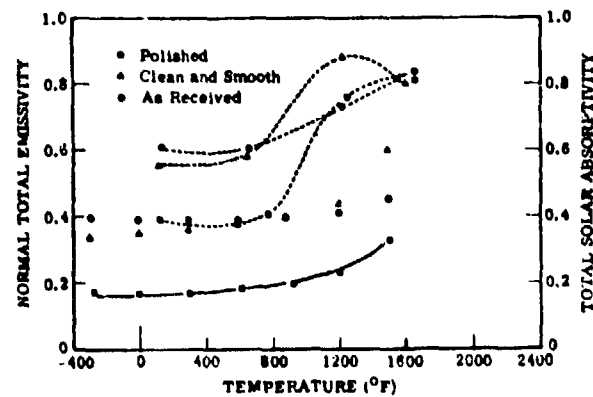


FIGURE A-20. NORMAL TOTAL EMISSIVITY AND TOTAL SOLAR ABSORPTIVITY FOR 347 STAINLESS STEEL. (Note: All measurements made at 100°F. Temperatures are those to which samples had been heated previous to tests.)

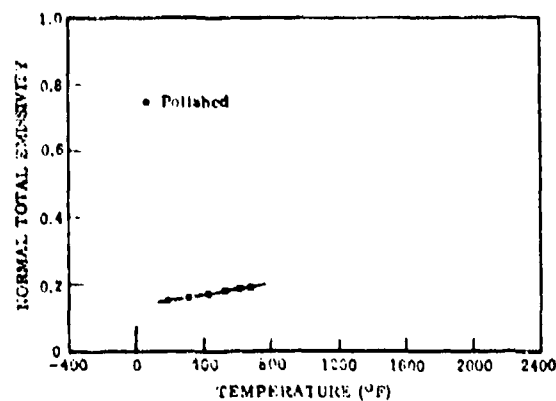


FIGURE A-21. NORMAL TOTAL EMISSIVITY FOR 18-8 STAINLESS STEEL

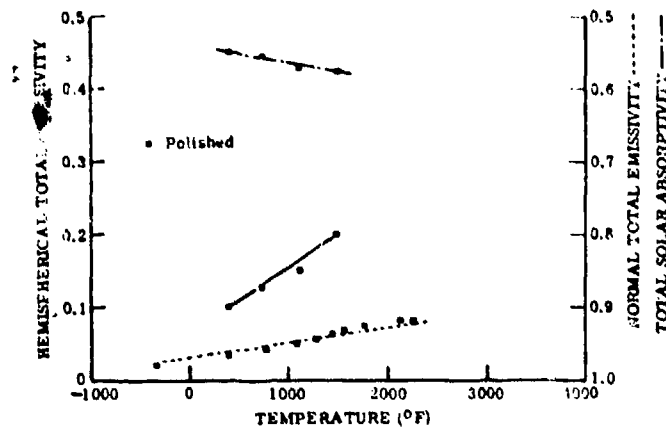


FIGURE A-22. HEMISPHERICAL TOTAL EMISSIVITY, NORMAL TOTAL EMISSIVITY, AND TOTAL SOLAR ABSORPTIVITY FOR TANTALUM

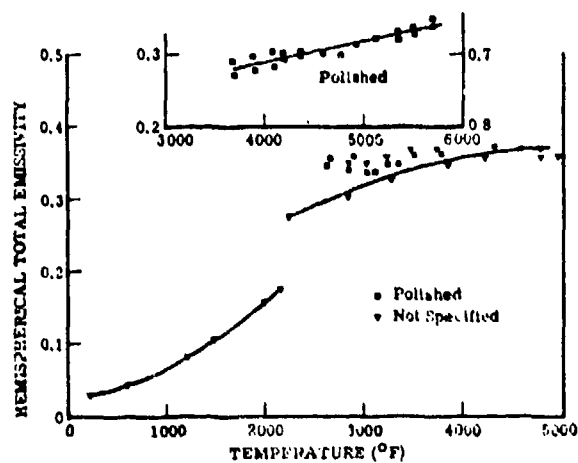


FIGURE A-23. HEMISPHERICAL TOTAL EMISSIVITY OF TUNGSTEN

FTD-CW-01-01-74
Vol. 1

June 1974

APPENDIX B
SPECTRAL CHARACTERISTICS OF BLACKBODY RADIATORS
AND SELECTED ILLUMINATORS

In this appendix the illuminance H or blackbody emittance W_{BB} is considered, which is needed in the radiant emission expressions for vehicle body radiations. We shall consider first radiation emitted by blackbodies in section B.1 and then illumination sources in section B.2.

B.1 BLACKBODY RADIATORS

According to Planck's Law, the emission from a blackbody can be expressed by the relation (Refs. 2 and 35):

$$\frac{dW(\lambda, T)}{d\lambda} = \frac{2\pi hc^2}{\lambda^5 \left[\exp\left\{hc/(k\lambda T)\right\} - 1 \right]} = \frac{3.741294 \times 10^8}{\lambda^5 \left[\exp(14,388.6/\lambda T) - 1 \right]} \cdot \frac{\text{Watts}}{\text{m}^2 \cdot \mu\text{m}} \quad (\text{B.1})$$

where λ is the wavelength in μm , T is in $^\circ\text{K}$, and we used $h = 6.6252 \times 10^{-27}$ erg-sec, $c = 2.99793 \times 10^{10}$ cm/sec, $k = 1.3804 \times 10^{-16}$ erg $^\circ\text{K}^{-1}$. The total radiation from all wavelengths is given by the Stefan-Boltzman relation:

$$W_{\text{tot}} = \int_{\lambda=0}^{\infty} \frac{dW(\lambda, T)}{d\lambda} d\lambda = 5.679 \times 10^{-8} T^4, \quad \frac{\text{Watts}}{\text{m}^2} \quad (\text{B.2})$$

The maximum value of $dW/d\lambda$ is given by:

$$\left(\frac{dW}{d\lambda} \right)_{\text{max}} = 1.90 \times 10^{-11} T^5, \quad \frac{\text{Watts}}{\text{m}^2 \cdot \mu\text{m}} \quad (\text{B.3})$$

June 1974

The wavelength λ_{\max} at which $\frac{dW}{d\lambda} = \left(\frac{dW}{d\lambda}\right)_{\max}$ is given by Wien's displacement law:

$$\lambda_{\max} T = 2897.8 \mu\text{m} \cdot ^\circ\text{K} \quad (\text{B.4})$$

Values for the total radiation from all wavelengths between 0 and λ , that is $W(\lambda, T) = \int_0^\lambda dW(\lambda, T)$ are tabulated in Table B-1, while Table B-2 lists values for $W_{\text{tot}} = \int_0^\infty dW(\lambda, T)$ and W_{\max} .

The total radiation in any wavelength interval between λ_1 and λ_2 , $H(\lambda_1 - \lambda_2, T)$, can be obtained from Tables B-1 and B-2 from the equation:

$$\int_{\lambda_1}^{\lambda_2} dW(\lambda, T) \equiv W(\lambda_2 - \lambda_1, T) = W(\lambda_2, T) - W(\lambda_1, T) \quad (\text{B.5})$$

Instead of the Planck function (B.1) which gives the emitted spectral radiance per unit wavelength interval, the radiance per unit wavenumber interval is often useful:

$$\frac{dW}{d\nu} = \frac{dW}{d\lambda} \frac{d\lambda}{d\nu} = \frac{2\pi h c \nu^3}{\left\{ \exp(hc\nu/kT) - 1 \right\}} = \frac{1.24796 \times 10^{-15} \nu^3}{\left[\exp(1.43886 \nu/T) - 1 \right]}, \quad \frac{\text{Watts}}{\text{m}^2 \cdot \text{Hz}} \quad (\text{B.6})$$

The spectral radiance per unit solid angle or spectral "steradian" is given by (Ref. 2):

$$N_\lambda(\lambda, T, \Omega) = \frac{dW}{d\lambda} \cdot f(\Omega), \quad \frac{\text{Watts}}{\text{m}^2 \cdot \mu\text{m} \cdot \text{ster}} \quad (\text{B.7})$$

TABLE B-1. BLACKBODY RADIATION FUNCTIONS

$\lambda T,$ $\mu\text{m} \cdot \text{deg}$	$\frac{dW/d\lambda}{(dW/d\lambda)_{\text{max}}}$	$\frac{\int_0^\lambda \frac{dW}{d\lambda} d\lambda}{\int_0^\infty \frac{dW}{d\lambda} d\lambda}$	$\lambda T,$ $\mu\text{m} \cdot \text{deg}$	$\frac{dW/d\lambda}{(dW/d\lambda)_{\text{max}}}$	$\frac{\int_0^\lambda \frac{dW}{d\lambda} d\lambda}{\int_0^\infty \frac{dW}{d\lambda} d\lambda}$
500	2.999×10^{-7}	1.316×10^{-9}	800	1.382×10^{-3}	1.657×10^{-5}
510	4.775×10^{-7}	2.184×10^{-9}	810	1.621×10^{-3}	1.997×10^{-5}
520	7.452×10^{-7}	3.552×10^{-9}	820	1.893×10^{-3}	2.395×10^{-5}
530	1.142×10^{-6}	5.665×10^{-9}	830	2.201×10^{-3}	2.859×10^{-5}
540	1.718×10^{-6}	8.871×10^{-9}	840	2.548×10^{-3}	3.398×10^{-5}
550	2.545×10^{-6}	1.366×10^{-8}	850	2.938×10^{-3}	4.020×10^{-5}
560	3.709×10^{-6}	2.068×10^{-8}	860	3.373×10^{-3}	4.735×10^{-5}
570	5.326×10^{-6}	3.084×10^{-8}	870	3.859×10^{-3}	5.555×10^{-5}
580	7.544×10^{-6}	4.532×10^{-8}	880	4.397×10^{-3}	6.491×10^{-5}
590	1.054×10^{-5}	6.568×10^{-8}	890	4.993×10^{-3}	7.556×10^{-5}
600	1.455×10^{-5}	9.395×10^{-8}	900	5.651×10^{-3}	8.763×10^{-5}
610	1.985×10^{-5}	1.327×10^{-7}	910	6.373×10^{-3}	1.013×10^{-4}
620	2.676×10^{-5}	1.853×10^{-7}	920	7.165×10^{-3}	1.166×10^{-4}
630	3.570×10^{-5}	2.558×10^{-7}	930	8.030×10^{-3}	1.339×10^{-4}
640	4.713×10^{-5}	3.493×10^{-7}	940	8.973×10^{-3}	1.532×10^{-4}
650	6.113×10^{-5}	4.721×10^{-7}	950	9.998×10^{-3}	1.747×10^{-4}
660	7.984×10^{-5}	6.319×10^{-7}	960	1.111×10^{-2}	1.986×10^{-4}
670	1.025×10^{-4}	8.380×10^{-7}	970	1.231×10^{-2}	2.252×10^{-4}
680	1.305×10^{-4}	1.101×10^{-6}	980	1.360×10^{-2}	2.546×10^{-4}
690	1.649×10^{-4}	1.435×10^{-6}	990	1.500×10^{-2}	2.870×10^{-4}
700	2.066×10^{-4}	1.856×10^{-6}	1000	1.649×10^{-2}	3.228×10^{-4}
710	2.571×10^{-4}	2.380×10^{-6}	1050	2.563×10^{-2}	5.591×10^{-4}
720	3.176×10^{-4}	3.030×10^{-6}	1100	3.785×10^{-2}	9.162×10^{-4}
730	3.897×10^{-4}	3.831×10^{-6}	1150	5.350×10^{-2}	1.431×10^{-3}
740	4.751×10^{-4}	4.810×10^{-6}	1200	7.281×10^{-2}	2.145×10^{-3}
750	5.757×10^{-4}	5.999×10^{-6}	1250	9.588×10^{-2}	3.099×10^{-3}
760	6.934×10^{-4}	7.436×10^{-6}	1300	1.227×10^{-1}	4.336×10^{-3}
770	8.304×10^{-4}	9.162×10^{-6}	1350	1.530×10^{-1}	5.897×10^{-3}
780	9.891×10^{-4}	1.122×10^{-5}	1400	1.866×10^{-1}	7.822×10^{-3}
790	1.172×10^{-3}	1.367×10^{-5}	1450	2.232×10^{-1}	1.015×10^{-2}

TABLE B-1. BLACKBODY RADIATION FUNCTIONS (Cont.)

$\lambda T,$ $\mu\text{m} \cdot \text{deg}$	$\frac{dW/d\lambda}{(dW/d\lambda)_{\text{max}}}$	$\frac{\int_0^\lambda \frac{dW}{d\lambda} d\lambda}{\int_0^\infty \frac{dW}{d\lambda} d\lambda}$	$\lambda T,$ $\mu\text{m} \cdot \text{deg}$	$\frac{dW/d\lambda}{(dW/d\lambda)_{\text{max}}}$	$\frac{\int_0^\lambda \frac{dW}{d\lambda} d\lambda}{\int_0^\infty \frac{dW}{d\lambda} d\lambda}$
1500	2.622×10^{-1}	1.290×10^{-2}	6200	3.453×10^{-1}	7.544×10^{-1}
1550	3.032×10^{-1}	1.610×10^{-2}	6400	3.193×10^{-1}	7.694×10^{-1}
1600	3.457×10^{-1}	1.979×10^{-2}	6600	2.956×10^{-1}	7.834×10^{-1}
1650	3.892×10^{-1}	2.396×10^{-2}	6800	2.737×10^{-1}	7.963×10^{-1}
1700	4.332×10^{-1}	2.862×10^{-2}	7000	2.537×10^{-1}	8.083×10^{-1}
1750	4.772×10^{-1}	3.379×10^{-2}	7200	2.354×10^{-1}	8.194×10^{-1}
1800	5.208×10^{-1}	3.946×10^{-2}	7400	2.185×10^{-1}	8.297×10^{-1}
1850	5.636×10^{-1}	4.561×10^{-2}	7600	2.030×10^{-1}	8.392×10^{-1}
1900	6.053×10^{-1}	5.225×10^{-2}	7800	1.888×10^{-1}	8.481×10^{-1}
1950	6.455×10^{-1}	5.935×10^{-2}	8000	1.758×10^{-1}	8.564×10^{-1}
2000	6.840×10^{-1}	6.690×10^{-2}	8200	1.638×10^{-1}	8.641×10^{-1}
2200	8.169×10^{-1}	1.011×10^{-1}	8400	1.528×10^{-1}	8.713×10^{-1}
2400	9.126×10^{-1}	1.405×10^{-1}	8600	1.426×10^{-1}	8.780×10^{-1}
2600	9.712×10^{-1}	1.834×10^{-1}	8800	1.332×10^{-1}	8.843×10^{-1}
2800	9.972×10^{-1}	2.282×10^{-1}	9000	1.246×10^{-1}	8.901×10^{-1}
3000	9.971×10^{-1}	2.736×10^{-1}	9200	1.166×10^{-1}	8.956×10^{-1}
3200	9.771×10^{-1}	3.185×10^{-1}	9400	1.093×10^{-1}	9.007×10^{-1}
3400	9.432×10^{-1}	3.621×10^{-1}	9600	1.024×10^{-1}	9.055×10^{-1}
3600	8.999×10^{-1}	4.040×10^{-1}	9800	9.613×10^{-2}	9.100×10^{-1}
3800	8.512×10^{-1}	4.438×10^{-1}	10,000	9.029×10^{-2}	9.143×10^{-1}
4000	7.997×10^{-1}	4.813×10^{-1}	11,000	6.679×10^{-2}	9.319×10^{-1}
4200	7.475×10^{-1}	5.164×10^{-1}	12,000	5.035×10^{-2}	9.451×10^{-1}
4400	6.961×10^{-1}	5.492×10^{-1}	13,000	3.862×10^{-2}	9.551×10^{-1}
4600	6.464×10^{-1}	5.796×10^{-1}	14,000	3.007×10^{-2}	9.629×10^{-1}
4800	5.990×10^{-1}	6.079×10^{-1}	15,000	2.375×10^{-2}	9.690×10^{-1}
5000	5.543×10^{-1}	6.341×10^{-1}	16,000	1.899×10^{-2}	9.738×10^{-1}
5200	5.125×10^{-1}	6.583×10^{-1}	17,000	1.536×10^{-2}	9.777×10^{-1}
5400	4.735×10^{-1}	6.807×10^{-1}	18,000	1.255×10^{-2}	9.808×10^{-1}
5600	4.375×10^{-1}	7.013×10^{-1}	19,000	1.035×10^{-2}	9.834×10^{-1}
5800	4.042×10^{-1}	7.204×10^{-1}	20,000	8.612×10^{-3}	9.856×10^{-1}
6000	3.735×10^{-1}	7.381×10^{-1}			

TABLE B-2. TOTAL BLACKBODY RADIATION

$T, ^\circ K$	$W_{\text{tot}} = \int_0^\infty \frac{dW}{d\lambda} d\lambda,$ Watt m^{-2}	$(dW/d\lambda)_{\text{max}},$ Watt $m^{-2} \mu m^{-1}$	$T, ^\circ K$	$W_{\text{tot}} = \int_0^\infty \frac{dW}{d\lambda} d\lambda,$ Watt m^{-2}	$(dW/d\lambda)_{\text{max}},$ Watt $m^{-2} \mu m^{-1}$
1	5.679×10^{-8}	1.290×10^{-12}	250	2.218×10^2	1.260×10
5	3.549×10^{-5}	4.030×10^{-8}	260	2.595×10^2	1.532×10
10	5.679×10^{-4}	1.290×10^{-6}	270	3.018×10^2	1.851×10
15	2.875×10^{-3}	9.794×10^{-6}	280	3.491×10^2	2.220×10
20	9.086×10^{-3}	4.127×10^{-5}	290	4.017×10^2	2.645×10
30	4.600×10^{-2}	3.134×10^{-4}	300	4.600×10^2	3.134×10
40	1.454×10^{-1}	1.321×10^{-3}	310	5.245×10^2	3.692×10
50	3.549×10^{-1}	4.030×10^{-3}	320	5.955×10^2	4.328×10
60	7.360×10^{-1}	1.003×10^{-2}	330	6.735×10^2	5.047×10
70	1.364	2.168×10^{-2}	340	7.589×10^2	5.860×10
80	2.326	4.226×10^{-2}	350	8.522×10^2	6.774×10
90	3.726	7.616×10^{-2}	360	9.538×10^2	7.799×10
100	5.679	1.290×10^{-1}	370	1.065×10^3	8.944×10
110	8.315	2.077×10^{-1}	380	1.184×10^3	1.022×10^2
120	1.178×10	3.209×10^{-1}	390	1.314×10^3	1.164×10^2
130	1.622×10	4.789×10^{-1}	400	1.454×10^3	1.321×10^2
140	2.181×10	6.936×10^{-1}	410	1.605×10^3	1.494×10^2
150	2.875×10	9.794×10^{-1}	420	1.768×10^3	1.686×10^2
160	3.722×10	1.352	430	1.942×10^3	1.896×10^2
170	4.743×10	1.831	440	2.128×10^3	2.127×10^2
180	5.961×10	2.437	450	2.328×10^3	2.380×10^2
190	7.401×10	3.194	460	2.542×10^3	2.656×10^2
200	9.086×10	4.127	470	2.771×10^3	2.958×10^2
210	1.105×10^2	5.267	480	3.015×10^3	3.286×10^2
220	1.331×10^2	6.647	490	3.274×10^3	3.643×10^2
230	1.590×10^2	8.301	500	3.549×10^3	4.030×10^2
240	1.885×10^2	1.027×10	520	4.152×10^3	4.904×10^2

TABLE B-2. TOTAL BLACKBODY RADIATION (Cont.)

$T, ^\circ K$	$W_{\text{tot}} = \int_0^\infty \frac{dW}{d\lambda} d\lambda,$ Watt m^{-2}	$(dW/d\lambda)_{\text{max}},$ Watt $m^{-2} \mu m^{-1}$	$T, ^\circ K$	$W_{\text{tot}} = \int_0^\infty \frac{dW}{d\lambda} d\lambda,$ Watt m^{-2}	$(dW/d\lambda)_{\text{max}},$ Watt $m^{-2} \mu m^{-1}$
540	4.829×10^3	5.922×10^2	1080	7.726×10^4	1.895×10^4
560	5.585×10^3	7.103×10^2	1100	8.315×10^4	2.077×10^4
580	6.426×10^3	8.465×10^2	1120	8.937×10^4	2.273×10^4
600	7.360×10^3	1.003×10^3	1140	9.591×10^4	2.483×10^4
620	8.392×10^3	1.182×10^3	1160	1.029×10^5	2.709×10^4
640	9.527×10^3	1.385×10^3	1180	1.101×10^5	2.951×10^4
660	1.078×10^4	1.615×10^3	1200	1.178×10^5	3.209×10^4
680	1.215×10^4	1.875×10^3	1220	1.258×10^5	3.486×10^4
700	1.364×10^4	2.168×10^3	1240	1.343×10^5	3.781×10^4
720	1.527×10^4	2.496×10^3	1260	1.432×10^5	4.096×10^4
740	1.703×10^4	2.862×10^3	1280	1.525×10^5	4.431×10^4
760	1.895×10^4	3.270×10^3	1300	1.622×10^5	4.789×10^4
780	2.102×10^4	3.724×10^3	1320	1.725×10^5	5.169×10^4
800	2.326×10^4	4.226×10^3	1340	1.832×10^5	5.572×10^4
820	2.567×10^4	4.782×10^3	1360	1.943×10^5	6.001×10^4
840	2.827×10^4	5.394×10^3	1380	2.059×10^5	6.455×10^4
860	3.106×10^4	6.067×10^3	1400	2.181×10^5	6.936×10^4
880	3.406×10^4	6.806×10^3	1420	2.309×10^5	7.446×10^4
900	3.726×10^4	7.616×10^3	1440	2.442×10^5	7.986×10^4
920	4.069×10^4	8.500×10^3	1460	2.580×10^5	8.556×10^4
940	4.434×10^4	9.465×10^3	1480	2.724×10^5	9.158×10^4
960	4.824×10^4	1.052×10^4	1500	2.875×10^5	9.794×10^4
980	5.239×10^4	1.166×10^4	1520	3.031×10^5	1.046×10^5
1000	5.679×10^4	1.290×10^4	1540	3.194×10^5	1.117×10^5
1020	6.147×10^4	1.424×10^4	1560	3.363×10^5	1.192×10^5
1040	6.644×10^4	1.569×10^4	1580	3.539×10^5	1.270×10^5
1060	7.170×10^4	1.726×10^4	1600	3.722×10^5	1.352×10^5

TABLE B-2. TOTAL BLACKBODY RADIATION (Cont.)

$T, ^\circ K$	$W_{tot} = \int_0^\infty \frac{dW}{d\lambda} d\lambda,$ Watt m^{-2}	$(dW/d\lambda)_{max},$ Watt $m^{-2} \mu m^{-1}$	$T, ^\circ K$	$W_{tot} = \int_0^\infty \frac{dW}{d\lambda} d\lambda,$ Watt m^{-2}	$(dW/d\lambda)_{max},$ Watt $m^{-2} \mu m^{-1}$
1620	3.912×10^5	1.439×10^5	2700	3.018×10^6	1.851×10^6
1640	4.108×10^5	1.530×10^5	2800	3.491×10^6	2.220×10^6
1660	4.312×10^5	1.626×10^5	2900	4.017×10^6	2.645×10^6
1680	4.524×10^5	1.726×10^5	3000	4.600×10^6	3.134×10^6
1700	4.743×10^5	1.831×10^5	3100	5.245×10^6	3.692×10^6
1720	4.971×10^5	1.942×10^5	3200	5.955×10^6	4.328×10^6
1740	5.206×10^5	2.057×10^5	3300	6.735×10^6	5.047×10^6
1760	5.450×10^5	2.178×10^5	3400	7.589×10^6	5.860×10^6
1780	5.701×10^5	2.305×10^5	3500	8.522×10^6	6.774×10^6
1800	5.961×10^5	2.437×10^5	3600	9.538×10^6	7.799×10^6
1820	6.231×10^5	2.575×10^5	3700	1.065×10^7	8.944×10^6
1840	6.509×10^5	2.720×10^5	3800	1.184×10^7	1.022×10^7
1860	6.797×10^5	2.871×10^5	3900	1.314×10^7	1.164×10^7
1880	7.094×10^5	3.029×10^5	4000	1.454×10^7	1.321×10^7
1900	7.401×10^5	3.194×10^5	4500	2.328×10^7	2.380×10^7
1920	7.718×10^5	3.365×10^5	5000	3.549×10^7	4.030×10^7
1940	8.044×10^5	3.544×10^5	5500	5.197×10^7	6.491×10^7
1960	8.381×10^5	3.731×10^5	6000	7.360×10^7	1.003×10^8
1980	8.729×10^5	3.925×10^5	6500	1.014×10^8	1.496×10^8
2000	9.086×10^5	4.127×10^5	7000	1.364×10^8	2.168×10^8
2100	1.105×10^6	5.267×10^5	7500	1.797×10^8	3.061×10^8
2200	1.331×10^6	6.647×10^5	8000	2.326×10^8	4.226×10^8
2300	1.590×10^6	8.301×10^5	8500	2.964×10^8	5.723×10^8
2400	1.885×10^6	1.027×10^6	9000	3.726×10^8	7.616×10^8
2500	2.218×10^6	1.260×10^6	9500	4.626×10^8	9.980×10^8
2600	2.595×10^6	1.532×10^6	10000	5.679×10^8	1.290×10^9

where $f(\Omega) = \frac{1}{2\pi}$ for an isotropically emitting surface and $f(\Omega) = (\cos\theta)/\pi$ for a diffusely emitting surface (θ = angle with the normal to the surface).

Values for $N_{\lambda}^0 = N_{\lambda}(\lambda, T, \theta=0) = \frac{1}{\pi} \frac{dW}{d\lambda}$ are plotted in Figure B-1, while in Figure B-2 curves for $N_{\nu}^0 = N_{\nu}(\nu, T, \theta=0) = \frac{1}{\pi} \frac{dW}{d\nu}$ are shown. Figure B-3 shows plots of the same functions on a linear scale instead of the logarithmic scale employed in Figures B-1 and B-2.

Instead of the energy flux expressions (B.1) through (B.6) it is often useful to employ photon flux or "fluence" expressions which are related to W , H , and N by a factor $1/h\nu$. For example the photon fluence $\Phi_{\lambda}(\lambda, T, \Omega) = \frac{1}{h\nu} N_{\lambda}(\lambda, T, \Omega)$ and $\Phi_{\nu}(\nu, T, \Omega) = \frac{1}{h\nu} N_{\nu}(\nu, T, \Omega)$. In Figures B-4 through B-6 curves of $\Phi_{\lambda}(\lambda, T, \theta=0)$ and $\Phi_{\nu}(\nu, T, \theta=0)$ are shown.

For so-called "gray bodies," Kirchhoff's Law states that the emission W_{GB} may be expressed by:

$$\frac{dW_{GB}}{d\lambda} = \epsilon(\lambda) \frac{dW_{BB}}{d\lambda}, \quad \frac{\text{Watts}}{\text{m}^2 \mu\text{m}}, \quad (\text{B.8})$$

where $\epsilon(\lambda)$ is the emissivity. If $\epsilon(\lambda) \approx \bar{\epsilon}$ is constant or may be averaged over the wavelength range from λ_1 and λ_2 , as is often the case, we can write:

$$W_{GB}(\lambda_1 - \lambda_2, T) = \bar{\epsilon} W_{BB}(\lambda_1 - \lambda_2, T) \quad (\text{B.9})$$

Values for $\bar{\epsilon}$ and $\epsilon(\lambda)$ are given in Appendix A.

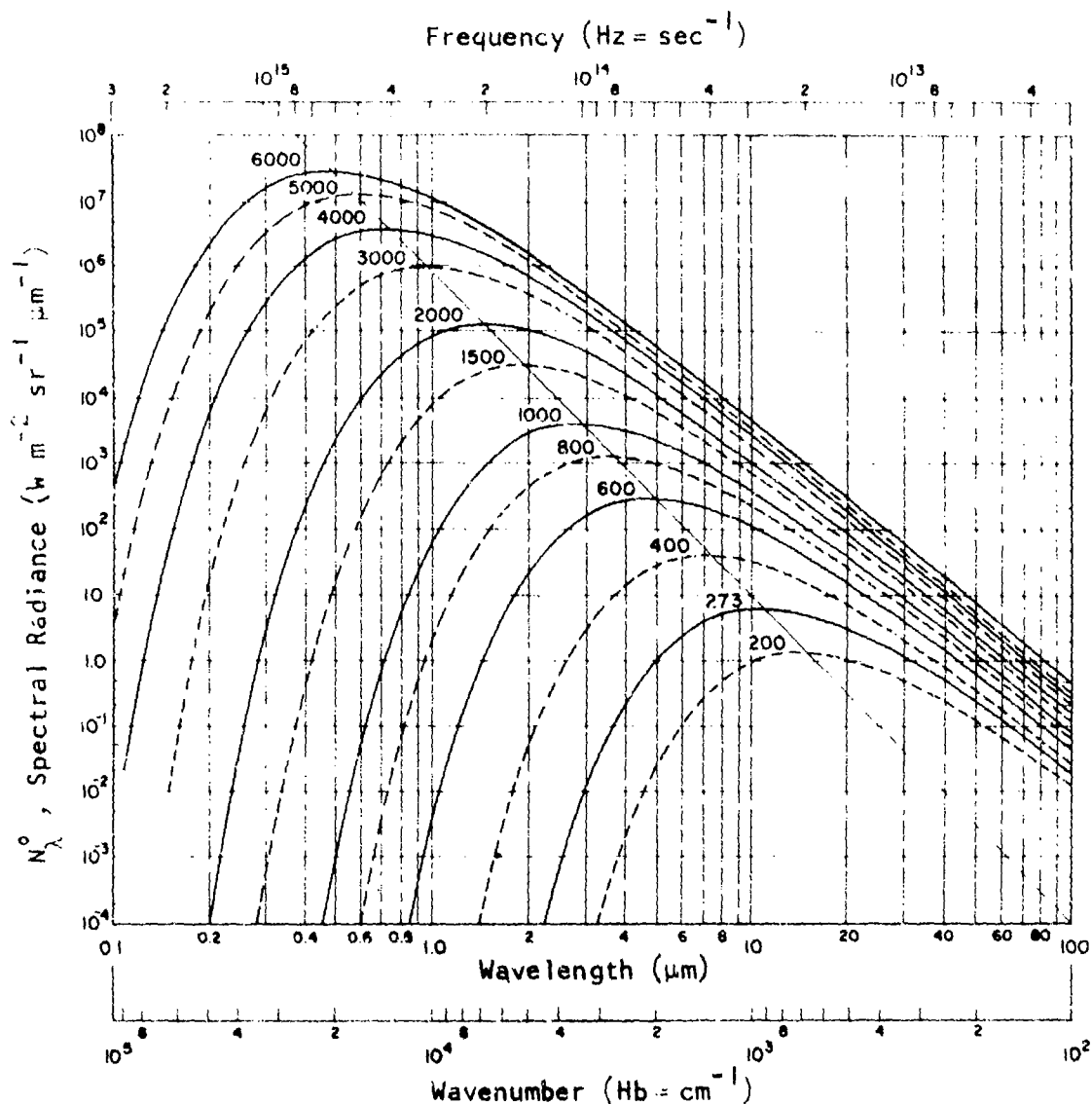


FIGURE B-1. SPECTRAL RADIANCE CURVES OF A BLACKBODY PER UNIT WAVELENGTH. The temperature in $^{\circ}\text{K}$ is shown on each curve; beyond $100 \mu\text{m}$ the curves continue to be linear (plotted on logarithmic scales). The diagonal line, intersecting the curves at their maxima, shows Wien's displacement law. Subdivision of the ordinate scale are at 2 and 5. (Figure after P. R. Gast, Ref. 24.)

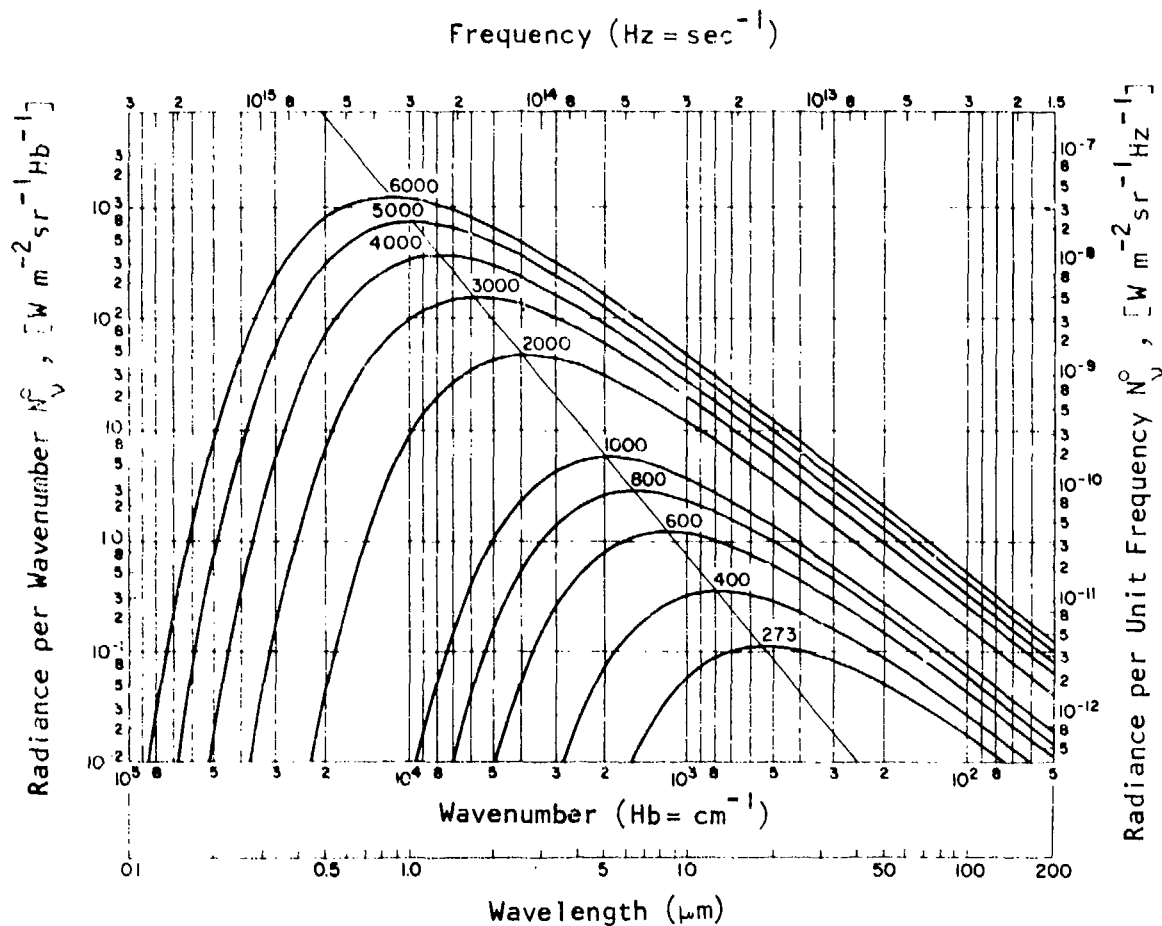


FIGURE B-2. SPECTRAL RADIANCE CURVES OF A BLACKBODY PER UNIT FREQUENCY. Temperatures are given in $^{\circ}\text{K}$ on each curve. At frequencies less than 3×10^{12} Hz or wavenumber 100 Hb, the curves continue to be linear (plotted on logarithmic scales). The diagonal line, intersecting the curves at their maxima, shows Wien's displacement law. (Figure from P. R. Gast, Ref. 24.)

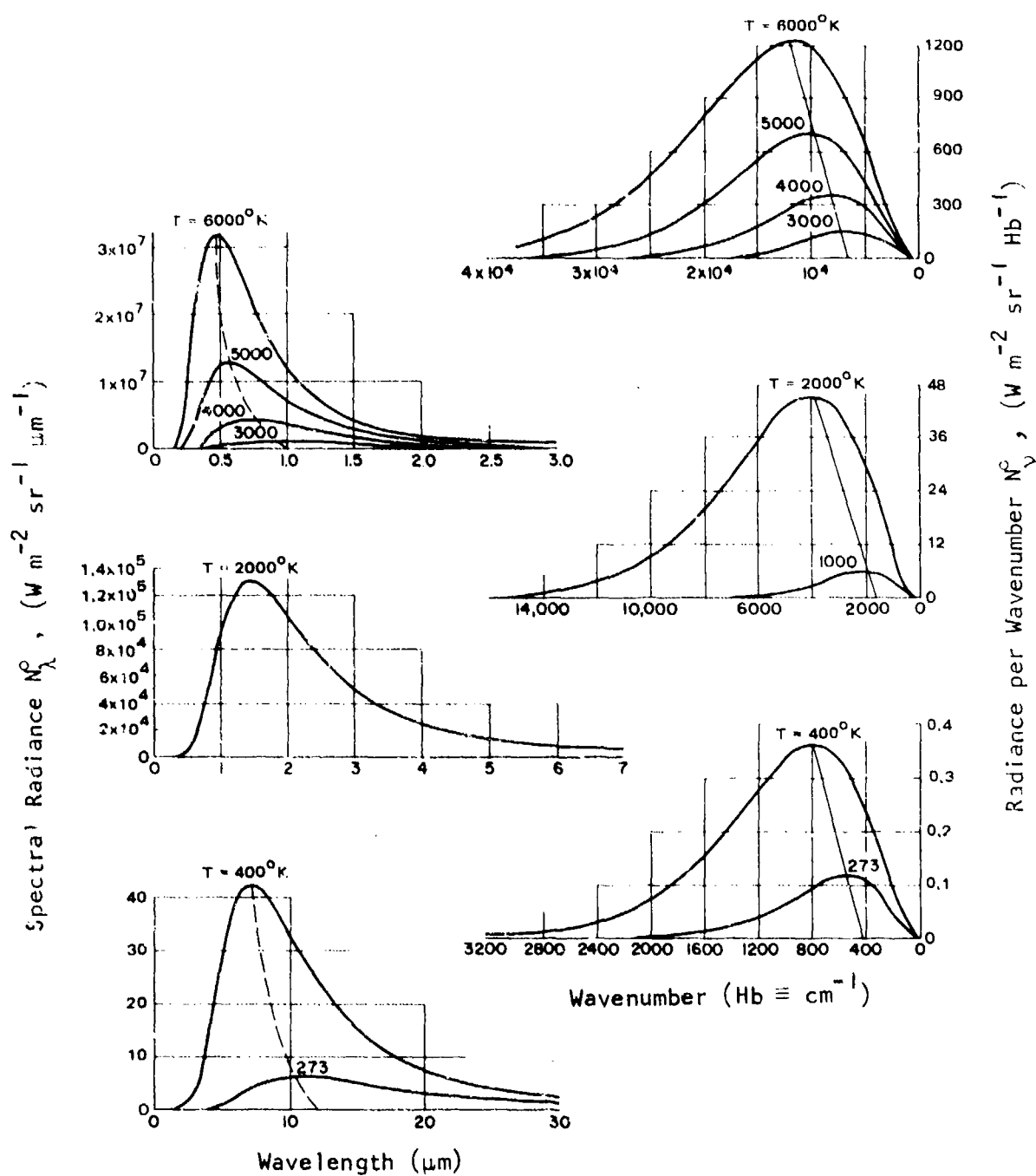


FIGURE B-3. SPECTRAL RADIANCES PER UNIT WAVELENGTH AND PER UNIT FREQUENCY FOR BLACKBODIES AT VARIOUS TEMPERATURES ($^{\circ}\text{K}$) PLOTTED ON ARITHMETIC SCALES. The dashed and diagonal lines show Wien's displacement law. (Figure from P. R. Gast, Ref. 24.)

June 1974

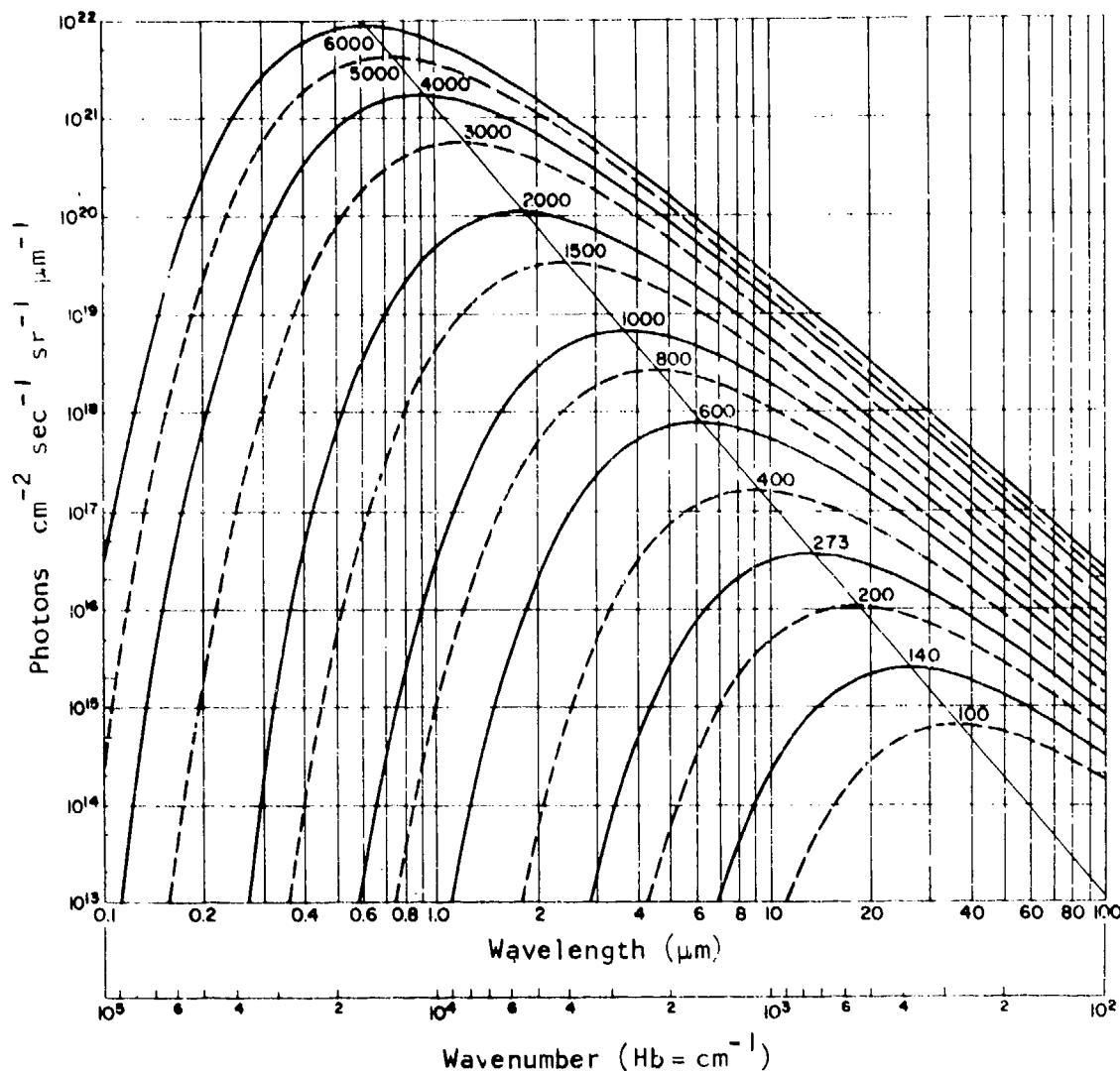


FIGURE B-4. SPECTRAL PHOTON FLUENCE PER UNIT WAVELENGTH FROM A BLACKBODY AT VARIOUS TEMPERATURES ($^{\circ}\text{K}$). The diagonal line, intersecting the curves at their maxima, shows Wien's displacement law. (Figure from P. R. Gast, Ref. 24.)

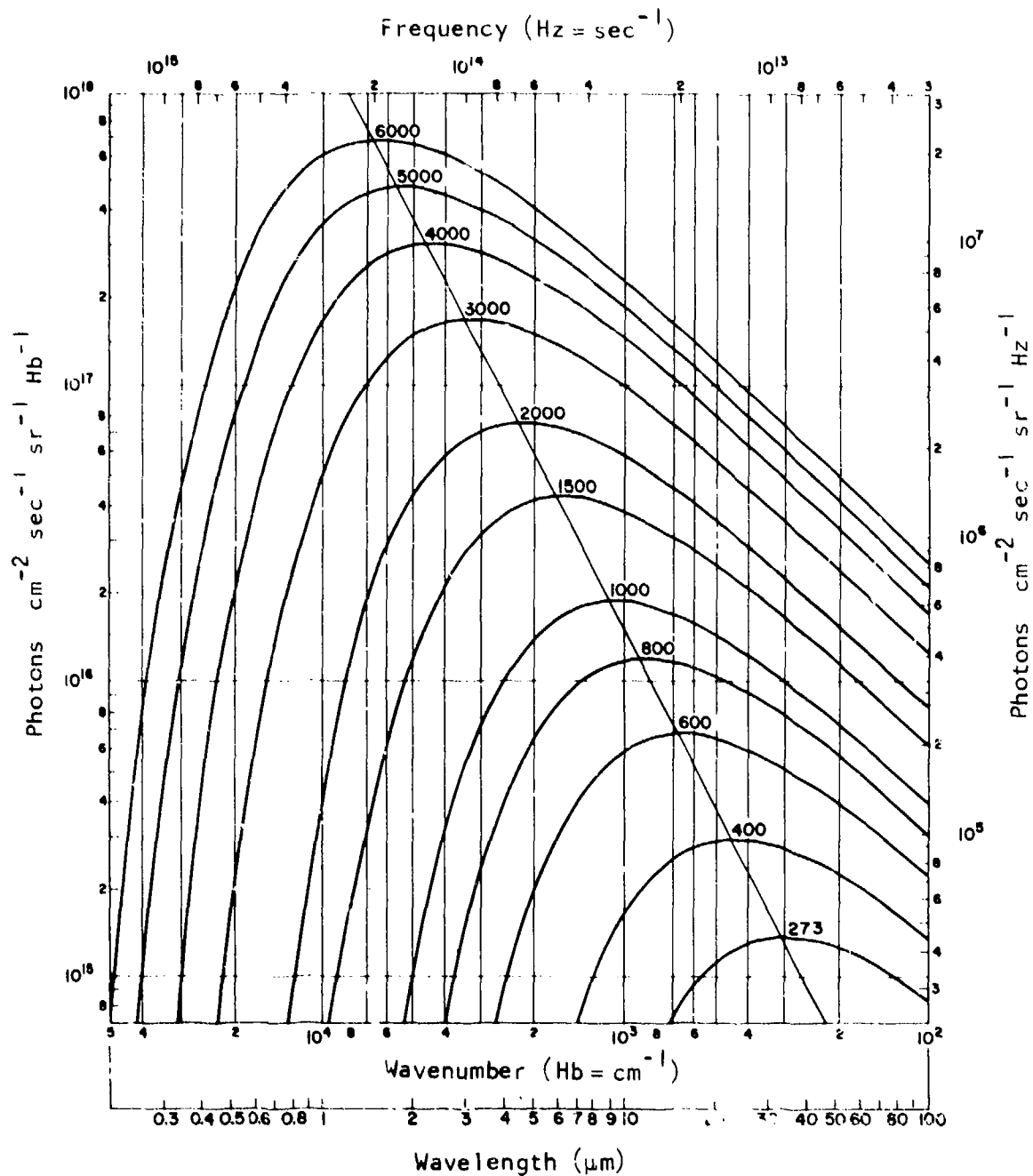


FIGURE B-5. SPECTRAL PHOTON FLUENCE PER UNIT FREQUENCY FROM A BLACKBODY AT VARIOUS TEMPERATURES ($^{\circ}\text{K}$). The diagonal line, intersecting the curves at their maxima, shows Wien's displacement law. (Figure from P. R. Gast, Ref. 24.)

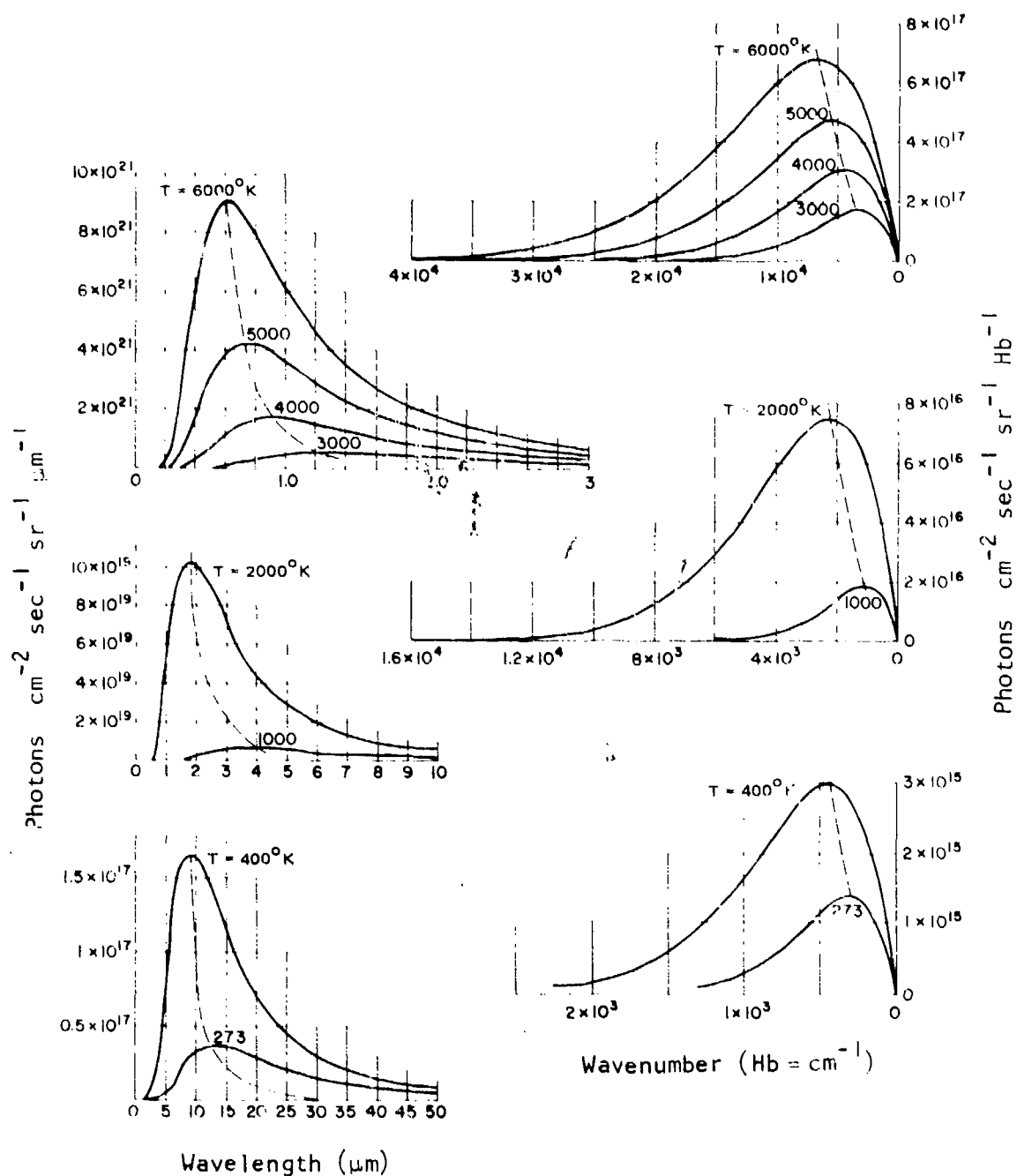


FIGURE B-6. PHOTON FLUENCES EMITTED BY BLACKBODIES AT VARIOUS TEMPERATURES ($^\circ\text{K}$) PLOTTED ON ARITHMETIC SCALES. (Figure from P. R. Gast, Ref. 24.)

B.2 SOLAR AND PLANETARY ILLUMINATORS

The main sources of illumination which will be encountered in space vehicle observation work are:

Natural Sources

- a. Sun
- b. Earthshine
- c. Moon, Planet, and Star Light

Man-made Sources

- d. Lasers
- Radars

In the following we shall briefly review the intensity and spectrum of natural illuminators.

The radiation received from the sun outside the earth's atmosphere has a spectral distribution as shown in Figures B-7 and B-8 (see also Figure 2-4 and Table 2-4 of section 2 of the main text). This distribution is close to that of a blackbody radiator at 5800°K. The radiation energy flux from the sun near the earth is $H_s = 1390 \text{ Watts/m}^2$. Since this radiation originated at a distance of 1.496×10^{11} meters or 92,950,000 miles from the earth from a source 6.95×10^8 meters (432,500 miles) in diameter, it may for all practical purposes be considered to propagate unidirectionally or parallel over the 1 to 100-meter dimensions of typical space vehicles.

Figure B-7 shows the approximately 40 percent of the solar irradiation is in the visible, 9 percent in the UV, and 51 percent in the infrared. We have thus that:

June 1974

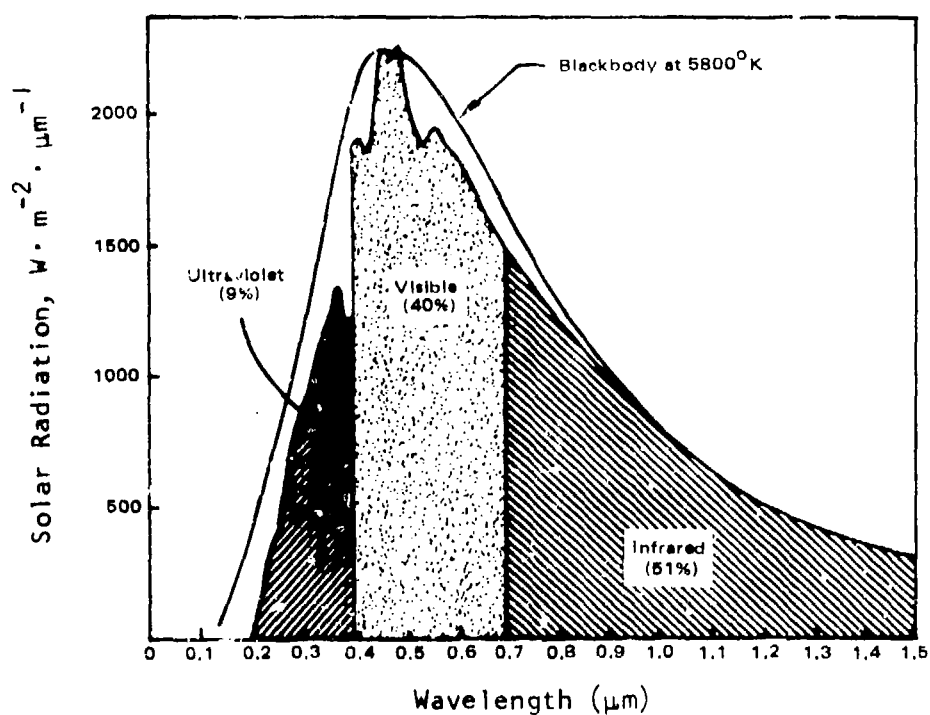
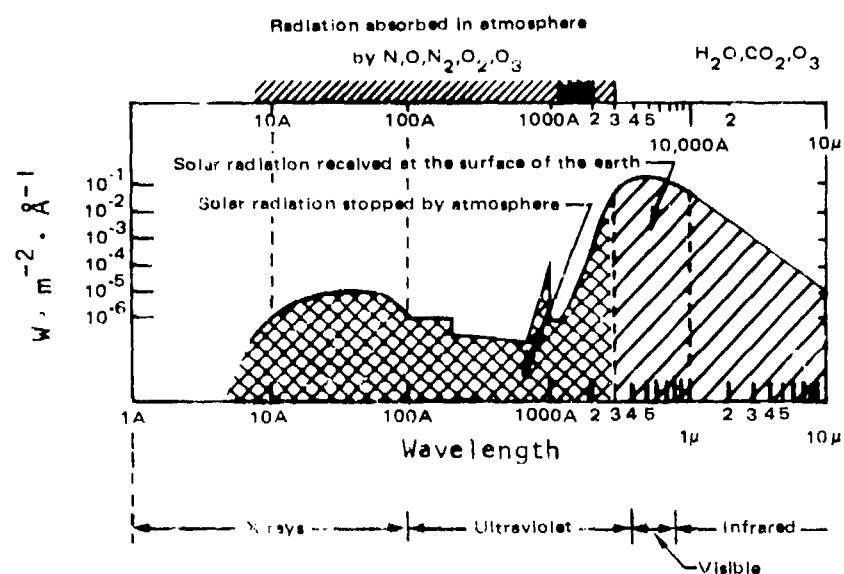


FIGURE B-7. SOLAR RADIATION INTENSITY ABOVE THE ATMOSPHERE AT EARTH'S DISTANCE FROM THE SUN. (After F. S. Johnson and J. C. New.)

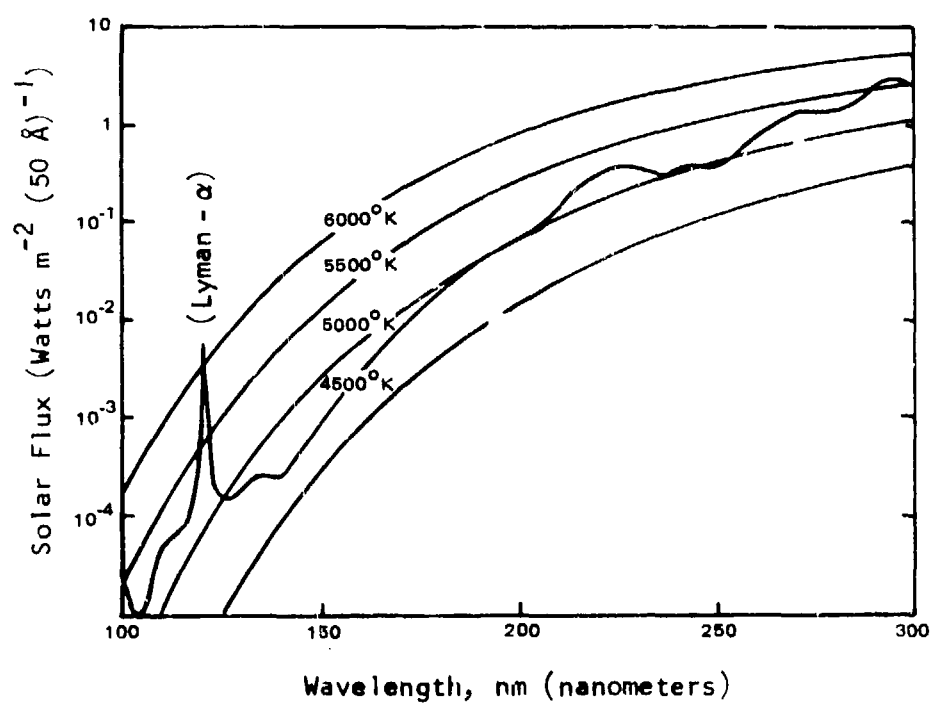


FIGURE B-8. SOLAR ULTRAVIOLET RADIATION OUTSIDE THE EARTH'S ATMOSPHERE. The measurements are smoothed over 50- \AA spectral intervals. Blackbody curves are shown for comparison. (After data reported by Johnson, 1954, and by Detwiler et al., 1961.)

June 1974

$$H_{s_{UV}} (1000 - 4000 \text{ \AA}) = 125 \text{ W/m}^2$$

$$H_{s_{visible}} (4000 - 7500 \text{ \AA}) = 556 \text{ W/m}^2$$

$$H_{s_{IR}} (0.75 - 100 \text{ \mu m}) = 709 \text{ W/m}^2$$

Since most space activities of significance occur within 500 miles from the earth, the above solar irradiation values may be assumed constant. Even at synchronous altitude of 35,880 kilometers or 22,300 miles, the solar constant only varies by:

$$\frac{\Delta H(\text{synchron altitude})}{H} = \pm 2 \left\{ \frac{(35.88 + 6.37) \times 10^6}{1.496 \times 10^{11}} \right\} = \pm 0.0565\% \quad (\text{B.10})$$

The irradiance due to solar light reflections from the earth were considered in section 3.2.2 where it was shown that:

$$\bar{H}_{\text{earth}} = a F H_{\text{sun}} \quad (\text{B.11})$$

The albedo a varies with wavelength and has values between 0.32 in July and 0.52 in October for the visible spectrum. An average value of 0.39 is often assumed. The irradiance factor F is plotted in Figure 3-8 of section 3.2.2. Since it has a maximum value of about 0.9 and an average value of about 0.44 at 100 miles altitude, a maximum and average value of respectively $H_{\text{earth}}^{\text{max}} \approx 195$ and $\bar{H}_{\text{earth}} \approx 98 \text{ Watts/m}^2$ may be assumed for earth-reflected radiation in the visible. In Figure B-9, some measured albedo spectra distributions are shown for various sky conditions.

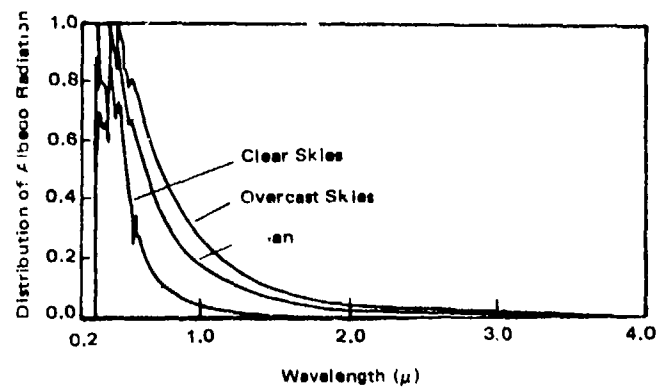


FIGURE B-9. RELATIVE SPECTRAL DISTRIBUTION OF ALBEDO RADIATION UNDER VARIOUS SKY CONDITIONS. (After Ref. 2.)

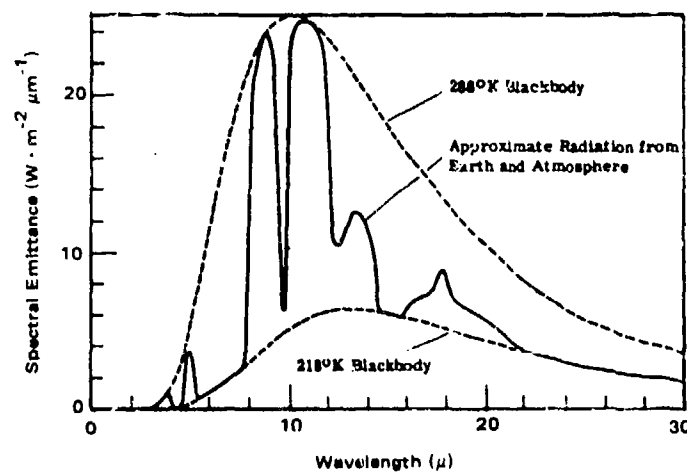


FIGURE B-10. A TYPICAL SPECTRAL EMISSIVE POWER CURVE FOR THE THERMAL RADIATION LEAVING THE EARTH. The 288 K blackbody curve approximates the radiation from the Earth's surface, and the 218 K blackbody curve approximates the radiation from the atmosphere in those spectral regions where the atmosphere is opaque. (After Ref. 2.)

June 1974

In addition to providing solar-reflected radiation, the earth also emits in the far infrared since it is a large blackbody at approximately 300°K. In Figure B-10, curves of the radiance due to thermal earthshine are given.

The irradiance in the visible at a space target due to moonlight or starlight can be shown to be:

$$H_{\text{full moon}} \approx 10^{-3} \text{ Watts/m}^2$$

$$H_{\text{all stars in hemisphere}} \approx 2 \times 10^{-6} \text{ Watts/m}^2$$

These levels are clearly insignificant compared to solar and earth-reflected intensities. The same comment applies to radiation in the UV or IR. If a 1.0 m² space target is to be detected by visible light of the full moon in the absence of solar radiation, a sensor at a distance of 25 miles from the target would observe it as a 13th magnitude source. Since most space sensor systems can at most detect 8th to 10th magnitude sources, lunar or stellar illumination may be dropped from further consideration as a means of space target detection.

The most promising source for space target illumination aside from the sun is the laser. Since a laser is man-made and can be controlled, many dependences imposed by nature such as the varying solar incidence and earth obscuration which limit the usefulness of the standard optical observation systems are absent.

The laser illumination of a target a large distance S away, is given by:

$$H_{\text{laser}} = \frac{P_{\text{laser}}}{\pi(\alpha S)^2} , \frac{\text{Watts}}{\text{cm}^2} \quad (\text{B.12})$$

where α is the laser beam divergence in radiance, S is the distance in cm, and P is the laser power in Watts. Laser beams with output powers $P = 10^3$ to 10^5 Watts and $\alpha \sim 10^{-3}$ to 10^{-5} radians exist today which can provide continuous illumination intensities of $\sim 2 \times 10^{-10}$ Watts/m² on a space target at a distance of 20 km, or $\sim 2 \times 10^{-2}$ Watts/m² in pulses of nanosecond durations (see Ref. 54).

FTD-CW-01-01-74
Vol. 1

June 1974

APPENDIX C
VIEW FACTORS FOR DIFFUSE EXHAUST PLUMES

C.1 PRELIMINARY CONSIDERATIONS

If a gaseous body such as a cylinder, sphere, or cone is viewed from a large distance, and if the photon fluence at the boundary of the gaseous body is constant, one can readily show* that the radiant emission from the surface must follow the well-known cosine law of diffusive reflection and emission. That is the emission intensity W (Watts/m²) per unit solid angle $d\Omega = 2\pi \sin\delta \, d\delta$ in direction δ is given by:

$$\frac{dW}{d\Omega} = W_{\text{tot}} \left(\frac{\cos \delta}{\pi} \right), \quad \frac{\text{Watts}}{\text{m}^2 \cdot \text{ster}}, \quad (\text{C.1})$$

where the angle δ is measured from the local normal to the surface and W_{tot} is the total hemispherical emission per unit area (Watts/m²). Thus if the body is viewed from a large distance, the effective emissive area is simply equal to the projected area of the body on a plane perpendicular to the field-of-view (fov) axis of the observer.

The "projected-area" law is evident if one considers that the photons that escape the plume in the direction of the viewer must be simply proportional to the projected surface area in the direction of the observer as defined before if the fluence inside the plume is to be homogeneous, isotropic, and constant.

*See Volume III, Rocket Radiation Handbook.

Now if the total surface area of the body of gas through which radiation escapes is $A_{\text{tot. esc.}}$ (m^2) and the total emission rate of radiation is P_{tot} (Watts) then clearly for constant surface fluence:

$$W_{\text{tot}} = \frac{P_{\text{tot}}}{A_{\text{tot. esc.}}} , \frac{\text{Watts}}{\text{m}^2} \quad (\text{C.2})$$

In general, for an irregular body with elementary surface areas dA_p , we must integrate to obtain $A_{\text{tot. esc.}}$, that is:

$$A_{\text{tot. esc.}} = \int_{A_{\text{tot. esc.}}} dA_p , \text{m}^2 \quad (\text{C.3})$$

The effective steradian $J = dP/d\Omega$ observed by a sensor whose viewing cone* intersects the body of gas (see Figure C-1) is then according to (C.1) and (C.2) given by:

$$J = \frac{dP}{d\Omega} = \int_{A_{\text{intersection}}} \frac{dW}{d\Omega} dA_p = \frac{P_{\text{tot}}}{4\pi} F_v(\alpha, D_s, \text{Gas Body Dim.}) , \text{Watts/ster} , \quad (\text{C.4})$$

where we define the dimensionless geometric view-factor $F(\alpha, D_s, \text{Body Dim.})$ by:

*The viewing cone may be approximated by a viewing cylinder for large distances between the sensor and radiation source.

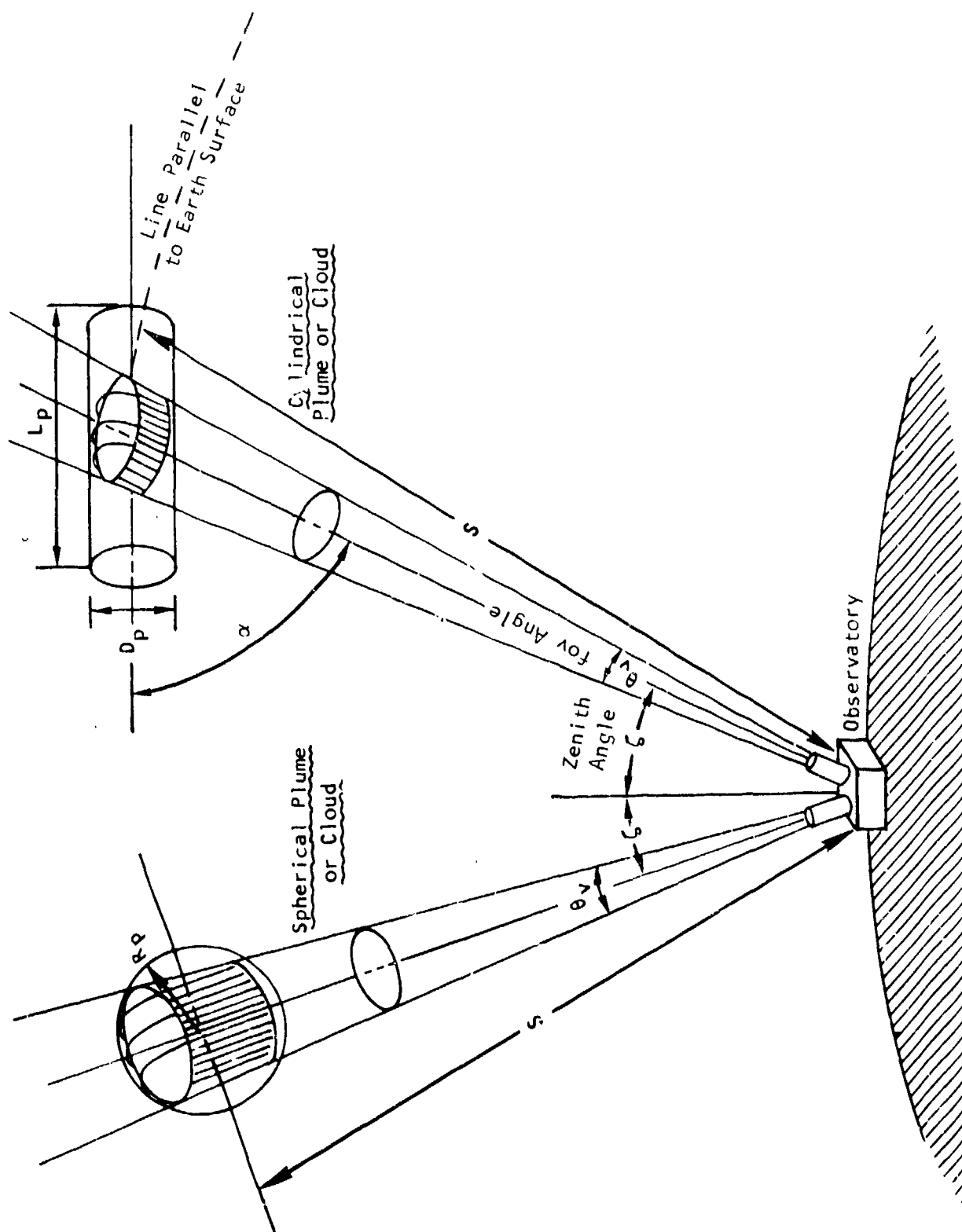


FIGURE C-1. ILLUSTRATION OF EXHAUST PLUME VIEWING SITUATION

June 1974

$$F_v(\alpha, D_s, \text{Gas Body Dim.}) = \frac{4\pi J}{P_{\text{tot}}} = \frac{\int_{A_{\text{intersection}}} \cos\{\delta(A_p)\} dA_p}{\int_{A_{\text{tot. esc.}}} dA_p} \quad (C.5)$$

Here:

- $A_{\text{intersection}}$ = Area on gaseous body surface intersected by the sensor's viewing cone (or cylinder) which faces the sensor, m^2
- $A_{\text{tot. esc.}}$ = Total surface area of gaseous body through which radiation escapes, m^2
- dA_p = Elemental surface area of gaseous body, m^2
- $\delta = \delta(A_p)$ = Angle between the local normal to the elemental surface area dA_p and the sensor line-of-sight
- α = Angle between major axis through gaseous body and the sensor line-of-sight
- D_s = Field-of-view diameter of sensor at the gaseous body, m
- Gas Body Dimensions = Three or two major dimensions of gaseous body which completely define it

Note that the view factor F_v is defined such that it represents the correction factor that one has to apply relative to the case that all gaseous radiation were emitted from an equivalent point source for which:

$$J_{\text{point source}} = \left(\frac{dP}{d\Omega} \right)_{\text{point source}} = \frac{P_{\text{tot}}}{4\pi} \text{ Watts/ster} \quad (C.6)$$

In the following sections we shall develop mathematical expressions for F_v for a sphere, cylinder, and cone.

C.2 SPHERICAL BODY OF GAS

It is clear that for a spherical gaseous body of diameter D_p , with constant surface fluence (i.e., an opaque diffuse body), one must have:

$$(W_{\text{tot}})_{\text{sphere}} = \frac{P_{\text{tot}}}{\pi D_p^2}, \quad \frac{\text{Watts}}{\text{m}^2} \quad (\text{C.7})$$

where P_{tot} is the total radiation emission rate of the gaseous body.

Now the sensor's fov diameter, D_s , at the gaseous body is given by:

$$D_s = 2S \tan(\theta/2) \approx S\theta \quad (\text{C.8})$$

where:

$\theta = \theta_v$ = Divergence or admittance angle of the sensor's fov.

S = Range or distance between the sensor and gaseous body, m

If the sensor's line-of-sight passes through the center of the spherical gas cloud and if $D_s < D_p$, we have the following relations between the various geometrical parameters illustrated in Figure C-2.

$$\beta' = \sin^{-1} \left(\frac{2S\theta'}{D_p} \right) \quad (\text{C.9})$$

$$\gamma' = \theta' + \beta' = \theta' + \sin^{-1} \left(\frac{2S\theta'}{D_p} \right) \quad (\text{C.10})$$

$$\beta = \sin^{-2} \left(\frac{2S\theta}{D_p} \right) \quad (\text{C.11})$$

$$\gamma = \theta + \beta = \theta + \sin^{-1} \left(\frac{2S\theta}{D_p} \right) \quad (\text{C.12})$$

June 1974

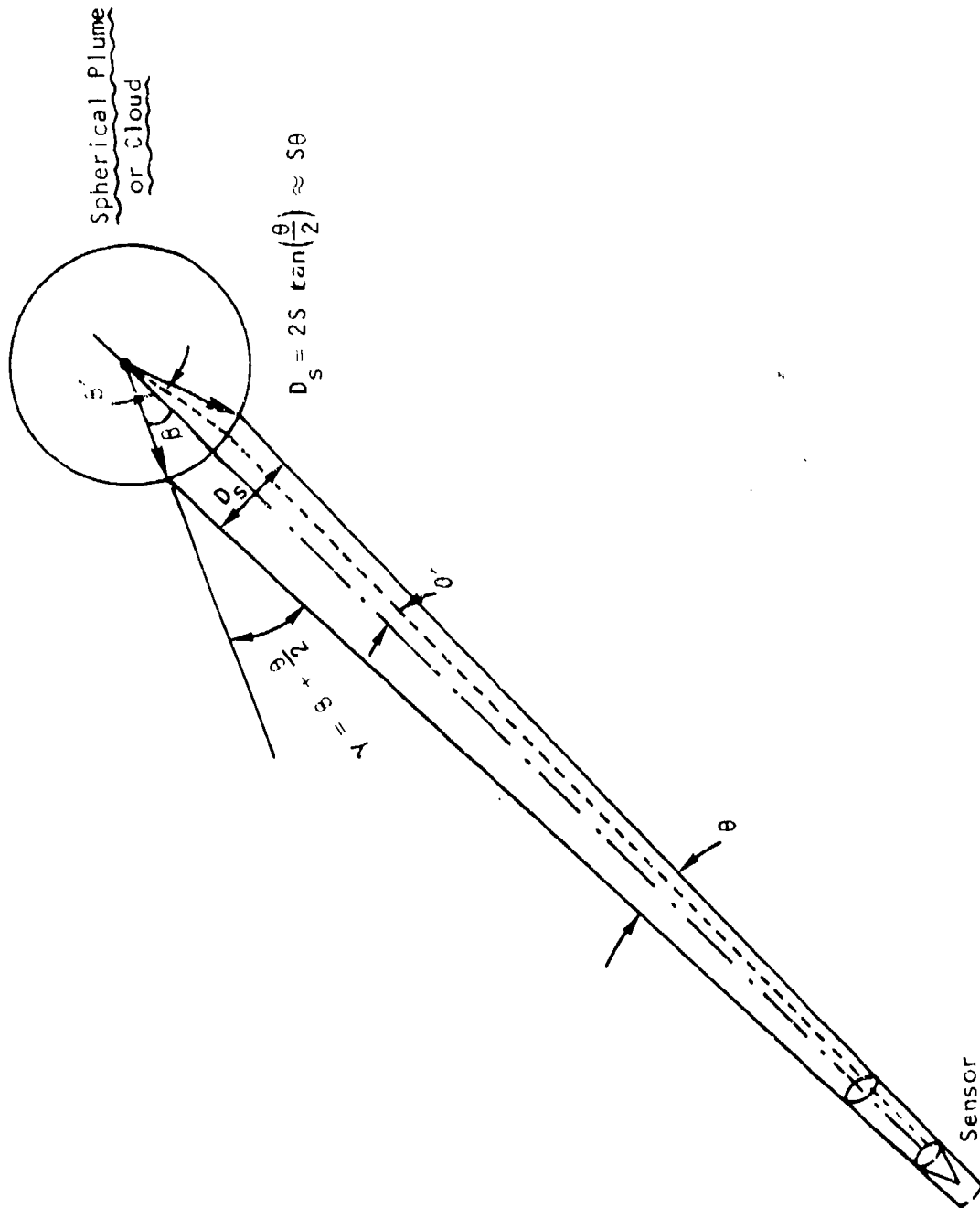


FIGURE C-2. DEPICTION OF SPHERICAL PLUME VIEWING GEOMETRY

June 1974

FTD-CW-01-01-74
Vol. I

The apparent steradian observed by the sensor is then:

$$J_{\text{sphere}} \left(\frac{dP}{d\Omega} \right)_{\text{sphere}} = W_{\text{tot}} \int_{\substack{\theta'=0 \\ \beta'=0}}^{\substack{\theta'=\tan^{-1}(D_s/2S) \\ \beta'=\sin^{-1}(D_s/D_p)}} \left\{ \frac{\cos(\theta'+\beta')}{\pi} \right\} 2\pi \left(\frac{D_p}{2} \right)^2 \sin\beta' d\beta', \quad \frac{\text{Watts}}{\text{ster}} \quad (\text{C.13a})$$

If $\theta' \ll \beta'$, that is if the sensor is very far from the sphere, we can set $\cos(\theta'+\beta') \approx \cos\beta'$ in (C.13a) and this equation can be shown to reduce to:

$$J_{\text{sphere}} = \frac{W_{\text{tot}} D_s^2}{4} = \frac{P_{\text{tot}}}{4\pi} \left(\frac{D_s}{D_p} \right)^2, \quad \frac{\text{Watts}}{\text{ster}}, \quad (\text{C.13b})$$

and thus the view factor becomes:

$$(F_v)_{\text{sphere}} = \left(\frac{D_s}{D_p} \right)^2, \quad (D_s < D_p) \quad (\text{C.14})$$

$\theta \ll \beta$

If the sensor is closer to the sphere, but still far enough such that we can approximate $\sin\theta' \approx \theta'$, the integration of (C.13a) becomes:

$$J_{\text{sphere}} = W_{\text{tot}} S D_p \int_{\theta'=0}^{\theta'=\tan^{-1}(D_s/2S)} \left[\cos \left\{ \theta' + \sin^{-1} \left(\frac{2S\theta'}{D_p} \right) \right\} \right] \frac{\frac{2S}{D_p} \theta' d\theta'}{\sqrt{1 - \left(\frac{2S}{D_p} \theta' \right)^2}} =$$

$$= 2S^2 W_{\text{tot}} \int_{\theta'=0}^{\theta'=\tan^{-1}(D_s/2S)} \left[\cos\theta' - \frac{\left(\frac{2S\theta'}{D_p} \right) \sin\theta'}{\sqrt{1 - \left(\frac{2S\theta'}{D_p} \right)^2}} \right] \theta' d\theta', \quad \frac{\text{Watts}}{\text{ster}} \quad (\text{C.15a})$$

which after writing it in terms of the view factor $F_v = \frac{4\pi J}{P_{tot}}$ and with the aid of (C.7) yields:

$$\begin{aligned} (F_v)_{\text{sphere}} &= \frac{8 S^2}{D_p^2} \left[\left\{ \frac{1}{1 + (D_s/2S)^2} \right\}^{1/2} - 1 + \left\{ \frac{(D_s/2S)^2}{1 + (D_s/2S)^2} \right\}^{1/2} \right. \\ &\quad \cdot \tan^{-1} \left(\frac{D_s}{2S} \right) - \frac{2}{3} \left(\frac{D_p}{2S} \right)^3 \left\{ 1 - \left[1 + \frac{1}{2} \left(\frac{2S}{D_p} \tan^{-1} \left(\frac{D_s}{2S} \right) \right)^2 \right] \right. \\ &\quad \left. \left. \cdot \left[1 - \left\{ \frac{2S}{D_p} \tan^{-1} \left(\frac{D_s}{2S} \right) \right\}^2 \right]^{1/2} \right\} \right] \end{aligned}$$

(C.15b)

If we assume that $(D_s/2S) \ll 1$ and $\tan^{-1}(D_s/2S) \approx D_s/2S$,

Eq. (C.15) reduces to:

$$\begin{aligned} (F_v)_{\text{sphere}} &= \frac{\pi W_{tot} D_s^2}{P_{tot}} \left[1 - \left(\frac{2 D_p^3}{3 D_s^2 S} \right) \left\{ 1 - \left(1 + \frac{1}{2} \frac{D_s^2}{D_p^2} \right) \left(1 - \frac{D_s^2}{D_p^2} \right)^{1/2} \right\} \right] = \\ &= \left(\frac{D_s^2}{D_p^2} \right) \left[1 - \left(\frac{2 D_p^3}{3 D_s^2 S} \right) \left\{ 1 - \left(1 + \frac{1}{2} \frac{D_s^2}{D_p^2} \right) \left(1 - \frac{D_s^2}{D_p^2} \right)^{1/2} \right\} \right], \end{aligned}$$

(C.16)

Equation (C.16) is seen to contain a second-order correction term over the expression given by (C.14) if the assumption that $\theta \ll \beta$ cannot be made, but

$(D_s/2S) \ll 1$ does apply. Equations (C.13) through (C.16) applied for $D_s < D_p$. For any value of D_s including $D_s > D_p$, we can combine our results and write:

$$(F_v)_{\text{sphere}} = \left[\left(1 - \frac{2 D_p}{3 S} \right) H(D_s - D_p) + \left(\frac{D_s}{D_p} \right)^2 \left\{ 1 - \left(\frac{2 D_p^3}{3 D_s^2 S} \right) \cdot \right. \right. \\ \left. \left. \cdot \left(1 - \left(1 + \frac{1}{2} \frac{D_s^2}{D_p^2} \right) \left(1 - \frac{D_s^2}{D_p^2} \right)^{1/2} \right) \right\} H(D_p - D_s) \right] \quad (\text{C.17})$$

where $H(x)$ is the Heaviside unit step function defined by:

$$H(x) = 1 \quad , \quad \text{for } x \geq 0 \quad (\text{C.18a})$$

$$H(x) = 0 \quad , \quad \text{for } x < 0 \quad (\text{C.18b})$$

The second-order terms with the factor $\left(\frac{2 D_p}{3 S} \right)$ and $\left(\frac{2 D_p^3}{3 D_s^2 S} \right)$ in (C.17) may be dropped in first-order calculations. Note also that for $D_p \ll R$ and $D_p \ll D_s$ which means that the sphere is essentially a point source, we have from (C.17) that $F_v = 1$ as it should.

C.3 CYLINDRICAL BODY OF GAS

Let the gaseous cylinder have a length L_p and diameter D_p^* and let the fov diameter be D_s again.** Let us also assume that the sensor is a large distance from the cylindrical cloud so that all rays from the sensor to all points on the cylinder axis make the same angle α with this axis (see Figure C-2). Then there are four possible situations, each one of which requires a slightly different integration over the cylinder's geometric boundaries:

- (a) $0 < D_s \leq D_p$, or $0 < \rho \leq 1$
- (b) $D_p < D_s \leq L_p \sin \alpha$, or $1 < \rho \leq \lambda \sin \alpha$
- (c) $L_p \sin \alpha < D_s \leq \sqrt{L_p^2 + D_p^2} \sin \alpha$, or $\lambda \sin \alpha < \rho \leq \sqrt{\lambda^2 + 1} \sin \alpha$.
- (d) $\sqrt{L_p^2 + D_p^2} \sin \alpha < D_s \leq \infty$, or $\sqrt{\lambda^2 + 1} \sin \alpha < \rho \leq \infty$

According to Eq. (C.2) we have that:

$$(W_{\text{tot}})_{\text{cyl.}} = \frac{P_{\text{tot}}}{A_{\text{cyl.}}} = \frac{P_{\text{tot}}}{\pi D_p (L_p + k_r D_p / 4)} , \quad \frac{\text{Watts}}{\text{m}^2} , \quad (\text{C.19})$$

where for a cylinder that can emit radiation through both ends and its sides $k_r = 2$, and for the case that radiation can only escape through the sides and one end, $k_r = 1$. For simplicity we set $k_r = 1$ in what follows (the case for a cylindrical rocket exhaust), keeping in mind that the correction factor $k_r = 2$ must be applied in the denominator, if both ends can emit.

*We shall assume throughout that $L_p > D_p$.

**The line-of-sight of the sensor is always assumed to pass through the center of the cylinder.

June 1974

FTD-CW-01-01-74
Vol. I

The radiance $J_{cyl.}$ and view factor $F_{v_{cyl.}}$ are given by (see section C.1):

$$J_{cyl.} = \frac{W_{tot} A_{proj}}{\pi} = \frac{P_{tot} A_{proj}}{\pi^2 D_p (L_p + D_p/4)}, \quad \frac{\text{Watts}}{\text{ster}} \quad (C.20)$$

$$(F_v)_{cyl.} = \frac{4\pi J_{cyl.}}{W_{tot} A_{cyl.}} = \frac{4 A_{proj}}{\pi D_p (L_p + D_p/4)} \quad (C.21)$$

Starting with case (a) and referring to Figure C-3, we have for the chord x (parallel to the gas-cylinder axis) of the three-dimensional circle-like surface cut out by the intersection of the fov cylinder with the gas cylinder that:

$$x = \frac{D_p}{\sin \alpha} \sqrt{\left(\frac{D_s}{D_p}\right)^2 - \sin^2 \gamma}, \quad (C.22)$$

where γ is an angle in the plane at right angles to the gas-cylinder axis as shown in Figure C-3. The differential area of a strip is then:

$$dA = \frac{D_p}{2} x d\gamma = \frac{D_p^2}{2 \sin \alpha} \sqrt{\left(\frac{D_s}{D_p}\right)^2 - \sin^2 \gamma} d\gamma \quad (C.23)$$

The radiation from the cloud as observed by the sensor is then given by:

$$J_{cyl.} = \left(\frac{dP}{d\Omega}\right)_{cyl.} = W_{tot} \int_{\gamma=0}^{\gamma=\sin^{-1}(D_s/D_p)} \left(\frac{\cos \delta}{\pi}\right) \cdot \frac{D_p^2}{\sin \alpha} \sqrt{\left(\frac{D_s}{D_p}\right)^2 - \sin^2 \gamma} d\gamma, \quad \frac{\text{Watts}}{\text{ster}} \quad (C.24)$$

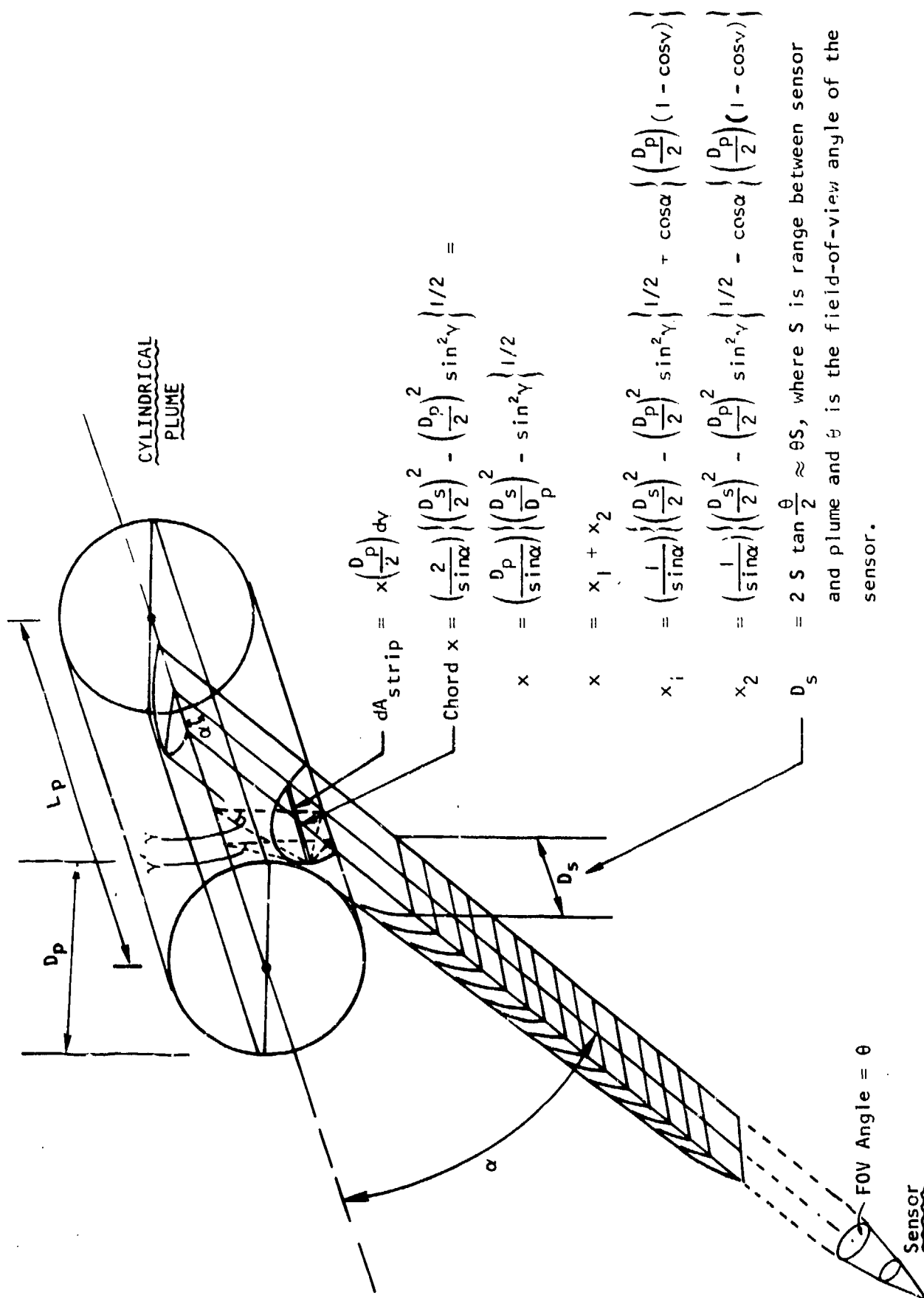


FIGURE C-3. ILLUSTRATION OF CYLINDRICAL PLUME VIEWING GEOMETRY

The angle δ is the angle between the local normal and the line-of-sight to elemental areas on the intersection surface. It is related to the angle γ by the equation:

$$\cos \delta = \cos \gamma \sin \alpha \quad (C.25)$$

With (C.25) substituted in (C.24), the integration yields:

$$J_{\text{cyl.}} \left(\frac{D_s < D_p}{D_s < D_p} \right) = \left(\frac{dP}{d\Omega} \right)_{\text{cyl.}} = \frac{W_{\text{tot}} D_p^2}{\pi} \int_{\gamma=0}^{\gamma=\sin^{-1}(D_s/D_p)} \sqrt{\left(\frac{D_s}{D_p} \right)^2 - \sin^2 \gamma} (\cos \gamma) d\gamma = \frac{W_{\text{tot}} D_s^2}{4}, \frac{\text{Watts}}{\text{ster}} \quad (C.26)$$

and thus according to (C.21):

$$(F_v)_{\text{cyl.}} \left(\frac{D_s < D_p}{D_s < D_p} \right) = \frac{\rho^2}{\lambda + 0.25} H(1-\rho) \quad (C.27)$$

where we define for convenience:

$$\rho = D_s/D_p \quad (C.28)$$

$$\lambda = L_p/D_p \quad (C.29)$$

For case (b), one finds similarly:

$$(F_v)_{\text{cyl.}} \left(1 < \rho \leq \lambda \sin \alpha \right) = \frac{2}{\pi} \left(\frac{\rho^2}{\lambda + 0.25} \right) \left[\frac{1}{\rho} \sqrt{1 - (1/\rho)^2} + \sin^{-1}(1/\rho) \right] \cdot H(\rho-1) H(\lambda \sin \alpha - \rho) \quad (C.30)$$

June 1974

Case (c) yields next:

$$\begin{aligned} (F_v)_{\text{cyl.}} &= \frac{2}{\pi} \left(\frac{1}{\lambda + 0.25} \right) \left[2\lambda \sin\alpha + \frac{\pi}{2} \cos\alpha + \right. \\ &(\lambda \sin\alpha < \rho \leq \sqrt{\lambda^2 + 1} \sin\alpha) \\ &+ \rho^2 \left\{ \frac{\pi}{2} - \xi \sqrt{1 - \xi^2} - \sin^{-1} \xi \right\} + \cos\alpha \left\{ \frac{\pi}{2} - \zeta \sqrt{1 - \zeta^2} - \sin^{-1} \zeta \right\} \cdot \\ &\cdot H(\rho - \lambda \sin\alpha) H(\sqrt{\lambda^2 + 1} \sin\alpha - \rho) \end{aligned} \quad (C.31)$$

where:

$$\zeta = \frac{L_p \sin\alpha - D_s}{D_p |\cos\alpha|} \cdot \frac{\sqrt{L_p^2 + D_p^2 - D_s^2} - \sqrt{L_p^2 - D_s^2 + \left(\frac{L_p \sin\alpha - D_s}{|\cos\alpha|} \right)^2}}{D_p \sin\alpha} \quad (C.32)$$

$$\xi = 1 - |\cot\alpha| \left\{ \sqrt{\frac{L_p^2 + D_p^2}{D_s^2} - 1} - \sqrt{\frac{L_p^2 + D_s^2}{D_s^2 \cos^2\alpha} - \frac{2 L_p |\tan\alpha|}{D_s} - 1} \right\} \quad (C.33)$$

Finally for case (d), one obtains:

$$\begin{aligned} (F_v)_{\text{cyl.}} &= \frac{|\cos\alpha| + 4/\pi \lambda \sin\alpha}{\lambda + 0.25} H(\rho - \sqrt{\lambda^2 + 1} \sin\alpha) \\ &(\sqrt{\lambda^2 + 1} \sin\alpha < \rho \leq \infty) \end{aligned} \quad (C.34)$$

The partial view factor relations given above can be combined into the one expression:

$$\begin{aligned}
 (F_v)_{cyl.} &= \left(\frac{\rho^2}{\lambda + 0.25} \right) \left[H(1-\rho) + \frac{2}{\pi\rho} \left\{ \sqrt{1-\rho^2} + \rho \sin^{-1}(\rho^{-1}) \right\} H(\rho-1) \cdot \right. \\
 &\quad \cdot H(\lambda \sin \alpha - \rho) + \frac{2}{\pi\rho^2} \left\{ 2\lambda \sin \alpha + \frac{\pi}{2} |\cos \alpha| + \rho^2 \left(\frac{\pi}{2} - \xi \sqrt{1-\xi^2} - \sin^{-1} \xi \right) - (|\cos \alpha|) \cdot \right. \\
 &\quad \cdot \left. \left(\frac{\pi}{2} - \zeta \sqrt{1-\zeta^2} - \sin^{-1} \zeta \right) \right\} H(\rho - \lambda \sin \alpha) \cdot \\
 &\quad \left. \cdot H \left(\sqrt{\lambda^2 + 1} \sin \alpha - \rho \right) + \frac{1}{\rho^2} \left\{ |\cos \alpha| + \left(\frac{4}{\pi} \right) \lambda \sin \alpha \right\} H \left(\rho - \sqrt{\lambda^2 + 1} \sin \alpha \right) \right] ,
 \end{aligned}$$

(C.35)

where $H(x)$ is the unit step function defined in (C.18), $\rho = D_s/D_p$, $\lambda = L_p/D_p$, and where for convenience we rewrite ξ and ζ in terms of ρ and λ :

$$\zeta = \frac{\lambda \sin \alpha - \rho}{|\cos \alpha|} + \frac{\sqrt{\lambda^2 - \rho^2 + 1} - \sqrt{\lambda^2 - \rho^2 + \frac{\lambda \sin \alpha - \rho}{|\cos \alpha|}}}{\sin \alpha}$$

(C.36)

$$\xi = 1 - |\cot \alpha| \left\{ \sqrt{\frac{\lambda^2 + 1}{\rho^2} - 1} - \sqrt{\frac{\lambda^2}{\rho^2} + \left(\frac{(\lambda/\rho) \sin \alpha - 1}{|\cos \alpha|} \right)^2 - 1} \right\}$$

(C.37)

For a cylinder that can emit from both ends (and its sides), the factor $(\lambda + 0.25)$ in the denominator of (C.35) should be replaced by $(\lambda + 0.50)$.

Equation (C.35) which is plotted in Figure C-4 (for $\lambda = 3$) may be assumed to apply at all angles α if there is no obscuration. In the case of

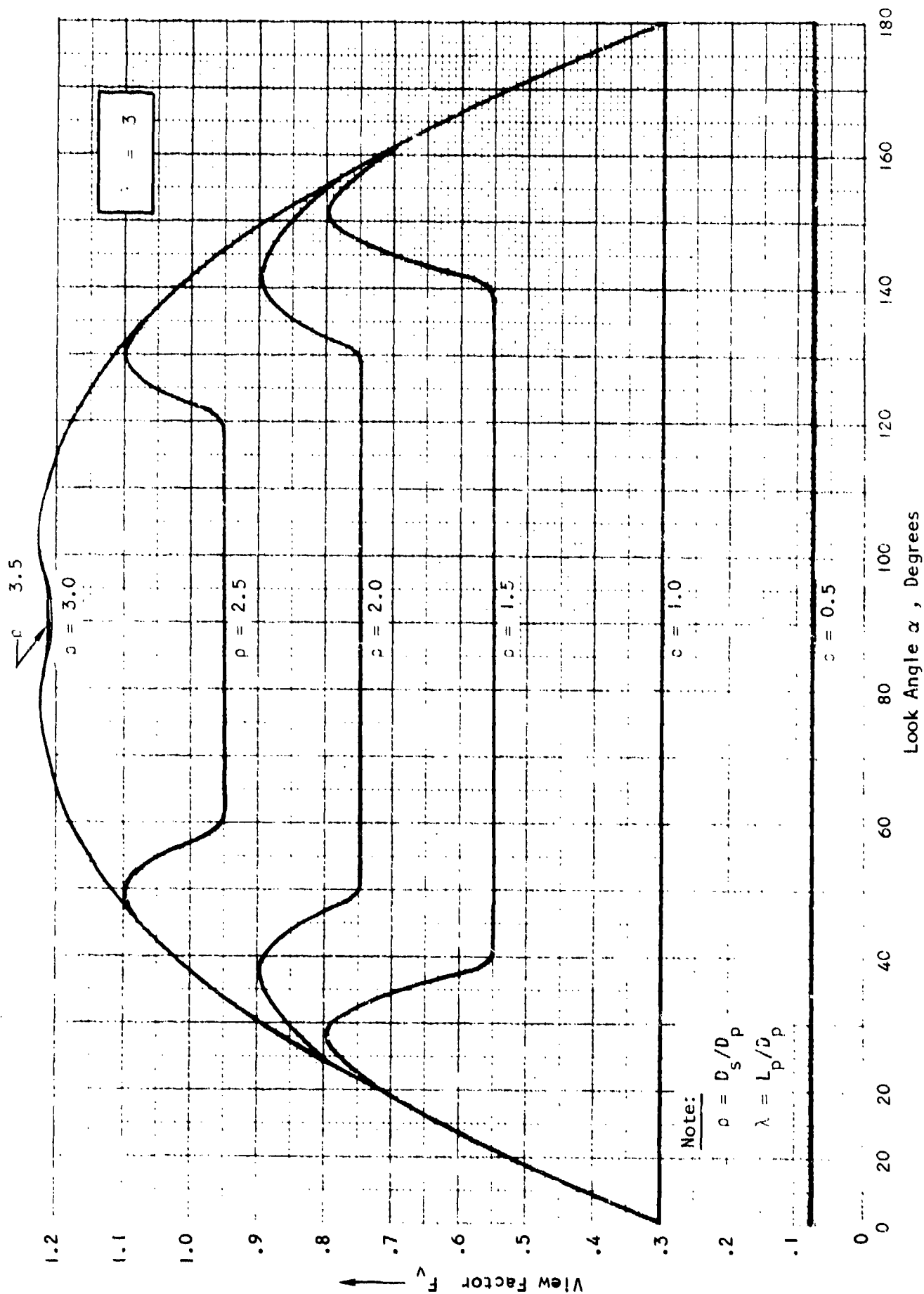


FIGURE C-4. VIEW FACTOR F_v FOR CYLINDRICAL PLUME WITH $\lambda = 3$

an equivalent cylindrical rocket plume, there is vehicle body obscuration in the forwards direction at small angles α . However at medium to high altitudes the obscuration is negligible, since the rocket body diameter D_r is much smaller than the plume diameter D_p , and Eq. (C.35) may be used at all angles α .*

At the lower altitudes a correction for small values of α is necessary to account for rocket-body obscuration. This correction amounts to subtracting out the plume-shadowing projected area of the rocket body in the direction of the sensor from the expressions given before. Assuming again that the line-of-sight of the observer passes through the center of the equivalent cylindrical plume, one obtains in the case that

$$D_s > \sqrt{L_p^2 + D_p^2} \sin \alpha :$$

$$\begin{aligned} (\Delta F_v)_{\text{cyl.}} &= - \frac{|\cos \alpha|}{\lambda + 0.25} H\left(\frac{\pi}{2} - \alpha\right) \left\{ \left(\frac{D_r}{D_p}\right)^2 + \left(\frac{D_q}{D_p}\right)^2 \right. \\ &\quad \left. (D_s > (\sin \alpha) \sqrt{L_p^2 + D_p^2}) \right. \\ &\quad \cdot \left. \left(\frac{1}{2} + \frac{1}{\pi} \sin^{-1} \sqrt{\frac{D_q^2 - D_p^2}{D_q^2}} \right) + \frac{1}{\pi} \sqrt{\frac{D_q^2 - D_p^2}{D_q^2}} - \frac{1}{2} \right\} H\left(p - (\sin \alpha) \sqrt{L_p^2 + 1}\right) \end{aligned} \quad (C.38)$$

The obscuration-corrected view-factor for $D_s > (\sin \alpha) \sqrt{L_p^2 + D_p^2}$ is then:††

$$\begin{aligned} (F_v)_{\text{cyl.}} &= \frac{H(p - (\sin \alpha) \sqrt{L_p^2 + 1})}{\lambda + 0.25} \left[|\cos \alpha| + \frac{4\lambda \sin \alpha}{\pi} - H\left(\frac{\pi}{2} - \alpha\right) |\cos \alpha| \right. \\ &\quad \left. (D_s > (\sin \alpha) \sqrt{L_p^2 + D_p^2}) \right. \\ &\quad \cdot \left. \left\{ \left(\frac{D_r}{D_p}\right)^2 + \left(\frac{D_q}{D_p}\right)^2 \left(\frac{1}{2} + \frac{1}{\pi} \sin^{-1} \sqrt{\frac{D_q^2 - D_p^2}{D_q^2}} \right) - \frac{1}{2} + \frac{1}{\pi} \sqrt{\frac{D_q^2 - D_p^2}{D_q^2}} \right\} \right] \end{aligned} \quad (C.39)$$

*For example at $h = 100$ km, $D_p \sim 200$ m, while $D_r \sim 10$ m, so that $D_r \ll D_p$.

††The obscuration corrections that follow are in part due to R. Chardon.

June 1974

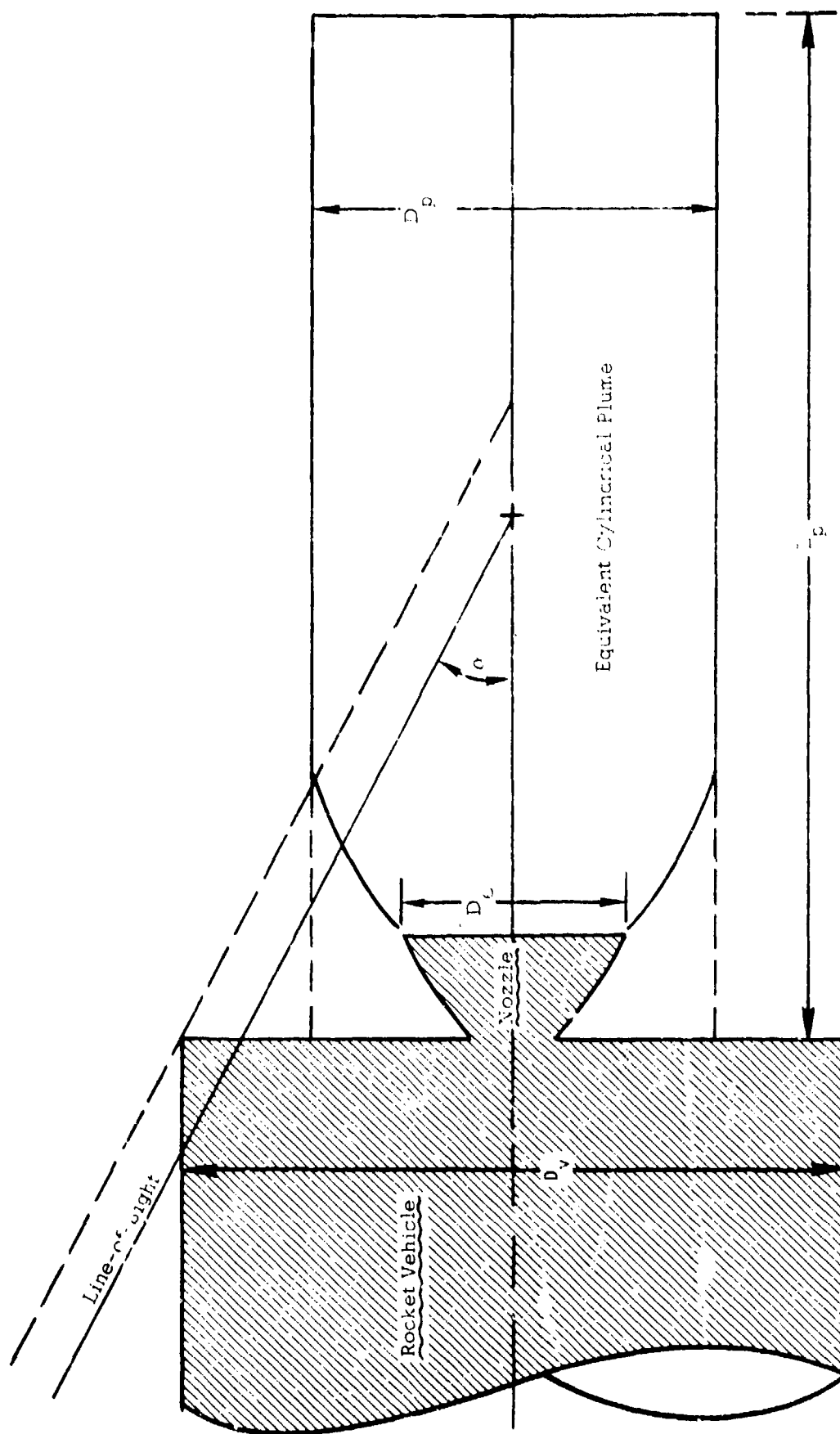


FIGURE C-5. ILLUSTRATION OF VEHICLE OBSCURATION PROBLEM WHEN $D_v > D_p$

Here the end- and side-obscuration diameters D_r and D_q are defined by:

$$D_r = D_v H(D_p - D_v) + D_p H(D_v - D_p), \text{ m} \quad (\text{C.40})$$

$$D_q = D_v H(D_v - D_p) + D_p H(D_p - D_v), \text{ m} \quad (\text{C.41})$$

The parameter D_v is the rocket vehicle skirt or body diameter as illustrated in Figure C-5. D_r is thus always less or equal to D_p , while D_q is larger or equal to D_p .

Making similar corrections to the other cases, the general obscuration-corrected view-factor may be written:

$$\begin{aligned} (F_v)_{\text{cyl.}} = & (\lambda + 0.25)^{-1} \left(H(1-p) \left[p^2 - H\left(\frac{\pi}{2} - \alpha\right) \cdot H(p - \lambda \sin \alpha + \rho \chi_v |\cos \alpha|) \cdot \right. \right. \\ & \cdot H(p + \lambda \sin \alpha - \rho \chi_v |\cos \alpha|) \cdot \left\{ p^2 \left(\frac{1}{2} + \frac{1}{\pi} \sin^{-1} \sqrt{1 - \chi_v^2 + \mu^2 \chi_p^2} \right) + \right. \\ & - \frac{1}{\pi} \sqrt{(-\chi_v^2 + \mu^2 \chi_p^2)(\chi_v^2 - \mu^2 \chi_p^2)} \left. \right\} + |\cos \alpha| \left(\frac{\chi_v}{\chi_p} \right)^2 \left(\frac{1}{2} + \frac{1}{\pi} \sin^{-1} \left(\frac{\mu \chi_p}{\chi_v} \right) + \right. \\ & \left. \left. - \left(\frac{\mu \chi_p}{\pi \chi_v} \right) \sqrt{1 - \left(\frac{\mu \chi_p}{\chi_v} \right)^2} \right) \right\} + H\left(\frac{\pi}{2} - \alpha\right) H(\rho \chi_v \cos \alpha - \lambda \sin \alpha - p) p^2 \right] + \end{aligned}$$

$$\begin{aligned}
 & \left\{ H(x_v - x_p) \left(\rho^2 \cdot \left(\frac{1}{2} + \frac{1}{\pi} \sin^{-1} \sqrt{1 - x_q^2} \right) - \frac{x_q}{\pi} \sqrt{1 - x_q^2} \right) + \frac{x_p}{\pi} \left(\sqrt{\frac{1 - x_q^2}{x_p^2}} + \right. \right. \\
 & + |\cos \alpha| \sqrt{\frac{x_q^2 - x_p^2}{x_p^2}} - 2\lambda \sin \alpha \left. \right) + |\cos \alpha| \left(\frac{x_q}{x_p} \right)^2 \left(\frac{1}{2} + \frac{1}{\pi} \sin^{-1} \sqrt{1 - (x_p/x_q)^2} + \right. \\
 & \left. \left. - \frac{x_p}{\pi x_q} \sqrt{1 - (x_p/x_q)^2} \right) \right) + H(x_p - x_v) \cdot H(\rho x_v |\cos \alpha| - \lambda \sin \alpha + \rho) \cdot \\
 & \cdot \left(\rho^2 \left(\frac{1}{2} + \frac{1}{\pi} \sin^{-1} \sqrt{1 - x_r^2 + \mu^2 x_p^2} - \frac{1}{\pi} \sqrt{(1 - x_r^2 + \mu^2 x_p^2)(x_r^2 - \mu^2 x_p^2)} \right) + \right. \\
 & \left. + |\cos \alpha| \left(\frac{x_r}{x_p} \right)^2 \cdot \left(\frac{1}{2} + \frac{1}{\pi} \sin^{-1} \left(\frac{\mu x_p}{x_r} \right) - \left(\frac{\mu x_p}{\pi x_r} \right) \sqrt{1 - \left(\frac{\mu x_p}{x_r} \right)^2} \right) \right) \left. \right\} + \\
 & + H(\rho - \lambda \sin \alpha) H(\sqrt{\lambda^2 + 1} \sin \alpha - \rho) \left[|\cos \alpha| + \frac{4\lambda \sin \alpha}{\pi} + \right. \\
 & + \rho^2 \left(1 - \frac{\xi \sqrt{1 - \xi^2} - \sin^{-1} \xi}{\pi/2} \right) - |\cos \alpha| \left(1 - \frac{\zeta \sqrt{1 - \zeta^2} - \sin^{-1} \zeta}{\pi/2} \right) - H\left(\frac{\pi}{2} - \alpha\right) \cdot \\
 & \cdot |\cos \alpha| \left\{ \left(\frac{x_r}{x_p} \right)^2 + \left(\frac{x_q}{x_p} \right)^2 \left(\frac{1}{2} + \frac{1}{\pi} \sin^{-1} \sqrt{1 - \left(\frac{x_p}{x_q} \right)^2} \right) - \frac{1}{2} + \frac{1}{\pi} \sqrt{\left(\frac{x_q}{x_p} \right)^2 - 1} \right\} + \\
 & - \frac{1}{2} H\left(\frac{\pi}{2} - \alpha\right) \left\{ \left(\frac{1}{x_r} \right)^2 \left(1 - \frac{\xi_r \sqrt{1 - \xi_r^2} - \sin^{-1} \xi_r}{\pi/2} \right) - |\cos \alpha| \left(1 - \frac{\zeta_r \sqrt{1 - \zeta_r^2} - \sin^{-1} \zeta_r}{\pi/2} \right) \right\} \left. \right]
 \end{aligned}$$

June 1974

FTD-CW-01-01-74
Vol. I

Here the additional dimensionless constants χ_p , χ_q , χ_r , χ_v , μ , ξ_r , and ζ_r were used for brevity, which are defined by:

$$\chi_p = D_p/D_s = 1/\rho \quad (C.43)$$

$$\chi_q = D_q/D_s \quad (C.44)$$

$$\chi_r = D_r/D_s \quad (C.45)$$

$$\chi_v = D_v/D_s \quad (C.46)$$

$$\mu = \lambda - \rho/(\sin\alpha) \quad (C.47)$$

$$\zeta_r = \zeta(D_p=D_r) = \frac{L_p \sin\alpha - D_s}{D_r |\cos\alpha|} + \frac{\sqrt{L_p^2 + D_r^2 - D_s^2} - \sqrt{L_p^2 + (L_p |\tan\alpha| - D_s |\sec\alpha|)^2 - D_s^2}}{D_r \sin\alpha} \quad (C.48)$$

$$\xi_r = \xi(D_p=D_r) = 1 - |\cot\alpha| \left\{ \sqrt{\lambda^2 \chi_p^2 + \chi_r^2 - 1} - \sqrt{\lambda^2 \chi_p^2 + (\lambda \chi_p |\tan\alpha| - |\sec\alpha|)^2 - 1} \right\} \quad (C.49)$$

Equation (C.42) which gives the obscuration-corrected view-factor may provide values that are significantly smaller than Eq. (C.35) at low

FTD-CW-01-01-74
Vol. I

June 1974

In carrying out computer calculations using the view-factors (C.35) or (C.42), the parameters ζ and ξ will approach limiting values when $(\cos\alpha) \rightarrow 0$, as $\alpha \rightarrow \pi/2$, which often give difficulties. For values of $|\cos\alpha|$ smaller than some suitable cut-off limit, say $|\cos\alpha| < 0.001$, one should assume ζ and ξ to take on the limiting values:

$$\xi_{(\cos\alpha \rightarrow 0)} = 1 + \left(\frac{L_p}{D_s} - 1 \right)^2 \quad (C.50)$$

$$\zeta_{(\cos\alpha \rightarrow 0)} = \left\{ 1 + \left(\frac{L_p}{D_p} \right)^2 - \left(\frac{D_s}{D_p} \right)^2 \right\}^{1/2} \quad (C.51)$$

$$\begin{aligned} \text{Tr}_6(\lambda, h, \theta_s) &= \exp - \left[\frac{2.40 (30 - h)}{\cos \theta_s} \exp - \left\{ \frac{3246.75}{\lambda} - 12.63 \right\}^2 \right] \\ (0_3) \end{aligned} \quad (\text{H.20})$$

$$\begin{aligned} \text{Tr}_7(\lambda, h, \theta_s) &= \exp - \left[\frac{5.34 \times 10^4}{\cos \theta_s} \left\{ \exp - \left(\frac{h}{3.86} \right) \right\} \cdot \exp - \left\{ \frac{3246.75}{\lambda} - 12.63 \right\}^2 \right] \\ (0_3) \end{aligned} \quad (\text{H.21})$$

$$\begin{aligned} \text{Tr}_8(\lambda, h, \theta_s) &= \exp - \left[\frac{0.381}{\cos \theta_s} \left\{ \exp - \left(\frac{h}{1.09} \right) \right\} \left\{ \exp - \left(\frac{\lambda - 200}{357} \right) \right\} \right] \\ (\text{aerosol}) \end{aligned} \quad (\text{H.22})$$

$$\begin{aligned} \text{Tr}_9(\lambda, h, \theta_s) &= \exp - \left[\frac{1.40 \times 10^{-3}}{\cos \theta_s} \exp - \left(\frac{\lambda - 200}{357} \right) \right] \\ (\text{aerosol}) \end{aligned} \quad (\text{H.23})$$

$$\begin{aligned} \text{Tr}_{10}(\lambda, h, \theta_s) &= \exp - \left[\frac{3.71 \times 10^{-5}}{\cos \theta_s} \exp - \left(\frac{\lambda - 200}{357} \right) \right] \\ (\text{aerosol}) \end{aligned} \quad (\text{H.24})$$

$$\begin{aligned} \text{Tr}_{11}(\lambda, h, \theta_s) &= \exp - \left[\frac{7 \times 10^{-5}}{\cos \theta_s} (30 - h) \exp - \left(\frac{\lambda - 200}{357} \right) \right] \\ (\text{aerosol}) \end{aligned} \quad (\text{H.25})$$

$$\begin{aligned} \text{Tr}_{12}(\lambda, h, \theta_s) &= \exp - \left[\frac{3.17 \times 10^7}{\cos \theta_s} \left\{ \exp - \frac{h}{1.09} \right\} \left\{ \exp - \left(\frac{\lambda - 200}{357} \right) \right\} \right] \\ (\text{aerosol}) \end{aligned} \quad (\text{H.26})$$

In Eqs. (H.15) through (H.26), we have:

h = Altitude, km

λ = Wavelength, nm

θ_s = Solar zenith angle, degrees or radians

Equations (H.15) through (H.26) are given in terms of the photon wavelength λ . Often it is more convenient to express these relations in terms of the photon frequency $\nu = c/\lambda$. If $\Delta\nu/\nu \ll 1$, we have that:

$$\frac{\Delta\nu}{\nu} = \frac{1}{\nu} \left(\frac{-c \Delta\lambda}{\lambda^2} \right) = -\frac{\Delta\lambda}{\lambda} \quad (\text{H.27})$$

Then since also:

$$\lambda(\text{nm}) = \frac{300,000}{\nu(\text{THz})}, \quad (\text{H.28})$$

we can reexpress Eqs. (H.15) through (H.26) in terms of ν as follows:

$$\begin{aligned} Tr_1(\nu, h, \theta_s) = \exp & \left[\frac{95}{\cos \theta_s} \left\{ \exp \left(-\frac{h}{6.78} \right) \right\} \left\{ \exp \left(-\frac{|\nu - 1500|}{150} \right) \right. \right. \\ (0_2) & \left. \left. + 5.70 \times 10^5 \exp \left(-\frac{(\nu - 2028.8)^2}{151.5} \right) + 7.86 \times 10^5 \exp \left(-\frac{(\nu - 3308)^2}{330.8} \right) \right\} \right] \quad (\text{H.29}) \end{aligned}$$

$$Tr_2(\nu, h, \theta_s) = \exp \left[\frac{1.543}{\cos \theta_s} \exp \left(-\frac{(\nu - 1167)^2}{92.4} \right) \right] \quad (\text{H.30})$$

(0₃)

$$Tr_3(\nu, h, \theta_s) = \exp \left[\frac{24}{\cos \theta_s} \exp \left(-\frac{(\nu - 1167)^2}{92.4} \right) \right] \quad (\text{H.31})$$

(0₃)

$$\text{Tr}_{4(0_3)}(v, h, \theta_s) = \exp - \left[\frac{22.2}{\cos \theta_s} \exp - \left(\frac{v - 1167}{92.4} \right)^2 \right] \quad (\text{H.32})$$

$$\text{Tr}_{5(0_3)}(v, h, \theta_s) = \exp - \left[\frac{1.543}{\cos \theta_s} \left\{ 1 - \exp \left(\frac{h - 20}{0.69} \right) \right\} \left\{ \exp - \left(\frac{v - 1167}{92.4} \right)^2 \right\} \right] \quad (\text{H.33})$$

$$\text{Tr}_{6(0_3)}(v, h, \theta_s) = \exp - \left[\frac{2.40 (30 - h)}{\cos \theta_s} \exp - \left(\frac{v - 1167}{92.4} \right)^2 \right] \quad (\text{H.34})$$

$$\text{Tr}_{7(0_3)}(v, h, \theta_s) = \exp - \left[\frac{5.34 \times 10^4}{\cos \theta_s} \left\{ \exp - \left(\frac{h}{3.86} \right) \right\} \left\{ \exp - \left(\frac{v - 1167}{92.4} \right)^2 \right\} \right] \quad (\text{H.35})$$

$$\text{Tr}_{8(\text{aerosol})}(v, h, \theta_s) = \exp - \left[\frac{0.667}{\cos \theta_s} \left\{ \exp - \left(\frac{h}{1.09} \right) \right\} \left\{ \exp - \left(\frac{840.3}{v} \right) \right\} \right] \quad (\text{H.36})$$

$$\text{Tr}_{9(\text{aerosol})}(v, h, \theta_s) = \exp - \left[\frac{2.45 \times 10^{-3}}{\cos \theta_s} \exp - \left(\frac{840.3}{v} \right) \right] \quad (\text{H.37})$$

$$\text{Tr}_{10(\text{aerosol})}(v, h, \theta_s) = \exp - \left[\frac{6.50 \times 10^{-5}}{\cos \theta_s} \exp - \left(\frac{840.3}{v} \right) \right] \quad (\text{H.38})$$

$$\text{Tr}_{11(\text{aerosol})}(v, h, \theta_s) = \exp - \left[\frac{12.26 \times 10^{-5}}{\cos \theta_s} (30 - h) \exp - \left(\frac{840.3}{v} \right) \right] \quad (\text{H.39})$$

June 1974

$$Tr_{12}(\nu, h, \theta_s) = \exp\left[-\frac{5.55 \times 10^7}{\cos\theta_s} \left\{ \exp\left(-\frac{h}{1.09}\right) \cdot \exp\left(-\frac{840.3}{\nu}\right) \right\}\right] \quad (H.40)$$

(aerosol)

In Eqs. (H.29) through (H.40), h is again in kilometers and:

$$\nu = \text{Photon Frequency, THz} (1 \text{ THz} = 10^{12} \text{ Hz})$$

Equations (H.14) through (H.26) provide a coarse (broad-band) relation for the solar attenuation in the earth atmosphere which may be used in evaluating SUAR radiation in section 3.3.7. Though approximate, Eq. (H.14) is at least better than assuming that all solar UV ($\lambda \leq 280 \text{ nm}$) starts at an altitude $h = 130 \text{ km}$ and is absent below this altitude. This latter type of assumption would have to be made as a zero-order approximation in the absence of any other data.

As better and finer spectral transmission data become available using tunable laser spectrometry, it should be possible to replace Eqs. (H.14) through (H.26) with much more accurate relations. In constructing analytical expressions for these future equations, the theory given in section 4.8 of Volume II and the general relations for atmospheric transmission given in Volume V of the Rocket Radiation Handbook would be needed.

APPENDIX I

EFFECTIVE THROAT AND PLUME DIAMETERS FOR MULTIPLE-NOZZLED ROCKETS*

In applying the radiant emission formulas of Chapter 3 to actual rockets, a difficulty arises when a rocket has more than one nozzle. The radiation expressions were developed for a one-nozzle jet and exhibit only one parameter D_t (the throat diameter), on the basis of which the nozzle exit diameter D_e and the plume diameter D_p may be calculated via the one-dimensional rocket-flow relations:

$$D_e = \sqrt{E} D_t, \text{ m} \quad (I.1)$$

$$E = \left(\frac{\gamma-1}{2}\right)^{1/2} \left(\frac{2}{\gamma+1}\right)^{\frac{\gamma+1}{2(\gamma-1)}} \left(\frac{p_c}{p_e}\right)^{\frac{1}{\gamma}} \left[1 - \left(\frac{p_e}{p_c}\right)^{\frac{\gamma-1}{\gamma}}\right]^{-1/2} \quad (I.2)$$

$$\frac{D_p}{D_t} \equiv F = \frac{D_{exh}}{D_t} = \left(\frac{\gamma-1}{2}\right)^{1/4} \left(\frac{2}{\gamma+1}\right)^{\frac{\gamma+1}{4(\gamma-1)}} \left(\frac{p_c}{p_a}\right)^{\frac{1}{2\gamma}} \left[1 - \left(\frac{p_a}{p_c}\right)^{\frac{\gamma-1}{\gamma}}\right]^{-1/4}, \text{ m}, \quad (I.3)$$

If the one-dimensional adiabatic flow relations which lead to (I.3) are inadequate, one may write more generally that:

*The material for this Appendix was provided by R. Chardon.

June 1974

$$\frac{D_p}{D_t} = F'(p_a, p_c, \gamma), \text{ m} \quad (1.4)$$

Here the function $F'(p_a, p_c, \gamma)$ may contain two-dimensional and other corrections.

The various parameters in the above relations are:

- D_t = Throat diameter, m
- E = Nozzle area ratio
- D_e = Nozzle exit diameter, m
- D_{exh} = Plume diameter assuming adiabatic expansion, m
- γ = Gas coefficient ($\gamma \sim 1.23$)
- p_e = Design pressure in nozzle exit plane, bars
- p_c = Rocket chamber pressure, bars
- p_a = Ambient atmospheric pressure, bars

To estimate the effective diameters D_p of rocket plumes with N_N nozzles, one approach is to add the flow-through areas of each nozzle and take an average diameter based on the total area according to the relation:

$$(D_t)_N = N_N^{1/2} D_t, \text{ m} \quad (1.5)$$

or more generally:

$$(D_t)_N = \left[\sum_{i=0}^{N_N} (D_t)_i^2 \right]^{1/2}, \text{ m} \quad (1.6)$$

Equation (1.5) or (1.6) may then be used in the radiation equations for D_t when multiple-nozzled rockets are considered. However it will be shown below that such a simple assumption, while reasonable at high altitudes, underestimates the plume diameter at the lower altitudes.

For reference purposes, diameters calculated according to the expressions (I.5) or (I.6) will be given the subscript N. Thus:

$$(D_t)_N = k_N (D_t)_{\text{one-nozzle}}, m \quad (I.7)$$

$$(D_e)_N = k_N (D_e)_{\text{one-nozzle}}, m \quad (I.8)$$

$$(D_p)_N = k_N (D_p)_{\text{one-nozzle}}, m, \quad (I.9)$$

where:

$$k_N = N_N^{1/2} \quad (I.10)$$

Note that all effective diameters, D_t , D_e , and D_p are scaled by the same factor k_N .

To estimate multi-nozzle effects at low altitudes more accurately, some simple geometric arguments will be used rather than a full-fledged fluid dynamics analysis.* Such a "modeling" approach is more than adequate for the purpose of radiance calculations.

Referring to Figures I-1 through I-9, a number of possible nozzle configurations are shown whose effective values D_t , D_e , and D_p will be estimated by geometric modeling. Key parameters for nozzle diameter modeling are the multiple nozzle circle diameter C_D (or rocket skirt diameter $D_r = C_D + D_e$ (Figure I-2)), and the separation between nozzles S_N (see Fig. I-9). In many cases S_N is small or zero and the additional complication of assuming a finite S_N may be neglected as was done in Figure I-1 through

*Because the flow is supersonic the outer regions of the multiple jets can initially not sense the internal interference shocks between jets. Hence the simple geometric considerations given here are adequate for the "early" part of the plume.

June 1974

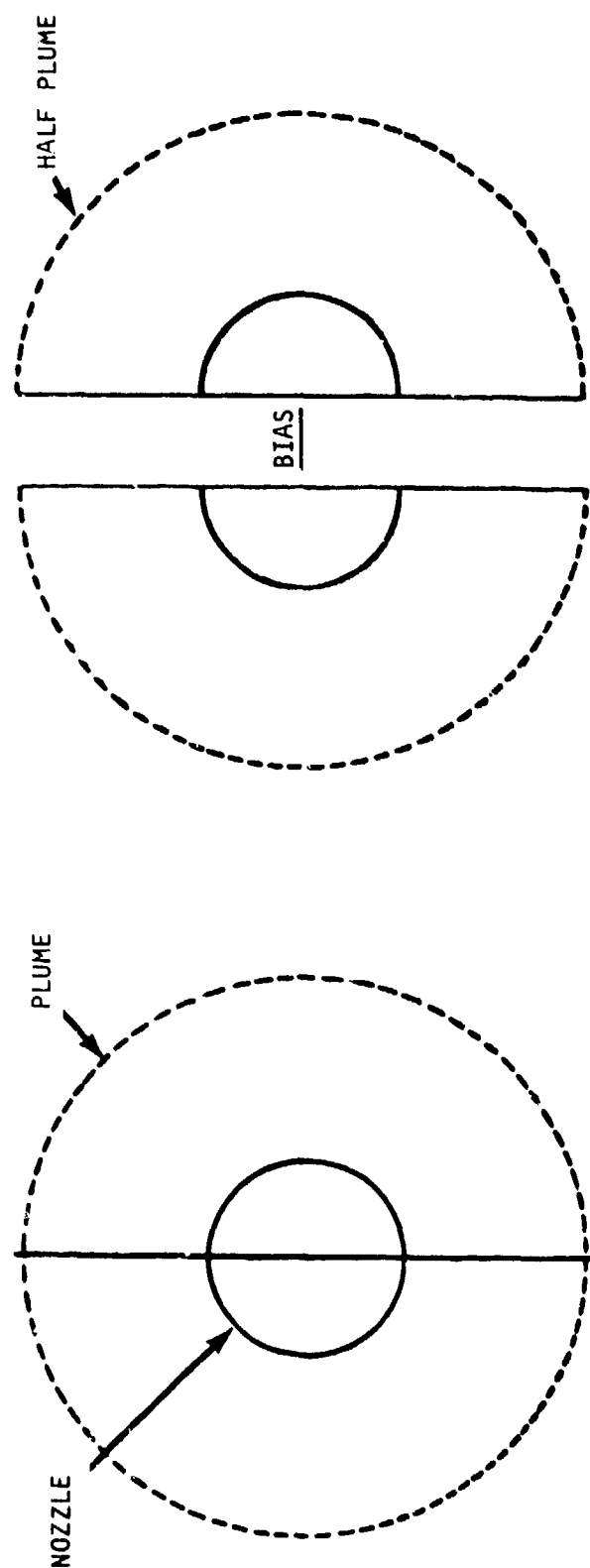


FIGURE I-1. ILLUSTRATION OF THE MODELING OF TWO EFFECTIVE HALF NOZZLES

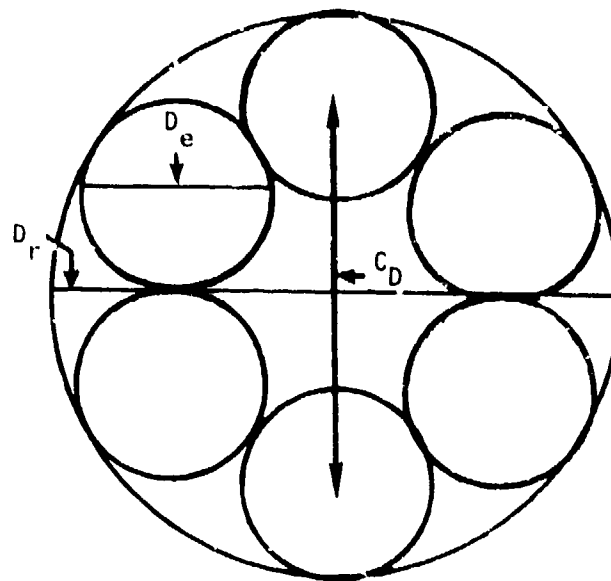


FIGURE I-2. MODEL FOR SIX NOZZLES

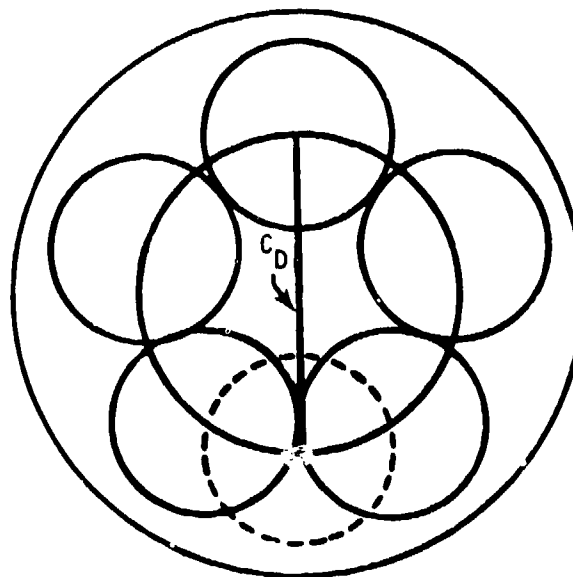


FIGURE I-3. MODEL FOR FIVE NOZZLES (PENTAGON)

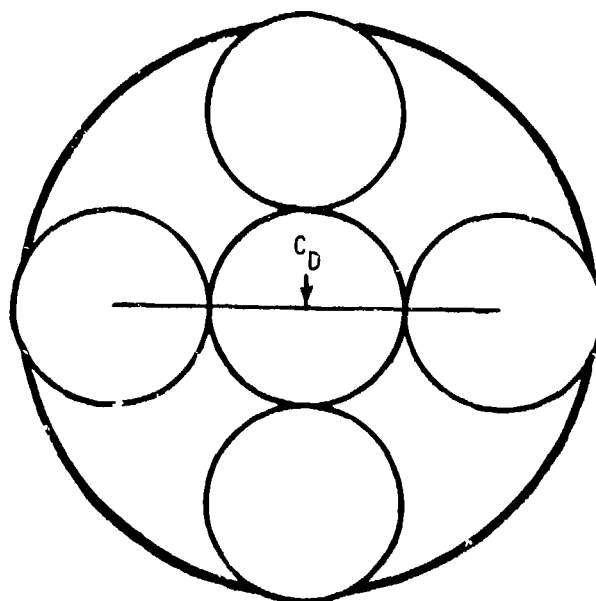


FIGURE I-4. MODEL OF FIVE NOZZLES (CROSS)

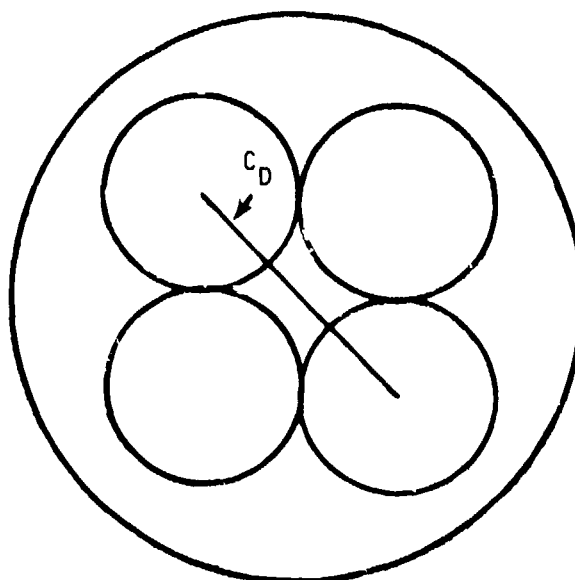


FIGURE I-5. MODEL OF FOUR NOZZLES

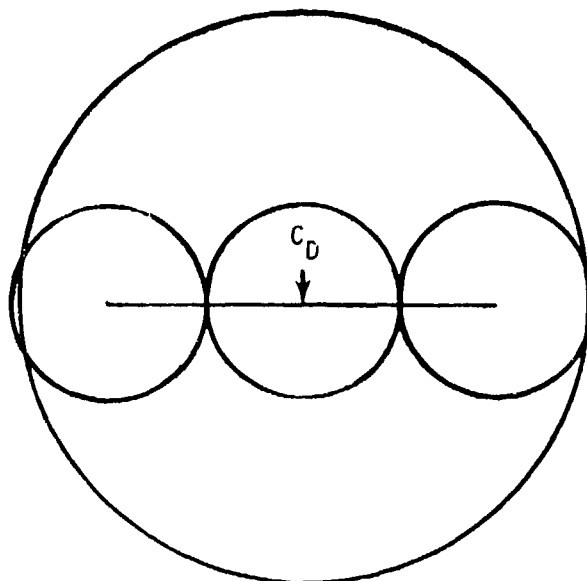


FIGURE I-6. MODEL OF THREE NOZZLES (LINEAR)

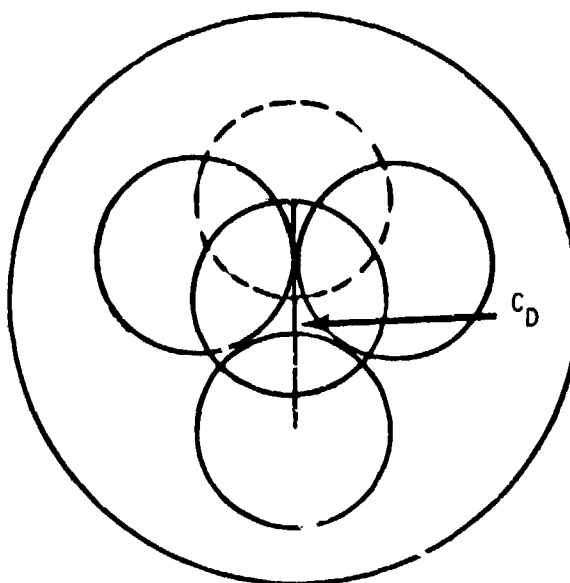


FIGURE I-7. MODEL OF THREE NOZZLES (TRIANGULAR)

June 1974

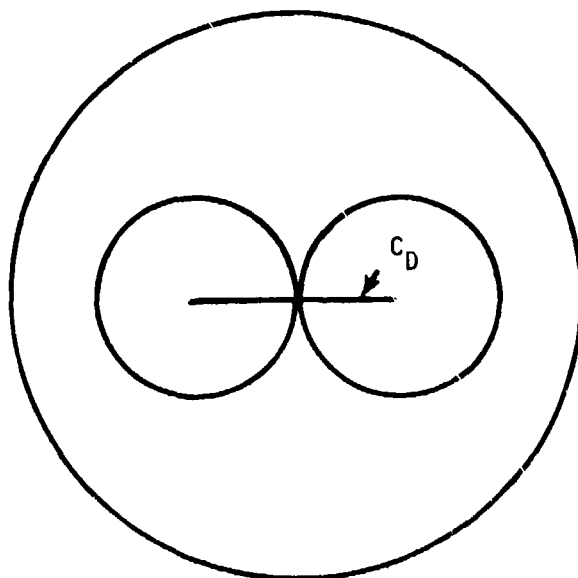


FIGURE I-8. MODEL OF TWO NOZZLES

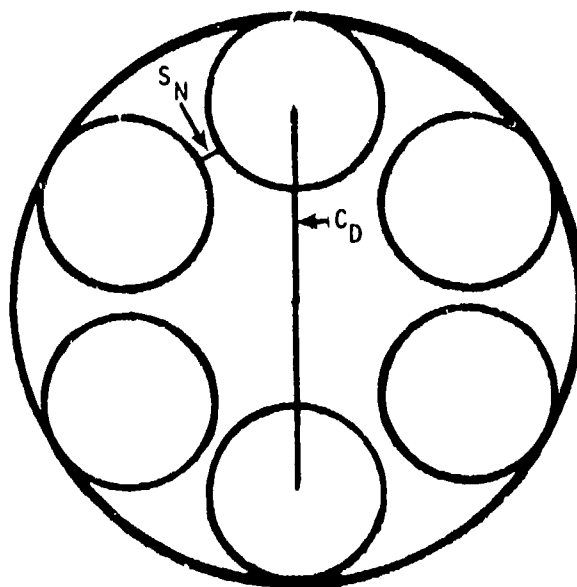


FIGURE I-9. GENERALIZATION OF MODEL TO INCLUDE
SEPARATION BETWEEN NOZZLES

June 1974

Figure I-8. However in the expressions that follow, the assumption of a finite value for S_N will be retained.

Starting with the six-nozzle configuration shown in Figure I-9, one has:

$$C_D = 2(D_E + S_N) = 2(D_t \sqrt{E} + S_N) \quad (I.11)$$

Since the geometric plume diameter $(D_p)_G$ is:

$$(D_p)_G = D_p + C_D, \quad (I.12)$$

one obtains for the case of:

a. Six Nozzles (Fig. I-9)

$$(D_p)_G = D_t (F(p_a, p_c, \gamma) + 2 \sqrt{E}) + 2 S_N \quad (I.13)$$

Here Eq. (I.4) was also used. For the other cases, one finds similarly:

b. Five Nozzles (Pentagon)

$$(D_p)_G = D_t (F(p_a, p_c, \gamma) + \sqrt{E} \csc(\frac{\pi}{5})) + S_N \csc(\frac{\pi}{5}) \quad (I.14)$$

c. Five Nozzles (Cross)

$$(D_p)_G = D_t (F(p_a, p_c, \gamma) + 2 \sqrt{E}) + 2 S_N \quad (I.15)$$

June 1974

d. Four Nozzles

$$(D_p)_G = D_t (F(p_a, p_c, \gamma) + \sqrt{2E}) + S_N \sqrt{2} \quad (I.16)$$

e. Three Nozzles (Linear)

$$(D_p)_G = D_t (F(p_a, p_c, \gamma) + 2\sqrt{E}) + 2 S_N \quad (I.17)$$

f. Three Nozzles (Triangular)

$$(D_p)_G = D_t (F(p_a, p_c, \gamma) + \sqrt{E} \sec(\frac{\pi}{6})) + S_N \sec(\frac{\pi}{6}) \quad (I.18)$$

g. Two Nozzles

$$(D_p)_G = D_t (F(p_a, p_c, \gamma) + \sqrt{E}) + S_N \quad (I.19)$$

From relations (I.14) through (I.19), it is clear that the separation of the nozzles S_N produces a direct additive effect on the plume diameter $(D_p)_G$. Calculations which ignore or neglect S_N will predict a plume diameter that is too small.

To illustrate what happens when the multiple-nozzle effect is more accurately accounted for by means of geometric modeling, some sample calculations are presented and a comparison is made with plume diameter calculations using the "averaging" relations (I.7) through (I.10). For convenience, it is assumed that $S_N \approx 0$ in these calculations, and the following typical values were chosen for the rocket parameters:

$$\left\{ \begin{array}{l} p_a = 1.014 \text{ bar} \\ p_c = 55.17 \text{ bar} \\ \gamma = 1.25 \end{array} \right\} \longrightarrow F(p_a, p_c, \gamma) = 2.619, \text{ using Eq. (I.3)}$$

$$D_t = 0.184 \text{ m}$$

$$E = 20$$

Example 1. Two Nozzles

a. Calculation by Eq. (I.19):

$$(D_p)_G = D_t (F(p_a, p_c, \gamma) + \sqrt{E})$$

$$(D_p)_G = 0.184 \{2.619 + 4.472\} \text{ m}$$

$$(D_p)_G = 1.305 \text{ m}$$

b. Calculation by Eq. (I.9):

$$(D_p)_N = D_t \sqrt{N} F(p_a, p_c, \gamma) = 0.184 (1.414) (2.619)$$

$$(D_p)_N = 0.681, \text{ m}$$

c. Comparison:

$$\frac{(D_p)_G}{(D_p)_N} = \frac{1.305}{0.681} = 1.916$$

Example 2. Three Nozzles (Linear)

a. Calculation by Eq. (I.18):

$$(D_P)_G = 0.184 \{2.619 + 2 (4.48)\}$$

$$(D_P)_G = 2.131 \text{ m}$$

b. Calculation by Eq. (I.9):

$$(D_P)_N = 0.184 \sqrt{3} (2.619)$$

$$(D_P)_N = 0.835 \text{ m}$$

c. Comparison:

$$\frac{(D_P)_G}{(D_P)_N} = \frac{2.131}{0.835} = 2.553$$

Example 3. Three Nozzles (Triangular)

a. Calculation by Eq. (I.17):

$$(D_P)_G = 0.184 \left(2.619 + \frac{4.48}{0.866} \right)$$

$$(D_P)_G = 1.434 \text{ m}$$

b. Calculation by Eq. (I.9):

$$(D_p)_N = 0.184 \sqrt{3} (2.619) \text{ m}$$

$$(D_p)_N = 0.835 \text{ m}$$

c. Comparison:

$$\frac{(D_p)_G}{(D_p)_N} = \frac{1.434}{0.835} = 1.718$$

For the four nozzle case one finds similarly that $\frac{(D_p)_G}{(D_p)_N} = 1.72$, while for the five nozzle pentagon this ratio is approximately 2.00, and for the six nozzle configuration the ratio is 1.82.

From the above illustrations it is evident that the calculation of the effective plume diameter via the "averaging" method of Eq. (I.9) yields a plume diameter that is too small by a factor of approximately two at the lower altitudes where p_a has values between 0.01 and 1 bar. At high altitudes however where $F(p_a, p_c, \gamma)$ becomes large, the opposite is true, and Eq. (I.9) gives values for D_p that are higher than those estimated by the geometric relations (I.13) through (I.19). For example at $p_a = 5.52 \times 10^{-9}$ bars (altitude = 140 km), one finds, assuming again $\gamma = 1.25$ and $p_c = 55.2$ bars, that $F(p_a, p_c, \gamma) = 5,473.25$. Thus for two nozzles, one obtains in this case $(D_p)_N = 1,424.22$ meters from Eq. (I.9), while Eq. (I.19) gives $(D_p)_G = 1,007.89$ meters. For more than two nozzles, $(D_p)_N$ is even much larger than $(D_p)_G$, and approximately $(D_p)_N / (D_p)_G \sim \sqrt{N_N}$ at high altitudes.

The geometric method fails to account for intermixing of the jets from different nozzles. It assumes that gas in the intermixing overlap regions of different jets, results in a gas at the same pressure and density as the gas in non-overlap regions, which is of course unphysical. The "averaging" method on the other hand assumes that the jets are completely and thoroughly mixed and issue from one "averaged" nozzle.

At high altitudes where the jets of the different nozzles have to travel a considerable distance before reaching the maximum diameter D_p , and where there is some time available for intermixing, the "averaging" method for calculating plume diameters should be quite adequate. At the lower altitudes however, where expansion to the maximum plume diameter is rapid and takes place before high-pressure interference shocks can travel and reach the boundaries of the jets, the simple geometric method outlined above should suffice. As a compromise therefore one may assume the following relation for the plume diameter of a multi-nozzle rocket:

$$(D_p)_{\text{eff}} = (D_p)_G H(D_{pG} - D_{pN}) + (D_p)_N H(D_{pN} - D_{pG}), \quad m \quad (I.20)$$

Here $H(x)$ is the unit step function ($H(x \geq 0) = 1$; $H(x < 0) = 0$), and (I.20) states thus simply that $(D_p)_{\text{eff}}$ is the larger of D_{pG} and D_{pN} . Expressions for $(D_p)_N$ and $(D_p)_G$ to be used in (I.20) are of course (I.9) and (I.13) through (I.19), depending on the number of nozzles.

NOMENCLATURE AND UNITS

The various symbols adopted in the Rocket Radiation Handbook constitute a compromise between those that are current in various disciplines. For example, the symbol σ , which was adopted for microscopic cross-sections (cm^2), is presently used by most applied atomic scientists and nuclear engineers, although theoretical nuclear physicists often prefer Q and some chemical kineticists employ S for this parameter. Since Q and S have already other well-established meanings in engineering, σ was chosen in this case for cross-sections. A determined effort was made throughout to stay as close as is practically possible to already established nomenclature.

The symbols adopted for radiometric quantities are, with few exceptions, in conformity with those recommended by the "Working Group on Infrared Backgrounds," Report No. 2389-3-S, Univ. of Michigan Institute of Science and Technology (1956). Further, the mks (meter, kilogram, second) system of units is used throughout, although in some instances a conversion to English units (foot, pound, second) is provided for the benefit of those that are still accustomed to it.

$a, a(\lambda)$	= Earth albedo or total solar reflectance (at wavelength λ) from earth atmosphere and surface.
\bar{a}	= Wavelength-averaged earth albedo
$a = (g_{H_2})_o$	= Concentration of H_2 entering AB reaction region (used in Appendix E only), moles per kgm of air plus exhaust.
a_e	= Original radius of axisymmetric exhaust plume, m.
a_o	= Radius of bottom face of a full cone, m.
a_1, a_2	= Radii of end faces of truncated cone, m.
A	= General surface area, m^2 .
A_e	= Rocket nozzle exit plane area, m^2 .
A_{exh}	= Plume maximum cross-sectional area, m^2 .
A_{proj}, A_p, dA_p	= Projected surface area, or element of projected surface area, of diffusely emitting object, m^2 .
A_s	= Sensor field-of-view area at target, m^2 .
A_t	= Rocket nozzle throat area, m^2 .
A_o	= Avogadro's number = 6.025×10^{23} molecules/mole.
A_i, A_i^o	= Einstein total radiative decay constant for excited level i ; $A_i^o = \sum_j A_{ij}^o$, sec^{-1} .
A_{ij}^o	= Einstein radiative decay constant for transitions $i \rightarrow j$, sec^{-1} .
AB	= Afterburning radiation mechanism occurring in rocket plumes (used as subscript and in abbreviation).
ABCD	= Combined afterburning and collisional deceleration radiation (used as subscript and in abbreviation).
ATMP	= Abbreviation for atmospheric pumping mechanism. Used also as subscript.

- $b \left(g_{O_2} \right)_o$ = Original concentration of O_2 entering ABCD region (used in Appendix E only), moles per kgm of air plus exhaust.
- $h(\nu, \nu_{ij}, \Delta\nu_{ij})$ = Dimensionless spectral band-shape or line-shape function for photon emissions of frequency ν from transitions $i \rightarrow j$ with frequency spread $\Delta\nu_{ij}$.
- B = Exhaust jet or plume parameter defined by Eq. (3.228).
- $B(X_i) = B_i$ = Stimulated deexcitation rate of excited levels of i of species X , sec^{-1} .
- c = Velocity of light = 2.99793×10^8 m/sec.
- c_c = Average molecular velocity of molecules escaping from the plume core region in deep space, m/sec.
- C, dC = Surface area, element of surface area, m^2 .
- C_e = Imaginary surface surrounding region in space where exhaust gases emit all radiation, m^2 .
- $C(X_i) = C_i$ = Resonant photon capture rate by species X resulting in the excitation of level i , sec^{-1} .
- C_a, C_e = Molar heat capacity of air and exhaust molecules (at constant pressure), $\text{Joules} \cdot (^\circ\text{K})^{-1}$ per mole or per molecule.
- C_{P_i} = Specific particle production factor for species i , particles/kgm.

June 1974

- CD = Collisional deceleration radiation mechanism occurring in rocket plumes (used as subscript and in abbreviation).
- CORE = Undisturbed core or mach cone radiation mechanism occurring in rocket plumes (used as subscript and in abbreviation).
- d_m, d_A, d_X = Collision diameters of general molecules m, of air molecules A, and exhaust molecules X, m or cm.
- $d_p, \bar{d}_p, \bar{d}_i, \bar{d}_X$ = Average particle diameter of solid entrained particles (of species i or X) in exhaust, m or μm .
- $D_a = D$ = Effective diameter of equivalent cylindrical AB chemical reactor, m.
- D_c = Truncated-cone largest body dimension defined by Eq. (C.41), m.
- D_e = Rocket nozzle exit diameter, m.
- D_{exh} = Exhaust gas diameter for adiabatic isentropic expansion to ambient pressure, m.
- D_h = Exhaust gas diameter for isentropic expansion to ambient pressure with radiation loss correction, m.
- D_r = Radiation-limited plume diameter defined by Eq. (3.361).
- D_p = Equivalent cylindrical diameter of rocket exhaust plume, m, defined by Eq. (C.40).
- D_q = DIAMETER USED IN VIEW-FACTOR CALCULATIONS, DEFINED BY EQ. (C.41)

D_s	=	Sensor field-of-view diameter at the target, m.
D_t	=	Rocket nozzle throat diameter, m.
D_v	=	Rocket vehicle body or skirt diameter, m.
D_1, D_2	=	Diameters of end faces of truncated cone ($D_2 > D_1$), m.
D_{ABCD}	=	Imaginary equivalent cylindrical diameter of ABCD emission region, m.
$D(X_i) \equiv D_i$	=	Photon emission rate by species X from excited level i, sec^{-1} .
DSPR	=	Deep space plume radiation mechanism occurring for rocket exhausts in the exosphere, used in subscripts and in abbreviation.
D, D_{X_i}, D_i, D_X	=	Diffusion coefficient, of molecules X_i or X, m^2/sec .
D_t	=	Turbulent diffusion coefficient, m^2/sec .
$D_{\text{tot}} \approx D + D_t$	=	Total diffusion coefficient due to molecular diffusion and turbulence, m^2/sec .
$E = \frac{A_e}{A_t}$	=	Nozzle area (or expansion) ratio.
$E(X_i) = E_i$	=	Photon emission rate due to deexcitations from level i, sec^{-1} .
E_{ion}	=	Ionization energy of an atom or molecule, Joules or eV.

- i_p = Weight fraction of condensable species in rocket exhaust.
- f_{ij} = Relative fractional probability for level i to deexcite to level j ; $f_{ij} = A_{ij}^0 \left[\sum_j A_{ij}^0 \right]^{-1}$.
- f_{rci} = Average probability that recombining electrons will cascade through level i .
- $f(\chi)$ = Special function defined by Eq. (G.6) or (G.8) used in formula for photoionization cross-sections (used in Appendix G only).
- $f(\xi)$ = AB reaction function for CO afterburning defined by Eq. (E.72)(used in Appendix E only).
- $f_r(\eta_s, \lambda)$ = Specular photon reflection function defined by Eq. (3.30), dependent on angle of incidence and photon wavelength.
- $f_{r\perp}, f_{r\parallel}$ = Specular photon reflection functions for perpendicular (\perp) and parallel (\parallel) polarized light, defined by Eqs. (3.31) and (3.32).
- $f(s), f(\psi)$ = Functions giving angular/geometry dependences of the photon reflectivity of a body's surface for sun-body-observer angle ψ (see Eq.(3.20) through (3.24) and section 2.2).
- fov = Field-of-view, used in abbreviation and as subscript.
- F = Rocket thrust, Mgm(F), kgm(F), or Newtons.
- F = Exhaust gas diameter expansion ratio defined by Eq. (3.367).
- F = Earthshine irradiance factor for a space body (see figure 3.8).

- F_v = Field-of-view factor to correct for aspect-angle dependence of radiant intensity, defined in Appendix C.
- $F(X_i) = F_i$ = Population rate of excited level i and species X due to radiative decay from higher levels $j > i$, sec^{-1} .
- FIR = Far-infrared part ($8 \leq \lambda \leq 20 \mu\text{m}$) of the electromagnetic spectrum. Used in abbreviation.
- \mathcal{J} = Reaction mass feed rate to equivalent AB chemical reactor region, kgm/sec .
- g_c = Concentration of propellant fuel burnt in rocket chamber, moles per kgm of total propellants.
- g_F = Concentration of unburnt fuel leaving rocket nozzle, moles per kgm of total exhaust.
- g_X = Concentration of exhaust species X ($X = \text{H}_2\text{O}$, CO , CO_2 , etc.) in rocket exhaust gas, moles per kgm of total exhaust.
- g_{X_i}, g_i = Concentration of exhaust species X at excited level i in rocket exhaust gas, moles per kgm of total exhaust.
- g_{p_i} = Concentration of condensable exhaust species i in rocket exhaust, moles per kgm of total exhaust.
- $g_{\text{tot}}, (g_{\text{tot}})_o$ = Total moles per kgm , at entry point (subscript o), of reactants (used in Appendix E only).
- $q(x)$ = AB reaction function defined by Eq. (E 44) (used in Appendix E only).

June 1974

- G = Total mass density of reactants in AB region, gm/cm^3 .
- $G(X_i) = G_i$ = Net influx or outflux of molecules X in excited state i due to transport, sec^{-1} .
- h = Altitude, km
- h = Planck's constant = 6.6252×10^{-27} erg.sec (when appearing next to frequency).
- h = Height of undisturbed Mach cone, m.
- $h(\xi) = h(\xi_{\text{H}_2\text{O}})$ = Reaction function for H_2O production by AB process defined by Eq. (E.50) (used in Appendix E only).
- H = Irradiance or illumination intensity, watts/m^2 .
- H_o = Total solar irradiance or illumination intensity from the sun in the vicinity of planet earth, watts/m^2 .
- $H_{\Delta\lambda}$ = Irradiance or illumination intensity in wavelength range $\Delta\lambda$, watts/m^2 .
- $H_B(\lambda)$ = Irradiance or illumination intensity at wavelength λ from background radiation, watts/m^2 .
- $H_E = H_E(\lambda)$ = Irradiance or illumination intensity due to earthshine (at wavelength λ), watts/m^2 .
- $H_I(\lambda)$ = Irradiance or illumination intensity at wavelength λ from a general illuminating source, watts/m^2 .
- $H_S(\lambda)$ = Irradiance or illumination intensity at wavelength λ from the sun, watts/m^2 .

$H_T(\lambda)$	= Irradiance or illumination intensity at wavelength λ from a radiating target, watts/m ² .
$\frac{dH}{d\lambda}$	= Spectral solar irradiance, W · m ⁻² · nm ⁻¹ .
$H(x)$	= Heaviside unit step function; $H(x) = 0$ for $x < 0$, $H(x) = 1$, for $x \geq 0$.
$H(T_e)$	= Enthalpy of exhaust gas in the nozzle exit plane, Joules/mole or kcal/mole.
$\Delta H_c, \Delta H_x$	= Molar heat of combustion of rocket fuel, or species X , Joules/mole or kcal/mole.
i	= Used as a subscript to indicate an excited level in an atom or molecule.
I_{sp}	= Rocket propellant specific impulse, sec.
IR	= Infrared part ($1 \leq \lambda \leq 20 \mu\text{m}$) of the electromagnetic spectrum. Used as subscript and in abbreviation.
ICO	= Integrated cloud observation viewing condition; used as subscript and in abbreviation.
j	= Used as a subscript to indicate an excited level in an atom or molecule.
J	= Radiant intensity, watts · ster ⁻¹ .

$J(\lambda)$	= Radiant intensity at wavelength λ , watts \cdot ster $^{-1}$.
$J(\nu)$	= Radiant intensity at frequency ν , watts \cdot ster $^{-1}$.
$dJ/d\lambda = dJ(\lambda)/d\lambda$	= Radiant intensity at wavelength λ per unit wavelength, watts \cdot ster $^{-1} \cdot \mu\text{m}^{-1}$.
$dJ/d\nu = dJ(\nu)/d\nu$	= Radiant intensity at frequency ν per unit frequency, watts \cdot ster $^{-1} \cdot \text{THz}^{-1}$, or watts \cdot ster $\cdot \text{Hb}^{-1}$.
J_{ABCD}	= Radiant intensity due to the ABCD mechanism in a rocket plume only, watts \cdot ster $^{-1}$.
J_{CORE}	= Radiant intensity due to the CORE mechanism in a rocket plume only, watts \cdot ster $^{-1}$.
J_{DSPR}	= Radiant intensity from a rocket plume in deep space, watts \cdot ster $^{-1}$.
J_{SUAR}	= Radiant intensity from a rocket plume due to solar ultraviolet absorption and reemission, watts \cdot ster $^{-1}$.
J_{ATMP}	= Radiant intensity due to atmospheric pumping, watts \cdot ster $^{-1}$.
J_{SOSP}	= Radiant intensity due solar photon scattering by particles in rocket exhaust, watts \cdot ster $^{-1}$.
$J_{\text{VBSR}}, J_{\text{VBER}}$	= Radiant intensity due to rocket vehicle body solar reflections (VBSR) and earthshine reflection (VBER), watts \cdot ster $^{-1}$.
k	= Used as a subscript to indicate a general excited level in an atom or molecule.

- k = Boltzmann's constant = 1.3804×10^{-23} Joule \cdot ($^{\circ}\text{K}$) $^{-1}$,
when appearing next to temperature T .
- k_d = Collision factor from the kinetic theory of gases;
 $k_d = 1.000$ for hard-sphere molecules, $k_d = 1.2652$ for
"inverse-fifth-power-repulsion" molecules (Ref. 34).
- k_{m_f}, k_{m_r} = Forward (f) and reverse (r) chemical reaction rate
constant for reaction m (used in Appendix E only),
 $\text{cm}^3 \cdot \text{mole}^{-1} \cdot \text{sec}^{-1}$ (first-order reactions) or
 $\text{cm}^6 \cdot \text{mole}^{-1} \cdot \text{sec}^{-1}$ (second-order reactions).
- K_o = Effective overall AB chemical rate constant (used in
Appendix E, $\text{cm}^3 \cdot \text{mole}^{-1} \cdot \text{sec}^{-1}$.
- l = Length of (truncated) cone, m.
- l_c = Mean free path for molecular collisions, m or cm.
- L = Length of cylindrical body, m.
- L_c = Longest linear dimension of optically dense plume
core in deep space, m.
- L_p = Equivalent cylindrical radiating plume length, m.
- $L(X_i) = L_i$ = Collisional deexcitation (V-T) rate of excited levels
of species X , sec^{-1} .
- \bar{L}_M, L_M = Average length of Mach core region, m.
- L_{ABCD} = Imaginary equivalent cylindrical length of ABCD mixing
region, m.

June 1974

- L_a, L = Length of equivalent cylindrical AB chemical reactor, m.
- L_m = Relative intensity of special solar spectral lines in the UV (see table 3-2).
- $L(\xi), L(\xi_{H_2O}), L(\xi_{CO_2})$ = Reaction length (defined by Eq. (E.49) or (E.71)) for conversion of H_2O and CO_2 in AB region to the limit values ξ_{H_2O} or ξ_{CO_2} (used in Appendix E only).
- m = Real part of the optical index of refraction of a material.
- m_a = Molar density of air, moles $\cdot m^{-3}$.
- m_e = Molar density of rocket exhaust, moles $\cdot m^{-3}$.
- m_I = Molar density in CORE/ABCD interface region, moles $\cdot m^{-3}$.
- m_{tot} = Total number of reactants per unit volume (used in Appendix E only), moles $\cdot cm^{-3}$.
- M = Molecular mass, amu (= molec. wt.) or grams.
- M_a, M_{air} = Average molecular weight of air, amu (= gms/mole) or kgm.
- M_e, \bar{M}_e = Average molecular weight of rocket exhaust in nozzle exit plane, amu (= gm/mole).
- M_p, M_{p_i} = Molecular weight of condensables (of species i) in rocket exhaust, amu (= gm/mole).
- $L(\lambda), L(\gamma)$ = CONTINUUM FUNCTION OF SPECIAL SOLAR UV LINE
DEFINED BY Eq. (3.292)

M_X	= Molecular weight of gaseous rocket exhaust species X, amu (= gm/mole).
$\bar{M}_X = M_{XY}$	= Reduced mass of molecules X-Y collisions, defined by Eq. 3.71, amu (= gm/mole).
MIR	= Mid-infrared part ($4 \leq \lambda \leq 8 \mu\text{m}$) of the electromagnetic spectrum. Used in abbreviation.
M_α	= Vibrational mass of normal vibration α , amu.
M_{ij}	= Effective vibrational mass for transition $i \rightarrow j$, amu.
n	= Molecular density, molecules/ m^3 .
n_X	= Molecular density of molecules X, molecules/ m^3 .
$n_{X_i}, n(X_i), n_i$	= Molecular density of molecules X in excited state i, molecules/ m^3 .
$n_a = n_{\text{air}} = n_a(h)$	= Molecular density of air, molecules/ m^3 .
n_o	= General background gas molecular density which diffuses into gaseous jet, molecules/ m^3 .
n_e	= Molecular density of exhaust in nozzle exit plane, molecules/ m^3 .
n_{tot}	= Total molecular density, molecules per m^3 .
n_F	= Molecular density of fuel molecules in exhaust, molecules per m^3 .
N	= Total radiance, watts $\cdot \text{m}^{-2} \cdot \text{sr}^{-1}$.

\dot{N}	= Flow rate of molecules, molecules $\cdot \text{sec}^{-1}$.
N_a	= Total number of air molecules in ABCD region of plume.
N_{exh}, N_e	= Total number of exhaust molecules in ABCD region of plume.
$N_i, N(X_i)$	= Total number of molecules of species X at excited level i.
N_{ij}	= Total number of excitations or deexcitations $i \rightarrow j$.
N_p	= Total number of condensed (liquid or solid) particles in rocket exhaust released in atmosphere.
N_X	= Total number of molecules of species X.
N_λ^o	= Spectral radiance, watts $\text{m}^{-2} \cdot \text{sr}^{-1} \cdot \mu\text{m}^{-1}$.
N^o	= Spectral radiance, watts $\cdot \text{m}^{-2} \cdot \text{sr}^{-1} \cdot \text{Hb}^{-1}$.
N_Y	= Number of photons.
N_{Y_i}	= Number of photons emitted from excited levels i.
NIR	= Near-infrared part ($0.7 \leq \lambda \leq 4 \mu\text{m}$) of the electromagnetic spectrum. Used in abbreviation.
p	= General gas pressure, bars.
$p = (g_{\text{CO}})_o$	= Moles of CO entering AB region per kgm of air plus exhaust, defined by Eq. (E.60)(used in Appendix E only).

$p_a = p_a(h)$	= Ambient air or atmospheric pressure, bars.
p_e	= Exhaust gas pressure in rocket nozzle exit plane, bars.
p_o	= Design pressure of exhaust gas in nozzle exit plane, bars.
p_c	= Rocket chamber gas pressure, bars.
p_{tot}	= Total pressure, bars.
p_i	= Average escape probability for photons emitted from level i to escape from plume without being reabsorbed.
p_{oi}	= Probability of exciting level i in a collision between an exhaust and air molecule in the AIMP process.
p_r	= Atmospheric pressure at altitude where radiation cloud diameter prevails (Eq. 3.361), bars.
P	= Radiant power = Total rate of energy emitted by a body, watts.
P_{CORE}	= Total radiant power emitted from the CORE region, watts.
$P(X_i) = P_i$	= Collisional excitation (T-V) rate of excited levels i of species X , sec^{-1} .
q_i, q_α	= Boltzmann exponent factor defined by Eq. (3.187).
$q = \left(g_{O_2} \right)_o$	= Moles of O_2 per kgm of exhaust plus air entering AB region, defined by Eq. (E.61)(used in Appendix E only).
Q	= Used as subscript on temperature T and velocity V for ABCD region.

June 1974

r	= Radius of cylindrical body, m.
\vec{r}	= General position vector, m.
r_f	= Radial distance from rocket plume axis to diffusion front, m.
r_A, r_X	= Collision radii of air (A) and exhaust (X) molecules, cm or m.
r_{H_2O}, r_{CO_2}	= Rate of reaction of H_2O and CO_2 production (used in Appendix E only), moles \cdot cm $^{-3}$ \cdot sec $^{-1}$.
$r_{\alpha, i}$	= Equilibrium separation for normal vibration α in electronic excited level i (used in vibronic band calculations), cm.
R	= Gas constant = 8.317 Joules \cdot ($^{\circ}K$) $^{-1}$ \cdot mole $^{-1}$.
R	= Radius of spherical body, m.
R	= Radius measured from center of earth, m or km
R_E	= Earth radius, m or km.
R_{ij}^2	= Transition ($i \rightarrow j$) matrix element, cm 2 .
$R(X_i) = R_i$	= Rate of excitation of levels i of species X due to V-V resonant potential energy transfer collisions, sec $^{-1}$.
Re	= Reynolds number.
RW	= Radarwave part ($20 \leq \lambda \leq 10,000 \mu m$) of the electromagnetic spectrum. Used in abbreviation.

- s = Moles of CO_2 produced due to CO afterburning in ABCD region per kgm of air plus exhaust (used in Appendix E only).
- $d\vec{s}$ = Unit surface element vector, m^2 .
- S = Distance between observer and rocket, m.
- S_{AP} = Length of rocket trail in the part of the atmosphere where the atmospheric pumping mechanism is active, m.
- S_{HACR} = Length of rocket trail in that part of the atmosphere where high-altitude chemical reactions are active, m.
- $S(X_i) = S_i$ = Rate of deexcitation of levels i of species X due to resonant V-V potential energy transfer collisions, sec^{-1} .
- S_s = Approximate solar UV atmospheric transmission factor defined by Eq. (3.300).
- $S(r')$ = Initial distribution of molecules (as a function of point r') in diffusion problem at time $t = 0$ (used only in Appendix D).
- S_o = Total number of molecules in diffusion problem (used only in Appendix D).
- SUAR = Solar ultraviolet absorption and reradiation mechanism occurring in rocket plumes at high altitudes (used as subscript and in abbreviation).
- SOSP = Scattering of solar photons by particles in rocket plume (used as subscript and in abbreviation).

June 1974

t	= Time, sec.
t'	= Time measured from rocket thrust cessation, sec.
t_b	= Rocket burn time, sec.
t_f	= Time of travel for the inwards moving turbulent diffusion front to reach the axis of the exhaust jet, starting at the nozzle exit plane, sec.
t_{AP}	= Rocket travel time in region of the atmosphere where atmospheric pumping is active, sec.
t_{HACR}	= Rocket travel time in region of the atmosphere where high-altitude chemical reactions are active, sec.
t_s	= Field-of-view transit time defined by Eq. (3.264), sec.
T	= General temperature of a body or gas, $^{\circ}\text{K}$.
T_a	= Temperature of ambient air or atmosphere, $^{\circ}\text{K}$.
T_c	= Rocket combustion chamber temperature, $^{\circ}\text{K}$.
T_e	= Rocket nozzle exit plane temperature, $^{\circ}\text{K}$.
T_{exh}	= Temperature of rocket exhaust gas after expansion to ambient pressures assuming adiabatic isentropic expansion, $^{\circ}\text{K}$.
T_h	= Temperature of rocket exhaust gas after expansion to ambient pressures assuming isentropic expansion with radiation corrections, $^{\circ}\text{K}$.
T_o	= Design temperature in rocket nozzle exit plane, $^{\circ}\text{K}$.
T_r	= Average temperature of exhaust and air in ABCD mixing region due to all possible effects, $^{\circ}\text{K}$.

T_Q	= Average temperature of exhaust gas entering the ABCD mixing region, °K.
T_I, \bar{T}_I	= Average interface temperature in boundary between CORE and ABCD region, °K.
T_{mix}	= Average temperature of exhaust gases at T_Q and air at T_a when mixed without AB or CD heating effects, °K.
ΔT_{AB}	= Mean temperature increase in ABCD mixing region due to afterburning, °K.
ΔT_{CD}	= Mean temperature increase in ABCD mixing region due to collisional deceleration, °K.
T_M	= Mean temperature in Mach core, °K.
$Tr = Tr(S, \lambda, h)$	= Atmospheric transmission for distance S , wavelength λ , and altitude h .
$Tr_s = Tr_s(h)$	= Transmission of solar UV from outer space into the atmosphere.
TT0	= Target tracking observation viewing condition; used as subscript and in abbreviation.
u, u_X	= Kinetic energy of a molecule (X), ergs or Joules.
U	= Energy, Joules or ergs.
UV	= Ultraviolet ($200 \leq \lambda \leq 380$ nm) part of the electromagnetic spectrum. Used as subscript and in abbreviation.

UVIR	= Ultraviolet-visible-infrared-radarwave ($0.1 \leq \lambda \leq 1000 \mu\text{m}$), or molecular emission part of the electromagnetic spectrum. Used in abbreviation.
UVIS	= Combined ultraviolet and visible ($200 \leq \lambda \leq 700 \text{ nm}$), of the electronic emission part of the electromagnetic spectrum. Used as subscript and in abbreviation.
\bar{v}	= Mean molecular velocity, m/sec or cm/sec.
$\bar{v}_{a/X}$	= Mean relative molecular velocity between air and exhaust molecules, m/sec or cm/sec.
v_{YX}	= Average molecular velocity of molecules Y with respect to molecules X, m/sec.
v	= Vibrational quantum number.
v_{α}, v_{α_i}	= Vibrational quantum number of normal vibration α , in state i .
Δv_{α}	= Change in the vibrational quantum number of normal vibration α in a transition $i \rightarrow j$; $\Delta v_{\alpha} = v_{\alpha_i} - v_{\alpha_j}$
V	= General bulk velocity, m/sec
V_a	= Average velocity of air relative to the plume, m/sec.
\bar{V}_c	= Mean bulk velocity (relative to the rocket) of the molecules in the core region of the plume in deep space, m/sec.
V_{*}	= Turbulent friction velocity, m/sec.

June 1974

V_e	= Nozzle exit plane velocity of rocket exhaust, m/sec.
V_o	= Design nozzle exit plane velocity, m/sec.
\bar{V}_{exh}, V_{exh}	= Average velocity of exhaust gas upon adiabatic isentropic expansion to ambient pressures relative to rocket, m/sec.
\bar{V}_f, V_f	= Average inwards diffusion front velocity of air moving into the plume, m/sec.
V_{fc}	= Inwards diffusion front velocity of air due to molecular diffusion only, m/sec.
V_{ft}	= Inwards diffusion front velocity of air due to turbulent diffusion only, m/sec.
\bar{V}_h	= Velocity of exhaust gas upon isentropic expansion to ambient pressures with radiation-correction accounted for, m/sec.
$\vec{V}_i = \vec{V}_i(\vec{r})$	= Bulk vector velocity of exhaust molecules X in excited level i at position \vec{r} , m/sec.
\bar{V}_r, V_r	= Mean velocity of exhaust molecules in Mach core relative to the atmosphere, m/sec.
$V_v = V_v(h)$	= Rocket vehicle velocity (dependent on altitude h), m/sec.
$V_k = (V_v - \tilde{V}_x)$	= Average air-relative exhaust velocity in ABCD region in axial (x) direction, m/sec.
V_M, \bar{V}_M	= Average bulk velocity of exhaust gas in Mach core region relative to the rocket, m/sec.
V_Q	= Mean velocity of exhaust gas in the ABCD region relative to the rocket, m/sec.

June 1974

V_x	= Mean velocity of exhaust gases in ABCD region in the axial x-direction relative to the rocket, m/sec.
V_y	= Mean velocity of exhaust gases in ABCD region in the y-direction perpendicular to the axial x-axis relative to the rocket, m/sec.
V_{ABCD}	= Average velocity of molecules (relative to the rocket) entering the ABCD region, m/sec.
VIS	= Visible region ($380 \leq \lambda \leq 700$ nm) of the spectrum. Used as subscript and in abbreviation.
VUV	= Vacuum ultraviolet part ($10 \leq \lambda \leq 200$ nm) of the electromagnetic spectrum. Used in abbreviation.
VBSR	= Vehicle body solar reflections, used as subscript and in abbreviation.
VBER	= Vehicle body earthshine reflections, used as subscript and in abbreviation.
VBSE	= Vehicle body self-emissions, used as subscript and in abbreviation.
w_i	= Statistical weight of excited level i.
W	= Rocket-expelled propellant mass, kgm.
\dot{W}	= Propellant mass expulsion rate, kgm/sec.
W_{BB}, W_{GB}	= Total radiant emittance per unit surface area (integrated over all solid angles and wavelengths) for a black-body (BB), gray-body (GB), $\text{watts} \cdot \text{m}^{-2}$

W_{tot} = Total radiant emittance per unit surface area
(integrated over all solid angles and wavelengths)
for a general solid or gaseous body, watts \cdot m⁻².

$W_{\text{BB}}(\lambda), W_{\text{tot}}(\lambda)$ = Total radiant emittance per unit surface area at
wavelength λ integrated over all solid angles, for
respectively a black-body and a general body,
watts \cdot m⁻².

x = X-direction along axis of jet or plume, m.

$x = \left(q_{\text{H}_2\text{O}} \right)_{\text{reaction product}}$ = Moles of H₂O produced per kgm of reactant mass in
AB region (used in Appendix E only).

x_{α} = Anharmonic constant of normal vibration α .

x_{ij} = Effective anharmonic constant for transition $i \rightarrow j$.

X, X_i = General designation for exhaust species ($X = \text{CO}_2$,
H₂O, CO, etc.), at internally excited level i .

y = Mole fraction.

y_{air} = Mole fraction of air.

y_X = Mole fraction of species X .

Y, Y_i = Designation for second molecular exhaust species
($Y = \text{H}_2\text{O}, \text{CO}_2$, etc.) in excited state i .

- $z_c^* = z_c^*(h)$ = Collisional excitation rate factor in the atmosphere for atmospheric pumping, sec^{-1} .
- $z_c^r = z_c^r(h)$ = Chemical reaction rate factor in the atmosphere for high-altitude chemical reactions, sec^{-1} .
- z_{Xd} = Photo-dissociation rate for molecules X in the exosphere under solar UV illumination, sec^{-1} .
- z_α = Dipole charge number of normal vibration α for infrared-active transitions.
- z_{ij} = Effective vibrational dipole charge number for transition $i \rightarrow j$.
- z_{eff} = Effective charge number for outer (ionizable) electrons in atom or molecules.
- z_q, z_v = Partition or "sum-of-states" function of internal energy modes.
- z_v = Partition function of the vibrational energy states of a molecule.
- α = Aspect angle, that is angle between line-of-sight and rocket vehicle trajectory, degrees or radians.
- α_s = Angle between space object axis and object-to-sun line, degrees or radians.
- α_o = Angle between space object axis and object-to-observer line, degrees or radians.
- $\alpha_I^{\text{eff}}, \alpha_I$ = (Effective) earthshine illumination angle between earth-center to target line and body axis defined by Eq. (3.50), degrees or radians.

- β = Dimensionless constant defined by Eq. (E.47) used in AB calculations (used in Appendix E only).
- β = Solar zenith angle, radians or degrees.
- β_E = Solar zenith angle at a point on earth surface (see fig. 3.7), radians or degrees.
- β_M = Radiative correction factor for expanding exhaust gases due to radiation in Mach core region, defined by Eq. 3.186.
- $\beta_{\alpha i}$ = Morse exponential coefficient for normal vibration α of electronic excited level i (used in vibronic band calculations).
- $\gamma = c_p/c_v$ = Gas coefficient or ratio of specific heats.
- γ = Used as subscript to indicate a photon.
- $\gamma = b/a$ = Dimensionless constant used in AB process calculations for H_2 , defined by Eq. (E.51)(used in Appendix E only).
- γ_s, γ_o = Special angles defined by Eq. (3.19) and the following discussion.
- δ = Dimensionless constant used in AB calculations defined by Eq. (E.46)(used in Appendix E only).
- $\delta = \delta(A_p)$ = Angle between local normal of an elemental surface area dA_p of the plume and the sensor's line-of-sight, degrees or radians.

June 1974

- δ = Apex half-angle of conically-shaped space body or plume, degrees or radians.
- $\delta(x)$ = Dirac delta function; $\delta(x) = 0$ for $x \neq 0$, $\delta(x) = 1$ for $x = 0$.
- $\epsilon = \epsilon(\lambda)$ = Emissivity of a body (at wavelength λ).
- $\bar{\epsilon}$ = Wavelength-averaged emissivity of a body.
- ϵ_γ = Photon energy, Joules, ergs, or eV.
- $\epsilon_{\gamma i}$ = Photon energy of photons emitted from level i , Joules, ergs, or eV.
- ϵ_i = Energy of level i in a molecule or atom, Joules, ergs, or eV.
- ϵ_{ij} = Energy difference between levels i and j in a molecule or atom, Joules, ergs, or eV.
- ϵ_d = Dissociation energy of a molecule, ergs, Joules, or eV.
- ζ = Hill-Draper plume parameter defined by Eq. (3.227).
- ζ_{ion} = Ionization factor defined by Eq. (G.12) used in Rayleigh scattering formula.

- μ * SPECIAL PARAMETER USED IN VIEW-FACTOR CALCULATIONS,
DEFINED BY EQ (C.47)
- η = Illuminator-target-observer angle, degrees or radians.
- η_s = Sun-target-observer angle, degrees or radians.
- η_{AB} = Efficiency or fractional degree of reaction of fuel
in exhaust with atmospheric oxygen.
- η_{AG} = Conversion efficiency of heat to airflow radiation
in vehicle body air friction mechanism.
- η_i = Fraction of molecules X excited to level i in ABCD
region due to the temperature increase by the ABCD
processes.
- θ = Rocket engine thrust angle relative to vehicle
direction of motion, degrees or radians.
- θ, θ_{fov} = Field-of-view angle, radians.
- $\theta, \theta_U, \theta_L$ = Special angles defined in figure 3.7 and by equation
(3.49).
- θ_s = Photon-particle scattering angle, $\theta_s = \pi - \eta_s$,
radians or degrees.
- Θ = Non-dimensionalized average temperature in ABCD region.
- Θ_1, Θ_2 = Non-dimensionalized temperatures for ABCD region to be
used in Boltzmann factor (subscript 1) and in band-
shape function (subscript 2) calculations. Always
 $\Theta_2 < \Theta_1$.
- θ_s = SOLAR ZENITH ANGLE, RADIAN OR DEGREES.

κ_0	= Imaginary part of the refractive index of a material.
λ	= Photon wavelength, μm or nm .
$\Delta\lambda$	= Small difference, deviation, or uncertainty in photon wavelength about the value λ , μm or nm .
λ_c	= Center wavelength of solar UV spectral line, nm .
$\Delta\lambda_c$	= Linewidth of solar UV spectral line, nm .
λ_i	= Wavelength corresponding to energy level i , μm or nm .
λ_{ij}	= Wavelength for transition $i \rightarrow j$, μm or nm .
λ_α	= Fundamental wavelength of normal vibration α , μm .
λ_{ion}	= Wavelength below which a molecule can be photo-ionized, nm .
λ_1, λ_2	= Wavelength of first, second electronic excitation level(s), nm .
λ_{pd}	= Wavelength below which predissociation of the molecule can occur, nm .
λ_d	= Wavelength corresponding to dissociation energy of a molecule, Hz or Hb .
$\lambda_{d\&i}$	= Wavelength at or below which a molecule is photo-dissociated and excited level i is created in one of the dissociation products, nm .
$\lambda = L_p/D_p$	= Non-dimensionalized plume length used in view-factor calculations

June 1974

FTD-CW-01-01-74
Vol. I

- $\mu = q/p$ = Dimensionless ratio used in AB process calculations for CO defined by Eq. (E.69) (used in Appendix E only).
- $\mu_{a/e}$ = Air to exhaust molar "mixing ratio" in the ABCD mixing region of the plume.
- ν = Photon frequency, Hz or Hb.
- ν_i = Frequency of level i , Hz or Hb.
- $\nu_{io} = \nu_i$ = Frequency of transition $i \rightarrow o$, Hz or Hb.
- ν_{ij} = Frequency difference between levels i and j , Hz or Hb.
- $\Delta\nu_{ij}$ = Frequency spread of emission band or line from transitions $i \rightarrow j$, Hz or Hb.
- ν_A, ν_B, ν_C = Rotational constants of molecules, Hz or Hb.
- ν_α = Fundamental frequency of normal vibration α , Hz or Hb.
- ν_{ion} = Frequency above which a molecule can be photo-ionized, Hz or Hb.
- ν_1, ν_2 = Frequencies of first, second, electronic excitation level(s) in molecule, Hz or Hb.
- ν_{pd} = Frequency above which a molecule can be predissociated by a photon, Hz or Hb.
- ν_d = Frequency corresponding to dissociation energy of a molecule, Hz or Hb.
- ν_{d+i} = Frequency at or above which a molecule is photo-dissociated and an excited level i is created in one of the dissociation products, Hz or Hb.
- ν_p, ν_q = Special vibronic frequencies defined by Eqn. (3.349) and (3.350), Hz or Hb.
- μ = SPECIAL PARAMETER USED IN VIEW GRAPH CALCULATIONS,
DEFINED BY ⁵¹⁵ EQ. (C.47)

June 1974

ξ_i = AB chemical reaction conversion parameter giving the number of excited states X_i produced due to combustion reactions of fuel molecules F with atmospheric oxygen, per fuel molecule F.

$\xi_{fr} = \xi_{fr}(h)$ = Freezing fraction = mole fraction of H_2O in exhaust that freezes out in the plume.

ξ_a = Limiting AB chemical conversion fraction for H_2 and CO defined by Eq. (3.216).

ξ_h = Limiting AB chemical conversion fraction for H_2 defined by Eq. (3.217).

ξ_c = Limiting AB chemical conversion fraction for CO defined by Eq. (3.218).

ξ_∞ = AB conversion fraction for an infinitely long plume.

ξ_B, ξ_{BC} = Rotational anharmonic coefficients of molecules.

$\rho, \rho(\lambda)$ = Reflectivity of a material for unpolarized light at normal incidence (at wavelength λ).

$\bar{\rho}$ = Wavelength-averaged reflectivity of a material or body.

$\rho_{||}, \rho_{\perp}$ = Reflectivity of a material for parallel and perpendicular polarized light.

ρ_{VIS}, ρ_{UV} = Average reflectivity of a material for unpolarized light in respectively the visible (VIS) and ultra-violet (UV) regions of the solar spectrum.

- ρ_e = Density of exhaust gas in nozzle exit plane, kgm/m^3 .
- $\rho_i, \rho_p, \rho_{p_i}$ = Density of solidified particles of species i in rocket exhaust, gms/cm^3 .
- ρ_i = Special cross-section ratio defined by Eq. (3.81).
- ρ_i = Dimensionless vibronic factor for electronic level i defined by Eq. (3.348) used in vibronic band calculations.
- $\rho_{\text{air}}, \rho_a$ = Density of atmospheric air, $\text{g} \cdot \text{cm}^{-3}$, $\text{kg} \cdot \text{m}^{-3}$, or $\text{kg} \cdot \text{cm}^{-3}$.
- ρ_I = Gas density in CORE/ABCD interface region, $\text{gms} \cdot \text{cm}^{-3}$ or $\text{kgm} \cdot \text{m}^{-3}$.
- $\rho = D_s/D_p$ = Dimensionless geometric ratio used in view factor calculations.
- σ = Electrical conductivity, ohm-cm.
- σ = General cross-section of a body, particle, or molecule, m^2 or cm^2 .
- $\bar{\sigma}_a, \sigma_a$ = (Wavelength averaged) photon absorption cross-section of molecules, m^2 or cm^2 .
- $\bar{\sigma}_p, \sigma_p$ = (Wavelength- and size-averaged) photon scattering cross-section of a solid microparticle, m^2 or cm^2 .
- $\sigma_s, \sigma_{\text{sc}}, \sigma_{\text{Rayleigh}}$ = Average photon scattering cross-section of molecules (Rayleigh scattering), m^2 or cm^2 .
- σ_s = Apparent or equivalent isotropic photon reflection cross-section of a vehicle or body in space, m^2 .

- σ_e = Apparent or equivalent isotropic emission cross-section of a vehicle or body in space, m^2 .
- $(\sigma_c)_m, \bar{\sigma}_{c_i}, \bar{\sigma}_{c_X}$ = Gas-kinetic collision cross-section of molecules m , i , or X , m^2 or cm^2 .
- $(\sigma_{jX})_i$ = Average resonant (V-V) energy transfer cross-section for collisional interactions between excited molecules Y_j and non-excited molecules X resulting in excited molecules X_i , m^2 .
- $(\bar{\sigma}_{YX})_i$ = Average collisional T-V excitation cross-section for collisional interactions between unexcited molecules Y and X resulting in the excitation of molecule X to level i , m^2 .
- $\sigma_{Yi} = \sigma_{Yi}(\lambda)$ = Absorption cross-section of photons of wavelength λ by molecules X resulting in excitation i , m^2 .
- $\sigma_{iY} = \sigma_{iY}(\lambda)$ = Stimulated deexcitation cross-section by photons of wavelength λ for excited molecules X_i resulting in their deexcitation, m^2 .
- $\sigma_{a/e} = \bar{\sigma}_{a/X} = \sigma_{a/X}$ = Average collision cross-section between air molecules and exhaust molecules, m^2 .
- σ_* = Collisional deexcitation cross-section, m^2 .
- σ_{ion} = Photo-ionization cross-section of an atom or molecule, m^2 or cm^2 .
- $\sigma_{abs} = \sigma_{abs}(\lambda)$ = Photo-absorption cross-section of an atom or molecule at wavelength λ , m^2 or cm^2 .
- $\Sigma_a = \Sigma_a(\lambda)$ = Macroscopic photon absorption cross-section (at wavelength λ), cm^{-1} or m^{-1} .
- $\Sigma_o = \Sigma_o(\lambda) = \Sigma_a + \Sigma_s$ = Total macroscopic photon extinction cross-section (at wavelength λ), cm^{-1} or m^{-1} .
- $\Sigma_s = \Sigma_s(\lambda)$ = Macroscopic photon scattering cross-section (at wavelength λ), cm^{-1} or m^{-1} .

- τ_i, τ_i^0 = Radiative decay time of excited level i of species X , sec.
- $\bar{\tau}_c, \tau_c$ = Mean dwell time of exhaust molecules in core region in deep space, sec.
- τ_{qi} = Mean or effective decay time of excited level i due to V-V transfer collisions with suppressant molecules, sec.
- τ_{i*} = Average regeneration time of excitation of level i in the ATMP process, sec.
- $(\tau_{a/X})_i$ = Mean time between collisions for excitation of level i of molecule X when the latter is in a cloud in the atmosphere, sec.
- τ_{Xd} = Mean time before photo-dissociation of molecules X occurs in exosphere due to solar UV, sec.
- τ_{CD} = Mean time of collisionless travel in a sensor's field of view for air molecules colliding with exhaust molecules, sec.
- τ_M = Mean dwell time of exhaust molecules in the core of the plume, sec.
- τ_r = Mean radiative decay time of excited species in Mach core region, sec.
- $\tau_s, \tau_{si}, \tau_{sX}$ = Effective field-of-view transit time defined by Eqs. (3.262) or (3.263). for molecules i or X , sec.
- $\tau_s^i, \tau_{si}^i, \tau_{sX}^i$ = Effective field-of-view transit time defined by Eqs. (3.271) and (3.272) for molecules i or X , when photo-dissociation is present.

- u, dv = Differential element of volume, m^3 .
- φ = Average flare angle of plume defined in Appendix F, degrees or radians.
- $\varphi_{\max}, (\varphi_{CD})_{\max}$ = Maximum average flare angle reached when the ambient pressure $p_a \rightarrow 0$, degrees or radians (see Appendix F).
- $\varphi_Y = \varphi_Y(\lambda)$ = Solar photon flux (at wavelength λ), photons $\cdot m^{-2} \cdot sec^{-1}$.
- $\frac{d\varphi_Y}{d\lambda}$ = Spectral solar photon flux (at wavelength λ), photons $\cdot m^{-2} \cdot nm^{-1}$.
- ϕ_i = Degrees of freedom of molecular species i ; for diatomic molecules $\phi_i = 5$ and for triatomic molecules $\phi_i \approx 7$.
- ϕ = Special parameter defined by Eq. (3.222), used in vibrational matrix element calculations.
- ϕ = Optical angle of incidence, degrees or radians.
- ϕ_o, ϕ_s = View angles defined in figure 3.1, degrees or radians.
- Φ_v, Φ_λ = Photon fluence per unit frequency, per unit wavelength, photons $cm^{-2} \cdot sec^{-1} \cdot Hz^{-1}$.

χ = Angle used in dielectric reflection calculations, defined by Eq. (3.39), degrees or radians.

χ = Special frequency ratio used in photoionization cross-section calculations, defined by Eq. (G.7).

$\chi_p, \chi_g, \chi_r, \chi_v$

= SPECIAL DIMENSIONLESS RATIOS USED IN VIEW-FACTOR CALCULATIONS: DEFINED BY EQS. (C.43) THROUGH (C.46).

ψ = Dihedral angle between planes of α_s and α_o (see Figure 3.1).

ψ_i = Gain in concentration of species i in exhaust due to creation by AB process, moles/kgm.

ψ_s = Sun-target-observ' angle, degrees or radians.

ω = Angle between direction of polarization and the plane of incidence, radians or degrees.

$\Omega, d\Omega$ = Solid angle, differential solid angle, steradians.

χ_c

= FACTOR USED TO CALCULATE THE AVERAGE CORE TEMPERATURE. SEE Eq. (3.115).

UNITS AND CONVERSION FACTORS

Prefix Scaling Values:

T	=	Tera-	=	10^{12}
G	=	Giga-	=	10^9
M	=	Mega-	=	10^6
k	=	kilo-	=	10^3
h	=	hecto-	=	10^2
da	=	deca-	=	10

Basic Unit = 1

d	=	deci-	=	10^{-1}
c	=	centi-	=	10^{-2}
m	=	milli-	=	10^{-3}
μ	=	micro-	=	10^{-6}
n	=	nano-	=	10^{-9}
p	=	pico-	=	10^{-12}
f	=	femto-	=	10^{-15}
a	=	atto-	=	10^{-18}

Examples: 1 pm = 10^{-12} meters; 1 MJ = 10^6 Joules; 1 heV = 100 electronvolts;
1 mTorr = 10^{-3} Torr; etc.

Length:

1 m	=	1 meter	=	100 cm
1 cm	=	1 centimeter	=	0.01 m
1 ft	=	1 foot	=	30.48 cm
1 in	=	1 inch	=	2.54 cm
1 nm	=	10^{-9} m	=	10^{-7} cm = 10° Å

PRECEDING PAGE BLANK NOT FILMED

1 Å	= 1 Angstrom = 10^{-8} cm = 10^{-10} m = 10^{-1} mm
1 μm	= 1 micrometer = 1 micron = 10^{-4} cm = 10^{-6} m
1 km	= 10^3 meter = 0.6215 mile
1 mi.	= 1 mile
1 n.mi.	= 1 nautical mile = 1.853 km

Area:

1 barn	= 10^{-24} cm ² = 10^{-28} m ²
1 a	= 1 are = 10^2 m ² = 10^6 cm ²
1 ha	= 1 hectare = 10^4 m ² = 10^8 cm ²
1 acre	= 43,560 ft ² = 0.4047 ha = 4046.8564 m ²

Volume:

1 ℓ	= 1 liter = 1000 cm ³ = 1.057 quart
1 ml	= 1 milliliter = 1 cm ³
1 gal	= 1 gallon = 4 quarts = 3.785 ℓ
1 qt	= 1 quart = 0.9461 ℓ
1 cu.ft.	= 1 ft ³ = 7.481 gal. = 28.32 ℓ
1 cu.in.	= 1 in ³ = 16.387 cm ³

Time:

1 s	= 1 sec = 1 second
1 ms	= 1 millisecond = 10^{-3} s
1 μs	= 1 microsecond = 10^{-6} s
1 ns	= 1 nanosecond = 10^{-9} s
1 year	= 365 days = 8760 hours =
1 year	= 525,600 minutes = 3.1536×10^7 seconds

Mass:

1 g	= 1 gm = 1 gram = 10^{-3} kg
1 kg	= 1 kilogram = 10^3 g
1 lb	= 1 pound = 453.59 g = 0.45359 kg
1 slug	= 32.174 lb = 14.594 kg
1 metric ton	= 10^3 kg = 10^6 g = 2205 lb
1 British ton	= 2000 lb = 907.2 kg
1 amu	= 1 atomic mass unit = 1.65983×10^{-24} g

Photon Frequency:

1 Hz	= 1 hertz = 1 s^{-1} = 1 cps = 1 cycle per second
1 Hz	= 33.356 pHb = 3.3356×10^{-11} Hb
1 MHz	= 1 megahertz = 10^6 Hz = 0.033 mHb
1 GHz	= 10^9 Hz = 33 mHb = 0.033 Hb
1 THz	= 1 terahertz = 10^{12} Hz = 33.36 Hb
1 Hb	= 1 herzberg = 1 cm^{-1} = 1 wavenumber
1 Kb	= 0.03 THz = 30 GHz
1 mHb	= 1 millihertzberg = 10^{-3} Hb = 10^{-3} cm^{-1}
1 pHb	= 1 picohertzberg = 10^{-12} Hb
1 mHb	= 30 Mhz

Energy:

1 erg	= 1 dyne-cm = $1 \text{ g} \cdot \text{cm}^2 \cdot \text{s}^{-2}$ = 10^{-7} J = = 6.2418×10^{11} eV
1 J	= 1 Newton-m = $1 \text{ kg} \cdot \text{m}^2 \cdot \text{s}^{-2}$ = 10^7 erg = = 6.2418×10^{18} eV
1 eV	= 1 electron-volt = 1.6021×10^{-12} erg = = 1.6021×10^{-19} Joules

June 1974

$$\begin{aligned} 1 \text{ cal} &= 1 \text{ calorie} = 4.18 \text{ J} = 4.18 \times 10^7 \text{ ergs} \\ 1 \text{ kcal} &= 1 \text{ Cal} = 1 \text{ kilocaloric} = 1000 \text{ cal} = 4,180 \text{ J} \\ 1 \text{ eV/molecule} &= 23.06 \text{ kcal/mole} \\ 1 \text{ BTU} &= 252 \text{ cal} = 778 \text{ ft} \cdot \text{lb} = 1055 \text{ J} \end{aligned}$$

Power:

$$\begin{aligned} 1 \text{ W} &= 1 \text{ watt} = 1 \text{ J} \cdot \text{s}^{-1} = 10^7 \text{ erg s}^{-1} \\ 1 \text{ kW} &= 1 \text{ Kilowatt} = 10^3 \text{ W} \\ 1 \text{ HP} &= 1 \text{ Horse Power} = 0.746 \text{ kW} \\ 1 \text{ BTU/hr} &= 0.29306 \text{ W} \end{aligned}$$

Pressure:

$$\begin{aligned} 1 \text{ atm} &= 1 \text{ atmosphere} = 760 \text{ Torr} = 1.0133 \text{ bar} = 14.696 \text{ psi} \\ 1 \text{ Torr} &= 1 \text{ mm Hg} = 1.3158 \times 10^{-3} \text{ atm} = 1333.2 \text{ dyne} \cdot \text{cm}^{-2} \\ 1 \text{ bar} &= 0.9869 \text{ atm} = 750 \text{ Torr} = 10^6 \text{ dyne} \cdot \text{cm}^{-2} = 10^3 \text{ pascal} \\ 1 \text{ pascal} &= 1 \text{ Newton} \cdot \text{m}^{-2} = 10^{-2} \text{ mbar} = 10 \text{ dyne} \cdot \text{cm}^{-2} \\ 1 \text{ psi} &= 1 \text{ lb} \cdot \text{in}^{-2} = 6.895 \times 10^4 \text{ dyne} \cdot \text{cm}^{-2} \\ 1 \text{ psf} &= 1 \text{ lb} \cdot \text{ft}^{-2} = 478.8 \text{ dyne} \cdot \text{cm}^{-2} \end{aligned}$$

Force:

$$\begin{aligned} 1 \text{ dyne} &= 10^{-5} \text{ newton} = 1 \text{ g} \cdot \text{cm} \cdot \text{s}^{-2} \\ 1 \text{ newton} &= 1 \text{ kg} \cdot \text{m} \cdot \text{s}^{-2} = 10^5 \text{ dyne} = 7.2330 \text{ poundal} \\ 1 \text{ poundal} &= 0.031081 \text{ lbs-force} \\ 1 \text{ lbs(f)} &= \text{pound-force} = 0.4536 \text{ kg(f)} = 4.445 \text{ Newton} \\ 1 \text{ g(f)} &= \text{gram-force} = 980 \text{ dyne} = 0.00980 \text{ Newtons} \\ 1 \text{ Mg(f)} &= 10^3 \text{ kg(f)} = 10^6 \text{ g(f)} = 9,800 \text{ Newtons} \end{aligned}$$

Temperature:

$$\begin{aligned}
 1^{\circ}\text{K} &= 1 \text{ degree Kelvin} = \frac{9}{5}^{\circ}\text{R} \\
 1^{\circ}\text{R} &= 1 \text{ degree Rankine} = \frac{5}{9}^{\circ}\text{K} \\
 x^{\circ}\text{C} &= (x + 273.16)^{\circ}\text{K} \\
 x^{\circ}\text{F} &= (x + 459.7)^{\circ}\text{R}
 \end{aligned}$$

Electrical

$$\begin{aligned}
 1 \text{ C} &= 1 \text{ coulomb} = 6.242 \times 10^{18} \text{ electrons} \\
 1 \text{ Faraday} &= 96,520.1 \text{ C} = 6.0247 \times 10^{23} \text{ electron charges} \\
 1 \text{ A} &= 1 \text{ amp} = 1 \text{ ampere} = 1 \text{ C} \cdot \text{s}^{-1} = \\
 &= 6.242 \times 10^{18} \text{ electrons} \cdot \text{s}^{-1} \\
 1 \text{ V} &= 1 \text{ volt} = 1 \text{ W} \cdot \text{A}^{-1} = 1 \text{ J} \cdot \text{C}^{-1} \\
 1 \Omega &= 1 \text{ ohm} = 1 \text{ V} \cdot \text{A}^{-1} \\
 1 \text{ F} &= 1 \text{ farad} \\
 1 \text{ H} &= 1 \text{ henry} \\
 1 \text{ esu} &= 1 \text{ electrostatic charge unit} = 1 \text{ erg}^{1/2} \text{ cm}^{1/2} = \\
 &= 1.6021 \times 10^{-19} \text{ C} \\
 1 \text{ debye} &= 1 \text{ dipole moment unit} = 10^{-18} \text{ erg}^{1/2} \text{ cm}^{3/2}
 \end{aligned}$$

BASIC PHYSICAL CONSTANTS

Avogadro's Number	A_o	$= 6.02471 \times 10^{23} \text{ molecules} \cdot (\text{mole})^{-1}$
Atomic Mass Unit	amu	$= A_o^{-1} = 1.65983 \times 10^{-24} \text{ g}$
Boltzmann Constant	k	$= 1.3804 \times 10^{-16}, \text{ erg} \cdot (^{\circ}\text{K})^{-1}$ $= 1.3804 \times 10^{-23}, \text{ Joule} \cdot (^{\circ}\text{K})^{-1}$ $= 0.86167 \times 10^{-4}, \text{ eV} \cdot (^{\circ}\text{K})^{-1}$
Gas Constant	R	$= 8.317 \times 10^7 \text{ erg} \cdot (^{\circ}\text{K})^{-1} \cdot (\text{mole})^{-1}$ $= 1.987 \text{ cal} \cdot (^{\circ}\text{K})^{-1} \cdot (\text{mole})^{-1}$ $= 83.17 \text{ bar} \cdot \text{cm}^3 \cdot (^{\circ}\text{K})^{-1} \cdot (\text{mole})^{-1}$ $= 82.08 \text{ atm} \cdot \text{cm}^3 \cdot (^{\circ}\text{K})^{-1} \cdot (\text{mole})^{-1}$
Planck's Constant	h	$= 6.6252 \times 10^{-27} \text{ erg/Hz}$ $= 6.6252 \times 10^{-34} \text{ Joules/Hz}$ $= 1.9862 \times 10^{-16} \text{ ergs/Hb}$ $= 1.9862 \times 10^{-23} \text{ Joules/Hb}$
Velocity of Light	c	$= 2.99793 \times 10^{10} \text{ cm/sec}$ $= 2.99793 \times 10^8 \text{ m/sec}$
Electronic Charge Squared	e^2	$= 2.3068 \times 10^{-19} \text{ erg} \cdot \text{cm}$ $= 2.3068 \times 10^{-28} \text{ Joule} \cdot \text{m}$ $= 1.440 \times 10^{-7} \text{ eV} \cdot \text{cm}$
Electronic Charge	e	$= 4.8029 \times 10^{-10} \text{ erg}^{1/2} \text{ cm}^{1/2}$ $= 4.8029 \times 10^{-10} \text{ esu}$
Electronic Mass	m_e	$= 0.54875 \times 10^{-3} \text{ amu}$ $= 0.91083 \times 10^{-27} \text{ g}$ $= 0.91083 \times 10^{-30} \text{ kg}$

Proton Mass	m_p	=	1.00759 amu
		=	1836.2 m_e
		=	1.67243×10^{-24} g
		=	1.67243×10^{-27} kg
Neutron Mass	m_n	=	1.00898 amu
		=	1838.7 m_e
		=	1.67474×10^{-24} g
		=	1.67474×10^{-27} kg
Hydrogen Atom Mass	m_H	=	1.00814 amu
		=	1837.1 m_e
		=	1.67334×10^{-24} g
		=	1.67334×10^{-27} kg
Earth Gravitational Constant	\bar{g}	=	$980.665 \text{ cm/sec}^2 = 9.80665 \text{ m/sec}^2$
	g_{pole}	=	$983 \text{ cm/sec}^2 = 9.83 \text{ m/sec}^2$
	g_{equator}	=	$978 \text{ cm/sec}^2 = 9.78 \text{ m/sec}^2$
Bohr Orbit (Hydrogen Atom) Radius	a_0	=	$a_H = h^2 / (4\pi^2 m_e e^2) =$
		=	0.52917×10^{-8} cm
		=	0.52917×10^{-10} m
Classical Electron Radius	a_e	=	$e^2 / (m_e c^2) =$
		=	0.28178×10^{-12} cm
		=	0.28178×10^{-14} m
Compton Electron Wavelength	λ_c	=	$h/m_e c = 2.42626 \times 10^{-10}$ cm
		=	2.42626×10^{-12} m

Fine Structure Constant	α	$= \frac{2\pi e^2}{hc} = \frac{1}{137.04}$
Planck/Boltzmann Ratio	h/k	$= 1.43886, (^{\circ}\text{K}) \cdot \text{Hb}^{-1}$ $= 4.79948 \times 10^{-11}, (^{\circ}\text{K}) \cdot \text{Hz}^{-1}$
Rydberg Energy (Ionization Energy of Hydrogen Atom)	R_y	$= \frac{e^2}{2a_c} = \frac{2\pi^2 m_e e^4}{h^2} = 13.605 \text{ eV}$ $= 2.1797 \times 10^{-11} \text{ erg}$ $= 2.1797 \times 10^{-18} \text{ Joules}$
Electron Rest Mass Energy	ϵ_e	$= m_e c^2 = 0.51098 \times 10 \text{ eV}$ $= 8.1864 \times 10^{-7} \text{ erg}$ $= 8.1864 \times 10^{-14} \text{ Joules}$
Electron Velocity in Bohr Orbit	v_H	$= \frac{2\pi e^2}{h} = 2.188 \times 10^8 \text{ cm/sec}$ $= 2.188 \times 10^6 \text{ m/sec}$
Thomson Electron Cross-Section	σ_T	$= \frac{8}{3} \pi a_e^2 = \frac{8\pi e^2}{3 m_e c^2}$ $= 0.6652 \times 10^{-24} \text{ cm}^2$ $= 0.6652 \times 10^{-28} \text{ m}^2$
Bohr Orbit (Hydrogen Atom) Cross-Section	σ_B	$= \pi a_0^2 = \frac{h^2}{4\pi m_e^2} =$ $= 0.8798 \times 10^{-16} \text{ cm}^2$ $= 0.8798 \times 10^{-20} \text{ m}^2$
Stefan-Boltzmann (Radiation) Constant	τ_{SB}	$= \frac{2\pi^5 k^4}{15 h^3 c^2} =$ $= 4.6687 \times 10^{-12} \text{ W} \cdot \text{cm}^{-2} \cdot (^{\circ}\text{K})^{-4}$

June 1974

FTO-CW-01-01-74
Vol. I

Photon Parameter Conversions
(Energy ϵ , Frequency ν ,
Wavelength λ)

(1 Hz = 1 sec⁻¹; 1 Hb = 1 cm⁻¹)

$$\nu = c \cdot \lambda^{-1}$$

$$\nu = \epsilon \cdot h^{-1}$$

$$\nu(\text{Hz}) = 2.99793 \times 10^{10} \cdot \lambda^{-1} (\text{cm})$$

$$\nu(\text{Hb}) = \lambda^{-1} (\text{cm})$$

$$\nu(\text{Hz}) = 1.5094 \times 10^{26} \cdot \epsilon (\text{erg})$$

$$\nu(\text{Hb}) = 5.0347 \times 10^{15} \cdot \epsilon (\text{erg})$$

$$\nu(\text{Hz}) = 2.4182 \times 10^{14} \cdot \epsilon (\text{eV})$$

$$\nu(\text{Hb}) = 8066.166 \cdot \epsilon (\text{eV})$$

REFERENCES

1. "Proceeding of the Third Symposium on Remote Sensing of Environment," held October 1964, Infrared Physics Lab., Inst. of Sc. Tech., Univ. of Michigan, Ann Arbor, Michigan, 1965.
2. Handbook of Military Infrared Technology, Chapters 3, 4, and 5, W. F. Wolfe, Editor, Office of Naval Research, Supt. of Documents, Washington, D.C., 1965.
3. "Photography of Chemiluminescent Studies of Upper Atmosphere Wind Phenomena," by J. Mazzotta, R. Proctor, and J. Latimer, Special Report No. 176, Smithsonian Institution Astrophysical Observatory, May 17, 1965.
4. "Chemical Releases at High Altitudes," by N. W. Rosenberg, Science, Vol. 152, No. 3725, p. 1017, May 20, 1966.
5. "Artificial Plasma Clouds in Space," by G. Haerendel and R. Lust, Scientific American, p. 81, Nov. 1968.
6. "Atmospheric Photochemistry," by R. D. Cadle and E. R. Allen, Science, Vol. 167, No. 3916, p. 243, Jan. 16, 1970.
7. "Photometry from Apollo Tracking," by C. A. Lundquist, Space Research X, North-Holland Publ. Co., Amsterdam, 1970.
8. "Baker-Nunn Observations of Apollo 9 S-IVB," Special Report 903-27, Smithsonian Institution Astrophysical Lab., March 7, 1969.
9. "Observations of the Apollo-12 Liquid Oxygen Cloud with a New Type of Spectrograph," by L. J. Lentwaard and H. Van de Stadt, J. of Physics E: Scientific Instruments 1971, Vol. 4, p. 879.
10. "Water and Oxygen Particles in Space from Apollo Missions," by R. D. Sharma, M. L. Kratage, and A. C. Buffalano, J. of Spacecraft, Vol. 8, No. 12, p. 1230, Dec. 1971.
11. "A Preliminary Review of the Upper Atmosphere Observations Made During the Saturn High Water Experiment," by K. H. Debus, W. G. Johnson, R. V. Hembree, and C. A. Lundquist, Proceedings of the XIIIth Internat. Astron. Congress, Varna 1962, p. 182; Springer-Verlag, 1964.

12. "Study on Exhaust Plume Radiation Predictions," Report No. GDC-DBE 66-017, General Dynamics Corp., Dec. 1966.
13. "Some Recent Developments on the Analysis of Exhaust Plume Afterburning," by R. Edelman and O. Fortune, General Applied Sciences Laboratory, Inc. Report P #176, 1968.
14. "Plume Analysis Study," by J. Rowe, R. Gilbert, and H. White, Aerospace Corp., San Bernardino, Calif., APP-0158 (S9990)-19, 1968.
15. "Spectral Emissivities and Integrated Intensities of the $2.7 \mu\text{m}$ H_2O Band Between 530°K and 220°K ," by C. C. Ferriso and C. B. Ludwig, J. of Qu. Spect. Rad. Trans., Vol. 4, pp. 205-222, 1964.
16. "Spectral Emissivities and Integrated Intensities of the $2.7 \mu\text{m}$ CO_2 Band Between 1200°K and 1800°K ," by C. C. Ferriso and C. B. Ludwig, J. of Opt. Soc. of Am., Vol. 54, No. 5, pp. 657-662.
17. "Thermal Radiation From the Exhaust Plume of an Aluminized Composite Rocket Propellant," by S. J. Morizumi and H. J. Carpenter, J. of Spacecraft and Rockets, Vol. 1, No. 5, p. 501, 1964.
18. "Particle Characteristics in Two-Phase Plumes," by L. J. Delaney, Martin-Marietta Corp., Internal Report, 1968.
19. "Analytical Approximation for the Flow From a Nozzle Into a Vacuum," by J. A. F. Hill and J. S. Draper, J. of Spacecraft and Rockets, Vol. 3, No. 10, p. 1552, Oct. 1966.
20. "Rarefaction Effects in Exhaust Plumes," by B. B. Hamel, E. P. Muntz, and B. L. Maguire, City Univ. of New York and General Electric Co., Pa., Internal Paper, July 1968.
21. "Highly Rarefied Rocket Exhaust Plume Flow Fields," by M. J. Wayte and J. A. Osida, The Boeing Company, Internal Report, 1968.
22. Handbook of Astronautical Engineering, edited by H. H. Koelle; "Propulsion Fundamentals," by R. C. Truax, Chapter 17, pp. 17-5 through 17-18, First Edition, McGraw-Hill, 1961.
23. "Intermediate Altitude Rocket Exhaust Plumes," by J. C. Tannehill and E. W. Anderson, J. of Spacecraft, Vol. 8, No. 10, p. 1052, Oct. 1971.
24. Handbook of Geophysics and Space Environments, edited by S. L. Valley, Air Force Cambridge Research Laboratories (AFCRL), 1965.

25. Radiation and Reentry , by S. S. Penner and D. B. Olfe, Academic Press, 1968.
26. Theoretical Evaluation of Chemical Propellants, by R. L. Wilkins, Prentice-Hall, 1963.
27. Propellant Performance and Gas Composition Handbook , by S. A. Johnston, E. A. Mathias, P. C. Hanzel, and L. Schieler, Aerospace Corp. Tech. Report No. TDR-930(2210-07) TN-1, 1962.
28. TRW Space Data, 3rd edition, J. B. Kendrick, Editor, TRW Public Relations Dept., 1967.
29. "Electro-Optical Techniques Study," ASD-TDR-63-821, prepared by Northrop Space Labs for AF AVIONICS Lab, October 1963.
30. Fundamentals of Optics, by F. A. Jenkins and H. E. White, 2nd edition, McGraw-Hill, 1950.
31. "Illumination of a Space Vehicle Surface Due to Sunlight Reflected From Earth," A. J. Dennison, Jr., ARS Journal, p. 635, April 1962.
32. "On the Angular Distribution of Photon Radiance of a Perfectly Reflective Spherical Satellite Irradiated by a Lambertian Earth," by R. A. Schmeltzer, J. Appl. Optics, 8 , 1, 179, January 1969.
33. An Introduction to Thermodynamics, the Kinetic Theory of Gases, and Statistical Mechanics, by F. W. Sears, Addison-Wesley, 1950.
34. Kinetic Theory of Gases, by E. H. Kennard, McGraw-Hill, 1938.
35. Quantitative Molecular Spectroscopy and Gas Emissivities, by S. S. Penner, Addison-Wesley, 1959.
36. "Some Studies of Axisymmetric Jets Exhausting from Sonic and Supersonic Nozzles Into Still Air and Into Supersonic Streams," by E. S. Love and C. E. Grigsby, NACA Report RML54L31, May 10, 1951.
37. Boundary Layer Theory , by H. Schlichting, McGraw-Hill, 1960.
38. Elementary Fluid Mechanics , by J. K. Vennard, 2nd ed., John Wiley, 1951.
39. "The Characteristics of the Turbulence in the Mixing Region of a Round Jet," by P.O.A.L. Davies, M. J. Fisher, and M. J. Barratt, J. Fluid Mech., 15 , 337.

40. "Initial Inclination of the Mixing Boundary Separating an Exhausting Supersonic Jet from a Supersonic Ambient Stream," by E. S. Love, NACA Report RML55J14, January 11, 1956.
41. Light Scattering by Small Particles, by H. C. Van de Hulst, Wiley, 1957.
42. "Proceedings of the Rocket Plume Phenomena Specialists Meeting," edited by B. Brown and A. Muraszew, Vols. I and II, Aerospace Corp. Report TDR-0200 (4413)-4, 14 February 1969.
43. Quantum Mechanics, by L. I. Schiff, 3rd edition, McGraw-Hill, 1968.
44. Atomic Theory of Gas Dynamics, by J. W. Bond, K. M. Watson, and J. A. Welch, Addison-Wesley, 1965.
45. Quantum Theory of Radiation, by W. Heitler, 3rd edition, Oxford, 1953.
46. The Identification of Molecular Spectra, by R. W. B. Pearse and A. G. Gaydon, 3rd edition, Chapman and Hall, Ltd., 1965.
47. Spectra of Diatomic Molecules, by G. Herzberg, Van Nostrand, 1950.
48. Electronic Spectra of Polyatomic Molecules, by G. Herzberg, Van Nostrand, 1966.
49. "The Chemical Kinetics and the Composition of the Earth's Atmosphere," prepared by M. Bortner and R. Kummier, Space Sciences Lab., General Electric, Report No. GE-9500-ECS-SR-1, July 1968.
50. "Aerosol Extinction Contribution to Atmospheric Attenuation in Infrared Wavelengths," by John A. Hodges, Appl. Optics 11, No. 10, 2304, October 1972.
51. Atomic Transition Probabilities - Hydrogen through Neon, Vol. I, and Sodium through Calcium, Vol. II; NSRDS-NBS4 and NSRDS-NBS22, U.S. Govt. Printing Office.
52. Atomic Energy Levels, Vol. I (1H-23V); Vol. II (24Cr-41Nb); Vol. III (42 Mo-57 La; 72 Hf-89 Ac); by C. E. Moore, Circular 467, NBS, U.S. Govt. Printing Office.
53. "Analysis of SAO Photographs of Apollo-7, Apollo-8, and Apollo-9 Visible Cloud Emissions," by J. W. Eerkens, Science and Technology Associates Report No. S&T 69/9L, 28 July 1969.
54. "Interrogation of Space Vehicle Exhaust Clouds With a Laser Illuminator/Detector System," by J. W. Eerkens, Science and Technology Associates Report No. S&T 69/35L, prepared under Contract NASW-1821 (Mod. 4), 15 September 1969.

June 1974

DISTRIBUTION

Commander
U. S. Army Missile Command
Attn: AMSMI-RNS/Mr. Fronefield
Redstone Arsenal, Alabama 35809

Director
Defense Advanced Research Projects
Agency
Attn: Program Management
Technical Information Office
Dr. R. Hoglund
Col. F. Baker, Jr.
Maj. R. L. Paulson
Mr. R. Zirkind
1400 Wilson Boulevard
Arlington, Virginia 22209

Office of the Director
Defense Research & Engineering
The Pentagon
Attn: Mr. D. Brockway
Mr. R. Moore
Mr. Makepeace
Washington, D. C. 20301

U. S. Army Advanced Ballistic
Missile Defense Agency
Attn: Dr. R. Ruffine
Dr. J. Jamieson
Dr. J. Gilstein
Commonwealth Building
1320 Wilson Boulevard
Arlington, Virginia 22209

U. S. Army Advanced Ballistic
Missile Defense Agency
Attn: RDMH-R/R. Heatherly
RDMH-O/Dr. W. O. Davies
RDMH-M/Mr. A. Carmichael
RDMH-O/Mr. R. Bowen
P. O. Box 1500
Huntsville, Alabama 35807

U. S. Army Research Office
Attn: Dr. Robert Mace
Box 011, Duke Station
Durham, North Carolina 27706

U. S. Army, Safeguard Systems Office
Attn: Mr. Bobby J. Sisco
1320 Wilson Boulevard
Arlington, Virginia 22209

Hq., USAF
Attn: Lt. D. M. Schlatter, RDSD
Washington, D. C. 20330

SAMSO, AFSC
Attn: Lt. C. Zimmerman
Lt. H. Harkleroad
A. F. Unit Post Office
Los Angeles, California 90045

Air Force Office of Scientific
Research, USAF
Attn: Dr. J. Masi
Cpt. L. R. Lawrence
1400 Wilson Boulevard
Arlington, Virginia 22209

Air Force Cambridge Research Lab.
Attn: Scientific Library
CRREL, Stop 29
Dr. N. W. Rosenberg
Dr. J. Garing
Dr. A. T. Stair
Dr. D. Golomb
Mr. B. P. Sanford/OPR
L. H. Hanscom Field
Bedford, Massachusetts 01731

Rome Air Development Center, AFSC
Attn: RALS
Griffiss Air Force Base
Rome, New York 13440

Air Force Rocket Propulsion Lab.
Attn: Dr. L. Quinn
Cpt. Nunn
Cpt. Lupton
Edwards, AFB, California 92523

AEDC
Attn: Dr. W. K. McGregor
Dr. D. Whitfield
Arnold AFS
Tullahoma, Tennessee

Air Force Avionics Laboratory, AFSC
Attn: Dr. A. Mantz
Dr. D. Parker
Ltc. J. Rudzki
Cpt. R. Weber
Wright-Patterson Air Force Base
Ohio 45433

Chief of Naval Operations
Department of the Navy
Attn: Commander G. R. McKee
Washington, D. C. 20360

Naval Ordnance Laboratory
Attn: Dr. L. Schindel
White Oak
Silver Spring, Maryland 20910

U. S. Naval Research Laboratory
Attn: Dr. T. Chubb
Washington, D. C. 20390

Office of Naval Research
Attn: Dr. R. Roberts
Washington, D. C. 20360

Central Intelligence Agency
Attn: Mr. Berquist
Washington, D. C. 20505

National Bureau of Standards
Attn: Dr. K. G. Kessler
Washington, D. C. 20234

U. S. ACDA
Department of State
Washington, D. C. 20451

Aerodyne Research, Inc.
Technical Operations Building
Attn: Dr. J. Draper
D. M. Moran
South Avenue
Burlington, Massachusetts 01803

AeroChem Research Labs., Inc.
Attn: Dr. A. Fountijn
Dr. W. Miller
P. O. Box 12
Princeton, New Jersey 08540

Aerospace Corporation
El Segundo Operations
Attn: Dr. F. Simmons
Dr. K. Horn
Mr. S. Evans
Dr. T. Taylor
Dr. D. Steward
Mr. R. Kuiper
P. O. Box 95085
Los Angeles, California 90045

Aerojet-General Corporation
Attn: Dr. S. Golden
Aerojet-Electrosystems
P. O. Box 296
Azusa, California 91702

AVCO-Everett Research Lab.
Attn: Dr. Raymond L. Taylor
Dr. J. Mayer
Dr. R. Weiss
2385 Revere Beach Parkway
Everett, Massachusetts 02149

Boeing Company
Aerospace Group
Attn: Dr. Y. Yoler/Mail Stop 41/25
P. O. Box 3999
Seattle, Washington, 98124

Calspan Corporation
Attn: Dr. C. Treanor
Dr. W. Wurster
Dr. P. Marrone
4455 Genesee Street
Buffalo, New York 14221

General Electric Company
Missiles and Space Division
Valley Forge Space Technology Center
Attn: Dr. J. Burns
Dr. D. Barr
Dr. J. Vent
P. O. Box 8555
Philadelphia, Pennsylvania 19101

General Research Corporation
Attn: Dr. W. Hamilton
1501 Wilson Boulevard
Arlington, Virginia 22209

June 1974

FTD-CW-01-01-74
Vol. I

General Research Corporation
Attn: Mr. W. W. Short
P. O. Box 3587
Santa Barbara, California 93105

General Motors Corporation
DELCO Electronics Defense Research Labs.
Attn: Dr. R. Hayami
6767 Hollister Avenue
Santa Barbara, California 93107

Geophysics Corporation of America
Attn: Dr. F. Marm
Burlington Road
Bedford, Massachusetts 01730

Advanced Research Associates of
Princeton (ARAP)
Attn: Dr. S. Fishborn
Princeton, New Jersey

Institute for Defense Analyses
Attn: Dr. P. Davis
Dr. H. G. Wolfhard
400 Army-Navy Drive
Arlington, Virginia 22202

Battelle
Strategic Technology Office
Information Analysis Center (STOLAC)
Room 10-311
505 King Avenue
Columbus, Ohio 42301

LTV Aerospace Corporation
Vought Missiles & Space Co.
Texad Vision
Attn: Mr. F. K. McGinnis
P. O. Box 6267
Dallas, Texas 75222

Lockheed Missiles & Space Co.
Attn: Mr. R. Capiaux
Dr. K. Wilson
Dr. C. E. Smith
3251 Hanover Street
Palo Alto, California 94304

McDonnell-Douglas Corporation
Attn: Dr. M. Thomas
5301 Balsa Avenue
Huntington Beach, Calif. 92646

Philco-Ford Corporation
Aeronutronics Division
Attn: J. J. Geanakos
Newport Beach, California 92663

Physical Dynamics, Inc.
Attn: Dr. E. Fisher
P. O. Box 604
College Park Station
Detroit, Michigan 48221

Physical Dynamics, Inc.
Attn: Mr. Frederick Boynton
125 University Avenue
Berkeley, California 94704

Polytechnic Institute of Brooklyn
Graduate Center
Attn: Dr. M. Bloom
Broad Hollow Road
Route 110
Farmingdale, L. I., New York 11735

R&D Associates
Attn: Dr. Forrest Gilmore
Mr. L. Wilson
P. O. Box 3580
Santa Monica, California 90403

Riverside Research Institute
Attn: Dr. G. Glaser
80 West End Avenue
New York, New York 10023

TRW Systems Group
Attn: Dr. F. Mastrup
Dr. L. Hromas
Dr. J. Stenbit
Mr. F. Vogenitz
One Space Park
Redondo Beach, California 90278

University of California
Attn: Dr. S. S. Penner
P. O. Box 109
La Jolla, California 92307

UNCLASSIFIED

SECURITY CLASSIFICATION OF THIS PAGE (When Data Entered)

REPORT DOCUMENTATION PAGE		READ INSTRUCTIONS BEFORE COMPLETING FORM										
1. REPORT NUMBER FTD-CW-01-01-74	2. GOVT ACCESSION NO.	3. RECIPIENT'S CATALOG NUMBER										
4. TITLE (and Subtitle) Rocket Radiation Handbook, Volume I "Rocket Radiation Phenomenology and Theory"		5. TYPE OF REPORT & PERIOD COVERED Volume I of Series										
		6. PERFORMING ORG. REPORT NUMBER Garrett No. 74-9903										
7. AUTHOR(s) Jozef W. Eerkens		8. CONTRACT OR GRANT NUMBER(s) F33657-72-C-0850										
9. PERFORMING ORGANIZATION NAME AND ADDRESS AiResearch Mfg. Co., Division of Garrett Corp. Torrance, Calif.		10. PROGRAM ELEMENT, PROJECT, TASK AREA & WORK UNIT NUMBERS N/A										
11. CONTROLLING OFFICE NAME AND ADDRESS Foreign Technology Division (AFSC) Wright-Patterson AFB, Ohio 45433		12. REPORT DATE June 1974										
		13. NUMBER OF PAGES 564 pages										
14. MONITORING AGENCY NAME & ADDRESS (if different from Controlling Office) Foreign Technology Division (AFSC) Wright-Patterson AFB, Ohio 45433		15. SECURITY CLASS. (of this report) Unclassified										
		15a. DECLASSIFICATION DOWNGRADING SCHEDULE										
16. DISTRIBUTION STATEMENT (of this Report) Distribution of this document is unlimited.												
17. DISTRIBUTION STATEMENT (of the abstract entered in Block 20, if different from Report) Distribution is unlimited.												
18. SUPPLEMENTARY NOTES												
19. KEY WORDS (Continue on reverse side if necessary and identify by block number)												
<table border="0"> <tr> <td>Rocket Radiation Phenomenology</td> <td>High-Altitude Radiation</td> </tr> <tr> <td>Rocket Radiation Signatures</td> <td>Atmosphere-Pumped Cloud Radiation</td> </tr> <tr> <td>Rocket Plume Radiation</td> <td>Solar Ultraviolet Luminescence</td> </tr> <tr> <td>Airshock/Collisional Radiation</td> <td>Particle-Scattered Radiation</td> </tr> <tr> <td>Afterburning Radiation</td> <td>Space-Vehicle-Reflected Radiation</td> </tr> </table>			Rocket Radiation Phenomenology	High-Altitude Radiation	Rocket Radiation Signatures	Atmosphere-Pumped Cloud Radiation	Rocket Plume Radiation	Solar Ultraviolet Luminescence	Airshock/Collisional Radiation	Particle-Scattered Radiation	Afterburning Radiation	Space-Vehicle-Reflected Radiation
Rocket Radiation Phenomenology	High-Altitude Radiation											
Rocket Radiation Signatures	Atmosphere-Pumped Cloud Radiation											
Rocket Plume Radiation	Solar Ultraviolet Luminescence											
Airshock/Collisional Radiation	Particle-Scattered Radiation											
Afterburning Radiation	Space-Vehicle-Reflected Radiation											
20. ABSTRACT (Continue on reverse side if necessary and identify by block number)												
See Reverse												

PRECEDING PAGE BLANK NOT FILMED

DD FORM 1 JAN 73 1473

EDITION OF 1 NOV 65 IS OBSOLETE

UNCLASSIFIED

SECURITY CLASSIFICATION OF THIS PAGE (When Data Entered)

UNCLASSIFIED

SECURITY CLASSIFICATION OF THIS PAGE(When Data Entered)

ABSTRACT

A review is given of various mechanisms responsible for the generation of infrared, visible, and ultraviolet radiation from aerospace rockets. Key mechanisms responsible for most of the observed radiation are identified by examining the order-of-magnitude of the energy that is fed to each one. For the exhaust, the major mechanisms are:

Undisturbed Core Relaxation (CORE); Afterburning (AB); Air Shock Collisional Deceleration (CD); Atmospheric Pumping (ATMP); Solar Scattering by Particles (SOSP); Solar Ultraviolet Absorption and Reradiation (SUAR),

while radiation from vehicle hardware is primarily caused by:

Vehicle Body Solar Reflections (VBSR); Vehicle Body Earth-shine Reflections (VBER); Vehicle Body Self-Emissions (VBSE).

The AB and CD mechanisms are coupled and abbreviated ABCD. CORE and ABCD radiation are produced in different regions of the rocket plume and it is shown that they can be analyzed separately; together they are responsible for most of the infrared emissions from a thrusting rocket. ATMP is a weak infrared afterglow radiation from the slowed-down exhaust cloud that is active only at medium-high altitudes. It decays slowly but is usually not observed because of its dilution and because it is outside the field-of-view of a vehicle-tracking sensor.

SOSP and SUAR are primarily operative in the visible part of the spectrum. SUAR is important at altitudes above 135 km and is shown to be the origin of several spectacular emissions in the visible observed during the Apollo space flights.

After a qualitative survey, detailed quantitative expressions are developed for each of the main mechanisms. These expressions provide the spectral radiance as a function of altitude for different types of fuel/exhaust species, rocket hardware parameters, and rocket trajectories. In the derivation of the analytical expressions for ABCD and CORE radiances, a new approach is presented which differs from most earlier techniques. The new approach consists of applying the conservation law to the rate of production and loss of excited states in the plume, the use of Gauss divergence theorem to the radiating region, and the application of generalized spectral broadening functions which are evaluated in Volume II. Although some inevitable approximations are used, the new technique appears to give results that are more tractable, more general, and more exact than those obtained by earlier methods.

Examples are finally presented on how to calculate altitude dependent rocket-radiation signatures in the infrared. Computer-calculated curves of the integrated radiation in selected spectral ranges of the $2.66 \mu\text{m}$ H_2O band and the $4.26 \mu\text{m}$ CO_2 band are shown as a function of flight time for two different rockets. Computer-calculated NIR and UVIS spectral emissions are also presented as a function of wavelength for a given altitude.

UNCLASSIFIED

SECURITY CLASSIFICATION OF THIS PAGE(When Data Entered)

where:

$$f(x) = 2\pi \left(\frac{\nu_{ion}}{\nu} \right)^{1/2} \left\{ \frac{\exp(-4x \cot^{-1} x)}{1 - \exp(-2\pi x)} \right\} \quad (G.6)$$

$$x = \left(\frac{\nu_{ion}}{\nu - \nu_{ion}} \right)^{1/2} \quad (G.7)$$

and where:

Z_{eff} = Effective charge number of atomic shell from which electron under consideration is removed in the ionization process (see Table G-1).

ν_{ion} = Ionization frequency for electron transition under consideration in atom or molecule, Hz

ν = Photon frequency, Hz

For frequencies ν such that $\nu_{ion} \lesssim \nu \lesssim 6\nu_{ion}$, Eq. (G.6) may be approximated with an accuracy of 1 percent by (Ref. 44):

$$f(x) = 0.115 \left(\frac{\nu}{\nu_{ion}} \right) - 0.010 \left(\frac{\nu}{\nu_{ion}} \right)^2 \quad (G.8)$$

$$(\nu_{ion} \lesssim \nu \lesssim 6\nu_{ion})$$

With (G.8) substituted in Eq. (G.5), one then obtains the useful relation:

$$\sigma_{ion} = 6.30 \times 10^{-18} \left(\frac{1}{Z_{eff}^2} \right) \left\{ \left(\frac{\nu_{ion}}{\nu} \right)^{5/2} - 0.087 \left(\frac{\nu_{ion}}{\nu} \right)^{3/2} \right\}, \text{ cm}^2$$

$$(\nu_{ion} \lesssim \nu \lesssim 6\nu_{ion}) \quad (G.8)$$

In Tables G-1 and G-2, values for Z_{eff} and ν_{ion} are listed for some atoms and molecules.

G.2 RAYLEIGH SCATTERING

To obtain theoretical relations for the Rayleigh scattering of photons by molecules, one requires again the theory of quantum mechanics. From Refs. 44 and 45, one finds that:

$$\frac{d\sigma_{sc}}{d\Omega} = \frac{8\pi}{3} z_{outer} \left(\frac{e^2}{m_e c^2} \right)^2 \left(\frac{\nu}{\nu_{ion}} \right)^4 \left(\frac{1 + \cos^2 \theta}{16 \pi/3} \right) =$$

$$= 3.9706 \times 10^{-26} z_{outer} \left(\frac{\nu}{\nu_{ion}} \right)^4 (1 + \cos^2 \theta), \frac{\text{cm}^2}{\text{ster}} \quad (G.9)$$

Here z_{outer} is the number of electrons in the outer valence shell and ν_{ion} is the average ionization frequency of the valence shell tabulated in Tables G-1 and G-2.

The total cross-section is obtained by integrating (G.9) over all solid angles ($d\Omega = 2\pi \sin\theta d\theta$). The result is:

TABLE G-1. EFFECTIVE CHARGE NUMBERS AND IONIZATION FREQUENCIES OF OUTER
(VALENCE) SHELL FOR THE FIRST 36 ELEMENTS OF THE PERIODIC TABLE

Element	Atomic Number, Z = N	Valence-Shell Principal Quantum Number, n_v	Ionization Energy, E_{ion} , eV	Ionization Frequency ν_{ion} , THz*	Effective Nuclear Charge, $Z_{eff} = n_v \sqrt{\frac{E_{ion}}{Ry}}$
H	1	1	13.595	3320.7	1.00
He	2	1	24.580	6003.9	1.35
Li	3	2	5.390	1316.6	1.25
Be	4	2	9.320	2276.5	1.66
B	5	2	8.296	2026.4	1.56
C	6	2	11.264	2751.3	1.82
N	7	2	14.54	3551.5	2.07
O	8	2	13.614	3325.4	2.00
F	9	2	17.42	4255.0	2.26
Ne	10	2	21.559	5266.0	2.52
Na	11	3	5.138	1255.0	1.84
Mg	12	3	7.644	1867.1	2.25
Al	13	3	5.984	1461.7	1.99
Si	14	3	8.149	1990.5	2.32
P	15	3	10.43	2547.6	2.62
S	16	3	10.357	2529.8	2.62
Cl	17	3	13.01	3177.8	2.93
A	18	3	15.755	3848.3	3.23
K	19	4	4.339	1059.8	2.26
Ca	20	4	6.111	1492.7	2.68
Sc	21	4	6.56	1602.3	2.78
Ti	22	4	6.83	1668.3	2.84
V	23	4	6.738	1645.8	2.82
Cr	24	4	6.76	1651.2	2.82
Mn	25	4	7.432	1815.3	2.96
Fe	26	4	7.896	1928.7	3.05
Co	27	4	7.86	1919.9	3.04
Ni	28	4	7.633	1864.4	3.00
Cu	29	4	7.723	1886.4	3.01
Zn	30	4	9.391	2293.8	3.32
Ga	31	4	5.97	1458.2	2.66
Ge	32	4	8.13	1985.8	2.09
As	33	4	10.05	2454.8	3.43
Se	34	4	9.750	2381.5	3.38
Br	35	4	11.84	2892.0	3.73
Kr	36	4	13.996	3418.7	4.06

*1 THz = 1 Terahertz = 10^{12} Hertz

TABLE G-2. EFFECTIVE CHARGE NUMBERS AND IONIZATION FREQUENCIES OF OUTER
(VALENCE) SHELL FOR MISCELLANEOUS MOLECULES

Molecule	Ionization Energy, E_{ion} , eV	Valence-Shell Equivalent Principal Quantum Number, n_v	Equivalent Principal Quantum Number for Lowest Excitations, n_m	Ionization Frequency ν_{ion} , THz	Effective Charge, $Z_{eff} = n_v \sqrt{\frac{E_{ion}}{Ry}}$
H ₂	15.422	1	2	3767.0	1.065
O ₂	12.2	3	3	2980.0	2.842
N ₂	15.576	3	3	3804.6	3.211
F ₂	15.7	3	4	3834.9	3.224
Cl ₂	11.48	4	4	2804.1	3.676
CO	14.009	3	3	3421.8	3.091
HCl	12.74	3	4	3111.9	2.904
HF	15.77	2	3	3852.0	2.154
NO	9.25	3	3	2259.4	2.475
OH	13.17	2	2	3216.9	1.968
HS	10.50	3	3	2564.7	2.636
H ₂ O	12.618	2	3	3082.1	1.927
CO ₂	13.769	4	4	3363.2	4.026
N ₂ O	12.893	4	4	3149.2	3.895
NO ₂	9.78	4	4	2388.9	3.393
SO ₂	12.34	4	4	3014.2	3.811
H ₂ S	10.472	3	4	2557.9	2.633
HCN	13.91	3	3	3397.7	3.035
OCS	11.24	4	4	2745.5	3.637
CS ₂	10.079	5	5	2461.9	4.305
O ₃	12.800	4	4	3126.5	3.881
NH ₃	10.154	2	3	2480.2	1.728
CH ₄	12.99	2	3	3172.9	1.955

$$\sigma_{sc} = 3.9706 \times 10^{-26} z_{outer} \left(\frac{\nu}{\nu_{ion}} \right)^4, \text{ cm}^2 \quad (G.10)$$

For most molecules $z_{outer} \approx 2$.

Often it is convenient to express (G.10) in terms of wavelength λ instead of frequency ν ($= c/\lambda$), and in terms of the ionization energy E_{ion} instead of ν_{ion} . In this case Eq. (G.10) becomes:

$$\sigma_{sc} = 5.3406 \times 10^{-29} \lambda_{(\mu m)}^{-4} \zeta_{ion}, \text{ cm}^2 \quad (G.11)$$

where:

$$\zeta_{ion} = \frac{z_{outer}}{2} \left(\frac{15.576}{E_{ion(eV)}} \right)^4 \quad (G.12)$$

Here the wavelength is in μm and we have normalized Eq. (G.11) to the value for the nitrogen molecule N_2 , for which $E_{ion} = 15.576$ eV, and $z_{outer} = 2$, and thus $\zeta_{ion} = 1$. Values for E_{ion} are also tabulated in Tables G-1 and G-2.

Comparing Eq. (G.10) with (G.8) it is clear that Rayleigh scattering is very weak (by a factor of $\sim 10^{-8}$) compared to photoionization for $\nu \sim \nu_{ion}$.

APPENDIX H
ATMOSPHERIC TRANSMISSION OF SOLAR ULTRAVIOLET
RADIATION AT HIGH ALTITUDES

To calculate ionization and excitation rates at high altitudes for the SUAR mechanism discussed in section 3.3.7, it is necessary to have an expression for the UV photon flux as a function of altitude. In the exosphere (above approximately 130 km), the UV intensity is essentially constant and as given by Eqs. (3.288) through (3.291) of section 3.3.7. However at lower altitudes these expressions must be multiplied by a transmission factor $Tr_s = Tr_s(\lambda, h, \theta_s)$ to account for the absorption losses suffered by solar photons while traveling from the exosphere to the atmospheric high-altitude point $h(\text{km})$ of interest (see Figure 2-4 of Chapter 2).

The atmospheric species responsible for most of the solar UV absorption in the atmosphere are oxygen (O_2), ozone (O_3), and aerosols. Other atmospheric species also absorb in the ultraviolet, but they are either present in much lower concentration, or their absorption cross-section is less. Removal due to scattering of solar UV photons also occurs, but the cross-section for UV scattering is much lower than that for absorption, as may be seen by comparing Figure H-1 with Figures H-2 through H-5 (see also Appendix G).

Figures H-2 through H-5 show consolidated plots of ultraviolet and visible absorption coefficients as reported in the literature (Refs. 24, 46, 47, and 48). These absorption curves are normalized to a molecular density of $n_0 = 2.55 \times 10^{19}$ molecules/cm³, and for other densities n the values shown in the graphs must be adjusted according to the relation:

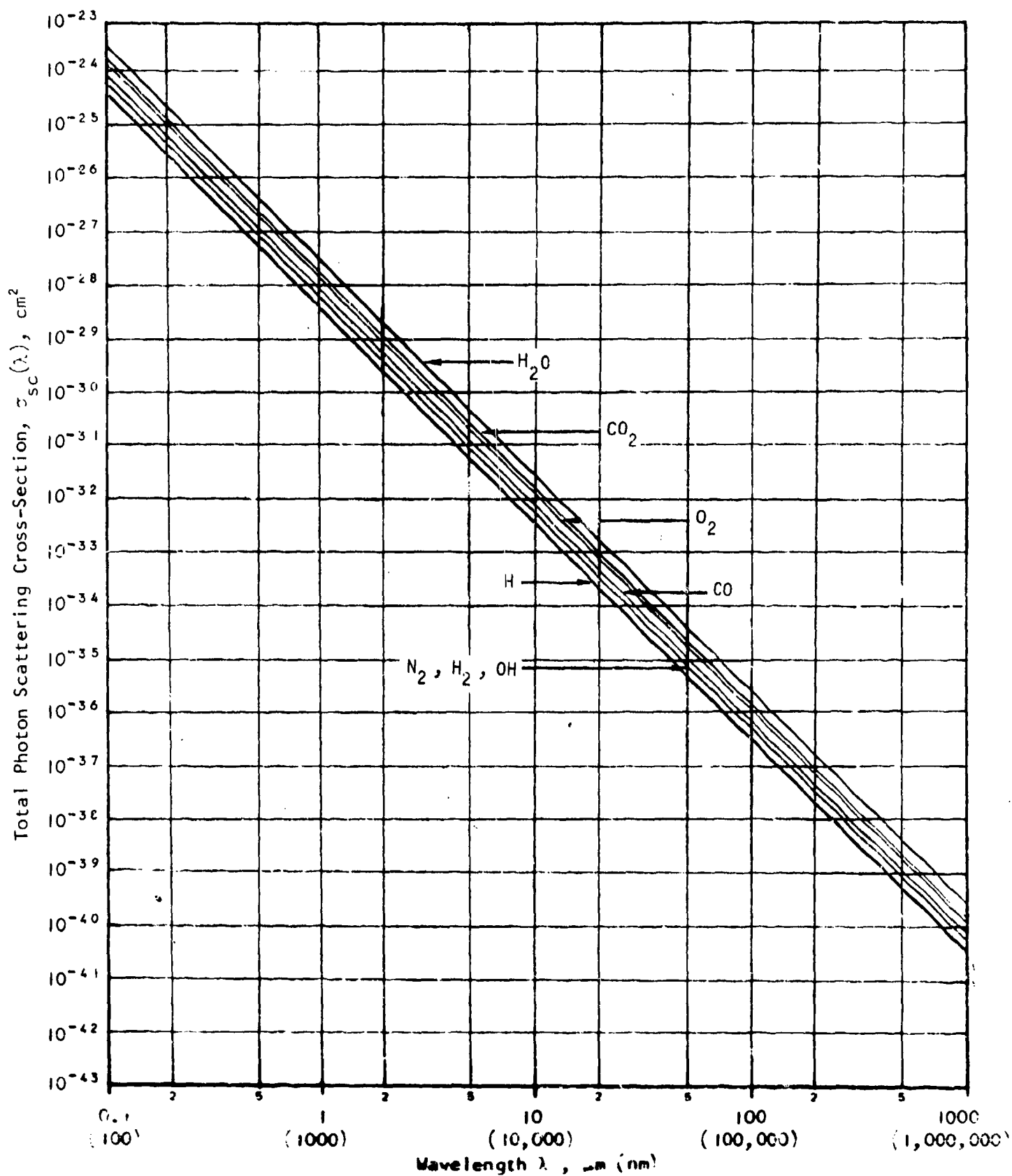
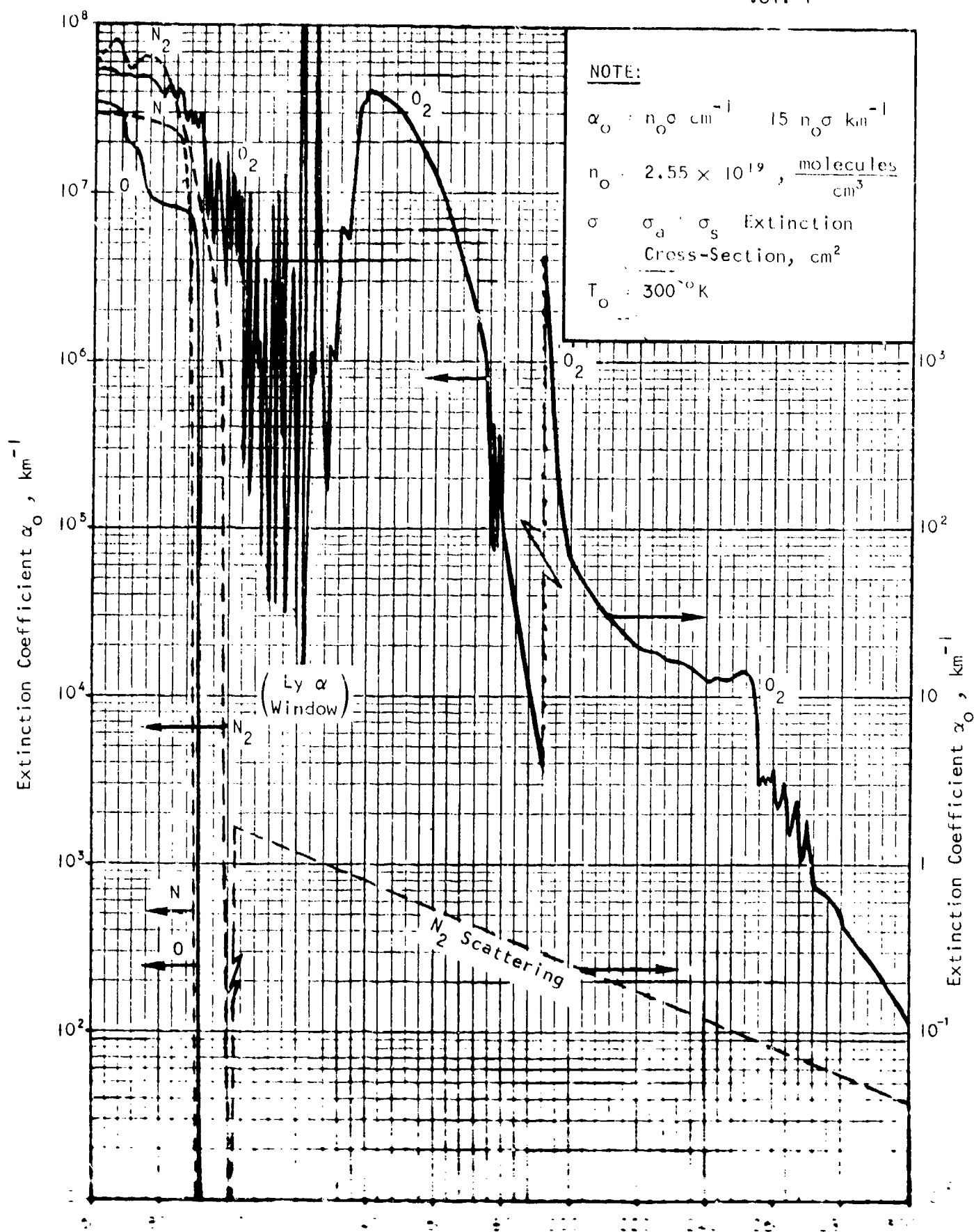


FIGURE K-1. PHOTON SCATTERING CROSS-SECTIONS

June 1974

FTD-CW-01-01-1/4
Vol. 1



June 19/4

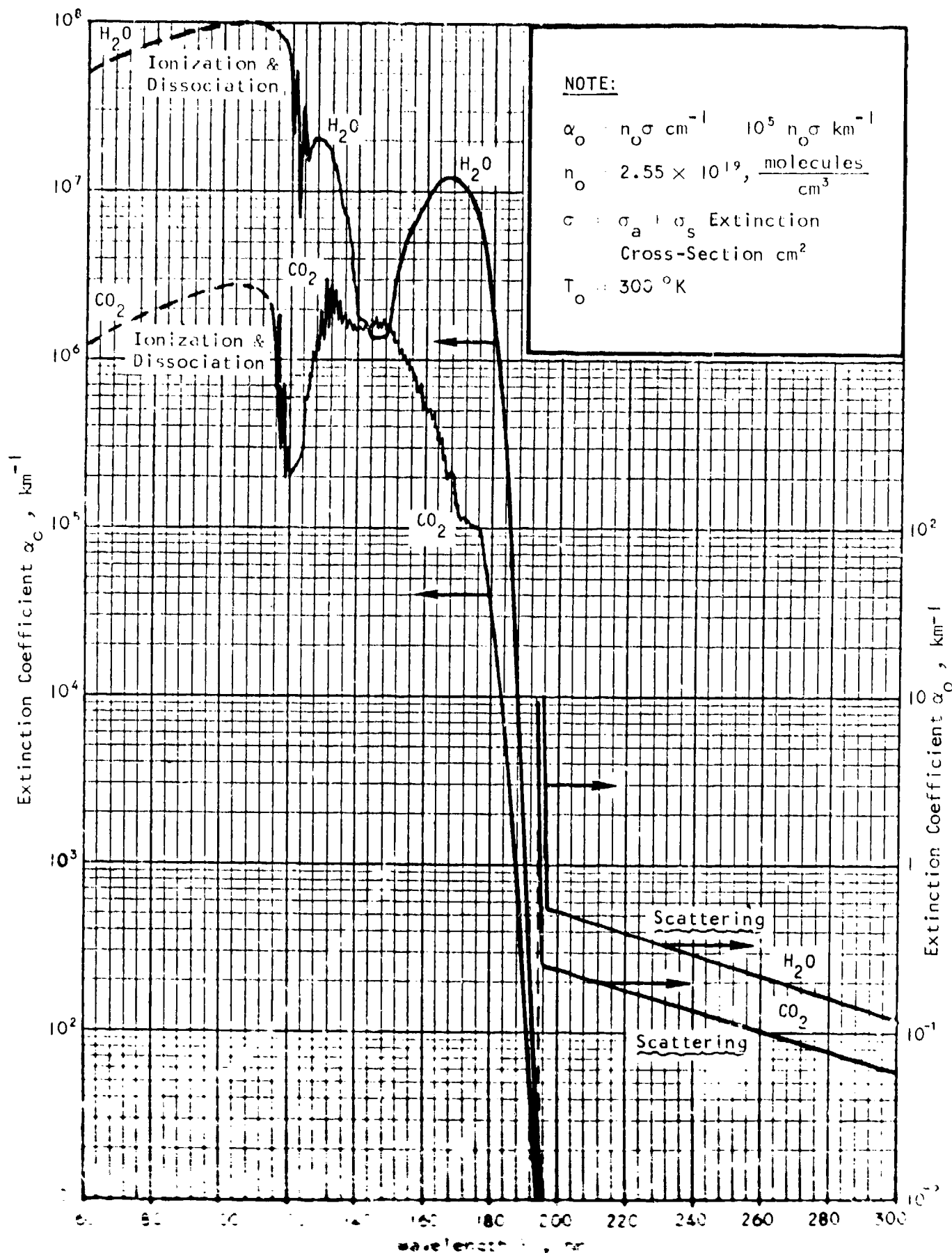


FIGURE 1-1. EXTINCTION COEFFICIENTS OF H₂O, CO₂